

# Characterization of MERISTEM DEFECTIVE as a splicing factor involved in the DNA damage response in plants

Dissertation submitted to the University of Hamburg  
Faculty of Mathematics, Informatics and Natural Sciences  
Department of Biology

presented by:

Cloe de Luxán Hernández

from Las Palmas de Gran Canaria

Hamburg, 2022





“Nada aprovecha tanto, ni se hace con más placer que aquello que uno mismo inventa y descubre, con la cooperación desde luego de una persona experta”

“Nothing is as rewarding or enjoyable as what we get to make and discover on our own, but in cooperation with an expert.”

Manuel Socorro Pérez, *La enseñanza del latín. Ensayo metodológico*, 35-36



**1. Referee: Prof. Dr. Stefan Hoth**

Institut für Pflanzenwissenschaften und Mikrobiologie, Universität Hamburg

**2. Referee: Prof. Dr. Óscar Lorenzo Sánchez**

Instituto Hispanoluso de Investigaciones Agrarias, Universidad de Salamanca

**Disputation date:** 28.10.2022



# TABLE OF CONTENTS

1. INTRODUCTION .....	21
<b>1.1 Plant Growth and Development.....</b>	<b>22</b>
1.1.1 Embryogenesis and Seed Germination.....	22
1.1.2 Apical meristems and post-embryonic growth.....	23
1.1.3 Vegetative and Reproductive growth.....	27
1.1.4 Senescence.....	30
<b>1.2 Cell proliferation .....</b>	<b>32</b>
1.2.1 Cell cycle phases .....	32
1.2.2 Regulation of cell cycle progression.....	33
1.2.3 Endoreplication .....	34
<b>1.3 Plant DNA damage response .....</b>	<b>35</b>
1.3.1 Types of DNA damage.....	35
1.3.2 Main components of the plant DDR.....	36
1.3.3 Cell cycle checkpoints.....	39
1.3.4 DNA repair mechanisms .....	40
1.3.5 Cell death induction.....	42
<b>1.4 Precursor-messenger RNA splicing .....</b>	<b>43</b>
1.4.1 Formation of the Plant Spliceosome.....	43
1.4.2 Alternative splicing.....	44
1.4.3 Splicing factors .....	45
1.4.4 RNA processing and DNA damage .....	48
2. AIMS OF THE DOCTORAL THESIS.....	55
3. MATERIAL AND METHODS .....	57
<b>3.1 Plant lineages .....</b>	<b>58</b>
3.1.1 Single mutant lines .....	58
3.1.2 Double mutant lines .....	60
3.1.3 Transgenic lines.....	61
<b>3.2 Plant phenotyping methods.....</b>	<b>70</b>

3.2.1	Monitoring of seed-related phenotypical traits.....	70
3.2.2	Phenotypical studies during seedling stage .....	70
3.2.3	Phenotypical studies of aerial tissues.....	71
3.2.4	Evaluation of cell cycle associated defects .....	72
<b>3.3</b>	<b>Differential expression and splicing analyses.....</b>	<b>74</b>
3.3.1	Differential expression analyses in selected targets .....	74
3.3.2	Genome-wide evaluation of expression and splicing changes .....	75
<b>3.4</b>	<b>Sensitivity assays to DNA damaging agents .....</b>	<b>77</b>
3.4.1	Primary root length and Adventitious root (AR) formation .....	77
3.4.2	True leaf formation .....	78
3.4.3	Cell death accumulation .....	78
3.4.4	Transcriptional induction of selected genes after genotoxic treatments .....	78
<b>3.5</b>	<b>Localization and interaction studies.....</b>	<b>80</b>
3.5.1	Transient expression in <i>Arabidopsis thaliana</i> protoplasts .....	80
3.5.2	Transient expression in <i>Nicotiana benthamiana</i> .....	81
3.5.3	Co-immunoprecipitation .....	82
3.5.4	BiFC.....	84
3.5.5	Co-localization and FLIM-FRET analyses.....	84
3.5.6	Yeast-Two-Hybrid.....	85
<b>3.6</b>	<b>Primers .....</b>	<b>87</b>
<b>4.</b>	<b>RESULTS.....</b>	<b>101</b>
<b>4.1</b>	<b><i>mdf</i> mutants display a pleiotropic phenotype that resembles constitutive activation of the plant DNA damage response.....</b>	<b>102</b>
4.1.1	Absence of MDF leads to reduced cell division and growth .....	102
4.1.2	The dwarf phenotype of <i>mdf</i> mutants is related to G2/M cell cycle arrest, increased endoreplication and cell death induction .....	105
4.1.3	<i>mdf</i> mutants exhibit growth arrest in later developmental stages .....	108
4.1.4	Seed production and germination is unaltered in <i>mdf</i> mutants.....	110
4.1.5	A putative C-terminal MDF truncated version restores some developmental defects associated to the absence of MDF in <i>mdf-2</i> mutants .....	111
4.1.6	Transgenic expression of <i>pMDFMDFg</i> restores the developmental defects present in <i>mdf</i> mutants .....	115

<b>4.2</b>	<b>MDF is localized in the spliceosome .....</b>	<b>118</b>
4.2.1	MDF is associated with the U4/U6.U5 tri-snRNP protein LSM8.....	118
4.2.2	MDF and LSM8 do not interact physically .....	120
4.2.3	Absence of MDF and LSM8 in <i>mdf-1lsm8-1</i> double mutants putatively results in embryo lethality.....	124
<b>4.3</b>	<b>MDF is required for the correct splicing and expression of numerous transcripts .....</b>	<b>128</b>
4.3.1	<i>mdf-1</i> mutants show splicing defects in genes important for transcriptional control and development .....	128
4.3.2	Absence of different components of the U4/U6.U5 tri-snRNP complex does not lead to equivalent defects in alternative splicing.....	129
4.3.3	Verification of the importance of MDF for the correct splicing of a subset of transcripts involved in splicing, DNA damage repair and transcriptional and cell cycle regulation.....	133
4.3.4	Genes involved in stress response, cell cycle and gene expression control and metabolism are commonly spliced and differentially expressed in <i>mdf-1</i> background	135
4.3.5	The pleiotropic defects observed in <i>mdf-1</i> mutants correlate with the abundant differential transcriptional changes.....	137
4.3.6	MDF controls the expression of genes associated to cell cycle control upon DNA damage.....	139
<b>4.4</b>	<b>MDF acts independently or downstream from DDR regulators SOG1 and ATM .....</b>	<b>144</b>
4.4.1	The cell cycle and growth arrest observed in <i>mdf</i> mutants is not rescued by the absence of SOG1 and ATM.....	144
4.4.2	The accumulation of dead cells in the RAM in <i>mdf</i> mutants occurs independently of SOG1 and ATM .....	146
4.4.3	Cell death accumulation in <i>mdf</i> and <i>mdfsog1-7</i> mutants is not influenced by temperature.....	148
4.4.4	Expression of SOG1-dependent DDR genes in meristematic tissues of <i>mdf</i> mutants is influenced by SOG1.....	149
<b>4.5</b>	<b>Analyses of the putative involvement of MDF in the plant DDR by assessing its response to different chemical treatments .....</b>	<b>151</b>
4.5.1	<i>mdf</i> mutants are hypersensitive to the DSB inducing drug zeocin .....	151
4.5.2	<i>mdf</i> mutants are insensitive to the replication inhibitor Hydroxyurea .....	161

4.5.3	<i>mdf</i> mutants are less sensitive to the oxidative stress induced by H <sub>2</sub> O <sub>2</sub> .....	164
4.5.4	<i>mdf-1</i> mutants are insensitive to the microtubule depolymerizing drug oryzalin	167
<b>4.6</b>	<b>The phosphorylation state of MDF influences its activity .....</b>	<b>170</b>
4.6.1	The phosphorylation of MDF is not essential for its nuclear localization....	170
4.6.2	The phosphorylation of MDF is important for its efficient function in cell division and growth control in the root.....	171
4.6.3	The phosphorylation state of MDF influences the aerial development of both <i>mdf</i> and WT transgenic plants.....	173
4.6.4	The growth arrest phenotype caused by expression of <i>35SMDF</i> in WT background is putatively dependent on ATM .....	176
4.6.5	The phosphorylation state of MDF does not influence the induction of cell death and DNA repair genes after DNA damage .....	178
4.6.6	Splicing efficiency of MDF seems to be regulated by its phosphorylation state in a developmental related manner .....	181
<b>5.</b>	<b>DISCUSSION .....</b>	<b>185</b>
<b>5.1</b>	<b>MDF strongly impacts Arabidopsis development.....</b>	<b>186</b>
5.1.1	MDF is a positive regulator of cell proliferation and plant growth .....	186
<b>5.2</b>	<b>MDF acts as a splicing and transcriptional regulator.....</b>	<b>190</b>
5.2.1	MDF is putatively associated to the U4/U6.U5 trisnRNP complex in the spliceosome.....	190
5.2.2	The pleiotropic phenotype of <i>mdf</i> mutants is correlated with numerous expression and splicing changes .....	192
<b>5.3</b>	<b>Loss of MDF leads to constitutive activation of the plant DDR and impaired response to DNA damaging drugs .....</b>	<b>195</b>
5.3.1	MDF has a putative role in the maintenance of genome stability by modulating the AS of important DDR regulators and regulating cell proliferation ....	195
5.3.2	<i>mdf</i> mutants exhibit altered sensitivity to genotoxic agents and SR-related proteins might have a conserved role in the plant DDR.....	197
5.3.3	The root growth phenotype is not recovered in <i>mdfsog1-7</i> and <i>mdfatm-2</i> double mutants .....	201
<b>5.4</b>	<b>The phosphorylation status of MDF influences Arabidopsis development.....</b>	<b>203</b>
<b>5.5</b>	<b>Conclusions.....</b>	<b>205</b>



6. SUMMARY .....	207
7. ADDITIONAL RESEARCH LINES .....	211
7.1 Analyses of the impact of the MAIN/MAIL1/PP7L complex in primary root growth and genome stability .....	212
7.2 Assessing the importance of the Translation Elongation complex eEF1B in cell division and plant development .....	213
ACKNOWLEDGEMENTS .....	215
REFERENCES .....	217
8. APPENDIX .....	239



# LIST OF ABBREVIATIONS

μL	Microlitre
3'SS	3' splicing site
5'SS	5' splicing site
9-1-1 complex	RAD9, RAD1, and HUS1
A. thaliana	Arabidopsis thaliana
A. tumefaciens	Agrobacterium tumefaciens
A3'SS	Alternative 3' splice site
A5'SS	Alternative 5' splice site
aa	Amino acid
ABA	Abscisic acid
ABC	Ammonium bicarbonate
ACN	Acetonitrile
Act-MYBs	Activator-type R1R2R3-Myb transcription factors
AD	Activating domain
adj	Adjusted
AG	AGAMOUS
AGC	Automatic gain control
AOX1C	ALTERNATIVE OXIDASE 1C
AP	APETALA
APC	Anaphase Promoting Complex/Cyclosome
AR	Adventitious roots
ARF8	AUXIN RESPONSE FACTOR 8
ARR	ARABIDOPSIS RESPONSE REGULATORS
AS	Alternative splicing
ASAP	Apoptosis and splicing associated
ATH13 PROTEIN 1	A. THALIANA OXIDATIVE STRESS-RELATED ABC1-LIKE
ATM	ATAXIA TELANGIECTASIA MUTATED
ATR	ATM AND RAD3- RELATED
ATRIP	ATR Interacting Protein
att	Attachment
BD	Binding domain

BER	Base excision repair
BiFC	Bimolecular fluorescence complementation
bp	Base pair
BRCA1	BREAST CANCER SUSCEPTIBILITY 1
Brr2p	Bad response to refrigeration 2 protein
BUD13	BUD SITESELECTION PROTEIN 13
bZIP	Basic leucine zipper
CAKs	CDK-activating kinases
CAPS	Cleaved Amplified Polymorphic Sequence
CD2B	CD2-binding protein-like protein
CDC26	CELL DIVISION CYCLE PROTEIN 26
CDKs	Cyclin dependent kinases
cDNA	Complementary DNA
CDS	Coding sequence
CHK1/2	CHECKPOINT KINASES 1 AND 2
CK	Cytokinins
CKIs	CDK inhibitors
CKL	CDC-like kinases
CLV3	CLAVATA 3
CMT3	CHROMOMETHYLASE3
CO	CONSTANS
Co-IP	Co-immunoprecipitation
Col-0	Columbia
CYC	Cyclin
CYCA	Cyclin type-A
CYCB	Cyclin type-B
CYCD	Cyclin type-D
CZ	Central zone
DAG	Days after germination
DAT	Days after transfer
dd	Double distilled
DDR	DNA damage response
DEG	Differentially Expressed Gene
DFD	DHFS-FPGS HOMOLOG D

D-loop	Displacement loop
dNTP	Deoxyribose nucleoside triphosphate
DOT2	DEFECTIVELY ORGANIZED TRIBUTARIES 2
DSBs	Double strand breaks
E. coli	Escherichia coli
EDTA	Ethylenediaminetetraacetic acid
EdU	5-Ethynyl-2'-deoxyuridine
EDZ	Elongation/differentiation zone
eff	Efficiency
EI	Endoreplication Index
EMS	Ethyl methanesulfonate
ERF115	ETHYLENE RESPONSE FACTOR 115
ES	Exon skipping
ESP3	ENHANCED SILENCING PHENOTYPE 3
ETH	Ethylene
EtOH	Ethanol
FBL17	F BOX-LIKE17
Fg	Fusarium graminearum
FLC	FLOWERING LOCUS C
FLIM	Fluorescence lifetime imaging
FPGS	Folylpolyglutamate synthetase
FRET	Fluorescence resonance energy Transfer
FT	FLOWERING LOCUS T
FULL	FRUITFULL
g	Gram
g	Genomic
G1	Gap phase 1
G2	Gap phase 2
GA	Gibberellins
GFP	Green Fluorescent Protein
GO	Gene ontology
h	hour
H, HIS	Histidine
HD-ZIP	HOMEODOMAIN-LEUCINE ZIPPER

het	Heterozygous
HIND	Hub1 interacting
hom	Homozygous
HR	Homologous Recombination
HSP101	HEAT SHOCK PROTEIN 101
HU	Hydroxyurea
HUB1	HOMOLOGOUS TO UBIQUITIN 1
HyD	Hybrid detector
Hyg	Hygromycin
ICK/KRP	Interactor/Inhibitor of cyclin dependent kinase/Kip-related protein
IM	Inflorescence meristem
IR	Intron retention
JA	Jasmonic acid
Kan	Kanamycin
L	Leucin
LB	Lysogeny broth
LEA	Late embryogenesis abundant
LFY	LEAFY
LSM	SM-like
M	Mitosis
M	Molar
MAC	MOS4-associated complex
MAIL1	MAIN-LIKE1
MAIN	MAINTENANCE OF MERISTEMS
MDF	MERISTEM DEFECTIVE
MDFL	MDF-LIKE
MET1	METHYLTRANSFERASE1
mg	Milligram
min	Minute
miRNAs	microRNAs
mL	Millilitre
mM	Millimolar
MMC	Mitomycin
MMR	Mismatch repair pathway

MP	MONOPTEROS
MPK4	MITOGEN-ACTIVATED PROTEIN KINASE 4
MRN complex	MRE11, RAD50 and NBS1
MS	Murashige and Skoog
MS	Mass spectrometry
MV	Methyl-viologen
MXE	Mutually exclusive exons
N. benthamiana	Nicotiana benthamiana
NADPH	Nicotinamide adenine dinucleotide phosphate (reduced form)
NASC	Nottingham Arabidopsis Stock Centre
NCH1	NRL PROTEIN FOR CHLOROPLAST MOVEMENT1
NER	Nucleotide excision repair
NHEJ	Non-Homologous End-Joining
nm	Nanometer
NMD	Nonsense-mediated decay
NoD	Nucleolar localization sequence Detector
NoLS	Nucleolar localization signals
NTC	NineTeen Complex
OC	Organizing center
°C	Degree Celsius
OE	Overexpression
ON	Overnight
ORF	Open reading frame
p	Promoter
PARP	POLY(ADP-RIBOSE) POLYMERASE
PAT1	PHYTOCHROME A SIGNAL TRANSDUCTION 1
PCD	Programmed cell death
PCR	Polymerase Chain Reaction
PEG	Polyethylenglycol
PI	PISTILLATA
PI	Propidium iodide
PLT	PLETHORA
PM	Proximal meristem
PMD	Plant mobile domain

PNF	POUND-FOOLISH
PNY	PENNYWISE
PP7L	PHOSPHATASE7-LIKE
pre-mRNA	Precursor-messenger RNA
PRL1	PLEIOTROPIC REGULATORY LOCUS 1
PRP	PRE-mRNA PROCESSING
PRP4	PRE-mRNA PROCESSING 4
PRR7	PSEUDO-RESPONSE REGULATOR 7
PTC	Premature termination codons
PZ	Peripheral zone
QC	Quiescent center
RAD51	RADIATION SENSITIVE 51
RAM	Root apical meristem
RBR	RETINOBLASTOMA
RBR	RETINOBLASTOMA RELATED
RCD1	RADICAL-INDUCED CELL DEATH1
RCF	RAD17-Replication factor C
Rep-MYBs	Repressor-type R1R2R3-Myb transcription factors
RID1	ROOT INITIATION DEFECTIVE1
RM	Rib meristem
RNA-seq	RNA sequencing
RNP	Ribonucleoprotein
RNSP1	RNA BINDING PROTEIN S1
ROS	Reactive oxygen species
RPA	Replication Protein A
RPKM	Reads Per Kilobase of exon model per Million mapped reads
rpm	Revolutions per minute
RPP1	RECOGNITION OF PERONOSPORA PARASITICA 1
RRM	RNA recognition motifs
rRNA	Ribosomal RNA
RT	Room temperature
RTEL1	DNA helicase Regulator of Telomere Length 1
RT-qPCR	Quantitative real-time-PCR
S	Synthesis



S22A	Serine substitution by Alanine
S22D	Serine substitution by Aspartate
SA	Salicylic acid
SAM	Shoot apical meristem
SAP18	SIN3-ASSOCIATED PROTEIN 18
SART1	SQUAMOUS CELL CARCINOMA ANTIGEN RECOGNIZED BY T CELLS1
SCF	Skp1-cullin-F-box-protein
SCN	Stem cell niche
SCR	SCARECROW
SD	Synthetic Defined
SDM	Site directed mutagenesis
SDS	Sodium dodecyl sulfate
seg	Segregating
SHR	SHORTROOT
SIM	Siamese
SMC5/6	Structural Maintenance of Chromosome
SMR	Siamese-related
sn	Small nuclear
SNI1	SUPPRESSOR OF NPR1 INDUCIBLE 1
SOC	Super Optimal broth with Catabolite repression
SOC1	SUPPRESSOR OF OVEREXPRESSION OF CONSTANS 1
SOG1	SUPPRESOR OF GAMMA RESPONSE 1
SPL	SQUAMOSA PROMOTER BINDING PROTEIN-LIKE
SR	Serine/arginine rich
SSBs	Single-strand DNA breaks
ssDNA	Single stranded DNA
SSP	Seed storage proteins
SYD	SPLAYED
TIE1	INTERACTOR CONTAINING EAR MOTIF PROTEIN 1
TTM3	TRIPHOSPHATE TUNNEL METALLOENZYME 3
TZ	Transition zone
UBL5	UBIQUITIN-LIKE PROTEIN 5
uORF	Upstream open reading frame

UTR	Untranslated region
UV	Ultraviolet
V	Volt
W	Tryptophan
WOX	WOX WUSCHEL-RELATED HOMEODOMAIN PROTEIN 4
WT	Wildtype
WUS	WUSCHEL
XRCC4	X-RAY CROSS COMPLEMENTATION PROTEIN 4
Y2H	Yeast-Two-Hybrid
YFP	Yellow Fluorescent Protein
Z, Zeo	Zeocin

# 1. INTRODUCTION



## 1.1 Plant Growth and Development

The plant life cycle comprises two major phases: embryogenesis and post-embryonic growth. While plant morphology is fundamentally dependent on the tight coordination of asymmetric cell division, cell expansion, cell fate specification and positional signalling during the post-embryonic stage; these processes are ultimately the reiteration of the developmental program defined during embryogenesis (ten Hove *et al.*, 2015).

### 1.1.1 Embryogenesis and Seed Germination

Plant embryogenesis constitutes the beginning of the diploid phase in higher plants and includes all processes that take place between the fertilization of the egg cell until the formation of the mature embryo (Goldberg *et al.*, 1994).

Embryo development is started by a morphogenesis phase, during which the basic body plan of the plant is defined after coordinated cell divisions and the establishment of an apical-basal polarity and radial pattern (Figure I-1) (Park and Harada, 2008; Nodine *et al.*, 2011). This is followed by a maturation phase that involves cell expansion and differentiation processes, accompanied by the storage of macromolecules and entry into metabolic quiescence. These last steps are essential to prepare the embryo for desiccation, germination and early seedling growth (Baud *et al.*, 2002; Park and Harada, 2008).

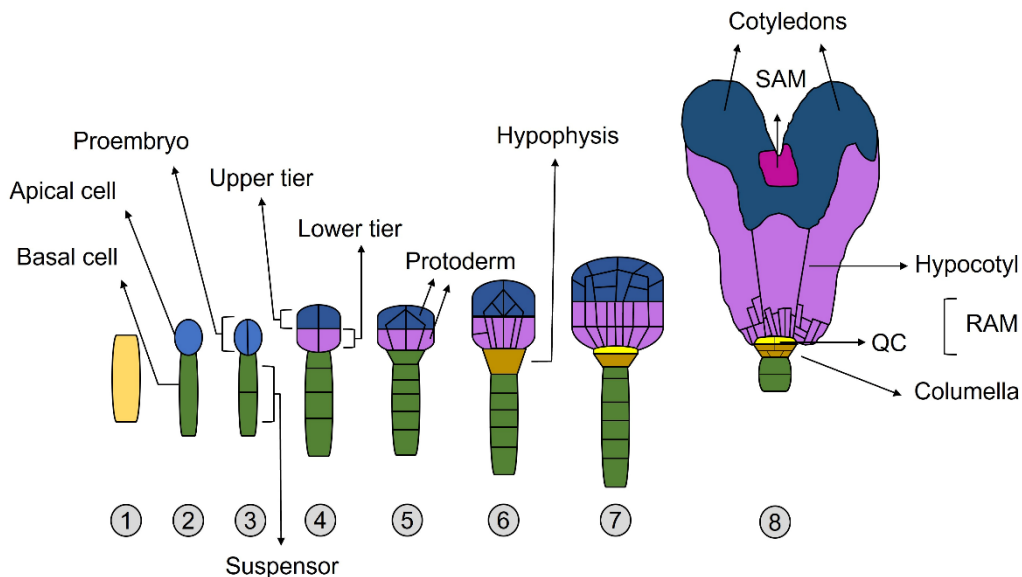


**Figure I-1.** Schematic simplified overview of early embryogenesis based on Capron *et al.*, 2009 and Llavata Peris *et al.*, 2010. (1) The zygote is formed after fertilization of the egg cell by one sperm cell. (2) The newly formed zygote elongates and divides asymmetrically to generate the apical (blue) and basal (green) cells. (3) In the 4-Cell state, a new division in the basal lineage generates the extra-embryonic suspensor (green), while the proembryo is generated after division of the apical lineage (blue). (4) Upper (dark blue) and lower tier (purple) are formed in the octant stage after division of all 4 cells. (5) In the dermatogen, radial patterning takes place

after a tangential division of each of the eight “octant” cells, resulting in the formation of the inner cells and the outer epidermis (protoderm) cells. (6) Subsequently, during globular stage, the hypophysis (orange) is generated after specification of the uppermost cell of the suspensor. (7) The hypophysis undergoes an asymmetric cell division and gives rise to a lens-shaped cell (yellow), from which the quiescent center (QC) will derive and a basal cell (orange), from which stem cells and columella cells of the root tip will be generated. (8) During the heart and torpedo stages, subsequent cell divisions will produce all structures necessary for seedling development including cotyledons, the shoot apical meristem (SAM), hypocotyl and root apical meristem (RAM).

There are diverse molecular mechanisms tightly regulating the specification of different cell identities during embryogenesis, including auxin signalling and transcriptional induction of the *WUSCHEL-RELATED HOMEODOMAIN* (*WOX*) transcription factors (ten Hove *et al.*, 2015). Apical and basal axis formation is correlated with the specific expression (in each daughter cell resulting from the first asymmetric zygotic division) of *WOX2* and *WOX8* respectively (Breuninger *et al.*, 2008). Apical cell fate is also associated with auxin activity, transport and the correct establishment of auxin maxima (Park and Harada, 2008). Consequently, loss of auxin transporters PIN1, PIN3, PIN4 and PIN7 in quadruple *pin1,3,4,7* mutant leads to severe defects in apical-basal organization (Friml *et al.*, 2003; Park and Harada, 2008).

A coordinated genetic regulation has also been documented during the maturation phase. For example, starting at the torpedo embryo stage, B3 domain and basic leucine zipper (bZIP) factors coordinate the expression of genes encoding seed storage proteins (SSPs) (Kroj *et al.*, 2003). Additionally, the establishment of a quiescent dehydrated state can cause cellular DNA damage, which is why several proteins, including heat shock and late embryogenesis abundant (LEA) proteins, are synthesized during the late maturation stage to prevent protein aggregation (Hoekstra *et al.*, 2001; Hundertmark and Hincha, 2008).

The reduced metabolic state acquired at the end of the maturation phase is called dormancy and enables the seed to delay germination until favourable environmental conditions. Dormancy break is mediated by two antagonistic phytohormones: abscisic acid (ABA), responsible for maintaining the seed in a dormant state, and gibberellins (GA), which promote seed germination and seedling growth (Li *et al.*, 2019). Moreover, due to the high levels of DNA double strand breaks (DSBs) accumulated during desiccation, the checkpoint DNA damage kinase ATAXIA TELANGIECTASIA MUTATED (ATM) was shown to limit and control germination in aged seeds (Waterworth *et al.*, 2016).

### 1.1.2 Apical meristems and post-embryonic growth

As previously discussed, the establishment of an apical-basal axis is essential during embryogenesis and is most prominent by the octant stage (Figure I-1), in which the three

distinctive domains from which all morphological structures will derive are formed. The top and bottom halves of the proembryo give rise to the apical and central domains, respectively, while the uppermost cell of the basal lineage (hypophysis), corresponds to the basal domain. The apical domain generates the shoot apical meristem (SAM) and most of the cotyledons, while the hypocotyl, radicle, part of the root apical meristem (RAM) and the rest of the cotyledons derive from the central domain. Finally, the basal domain produces the quiescent center (QC) and central root cap initials of the RAM (Parker and Harada, 2008).

Apical meristem formation is particularly important in higher plants because organ morphogenesis throughout their entire life cycle is dependent on the activity of the RAM, from which the root system is derived, and the SAM, which produces all above ground organs (Weigel and Jürgens, 2002). These meristems are reservoirs of pluripotent stem cells, which are able to self-maintain and produce all cells required for organ initiation (Mayer, *et al.*, 1998).

#### 1.1.2.1 Root apical meristem

The RAM sustains root growth and development and is responsible of the root architecture. A pool of pluripotent cells is localized at the tip of the root meristem surrounding a small group of undifferentiated cells called the quiescent center (QC). Together they conform the stem cell niche (SCN) (Figure I-2). Self-maintenance of the stem cells is regulated by signals from the QC, which acts as an organizing center that inhibits differentiation of the stem cells so that they remain competent for cell division (Laux, 2003; Scheres, 2007; Perilli *et al.*, 2012). Post-embryonically, stem cells undergo asymmetric cell divisions which generate self-renewing cells and daughter cells that go through several rounds of cell division and constitute the proximal meristem (PM). Subsequently, stem cells exit the cell cycle and differentiate to acquire tissue-specific traits in the elongation/differentiation zone (EDZ). The transition zone (TZ) is found in between the PM and the EDZ and defines the boundary between dividing and expanding cells (Perilli *et al.*, 2012).

RAM organization and specification is highly dynamic and requires a tight regulation during the transition from a pluripotent to a differentiated state in the stem cells (Drisch and Stahl, 2015). Thus, complex regulatory mechanisms take place in the RAM, including the transcriptional repression of III HOMEODOMAIN-LEUCINE ZIPPER (HD-ZIP III) transcription factors - master regulators of embryonic apical fate - mediated by transcription factors of the PLETHORA family (PLT), which are responsible for root pole specification. Likewise, SAM specification is dependent on the inhibition of PLT factors by HD-ZIP III (reviewed in Perilli *et al.*, 2012). PLT proteins also enhance the expression of auxin PIN transporters, which are necessary to establish the apical-basal auxin gradient required for SCN maintenance and root formation (Blilou *et al.*, 2005; Perilli *et al.*, 2012). Therefore, while loss of PLT transcription factors leads to severe developmental alterations in the RAM

such as shorter meristem size and loss of QC specification in *plt1plt2* double mutants (Aida *et al.*, 2004; Drisch and Stahl, 2015), ectopic overexpression results in higher accumulation of stem cells and abnormal production of ectopic roots from the shoot apex (Galinha *et al.*, 2007; Drisch and Stahl, 2015).

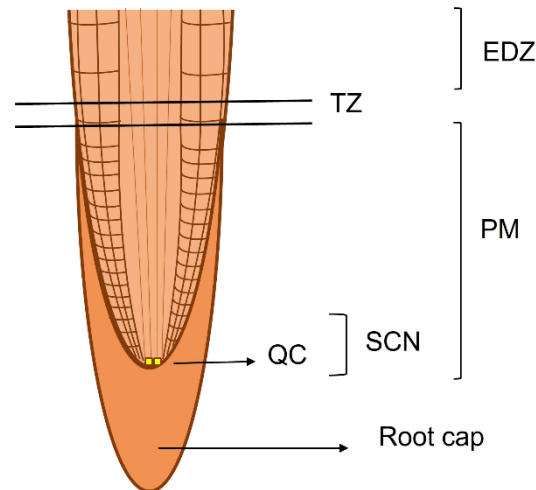


**Figure I-2. Schematical representation of the root apical meristem in *Arabidopsis thaliana* based on Perilli *et al.*, 2012.** QC: quiescent center (yellow); SCN: stem cell niche; PM: proximal meristem; TZ: transition zone and EDZ: elongation/differentiation zone are pointed out. The root cap is represented in darker orange.

SCN maintenance and QC specification is regulated in parallel by the GRAS-transcription factors SCARECROW (SCR) and SHORTROOT (SHR), whose loss of function mutants present arrested root development and aberrant QC (reviewed in Drisch and Stahl, 2015).

Additionally, the homeodomain WUS-RELATED HOMEODOMAIN 5 (WOX5) transcription factor, whose expression is controlled by SCR transcription factors, is also essential for stem cell maintenance signalling in the RAM, playing an analogous role as its homolog WUSCHEL (WUS) in the SAM (Sarkar *et al.*, 2007; Perilli *et al.*, 2012). Furthermore, WOX5 arrests cell division in the QC by repressing *CYCD3;3* expression and is therefore important for preserving the quiescence of the RAM organizing center (Forzani *et al.*, 2014; Drisch and Stahl, 2015). Consequently, loss of WOX5 function results in premature differentiation of stem cells in the proximal meristem (Sarkar *et al.*, 2007).

#### 1.1.2.2 Shoot apical meristem

The SAM provides all cells necessary for the development of above ground tissues such as leaves, flowers, branches or internodes (Perales and Reddy, 2012). It is a dome shaped structure which contains a pool of slowly dividing stem cells at the tip that constitute the central zone (CZ) (Figure I-3). As it happened in the RAM, there is a distinctive domain called the organizing center (OC) located below the CZ, which provides cues for stem cell



specification and is defined by the expression of the stem cell regulator *WUS* (Perales and Redy, 2012; Fuchs and Lohmann, 2020). When stem cells in the CZ undergo cell division, they are passively pushed laterally towards the peripheral zone (PZ) or basally towards the rib meristem (RM). Cells in both the PZ and RM divide more rapidly and, after specific spatio-temporal signals such as auxin (Ma *et al.*, 2019), differentiate into lateral organs and meristems (e.g., leaves or flowers) at the organ primordia, or become part of the stem and vascular tissues, respectively (Perales and Redy, 2012; Fuchs and Lohmann, 2020).

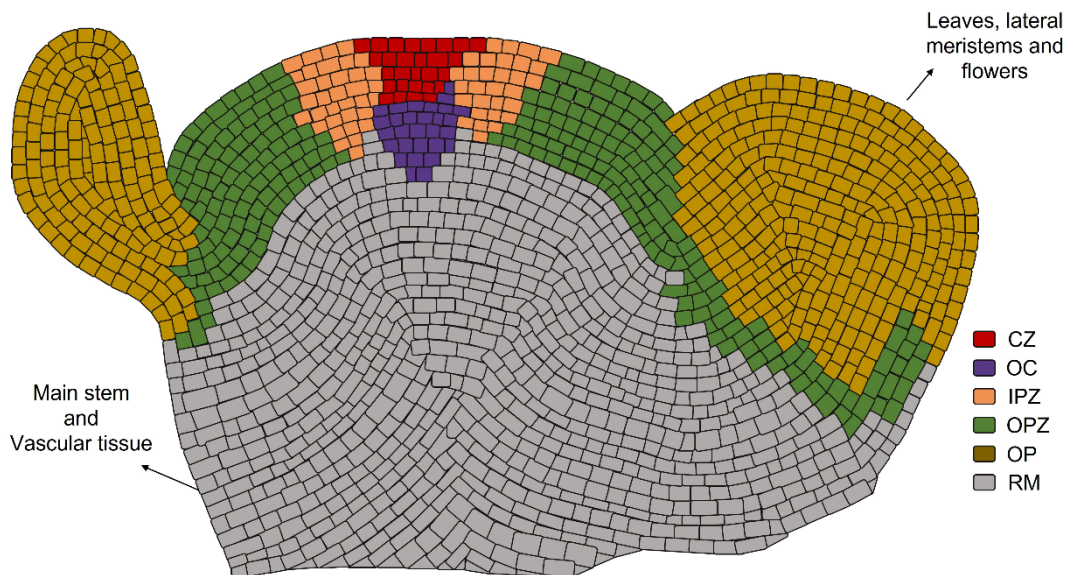


**Figure I-3.** Schematical representation of the shoot apical meristem in *Arabidopsis thaliana* based on Perales and Reddy, 2012. CZ: Central zone (red); OC: Organizing center (purple); IPZ: Inner peripheral zone (pink); OPZ: Outer peripheral zone (green); Organ primordia (yellow) and RB: Rib meristem (grey) are indicated. Organ primordia differentiate into leaves, lateral meristems and flowers, while cells in the rib meristem will conform the stem and vascular tissue after differentiation. The IPZ can de-differentiate upon downregulation of *CLV3*, while the OPZ remains differentiated even when *CLV3* is expressed at low levels.

*WUS* was identified to act in a negative feedback loop with *CLAVATA 3* (*CLV3*). Genetic studies have shown how specific *WUS* expression in the OC positively regulates *CLV3* expression in overlying cells of the CZ, which subsequently promotes cell differentiation. Additionally, *CLV3* restricts *WUS* expression and limits it to the OC. Therefore, the *WUS/CLV3* negative feedback loop regulates the size of the SAM by coordinating the balance between stem cell fate and differentiation (Perales and Reddy, 2012; Fuchs and Lohmann, 2020).

A similar negative feedback regulation takes place during flower formation in the flower meristem: *WUS* activates the expression of *AGAMOUS* (*AG*), which regulates floral organ identity and proliferation. In turn, *AG* represses *WUS* expression and thus prevent over-accumulation of floral stem cells (Fuchs and Lohmann, 2020).



Finally, WUS transcriptional activation is also dependent on cytokinin and auxin signalling, which antagonistically regulate *ARABIDOPSIS RESPONSE REGULATORS* (*ARRs*) 7 and 15 expression. ARR7/ARR15 mediated cytokinin signalling induces WUS levels via CLV-dependent and CLV-independent feedback loops. Per contra, auxin modulates this response by inhibiting ARR7 and ARR15 via the transcription factor AUXIN RESPONSE FACTOR 5/MONOPTEROS (MP) (Fuchs and Lohmann, 2020). Additionally, WUS also influences auxin signalling and response in the SAM to ensure the balance between stem cell fate and differentiation. Consequently, in *clv3* mutants, where *WUS* is overexpressed, the increase of stem cells in the SAM is accompanied by a reduction of auxin levels (Ma *et al.*, 2019).

### 1.1.3 Vegetative and Reproductive growth

Plant development is defined as the sequential combination of qualitative (germination, flowering, etc.) and quantitative (number of leaves, number of siliques, etc.) changes in plant structures. Researchers distinguish two major developmental phases: vegetative and reproductive (Figure I-4) (Dramberville *et al.*, 2015).

#### 1.1.3.1 Vegetative growth

After germination is completed, plants undergo a series of events where their size, mass and photosynthetic capacity is rapidly increased. This process is collectively called vegetative growth and is usually further divided into the juvenile phase, in which true leaves and axillary buds are formed, and the adult vegetative phase.

The juvenile to adult transition is characterized by a change in growth pattern and body form and the acquisition of flower competence (Huijser and Schmid, 2011). Representative phenotypical traits of the juvenile to adult transition in *Arabidopsis* are the formation of trichomes on the abaxial side of the leaf blade, an increase in the leaf length/width ratio, a decrease in cell size and an enhancement in the degree of serration on the leaf margins (Guo *et al.*, 2017). During the vegetative transformation both juvenile and mature shoots are produced on the same plant, a phenomenon known as heteroblasty (Huijser and Schmid, 2011).

microRNAs (miRNAs) miR156 and miR159 antagonistically coordinate the timing of the juvenile to adult transition in *Arabidopsis*: While miR156 acts as a repressor of several transcription factors involved in the vegetative phase change such as SQUAMOSA PROMOTER BINDING PROTEIN-LIKE (SPL) proteins; miR159 inhibits miR156, predominantly via the R2R3 MYB domain transcription factor MYB33. Hence, miR159 facilitates vegetative phase change by preventing the activation of miR156 by MYB33. Moreover, miR156 levels are controlled by exogenous cues such as temperature or CO<sub>2</sub> concentration (Guo *et al.*, 2017). Recent publications also report the importance of glucose-

and sucrose-signalling modules in the juvenile to adult transition by decreasing miR156 levels (Meng *et al.*, 2021).

Additionally, the miRNA miR172 also impacts the juvenile-adult transition in an opposite way of miR156, with higher levels of miR172 accelerating the production of characteristic adult stage traits such as the formation of abaxial trichomes (Huijser and Schmid, 2011).

### 1.1.3.2 Reproductive growth

Once flower competency is acquired, plants undergo another phase transition termed reproductive phase change which marks the transition from vegetative to reproductive growth (Huijser and Schmid, 2011). Following the reproductive phase change, the SAM changes its identity by converting into an inflorescence meristem (IM) and ceasing to produce vegetative leafy shoots. The IM can remain on an indeterminate state, characterized by the production of lateral meristems that may convert to floral meristems or self-convert into a floral meristem (Huijser and Schmid, 2011). A single flower that bears both male (stamen) and female (pistil) reproductive organs is generated by each floral meristem (Walker *et al.*, 2021).

Timing and transition to flowering is strongly regulated since it has a strong impact on the plant fitness (Huijser and Schmid, 2011). A complex regulatory network including five major genetically defined pathways (photoperiod, ambient temperature, age, autonomous and GA-dependent pathways) has been described to adapt flowering time to different environmental and endogenous cues in *Arabidopsis* (Figure I-4) (Yamaguchi *et al.*, 2012).

The photoperiod pathway coordinates the reproductive phase change based on day length, with longer day conditions accelerating flowering through the induction of the FLOWERING LOCUS T (FT) protein by circadian clock regulated zinc finger protein CONSTANS (CO) (Song *et al.*, 2013; Cho *et al.*, 2017). FT is produced in the leaf phloem and, after translocation to the SAM, promotes the meristem identity switch from vegetative into inflorescence by activating SUPPRESSOR OF OVEREXPRESSION OF CONSTANS 1 (SOC1) via its interaction with the bZIP transcription factor FD (Huijser and Schmid, 2011; Cho *et al.*, 2017). The FT/FD and SOC1 complex subsequently activates floral meristem identity regulators LEAFY (LFY), APETALA1 (AP1) and FRUITFULL (FULL). These proteins further activate each other, whereas they negatively impact *SOC1* expression, thereby promoting the transformation of the indeterminate IM into a floral meristem. This phenomenon is restricted to lateral meristems, since specific expression of *TERMINAL FLOWER1* in the *Arabidopsis* inflorescence maintains its indeterminate state (Huijser and Schmid, 2011). *SOC1* and *LFY* expression is also activated by gibberellins (Kim *et al.*, 2009).

Long exposure to cold temperatures, known as vernalization, also promotes flowering in *Arabidopsis* by repressing the expression of *FLOWERING LOCUS C (FLC)*. Lack of *FLC* function in the SAM enhances the transcription of several transcription factors important for

floral transition including FT and SOC1 (Yamaguchi *et al.*, 2012; Cho *et al.*, 2017). Autonomous pathway genes also modulate FLC repression mostly by RNA binding/processing or chromatin remodelling, independently of the photoperiod and vernalization pathways (Kim *et al.*, 2009; Yamaguchi *et al.*, 2012; Cho *et al.*, 2017).

Finally, the aging pathway comprises the biological endogenous processes that influence the acquisition of floral competency and is strongly regulated by miRNAs miR156 and miR172 (Yamaguchi *et al.*, 2012; Cho *et al.*, 2017). As previously mentioned, miR156 stimulates juvenile vegetative growth during early development. As the plant matures, it steadily decreases its levels, which thereby promotes the acquisition of adult leaf traits by allowing the expression of SPL9 and SPL10 proteins (Huijser and Schmid, 2011). Concomitantly, SPL9 and SPL10 induce miR172 levels, which results in the downregulation of six AP2-like flowering repressing transcription factors. In addition to SPL9 and SPL10, reduced levels of miR156 also release the repression of SPL3, SPL4 and SPL5, which confer floral competency so that the transition to the reproductive stage can take place (Huijser and Schmid, 2011) (Figure I-4).

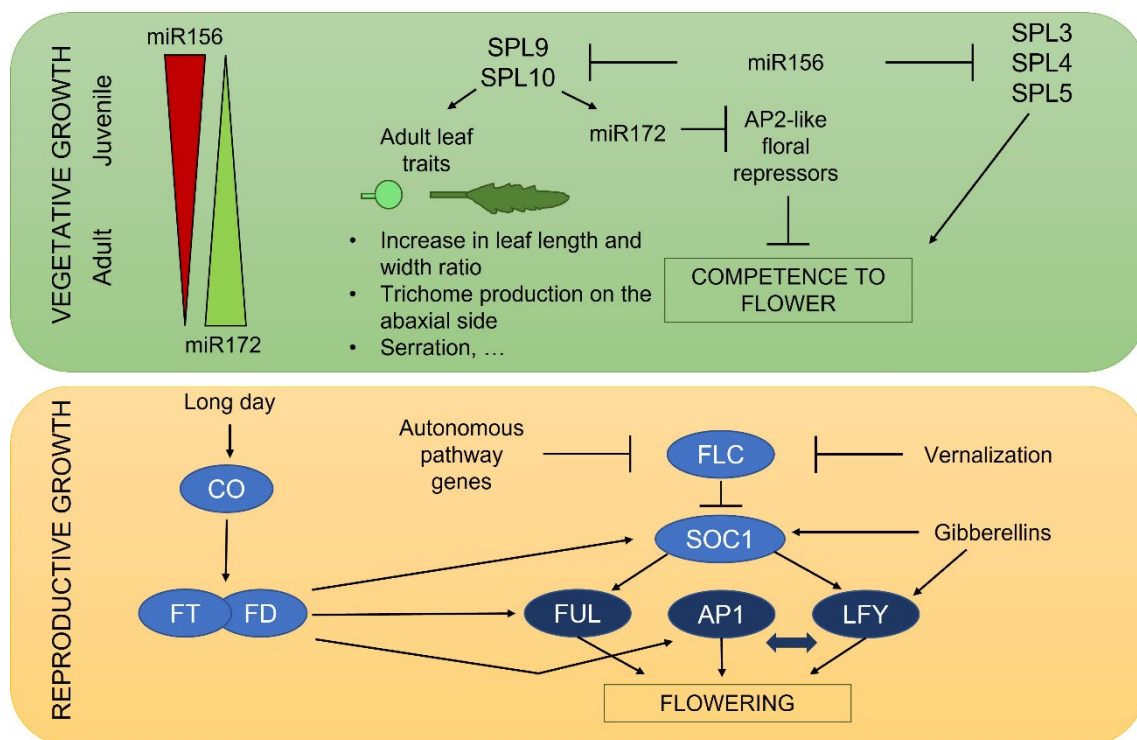


**Figure I-4.** Schematical representation of the juvenile to adult transition during vegetative growth and the vegetative phase change into reproductive development after acquisition of floral competency based on Kim *et al.*, 2009 and Huijser and Schmid, 2011 as described in sections 1.1.3.1 and 1.1.3.2. Red and green triangles on the upper left corner represent the steady decrease and increase of miR156 and miR172 levels respectively throughout Arabidopsis vegetative growth. SPL: SQUAMOSA PROMOTER BINDING PROTEIN-LIKE; miRNA: microRNA; AP: APETALA; CO: CONSTANS; FT: FLOWERING LOCUS T; SOC1: SUPPRESSOR OF OVEREXPRESSION OF CONSTANS 1; FLC: FLOWERING LOCUS C; FUL: FRUITFULL; LFY: LEAFY.

### 1.1.3.3 Flower patterning

Flower patterning follows the ABC model, which states that the combined interaction of the “A”, “B” and “C” homeotic functions determines the fate of the floral organs (Figure I-5) (Huijser and Schmid, 2011). In brief, “A” function is coded by *APETALA1* (*AP1*) and *APETALA2* (*AP2*) genes and specifies sepal identity in the outermost whorl. Combination of “A” and “B” class protein activity, which is determined by *PISTILLATA* (*PI*) and *APETALA3* (*AP3*) generates the petals in the second whorl. Similarly, the overlap of “B” activity and the “C” class *AGAMOUS* (*AG*) protein generates the stamens in the third whorl. Lastly, the carpels, located in the innermost whorl, are determined by the “C” function provided by *AG* (Huijser and Schmid, 2011).

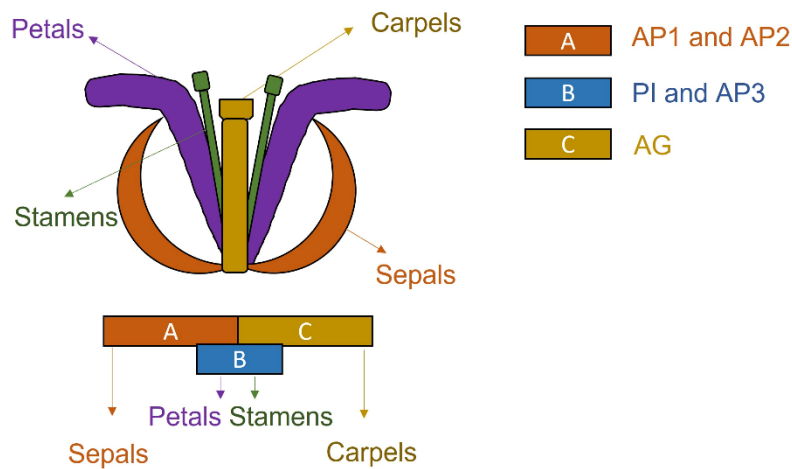


**Figure I-5.** Schematic representation of the ABC model based on Huijser and Schmid, 2011 and Irish *et al.*, 2017. “A” function specified by AP1: *APPETALA1* and AP2: *APPETALA2*. “B” function specified by PI: *PISTALLATA* and AP3: *APPETALA3*. “C” function specified by AG: *AGAMOUS*.

### 1.1.4 Senescence

Senescence constitutes the final stage of plant development and involves the programmed disassembly and degeneration of cells, tissues, organs, or whole organisms. It occurs most distinctively at the leaves, where it is regulated by various endogenous and exogenous factors including hormonal signalling (Kim *et al.*, 2017; Zhang *et al.*, 2020). While abscisic acid (ABA), ethylene (ETH), jasmonic acid (JA), salicylic acid (SA) and strigolactones promote leaf senescence; cytokinins (CK), gibberellic acid (GA) and auxin have an inhibitory function (Zhang *et al.*, 2020).

The induction of the senescence associated developmental program at the leaf results in leaf yellowing and remobilization of nutrients to support growth in younger vegetative organs and reproductive tissues. Furthermore, precocious senescence, which results in reduced seed set, can take place under unfavourable environmental conditions as a mechanism of evolutionary fitness (Zhang *et al.*, 2020).

Given its biological relevance, leaf senescence is regulated by multiple and cross-linking pathways, some of which are linked to stress responses, including oxidative, salt and drought stress signalling, and involve genes encoding transcription factors of the WRKY, NAC, DREB, MYB and bZIP family (Kim *et al.*, 2016b; Zhang *et al.*, 2020).

## 1.2 Cell proliferation

Plant postembryonic development is sustained by cell division and cell expansion. Therefore, regulation of cell cycle progression at the molecular level is essential for plant growth and organogenesis (Li *et al.*, 2005; Shimotohno *et al.*, 2021).

### 1.2.1 Cell cycle phases

In brief, the cell cycle consists of a synthesis (S) phase where DNA is replicated, and a mitotic (M) phase followed by cytokinesis, where the genetic material is partitioned between two daughter cells. Preceding and separating these two processes are two gap phases: G2 (gap between DNA replication and mitosis) and G1 (gap between mitosis and DNA replication) (Gutierrez, 2009; Nayeri, 2014). During G1, the number of organelles is increased and the protein complexes necessary for the activation of DNA replication origins are assembled. In G2, per contra, genome integrity is monitored, and cells are prepared for mitosis (Echevarría *et al.*, 2021). Thus, the mitotic cell cycle is a unidirectional sequence of consecutive regulated events (Figure I-6) (Goldy *et al.*, 2021).

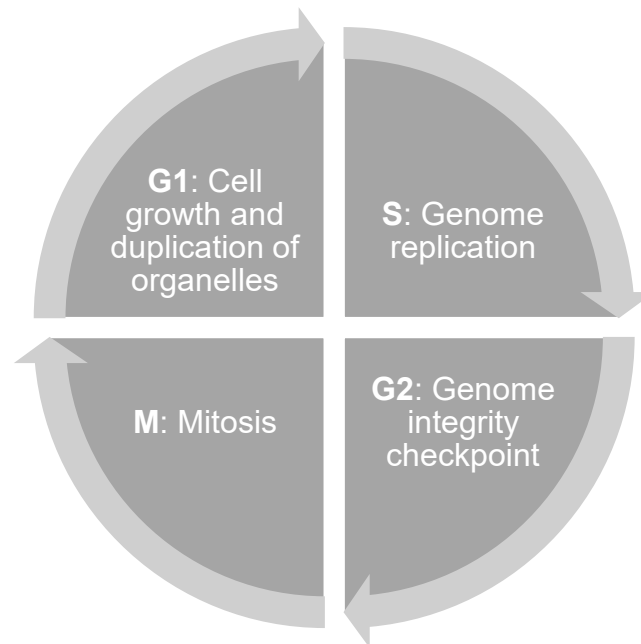


**Figure I-6.** Schematic representation of the cell cycle progression in plants. G1: gap phase 1; S: synthesis phase; G2: gap phase 2; M: mitosis phase.

### 1.2.2 Regulation of cell cycle progression

Phase transitions during the plant cell cycle are strongly regulated by the activity of conserved complexes formed by cyclin dependent kinases (CDKs) and their regulatory cyclin (CYC) subunits (Vieira and de Almeida Engler, 2017; Shimotohno *et al.*, 2021).

CDK-CYC-dependent phosphorylation mediated cell cycle control integrates endogenous information such as nutrient availability or hormone signalling with biotic and abiotic environmental conditions and allows the onset of DNA replication and chromosome segregation during G1/S and G2/M transitions (Noir *et al.*, 2015; Gentric *et al.*, 2021).

CDKs are Serine/Threonine kinases classified into eight distinctive groups in plants: CDKA-CDKG and CDC-like kinases (CKL) (Vandepoele *et al.*, 2002; Shimotohno *et al.*, 2021). Among them, the A and B-type CDKs have been most extensively studied. CDKA transcripts regulate both G1/S and G2/M transitions, whereas CDKB proteins are mostly involved in the G2/M checkpoint (Vandepoele *et al.*, 2002). Additionally, CDKB seem to be plant-specific and hence coordinate plant-specific developmental processes such as stomata formation and stem cell niche organization in the SAM (Shimotohno *et al.*, 2021).

Kinase activity of both A and B-type CDKs is controlled by binding to cyclins, and it is enhanced upon phosphorylation by CDK-activating kinases (CAKs) (Takatsuka *et al.*, 2009). Similarly, CDK activity can also be modulated upon interaction with CDK inhibitors (CKIs), which negatively regulate cell cycle progression (Kumar and Larkin, 2017). Two main groups of CKIs have been identified in plants: Interactor/Inhibitor of cyclin dependent kinase/Kip-related protein (ICK/KRP) family, which shares similarity to mammalian Cip/Kip family, and the plant-specific Siamese (SIM) and Siamese-related (SMR) proteins (Shimotohno *et al.*, 2021).

From the more than 50 cyclin genes identified in Arabidopsis, a major cell cycle regulatory role has been attributed to type-A (CYCA), type-B (CYCB) and type-D (CYCD). CYCA and CYCB function during G2/M transition, although some CYCA members, such as CYCA3;1 and CYCA3;2, are also highly expressed from late G1 to mid M phase, which suggests a role in G1/S progression. CYCDs have also been associated with the G1/S transition and are thought to be essential for plant development (Shimotohno *et al.*, 2021).

Since cell cycle related genes and their encoded proteins are frequently not essential in non-proliferating differentiated cells, plants have evolved several molecular mechanisms to repress the cell cycle machinery and allow cells to exit the cell cycle (Fisher and Müller, 2017).

In this context, cell cycle progression is influenced by the activity of three Myb repeat-containing plant proteins, also known as MYB3R, which directly modulate the expression of numerous G2/M-specific genes. Five genes encoding MYB3R transcription factors have been identified in Arabidopsis: MYB3R3 and MYB3R5 (Rep-MYBs) directly suppress the expression of genes involved in the transition to mitosis, whereas MYB3R4 (Act-MYB)



transcriptionally activates G2/M-specific genes such as *CYCB1*, *CYCB2* or *CDKB2*. Lastly, MYB3R1 has a dual role as activator and repressor of cell proliferation (Kobayashi *et al.*, 2015). Moreover, MYB3R association with E2Fs and the RETINOBLASTOMA (RBR) protein in Arabidopsis generates protein complexes homologous to the mammalian multi-subunit DREAM (DP, RB-like protein, E2F and Muv core) complex. Different plant-like DREAM complexes with opposite roles in cell division control are formed by the incorporation of Act- or Rep-MYBs (Kobayashi *et al.*, 2015; Ning *et al.*, 2020).

Additionally, CDKs activity is also controlled in a post-translational way by the ubiquitin-mediated proteolysis of key regulators such as cyclins and CKIs by the Anaphase Promoting Complex/Cyclosome (APC) or the Skp1-cullin-F-box-protein (SCF) FBL17 complex respectively (Kim *et al.*, 2008; de Lyra Soriano Saleme *et al.*, 2021).

### 1.2.3 Endoreplication

Endoreplication (also known as endoreduplication or endopolyploidization) is a variation in the classical cell cycle in which cells undergo genome replication without subsequent cell division due to the repression of CDK-CYC mitotic promoting complexes. As a consequence, DNA content and ploidy level are increased. (Lang and Schnittger, 2020; Hendrix, 2022).

This alternative cell cycle has been associated to growth and developmental processes in specific cells such as trichomes. It is believed to play an important role during plant stress responses and to be specifically activated upon genotoxic stress (Adachi *et al.*, 2011; Lang and Schnittger, 2020).



### 1.3 Plant DNA damage response

Plant genome integrity is constantly threatened by both endogenous DNA metabolic processes (e.g., DNA replication and repair) and, due to their sessile nature, exogenous environmental stresses such as heat or drought. Thus, DNA damage occurs under normal conditions, but is even more abundant after stress conditions (Nisa *et al.*, 2019). Plants have consequently evolved various mechanisms to protect their genome stability collectively known as the plant DNA damage response (DDR). This sophisticated signalling process involves the induction of DNA repair pathways and the activation of cell cycle checkpoints that transiently arrest cell proliferation so that lesions can be repaired before the cell divides. However, higher dosages of DNA damage and inefficient repair of DNA lesions promote endoreplication and programmed cell death (PCD) to avoid the propagation of cells with a compromised genome (Figure I-7) (Hu *et al.*, 2016; Nisa *et al.*, 2019).

#### 1.3.1 Types of DNA damage

Two major kinds of DNA damage activate the plant DDR: single- and double stranded. While the first category refers to lesions affecting only one DNA strand, including base loss, intra-strand cross-links or single-strand DNA breaks (SSBs); the second one comprises more severe lesions that disturb both DNA strands such as inter-strand cross-links and double-strand DNA breaks (Manova and Gruszka, 2015).

##### 1.3.1.1 DNA damage induced by endogenous factors

Reactive oxygen species (ROS) are produced not only upon environmental stresses, but also as a byproduct of metabolic pathways including the  $\beta$ -oxidation of fatty acids in the peroxisomes, or due to the leakage of electrons onto O<sub>2</sub> from the electron transport activities of chloroplasts, mitochondria and plasma membranes. Excessive ROS levels have deleterious effects on the plant fitness including oxidation of proteins, PCD activation and nucleic acid damage, triggering both SSBs and DSBs. Furthermore, loss of function mutants for antioxidant enzymes *apx1* and *cat1* exhibit increased levels of DNA damage, further confirming the impact of oxidative stress on genome stability (Sharma *et al.*, 2012; Raina *et al.*, 2021).

In addition to ROS-derived endogenous DNA damage, DNA mutations also take place during internal DNA metabolic processes such as DNA replication and DNA repair due to the small but still occurring error rate of both DNA replicative polymerases and proof-reading polymerases respectively (Nisa *et al.*, 2019).

### 1.3.1.2 DNA damage induced by exogenous factors

Due to the sessile lifestyle of plants, numerous environmental factors compromise their genome integrity. Some examples are the exposure to UV light (Gill *et al.*, 2015), heavy metals such as cadmium (Hendrix *et al.*, 2020) or high temperatures (Han *et al.*, 2021). Moreover, abiotic and biotic stress conditions frequently threaten DNA maintenance by the production of extracellular ROS mostly by plasma membrane-localized NADPH oxidases (Qi *et al.*, 2018).

In spite of their negative impact on plant development and survival, the exogenous application of DNA damage inducing agents is a common tool in molecular biology studies. For example, plant reverse genetic studies often rely on the mutagenic potential of alkylating agents, such as the monofunctional alkylator EMS, to generate a collection of mutagenized plants with small base damage caused by the methylation of DNA bases (Manova and Gruszka, 2015). Additionally, sensitivity assays to genotoxic drugs are also frequently employed to evaluate the impact of disrupting a specific molecular mechanism in different mutant backgrounds. To this end, effective blocking of the replication machinery is achieved after mitomycin C or hydroxyurea treatment and DSBs are mimicked upon incubation in bleomycin or zeocin.

### 1.3.2 Main components of the plant DDR

The plant DNA damage signalling cascade is dependent on the activation of two protein kinases conserved between animals and plants named ATAXIA TELANGIECTASIA MUTATED (ATM) and ATM AND RAD3- RELATED (ATR). ATM is primarily triggered after double-strand DNA lesions, whereas ATR is mostly responsible of the activation of the plant DDR upon single-strand DNA lesions and defects in replication fork progression (Figure I-7) (Yoshiyama *et al.*, 2013b). This was verified by the increased sensitivity displayed by *atm* mutants to DSB-inducing agents like zeocin and the increased susceptibility of loss of function mutants for ATR to replication stress-inducing agents such as hydroxyurea (HU) (Yoshiyama *et al.*, 2013a). Interestingly, in contrast to animals, where the *atr* mutation is embryo lethal and mutations in ATM lead to multiple growth defects and infertility, absence of ATM and ATR in Arabidopsis does not cause severe phenotypical alterations, except for partial sterility in the *atm* mutant (Yoshiyama *et al.*, 2013b). Both ATM and ATR mediated signalling enhance the accumulation of  $\gamma$ H2AX (a phosphorylated histone variant) at DNA damage sites, which contributes to the recruitment of signalling and repair DDR factors (Nisa *et al.*, 2019).

Since ATM and ATR sense different kinds of DNA damage, their activating mechanisms are also different. The MRN complex, consisting of MRE11, RAD50 and NBS1, is responsible of ATM activation upon recognition of DSBs (Nisa *et al.*, 2019). Per contra, the coordinated function of Replication Protein A (RPA) proteins, that coat and protect single-stranded DNA behind the helicase (Pedroza-García *et al.*, 2019), recruits the ATR Interacting Protein

(ATRIP), that is bound to an inactive ATR, to single-stranded lesion sites. In parallel, RPA also attracts the RAD17-Replication factor C (RCF) complex, which subsequently loads the 9-1-1 (RAD9, RAD1, and HUS1) complex to the DNA damage site, resulting in the activation of ATR. Additionally, the plant DNA polymerase  $\epsilon$  putatively impacts also replicative stress sensing upstream of ATR, as it was shown in yeast (Figure I-7) (Nisa *et al.*, 2019; Pedroza-García *et al.*, 2022). Both DSB and ssDNA recognition methods have not been biochemically proven in plants, but the existence of orthologous genes to the animal and yeast components, accompanied by the hypersensitivity to DNA damaging agents displayed by their corresponding loss of function mutants, suggests functional conservation of DNA damage sensing mechanisms among eukaryotes (Nisa *et al.*, 2019; Pedroza-García *et al.*, 2022).

Unlike in animals, ATM and ATR signalling converge with the activation of SUPPRESSOR OF GAMMA RESPONSE 1 (SOG1) by rapid phosphorylation upon DNA damage. SOG1 is a plant specific NAC transcription factor predominantly expressed in meristems and vascular tissues. It is believed to be the central integrator of the plant DDR and acts as a functional homolog of the animal tumour suppressor p53 (Yoshiyama *et al.*, 2013a; Yoshiyama *et al.*, 2013b; Nisa *et al.*, 2019). Moreover, SOG1 mediated transcriptional activation coordinates most of the downstream signalling cascade of both ATM and ATR such as transient cell cycle arrest, activation of DNA repair processes and PCD (Figure I-7) (Pedroza-García *et al.*, 2022).

Surprisingly, opposite to p53, SOG1 is a direct target of the ATM and ATR kinases since Arabidopsis lacks orthologous genes for the canonical signal transducer kinases CHECKPOINT KINASES 1 AND 2 (CHK1/2) that receive the signals from ATM and ATR in the animal kingdom (Yoshiyama *et al.*, 2013b; Pedroza-García *et al.*, 2022).

Another important component of the plant DDR is the WEE1 kinase which, like its animal homolog, plays a fundamental role in the regulation of cell cycle progression by inhibiting mitotic entry after activation upon both DNA damage and DNA replication arrest in an ATM an ATR dependent manner (Figure I-7) (Hu *et al.*, 2016). In particular, WEE1 kinase mostly regulates the inactivation of CDKs. Accordingly, *wee-1* mutants lacking WEE1 display increased sensitivity to replication stress agents and do not accumulate phosphorylated CDKs (De Schutter *et al.*, 2007).

### 1.3.2.1 SOG1 independent pathways

Although SOG1 is the central regulator of the plant DDR, recent investigations have described various mechanisms that modulate the induction of DNA repair proteins and cell cycle arrest in response to DNA damage independently of SOG1.

One well known example is the Arabidopsis RETINOBLASTOMA RELATED (RBR) protein, which has a conserved role in cell proliferation, differentiation, and stem cell niche

maintenance mostly by repressing E2F-dependent transcription of cell cycle genes (Horvath *et al.*, 2017). RBR modulates not only G1/S transition upon phosphorylation by CDKs but also the G2/M transition, as part of DREAM complexes (Desvoyes and Gutierrez, 2020). Besides its conserved role in cell cycle regulation, it was shown to contribute to the maintenance of genome stability by recruiting important DDR repair genes such as RADIATION SENSITIVE 51 (RAD51) and BREAST CANCER SUSCEPTIBILITY 1 (BRCA1) to DNA damage sites in an ATM/ATR dependent manner (Figure I-7) (Biedermann *et al.*, 2017; Horvath *et al.*, 2017). Additionally, RBR and SOG1 might play antagonistic roles in PCD, based on the enhanced cell death accumulation observed in *rbr1* mutants after genotoxic stress (Biedermann *et al.*, 2017) and the accumulation of dead cells in Arabidopsis root tips at normal conditions after RBR silencing (Horvath *et al.*, 2017; Nisa *et al.*, 2019).

RBR also binds to the promoter of several DDR genes, including RAD51 and BRCA1, thereby regulating their expression independently of SOG1 (Biedermann *et al.*, 2017; Horvath *et al.*, 2017; Bouyer *et al.*, 2018). Interestingly, the WEE1 kinase was also found among these targets (Bouyer *et al.*, 2018), which led to the hypothesis that RBR/E2F complexes might control the G1/S cell cycle transition after DNA damage by modulating *WEE1* expression (Nisa *et al.*, 2019).

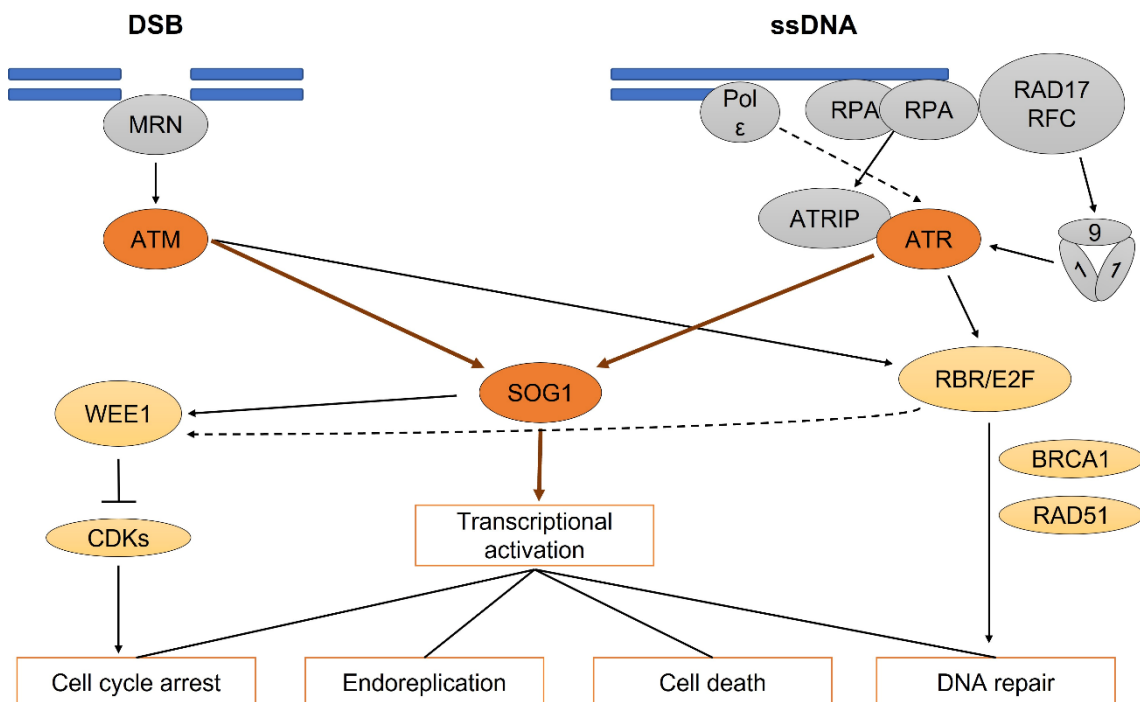


**Figure I-7.** Schematical representation of the major components and responses activated upon DNA damage in the plant DNA damage response as described in sections 1.3.1 and 1.3.2. Based on Nisa *et al.*, 2019. DSB: double strand breaks; MRN: MRE11, RAD50 and NBS1 complex; ATM: ATAXIA TELANGIECTASIA MUTATED; CDK: Cyclin dependent kinases; SOG1: SUPPRESOR OF GAMMA RESPONSE 1; Pol: polymerase; RPA: Replication Protein A; RCF: Replication Factor C; ATR: ATM AND RAD3- RELATED; 9-

1-1: RAD9, RAD1, and HUS1 complex; RBR: Retinoblastoma related; BRCA1: BREAST CANCER SUSCEPTIBILITY 1; RAD51: RADIATION SENSITIVE 51.

Recent publications point out also the importance of SNI1 (SUPPRESSOR OF NPR1 INDUCIBLE 1) in the plant DDR. SNI1 is a subunit of the Structural Maintenance of Chromosome (SMC5/6) complex that, after recruitment to DNA damage sites, enhances homologous recombination DNA repair mechanisms (Wang *et al.*, 2018). Similar to RBR, SNI1 proteins bind to E2F transcription factors, thereby suppressing the expression of several regulators of cell cycle progression. Phenotypical analyses of *sni1* mutants also revealed the accumulation of dead cells in the root tip, which is abolished in the additional absence of E2Fs (Wang *et al.*, 2018).

Unlike the RBR/E2F complex, E2Fs and SNI1 appear to form a negative feedback loop, where E2Fs further activate the expression of their negative regulator SNI1 (Wang *et al.*, 2018).

### 1.3.3 Cell cycle checkpoints

The coordinated activation of cell cycle checkpoints after DNA damage is essential to avoid the transmission of DNA lesions after cell division and for the maintenance of genome integrity (Pedroza-García *et al.*, 2022). Depending on the type of lesion, two main cell cycle checkpoints are activated: the G2/M checkpoint (triggered by DSBs) and the replication checkpoint (initiated after obstructions to replication fork progression) (Pedroza-García *et al.*, 2022).

#### 1.3.3.1 The G2/M checkpoint

SOG1 is the main regulator of the G2/M checkpoint in response to DSBs. Its phosphorylation by ATM/ATR leads to the transcriptional activation of several CKIs, such as SMR4, SMR5 and SMR7, which inhibit CDK activity. The absence of CDK complexes suppresses the proteasomal degradation of Rep-MYB3Rs, which in turn inhibit G2/M progression. The transcriptional repression of SOG1 over Act-MYB3Rs also putatively contributes to an additional repression of mitotic genes (Chen *et al.*, 2017). Moreover, the NAC transcription factors ANAC044 and ANAC085, which are direct targets of SOG1, were shown to further enhance Rep-MYB3Rs accumulation in response to DNA damage and heat stress (Takahashi *et al.*, 2019).

Additional G2-specific components, such as CDKB2;1 have been shown to be directly repressed after DNA damage in a SOG1 and proteasome dependent manner upon treatment with the DSB inducing drug zeocin (Adachi *et al.*, 2011; Pedroza-García *et al.*, 2022).

### 1.3.3.2 The replication checkpoint

Reduced availability of nucleotides, and formation of R loops or collisions between the transcription and replication machinery are among the numerous events that specifically impede replication fork progression and activate replication checkpoints (Pedroza-García *et al.*, 2022).

One of the best characterized elements of this cell cycle checkpoint is the already mentioned WEE1, whose activation upon replication stress seems to be partially SOG1 (Ogita *et al.*, 2018) and RBR/E2F (Bouyer *et al.*, 2018) dependent. WEE1 mostly activates G1/S specific arrest by phosphorylation of CDK, but also, as recent publications suggest, of non-CDK targets such as the splicing protein PLEIOTROPIC REGULATORY LOCUS 1 (PRL1) or the E3 ubiquitin ligase F BOX-LIKE17 (FBL17) (Wang *et al.*, 2021; Pan *et al.*, 2021).

PRL1, which is a subunit of the evolutionary conserved MOS4-associated complex (MAC) complex involved in RNA splicing, was shown to be directly phosphorylated by WEE1, which promotes PRL1 ubiquitination and subsequent degradation (Wang *et al.*, 2021). The absence of PRL1 is linked to alternative splicing of cell cycle regulators *CYCD3;1* and *CYCD1;1*, which have been characterized to function in both G1/S and G2/M transitions (Wang *et al.*, 2021).

On the other hand, FBL17 is an E3 ubiquitin ligase that specifically targets CKIs like KRP7 for degradation. Therefore, its proteasomal degradation upon WEE1 phosphorylation suppresses CKIs inhibition and negatively impacts cell cycle progression (Pan *et al.*, 2021). FBL17, in combination with RBR, has also been characterized to function in DNA damage signalling and repair. Accordingly, loss of function mutants for FBL17 displayed constitutive activation of DDR genes in a SOG1-independent manner (Gentric *et al.*, 2020)

### 1.3.4 DNA repair mechanisms

Transient cell cycle arrest in the plant DDR is usually linked to the activation of DNA repair processes. Depending on the type of DNA damage lesions, different DNA repair mechanisms are induced, including the nucleotide and base excision repair pathways (NER and BER), the mismatch repair pathway (MMR) and the Non-Homologous End-Joining (NHEJ) and Homologous Recombination (HR) pathways triggered by DSBs (Gentric *et al.*, 2021).

Since DSBs constitute the most severe type of DNA damage (Raina *et al.*, 2021; Gentric *et al.*, 2021), the NHEJ and HR repair mechanisms are of especial importance during the plant DDR.

The HR repair pathway relies on the homologous recombination principle by which nucleotide sequences between two related or identical DNA molecules are exchanged. Therefore, upon DSBs during the S/G2 phase transition, the undamaged sister chromatid is used as a template to restore the genetic information caused by the DNA lesions via HR (Raina



*et al.*, 2021; Gentric *et al.*, 2021). In contrast, the NHEJ repair pathway directly ligates the two broken ends without the need for a homologous sequence, what leads to the loss of genetic information. It constitutes the most frequent DSB repair mechanism and while it is active throughout the whole cell cycle, it is especially active during G1 (Raina *et al.*, 2021; Gentric *et al.*, 2021).

It is believed that meiotic and mitotic cells repair DSBs via the “error-free” HR pathway to avoid the loss of genetic information to be transmitted, whereas differentiated somatic cells use the NHEJ pathway (Gentric *et al.*, 2021).

#### 1.3.4.1 Components of the plant DDR repair pathways

The HR pathway is based on the activity of the MRN complex (MRE11, RAD50 and NSB1) for the recruitment of DNA repair proteins and ATM/ATR kinases to the DNA damage sites. In parallel, MRN activity at the DSBs is important for initiating the processing of the DNA ends by the exonucleolytic degradation of the 3' end. Activation of ATM/ATR kinases also initiate a signalling cascade that culminates with the activation of multiple proteins involved in DSB repair and checkpoint activation (Roy and Das, 2017; Raina *et al.*, 2021). Among these proteins BRCA1 is of essential importance because it is responsible of the recruitment of RAD51 to the DNA damage sites, which after coating the ssDNA overhangs, facilitates the strand invasion into the homologous template to generate the displacement loop (D-Loop) (Raina *et al.*, 2021).

Cell cycle regulation is also critical for the coordination and activation of the HR repair pathway (Gentric *et al.*, 2021). As such, one prominent example of this interconnection is the CDKB1/CYCB1;1 module activated after DNA damage in a SOG1 dependent manner (Gentric *et al.*, 2021; Pedroza-García *et al.*, 2022). SNI1, FBL17, RBR and E2F transcription factors constitute additional nodes of regulation between cell cycle checkpoints and DNA damage repair pathways independently of SOG1, as previously discussed in sections 1.3.2 and 1.3.3.

Per contra, the NHEJ pathway relies on the activity of the KU70/80 heterodimer for the detection of DSBs. Afterwards, gap filling DNA synthesis is carried out by the DNA polymerase  $\lambda$ , followed by joining of the DNA ends by the DNA ligase 4-XRCC4 (X-RAY CROSS COMPLEMENTATION PROTEIN 4) complex (Roy and Das, 2017). However, an alternative to the classical KU-dependent NHEJ pathway often called back-up NHEJ, has been shown to becomes active in the absence of core elements of the classical NHEJ. Among the major components of this back-up NHEJ are the POLY(ADP-RIBOSE) POLYMERASE 1 AND 2 (PARP1 and PARP2) proteins (Jia *et al.*, 2013), which, upon DNA breaks, transfer ADP-ribose units onto themselves or other target proteins using NAD<sup>+</sup> as a substrate. This

posttranslational modification is essential for the activation of DNA damage responses (Rissel and Peiter, 2019).

### 1.3.5 Cell death induction

Unsuccessful repair of DSBs triggers the induction of cell death (Hu *et al.*, 2016). This DNA damage induced programmed cell death (PCD) is found on the stele initials and immediate daughter cells in Arabidopsis root meristems and is SOG1 mediated (Johnson *et al.*, 2018).

Since RAM stem cells are the progenitors of all root cells, preventing the accumulation of DNA damage is essential. Thus, stem-cell specific PCD is important to avoid the propagation of deleterious mutations (Fulcher and Sablowski, 2009). The stem cell pool will subsequently be replenished after division of QC cells and other stem cells in direct contact with the damaged cells, following induction by the heterodimeric transcription factor complex ETHYLENE RESPONSE FACTOR115 (ERF115)-PHYTOCHROME A SIGNAL TRANSDUCTION1 (PAT1) (Heyman *et al.*, 2016).

While PCD in stem cells is SOG1 dependent, non-stem cell death takes place also in the absence of SOG1 (Yoshiyama *et al.*, 2014). In this context, accumulation of dead cells in the RAM of *sog1-1* mutants was suggested to be caused by uncontrolled DNA damage due to inefficient activation of the plant DDR (Yoshiyama *et al.*, 2014).



## 1.4 Precursor-messenger RNA splicing

Precursor-messenger RNA (pre-mRNA) splicing is a conserved mechanism in eukaryote organisms involved in constitutive and regulated gene expression. It consists on the removal of introns and subsequent ligation of exons to generate the translationally competent mRNAs and is mediated by the spliceosome, a large ribonucleoprotein (RNP) complex (Lorkovic *et al.*, 2000).

### 1.4.1 Formation of the Plant Spliceosome

Most eukaryotic organisms contain two distinctive spliceosomes: the U2- and the U12-dependent spliceosomes, which catalyse the removal of U2- and U12-type introns respectively. U12-type introns are less abundant, which is why U12 spliceosomes are only present in some eukaryote organisms (Will and Lührmann, 2011).

Most introns are recognized by the U2-type spliceosome, which is a RNP complex formed by the coordinated association of five snRNPs (U1, U2, U5, and U4/U6) and various non snRNP proteins (Brown and Simpson, 1998; Will and Lührmann, 2011). Each snRNP contains a specific small nuclear RNA, a heptameric ring of seven Sm or Lsm proteins and a subset of spliceosomal accessory proteins (Schlaen *et al.*, 2015).

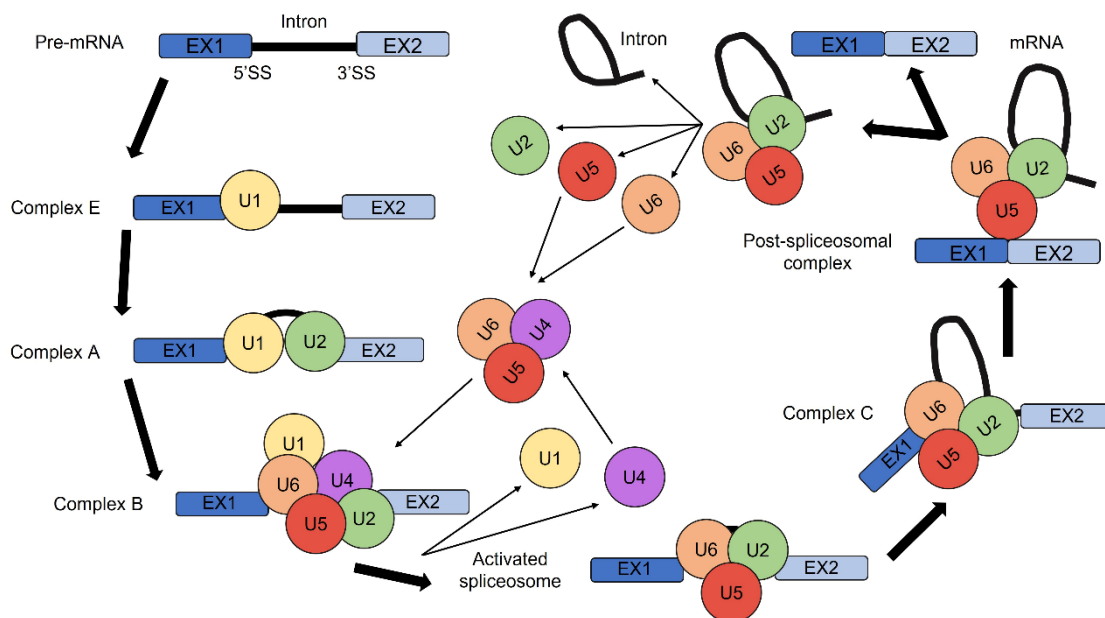


**Figure I-8.** Schematic simplified representation of the U2-type spliceosome assembly based on Will and Lührman, 2011. Pre-mRNA: precursor-messenger RNA; 5'SS: 5' splicing site; 3' SS: 3' splicing site; EX: exon; U1- U6: U1-U6 snRNP.

In brief, the canonical splicing cycle starts by the formation of the complex E after recruitment of the U1snRNP to the 5' splicing site. This is followed by the association of the U2snRNP to the branching point, thereby forming the complex A, also known as pre-spliceosome. A pre-assembled U4/U6.U5 tri-snRNP complex is afterwards recruited, generating the precatalytic complex B. This is followed by several rearrangements in RNA-RNA and RNA-protein interactions that facilitate the dissociation of the U1 and U4 snRNP, giving rise to the activated spliceosome. After catalytic activation and successful completion of the two transesterification reactions that are necessary to excise the intron and join together the exons, the spliceosome dissociates and the released snRNPs are available to catalyse the removal of another intron (Figure I-8) (Will and Lührmann, 2011; Shang *et al.*, 2017).

### 1.4.2 Alternative splicing

Single pre-mRNAs can generate more than one mRNA through the use of alternative splicing sites in a phenomenon known as alternative splicing (AS). AS strongly impacts transcriptome and proteome diversity. On one hand, transcript levels of specific genes can be altered by the synthesis of new unstable mRNA isoforms that will subsequently be degraded by the nonsense-mediated decay (NMD) machinery. On the other hand, AS can lead to the formation of alternate functional mRNAs that will afterwards generate alternative protein isoforms that may differ in subcellular localization, stability or even function, due to changes in domain organization motivated by the introduction of premature termination codons (PTC), intron retention or alternative 5' or 3' splice site selection. Additionally, newly generated isoforms can negatively regulate expression levels of the canonical protein through a dominant negative inhibition (Shang *et al.*, 2017).

#### 1.4.2.1 Types of AS events

Differential splice site selection leads to five major AS events: exon skipping/inclusion (ES), in which one or multiple exons are spliced out or retained, mutually exclusive exons (MXE), where only one of two exons is retained, intron retention (IR), in which an intron is not spliced out and consequently is retained in the mature transcript and alternative 5' (A5'SS) or 3' splice site (A3'SS), in which the boundary of the exons is altered (Figure I-9) (Chaudhary *et al.*, 2019).

While ES is the most prevalent AS events in animals, diverse AS studies suggest that IR is the most predominant type of AS in land plants (Reddy *et al.*, 2013).

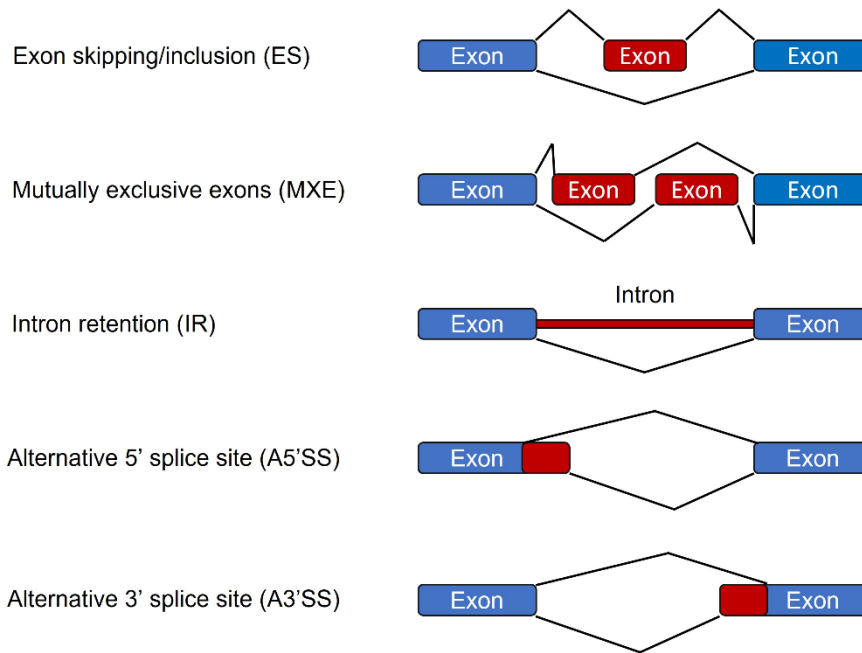


**Figure I-9.** Schematical representation of the different AS events based on Chaudhary *et al.*, 2019. Retained regions in the mature transcript are marked by black bars.

### 1.4.3 Splicing factors

Spliceosomal assembly and AS is mediated by splicing factors that recognize the cis sequences present in the pre-mRNAs, including the splice sites or the branch point, to facilitate the splicing process and are frequently rapidly transcriptionally induced after different environmental stress (Syed *et al.*, 2012; Zhang *et al.*, 2020; Liu *et al.*, 2022). Therefore, numerous evidence suggests that, besides its direct function in the regulation of gene expression, AS mechanisms, which allow a rapid adjustment of transcript abundance and function, are frequently used by plants to adapt to different stresses (Liu *et al.*, 2022).

#### 1.4.3.1 Serine/arginine rich proteins

Serine/arginine rich (SR) proteins are splicing factors with described functions in both constitutive and alternative splicing that are evolutionary conserved among eukaryotes, including the metazoan and plant kingdom. They contain two distinctive elements: one or two RNA recognition motifs (RRM) situated on the N-terminus and a serine/arginine rich domain known as RS domain at the C-terminus. While the RRM is needed for recognition and binding to specific exon and intron motifs, the RS C-terminal domain is believed to be important for protein-protein interactions (Kalyna and Barta, 2004; Yan *et al.*, 2017).

Based on domain organization and evolutionary relationships, SR proteins and SR-like proteins are divided into four groups: single-RRM, single-RRM Zink-like, dual RRM and RNPS1-like (Figure I-10) (Zhang *et al.*, 2020).



**Figure I-10.** Types of SR and SR-like proteins in *Arabidopsis* based on Zhang *et al.*, 2020. Green boxes represent the RNA recognition motif (RRM). Pink boxes represent the RS (arginine/serine rich) domain. Blue boxes represent a charged extension of the RRM domain. Yellow boxes represent the Zink knuckle. Dark grey boxes represent a SP (serine/proline) region. Light grey boxes represent a pseudo RRM domain containing a SWQDLKD motif.

*Arabidopsis* SR proteins can be further classified into six subfamilies: SC, SCL, RSZ, RS2Z, SR and RS. While members of the SR, SC and RSZ subfamilies and the SR-like SR45 protein have orthologous counterparts in humans; RS, SCL and RS2Z subfamilies are thought to be plant specific due to the acquisition of novel properties such as the duplication of the Zink knuckle or an acidic C-terminal region rich in serine and proline residues in RS2Z proteins (Zhang *et al.*, 2020).

Transient expression analyses of SR proteins fused to fluorescent markers in tobacco plants revealed, similar to their mammalian counterparts, a highly dynamic nuclear localization in

both nucleoplasm and nuclear speckles subnuclear regions (Zhang *et al.*, 2020). Upon transcriptional activation, some SR proteins like SR45 and SR34 have been shown to be recruited from the nuclear speckles (which act as storage sites for splicing factors) to the active transcription and splicing sites in the nucleoplasm. This phenomenon seems to be influenced by the phosphorylation status of their RS domain (Lamond and Spector, 2003; Ali *et al.*, 2003; Tillemans *et al.*, 2005; Zhang *et al.*, 2020). Furthermore, besides their predominant nuclear localization, SR34, SR34a and RSZ22 also possess a nucleocytoplasmic shuttling activity first described in their human orthologs (Zhang *et al.*, 2020).

Complex interactions between SR proteins by their RS domains have been predicted to be essential for the formation of different SR complexes that could determine the substrate specificity for their splicing function (Tillemans *et al.*, 2005; Zhang *et al.*, 2020). In this context, SR proteins have also been described to regulate the AS of other members of the SR family. For example, phenotypical defects in *sr45-1* mutants were associated with altered levels of SR protein isoforms (Ali *et al.*, 2007).

Besides their canonical function in splicing, SR proteins appear to play important roles in other RNA-related processes such as microRNA biogenesis (Chen *et al.*, 2015), mRNA export (Köhler and Hurt, 2007) and transcription (Yan *et al.*, 2017). Moreover, SR proteins are also involved in developmental processes (Kalyna *et al.*, 2003; Ali *et al.*, 2007; Yan *et al.*, 2017; Zhang *et al.*, 2020) and in the response to different abiotic stress conditions including cadmium, abscisic acid (ABA), or salt (Zhang *et al.*, 2020).

#### 1.4.3.2 LSM2-8 complex

SM-like (LSM) proteins are evolutionary conserved RNA-binding proteins with multiple roles in RNA metabolism (Perea-Resa *et al.*, 2012). Arabidopsis genome contains 11 genes encoding for 8 LSM (LSM1-LSM8) proteins. Each gene codifies for one LSM protein with the exception of LSM1, LSM3 and LSM6, where two highly similar genes encode for the same protein (Perea-Resa *et al.*, 2012).

The association of Arabidopsis LSM proteins generates two distinctive heptameric complexes: LSM1-7 and LSM2-8, where complex specificity is conferred by LSM1 and LSM8, while the other subunits are indistinguishable between both complexes (Figure I-11). While the LSM1-7 complex functions in mRNA decay in the cytosol, the LSM2-8 complex is a nuclear localized core component of the spliceosome that stabilizes the U6 snRNA contained inside the U6 snRNP and thus plays an essential role during pre-mRNA splicing (Perea-Resa *et al.*, 2012).

Interestingly, phenotypical analyses of *lsm8-1* and *lsm8-2* mutants revealed multiple growth defects in seed, cotyledon, and leaf morphology as well as in primary root growth and lateral root formation. These observations suggested that LSM8 was required during Arabidopsis

developmental transitions (Perea-Resa *et al.*, 2012). Additionally, different abiotic stress conditions such as draught or cold specifically induced AS in the absence of LSM8, which proofed the role of the LSM2-8 complex in Arabidopsis adaptation to different environmental conditions (Carrasco-López *et al.*, 2017).

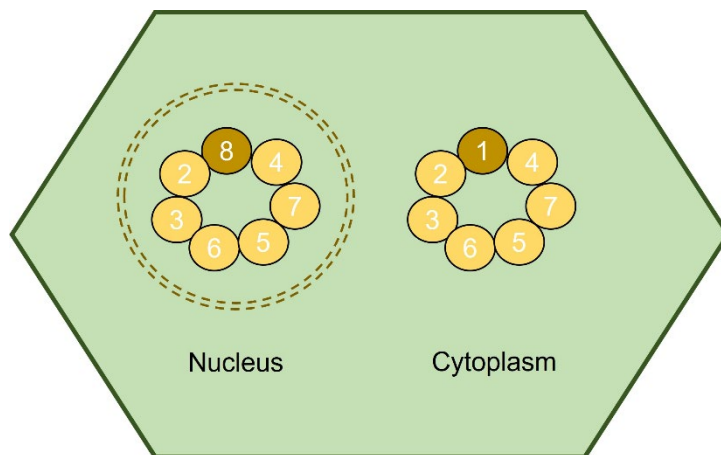


**Figure I-11.** Schematical representation of the LSM heptameric complexes organization and subcellular localization based on Perea-Resa *et al.*, 2012. LSM2-8 is nuclear localized, while LSM1-7 is found in the cytoplasm. 1-8 represents LSM1-8 proteins. LSM8 and LSM1 are marked in darker colour to indicate its role in defining the complex configuration.

#### 1.4.4 RNA processing and DNA damage

Numerous studies in the animal field highlight the importance of post transcriptional regulating factors, and in particular of splicing proteins, in the DNA damage response (Naro *et al.*, 2015). As such, genotoxic stresses have been shown to enhance AS events in important genes activated during the DDR, which thereby modify their mRNA stability and the availability of different protein isoforms, consequently altering their protein activity (Dutertre *et al.*, 2011; Naro *et al.*, 2015).

Additionally, beyond their canonical splicing function, animal splicing factors are thought to be directly involved in the maintenance of genome stability by preventing the occurrence of RNA-processing defects that can threaten the genetical information, safeguarding the chromosomal integrity and by directly sensing and repairing DNA lesions (Naro *et al.*, 2015).

Notably, SR proteins such as SRSF1 (ASF/SF2), SRSF2 (SC35) and SRSF3 (SRp20) have been associated to the preservation of genome integrity by preventing the accumulation of R-loops, which are three-stranded DNA:RNA hybrids often converted into DSBs (Li and Manley, 2005; Naro *et al.*, 2015).

Regarding the safekeeping function of chromosomal integrity, several splicing factors such as hnRNP A1 were described to participate in both protection and replication of telomeres, which are prone to be recognized as DNA breaks by the DNA repair machinery (Naro *et al.*,

2015). Moreover, defective splicing mutants lacking hnRNP U or PRP19 exhibited spindle abnormalities and thus altered chromosomal stability (Naro *et al.*, 2015).

There is also evidence of animal splicing factors being recruited to DNA damage sites possibly by posttranslational modifications such as phosphorylation or parylation and by doing so reducing the sensitivity of cells to DNA damage treatments (Naro *et al.*, 2015). Furthermore, the recruited splicing factors can also promote DNA repair processes such as HR or oxidized base repair at the DNA damage sites by enhancing the activity of RAD51 (Morozumi *et al.*, 2009) and NEIL1 (Hedge *et al.*, 2012) respectively (Naro *et al.*, 2015).

Finally, the splicing factor PRP19, a component of the PRP19 complex also known as the NineTeen (NTC) Complex, homologous to the MAC complex in Arabidopsis, is believed to sense single strand breaks by its interaction with RPA and thus constitutes one example of the role of pre-mRNA splicing in DNA damage sensing and signalling (Naro *et al.*, 2015).

Despite the numerous examples in mammalian cells indicating that pre-mRNA splicing might have an important role in genome stability, less studies support the role of splicing factors in the plant DDR (Nimeth *et al.*, 2020). Nevertheless, as it has been described in animals (Naro *et al.*, 2015); pre-mRNA splicing and other RNA binding processing factors are subject of posttranslational modifications during the plant DDR. In this context, 22 RNA binding proteins were found to be phosphorylated in an ATM/ATR dependent manner after DNA damage in Arabidopsis (Roitinger *et al.*, 2015). Among them, MERISTEM DEFECTIVE (MDF) (see Section 1.4.4.1) and 11 additional proteins were associated to splicing related processes (Table I-1).

Over 100 DDR repair genes were also found to undergo AS in Arabidopsis (Nimeth *et al.*, 2020), further underlining the importance of splicing regulation during the plant DDR.

**Table I-1.** Description of the molecular function and phenotypical alterations associated to the loss or enhancement of 11 RNA binding proteins associated to pre-mRNA splicing that are phosphorylated upon DNA damage in an ATM/ATR dependent manner. Based on the proteomics analyses performed by Roitinger *et al.*, 2015.

Protein	Relevant information	Phenotype
<b>ENHANCED SILENCING PHENOTYPE 3 (ESP3)</b>	Putative DEAH RNA helicase which negatively regulates Glc-induced ABA signalling and RNA silencing. Homologue of the yeast PRP2 RNA splicing cofactor (Herr <i>et al.</i> , 2006; Zheng <i>et al.</i> , 2019).	<i>esp3-1</i> (EMS line in C24 background) mutants have reduced size, altered leaf morphology, enhanced RNA silencing and an early flowering phenotype (Herr <i>et al.</i> , 2006).  <i>rsw12</i> (EMS line in Col-0 background) mutants present a temperature-sensitive radial swelling growth defect when grown



		<p>at 31°C with a root swelling phenotype, reduced growth and cell death. Reduced levels of cellulose were described in the mutant (Howles <i>et al.</i>, 2016).</p> <p><i>gsm1-1</i> (T-DNA insertion line in Col-0 background) mutants are Glc and ABA sensitive and exhibit reduced germination and impaired cotyledon development (Zheng <i>et al.</i>, 2019).</p>
<p><b>MOS4-ASSOCIATED COMPLEX 3A and 3B (MAC3A and MAC3B)</b></p>	<p>U-box E3 ubiquitin ligase subunits of the MOS4-Associated Complex (MAC) a highly conserved complex among eukaryotes. They share 82% identity at the amino acid level. Its orthologs are known as the NINETEEN COMPLEX (NTC) in human and the Prp19 complex (Prp19C) in yeast.</p> <p>It associates with the spliceosome and has a conserved role in splicing and are important for plant development and immunity. The MAC complex also promotes microRNA biogenesis and is important for the plant response to abiotic stresses and regulation of flowering time. (Monaghan <i>et al.</i>, 2009; Johnson <i>et al.</i>, 2011; Koncz <i>et al.</i>, 2012; Deng <i>et al.</i>, 2016; Jia <i>et al.</i>, 2017; Feke <i>et al.</i>, 2020).</p>	<p><i>mac3amac3b</i> double mutants (generated by crossing two T-DNA insertion lines) exhibit pleiotropic developmental phenotypes (short roots and siliques, small stature, and increased number of aborted seeds), reduced microRNA levels and global intron retention defects. They also present increased susceptibility to <i>P. syringae</i> infection and a delayed flowering time phenotype (Monaghan <i>et al.</i>, 2009; Weihmann <i>et al.</i>, 2012; Jia <i>et al.</i>, 2017; Li <i>et al.</i>, 2018; Feke <i>et al.</i>, 2020).</p>
<p><b>BUD SITESELECTION PROTEIN 13 (BUD13)</b></p>	<p>AtBUD13 is important in early embryo development by controlling pre-mRNA splicing of especially shorter introns (&lt;100bp). Homolog of yeast Bud13p (bud-site selection protein 13), which is part of the REtention and Splicing (RES) complex, a non-snRNP heterotrimeric complex identified in yeast and human that regulates splicing of a subset of transcripts (Xiong <i>et al.</i>, 2019).</p>	<p><i>atbud13-1</i> (GABI T-DNA insertion line) and <i>atbud13-2</i> (SALK T-DNA insertion line) are embryo-lethal (Xiong <i>et al.</i>, 2019).</p>
<p><b>AT3G02710</b></p>	<p>Encodes a protein with a putative role in mRNA splicing (Source: TAIR)</p>	<p>No phenotype described</p>
<p><b>AT3G49601</b></p>		<p>No phenotype described</p>



	Encodes a pre-mRNA-splicing factor (Source: TAIR)	
<b>PRE-mRNA PROCESSING 39a (PRP39a)</b>	Encodes a tetratricopeptide repeat protein similar to the yeast mRNA processing protein Prp39p and is part of the U1 snRNP. Together with RBP45d facilitates temperature induced AS of FLM to induce flowering at higher temperature (Wang <i>et al.</i> , 2007; Kanno <i>et al.</i> , 2017; Chang <i>et al.</i> , 2022).	<i>prp39-1</i> (T-DNA insertion line) mutants display late flowering under both short- and long-day conditions and defects in temperature-induced flowering (Wang <i>et al.</i> , 2007; Chang <i>et al.</i> , 2022).  <i>prp39a-3</i> and <i>prp39a-4</i> (BC1F3 generation) mutants present a mild developmental phenotype with shorter stature, and reduced seed set. Flowering time is increased in both lines and the mutations also affected the splicing of hundreds of pre-mRNAs, including proteins involved in transcription and PRP39 itself (Kanno <i>et al.</i> , 2017).
<b>AT4G21660</b>	Encodes a proline-rich spliceosome-associated (PSP) family protein (Source: TAIR)	No phenotype described
<b>CD2-binding protein-like protein (CD2B)</b>	Encodes a CD2-binding protein-like protein part of the U5 snRNP (Source: TAIR)	No phenotype described
<b>U1-70K</b>	Central component of the U1 snRNP with a conserved molecular function in eukaryotes by having an important role in response to environmental stresses. (Chen <i>et al.</i> , 2020).	<i>u1-70k-1</i> (SAIL T-DNA insertion line) displays mild increased tolerance to mannitol, by exhibiting slightly longer roots. No obvious phenotype at control conditions. (Chen <i>et al.</i> , 2020).  <i>u1-70k-2</i> (SALK T-DNA insertion line) is an enhancement mutation that phenocopies an OE-U1-70K line that has mild increased sensitivity to mannitol by exhibiting slightly shorter roots. No obvious phenotype at control conditions (Chen <i>et al.</i> , 2020).
<b>AT2G29210</b>	Encodes a splicing factor PWI domain-containing protein (Source: TAIR). It interacts with GDS1, a CH3-type zinc finger protein which is localized in nuclear speckles and is essential for normal growth and development (Kim <i>et al.</i> , 2016)	No phenotype described

#### 1.4.4.1 MERISTEM DEFECTIVE and SART1 family proteins

MERISTEM DEFECTIVE (MDF) is a putative splicing factor homologous to the human protein SQUAMOUS CELL CARCINOMA ANTIGEN RECOGNIZED BY T CELLS 1 (SART1) and hence a member of the SART1 family of proteins.

Human SART1 has been characterized to have a role during spliceosome assembly by facilitating the association of the U4.U6/U5 tri-snRNP complex (Makarova *et al.*, 2001). It physically interacts with various U5- and U4/U6-associated proteins such as human Brr2, Prp6 and Prp3 (Liu *et al.*, 2006). Thus, it locates on the interface between U5 and U4/U6 in the tri-snRNP complex (Liu *et al.*, 2006).

The predominant protein isoform of SART1 is expressed in the nucleus of proliferating cells and contains 800 amino acids. A less abundant SART1 protein isoform of 259 amino acids is generated after a frame shift in an internal ribosomal entry site and was found to localize in the cytoplasm of epithelial cancer cells (Hosokawa *et al.*, 2005; Henson and Taylor, 2020). Beyond its function in pre-mRNA splicing, SART1 transduction was associated to growth inhibition, cell cycle arrest and apoptosis (Hosokawa *et al.*, 2005). Furthermore, studies in Zebrafish revealed that an overexpression of SART1 caused by a point mutation in exon 12 led to an upregulation of apoptosis related genes, downregulation of genes involved in eye development, defective splicing in the brain and induction of cell death in the eyes (Henson and Taylor, 2020). Interestingly, the reduction of SART1 levels via small interference RNA (siRNA) based silencing also resulted in mitotic arrest and abnormal spindle formation (Kittler *et al.*, 2004).

Another well-known member of the SART1 family is MDF's homolog in yeast Snu66. Like human SART1, it was also found to be associated to the U4.U6/U5 tri-snRNP complex (Gottschalk *et al.*, 1999; Stevens and Abelson, 1999). It interacts with U5 snRNP components Bad response to refrigeration 2 protein (Brr2p), Prp6p (van Nues and Beggs, 2001) and Prp8 (Nguyen *et al.*, 2016). Furthermore, its role in pre-mRNA splicing is supported by the overall reduction of splicing at low temperatures in the absence of Snu66 (van Nues and Beggs, 2001). This splicing activity in both mammalian SART1 and yeast Snu66 is modulated by the non-covalent binding of the ubiquitin-related protein Hub1 to their conserved Hub1 interacting (HIND) domain (Mishra *et al.*, 2011). Additional studies on other organisms such as the pathogenic fungi *Fusarium graminearum* have further confirmed the importance of Snu66 in splicing through its functional relation with the spliceosome kinase FgPrp4 (Sun *et al.*, 2018).

Based on the presence of and N-terminal RS rich domain, consisting of arginine residues forming dipeptides with serine, glutamate or aspartate; SART1 family proteins, including Arabidopsis MDF, are considered SR-related proteins (Makarova *et al.*, 2001; Casson *et al.*, 2009).

The impact of MDF on Arabidopsis development was investigated by analysing the phenotype of two different null T-DNA insertion mutant lines: *mdf-1* and *mdf-2* (Casson *et al.*, 2009). Loss of MDF led to alterations in embryogenesis patterning (Casson *et al.*, 2005) and severe growth arrest in root and vegetative tissues, ultimately leading to the death of the plants 20-25 days after germination (Casson *et al.*, 2009). The dwarf and lethal phenotype of *mdf* mutants was correlated with loss of stem cell activity, decreased cell division and perturbations in the auxin maxima in the meristems. These defects were associated with the miss expression of auxin PIN transporters and a subset of transcription factors required for RAM and SAM formation and maintenance (Casson *et al.*, 2009).

Phenotypical analyses of an additional *mdf* mutant known as *dot2-1* generated by a single base-pair change (from A to T) at the end of exon 8 leading to the formation of a premature stop codon, reported that, in addition to the already described root growth arrest and dwarf phenotype, absence of MDF lead to disrupted vein patterning and cotyledon number, smaller and serrated leaves with an increase in cell number and reduced plant stature (Petricka *et al.*, 2008).

Opposite to their mammalian and yeast homologs, MDF does not possess a HIND element and thus does not bind to Hub1. Alternatively, Hub1 was shown to regulate AS in Arabidopsis by its binding to the C-terminal HIND domain of PRP38, another putative SR related splicing factor (Schütze *et al.*, 2016; Watanabe *et al.*, 2019).



## 2. AIMS OF THE DOCTORAL THESIS



MERISTEM DEFECTIVE (MDF) is a putative splicing factor of the SART1 family of proteins with an essential role in the maintenance and organization of stem cells in the apical meristems. Since the root and shoot apical meristems (RAM and SAM) sustain plant development, loss of meristematic activity was linked to growth arrest in root and vegetative tissues in *mdf* mutants (Casson *et al.*, 2009).

Based on the presumed phosphorylation of MDF upon DNA damage in an ATM/ATR dependent manner (Roitinger *et al.*, 2015), the importance of safeguarding genome integrity in the meristems and the accumulating evidence of pre-mRNA splicing functioning during the DNA damage response (DDR) in animals, it was proposed that:

**MDF has an essential role in the maintenance of genome stability in both apical meristems.**

This hypothesis was addressed by:

1. Exhaustive phenotypical analyses of *mdf-1* and *mdf-2* T-DNA insertion mutants with special focus on developmental traits previously described in mutants with compromised genome integrity.
2. Interaction studies with a known splicing factor to confirm its predicted location in the spliceosome.
3. RNA sequencing experiments that evaluated the putative function of MDF in pre-mRNA splicing and transcriptional control, specifically in plant DNA damage related pathways.
4. Generating double mutants with important components of the plant DDR to figure out the prospective regulatory mechanisms that modulate MDF's activity in genome stability.
5. Investigating the sensitivity and response of *mdf* seedlings and additional splicing mutants to genotoxic drugs.
6. Assessing the biological relevance of MDF phosphorylation in plant development and genome stability by creating phosphomimic variants of MDF OE constructs that emulated a constitutively phosphorylated and dephosphorylated state

# 3. MATERIAL AND METHODS



### 3.1 Plant lineages

*Arabidopsis thaliana*'s ecotype Columbia (Col-0) was selected as wildtype (WT) for all experiments. Correspondingly, every mutant and transgenic line used during this study was in Col-0 background.

#### 3.1.1 Single mutant lines

All mutants were T-DNA insertion lines provided by the Nottingham Arabidopsis Stock Centre (NASC) with the exception of the Ethyl methanesulfonate (EMS) *sog1-7* mutant line. Further details are described in Table M-1.

**Table M-1.** Description of the single mutant lines used during this study.

Line	Gene	Description	Reference
<i>mdf-1</i>	AT5G16780	SALK_040710	Casson <i>et al.</i> , 2009
<i>mdf-2</i>	AT5G16780	SAIL_775_F10	Casson <i>et al.</i> , 2009
<i>lsm8-1</i>	AT1G65700	SALK_025064	Perea-Resa <i>et al.</i> , 2012
<i>sr45-1</i>	AT1G16610	SALK_004132	Ali <i>et al.</i> , 2007
<i>sr34</i>	AT1G02840	SALK_125757	No SR34 transcript was found. Additional available lines for SR34 are described in Yan <i>et al.</i> , 2017.
<i>sr34b</i>	AT4G02430	SALK_055412	Yan <i>et al.</i> , 2017
<i>sog1-7</i>	AT1G25580	EMS mutagenized suppressor of <i>als3-1</i>	Sjogren <i>et al.</i> , 2015
<i>atm-2</i>	AT3G48190	SALK_006953	Garcia <i>et al.</i> , 2003
<i>atr-2</i>	AT5G40820	SALK_032841	Vespa <i>et al.</i> , 2005
<i>wee-1</i>	AT1G02970	GABI_270E05	De Schutter <i>et al.</i> , 2007

##### 3.1.1.1 Genotyping of T-DNA insertion mutant lines

Following the user's Guide to the Arabidopsis T-DNA Insertional Mutant Collections provided by the SALK institute (<http://signal.salk.edu/cgi-bin/tdnaexpress>), a two-step Polymerase Chain Reaction (PCR) genotyping assay was the selected method to identify homozygous plants for any T-DNA insert (O' Malley *et al.*, 2015).

##### DNA isolation

The DNA material necessary to perform the genotyping PCRs was obtained by grinding the selected tissue (complete seedlings, cotyledons, or rosette leaves) in a 1,5 mL tube with a sterile plastic pestle.

Afterwards, the disrupted tissue was dissolved in 200  $\mu$ L of Lysis buffer (Table M-2) and centrifuged for 5 min at 14.000 rpm (Eppendorf centrifuge 5424 R). Pellet was subsequently



discarded, and supernatant was resuspended in 150  $\mu$ L of Isopropanol and stored in between 1 and 2 hours at -20 °C.

**Table M-2.** Lysis buffer composition for plant quick DNA extraction

Lysis buffer composition for DNA extraction	
Tris-HCl (VWR Chemicals Prolabo®-EMSURE®)	200mM (pH 7,5-8)
NaCl (CHEMSOLUTE®)	250mM
EDTA (Carl ROTH®)	25mM (pH 8)
SDS (Carl ROTH®)	0,5%
In ddH2O	

This precipitation step was followed by another centrifugation of 8 min at 14.000 rpm in which the resulting supernatant was discarded. Pellet was washed with 500  $\mu$ L of 70% ethanol (EtOH) (CHEMSOLUTE®), vortexed and centrifuged for 3 min at 14.000 rpm. Supernatant was removed and the tube was placed in a Thermoblock (Thermo mixer compact Eppendorf) for 5 min at 50°C in order to dry the pellet and remove the residual ethanol. After completion of the incubation time, pellet was dissolved in 50 $\mu$ L of ddH2O and incubated for 10 min at 50°C to favour the dissolution. Finally, a 3 min centrifugation at 14.000 rpm was performed followed by the transfer of the supernatant to a fresh sterile tube. Isolated DNA was either used right away or stored at 4°C.

#### Polymerase Chain Reaction (PCR)

A two-step genotyping PCR was performed with a first PCR using appropriate primers to identify the inserted T-DNA, followed by a second PCR with a primer pair designed to amplify the WT locus. Annealing conditions and extension times were adjusted to enhance the efficacy of each primer pair. Protocol and cycling conditions for a standard PCR are described on Table M-3 and M-4.

**Table M-3.** Pipetting scheme of a standard PCR

Component	Volume ( $\mu$ L)
10 X Dream Taq Green Buffer (Thermo Fisher Scientific)	2
10 mM dNTPs (Thermo Fisher Scientific)	0,4
10 mM Forward Primer (Eurofins Genomics)	1
10 mM Reverse Primer (Eurofins Genomics)	1
Dream Taq DNA polymerase (Thermo Fisher Scientific)	0,1
Template	2
ddH2O	ad 20 $\mu$ L

**Table M-4.** Standard PCR Program

Cycle step	Temperature (°C)	Time (min)
Initial Denaturation	95	3

## MATERIAL AND METHODS

Denaturation	95	00:30	X 34
Annealing	55	00:30	
Extension	72	1	
Final Extension	72	5	
Hold	4	∞	

### Agarose gel electrophoresis

Amplified PCR products were loaded on 1% agarose (Genaxxon bioscience GmbH) gels prepared by diluting 1 g of agarose in 100 mL of 1x TAE buffer (Table M-5) supplemented with 4  $\mu$ L of a 1mg/mL EtBr (Roche Diagnostics GmbH) solution. DNA separation was carried out via electrophoresis by applying a current of 120 V for at least 30 min in an electrophoretic chamber filled with 1x TAE running buffer. Amplicons were detected after UV light exposition using a PEQLAB E-BOX VX2 device.

**Table M-5.** TAE buffer composition for electrophoresis.

TAE buffer 50X for electrophoresis separation (2 L)	
Tris (VWR Chemicals Prolabo®)	484 g
Glacial Acetic Acid (AnalaR NORMAPUR®)	114,2 mL
EDTA (Carl ROTH®)	18,6
In ddH <sub>2</sub> O	

#### 3.1.1.2 Genotyping of *sog1-7* mutants

As reported in Sjogren *et al.*, 2015, the *sog1-7* mutation was genotyped using Cleaved Amplified Polymorphic Sequence (CAPS) PCR followed by DdeI restriction enzyme digest.

To this end, after DNA isolation using the same protocol described in section 3.1.1.1; contrary to T-DNA insertion mutants, only one primer pair was used to amplify the EMS mutagenized region using the *sog1-7* CAPS primers described in Table M-23.

Subsequently, 10  $\mu$ L of the finished PCR reaction were transferred to a new tube, mixed with 2  $\mu$ L of CutSmart Buffer (NEB), 0,25  $\mu$ L DdeI restriction enzyme and 7,75  $\mu$ L of ddH<sub>2</sub>O and incubated for 1 hour at 37°C.

Both the undigested and digested PCR reactions were loaded on a 2% Agarose gel and separated for at least 1 hour with a current of 120 V in an electrophoretic chamber. Only WT samples contained the unmuted sequence recognized by the DdeI restriction enzyme and showed consequently a size difference between the digested and undigested sample.

#### 3.1.2 Double mutant lines

All double mutants were generated by crossing of individual single mutants (Table M-1). Table M-6 contains a list of every double mutant line generated during this study.

First, mature siliques and open flowers were removed from the plant providing the female organ in each specific crossing. Afterwards, under a Leica LED2500 binocular, closed flower buds were opened and emasculated using fine forceps. Naked pollen free stigmas were afterwards pollinated by tapping them with the anthers (and thereby with pollen) of an open mature flower from a plant containing the mutation we wished to incorporate. After several days, a young silique containing heterozygous seeds for both mutations developed from the manually pollinated stigma.

**Table M-6.** Description of the double mutant lines used during this study.

Line	Genes
<i>mdf-1sog1-7</i>	<i>AT5G16780</i> and <i>AT1G25580</i>
<i>mdf-1atm-2</i>	<i>AT5G16780</i> and <i>AT3G48190</i>
<i>mdf-1lsm8-1</i>	<i>AT5G16780</i> and <i>AT1G65700</i>
<i>mdf-2sog1-7</i>	<i>AT5G16780</i> and <i>AT1G25580</i>
<i>mdf-2atm-2</i>	<i>AT5G16780</i> and <i>AT3G48190</i>

### 3.1.3 Transgenic lines

*Arabidopsis thaliana* stable transformants were obtained by floral dipping using the *Agrobacterium tumefaciens* C58C1 strain carrying the different MDF constructs as described below. A list of all transgenic lines generated during this study is included in Table M-7.

**Table M-7.** List of transgenic lines generated during this study.

Line	Entry vector	Destination vector	Resistance in plants	Description
<i>mdf-1::pMDFMDFgGFP</i>	pDONR221 (Thermo Fisher Scientific)	pMDC107 (Curtis and Grossniklaus, 2003)	Hyg	Complementation line carrying MDF native promoter fused to genomic MDF and GFP. Promoter region was defined based on Casson <i>et al.</i> , 2009.
<i>mdf-2::pMDFMDFgGFP</i>	pDONR221 (Thermo Fisher Scientific)	pMDC107 (Curtis and Grossniklaus, 2003)	Hyg	Complementation line carrying MDF native promoter fused to genomic MDF and GFP. Promoter region was defined based on Casson <i>et al.</i> , 2009.
<i>mdf-1::p35SMDFCDSYFP</i>	pENTR-D-TOPO (Thermo Fisher Scientific)	pEarlyGate101 (Earley <i>et al.</i> , 2006)	BASTA	Transgenic line carrying MDF CDS under the 35S constitutive promoter fused to YFP.

MATERIAL AND METHODS

<i>mdf-1:: p35SMDFCDS S22AYFP</i>	pENTR-D- TOPO (Thermo Fisher Scientific)	pEarlyGate101 (Earley <i>et al.</i> , 2006)	BASTA	Transgenic line carrying MDF CDS containing the S22A aa exchange under the 35S constitutive promoter fused to YFP. Putative dephosphorylated MDF version.
<i>mdf-1:: p35SMDFCDS S22DYFP</i>	pENTR-D- TOPO (Thermo Fisher Scientific)	pEarlyGate101 (Earley <i>et al.</i> , 2006)	BASTA	Transgenic line carrying MDF CDS containing the S22D aa exchange under the 35S constitutive promoter fused to YFP. Putative phosphorylated MDF version.
WT:: p35SMDFCDS YFP	pENTR-D- TOPO (Thermo Fisher Scientific)	pEarlyGate101 (Earley <i>et al.</i> , 2006)	BASTA	Transgenic line carrying MDF CDS under the 35S constitutive promoter fused to YFP.
WT:: p35SMDFCDS S22AYFP	pENTR-D- TOPO (Thermo Fisher Scientific)	pEarlyGate101 (Earley <i>et al.</i> , 2006)	BASTA	Transgenic line carrying MDF CDS containing the S22A aa exchange under the 35S constitutive promoter fused to YFP. Putative dephosphorylated MDF version.
WT:: p35SMDFCDS S22DYFP	pENTR-D- TOPO (Thermo Fisher Scientific)	pEarlyGate101 (Earley <i>et al.</i> , 2006)	BASTA	Transgenic line carrying MDF CDS containing the S22D aa exchange under the 35S constitutive promoter fused to YFP. Putative phosphorylated MDF version.
<i>atm-2:: p35SMDFCDS YFP</i>	pENTR-D- TOPO (Thermo Fisher Scientific)	pEarlyGate101 (Earley <i>et al.</i> , 2006)	BASTA	Transgenic line carrying MDF CDS under the 35S constitutive promoter fused to YFP.
<i>atr-2:: p35SMDFCDS YFP</i>	pENTR-D- TOPO	pEarlyGate101 (Earley <i>et al.</i> , 2006)	BASTA	Transgenic line carrying MDF CDS under the

	(Thermo Fisher Scientific)			35S constitutive promoter fused to YFP.
<i>sog1-7:: p35SMDFCDS YFP</i>	pENTR-D-TOPO (Thermo Fisher Scientific)	pEarlyGate101 (Earley <i>et al.</i> , 2006)	BASTA	Transgenic line carrying MDF CDS under the 35S constitutive promoter fused to YFP.
<i>atm-2:: p35SMDFCDS S22DYFP</i>	pENTR-D-TOPO (Thermo Fisher Scientific)	pEarlyGate101 (Earley <i>et al.</i> , 2006)	BASTA	Transgenic line carrying MDF CDS containing the S22D aa exchange under the 35S constitutive promoter fused to YFP. Putative phosphorylated MDF version.
<i>sog1-7:: p35SMDFCDS S22DYFP</i>	pENTR-D-TOPO (Thermo Fisher Scientific)	pEarlyGate101 (Earley <i>et al.</i> , 2006)	BASTA	Transgenic line carrying MDF CDS containing the S22D aa exchange under the 35S constitutive promoter fused to YFP. Putative phosphorylated MDF version.
<i>mdf-1:: p35SMDFCDS GFP</i>	pENTR-D-TOPO (Thermo Fisher Scientific)	pABindGFP (Bleckmann <i>et al.</i> , 2010)	Hyg	Transgenic line carrying MDF CDS under the 35S estradiol inducible promoter fused to GFP.
<i>mdf-1:: p35SMDFCDS S22AGFP</i>	pENTR-D-TOPO (Thermo Fisher Scientific)	pABindGFP (Bleckmann <i>et al.</i> , 2010)	Hyg	Transgenic line carrying MDF CDS containing the S22A aa exchange under the 35S estradiol inducible promoter fused to GFP. Putative dephosphorylated MDF version.
WT:: p35SMDFCDS GFP	pENTR-D-TOPO (Thermo Fisher Scientific)	pABindGFP (Bleckmann <i>et al.</i> , 2010)	Hyg	Transgenic line carrying MDF CDS under the 35S estradiol inducible promoter fused to GFP.
WT:: p35SMDFCDS S22AGFP	pENTR-D-TOPO	pABindGFP (Bleckmann <i>et al.</i> , 2010)	Hyg	Transgenic line carrying MDF CDS containing

## MATERIAL AND METHODS

	(Thermo Fisher Scientific)			the S22A aa exchange under the 35S estradiol inducible promoter fused to GFP. Putative dephosphorylated MDF version.
--	----------------------------	--	--	--

### 3.1.3.1 Fragment amplification

Amplification of MDF genomic region with its upstream native promoter (Casson *et al.*, 2009) and MDF full length CDS excluding the STOP codon were achieved by performing Phusion High Fidelity PCR using the appropriate primers described in Table M-23.

DNA isolated from 7-day-old seedlings was used as source for MDF genomic amplification, whereas MDF CDS was amplified from the pda 30004 plasmid, which contained MDF CDS inside the RAFL15 vector and was generated by the RIKEN Bioresource Research Center.

Protocol and cycling conditions of a standard Phusion PCR are described on Tables M-8 and M-9.

**Table M-8.** Pipetting scheme of a standard Phusion PCR

Component	Volume (µL)
High Fidelity Buffer (Thermo Fisher Scientific)	10
10 mM dNTPs (Thermo Fisher Scientific)	1
10 mM Forward Primer (Eurofins Genomics)	2,5
10 mM Reverse Primer (Eurofins Genomics)	2,5
DMSO (VWR BDH Prolabo®)	1,5
High-Fidelity DNA Phusion polymerase (Thermo Fisher Scientific)	0,5
Template	1,25
ddH <sub>2</sub> O	ad 50 µL

**Table M-9.** Standard Phusion PCR Program

Cycle step	Temperature (°C)	Time (min)	
Initial Denaturation	98	00:30	X 39
Denaturation	98	00:10	
Annealing	60	00:30	
Extension	72	1:30	
Final Extension	72	8	
Hold	4	∞	

The finalized PCR reaction was run on an electrophoresis gel, cut and purified with the HiYield® PCR Clean-up/ Gel extraction (SLG®) kit. Afterwards, concentration and quality of the purified PCR product was measured using a NanoDrop2000 Spectrophotometer (Thermo Fisher Scientific).

### 3.1.3.2 Gateway cloning and *Escherichia coli* transformation

#### BP reaction

The selected cloning method for obtaining the different transgenic constructs was Gateway cloning which, in brief, consists of two concatenated reactions named BP and LR in which conserved sequences known as attachment or att sites are recombined to allow the transfer of DNA material.

Therefore, during fragment amplification, attachment sites were also added to the different amplicons, allowing thereby its subsequent recombination inside a Gateway cloning entry vector during the BP reaction as summarized in Table M-10.

**Table M-10.** Pipetting scheme of a standard BP reaction

Component	Volume (µL)
Purified PCR product	1-2 (≈100 ng)
Gateway® BP Clonase™ II (Invitrogen)	0,5
Entry vector (pDONR221 or pENTR-D-TOPO)	1 (≈150 ng)
TE buffer	1

After 1 hour incubation at room temperature or ON incubation at 16°C, the BP product was introduced in *E. coli* strains DH5α or TOP10 via Heat shock transformation as described in Table M-11.

**Table M-11.** Standard protocol for *E. coli* Heat shock transformation

<i>E. coli</i> Heath shock transformation
1. Mix BP product with 25µL of <i>E. coli</i> chemical competent cells
2. Incubation on ice for 30 minutes
3. Heat shock at 42°C for 40 seconds (Thermomixer Compact Eppendorf)
4. Incubation on ice for 1 minute
5. Add 250 µL of SOC liquid medium
6. Regeneration at 37°C 550 rpm for 1 hour
7. Plate 50-150 µL on LB plates supplemented with Kanamycin (Carl ROTH®)
8. Incubation at 37 °C ON or over the weekend at RT

**Table M-12.** SOC medium composition

Super Optimal broth with Catabolite repression (SOC) Medium	
Tryptone (Carl ROTH®)	20 g/L
Yeast Extract (Panreac Applichem)	5 g/L
NaCl (CHEMSOLUTE®)	0,6 g/L



## MATERIAL AND METHODS

KCl (AnalaR NORMAPUR®)	0,2 g/L
After autoclaving add 10 mL/L of 2 M Mg <sup>2+</sup> solution	

**Table M-13. LB medium composition**

Luria-Bertani (LB) Medium (1L)	
Tryptone/Peptone (Carl ROTH®)	10 g
Yeast Extract (Panreac Applichem)	5 g/L
NaCl (CHEMSOLUTE®)	10 g
Agar-Agar Kobe I (Carl ROTH®)	15 g
Autoclave for sterilisation	

### Colony PCR

Successful *E. coli* transformation led to the selective growth of several colonies carrying the antibiotic resistance due to the incorporation and expression of the entry vector. Single colonies were picked and tested by Colony PCR (Standard conditions defined in Tables M-3 and M-4) using appropriate primers targeting the vector regions upstream or downstream the insertion site as well as the transgene itself (Table M-23), to verify a correct insertion and orientation inside the entry vector.

Afterwards, ON cultures of the positive clones were prepared to obtain material for Plasmid DNA isolation the day after using the HiYield ® Plasmid Mini Kit Protocol (SLG®) kit. Lastly, the quality of the isolated Plasmid DNA was evaluated with a NanoDrop2000 Spectrophotometer (Thermo Fisher Scientific) and Sanger sequencing (Eurofins Genomics and GENEWIZ Inc.).

### Site directed mutagenesis (SDM) PCR

For the creation of stable transformants carrying phosphomimic variants of MDFCDS, an SDM Phusion PCR was performed using as template the MDFCDS\_pENTR-D-TOPO plasmid created during the BP reaction. To this end, appropriate complementing primers harbouring the desired nucleotide mutations to exchange serine 22 for alanine or aspartic acid (S22A and S22D), were used during the PCR (Table M-23). Pipetting scheme was previously defined in Table M-8. Table M-14 describes the specific Phusion PCR cycling conditions for MDFCDS SDM Phusion PCRs.

**Table M-14. Standard Phusion MDF SDM PCR Program.** Annealing temperature was increased from 54 until 60 °C gradually after each cycle.

Cycle step	Temperature (°C)	Time (min)	
Initial Denaturation	98	00:30	X 19
Denaturation	98	00:10	
Annealing	54-60	00:20	
Extension	72	3	
Final Extension	72	2	
Hold	4	∞	



20  $\mu$ L of SDM PCR product were transferred to a new tube, mixed with 1  $\mu$ L of the methylation specific DpnI restriction enzyme and incubated for 1 hour at 37°C.

Since plasmid DNA isolated from most *E. coli* strains is methylated, it will be digested, opposite to the newly mutagenized synthesized DNA. This means that only the MDF phospho-mutants were subsequently transformed into *E. coli* TOP10 strain via Heat shock (Table M-11) by mixing 15  $\mu$ L of the DpnI digested PCR product with 200  $\mu$ L of chemically competent cells.

### LR reaction

After verification via sequencing of the lack of mutations in the pMDFMDFg, pDONR221 and MDFCDS\_pENTR-D-TOPO plasmids, and the incorporation of the aa exchanges in the MDFCDS\_pENTR-D-TOPO phospho-mutants, isolated DNA from all constructs was recombined in different destination vectors during the LR reaction (Tables M-15 and M-16).

**Table M-15.** Description of the destination vectors used during this study.

Destination vector	Description	Purpose
pMDC107 (Curtis and Grossniklaus, 2003)	C-terminal GFP tag Confers Kanamycin resistance Valid for plant expression studies	Creation of <i>mdf-1</i> and <i>mdf-2</i> complementation lines.
pEarlyGate101 (Earley <i>et al.</i> , 2006)	35S promoter C-terminal YFP tag Confers Kanamycin resistance Valid for plant expression studies	Creation of <i>mdf-1</i> and WT MDFCDS/MDFCDS phospho-mutant overexpression lines.
pABindGFP (Bleckmann <i>et al.</i> , 2010)	35S estradiol inducible promoter C-terminal GFP tag Confers Spectinomycin resistance Valid for plant expression studies	Creation of inducible <i>mdf-1</i> and WT MDFCDS/MDFCDS phospho-mutant overexpression lines.

**Table M-16.** Pipetting scheme of a standard LR reaction.

Component	Volume ( $\mu$ L)
Purified BP product	1-2 ( $\approx$ 150 ng)
Gateway® LR Clonase™ II (Invitrogen)	0,5
Destination vector (pMDC107, pEarlyGate101 or pABindGFP)	1-2 ( $\approx$ 150 ng)
TE buffer	1

After ON incubation at 16°C, the LR product was introduced in *E. coli* strains DH5 $\alpha$  or TOP10 via Heat shock transformation as described in Table M-11 and plated on LB plates

supplemented with the corresponding antibiotic (Kanamycin (Carl ROTH®) and Spectinomycin (Duchefa Biochemie)). Positive clones were tested via Colony PCR and Sanger sequencing (see above).

### 3.1.3.3 *Agrobacterium tumefaciens* transformation

Prior to plant transformation, the different MDF constructs introduced in the destination vectors in *E. coli* were electroporated in *A. tumefaciens* C58C1 strain due to its ability of transferring foreign genes into a wide variety of host plants, including *Arabidopsis thaliana*. The protocol for *A. tumefaciens* transformation is summarized in Table M-17.

**Table M-17.** Standard protocol for *A. tumefaciens* electroporation transformation

<i>A. tumefaciens</i> electroporation	
1.	Mix 3-8 $\mu$ L of LR product with 80-100 $\mu$ L of <i>A. tumefaciens</i> electrocompetent C58C1 cells
2.	Apply a pulse of 1440 V with an Eporator (Eppendorf)
3.	Add 250 $\mu$ L of SOC liquid medium
4.	Incubation on ice for 2 hours
5.	Plate 100 $\mu$ L on LB plates supplemented with Kanamycin (Carl ROTH®) or Spectinomycin (Duchefa Biochemie) and incubate for $\approx$ 48 hours at 28°C

Positive clones were tested via Colony PCR and Sanger sequencing (see above). Additionally, transient expression on *Nicotiana benthamiana* leaves was also used to verify the expression of the construct by monitoring the appearance of fluorescent derived signals as a consequence of successful *A. tumefaciens* transformation (Table M-23)

### 3.1.3.4 *Arabidopsis thaliana* transformation

An adaptation of the Floral dipping protocol from Clough and Bent, 1998 was followed for efficient transformation of *Arabidopsis thaliana* with the different constructs successfully introduced in *A. tumefaciens*.

To this end, 7 days prior to the transformation, bolts and flowers were removed from the 4–5-week-old *Arabidopsis* plants to trigger the formation of additional bolts and hence improve the transformation efficiency. Later, 2 days before the transformation, a pre-pre-culture was generated by adding a single *Agrobacterium* transformed colony to 5 mL of LB liquid medium supplemented with the appropriate antibiotic and incubated ON at 28°C and 180 rpm. This was followed, by the set-up of a pre-culture one day prior to the transformation by mixing 2,5 mL of the pre-pre-culture with 50 mL of fresh LB liquid media and the appropriate antibiotic. After ON incubation at 28°C and 180 rpm, cells were harvested by centrifugation at 4700 rpm for 5-10 min (Eppendorf Centrifuge 5810R). Supernatant was discarded and pellet was resuspended in 50 mL of Sucrose-Silwet solution (Table M-18). Finally, the bacterial solution

was applied to the closed buds of the plants with a paintbrush, instead of the canonical dipping of the entire plant, to reduce the stress of the plant during the entire process. After at least three rounds of painting, the pot was covered for two days with a small autoclaving bag to increase the humidity and favour the survival of the bacteria.

Seeds produced by the floral painted plants were pooled and positive transformants were selected on Hygromycin B (Carl ROTH®) after stable insertion of pMDF107 and pABindGFP constructs or BASTA (Bayer) in the case of pEarlyGate101 constructs.

**Table M-18.** Sucrose-Silwet solution composition for *Arabidopsis thaliana* transformation.

Sucrose-Silwet solution (50 mL)	
Sucrose (Carl ROTH®) 5%	2,5 g
Silwet-77 (Momentive Performance Materials GmbH) 0,05%	25 µL
Ad 50 mL ddH2O	

## 3.2 Plant phenotyping methods

Plants were grown either on potting soil (Flormaris®) mixed with sand and volcanic soil in a 4:2:1 proportion or Murashige and Skoog (MS) (Duchefa Biochemie) plates containing 1% sucrose (Carl ROTH®) and 1% (w/v) phytoagar (Duchefa Biochemie). Standard growth cycles of 16 h light, 22°C/ 8 h dark, 18°C were adjusted in climate chambers (CLF climatics).

In order to remove bacterial or fungi contaminants, seeds were vapor sterilized with a mixture of 2,3 mL of 32% HCl (EMSURE®) and 50 mL of NaOCl (CHEMSOLUTE®) for 3 hours.

### 3.2.1 Monitoring of seed-related phenotypical traits

Seed counting and seed germination analyses were conducted to evaluate the impact of MDF and LSM8 on embryogenesis and dormancy break.

#### 3.2.1.1 Seed counting

Defects during seed formation were assessed by counting the number of seeds contained inside individual mature siliques from the main shoot of 5–7-week-old Arabidopsis plants using a Leica LED2500 binocular.

The first five incompletely developed siliques of the main inflorescence axis were not considered for the calculations (Jiang *et al.*, 2020).

The distribution of seeds inside individual siliques of *mdf-1lsm8-1* (heterozygous/homozygous) and *mdf-1lsm8-1* (segregating WT/homozygous) siliques was documented with an Olympus MVX10 Macrocope Fluorescence Microscope.

#### 3.2.1.2 Seed germination

Seeds were sown on MS sucrose plates and stratified for 2 days at 4°C and dark conditions. 48 hours after transfer to light, the percentage of germinating seeds was calculated for the indicated number of plants in each specific experiment. Seeds were considered to have germinated after radicle emergence.

### 3.2.2 Phenotypical studies during seedling stage

A wide range of phenotypical traits were monitored between day 1 after germination (DAG) and day 17. Germination was estimated and normalized to 24 hours. Thus, 1 DAG equals to 2 days after transfer to light.

### 3.2.2.1 Cell death accumulation

The accumulation of dead cells in the root apical meristem (RAM) was monitored by propidium iodide (PI) staining of 2 and 3 DAG root tips by incubation in a 10 µg/ml PI solution (Sigma-Aldrich). After 1-to-10-minute incubation time, imaging was carried out by confocal microscopy (Leica TCS SP8 Confocal Microscope. Excitation: 561 nm/ Detection: 600-636 nm). Layer specification was set based on the visualization of the quiescent center (QC) and cell death area was quantified using the ImageJ software.

### 3.2.2.2 Primary root length

Primary root growth was assessed by germination and growth on MS sucrose vertical plates. Plates were scanned (Epson Perfection V700 Photo Scanner) at the indicated timepoints and root length was quantified using the ImageJ software.

An Olympus MVX10 Macroscopic Fluorescence Microscope was used to document the growth arrest phenotype of *mdf* mutants 3 DAG.

### 3.2.2.3 True leaf formation

For true leaf formation experiments, plants were germinated and grown on MS sucrose horizontal plates. Percentage of plants showing true leaves 9 DAG was calculated for the indicated number of plants in each specific experiment. Plants with visible but still unfolded true leaves were included in the calculations.

### 3.2.2.4 Adventitious root formation

Adventitious rooting was evaluated by counting the number of plants that formed roots in the hypocotyl at the indicated timepoints for each specific experiment. Plants were germinated and grown on MS sucrose horizontal plates.

## 3.2.3 Phenotypical studies of aerial tissues

Defects in vegetative growth were examined by monitoring rosette and shoot development.

### 3.2.3.1 Number and diameter of rosette leaves

Leaf formation at later developmental stages was assessed by counting the number of rosette leaves formed by different plant lines four weeks after germination in soil under the previously defined standard growth conditions.

Additionally, rosette growth was followed and documented with a Canon EOS 600D Digital Camera at different timepoints. Vertical photographs taken with the camera directed straight down towards the ground at a right angle were afterwards processed with the ImageJ software. Rosette diameter between the two farthest leaves was determined.

### 3.2.3.2 Plant stature

Similar to rosette growth, development of the main shoot was also followed and documented with a Canon EOS 600D Digital Camera at different timepoints. Horizontal pictures taken with the camera straight directed towards the lateral sides of the pots at a right angle were used to measure the main shoot length with the ImageJ software.

## 3.2.4 Evaluation of cell cycle associated defects

Diverse experimental approaches were followed to evaluate the impact of MDF on cell cycle regulation.

### 3.2.4.1 Counting of dividing cells in the RAM

Cell division in the root apical meristem (RAM) was determined by counting the amount of cortex cells within the dividing zone of the RAM after Propidium iodide (PI) staining of 3DAG seedlings. To this end, root tips were excised and incubated for 1 min in 10 µg/ml PI solution (Sigma-Aldrich). Afterwards, imaging was carried with a confocal microscope (Leica TCS SP8. Excitation: 561 nm/ Detection: 600-636 nm). Layer specification was set based on the visualization of the quiescent center (QC) and the division zone was determined as the population of small and round stem cells and progenitors located underneath the first elongated cell.

### 3.2.4.2 EdU staining

EdU (5-Ethynyl-2'-deoxyuridine) labelling of replicating cells in 7 DAG seedlings was carried out at the Institute of Microbiology of the Czech Academy of Sciences in Prague by Pavla Binarova, Hana Kourova and Jana Chumova. The Click-iT EdU Alexa Fluor 488 HCS Assay (Molecular Probes) was used as previously reported (Kállai *et al.*, 2020) and seedlings were incubated in liquid medium with an EdU pulse at a dilution of 1:1000 for 3 h.

### 3.2.4.3 Immunostaining

Immunolabelling of microtubules in root tip cells of WT, *mdf-1* and *mdf-2* 6 DAG plants was performed at the Institute of Microbiology of the Czech Academy of Sciences in Prague by

Pavla Binarova, Hana Kourova and Jana Chumova following a previously published protocol (Horvath *et al.*, 2017). Mitotic microtubular arrays were visualized with the anti- $\alpha$ -tubulin (Abcam, 1:1000) and anti-mouse Alexa Fluor 488 (1:600) antibodies. Chromatin was counterstained with DAPI. Imaging was carried out with FV10 ASW2.0 and confocal IX-81 FV-1000 Olympus microscopes.

#### 3.2.4.4 Endoreplication Index

In order to assess whether MDF was not only important for promoting cell cycle arrest but also during endocycle activation, endoreplication levels were quantified at the Institute of Microbiology of the Czech Academy of Sciences in Prague by Pavla Binarova, Hana Kourova and Jana Chumova. To this end, as previously published, DNA content was determined using flow cytometry (Kallai *et al.*, 2020). Nuclei were isolated from 10 DAG WT, *mdf-1* and *mdf-2* seedlings (Partec CyStain UV precise P kit) and analysed on a BD LSRII Flow cytometer (BD Biosciences) with a solid-state laser (Excitation 405 nm) and 450/50 band pass filter. Data evaluation was performed with the FlowJo software. Endoreplication index (EI) was determined from percentage values of each C-level (cellular DNA content).

### 3.3 Differential expression and splicing analyses

#### 3.3.1 Differential expression analyses in selected targets

Quantitative real-time-PCR (RT-qPCR) experiments were performed to determine the expression levels of specific genes in *mdf* background.

##### 3.3.1.1 RNA isolation

Seedlings, rosette leaves or root tips from the indicated ages were frozen in liquid nitrogen and grinded in a Tissue Lyser (Qiagen). Afterwards, RNA isolation was carried out with the innuPREP Plant Kit from Analytik jena Biometra following manufacture's specifications.

##### 3.3.1.2 cDNA synthesis

RNA was converted to cDNA using the QuantiTect® Reverse Transcription kit (Qiagen). Initial RNA amount for cDNA synthesis was normalized to 300 ng when complete seedlings or leaves were used, whereas only 100 ng were used for experiments having root tips as tissue source.

##### 3.3.1.3 Quantitative real-time PCR

RT-qPCRs were performed in a Rotor-Gene Q (Qiagen) in reaction volumes of 10  $\mu$ L that contained 5  $\mu$ L of a QuantiFast SYBR Green PCR Master Mix (Qiagen), 0,5  $\mu$ L of each primer (10 mM) and 4  $\mu$ L of newly synthesized cDNA. Gene expression quantification and normalization against the reference genes *FASS* (*AT5G18580*) and *SAND* (*AT2G28390*) was done with the qbasePLUS software (Hellemans *et al*, 2007). Standard cycling conditions are listed in Table M-19.

**Table M-19.** Standard RT-PCR Program used in this study.

Cycle step	Temperature (°C)	Time (min)	
PCR initial activation step	95	5	
Denaturation	95	00:10	X 39
Combined annealing/extension	60	00:30	
Melting curve analyses	65-95	-	



### 3.3.2 Genome-wide evaluation of expression and splicing changes

RNA sequencing experiments were performed as described in a manuscript containing some of the results included in this thesis (de Luxán Hernández *et al.*, 2022 in revision in the Life Science Assembly Journal. See Appendix)

Total RNA was extracted from 3 different biological replicates of 12-day-old WT and *mdf-1* seedlings using the innuPREP Plant RNA kit (Analytik Jena Bio solutions) as described in section 3.3.1.1.

RNA quality assessment, library preparation, sequencing and bioinformatic analyses were performed by Novogene Co. Integrity and quantitation of the extracted RNA were measured using the RNA Nano 6000 Assay Kit of the Bioanalyzer 2100 system (Agilent Technologies, CA, USA). With 1 µg RNA per sample as input material, sequencing libraries were subsequently generated using NEBNext® Ultra™ RNA Library Prep Kit for Illumina® (NEB) following the manufacturer's recommendations. Index codes were also added to attribute sequences to each sample. Clustering of the index-coded samples was carried out on a cBot Cluster Generation System using PE Cluster Kit cBot-HS (Illumina) following manufacturer's instructions. Afterwards, library preparations were sequenced on an Illumina NovaSeq 6000 platform and approximately 50 million 150 paired end reads per sample were generated. To ensure the high quality of the samples, only clean data was used for subsequent analyses. This was achieved after the removal of reads containing adapter and poly-N sequences and reads with low quality from the raw data. Mapping against the Arabidopsis TAIR10 reference genome was performed using the HISAT2 software. Reads Per Kilobase of exon model per Million mapped reads (RPKM) of each gene was calculated based on the length of the gene and reads count mapped to this gene. Differential expression analyses between *mdf-1* and WT were carried out using the DESeq2 R package with the Benjamini and Hochberg's approach for adjusting p values according to the False Discovery Rate (FDR). Genes with adjusted p-value < 0.05 were considered as differentially expressed. Validation of differential expression events was performed via RT-qPCR with appropriate primers targeting the differentially expressed area.

Gene ontology (GO) enrichment analyses were performed using the GO-term finder software from Princeton University (Boyle *et al.*, 2004) and the degree of significancy of selected relevant terms ( $-\log_{10} \text{padj}$ ) was graphically represented together with the number of genes (n) found in the different categories.

Alternative splicing (AS) analysis was performed with the rMATS software. Events with adjusted p-value < 0.05 were considered as alternatively spliced. Validation of differential splicing events was performed via RT-qPCR. Two different primers pairs were designed to specifically detect intron and exon transcripts. Exon primers annealed to the exon junction,

while intron-specific primers annealed inside the retained intron. Intron retention was afterwards measured by dividing intron expression by exon-specific expression.

Visualization of the degree of overlap between different conditions or mutant lines was achieved by the generation of Venn diagrams with the online software Venny 2.1 generated by Juan Carlos Oliveros (BioinfoGP, CNB-CSIC). Statistical significance was calculated based on a normal approximation of a hypergeometric probability formula implemented at the web tool [http://nemates.org/MA/progs/overlap\\_stats.html](http://nemates.org/MA/progs/overlap_stats.html). Arabidopsis reference number of protein-coding genes was set to 27474 (Source: Uniprot). Additional information about the calculations can be found in [http://nemates.org/MA/progs/representation\\_stats.html](http://nemates.org/MA/progs/representation_stats.html).

The genome wide RNAseq data presented in this study was deposited at the Gene Expression Omnibus database under the identification GSE197898 and will be accessible after publication of a manuscript that describes the major findings of this thesis (de Luxán-Hernández *et al.*, 2022 in revision in the Life Science Assembly Journal. See Appendix).

### 3.4 Sensitivity assays to DNA damaging agents

Short and long-term experiments with different chemicals that compromise Arabidopsis DNA integrity (zeocin (Invitrogen), bleomycin (Sigma-Aldrich), hydroxyurea (Sigma-Aldrich), H<sub>2</sub>O<sub>2</sub> (CHEMSOLUTE®) and oryzalin were carried out in WT and mutant lines.

#### 3.4.1 Primary root length and Adventitious root (AR) formation

##### 3.4.1.1 Primary root length

The impact of zeocin and hydroxyurea (HU) on primary root length was evaluated by germinating and growing WT and mutant plants on MS sucrose vertical plates for 5 days. Afterwards, seedlings were transferred to either control plates (without chemicals) or plates containing either zeocin 20 µg/mL or HU 1,5 mM for 6 additional days. Plates were scanned (Epson Perfection V700 Photo Scanner) 3 DAG and 2, 4 and 6 days after transfer (DAT). Primary root length was measured at each time point using the ImageJ software and growth for each timepoint was determined by subtracting the length of the previous timepoint. Relative growth values were obtained by dividing the growth at each timepoint by the initial root length measured before transfer.

The effect of H<sub>2</sub>O<sub>2</sub> on primary root length was also assessed by transferring 5-day-old WT and mutant plants to MS medium containing H<sub>2</sub>O<sub>2</sub> 0,8 mM or MS medium without chemical supplements (Control). Plates were scanned (Epson Perfection V700 Photo Scanner) before transfer and 7 and 10 DAT and primary root length was measured at each time point using the ImageJ software. Relative root growth was calculated in relation to the root length measured before transfer. Alternatively, WT and mutant plants were germinated and grown directly in MS medium (Control) or MS medium supplemented with H<sub>2</sub>O<sub>2</sub> 0,8 mM. Root length was evaluated after 3, 5 and 12 days in light using the ImageJ software.

Additionally, primary root length was also measured in 2 DAG WT and mutant plants germinated and grown on vertical MS sucrose plates (Control) or MS sucrose plates supplemented with oryzalin 100 nM using the ImageJ software.

##### 3.4.1.2 AR formation

The same plants used for primary root length analyses were also monitored for AR formation after zeocin or H<sub>2</sub>O<sub>2</sub> treatment.

Regarding the zeocin studies, the percentage of plants that formed roots in the hypocotyl in plants transferred to MS sucrose (Control conditions) or MS sucrose supplemented with zeocin 20 $\mu$ g/mL was quantified at 10, 13 and 17 DAG.

Following the same methodological approach, the percentage of plants forming AR in the presence and absence of H<sub>2</sub>O<sub>2</sub> 0,8 mM 10 DAT was also calculated.

### 3.4.2 True leaf formation

True leaf formation assays were carried out by germinating and growing WT and mutant plants on MS sucrose horizontal plates containing no zeocin (Control), zeocin 25  $\mu$ g/mL (Zeocin 25) and zeocin 50  $\mu$ g/mL (Zeocin 50) for 10 days. Percentage of plants showing true leaves was calculated for each of the conditions in at least three independent experiments with a minimum of 15 plants per line, condition, and experiment. Plants with visible but still unfolded true leaves were included in the calculations.

### 3.4.3 Cell death accumulation

Cell death induction in WT and mutant plants was determined in 3 DAG root tips after ON incubation in MS medium (Control) or MS medium supplemented with Zeocin 15 $\mu$ M.

Additionally, accumulation of dead cells in the RAM of 2 DAG WT, *sog1-7* and *mdf* mutants was measured after growth in MS sucrose vertical plates (Control) or MS sucrose plates containing 100nM or 200nM oryzalin.

Cell death visualization and quantification in both cases was executed as described in section 3.2.2.1.

### 3.4.4 Transcriptional induction of selected genes after genotoxic treatments

Transcriptional changes were evaluated with RT-qPCR experiments as described in section 3.3.1. Different chemical incubation times and conditions are listed below.

#### 3.4.4.1 DDR associated genes

The expression of different DNA damage related genes in 3 DAG root tips or 7-day-old WT and mutant seedlings was measured after 2-hour incubation in MS liquid supplemented with zeocin 100 $\mu$ M.

DDR transcriptional analyses using the 35SMDFCDS estradiol inducible transgenic plants required additional induction steps. For this reason, after 6 days growth in light, seedlings

were transferred ON to MS sucrose plates supplemented with estradiol 5  $\mu\text{M}$  (Sigma-Aldrich). Estradiol 20  $\mu\text{M}$  was also added the next day to the MS-liquid medium during the 2-hour zeocin 100 $\mu\text{M}$  incubation. The efficient induction of the MDFCDS transgenic constructs was monitored by the accumulation of fluorescence signal in the transformants, which was visualized using an Olympus MVX10 Macroscopic Fluorescence Microscope. Moreover, MDF expression levels were also assessed via RT-qPCR in comparison to WT and non-transformant plants to verify the correct induction of the transgene.

Alternatively, DDR genes expression was also evaluated in 7-day-old WT and mutant seedlings incubated for 12 hours in MS liquid medium (Control conditions) or 0,6  $\mu\text{g/mL}$  bleomycin containing medium.

#### 3.4.4.2 MDF

MDF transcriptional induction was also assessed after genotoxic treatments. To this end, MDF expression levels were calculated in 3DAG WT and *sog1-7* root tips incubated for 2 hours in zeocin 100 $\mu\text{M}$  and in 7-day-old WT and *wee-1* seedlings after ON growth in HU 1mM.

#### 3.4.4.3 Oxidative related genes

Finally, transcriptional analyses of ROS-responsive genes were carried out in 5-day-old WT, *mdf-1* and *mdf-2* seedlings after 2-hour incubation in MS sucrose liquid medium supplemented with or without 0,5mM  $\text{H}_2\text{O}_2$ .

### 3.5 Localization and interaction studies

#### 3.5.1 Transient expression in *Arabidopsis thaliana* protoplasts

35SMDFCDSYFP and 35SMDFCDS22AYFP constructs were transiently transformed in *Arabidopsis* mesophyll protoplasts to investigate the impact of MDF's phosphorylation on its subcellular localization.

##### 3.5.1.1 Protoplast isolation

*Arabidopsis thaliana* plants were grown for 6-8 weeks in short light conditions (8 h light, 22°C/ 16 h dark, 18°C cycles) to trigger the generation of rosette leaves. Individual leaves were sliced in small pieces of approximately 2 mm width and transferred to a petri dish filled with MCP buffer (Table M-20) and H<sub>2</sub>O in a 1:1 proportion. Once the whole surface was covered with leaf slices, the MCP buffer / H<sub>2</sub>O mix was removed and exchanged with 20 mL of digestion buffer (Table M-20). After 2-hour incubation in the dark at 55-60 rpm inside the enzymatic solution, protoplasts were released by shaking the mix for 1 minute at 80 rpm.

Next, protoplasts were carefully pipetted to a 50 µm nylon net fixed into a funnel (previously moist with MaMg buffer (Table M-20)) placed inside a 50 mL reaction tube, where protoplasts were collected. (Note that cutting off the top of the plastic tip prevents damaging the protoplasts). This step was repeated until all protoplasts were transferred from the petri dish to the reaction tube. Additional washing of the petri dish with MaMg buffer was performed to increase the number of isolated protoplasts.

Afterwards, the protoplast mix was centrifuged at 700 rpm and 23°C for 3 min (Eppendorf centrifuge 5810R) with acceleration level 4 and brake level 1. Supernatant was discarded and protoplasts were carefully resuspended in 20 mL of MaMg buffer by horizontally rotating the reaction tube. This was followed by an additional centrifugation step under the previously described conditions. Supernatant was removed and protoplasts were resuspended in 2-5 mL of MaMg buffer.

**Table M-20.** Composition of the different buffers used during protoplast isolation.

<b>MCP buffer (200 mL)</b>	
Sorbitol (SERVA) 500 mM	18,22 g
CaCl <sub>2</sub> (Panreac Applichem) 1 mM	200 µL from a 1 M solution
MES (Carl ROTH®) 10 mM pH 5,7	4 mL from a 0,5 M solution
In ddH <sub>2</sub> O	
Adjust pH to 5,6 with HCl 4% and autoclave	
<b>Digestion buffer (20 mL)</b>	
Mazerozym (Thermo Fisher Scientific) 0,25%	50 mg
Cellulase (Thermo Fisher Scientific) 1%	200 mg

In MCP buffer	
Incubate 10 minutes at 55°C to inhibit the proteases and cool down at RT before use	
<b>MaMg buffer (200 mL)</b>	
Sorbitol (SERVA) 450 mM	16,4 g
MgCl <sub>2</sub> (Carl ROTH®) 15 mM	3 mL from a 1 M solution
MES (Carl ROTH®) 5 mM pH 5,7	2 mL from a 0,5 M solution
In ddH <sub>2</sub> O	
Adjust pH to 5,6 with HCl 4% and autoclave	

### 3.5.1.2 Protoplast transformation

150 µL of the freshly made protoplasts were transferred into a Greiner tube (Greiner #187261) and mix with 20 µg of plasmid DNA containing the destination vector and 165 µL of PEG-Ca-Buffer (Table M-21). After 20 seconds of gentle rotation, the transformation mix was incubated for 30 min at RT in the dark.

Once the incubation time was finished, 3 mL of W5 Buffer (Table M-21) were added progressively: first 500µL, then 1 mL and finally 1,5 mL. (Note that a careful rotation of the tube is necessary after every step to ensure an efficient mix of all components). Next, a 3 min centrifugation at 23°C and 60 g was performed. Supernatant was discarded and protoplasts were resolved in 3 mL of W5 Buffer. Centrifugation and resolving steps were repeated to wash away the remaining PEG. Finally, protoplasts were poured on a small petri dish and left ON at RT in the dark.

Transformed protoplasts were imaged using a confocal microscope (Leica TCS SP8. Excitation: 488 nm/ Detection: 520-540 nm).

**Table M-21.** Composition of the different buffers used during protoplast transformation.

<b>PEG-Ca buffer (6,5 mL)</b>	
PEG 4000 (Fluka)	4 g
ddH <sub>2</sub> O	3 mL
Mannitol (Sigma-Aldrich) 0,8 M	2,5 mL
CaCl <sub>2</sub> (Panreac Applichem) 1 M	1 mL
<b>W5 buffer (200 mL)</b>	
NaCl (CHEMSOLUTE®) 154 mM	6,16 mL from a 5 M solution
CaCl <sub>2</sub> (Panreac Applichem) 125 mM	25 mL from a 1 M solution
KCl (AnalaR NORMAPUR®) 5 Mm	500 µL from a 2 M solution
Glucose (Panreac Applichem) 5 mM	500 µL from a 2 M solution
MES (Carl ROTH®) 2 mM	800 µL from a 0,5 M solution
In ddH <sub>2</sub> O	
Autoclave	

### 3.5.2 Transient expression in *Nicotiana benthamiana*

35SMDFCDSYFP and 35SMDFGFP constructs and their phospho-mutants were, prior to Arabidopsis transformation, transiently expressed in tobacco leaves to verify their correct cellular localization.

To this end, liquid cultures of *Agrobacterium tumefaciens* C58C1 successfully transformed single colonies were prepared in 4 mL of SOC liquid medium (Table M-12) with the appropriate antibiotics and incubated ON at 28°C and 180 rpm. Additionally, an ON culture of *Agrobacterium* transformed with the P19 gene silencing suppressor protein was also prepared.

The next day, all ON liquid cultures were poured on to 15 mL reaction tubes and centrifugated for 20 minutes at 4°C and 4000 rpm (Eppendorf centrifuge 5424 R). Supernatant was discarded and pellet was resuspended in 10 mL of infiltration solution (Table M-22). Afterwards, tubes were incubated for 2 hours at 28°C and 60-70 rpm to favour *Agrobacterium* growth.

ON cultures of 35SMDFCDS transformed constructs were poured on to a small petri dish and mixed in a 1:1 proportion with the P19 containing ON culture. The mix was afterwards carefully introduced through the leaf stomata of 4–6-week-old *Nicotiana benthamiana* leaves with a small syringe.

After approximately 48 hours, YFP signal derived from successful *Nicotiana benthamiana* transformation was monitored with an Olympus MVX10 Macroscope Fluorescence Microscope using a GFP filter.

Since 35SMDFGFP constructs were under an estradiol inducible promoter, 48 hours after *Agrobacterium* transformation, the infiltrated leaves were sprayed with a 15 µM estradiol (Sigma-Aldrich) solution. 24 hours later, GFP derived signal in transformed leaves was monitored with an Olympus MVX10 Macroscope Fluorescence Microscope using a GFP filter.

**Table M-22. Infiltration solution composition for *Nicotiana benthamiana* transformation.**

Infiltration solution (10 mL)	
Na-P-buffer 0,1 M pH 7	10 mL
MgCl <sub>2</sub> 2 M (Carl ROTH®)	100 µL
Acetosyringone (Sigma-Aldrich) 0,1 M	20 µL

### 3.5.3 Co-immunoprecipitation

Eduardo Tranques Montes in the group of Julio Salinas at the Centro de Investigaciones Biológicas "Margarita Salas" (CSIC) in Madrid performed different Co-immunoprecipitation (Co-IP) experiments using LSM8-GFP as bait and an anti-GFP antibody followed by tandem mass spectrometry (IP-MS/MS) to elucidate the interaction partners of LSM8 under different abiotic stress conditions. Three independent Co-IP experiments showed co-purification of MDF and LSM8 at control conditions. The experimental procedure is summarized below as



described in a manuscript containing some of the results presented in this thesis (de Luxán-Hernández *et al.*, 2022 in revision in the Life Science Assembly Journal. See Appendix.).

Fifteen grams of 3-week-old *c-lsm8* plants (Perea-Resa *et al.*, 2012) were cross-linked with 1% formaldehyde in PBS, two times for 10 min by vacuum infiltration, followed by 5 min vacuum with glycine to a final concentration of 125 mM. Plant material was rinsed 6 times with precooled water and frozen in liquid nitrogen. Nuclei isolation was performed as reported previously (Locascio *et al.*, 2013) and LSM8-GFP was immunoprecipitated using GFP-Trap agarose system (Chromotek) following the manufacturing indications. SDS-PAGE (10% polyacrylamide) was run till the whole proteome had penetrated in the resolving gel (about 1 cm of total migration). Gels were stained with Colloidal Blue Staining Kit (Invitrogen). Each proteome was excised and divided in 2 fractions (“up” and “down”). These fractions were cut in small pieces prior to manual in-gel digestion with trypsin. Excised bands were separately destained with 50 mM ammonium bicarbonate (ABC) (Sigma-Aldrich) and 50% acetonitrile (ACN) (Fisher Chemical). Samples were then reduced with 10 mM dithiothreitol (Bio-Rad) in 50 mM ABC and alkylated with 55 mM iodoacetamide (GE Healthcare Life Sciences) in 50 mM ABC. Then, gel pieces were digested with porcine trypsin (Thermo Fisher Scientific), at a final concentration 12.5 ng/ml in 50 mM ABC, overnight at 37°C. Peptides were extracted using 100% ACN and 0.5% trifluoroacetic acid, (Sigma-Aldrich), purified using a Zip Tip (Millipore, Sigma-Aldrich), and dried (Käll *et al.*, 2007). Finally, samples were reconstituted in 10 µl of 0.1% formic acid before their analysis by nanosystem liquid chromatography-tandem mass spectrometry (nLC-MS/MS). All peptide separations were carried out on an Easy-nLC 1000 nano system (Thermo Scientific). For each analysis, the sample was loaded into a precolumn Acclaim PepMap 100 (Thermo Scientific) and eluted in a RSLC PepMap C18, 15 cm long, 50 µm inner diameter and 2 µm particle size (Thermo Scientific). The mobile phase flow rate was 300 nL/min using 0.1% formic acid in water (solvent A) and 0.1% formic acid and 100% acetonitrile (solvent B). The gradient profile was set as follows: 0%–35% solvent B for 90 min, 35%-100% solvent B for 4 min, 100% solvent B for 8 min. Four microliters of each sample were injected. MS analysis was performed using a Q Exactive mass spectrometer (Thermo Scientific). For ionization, 2000 V of liquid junction voltage and 270 °C capillary temperature was used. The full scan method employed a  $m/z$  400–1500 mass selection, an Orbitrap resolution of 70,000 (at  $m/z$  200), a target automatic gain control (AGC) value of  $3e6$ , and maximum injection times of 100 ms. After the survey scan, the 15 most intense precursor ions were selected for MS/MS fragmentation. Fragmentation was performed with a normalized collision energy of 27 eV and MS/MS scans were acquired with a starting mass of  $m/z$  100, AGC target was  $2e5$ , resolution of 17,500 (at  $m/z$  200), intensity threshold of  $8e3$ , isolation window of 2  $m/z$  units and maximum IT was 100 ms. Charge state screening was enabled to reject unassigned, singly charged, and equal or more than seven protonated ions. A dynamic exclusion time of 20s was used to discriminate against previously selected ions. MS data were analysed with Proteome Discoverer (version

1.4.1.14) (Thermo Scientific) using standardized workflows. Mass spectra \*.raw files were searched against Swissprot *Arabidopsis thaliana* (thale cress) database (14986 sequences protein entries) using Mascot (version 2.6.0, Matrix Science) search engine. Precursor and fragment mass tolerance were set to 10 ppm and 0.02 Da, respectively, allowing 2 missed cleavages, carbamidomethylation of cysteines as a fixed modification, methionine oxidation as a variable modification. Identified peptides were filtered using Percolator algorithm (Käll *et al.*, 2007) with a q-value threshold of 0.01.

### 3.5.4 BiFC

The association between LSM8 and MDF found by Co-IP experiments was verified by Eduardo Tranque Montes at the Centro de Investigaciones Biológicas "Margarita Salas" (CSIC) in Madrid using bimolecular fluorescence complementation (BiFC) assays. To this end, as explained in section 3.1.3.1, the coding sequences of MDF, LSM8 and LSM1a (which served as a negative control) were amplified from a pool of *Arabidopsis* cDNAs with appropriated primers (Table M-23). Following the gateway cloning approach described in section 3.1.3.2, the amplified fragments obtained by Phusion PCR were introduced inside the pDONR207 vector, which served as an entry vector and had gentamycin resistance. Afterwards, the constructs were recombined into the destination vectors pYFN43 and pYFC43. These are specific BiFC assay vectors which possess the N-terminal half of YFP (pYFN43) and the C-terminal half of YFP (pYFC43) N-terminally fused and confer Kanamycin resistance upon efficient transformation in *E. coli*.

These constructs were subsequently used to transform *Agrobacterium tumefaciens* strain GV3101 cells as described in section 3.1.3.3. Leaves of 3-week-old *Nicotiana benthamiana* plants grown at 23°C were infiltrated (see section 3.5.2) and reconstitution of YFP was monitored by confocal microscopy (TCS SP5 confocal laser scanning microscope (Leica Microsystems) Excitation: 514 nm)) 3 days later. Analyses were performed at least in triplicate with independent samples.

### 3.5.5 Co-localization and FLIM-FRET analyses

To verify the interaction found by Eduardo Tranque Montes by Co-IP and BiFC experiments, co-localization and FLIM-FRET assays were carried out with the technical assistance of Judith Mehrmann and Magdalena Weingartner.

As described in a manuscript containing part of the results discussed in this thesis (de Luxán-Hernández *et al.*, 2022 in revision in the Life Science Assembly Journal. See Appendix), these constructs were generated by amplifying the CDS excluding the STOP codon of MDF, LSM8 and LSM2 (that served as positive control) by Phusion PCR (see section 3.1.3.1). Then, by gateway cloning, MDFCDS was introduced into the pENTR-D-TOPO entry vector and

LSM2CDS and LSM8CDS were inserted in the pDONR221 entry vector. Both entry vectors conferred Kanamycin resistance upon successful *E. coli* DH5 $\alpha$ /TOP10 transformation. The BP reaction was followed by LR recombination (see section 3.1.3.2) into the destination vectors pABindGFP and pABindmCherry (Bleckmann *et al.*, 2010). Both vectors contain a 35S estradiol inducible promoter, confer Spectinomycin resistance and possess either GFP or mCherry C-terminally tagged.

Following the experimental procedure described in sections 3.1.3.3 and 3.5.2, all constructs were electroporated in *Agrobacterium tumefaciens* C58C1 and transiently expressed in 4–6-week-old *Nicotiana benthamiana* leaves.

For co-localization experiments, imaging was performed by confocal microscopy (Leica TCS SP8) with Excitation/Detection ranges of 488 nm/496-514 nm for pABindGFP constructs and 561/590-630 nm for pABindmCherry constructs.

Regarding the FLIM-FRET assays, fluorescence lifetime was also acquired with a Leica TCS SP8 Confocal microscope (40 $\times$  Water immersion objective). Time-correlated single photon counting was performed with picosecond resolution (PicoQuant Hydra Harp 400). Fluorophores were excited with a 470 nm (r LDHPC470B, 40 MHz) or 485 nm (LDH-D-C-485, 32 MHz) pulsed polarized diode laser with a power of 1  $\mu$ W at the objective lens. For detection of emitted light, a SMD-adjusted Hybrid detector (HyD SMD3) (wavelength set to 500 – 520 nm) and a TCSPC modul PicoHarp 300 (PicoQuant) was used. Image acquisition was done at zoom 6 with a resolution of 256x256 pixel with a dwell time of 20 $\mu$ s, and photons were collected over 50-60 frames. Fluorescence decay was analysed in Symphotime 64 (version 2.4; PicoQuant) using the Lifetime FRET Image analysis tool. TCSPC channels were binned by eight, count threshold was set so that the background was removed, Fluorescence decay was fitted using a multi-exponential decay, and the amplitude-weighted lifetime was considered as the sample's apparent lifetime. FRET efficiency was calculated as the lifetime of the FRET sample over the arithmetic mean of the lifetimes of the donor only samples measured in the same experiment:  $FRET_{eff} = 1 - (\tau_{FRET} / \tau_{donor})$ . All measurements were done in three independent experiments (n = 8).

### 3.5.6 Yeast-Two-Hybrid

Yeast-Two-Hybrid (Y2H) assays were also carried out to evaluate the interaction between MDF and LSM8. The experimental protocol was described on a manuscript containing some of the results included in this thesis and is cited below (de Luxán-Hernández, *et al.*, 2022 in revision in the Life Science Assembly Journal. See Appendix).

Full length CDS of MDF, LSM8 and LSM2 were amplified (see section 3.1.3.1) and cloned into pDONR221 plasmids (see section 3.1.3.2). The Gateway compatible versions of the GAL4 DNA-binding domain vector pGBT-9 (Bleckmann *et al.*, 2010) and the activation

domain vector pGAD424 (Clontech, [www.takarabio.com](http://www.takarabio.com)) were used as destination vectors. Additionally, since LSM8 pGBT-9 gave autoactivation, full length CDS versions without the STOP codon of MDF and LSM8 were also amplified and cloned into the pDONR221 vector and recombined into the pGBKcG and pGADcG Y2H destination vectors (Stellberger *et al*, 2010). These vectors contain the binding and activation domain respectively C-terminally tagged, opposite to the N-terminally tagged pGBT9 and pGAD424.

*Saccharomyces cerevisiae* strain AH109 was transformed as previously published (Gietz *et al*, 1997). Positive transformants were selected on yeast minimal medium (SD medium: 0.66% yeast nitrogen base without amino 244 acids, 0.066% amino acid mix, 2% glucose) lacking leucine and tryptophan (SD-LW). Single positive colonies were cultured ON in liquid SD-LW at 30°C and continuous shaking. The day after, a pre-culture with OD600=0.3 was inoculated using the ON culture as the starter material. After 3h under continuous shaking at 30°C, optical density was adjusted to OD600=4 and a dilution series from 10<sup>-1</sup> to 10<sup>-3</sup> was made. Spotting of the pre-culture and dilutions was carried out on selection plates containing either SD-LW (Growth control) or SD-LWH (Interaction test). Plates were incubated for 3 days at 28°C. After co-transformation of both putative interacting proteins fused to either the activation or binding domain of the GAL4 transcription factor, only positive interaction resulted in the transcriptional activation of our reporter gene, histidine (H), enabling growth in the SD-LWH media.

Additional interaction studies were performed with shorter MDFCDS fragments putatively representing the different MDF domains as described in section 4.2.2.

### 3.6 Primers

All primers used during this study were generated by Eurofins Genomics and are listed in Table M-23

**Table M-23.** Description of the primers used during this study.

Name	Gene	Sequence	Purpose
RP-mdfsalkF	AT5G16780	CTGATGAGGCATCCA GGCTAC	Genotyping
Lba1-mdfsalk	AT5G16780	TGGTTCACGTAAGT GGCCATCG	Genotyping
RP-mdfsailR	AT5G16780	CTTTCAGGCTTCCGC ACATCTG	Genotyping
LB1Sail	AT5G16780	GCCTTTTCAGAAATG GATAAATAGCCTTGC TTCC	Genotyping
lsm8-1_fw	AT1G65700	ACTAACTGGCCTCTG AATGGAAG	Genotyping
lsm8-1_rev	AT1G65700	AAGAAGACCCAAGA CTCCGATG	Genotyping
lsm8-1_LB	AT1G65700	GGCAATCAGCTGTT GCCGTCTCACTGGTG	Genotyping
RP_sr45fw	AT1G16610	GATTGGAGATCTTCT GGGAGG	Genotyping
LP_sr45rv	AT1G16610	TTTTGTTTTTCCTTGT GTTGGC	Genotyping
LP_sr34bFW	AT4G02430	AGTTTGAGGATGCTC GTGATG	Genotyping
RP_sr34bRV	AT4G02430	CTCGATGTAGATTTT GCAGGC	Genotyping
SR34_LPfw	AT1G02840	TTTCTCGCAAGTGTA CCGTG	Genotyping
SR34_RPrev	AT1G02840	CCCAAGAGAACCCAG ATTCC	Genotyping
sog1-7CAPS-F	AT1G25580	CAGGTCAGGCAATA CAGGTTTC	Genotyping
sog1-7CAPS-R	AT1G25580	CAGAGACTTCCTGTT CAG	Genotyping
ATM-F1	AT3G48190	GCTTCAAGGTTGGG CAGTTC	Genotyping
ATM-R1	AT3G48190	GCAAACAGCATAACA AAACACTTCC	Genotyping
Lbc1	AT3G48190	TGGACCGCTTGCTGC AACTCT	Genotyping
MDF+877qF	AT5G16780	AATTGGAGAACAGA AGCGCC	MDF expression via RT-qPCR in <i>mdf</i> mutants
MDF+963qR	AT5G16780	CATCTTCTTTTCTGC CCCGG	MDF expression via RT-qPCR in <i>mdf</i> mutants
MDF+1986qF	AT5G16780	TTGTGGATGATGAT GGAGGT	MDF expression via RT-qPCR in <i>mdf</i> mutants
MDF+2072qrev	AT5G16780	TTTTGGAGTTAAAGT TCTAC	MDF expression via RT-qPCR in <i>mdf</i> mutants
MDFg+2665fw	AT5G16780	ATGTGCGGAAGCCT GAAAGT	MDF expression via RT-qPCR in

MATERIAL AND METHODS

			complementing lines
MDFg+2854rev	AT5G16780	TGCACCAGATAATCC TTTTCC	MDF expression via RT-qPCR in complementing lines
MDFqR	AT5G16780	TGTCTCAGGGCACA GAACAT	MDF 3' UTR expression via RT-qPCR in <i>mdf</i> mutants
MDFqF	AT5G16780	TCGTTTAGTTTTGGC CGCAA	MDF 3' UTR expression via RT-qPCR in <i>mdf</i> mutants
3UTR_MDF1_qPCR _fw	AT5G16780	ACACAACAAGGTTGC GTCAC	MDF 3' UTR expression via RT-qPCR after HU treatment
3UTR_MDF1_qPCR _rev	AT5G16780	TCTTGACTATCCCAA GCCGA	MDF 3' UTR expression via RT-qPCR after HU treatment
3UTR_MDF2_qPCR _fw	AT5G16780	GGCTATAAGCTGCG GGAGAG	MDF 3' UTR expression via RT-qPCR after HU treatment
3UTR_MDF2_qPCR _rev	AT5G16780	GAAGGTGGTCGTCG ATAGCC	MDF 3' UTR expression via RT-qPCR after HU treatment
3UTR_MDF3_qPCR _fw	AT5G16780	TGGGTTTGGTTTCAG TTCTGT	MDF 3' UTR expression via RT-qPCR after HU treatment
3UTR_MDF3_qPCR _rev	AT5G16780	GGCACAGAACATCTT CGCAC	MDF 3' UTR expression via RT-qPCR after HU treatment
SR+RRM_qPCRnew _fw	AT5G16780	ATGGAAGTGGAGAA GTCTAAA	MDF SR domain expression via RT-qPCR after HU treatment
SR+RRM_qPCRnew _rev	AT5G16780	AGAGATCTCCTTCTC AGTGT	MDF SR domain expression via RT-qPCR after HU treatment
SART1_qPCR_fw	AT5G16780	GGCCATGTCAAACCA GGTA	MDF SART1 domain expression via RT-qPCR after HU treatment
SART1_qPCR_rev	AT5G16780	CGCAAACCCACTCTG AGGAT	MDF SART1 domain expression via RT-qPCR after HU treatment
MDFCDSfw	AT5G16780	ggggacaagttgtacaaaaa gcaggcttcATGGAAGTG GAGAAGTCTAA	BiFC and Y2H
MDFCDS+STOPrev	AT5G16780	ggggaccactttgtacaagaaa gctgggtTCAAGGCTTT GGTCTCTTT	BiFC and Y2H



GW-LSM8.1-F	AT1G65700	ggggacaagttgtacaaaaaa gcaggcttcATGGCGGCA ACTACT	BiFC
GW-LSM8.1-R	AT1G65700	ggggaccactttgtacaagaaa gctgggtcTCAATGCACT ACGGGT	BiFC
F LSM1a	AT1G19120	ggggacaagttgtacaaaaaa gcaggctATGTCCTGGG CTGCTCCTGATG	BiFC
R LSM1a	AT1G19120	ggggaccactttgtacaagaaa gctgggTCATGGAGTTC CTTGATCTCGAT	BiFC
MDFcF	AT5G16780	CACCATGGAAGTGG AGAAGTCTA	Co-localization, FLIM FRET and Y2H
MDFcR	AT5G16780	AGGCTTTGGTCTCTT TGGTGGTGTA	Co-localization, FLIM FRET and Y2H
LSM8CDSCTermfw	AT1G65700	ggggacaagttgtacaaaaaa gcaggctATGGCGGCAA CTACTGGACT	Co-localization, FLIM FRET and Y2H
LSM8CDSCTermrev	AT1G65700	ggggaccactttgtacaagaaa gctgggtcATGCACTAC GGGTTTCAACG	Co-localization, FLIM FRET and Y2H
LSM2CDSCTermfw	AT1G03330	ggggacaagttgtacaaaaaa gcaggctATGTTGTTCT TTTCTTACTTCAAG	Co-localization and FLIM FRET
LSM2CDSCTermrev	AT1G03330	ggggaccactttgtacaagaaa gctgggtcGCCACCCCTA GCTTCTCTT	Co-localization and FLIM FRET
LSM8CDSNtermfw	AT1G65700	ggggacaagttgtacaaaaaa gcaggcttcATGGCGGCA ACTACTGGACT	Y2H
LSM8CDSNtermrev	AT1G65700	ggggaccactttgtacaagaaa gctgggtTCAATGCACT ACGGGTTTCA	Y2H
LSM2CDSNtermfw	AT1G03330	ggggacaagttgtacaaaaaa gcaggcttcATGTTGTTT TTTTCTTACTTCAAG	Y2H
LSM2CDSNtermrev	AT1G03330	ggggaccactttgtacaagaaa gctgggtTCAGCCACCC CTAGCTTCT	Y2H
SR+RRM_MDF_Ntermfw	AT5G16780	ggggacaagttgtacaaaaaa gcaggcttcATGGAAGTG GAGAAGTCTAA	Y2H MDF SR domain
SR+RRM_MDF_Ntermrev	AT5G16780	ggggaccactttgtacaagaaa gctgggtTCATCTCTCCT TGACTCTTGC	Y2H MDF SR domain
SART1_MDF_Ntermfw	AT5G16780	ggggacaagttgtacaaaaaa gcaggcttcGGITTTGACA GAAGTAAATGA	Y2H MDF SART1 domain
SART1_MDF_Ntermrev	AT5G16780	ggggaccactttgtacaagaaa gctgggtTCAAGGCTTT GGTCTCTT	Y2H MDF SART1 domain
CYCP3-2_EX_fw	AT3G60550	TCGAAGATTTGAACT ATAGGA	Intron retention validation via RT-qPCR
CYCP3-2_EX_rev	AT3G60550	CATCAAGAACAGAAA CTCTAA	Intron retention validation via RT-qPCR
CYCP3-2_IR_fw	AT3G60550	TGGTGGTTTTTCAGG AACTAT	Intron retention validation via RT-qPCR

MATERIAL AND METHODS

CYCP3-2_IR_rev	AT3G60550	ACACTCACATTCACA TGTAG	Intron retention validation via RT-qPCR
CYCB2-2_EX_fw	AT4G35620	TCAACTCCTAGAATG TTGTAG	Intron retention validation via RT-qPCR
CYCB2-2_EX_rev	AT4G35620	TCATACTTTTGGTTGCT ATGTA	Intron retention validation via RT-qPCR
CYCB2-2_IR_fw	AT4G35620	TACCCATTAGCACCT ATAAAG	Intron retention validation via RT-qPCR
CYCB2-2_IR_rev	AT4G35620	CAGCTTTTCTGATGTA GTCTCA	Intron retention validation via RT-qPCR
KRP6_qPCRfw	AT3G19150	AGAAGCAATTCATAG AAAA	Intron retention and gene expression validation via RT-qPCR
KRP6_qPCRrev	AT3G19150	TTGACAATATCGAAG TTGTAC	Intron retention and gene expression validation via RT-qPCR
KRP6_IR_rev	AT3G19150	ACTCACATTCCTCTC TCTCT	Intron retention validation via RT-qPCR
KRP2_EX_fw	AT3G50630	GGAATGTTCTATGAA GTATAA	Intron retention validation via RT-qPCR
KRP2_EX_rev	AT3G50630	ATAAGTACTTTGGTG AAAACA	Intron retention validation via RT-qPCR
KRP2_IR_fw	AT3G50630	TGATAATGAATTTGT TGTTAG	Intron retention validation via RT-qPCR
KRP2_IR_rev	AT3G50630	ATAAGTACTTTGGTG AAAAC	Intron retention validation via RT-qPCR
SKP2B_EX_fw	AT1G77000	TAATCACAGATGAGA GTGT	Intron retention validation via RT-qPCR
SKP2B_EX_rev	AT1G77000	TGAGCTAAAGAGTA CATTG	Intron retention validation via RT-qPCR
SKP2B_IR_fw	AT1G77000	GTTTCTTTGTTCATCT CTTAA	Intron retention validation via RT-qPCR
SR30_EX_fw	AT1G09140	CGACTTCGGGTTGA GATTGC	Intron retention validation via RT-qPCR
SR30_EX_rev	AT1G09140	CTTAAGGTCCTGCCA CGAAG	Intron retention validation via RT-qPCR
SR30_IR_fw	AT1G09140	TAGTAAACGCATGAT GAAAG	Intron retention validation via RT-qPCR
SR30_IR_rev	AT1G09140	CGGTAGTCAGAGCG TCTTGA	Intron retention validation via RT-qPCR
SR45new_EX_fw	AT1G16610	CCGCAGTCCTAAGAG GCCA	Intron retention validation via RT-qPCR



SR45new_EX_rev	AT1G16610	TTAAGTTTTACGAGG TGGAG	Intron retention validation via RT-qPCR
SR45new_IR_fw	AT1G16610	TCTGTCTTAACACTA ATCCTCG	Intron retention validation via RT-qPCR
SR45new_IR_rev	AT1G16610	CAGATGTTTATGCTA TGTCITT	Intron retention validation via RT-qPCR
RS2Z33new_EX_fw	AT2G37340	TATGCTTTCGTTGAA TTTGGTG	Intron retention validation via RT-qPCR
RS2Z33_EX_rev	AT2G37340	AACTCCACAGTGATG CGACT	Intron retention validation via RT-qPCR
RS2Z33_IR_fw	AT2G37340	TAACCTGAGCTTTCG ATTT	Intron retention validation via RT-qPCR
RS2Z33_IR_rev	AT2G37340	AATGTCTTGCATCAT CAGC	Intron retention validation via RT-qPCR
PFA4_EX_fw	AT1G61660	CAAGTCACTGTTCTA AGCA	Intron retention validation via RT-qPCR
PFA4_EX_rev	AT1G61660	ACTCTTCGATTTACC AGAT	Intron retention validation via RT-qPCR
PFA4_IR_fw	AT1G61660	TCTCCTAACTCACTG AATT	Intron retention validation via RT-qPCR
MYB4R1_EX_fw	AT3G18100	AAGCAGATCACGGG AAATCAG	Intron retention validation via RT-qPCR
MYB4R1_EX_rev	AT3G18100	CTTGTGTTTCTCGTT CTGCTC	Intron retention validation via RT-qPCR
MYB4R1_IR_fw	AT3G18100	TCATGAATGATTCTC ACGG	Intron retention validation via RT-qPCR
MYB4R1_IR_rev	AT3G18100	AAAGCTTTCACAAGT ATTAGATC	Intron retention validation via RT-qPCR
MYB3R3_EX_fw	AT3G09370	GAACATAGCGAAATC TTTC	Intron retention validation via RT-qPCR
MYB3R3_EX_rev	AT3G09370	CTCATGTGTCCAAGG TCCC	Intron retention validation via RT-qPCR
MYB3R3_IR_fw	AT3G09370	TATTAACAAGAGTAA TGTCAGTG	Intron retention validation via RT-qPCR
MYB3R3_IR_rev	AT3G09370	ATGCTTCACGGAACA AAA	Intron retention validation via RT-qPCR
MYBlikeHTH_EX_fw	AT5G06800	TGAGTCTCAAGAAG GCAAGTTT	Intron retention validation via RT-qPCR
MYBlikeHTH_EX_rev	AT5G06800	CTGAAGTGCCTCTTT AATTTG	Intron retention validation via RT-qPCR
MYBlikeHTH_IR_fw	AT5G06800	GAAGGTACACTAATA AATCTCTG	Intron retention validation via RT-qPCR

MATERIAL AND METHODS

MYBLikeHTH_IR_rev	AT5G06800	GTTCTTGTGTCAAGC TGAGA	Intron retention validation via RT-qPCR
REM30_EX_fw	AT2G24680	AGTAGACGGTATCTT CCGT	Intron retention validation via RT-qPCR
REM30_EX_rev	AT2G24680	ACAATTCTTCCTGAG GCTTC	Intron retention validation via RT-qPCR
REM30_IR_fw	AT2G24680	AAAGTAGACGGGTG AGTTCATC	Intron retention validation via RT-qPCR
REM30_IR_rev	AT2G24680	TCTACCAGTTTTGCC CAACA	Intron retention validation via RT-qPCR
RAD51D_EX_fw	AT1G07745	CGCTATACTGGTGAC AAAT	Intron retention validation via RT-qPCR
RAD51D_EX_rev	AT1G07745	ATGTGTGTTTTAAGA TGGA	Intron retention validation via RT-qPCR
RAD51D_IR_fw	AT1G07745	TCAGGCCATTAAGCG TGT	Intron retention validation via RT-qPCR
RAD51D_IR_rev	AT1G07745	CAGCACCCACCGTGT GAT	Intron retention validation via RT-qPCR
SYD_EX_fw	AT2G28290	GCCAATGGAAGTTG TGCA	Intron retention validation via RT-qPCR
SYD_EX_rev	AT2G28290	GTTGAACATCCGGAA GGGA	Intron retention validation via RT-qPCR
SYD_IR_fw	AT2G28290	GCCAATGGAAGGTA CACA	Intron retention validation via RT-qPCR
SYD_IR_rev	AT2G28290	GTTTGCACA ACTATA AGAGAA	Intron retention validation via RT-qPCR
ARF8_EX_fw	AT5G37020	TGTTACAATGCATGC AGAT	Intron retention validation via RT-qPCR
ARF8_EX_rev	AT5G37020	AAATGTTTCCTTCTG CTCCT	Intron retention validation via RT-qPCR
ARF8_IR_fw	AT5G37020	GTTACAATGCATGTG CGTA	Intron retention validation via RT-qPCR
ARF8_IR_rev	AT5G37020	AACATCTGCCTGAAA TAGT	Intron retention validation via RT-qPCR
TIE1_EX_fw	AT4G28840	TCTTACATGAGGATC AGAGA	Intron retention validation via RT-qPCR
TIE1_EX_rev	AT4G28840	TTACAATCTCAATTC CAA	Intron retention validation via RT-qPCR
TIE1_IR_fw	AT4G28840	TCTTACATGAGGTTA TTACTT	Intron retention validation via RT-qPCR
TIE1_IR_rev	AT4G28840	GATTTTGAAGAATT AACAC	Intron retention validation via RT-qPCR

ANAC044_qPCRfw	AT3G01600	GAGCGCTAGAAAGG GAACGA	Expression changes validation via RT-qPCR. Taken from Takahashi <i>et al.</i> , 2019
ANAC044_qPCRrev	AT3G01600	CCCCGGAACTACTCT CACCTTC	Expression changes validation via RT-qPCR. Taken from Takahashi <i>et al.</i> , 2019
ANAC085_qPCRfw	AT5G14490	AGCACACCGAAAACCT AGTAC	Expression changes validation via RT-qPCR. Taken from Takahashi <i>et al.</i> , 2019
ANAC085_qPCRrev	AT5G14490	CTTCAATAACACTCA CATTCCC	Expression changes validation via RT-qPCR. Taken from Takahashi <i>et al.</i> , 2019
CYCB1;2_qPCRfw	AT5G06150	ATTACGACACCTTGA CGTTCTGTC	Expression changes validation via RT-qPCR. Taken from Takahashi <i>et al.</i> , 2019
CYCB1;2_qPCRrev	AT5G06150	TTTGAGCAGTCCATA ATCTCAGAC	Expression changes validation via RT-qPCR. Taken from Takahashi <i>et al.</i> , 2019
EDE1_qPCRfw	AT2G44190	AGAAAGCACAAAGCT GAGAGAATG	Expression changes validation via RT-qPCR. Taken from Kobayashi <i>et al.</i> , 2015
EDE1_qPCRrev	AT2G44190	TCCAAAGAAGGAGT TTGTGACTC	Expression changes validation via RT-qPCR. Taken from Kobayashi <i>et al.</i> , 2015
CDC20;1_qPCRfw	AT4G33270	ATATATGGCCCAGAG TCCAGA	Expression changes validation via RT-qPCR. Taken from Kobayashi <i>et al.</i> , 2015
CDC20;1_qPCRrev	AT4G33270	TCTGTATCATGGGTT TCCTTGTC	Expression changes validation via RT-qPCR. Taken from Kobayashi <i>et al.</i> , 2015
CYCA2-3_qPCRfw	AT1G15570	AGGACGCGGTCATG GATT	Expression changes validation via RT-qPCR

MATERIAL AND METHODS

CYCA2-3_qPCRrev	AT1G15570	AGGTTTCCTGCTGTA TTTGATG	Expression changes validation via RT-qPCR
CYCD3-1_qPCRfw	AT4G34160	TCGGAAGGAGGAAG AAAGTA	Expression changes validation via RT-qPCR
CYCD3-1_qPCRrev	AT4G34160	GAAGAGTTTTCTTCA ACTTCT	Expression changes validation via RT-qPCR
IMK2new_qPCRfw	AT3G51740	TGGTGACTCAGGCG AACTAT	Expression changes validation via RT-qPCR
IMK2new_qPCRrev	AT3G51740	TCGGAGGCATTTGAT TCCAG	Expression changes validation via RT-qPCR
SCL28new_qPCRfw	AT1G63100	TGAAGCAGTAGCAG CAACAT	Expression changes validation via RT-qPCR
SCL28new_qPCRrev	AT1G63100	AGTTTCCTTGCGAGA GAAGC	Expression changes validation via RT-qPCR
MDFS22Acomp_Fw	AT5G16780	CTACGAGGGTgCGCC TGTTAG	Site-directed mutagenesis
MDFS22Acomp_Rv	AT5G16780	CTAACAGGCGCACCC TCGTAG	Site-directed mutagenesis
MDFS22Dcomp_Fw	AT5G16780	GACTACGAGGGTgatC CTGTTAGAG	Site-directed mutagenesis
MDFS22Dcomp_Rw	AT5G16780	CTCTAACAGGATCAC CCTCGTAGTC	Site-directed mutagenesis
FASSqF	AT5G18580	GGTGAAACCGTCTG ACCCAT	Reference gene RT-qPCR
FASSqR	AT5G18580	TCTCACGGTTGTCAT GAGCC	Reference gene RT-qPCR
SAND_fw	AT2G28390	AACTCTATGCAGCAT TTGATCCAC	Reference gene RT-qPCR
SAND_rev	AT2G28390	TGATTGCATATCTTT ATCGCCATC	Reference gene RT-qPCR
PARP 2 fw	AT4G02390	ATCGTCTACGATACA GCCAGGT	DDR gene expression RT- qPCR
PARP 2 rev	AT4G02390	TGGTTCAGGCTCATC TCTTGTGC	DDR gene expression RT- qPCR

PARP1F	AT2G31320	ATGCTACTCTGGCAC GGTTCAC	DDR gene expression RT- qPCR
PARP1R	AT2G31320	AGGAGGAGCTATTC GCAGACCTTG	DDR gene expression RT- qPCR
RAD51_F	AT5G20850	TTCCGCTCTGGAAAG ACTCAGC	DDR gene expression RT- qPCR
RAD51_R	AT5G20850	ACCTCCTTGATCCAT GGGAAGTTG	DDR gene expression RT- qPCR
ATBRCA1_F	AT4G21070	GTTGCCCTGTGAAG AGGCTAATTC	DDR gene expression RT- qPCR
ATBRCA1_R	AT4G21070	TAGGCTGAGAGTGC AGTGGTTC	DDR gene expression RT- qPCR
ERF115q3F	AT5G07310	CTCGGGACATTTGA GACTGC	DDR gene expression RT- qPCR
ERF115q3R	AT5G07310	GTTTGGCTTTGCTTC CTTTG	DDR gene expression RT- qPCR
ERF109qF	AT4G34410	GCCAAGGGCTAAAC TCAACT	Oxidative stress gene expression via RT-qPCR
ERF109qR	AT4G34410	GCTATCATCAGCAGC AACAGGA	Oxidative stress gene expression via RT-qPCR
AOX1CqF	AT3G27620	GGCATCCGATATTCA CTACCAA	Oxidative stress gene expression via RT-qPCR
AOX1CqR	AT3G27620	GCAAAGAAATCTGG ACCGTGTTA	Oxidative stress gene expression via RT-qPCR
DOX1qF	AT3G01420	CTCAACGTCGGTCAA ACTCC	Oxidative stress gene expression via RT-qPCR
DOX1qR	AT3G01420	ACTATTTTGACTGCC GACGC	Oxidative stress gene expression via RT-qPCR
HSP20-likeqF	AT2G19310	CACCGGAGAAAGAA GATAAGAATG	Oxidative stress gene expression via RT-qPCR
HSP20-likeqR	AT2G19310	TCAACACACCATTCT CCATC	Oxidative stress gene expression via RT-qPCR
GSTU24qF	AT1G17170	GGCGAGTATGTTTG GGATG	Oxidative stress gene expression via RT-qPCR
GSTU24qR	AT1G17170	TTCATCTCGAGGAGC AAGG	Oxidative stress gene expression via RT-qPCR
NDB3-F	AT4G21490	GGCCAGGTATAGAC ATTTGGGACA	Oxidative stress gene expression via RT-qPCR
NDB3-R	AT4G21490	GGCTCACTTGCTTAC TAGCGTA	Oxidative stress gene expression via RT-qPCR
NDA1-F	AT1G07180	GCCAGGTGGAAGGA TTGGTATT	Oxidative stress gene expression via RT-qPCR

MATERIAL AND METHODS

NDA1-R	AT1G07180	CTGTGCAAGTGCAG GAAGTGT	Oxidative stress gene expression via RT-qPCR
fmo1-1slk-LP	AT1G19250	CTTTTCGGTTGGACT TGGAAC	Oxidative stress gene expression via RT-qPCR
fmo1-1slk-RP	AT1G19250	CTGCTTTGGACGTAT CCTACG	Oxidative stress gene expression via RT-qPCR
AT5G35170- F_qPCR-EXP	AT5G35170	GTGGTAAAGAAGTT GATGAAGAAGA	Intron retention validation via RT-qPCR. Taken from Carrasco- López <i>et al.</i> , 2017
AT5G35170- R_qPCR-EXP	AT5G35170	TAATACAGTTTCCAA CGGCA	Intron retention validation via RT-qPCR. Taken from Carrasco- López <i>et al.</i> , 2017
AT5G35170- F_qPCR-IR	AT5G35170	CCACAAAATGCCGTT GGAAA	Intron retention validation via RT-qPCR. Taken from Carrasco- López <i>et al.</i> , 2017
AT5G35170- R_qPCR-IR	AT5G35170	ACAAACGAATCCGGT ATATTCT	Intron retention validation via RT-qPCR. Taken from Carrasco- López <i>et al.</i> , 2017
CESA5-F_qPCR- EXP	AT5G09870	AATGTGCTTTCCTG TCTGT	Intron retention validation via RT-qPCR. Taken from Carrasco- López <i>et al.</i> , 2017
CESA5-R_qPCR- EXP	AT5G09870	AACGAGTTTTGCACT GAGGA	Intron retention validation via RT-qPCR. Taken from Carrasco- López <i>et al.</i> , 2017
CESA5-F_qPCR-IR	AT5G09870	ACCAATCTTGTCCTC AGTGC	Intron retention validation via RT-qPCR. Taken from Carrasco- López <i>et al.</i> , 2017
CESA5-R_qPCR-IR	AT5G09870	CAGATACATAAGATC AGACAAAGGT	Intron retention validation via RT-qPCR. Taken from Carrasco- López <i>et al.</i> , 2017
DFD-F_qPCR- EXP/IR	AT3G55630	TGCGGAGTCTATTCT TCGTT	Intron retention validation via RT-qPCR. Taken from Carrasco- López <i>et al.</i> , 2017

DFD-R_qPCR-EXP	AT3G55630	AAGACGGAATCTCTC TCGGA	Intron retention validation via RT-qPCR. Taken from Carrasco-López <i>et al.</i> , 2017
DFD-R_qPCR-IR	AT3G55630	TCGTTGAGATGAGT GTATGTT	Intron retention validation via RT-qPCR. Taken from Carrasco-López <i>et al.</i> , 2017
ATH13-F_qPCR-EXP	AT5G64940	TGCTGCACAAAGAAA GGAGA	Intron retention validation via RT-qPCR. Taken from Carrasco-López <i>et al.</i> , 2017
ATH13-R_qPCR-EXP	AT5G64940	AGCCGCAATGGCTA ATAAGT	Intron retention validation via RT-qPCR. Taken from Carrasco-López <i>et al.</i> , 2017
ATH13-F_qPCR-IR	AT5G64940	CCGCCACATTCACAT TTGTT	Intron retention validation via RT-qPCR. Taken from Carrasco-López <i>et al.</i> , 2017
ATH13-R_qPCR-IR	AT5G64940	CTGCAGAAGAAAGT AACCATTAGT	Intron retention validation via RT-qPCR. Taken from Carrasco-López <i>et al.</i> , 2017
DFL2-F_qPCR-EXP	AT4G03400	GAACGGCCACAACAC ATTAC	Intron retention validation via RT-qPCR. Taken from Carrasco-López <i>et al.</i> , 2017
DFL2-R_qPCR-EXP	AT4G03400	ATACGTGCACTGACC GAAAT	Intron retention validation via RT-qPCR. Taken from Carrasco-López <i>et al.</i> , 2017
DFL2-F_qPCR-IR	AT4G03400	TCCGATTATCAGCGG CTTAC	Intron retention validation via RT-qPCR. Taken from Carrasco-López <i>et al.</i> , 2017
DFL2-R_qPCR-IR	AT4G03400	AGAAAGCATAGTAG GAATTTATGAGA	Intron retention validation via RT-qPCR. Taken from Carrasco-López <i>et al.</i> , 2017
CAC2-F_qPCR-EXP	AT5G35360	GGGGATTCCTTGTG TTGCTG	Intron retention validation via RT-qPCR. Taken from Carrasco-

MATERIAL AND METHODS

			López <i>et al.</i> , 2017
CAC2-R_qPCR-EXP	AT5G35360	GGAGCTTCACCAATA CAAACAGC	Intron retention validation via RT-qPCR. Taken from Carrasco- López <i>et al.</i> , 2017
CAC2-F_qPCR-IR	AT5G35360	AGTTTTTGCATGTCA AGAGAAGTC	Intron retention validation via RT-qPCR. Taken from Carrasco- López <i>et al.</i> , 2017
CAC2-R_qPCR-IR	AT5G35360	ATCTCATTGGCGACC CTGAC	Intron retention validation via RT-qPCR. Taken from Carrasco- López <i>et al.</i> , 2017
RH3-F_qPCR-EXP	AT5G26742	GCTTGCTGTTGGGTT TGAGG	Intron retention validation via RT-qPCR. Taken from Carrasco- López <i>et al.</i> , 2017
RH3-R_qPCR-EXP	AT5G26742	CCTCGCCAACTTCTT AACCCA	Intron retention validation via RT-qPCR. Taken from Carrasco- López <i>et al.</i> , 2017
RH3-F_qPCR-IR	AT5G26742	ACCATTTGTTTAGAT GTGACCTTT	Intron retention validation via RT-qPCR. Taken from Carrasco- López <i>et al.</i> , 2017
RH3-R_qPCR-IR	AT5G26742	ACTTAGGAAGACGA CCAGACC	Intron retention validation via RT-qPCR. Taken from Carrasco- López <i>et al.</i> , 2017
RPP1-F_qPCR-EXP	AT3G44480	AGTAAGTCGATCGG TCCTGA	Intron retention validation via RT-qPCR. Taken from Carrasco- López <i>et al.</i> , 2017
RPP1-R_qPCR-EXP	AT3G44480	CACCATTTGCCTGCA TTTCA	Intron retention validation via RT-qPCR. Taken from Carrasco- López <i>et al.</i> , 2017
RPP1-F_qPCR-IR	AT3G44480	TCCATTCACATAAAG GCCATCT	Intron retention validation via RT-qPCR. Taken from Carrasco- López <i>et al.</i> , 2017
RPP1-R_qPCR-IR	AT3G44480	TTTGTAAAGCTACG GCTGC	Intron retention validation via



			RT-qPCR. Taken from Carrasco-López <i>et al.</i> , 2017
--	--	--	---



# 4. RESULTS



## 4.1 *mdf* mutants display a pleiotropic phenotype that resembles constitutive activation of the plant DNA damage response

### 4.1.1 Absence of MDF leads to reduced cell division and growth

Absence of MDF in *mdf-1* and *mdf-2* T-DNA insertion mutants led to primary root growth arrest and loss of stem cell and meristematic activity in both root and vegetative tissues (Casson *et al.*, 2009). These defects were associated with misexpression of genes involved in auxin regulation, such as the PIN family of auxin transporters, and transcription factors important for correct root and shoot meristem formation, like members of the PLETHORA and WUSCHEL family (Casson *et al.*, 2009).

To analyse in further detail the phenotype associated to the loss of MDF in the root system, primary root length of both T-DNA insertion mutants and WT plants was monitored from 1 until 10 days after germination (DAG) (Figures R-1A and B). Reduced root growth was already observed 1 DAG in both mutant lines (Figure R-1B). Interestingly, a significant difference in primary root length between *mdf-1* and *mdf-2* seedlings was also measured starting 1 DAG and became more prominent over time. At 10 DAG, for example, the primary root of *mdf-2* with  $0.74 \pm 0.14$  cm (n=50) was approximately double as long as the one from *mdf-1* with  $0.35 \pm 0.09$  cm (n=46). Moreover, while *mdf-2* and WT continuously grew over time, *mdf-1* primary root growth was putatively completely arrested at 9 DAG, with no significant increase in root length at 10 DAG (Figure R-1B).

After germination, plant postembryonic growth is driven by the activity of the apical meristems: shoot apical meristem (SAM), giving rise to all aboveground organs, and root apical meristem (RAM), that generates the root system. Thus, the correct formation of organs throughout the plant life requires a precise balance between stem-cell proliferation and differentiation in the meristems (Weigel and Jürgens, 2002). Previous experiments showed how cell division was impaired in *mdf-1* mutants, which exhibited a reduced area of dividing cells in the RAM at both 2 and 7 DAG in comparison to WT (Casson *et al.*, 2009). Using confocal microscopy, the correlation between defective cell division and impaired primary root growth was further investigated by quantifying the number of dividing cells in the RAM of both *mdf-1* and *mdf-2* mutants. To this end, root tips were excised from 3 DAG seedlings and incubated for 1 minute in a 10  $\mu$ g/ml Propidium iodide (PI) solution. PI is a fluorescent dye that intercalates between DNA bases and is not membrane permeable. Thus, based on membrane integrity, it is frequently used to detect dead cells, but also traditionally used in *A. thaliana* studies for cell wall staining and subsequent observation of root meristem structures. PI staining of 3 DAG *mdf-1* and *mdf-2* seedlings revealed that the population of small non elongated cells in the cortical layer of the proximal meristem was decreased in comparison to

WT (Figures R-1C and E). Therefore, it was confirmed that loss of MDF led to reduced cell division not only in *mdf-1*, but also in *mdf-2*.

Jana Chumova and Pavla Binarova from the Institute of Microbiology of the Czech Academy of Sciences in Prague verified these findings by 5-Ethynyl-2'-deoxyuridine (EdU) staining of 7 DAG WT and *mdf-1* roots (Figure R-1D). EdU is a thymidine analogue that gets incorporated into newly synthesized DNA, and after covalent crosslink to a fluorescent azide (such as iFluor-488) in a “click” chemistry reaction, can be detected by fluorescence microscopy<sup>1</sup>. Therefore, it is commonly used in cell proliferation assays to detect replicating cells. After incubating WT and *mdf-1* 7 DAG seedlings in liquid medium with an EdU pulse at a dilution of 1:1000 for 3 h, a decrease in fluorescence signal was observed in *mdf-1* compared to WT. This means that, as previously demonstrated, loss of MDF negatively impacts proximal meristem size by repressing cell division.

Mutants with altered primary root growth were shown to produce more adventitious roots (AR) (Pérez-Pérez, 2020). These are roots originated from non-root tissues such as leaves, stems or hypocotyls, whose formation requires cell de-differentiation and subsequent reprogramming to enable the establishment of a new root primordia (Huang *et al.*, 2020). To assess whether loss of MDF enhanced adventitious rooting, the number of plants that developed AR at the root/hypocotyl junction was monitored 10 DAG (Figure R-1F). While approximately 50% of the *mdf-2* mutants and WT plants exhibited adventitious rooting, almost all *mdf-1* seedlings failed to form AR. This abnormal AR development could be explained by *mdf-1* defects in cell division, since efficient AR formation requires active cell division (Huang *et al.*, 2020). Additionally, adventitious rooting is dependent on auxin biosynthesis, transport and signalling (Canher *et al.*, 2020), which was shown to be altered in *mdf-1* (Casson *et al.*, 2009). For this reason, deficient AR formation in *mdf-1* could also be caused by auxin related defects. Altogether these analyses revealed that *mdf-1* is more affected than *mdf-2* in both primary and adventitious root growth.

Reduced *WUSCHEL* (*WUS*) levels and increased *CLAVATA 3* (*CLV3*) expression resulted in loss of stem cell activity in the SAM of *mdf-1* mutants (Casson *et al.*, 2009). Therefore, the influence of MDF on SAM activity was also assessed by quantifying the number of plants that developed true leaves 10 days after transfer to light in both *mdf* mutants and WT (Figures R-1G). The first pair of leaves, opposite to the cotyledons, is directly originated from the SAM and depends among other processes on cell division (Kalve *et al.*, 2014). A significant reduction in true leaf formation in comparison to WT was only detected in *mdf-1*, which indicates that cell division is also strongly impaired in the SAM in this mutant.

---

<sup>1</sup> <https://www.abcam.com/edu-assay--edu-staining-proliferation-kit-ifluor-488-ab219801.html>. Consulted on the 5<sup>th</sup> of June 2022.

## RESULTS

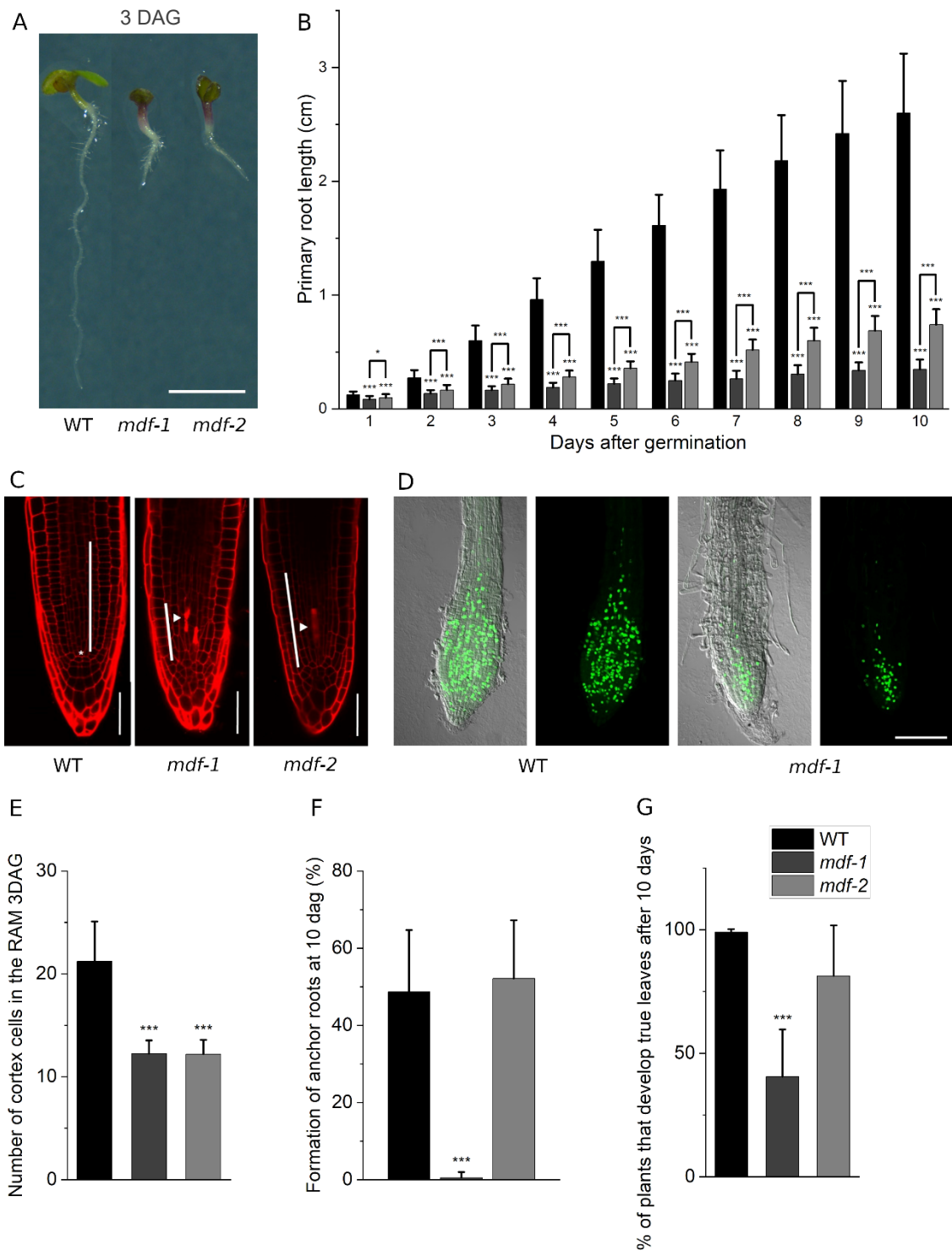


**Figure R-1. Absence of MDF leads to reduced cell division and growth** (A) Representative pictures of WT, *mdf-1* and *mdf-2* seedlings at 3 days after germination (DAG). Scale bar: 2 mm. (B) Primary root length from 1 until 10 DAG of WT (n=62, 137, 97, 74, 74, 75, 75, 74 and 75), *mdf-1* (n=48, 65, 69, 55, 53, 41, 50, 44 and 45) and *mdf-2* (n=46, 57, 63, 51, 51, 51, 50, 52, 49 and 50). Statistical significance was determined in comparison to WT and *mdf-1*. (C) Representative confocal images of propidium iodide-stained root tips of WT, *mdf-1* and *mdf-2* 3 DAG seedlings. Asterisk shows the quiescent center (QC). White bar indicates the division zone. Scale bar: 50  $\mu$ m. (D) Representative images of EdU labelling (3 h pulse) in roots of 7 DAG WT and *mdf-1*. Scale bar: 200  $\mu$ m. This experiment was carried out and analysed by Jana Chumova and Pavla Binarova from the Institute of

Microbiology of the Czech Academy of Sciences in Prague (E) Number of dividing cells in the cortical layer of 3 DAG seedlings of WT (n=40), *mdf-1* (n=36) and *mdf-2* (n=21). Statistical significance was determined in comparison to WT. (F) Percentage of plants developing anchor roots (AR) at 10 DAG for WT, *mdf-1* and *mdf-2* from 3 independent experiments with at least 15 plants per line and experiment. Statistical significance was determined in comparison to WT (G) Percentage of plants developing true leaves after 10 days for WT, *mdf-1* and *mdf-2* from 3 independent experiments with at least 15 plants per line and experiment. Statistical significance was determined in comparison to WT. Average  $\pm$  Standard deviation is represented. \*P < 0.05; \*\*P < 0.005; \*\*\*P < 0.0005 as determined by a two-tailed Student's t-test.

#### 4.1.2 The dwarf phenotype of *mdf* mutants is related to G2/M cell cycle arrest, increased endoreplication and cell death induction

To better understand at which stage of cell division meristematic cells were arrested, immunolabelling of microtubules in root tip cells of WT, *mdf-1* and *mdf-2* 6 DAG plants was performed. Quantification of microtubule arrays revealed a reduced number of cells exhibiting mitotic microtubular arrays in both mutants compared to WT. In contrast, more cells showing a preprophase band, which marks the G2/M transition, were detected in *mdf* samples (Figure R-2A). This indicates that in *mdf-1* and *mdf-2* the transition from G2 to mitosis was impaired.

Due to their sessile nature, plants have evolved different mechanisms to adapt to environmental and internal metabolic stresses that threaten their genome integrity. A common mechanism upon environmental stresses or after pathogen infection is to halt plant growth by suppressing cell division, so that energy and resources are redirected into other metabolic processes. In this context, DNA damage is also known to induce a temporary cell cycle arrest to allow DNA repair to take place before DNA replication or mitosis begin (Hu *et al.*, 2016). Moreover, previous studies have shown that SOG1, which is a transcription factor that regulates the expression of most genes induced by double strand breaks (DSBs) (Yoshiyama *et al.*, 2009) promotes G2 arrest in the meristem and enhances the transition from cell division to endoreplication (replication of a cell's nuclear genome without subsequent cytokinesis) as well as the induction of cell death (Furukawa *et al.*, 2010; Adachi *et al.*, 2011).

Based on the previously published phosphorylation of MDF at Serine 22 upon DNA damage (Roitinger *et al.*, 2015), MDF's function in the maintenance of meristems (Casson *et al.*, 2009), which sustain Arabidopsis post-embryonic growth and are thus more sensitive to DNA damaging conditions; together with the accumulating evidence of pre-mRNA splicing factors participating in the DNA damage response (DDR) in animals, it was proposed that the *mdf* phenotype could be caused by constitutive DNA damage.

To investigate whether the cell cycle arrest observed in *mdf* mutants was indeed linked to genome instability, nuclear DNA content was measured by flow cytometry in 10 DAG WT, *mdf-1* and *mdf-2* seedlings (Figure R-2B). Peaks corresponding to higher DNA contents of 32C, and even 64C in the case of *mdf-1*, were found in the absence of MDF. These higher DNA contents were associated with increased levels of endoreplication in both *mdf* lines

(Figure R-2C), a phenomenon previously characterized to occur upon DNA damage in WT plants (Adachi *et al.*, 2011). Activation of the endocycle is represented by significantly higher endoreplication indexes (EI) in *mdf* mutants in comparison to WT, which were calculated by determining the average number of endocycles per cell based on the cellular DNA content (C-value) measured by flow cytometry (For further details of EI calculation see section 6.7 of the experimental protocol described in Laimbeer *et al.*, 2018).

Experimental work, analyses and interpretation of the data presented in Figures R-2A, 2B and 2C were carried out by our collaboration partners from the Institute of Microbiology of the Czech Academy of Sciences in Prague.

To further analyse whether loss of MDF constitutively activates the plant DDR, the accumulation of dead cells in WT and *mdf* mutants was monitored by calculating the cell death area and occurrence of cell death in the RAM at 2 and 3DAG (Figures R-2D, E and F). As expected, WT plants showed no cell death for both timepoints. In contrast, propidium iodide (PI) staining revealed that the absence of MDF led to the accumulation of dead cells in the cell division zone of both mutant lines in approximately 50% of the plants analysed at 2 DAG (Figures R-2E and F). Interestingly, *mdf-1* plants showed again a stronger phenotype, with a significant increase in frequency of cell death and area of dead cells at 3 DAG in comparison to *mdf-2* (Figures R-2E and F).

These results suggest that the absence of MDF impairs genome stability resulting in cell cycle arrest and increased endoreplication accompanied by spontaneous cell death.



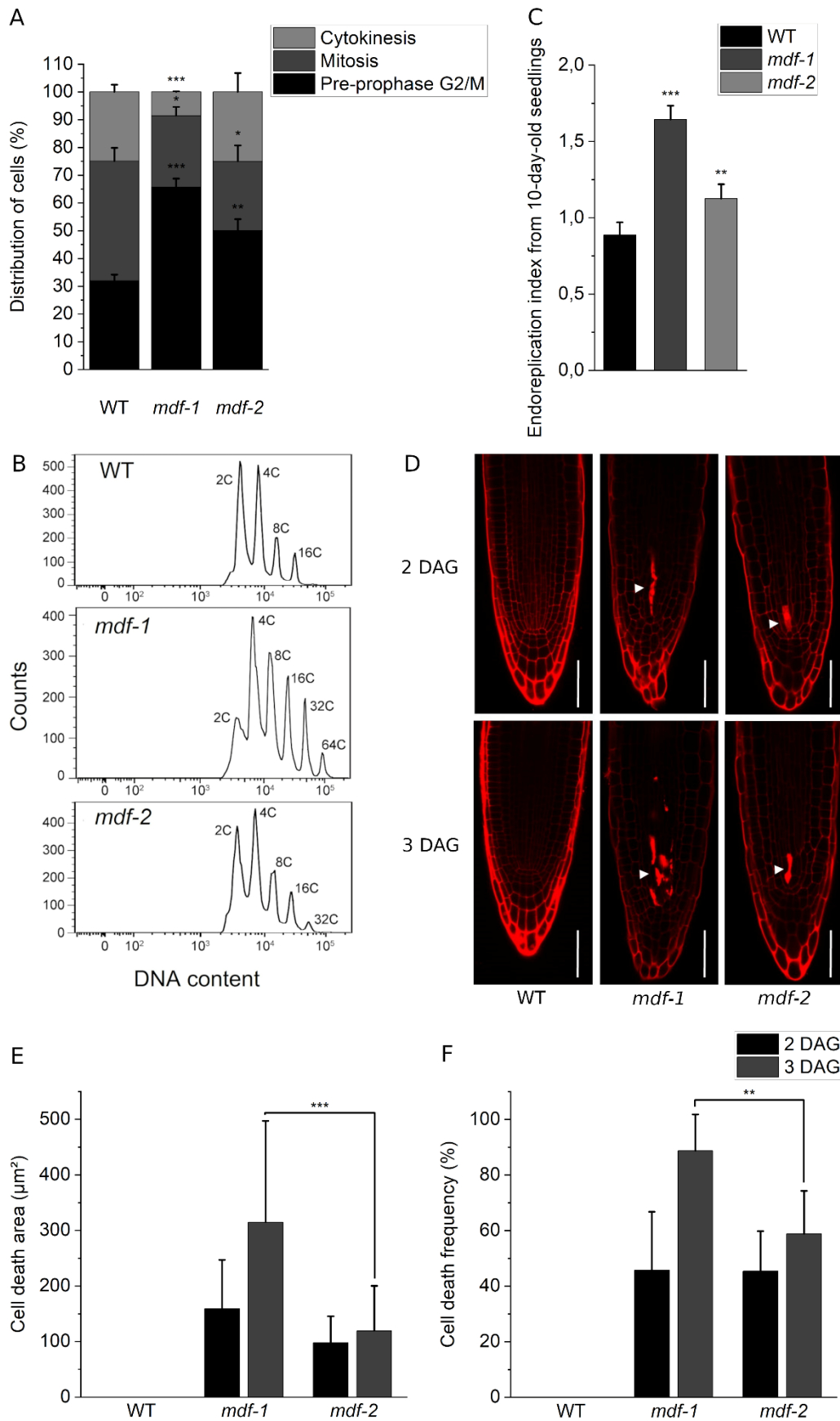


**Figure R-2.** The dwarf phenotype of *mdf* mutants is related to G2/M cell cycle arrest, increased endoreplication and cell death induction (A) Analyses of immunolabeled mitotic microtubular arrays in root tips of WT (n=348),

*mdf-1* (n=269) and *mdf-2* (n=284) 6 DAG seedlings. Percentual distribution of cells accumulated in G2/M with preprophase bands (G2/M - pre-prophase), pro, meta and anaphase spindle (mitosis) and with phragmoplast (cytokinesis) was determined. Statistical significance was determined in comparison to WT. (B) Representative DNA content histograms determined by flow cytometry of WT (n=7), *mdf-1* (n=3) and *mdf-2* (n=4) 10 DAG seedlings. (C) Endoreduplication index (EI) determined from the flow cytometry data measured in (B). Statistical significance was determined in comparison to WT. (A), (B) and (C) experiments were carried out and interpreted by Jana Chumova and Pavla Binarova from the Institute of Microbiology of the Czech Academy of Sciences in Prague. (D) Representative confocal images of PI-stained root tips of WT, *mdf-1* and *mdf-2* at 2 and 3 DAG. The white arrowhead indicates dead cells. Scale bar: 50  $\mu$ m. (E) Quantification of the cell death area and (F) percentage of plants containing dead cells in root tips of WT (n=21 and n=22), *mdf-1* (n=21 and n=95) and *mdf-2* (n=33 and n=59) lines at 2 and 3 DAG. Statistical significance was determined in comparison to *mdf-1*. Average  $\pm$  Standard deviation is represented. \*P < 0.05; \*\*P < 0.005; \*\*\*P < 0.0005 as determined by a two-tailed Student's t-test.

#### 4.1.3 *mdf* mutants exhibit growth arrest in later developmental stages

Analyses of true leaf formation in *mdf-2* revealed no apparent defects in SAM-derived organ formation, in contrast to the strongly impaired *mdf-1* (Figures R-1G). To further understand the role of MDF in the maintenance of the SAM, we monitored the aboveground growth of both mutant lines in comparison to WT for 5 weeks (Figures R-3A and B). A severe growth delay was detected in both mutants 2 weeks after germination. Nonetheless, *mdf-1* mutants exhibited a stronger phenotype with a significant reduction in rosette diameter in comparison to both WT and *mdf-2* mutants already 1 week after germination, as well as a complete arrest of aerial development after 3 weeks (Figure R-3C). Moreover, *mdf* mutants not only had smaller but also fewer rosette leaves, as it was found after counting the number of leaves after 4 weeks of growth in both mutants and WT plants (Figure R-3D).

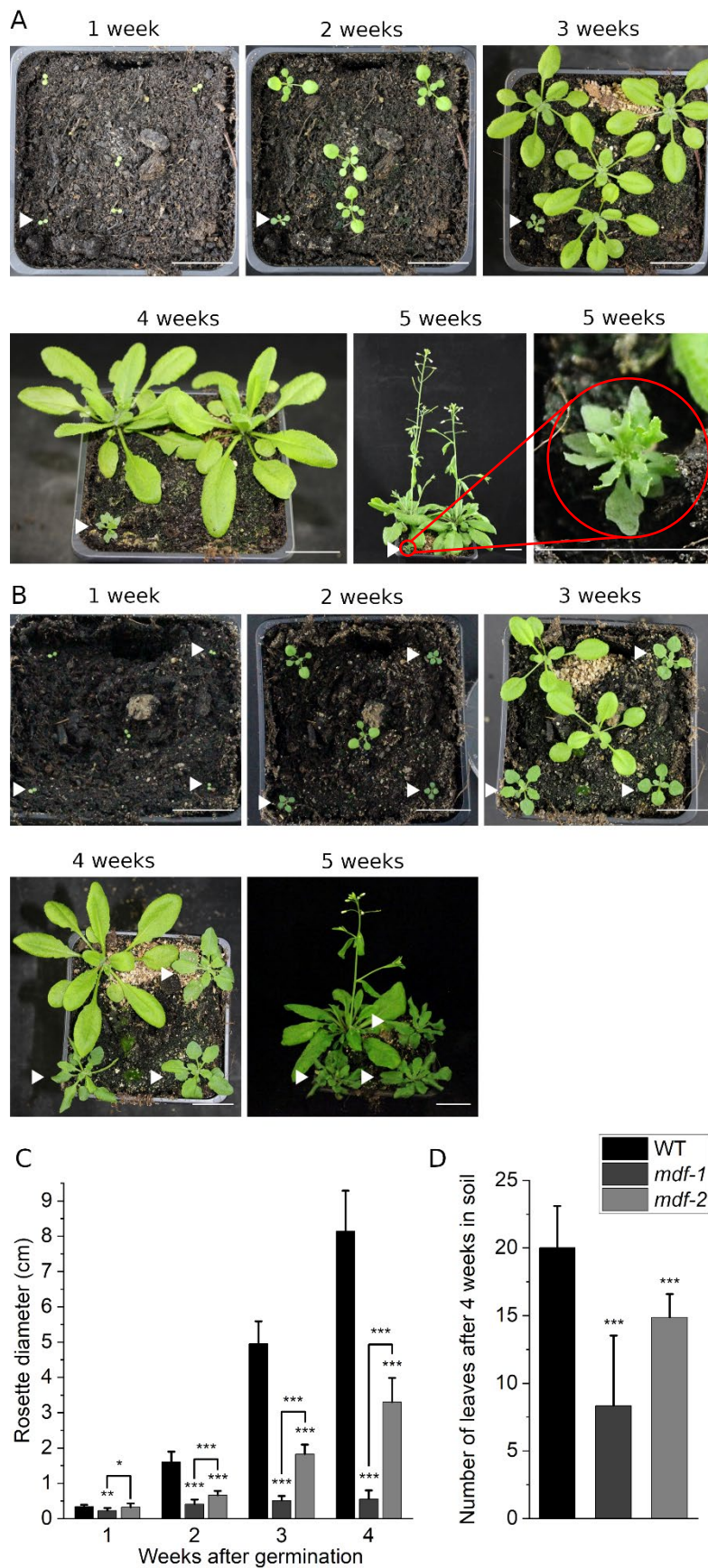


**Figure R-3.** *mdf* mutants exhibit severe growth arrest in above ground tissues. (A) Representative pictures of *mdf-1* and WT plants 1, 2, 3, 4 and 5 weeks after germination in soil. Arrowheads point out *mdf-1* plants. Non

marked plants are either heterozygous or segregating WT *mdf-1* plants. Scale bar: 2 cm. (B) Representative pictures of *mdf-2* and WT plants 1, 2, 3, 4 and 5 weeks after germination in soil. Arrowheads point out *mdf-2* plants. Non marked plants are either heterozygous or segregating WT *mdf-2* plants. Scale bar: 2 cm. (C) Quantification of the rosette diameter at 1, 2, 3 and 4 weeks after germination of WT (n= 68, 65, 63 and 31), *mdf-1* (n= 10, 9, 11 and 8) and *mdf-2* (n= 10, 15, 13 and 13) plants. (D) Quantification of the number of leaves formed in WT (n=61), *mdf-1* (n=15) and *mdf-2* (n=15) plants 4 weeks after germination. Average  $\pm$  Standard deviation is represented. \*P < 0.05; \*\*P < 0.005; \*\*\*P < 0.0005 as determined by a two-tailed Student's t-test in comparison to WT.

Interestingly, the *mdf-1* and *mdf-2* mutations had been previously described as lethal with 100% lethality between 20 and 25 DAG (Casson *et al.*, 2009). However, at long day conditions and 24°C, these mutants seem to be able to survive even longer than the WT, with some plants still conserving green photosynthetic tissue 3 months after germination (Data not shown). Nevertheless, they both remain sterile and are not able to produce seeds.

These findings confirm the importance of MDF for plant development not only in the root system, but also in aerial tissues.

#### 4.1.4 Seed production and germination is unaltered in *mdf* mutants

Cell division is not only essential during postembryonic growth, but also during embryogenesis. Asymmetric cell divisions followed by intense cell proliferation and endoreplication have to take place in a coordinated and sequential manner to ensure correct seed development (Dante *et al.*, 2014). To evaluate the prospective impact of MDF on cell division during seed development, the number of seeds inside individual siliques of WT and *mdf-1* and *mdf-2* heterozygous plants was counted (Figure R-4A). No significant difference was found in between the three lines, which suggests that MDF is not essential during embryogenesis.

Moreover, based on the nearly 100% germination ratio observed in both *mdf* heterozygous lines (Figure R-4B), homozygous *mdf* seeds seem to be as viable as WT seeds. However, since the *mdf-1* mutant was described to exhibit embryonic defects such as abnormal cell divisions at the basal pole at pre-globular stages (Casson *et al.*, 2005), the survival rate of *mdf-1* and *mdf-2* mutants was further assessed by calculating the distribution of homozygous seedlings among the progeny of *mdf* heterozygous plants (Figure R-4C). In accordance with previous findings, the *mdf-1* and *mdf-2* mutations followed a Mendelian segregation with approximately 25% of homozygous plants. These data suggest that the previously characterized cell division defects during embryo development associated to the loss of MDF (Casson *et al.*, 2005) are not lethal.

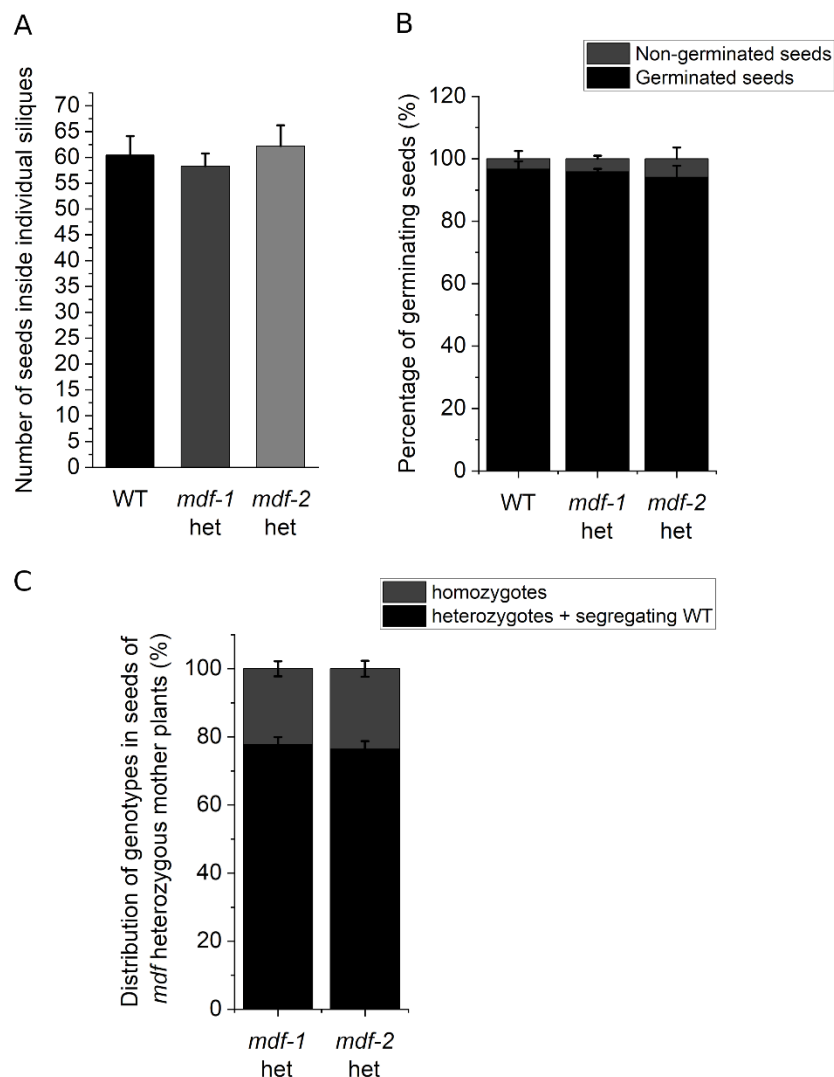


**Figure R-4. Seed production and germination is unaltered in *mdf* mutants.** (A) Quantification of the number of seeds inside individual siliques of 6-week-old WT (n=30), *mdf-1* heterozygous (n=30) and *mdf-2* heterozygous (n=30) plants. (B) Percentage of germinating seeds after 4 days in light for WT, *mdf-1* heterozygous and *mdf-2* heterozygous plants from 4 independent experiments with at least 75 plants per line and experiment. Statistical significance was determined in comparison to WT. (C) Percentage of homozygous and heterozygous /segregating WT after 4 days in light for *mdf-1* heterozygous and *mdf-2* heterozygous plants from 6 independent experiments with at least 130 plants per line and experiment. Average  $\pm$  Standard deviation is represented.

#### 4.1.5 A putative C-terminal MDF truncated version restores some developmental defects associated to the absence of MDF in *mdf-2* mutants

As previously published, in *mdf* mutant T-DNA insertion lines, the insertion lies within exon 9 in *mdf-2*, while it is located approximately 250 bases downstream within intron 9 in *mdf-1* (Casson *et al.*, 2009). Moreover, wild-type MDF transcript could not be detected in plants homozygous for either *mdf-1* or *mdf-2* by RT-PCR, which indicated that these are putative null mutations (Casson *et al.*, 2009).

During the phenotypical characterization of both *mdf* mutants, it was noticed how the *mdf-1* mutation had a strong impact on plant development in both root and aerial tissues (Figures R-1 to 3), whereas *mdf-2* mutants displayed a milder phenotype in above ground organs (Figure R-3). To further characterize the differences between both mutants, *MDF* transcript levels before and after the insertion sites were assessed by RT-qPCR experiments (Figure R-5A and B). Whereas the region upstream of the T-DNA insertion sites was still expressed in both mutant lines, the C-terminal part of *MDF*, located downstream the insertion sites, as well as the 3' UTR region, were not expressed in *mdf-1*, but still highly accumulated in *mdf-2*.

Interestingly, within this C-terminal truncated version of *MDF* lies the region that shares high homology with the human protein SART1 (Casson *et al.*, 2009) and, thus, qualifies *MDF* as a SART1 family protein. Therefore, the retained *MDF* transcript in *mdf-2* plants might still be partially functional and account for the phenotypical differences between *mdf-1* and *mdf-2* (Figures R-1 to 3). Additionally, this SART1 homologous region is putatively essential for the maintenance of the SAM since *mdf-2* plants are able to shoot after six weeks in soil and even flower (Figures R-5C and D). However, these mutants remain infertile since they are male sterile.

After close inspection of the flower buds formed in *mdf-2* mutants, no stamens or petals, but only carpels and sepals were found in these abnormally dwarf flower buds (Figure R-5E to G). This flower organization has been previously described according to the ABC model -that explains the organization of the 4 floral organ types- as the “AC” conformation (Figure R-6), in which only sepals and carpels are formed, due to the absence of the “B” function (reviewed in Irish, 2017).

The MADS box genes *APETALA3* (*AP3*) and *PISTILLATA* (*PI*) are responsible for the “B” function. Moreover, *ap3-1* mutants present a similar phenotype than *mdf-2* plants in terms of flower formation, with carpelloid stamens and male sterile flowers due to splicing defects in *AP3* that led to frequent exon 5 skipping (Yi and Jack, 1998). Hence, based on the presumed role of *MDF* in mRNA splicing, the *mdf-2* flower phenotype could be caused by splicing defects in genes responsible for the “B” function such as *AP3*.



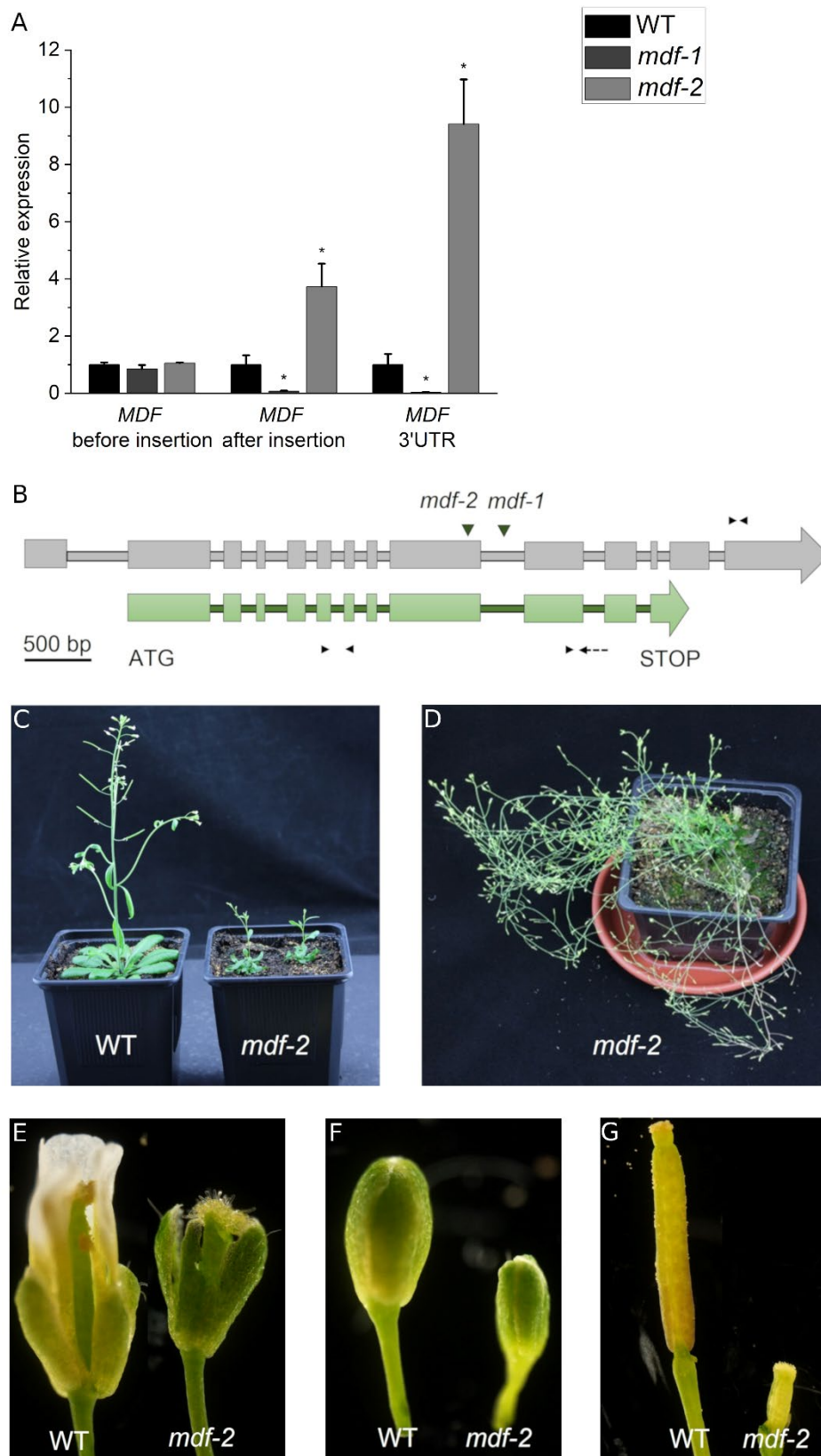


**Figure R-5.** A putative C-terminal MDF truncated version restores some developmental defects associated to the absence of *MDF* in *mdf-2* mutants. (A) RT-qPCR analysis of *MDF* expression in 3 biological replicates of 3 DAG root tips of WT, *mdf-1* and *mdf-2*. \* $P < 0.05$  as determined in comparison to WT by One way ANOVA-test post hoc Tukey Kramer. Average  $\pm$  Standard deviation is shown. (B) Schematic representation of *MDF*

## RESULTS

coding sequence. Big light green boxes represent exons and small dark green boxes represent introns. T-DNA insertion positions for *mdf-1* and *mdf-2* are represented by green arrowheads. Black arrowheads indicate approximate annealing positions of the primers used for testing MDF expression in (A). The dashed line on the reverse primer for testing the expression after the T-DNA insertion shows that this primer only binds to exonic regions. (C) Representative picture of WT and *mdf-2* plants 6 weeks after germination in soil. (D) Representative picture of *mdf-2* mutants 9 weeks after germination in soil taken by Wiebke Hellmeyer. (E-F) Representative pictures of WT and *mdf-2* flower buds. (G) Representative picture of WT and *mdf-2* naked pistils.

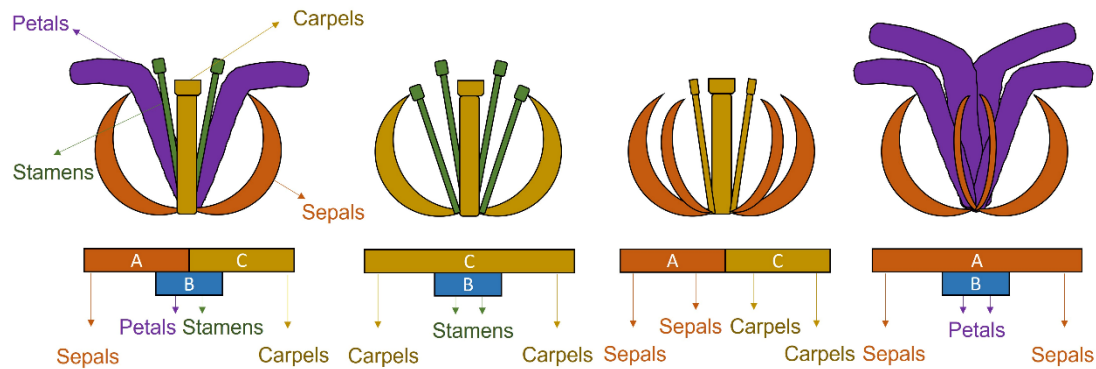


**Figure R-6. Graphical representation of the ABC model** based on Irish, 2017. Domains representing the ABC gene function are represented below. “A” function specifies sepal identity (Red) and a combination of “A” (red) and “B” (blue) specifies petal identity (purple). “B” function (blue) in combination with “C” (yellow) leads to the formation of stamens (green). “C” function (yellow) specifies carpel identity.

To verify that the “C” function was not compromised, and the female gametophyte was fully functional in *mdf-2*, naked pistils from this mutant (Figure R-5G) were pollinated with pollen from a heterozygous *mdf-2* plant. This pollination resulted in the formation of siliques (Figure 7H) which formed viable seeds that germinated and developed normally (Figure R-7I).

Since all the pollinated ovules were homozygous, we expected nearly a 1:1 segregation ratio. While approximately 50% of the seedlings were confirmed as heterozygous, this percentage was reduced in the case of the homozygous population, with around 33% (Figure R-7J). However, it should be considered that a low number of seeds were available due reduced seed production, with only 15 seeds in comparison to the average of 60 obtained in WT plants. Furthermore, when considering the non-germinating seeds as homozygous, the percentage of homozygous plants increases to almost the presumed 50%.





**Figure R-7. The female gametophyte in *mdf-2* mutants is viable.** (A) Representative picture of the formed siliques after *mdf-2* homozygous pollination with pollen from a *mdf-2* heterozygous plant. (B) Representative picture of a heterozygous *mdf-2* plant germinated from a seed obtained after pollination of *mdf-2*. (C) Genotype distribution of the progeny from the siliques represented in (A).

#### 4.1.6 Transgenic expression of *pMDFMDFg* restores the developmental defects present in *mdf* mutants

A previous publication showed that the introduction of a nuclear localized *MDF* cDNA construct under *MDF*'s native promoter complemented the defective RAM phenotype of *mdf-1* mutants, confirming that *MDF* had a function in the maintenance of the RAM (Casson *et al.*, 2009).

Using the same primers to define the promoter region, a construct containing *MDF* genomic region, including 3000 bp upstream of the start ATG, fused at the C-terminus to GFP was transformed into both *mdf-1* and *mdf-2* mutant background. The stable transformant lines *mdf-1::pMDFMDFg* and *mdf-2::pMDFMDFg* exhibited GFP-derived fluorescent nuclear signal and full complementation of the defective RAM phenotype (Figure R-8A). Moreover, opposite to both *mdf* mutants, the complemented transgenic lines had rosette leaf sizes and overall statures equivalent to WT plants (Figure R-8A).

The unfertile phenotype associated to the *mdf* mutations was also restored (Figure R-8A), further confirming that also the defective flower formation described in *mdf-2* plants is dependent on *MDF*.

Additional analyses confirmed that the developmental defects associated to the root system in *mdf* mutants such as cell death accumulation (Figure R-8B), reduced cell division (Figure R-8C) and arrested primary root growth (Figure R-8D) were recovered after the introduction of *pMDFMDFg*. These experiments were only performed with *mdf-1::pMDFMDFg* plants, based on the stronger phenotype displayed by *mdf-1* in comparison to *mdf-2* mutants (Figures R1 to 3).

## RESULTS

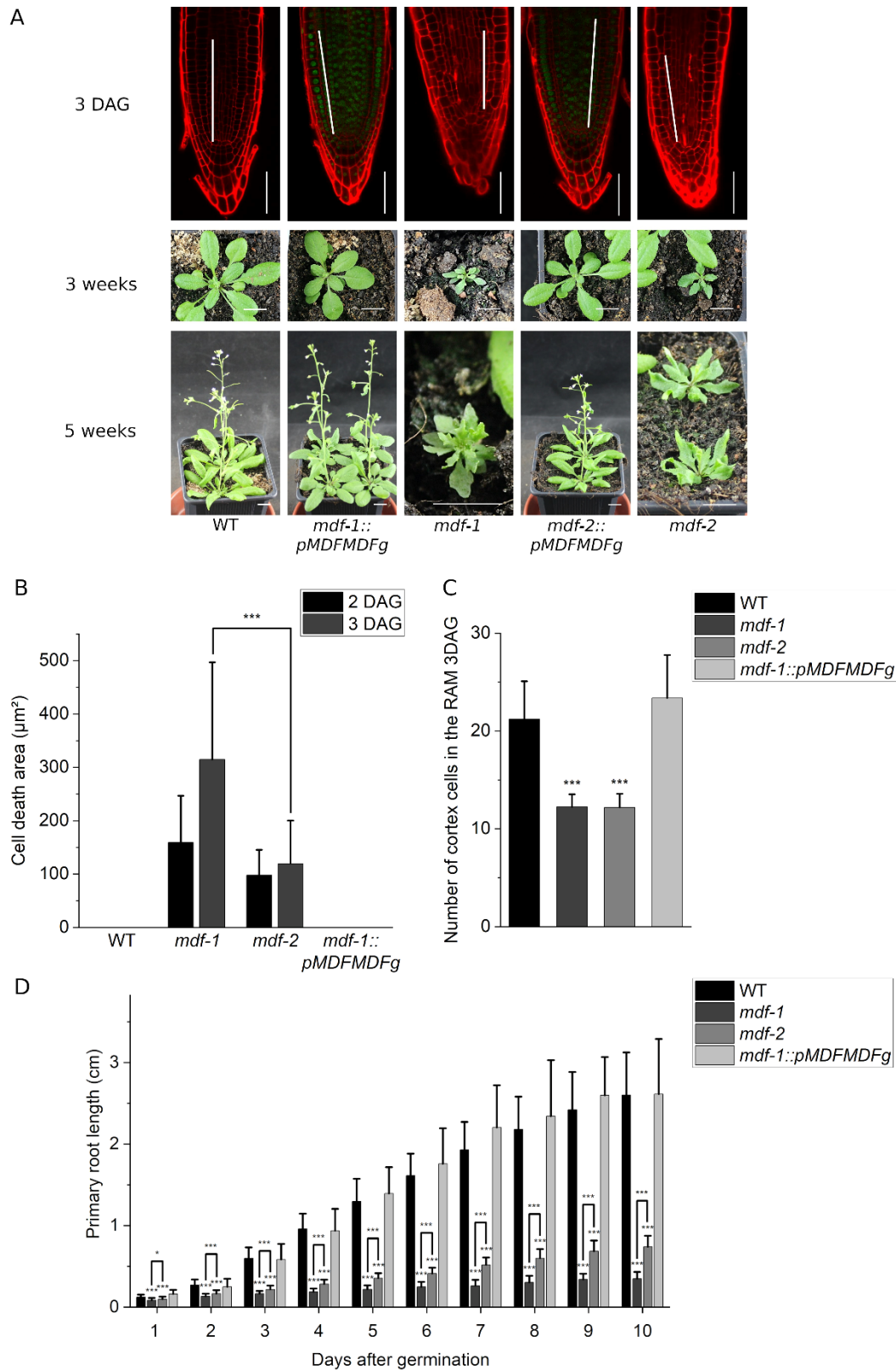


**Figure R-8.** Transgenic expression of *pMDFMDFg* restores the developmental defects present in *mdf* mutants. (A) Representative pictures of 3 DAG PI-stained root tips (Upper panel. White bar indicates the division zone. Scale bar: 50µm), 3-week-old (Middle panel. Scale bar: 1 cm) and 5-week-old (Lower panel. Scale bar: 1 cm) plants from WT, *mdf-1*, *mdf-1::pMDFMDFg*, *mdf-2* and *mdf-2::pMDFMDFg* lines. (B) Quantification of the

cell death area of root tips of WT (n=21 and n=22), *mdf-1* (n=21 and n=95), *mdf-2* (n=33 and n=59) and *mdf-1::pMDFMDFg* (n=19 and n=25) lines at 2 and 3 DAG. Statistical significance was determined in comparison to *mdf-1*. (C) Number of dividing cells in the cortical layer of 3 DAG seedlings of WT (n=40), *mdf-1* (n=36), *mdf-2* (n=21) and *mdf-1::pMDFMDFg* (n=24). Statistical significance was determined in comparison to WT. (D) Primary root length from 1 until 10 DAG of WT (n=62, 137, 97, 74, 74, 75, 75, 74 and 75), *mdf-1* (n=48, 65, 69, 55, 53, 41, 50, 44 and 45), *mdf-2* (n=46, 57, 63, 51, 51, 51, 50, 52, 49 and 50) and *mdf-1::pMDFMDFg* (n=72, 160, 161, 166, 223, 68, 66, 63 and 148). Statistical significance was determined in comparison to WT and *mdf-1*. Average  $\pm$  Standard deviation is represented. \*P < 0.05; \*\*P < 0.005; \*\*\*P < 0.0005 as determined by a two-tailed Student's t-test.

## 4.2 MDF is localized in the spliceosome

### 4.2.1 MDF is associated with the U4/U6.U5 tri-snRNP protein LSM8

The human homolog of MDF, SART1, is known to be part of the U4/U6.U5 tri-snRNP complex necessary for its association with the pre-spliceosome (Makarova *et al.*, 2001). To assess whether MDF is also associated to U4/U6.U5 tri-snRNP in plants, interaction studies with LSM8, a core component of the tri-snRNP complex, were conducted. LSM8 is a nuclear protein that confers specificity to the LSM2-8 heteroheptameric ring complex, required for efficient precursor mRNA splicing through U6 small nuclear RNA (snRNA) stabilization (Perea-Resa *et al.*, 2012).

Independently from our research, Eduardo Tranque Montes, a PhD candidate in the research group from Julio Salinas at the Centro de Investigaciones Biológicas "Margarita Salas" (CSIC) in Madrid, performed several Co-immunoprecipitation (Co-IP) experiments using LSM8-GFP as bait and an anti-GFP antibody followed by tandem mass spectrometry (IP-MS/MS) to elucidate the interaction partners of LSM8 under different abiotic stress conditions (Eduardo Tranque personal communication). Curiously, three independent Co-IP experiments showed co-purification of MDF and LSM8 at control conditions. Score, coverage and sequence of the MDF peptides that were identified to co-purify at control conditions in each of the three experiments using LSM8-GFP as bait are listed on Table R-1.

**Table R-I. Mass spectrometry results of MDF protein co-immunoprecipitating with LSM8-GFP. Results of the MS analyses showing the Score, coverage and sequence of the peptides that were identified for MDF in each of the three experiments using LSM8-GFP as bait.** Experimental design, performance and analyses were carried out by Julio Salinas and Eduardo Tranque from the Centro de Investigaciones Biológicas "Margarita Salas" (CSIC) in Madrid.

Experiment	Score	Coverage
1	162,4486099	6,59
Detected sequences	GLNEGGDNVDAASSGK	
	IQGQTTHTFEDLNSSAK	
	NSDTPSQSVQR	
	EASALDLQNR	
Experiment	Score	Coverage
2	198,5233817	7,93
Detected sequences	GLNEGGDNVDAASSGK	

	IFEEQDNLNQGENEDGEDGEHLSGVK	
	NSDTPSQSVQR	
	VVEGGAVILTLK	
Experiment	Score	Coverage
3	210,6966728	12,2
Detected sequences	GLNEGGDNVDAASSGK	
	IFEEQDNLNQGENEDGEDGEHLSGVK	
	NSDTPSQSVQR	
	mLPQYDEAATDEGIFLDAK	
	VVEGGAVILTLK	
	KPESEDVfMEEDVAPK	

This putative interaction was verified by Eduardo Tranque using bimolecular fluorescence complementation (BiFC) assays in which MDF and LSM8 open reading frames (ORF) were fused at its N-terminus to either the N-terminal or C-terminal half of YFP. These constructs were co-transformed in *Nicotiana benthamiana* leaves and reconstitution of YFP-derived fluorescence – as a consequence of the interaction between the two proteins- was analysed by confocal microscopy. Both combinations in which LSM8 and MDF were co-expressed, generated a strong nuclear YFP-derived fluorescence signal. The interaction of MDF and LSM1a, which is one of the two proteins that defines and confers the identity to the cytoplasmic localized LSM1-7 heteroheptameric complex involved in mRNA decay (Perea-Resa *et al.*, 2012), was also assessed to validate the method. As expected, no fluorescence was detected in these experiments (Figure R-9A).

Colocalization between MDF and LSM8 was also tested. To this end, MDFCDS-GFP and LSM8CDS-mCherry constructs were co-transformed in *Nicotiana benthamiana* leaf epidermis cells. In agreement with previous experiments, MDF and LSM8 signals overlapped in the nucleoplasm and in internal nuclear structures that appear to be nuclear speckles. MDF concentrated also in the nucleolus (Figure R-9B).

snRNPs and other non-snRNP protein splicing factors are known to accumulate in nuclear speckles (reviewed in Spector and Lamond, 2011). Therefore, the co-localization of LSM8 and MDF in these nuclear domains, further supports the presumed association of MDF to the spliceosome.

Regarding MDF specific nucleolar localization, it must be noted that new functions besides the canonical role in ribosomal RNA (rRNA) synthesis and ribosome biogenesis, have been attributed to the nucleolus. Those include cell cycle regulation, growth and development, senescence, gene silencing, response to stresses and biogenesis of various ribonucleoprotein particles (reviewed in Kalinina *et al.*, 2018). For example, Arabidopsis *ROOT INITIATION DEFECTIVE1 (RID1)*, a DEAH-Box RNA Helicase involved in pre-mRNA Splicing, essential

for plant developmental processes such as root and leaf morphogenesis and meristem maintenance, was characterized to also have a nucleolar localization (Ohtani *et al.*, 2013). Nevertheless, MDF putative localization in the nucleolus should be further verified by the use of an MDF construct under its native promoter.

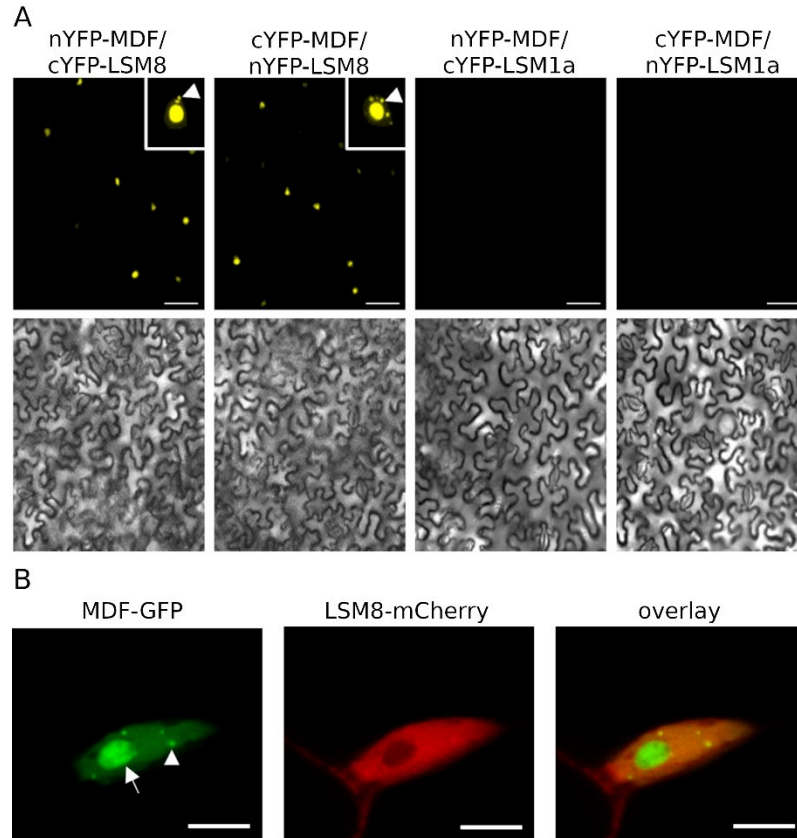


**Figure R-9. MDF is associated with the U4/U6.U5 tri-snRNP protein LSM8.** (A) Representative confocal images of BiFC assays showing reconstitution of YFP fluorescence in the nucleus of epidermal cells of *Nicotiana benthamiana* leaves in which nYFP-MDF and cYFP-LSM8, as well as cYFP-MDF and nYFP-LSM8, are co-expressed. No fluorescence is seen upon co-expression of nYFP-MDF and cYFP-LSM1a or cYFP-MDF and nYFP-LSM1a. Upper panels show fluorescence images and lower panels show bright field images. Scale bar: 75  $\mu$ m. Arrowheads point to putative nuclear speckles. Experimental design, performance and analyses were carried out by Julio Salinas and Eduardo Tranque from the Centro de Investigaciones Biológicas "Margarita Salas" (CSIC) in Madrid. (B) Representative confocal images showing GFP (green) and mCherry (red)-derived fluorescence upon co-expression of MDF-GFP and LSM8-mCherry in *Nicotiana benthamiana* leaf epidermis cells. MDF localises to the nucleolus (arrow) and co-localizes with LSM8-mCherry in the nucleoplasm and nuclear speckles (arrowheads). Scale bar: 9,7  $\mu$ m. Confocal microscopy was performed by Judith Mehrmann.

#### 4.2.2 MDF and LSM8 do not interact physically

The same constructs used during co-localization studies were also used to assess the physical interaction between MDF and LSM8 by fluorescence resonance energy Transfer (FRET)-based fluorescence lifetime imaging (FLIM). Constructs fused to GFP were used as donors and plasmids containing the fluorescent mCherry tag acted as acceptors. After co-expression



of both donor and acceptor in *Nicotiana benthamiana* leaf epidermis cells, fluorescence lifetime of the donor was measured. Subsequently, FRET efficiency was determined from the change in the fluorescence lifetime of the donor, which decreases in the presence of the acceptor in a distance dependent manner. Combinations in which the donor fluorescence lifetime is unchanged in comparison to donor-only samples are considered as non-interacting.

There was no significant difference in the fluorescence lifetime of LSM8-GFP in cells expressing LSM8-GFP alone compared to those expressing both LSM8-GFP and MDF-mCherry. Likewise, no change occurred when expressing MDF-GFP alone or in combination with LSM8-mCherry. The experimental design was validated by the confirmation of the interaction between LSM8 and LSM2 (Perea-Resa *et al.*, 2012) when using LSM8 as donor and LSM2 as acceptor (Figure R-10A). These measurements were carried out by Judith Mehrmann and analysed by Magdalena Weingartner.

Additionally, GAL4-based Yeast Two Hybrid (Y2H) experiments were performed with MDF and LSM8 CDS constructs N-terminally tagged to the binding (BD) and activating (AD) domains of the GAL4 transcription factor (Figure R-10B). Transformation of *Saccharomyces cerevisiae* AH109 strain with LSM2 fused to the BD and LSM8 fused to the AD served as positive control. The physical interaction of both LSM proteins led to the transcriptional activation of our reporter gene, histidine (HIS). Hence, the histidine deficient yeast strain was able to grow not only in the growth control (+HIS), but also in the absence of this amino acid (-HIS). Experiments in which MDF or LSM8 fused to either the AD and BD domain were co-transformed with citrine fused to the complementing BD and AD domain respectively, served as negative controls. Furthermore, they revealed that transformation of *Saccharomyces cerevisiae* AH109 with LSM8 N-terminally fused to the BD led to autoactivation of the GAL4 transcription factor irrespective of the presence of a physical interaction partner. Therefore, yeast growth in the -HIS plates after co-transformation of LSM8 and MDF fused to the binding and activating domains respectively, should be interpreted as a false positive.

72 hours after co-transformation of the different MDF and LSM8 N-terminally fused constructs, no growth was detected on the selective media (-HIS) (Figure R-10B), which indicated that MDF and LSM8 do not interact physically.

To minimize the risk of false negative interactions that can be originated by the steric hindrance effect of fusion tags by covering the potential interaction sites (Stellberger *et al.*, 2012), co-transformation of MDF and LSM8 C-terminally fused to either AD or BD domains was also performed (Figure R-10B). Unfortunately, no positive interacting combination was observed after C-terminal fusion of the AD and BD tags.

On the other hand, several publications have pointed out the advantages of using smaller sub-regions in addition to full-length proteins during Y2H studies (Galletta and Rusan, 2015). These include the removal of regions not valid for Y2H experiments due to its potential toxicity in yeast or its ability to induce auto-activation of the Y2H reporter gene. Additionally,

improper folding in yeast of full-length proteins as well as the lack of specific cellular events such as post-translational modifications might also yield false negative interactions (Galletta and Rusan, 2015). For this reason, Y2H experiments were also conducted between LSM8, LSM2 and different domains of MDF (Figure R-10C). The N-terminal Serine- Arginine (SR) domain was defined by a BLAST alignment against the SR protein SR34 (based on Stankovic *et al.*, 2016) and the predicted RNA recognition motif (RRM) region was delimited as described in Casson *et al.*, 2009. The C-terminal SART1 domain was determined according to a BLAST alignment against human SART1. No combination tested led to the growth of the co-transformed yeast strain in the absence of histidine (Figure R-10C).

These results verified that LSM8 and MDF do not interact physically but co-localize in the nucleoplasm and presumably also in nuclear speckles. The co-purification and association found by Co-IP and BiFC assays confirmed that, as shown in the animal field, they are part of the same complex by its association to the U4/U6.U5 tri-snRNP.



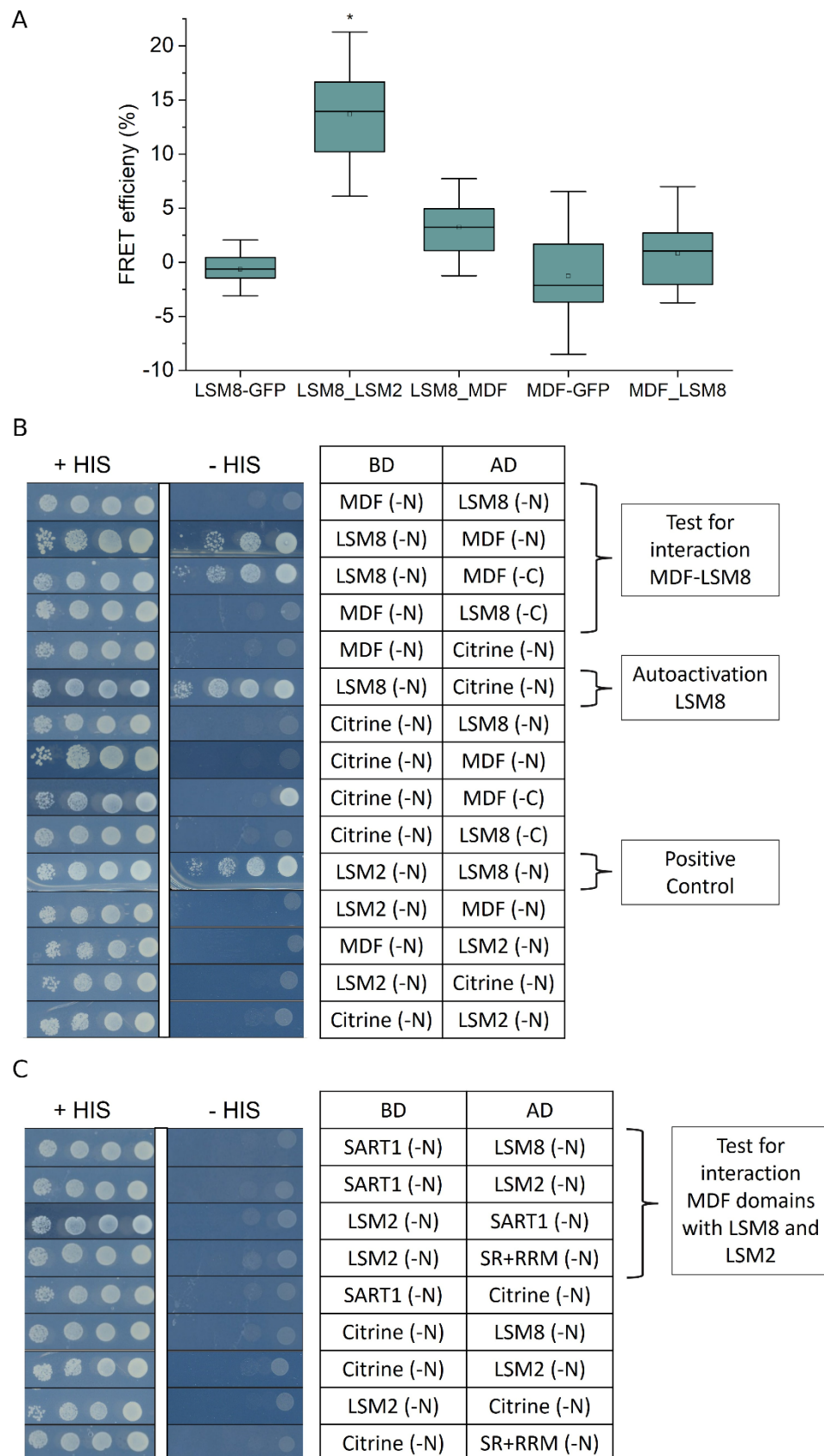


**Figure R-10. MDF and LSM8 do not interact physically.** Box graphs representing FLIM-FRET efficiencies (%) measured in *Nicotiana benthamiana* leaf epidermis cells expressing LSM8-GFP alone or in combination with LSM2-mCherry or MDF-GFP alone or together with LSM8-mCherry. FRET efficiency was significantly higher in samples co-expressing LSM8-GFP and LSM2-mCherry (\* $P < 0.0001$ ; two-tailed Student's t-test). FLIM-

## RESULTS

FRET measurements were performed by Judith Mehrmann and analysed by Magdalena Weingartner. (B-C) Yeast-two-hybrid (Y2H) assay confirming physical interaction between LSM8 and LSM2, but not between LSM8 and MDF complete CDS or its SR+RRM and SART1 domains. Growth of serial dilutions of yeast colonies was followed on medium without tryptophan and leucine (+HIS) and selective medium without tryptophan, leucine and histidine (-HIS) supplemented with 3-amino-1,2,4-triazole (3-AT). BD: DNA-binding domain; AD: activation domain; N: N-terminally tagged; C: C-terminally tagged. Interactions with BD and AD vectors containing citrine were used as negative controls. Interaction between LSM8 and LSM2 was used as positive control. LSM8 shows autoactivation in the BD vector. Visual representation of the SR+RRM and SART1 domains can be found in Figure R-32C.

### 4.2.3 Absence of MDF and LSM8 in *mdf-1lsm8-1* double mutants putatively results in embryo lethality

The interaction of MDF and LSM8 was investigated in more detail by the generation of *mdf-1lsm8-1* double mutants by crossing the already characterized *mdf-1* (Casson *et al.*, 2009) and *lsm8-1* (Perea-Resa *et al.*, 2012) T-DNA insertion lines. After finding no double homozygotes for both mutations among the progeny of an F2 *mdf-1lsm8-1* (het/hom) plant, it was speculated that the absence of both proteins could be lethal in Arabidopsis. To test this hypothesis, the number of seeds contained in more than 20 individual siliques of *mdf-1lsm8-1* (het/hom) and *mdf-1lsm8-1* (seg. WT/hom) mother plants was counted (Figure R-11A).

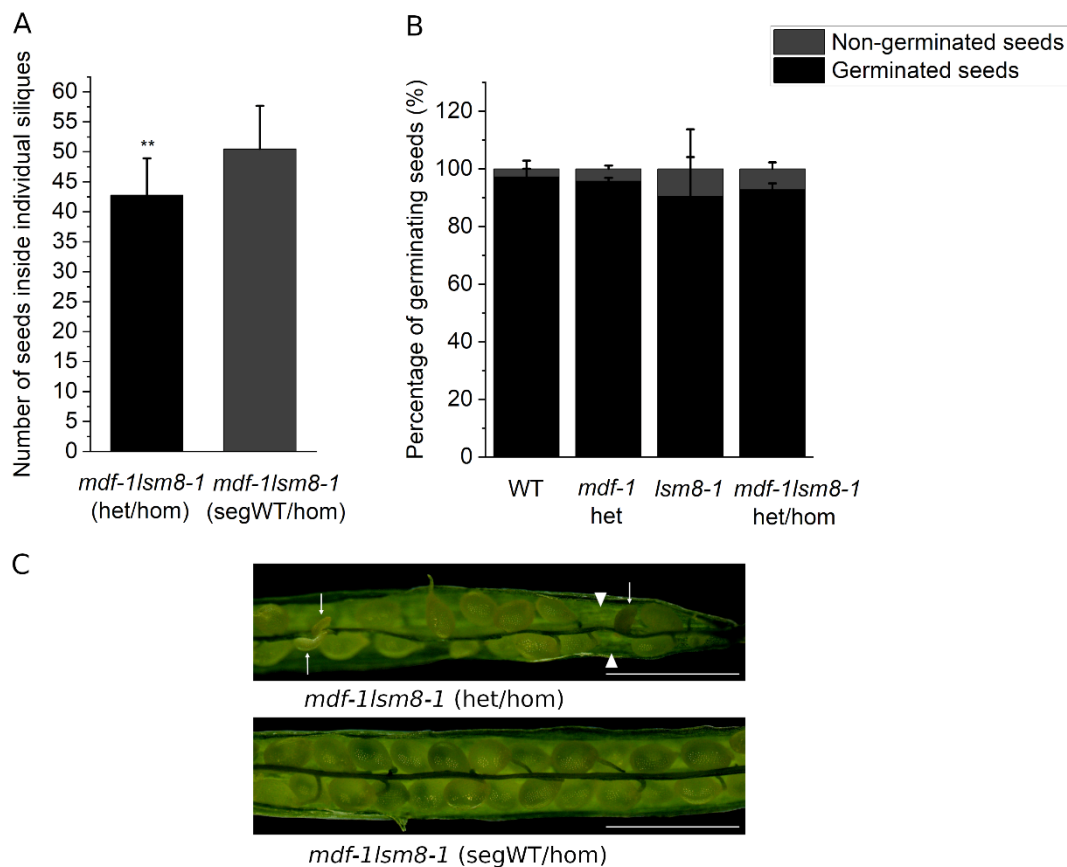


**Figure R-11.** Absence of MDF and LSM8 in *mdf-1lsm8-1* double mutants putatively results in embryo lethality. (A) Quantification of the number of seeds contained inside at least 20 individual siliques of *mdf-1lsm8-1* (heterozygous/homozygous) and *mdf-1lsm8-1* (segregating WT/homozygous). Statistical significance was

determined in comparison to *mdf-1lsm8-1* (het/hom). \*\*P < 0.005 as determined by a two-tailed Student's t-test. (B) Percentage of germinating seeds after 4 days in light for WT, *mdf-1* heterozygous, *lsm8-1* and *mdf-1lsm8-1* (het/hom) plants from 3 independent experiments with at least 75 plants per line and experiment. Average  $\pm$  Standard deviation is represented. (C) Representative pictures of *mdf-1lsm8-1* (het/hom) and *mdf-1lsm8-1* (seg. WT/hom) siliques. Arrowheads indicate empty spaces. Arrows point to aberrant seeds. Scale bar: 1 mm.

Plants containing the *lsm8-1* mutation in homozygosis in combination with the *mdf-1* mutation in heterozygosis produced significantly less seeds than plants having no mutant allele for the *mdf-1* mutation (Figure R-11A). These results indicate that the reduced seed set could be a consequence of the unviability of this double mutation, potentially resulting in embryo lethality.

Germination ratio of *mdf-1lsm8-1* (het/hom) was also evaluated in comparison to *mdf-1* heterozygous, *lsm8-1* homozygous and WT plants (Figure R-11B). For all lines, the percentage of germinating seeds was above 90%. This suggests that the combined loss of MDF and LSM8, arrests Arabidopsis development in early embryogenesis stages (Figure R-11A) and that most of the fully developed seeds can go through germination normally (Figure R-11B).

The embryo lethality of the *mdf-1lsm8-1* double mutation was further verified by the presence of gaps and aberrant seeds inside individual siliques from *mdf-1lsm8-1* het/hom plants (Figure R-11C).

LSM8 was shown to be important for ensuring the correct expression of developmental-related genes and for plant adaptation to different abiotic stresses (Perea-Resa *et al.*, 2012; Carrasco-López *et al.*, 2017). Consequently, *lsm8-1* mutants present severe developmental defects including altered cotyledon shape and number, smaller rosette leaves with shorter petioles, reduced primary root length and formation of secondary roots and reduced seed set with frequently aborted seeds (Perea-Resa *et al.*, 2012). Some of these phenotypical alterations have been associated to the *mdf-1* mutation, such as the abnormal number of cotyledons and arrested root growth (Casson *et al.*, 2009). In addition, *mdf-1* mutants also exhibited a disorganized RAM associated to cell cycle arrest in the G2/M checkpoint and accumulation of dead cells, as well as severe developmental defects in the aerial tissues (Figures R-1 to 3). To better understand the putative lethality of the *mdf-1lsm8-1* double mutation in Arabidopsis, phenotypical comparison analyses were carried out between *mdf-1* and *lsm8-1* for some of the traits associated to the absence of MDF (Figure R-12A to D).

Contrary to *mdf-1*, confocal experiments with 3 DAG *lsm8-1* root tips revealed no dead cells in the RAM (Figure R-12A). Quantification of the number of dividing cells in the cortical layer revealed a slight but significant reduction in cell division (Figure R-12B). However, the

## RESULTS

decreased cell division documented in *mdf-1* mutants was more acute, which could explain the milder root growth delay measured in *lsm8-1* seedlings 3 DAG (Figure R-12C).

Finally, aerial development was also evaluated in both mutant lines (Figure R-12D and E). *lsm8-1* plants, like *mdf-1* mutants, exhibited less rosette leaves than the WT after four weeks in soil at long-day conditions and 24°C (Figure R-12D). Nevertheless, while *mdf-1* mutants displayed a strong dwarf phenotype and complete sterility, *lsm8-1* plants were able to shoot and develop functional flowers (Figure R-12E) as previously published (Perea-Resa *et al.*, 2012).

Thus, evidence suggests that the combination of the *mdf-1* and *lsm8-1* mutations has an additive effect. *lsm8-1* alterations in seed production together with *mdf-1* associated defects in the SAM and RAM, and the importance of both proteins in the root system, potentially leads to embryo lethality, further confirming the importance of both splicing factors in plant development.

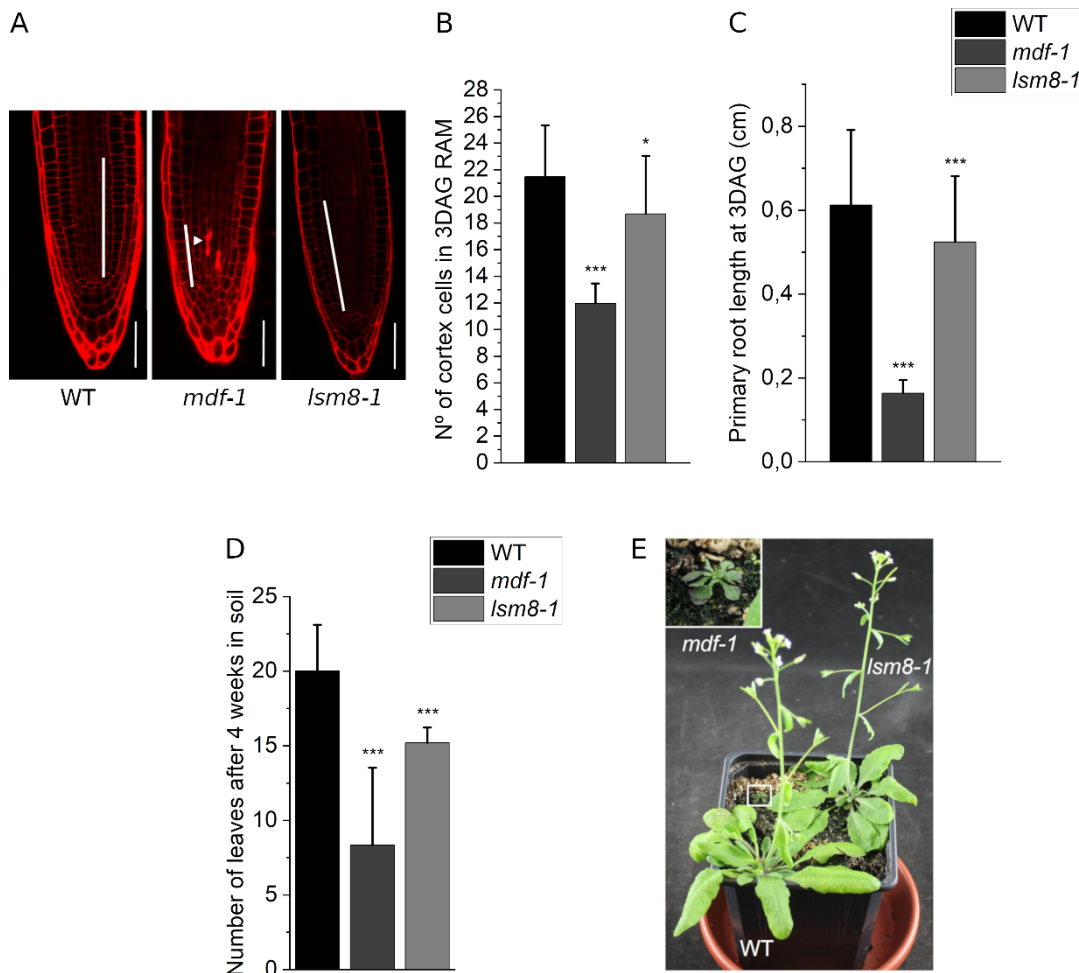


**Figure R-12. Phenotypic analyses between *mdf-1* and *lsm8-1* mutants.** (A) Representative confocal pictures of 3 DAG WT, *mdf-1* and *lsm8-1* PI-stained root tips. White bar indicates the division zone. Arrowheads point to dead cells. Scale bar: 50µM. (B) Number of dividing cells in the cortical layer of WT (n=40), *mdf-1* (n=36) and *lsm8-1* (n=16) 3 DAG seedlings. (C) Primary root length of WT (n=403), *mdf-1* (n=185) and *lsm8-1*

(n=241) 3 DAG seedlings. (D) Number of leaves developed after 4 weeks in soil at long-day conditions in WT (n=61), *mdf-1* (n=15) and *lsm8-1* (n=10) plants. (E) Representative picture of 5-week-old WT, *lsm8-1* and *mdf-1*. The closeup for *mdf-1* on the upper left corner represents the area marked with a white square on the original picture. Average  $\pm$  Standard deviation is represented. Statistical significance was determined in comparison to WT. \*P < 0.05; \*\*P < 0.005; \*\*\*P < 0.0005 as determined by a two-tailed Student's t-test.

### 4.3 MDF is required for the correct splicing and expression of numerous transcripts

#### 4.3.1 *mdf-1* mutants show splicing defects in genes important for transcriptional control and development

As stated previously, MDF belongs to the SART1 family of proteins. Other members include SART1 and Snu66: MDF's homologues in humans and yeast respectively. Both SART1 and Snu66 have been identified as components of the U4/U5.U6 tri-snRNP (Gottschalk *et al.* 1999; Stevens and Abelson, 1999; Makarova *et al.*, 2001). Furthermore, Snu66 was shown to be required for in vivo splicing at low temperatures (Van Nues and Beggs, 2001).

To investigate if MDF loss of function was associated with defects in pre-mRNA splicing, we performed a high-coverage RNA-seq analysis on 3 biological replicates from 12-days-old WT and *mdf-1* seedlings. Approximately 50 million 150 base pair (bp) paired-end reads per sample were generated in a NovaSeq 6000 platform in the European facility of Novogene Co. 2945 differential splicing (AS) events corresponding to 2037 genes were identified in *mdf-1* background (Figures R-13A and B). The majority of the altered splicing defects, approximately 64%, corresponded to intron retention (IR) events, in accordance with the notion that IR is the most prevalent AS form in plants (Reddy *et al.*, 2012). The categories exon skipping (ES), alternative 5' splice site (A5' SS), alternative 3' splice site (A3' SS) and mutually exclusive exon (MXE) were consequently much less abundant.

To gain insight into the regulatory function of MDF, a Gene Ontology (GO) term enrichment analysis based on the biological process ontology, was performed with the online tool GO term finder from Princeton University for genes showing AS in *mdf-1* (Figure R-13C). Among the top 25 most representative categories biological processes associated to metabolism, gene expression and transcription, stress responses, cell cycle, DNA damage and repair and developmental processes including reproduction were found.

These data suggest that the severe developmental alterations observed in *mdf* mutants (Figures R1 to 3) could be related to AS defects in genes involved the abovementioned biological processes and further supports the so far never proven role of MDF in splicing regulation.



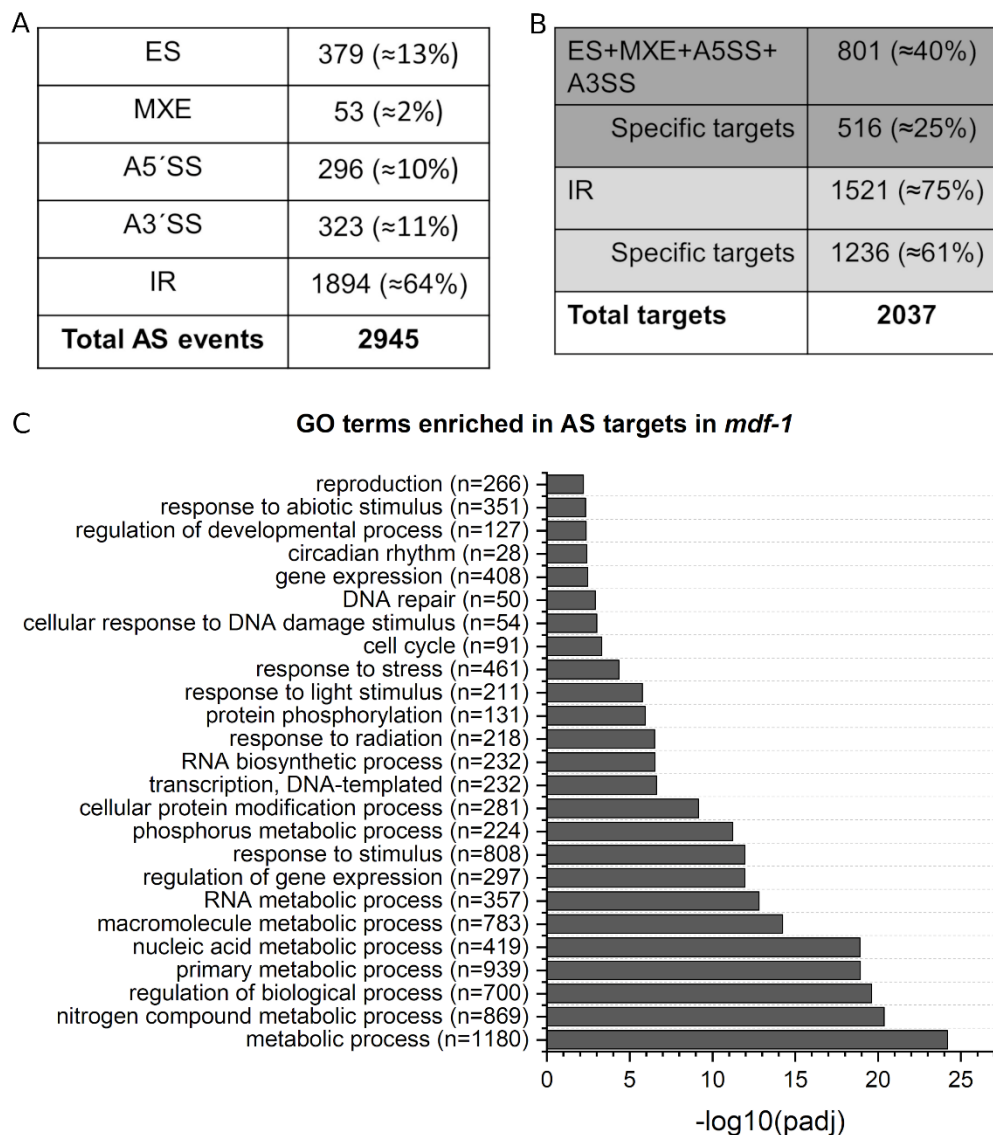


**Figure R-13.** *mdf-1* mutants show alternative splicing in genes important for transcriptional control and development. (A) Quantification and percentual distribution of alternative splicing (AS) events (ES: Exon skipping, MXE: Mutually exclusive exon, A5' SS: Alternative 5' splice site, A' 3SS: Alternative 3' splice site, IR: Intron retention) identified in *mdf-1* in respect to WT. (B) Quantification and percentual distribution of targets showing AS identified in *mdf-1* in respect to WT. Specific targets are defined as targets subject of one form of AS that do not contain other forms of AS. (C) 25 most representative top significant Biological Process GO terms enriched in AS targets identified in *mdf-1*.

#### 4.3.2 Absence of different components of the U4/U6.U5 tri-snRNP complex does not lead to equivalent defects in alternative splicing

To better understand the role of MDF in splicing regulation, AS targets identified in *mdf-1* were compared to AS genes found in previously published RNA-sequencing experiments from mutants for three other splicing factors associated to the plant tri-snRNP. These were loss of function mutants for the already introduced SM-like protein LSM8 (*lsm8-1*), the

U4/U6 snRNP pre-mRNA splicing factor 3 (PRP3) (*rdm16-4*) and the BRR2a helicase associated to the tri-snRNP (*brr2a-2*) (Mahrez *et al.*, 2016; Carrasco-López *et al.*, 2017; Lv *et al.*, 2021). In each of these experiments, light grown seedlings of similar age were used as plant material to generate the AS data. Since IR was the most abundant event in all cases, only genes with increased IR were used for the comparative analyses (Figures R-14A and B).

As observed in the Venn Diagram, with only three commonly spliced genes, no representative overlap was found for these splicing mutants (Figure R-14A). Besides, these overlapping genes (*AT4G24590*, *AT5G67385* and *AT5G02810*) have no apparent common biological function. While *AT4G24590* encodes for a RING finger protein that has not been characterized yet, *AT5G67385* gives rise to NRL PROTEIN FOR CHLOROPLAST MOVEMENT1 (NCH1), a protein necessary for phototropin-dependent chloroplast accumulation responses to optimize photosynthetic efficiency and ensure plant survival (Suetsugu *et al.*, 2016; Wang *et al.*, 2021). Finally, PSEUDO-RESPONSE REGULATOR 7 (PRR7) is encoded by *AT5G02810* and functions in circadian clock regulation (Kaczorowski and Quail, 2003).

The lack of significant overlap indicated that different splicing factors seem to have distinctive functions in splicing regulation. While approximately half of the detected splicing defects were specific to *mdf-1*, with enrichment in GO terms associated to metabolism and stress responses, specific GO categories relevant for its putative role in cellular signalling and transcriptional control were shared with other splicing mutants (Figure R-14B). Those were “regulation of biological process” with *lsm8-1*, “protein phosphorylation” with *rdm16-4* and “RNA biosynthetic process” with *brr2a-2*. Thus, although not all splicing proteins associated to the tri-snRNP regulate the same mechanisms, genes involved in important biological processes essential for plant survival are commonly regulated by more than one splicing factor.

To investigate in more detail the common regulation by two different splicing factors of genes important for plant survival, intron retention of several known splicing targets of LSM8 (Carrasco-Lopez *et al.*, 2017) was analysed in *mdf* mutants by RT-qPCR (Figure R-14C). To this end, six genes (*AT5G35170*, *CESA5*, *DFD*, *ATH13*, *DFL2* and *RPPI1*) associated to multiple GO biological processes including “response to cadmium”, “regulation of response to reactive oxygen species”, “response to light stimulus” or “cellulose biosynthetic process” (Source: TAIR) were selected for the analyses. All targets were previously shown to exhibit increased intron retention in *lsm8-1* mutants in comparison to WT plants and were classified as constitutive splicing defects (Carrasco-Lopez *et al.*, 2017). Two additional targets (*RH3* and *CAC2*) in which splicing defects were not found in *lsm8-1* mutants served as negative controls (Carrasco-Lopez *et al.*, 2017).

While RT-qPCR analyses revealed no significant intron retention in the genes used as negative controls (Figure R-14C), splicing defects in *lsm8-1* mutants were only verified in *AT5G35170*



and *RPP1*. The discrepancy with the previously published data (Carrasco-López *et al.*, 2017) could be explained by changes in plant age and growth conditions. Instead of 2-week-old seedlings grown in soil at 20°C, 3 DAG young seedlings grown in MS-sucrose plates at 22°C were used in this study.

Interestingly, 3 out of the 6 tested targets were found to be significantly intron retained in *mdf-2*, including the two genes in which splicing defects were also confirmed in *lsm8-1*. In contrast, only *DFD* showed mis-splicing in *mdf-1*. Differences between both *mdf* mutant lines might be caused by a higher biological variability within the three *mdf-1* biological replicates, as observed by the larger error bars.

Commonly intron retained genes *AT5G35170* and *RECOGNITION OF PERONOSPORA PARASITICA1 (RPP1)* in both *lsm8-1* and *mdf-2* encode for an adenylate kinase and an NLR protein respectively (Source: TAIR). *AT5G35170* is predicted to be involved in nucleoside triphosphate biosynthesis and regulation of light responses (Source: TAIR), whereas *RPP1* participates in plant immunity, specifically in the activation of programmed cell death (Schreiber *et al.*, 2016).

In addition to *AT5G35170* and *RPP1*, significant intron retention was also found for *A. THALIANA OXIDATIVE STRESS-RELATED ABC1-LIKE PROTEIN 1 (ATH13)* in *mdf-2*. *ATH13*, also known as *ABC1K8*, is a protein kinase of the *ABC1K* family with a role in chloroplast lipid biosynthesis and accumulation, that regulates chloroplast membrane composition upon stress responses (Manara *et al.*, 2015).

Finally, splicing defects in *mdf-1* were only detected in *DHFS-FPGS HOMOLOG D (DFD)*, which encodes the cytosolic folylpolyglutamate synthetase (FPGS) isoform (Srivastava *et al.*, 2011). FPGSs catalyse the attachment of glutamate residues to the folate molecules (vitamin B9) in plants. Based on their involvement as cofactors in carbon one (C1) metabolism, a metabolic pathway essential for efficient biosynthesis of essential amino acids and nucleotides, FPGSs play an important role in plant development (Srivastava *et al.*, 2011). Curiously, loss of function mutants for the plastid FPGS isoform (*DFB*), exhibit, similar to *mdf-1*, defects in RAM maintenance including loss of QC identity, which was attributed to the importance of C1 metabolism during cell division and expansion (Srivastava *et al.*, 2011).

Altogether, these analyses indicated that *LSM8* and *MDF* modulate the constitutive splicing of a subset of mRNAs involved in metabolism and stress responses during early seedling development. Since significant intron retention was not verified in *lsm8-1* for the majority of the tested targets, it could be argued that *LSM8* splicing control is more relevant at later growth stages. Moreover, the additional intron retention found in *mdf-1* for *DFD* and *mdf-2* for *ATH13*, highlights the importance of *MDF* in early development and correlate with the more severe phenotypical alterations found in 3 DAG *mdf* mutants in comparison to *lsm8-1* (Figures R-12A to C).

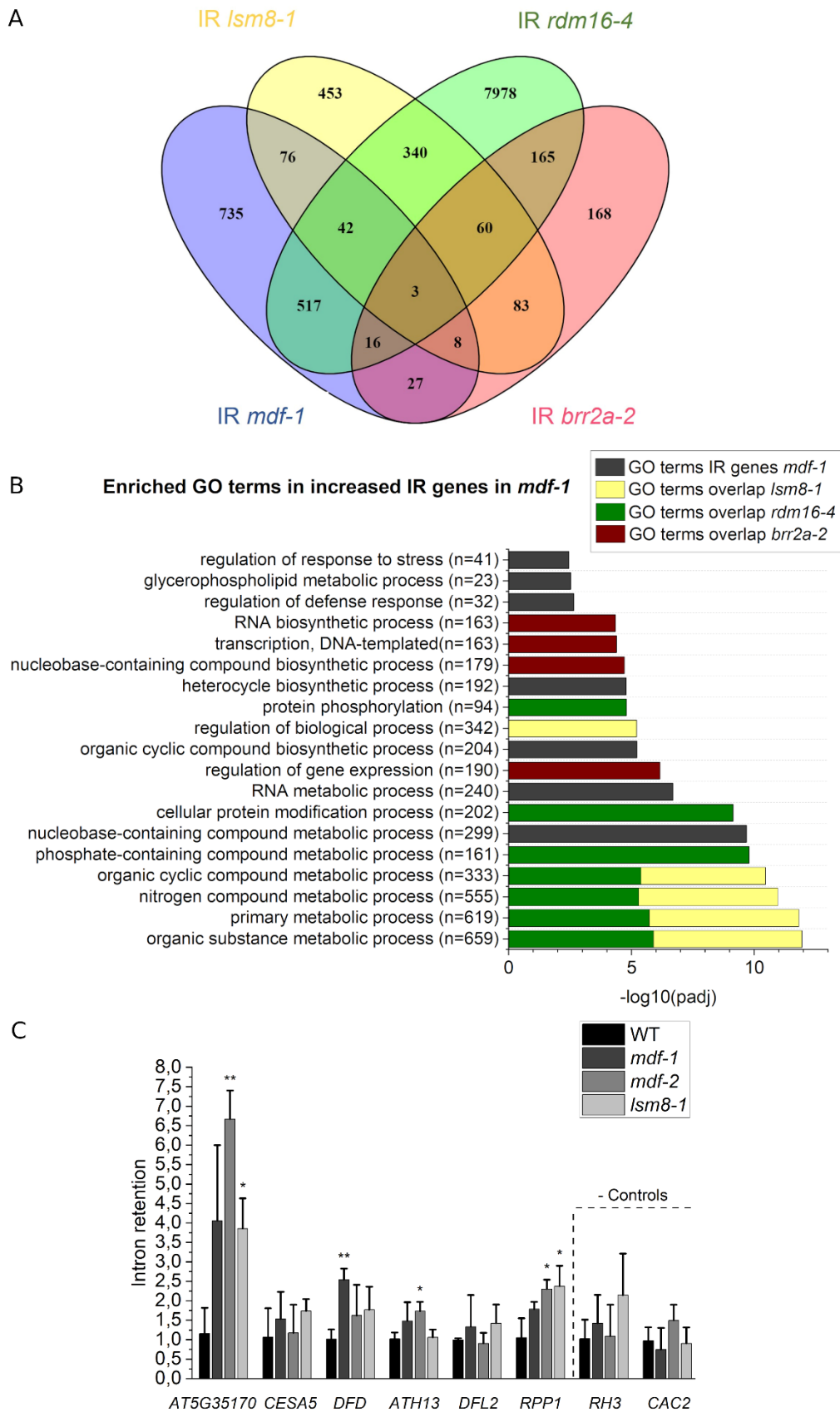


**Figure R-14. Absence of different components of the U4/U6.U5 tri-snRNP complex does not lead to equivalent defects in alternative splicing.** (A) Venn diagram representing the overlap between significantly increased IR targets between *mdf-1*, *lsm8-1*, *rdm16-4* and *brr2a-2*. (B) 20 most representative top significant Biological Process GO terms enriched in increased intron retained targets identified in *mdf-1*. Colouring indicates enriched

biological processes found in targets showing IR in *mdf-1* and *lsm8-1* (yellow), *mdf-1* and *rdm16-4* (green) and *mdf-1* and *brr2a-2* (red). (C) Verification of intron retention events found in *lsm8-1* (Carrasco-López *et al.*, 2017) in WT, *mdf-1*, *mdf-2* and *lsm8-1* 3 DAG seedlings. *RH3* and *CAC2* were used as negative controls. Average  $\pm$  standard deviation is represented. Statistical significance was determined in comparison to WT. \*P < 0.05; \*\*P < 0.005; \*\*\*P < 0.0005 as determined by a two-tailed Student's t-test.

#### 4.3.3 Verification of the importance of MDF for the correct splicing of a subset of transcripts involved in splicing, DNA damage repair and transcriptional and cell cycle regulation

Validation of the RNA-sequencing analyses was carried out by assessing specific intron retention events increased in *mdf-1* background, which constituted more than 90% of the total intron splicing defects found (Figure R-15A). To this end, RT-qPCR experiments were performed on RNA samples isolated from 12-day-old seedlings of WT, *mdf-1*, *mdf-2* and the complemented line (*mdf-1::pMDFMDFg*). Out of the selected genes, five were involved in cell cycle regulation (*CyclinP3-2*, *CyclinB2-2*, *KRP6*, *KRP2* and *SKP2B*) (Figure R-15B), three had a role in splicing (*SR30*, *SR45* and *RSZ33*) (Figure R-15C), five were known as transcriptional regulators (*PFA4*, *MYB4R1*, *MYB3R3*, *MYBL* and *REM30*) (Figure R-15D) and one was associated to DNA repair processes (*RAD51D*) (Figure R-15E).

Increased IR was verified for all targets in *mdf-1* mutant background, whereas only 8 targets exhibited also significant IR in *mdf-2* seedlings. In 13 out of the 14 tested genes, IR was reversed in the complemented line, further verifying that the splicing defects observed in these genes are very likely caused by the absence of MDF (Figure R-15B to E).

These data showed that MDF, like its homologs in other eukaryotic organisms, acts as a pre-mRNA splicing factor in Arabidopsis. Moreover, the putative truncated C-terminal MDF domain still present in *mdf-2* could be important for MDF's splicing function. This could explain the less pronounced splicing defects observed in *mdf-2* (Figure R-15B to E).

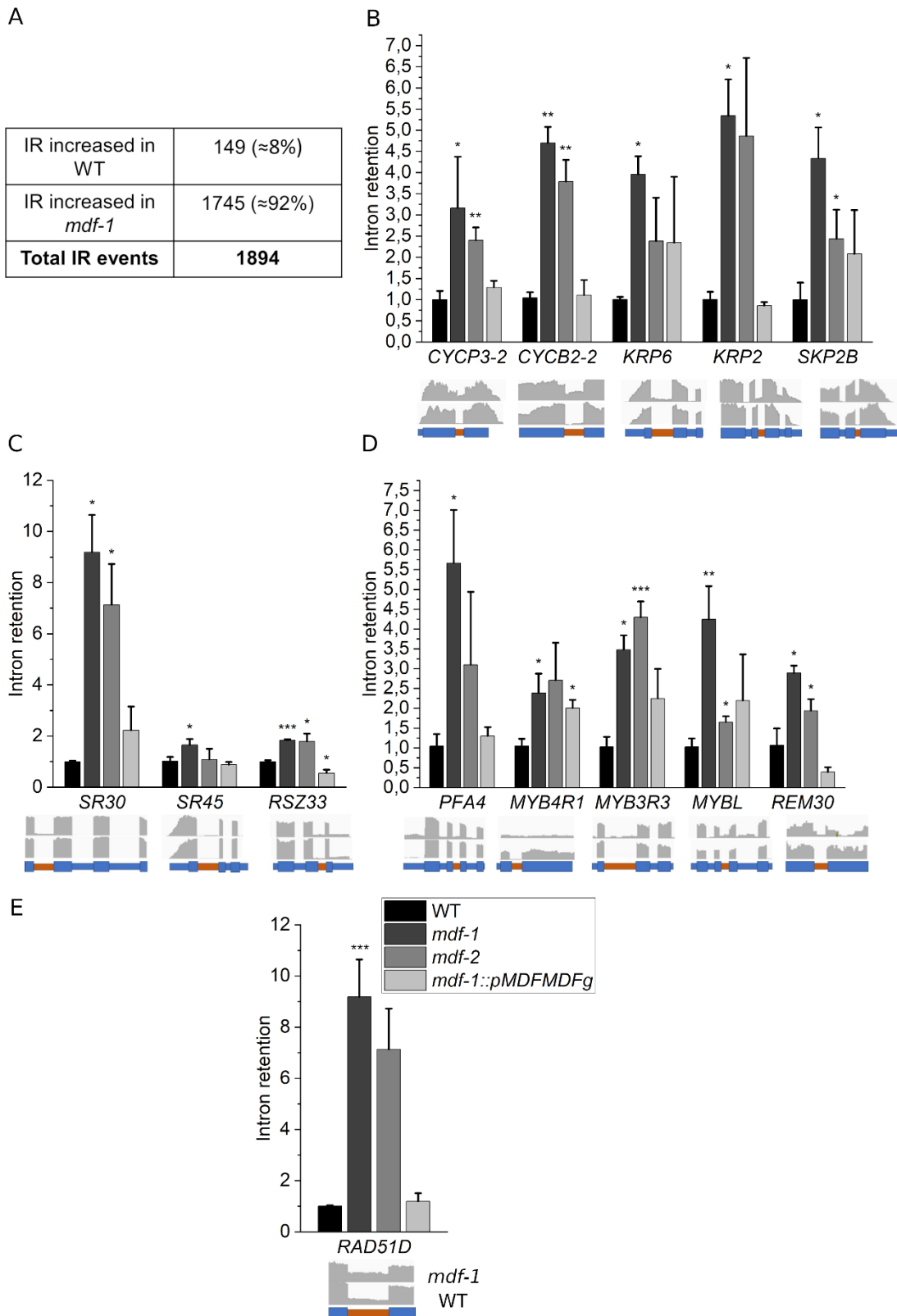


**Figure R-15.** Verification of the importance of MDF for the correct splicing of a subset of transcripts involved in splicing, DNA damage repair and transcriptional and cell cycle regulation. (A) Quantification and percentual distribution of the differential intron retention events increased in WT and *mdf-1* found by RNA-seq. (B-E) RT-qPCR analysis to confirm increased IR events found by RNA-seq in seedlings of WT, *mdf-1*, *mdf-2* and *mdf-1::pMDFMDFg* on genes involved in cell cycle (B), pre-mRNA splicing (C), transcription (D) and DNA repair (E). Captures from the IGV software corresponding to the read coverage tracks for *mdf-1* (upper lines) and WT

(lower line) are represented below each graph. Wide blue boxes represent exons and narrow blue boxes represent introns. Intron retention events verified by RT-qPCR are highlighted in orange. Average  $\pm$  Standard deviation of 2-3 independent biological replicates is represented. \*P < 0.05; \*\*P < 0.005; \*\*\*P < 0.0005 in comparison to WT as determined by a two-tailed Student's t-test.

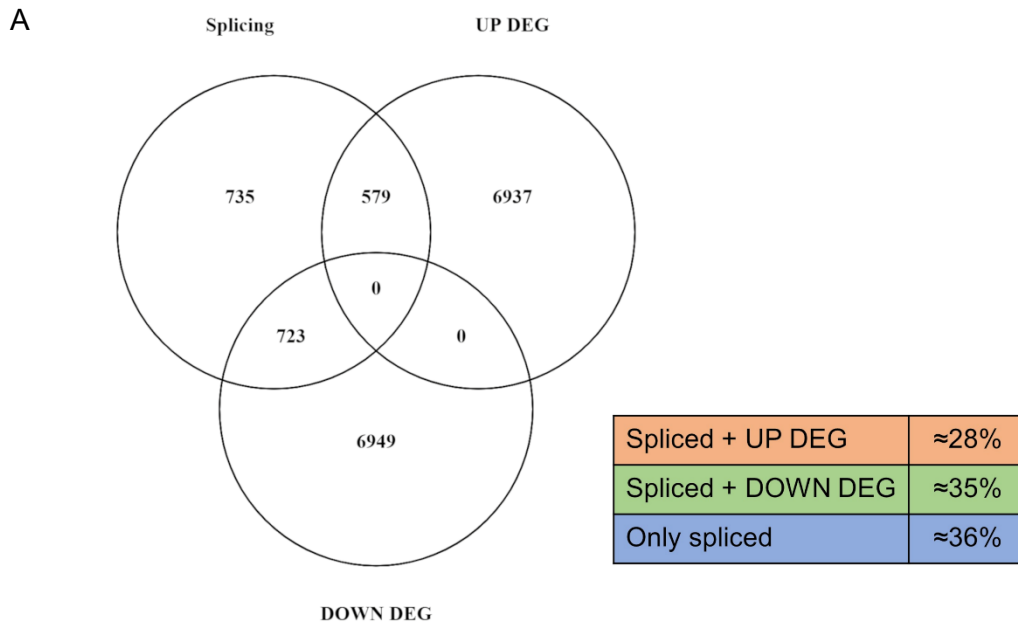
#### 4.3.4 Genes involved in stress response, cell cycle and gene expression control and metabolism are commonly spliced and differentially expressed in *mdf-1* background

Alternative splicing (AS) leads to the formation of a subset of mRNA isoforms derived from a single locus, which increases gene-coding capacity and subsequently also protein diversity (Rigo *et al.*, 2020). Additionally, AS regulates transcript abundance by the introduction of premature termination codons (PTC) in specific isoforms that activate the nonsense-mediated decay (NMD) machinery (Rigo *et al.*, 2020). AS mediated gene expression regulation was reported to be important for plant development and adaptation to different stress responses (reviewed in Reddy *et al.*, 2013).

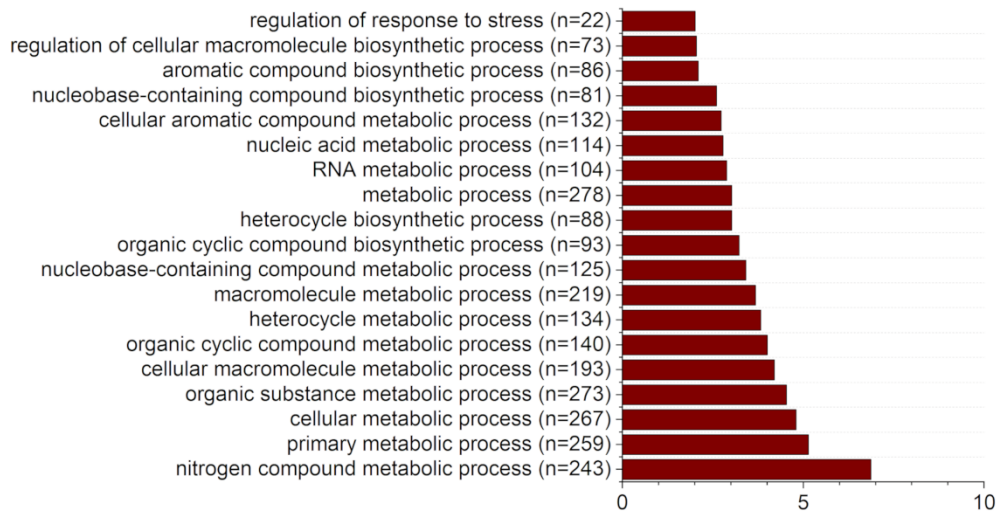
To evaluate the direct impact of the splicing defects associated to the *mdf-1* mutation in gene expression, the overlap between splicing regulated targets and genes undergoing transcriptional changes found by RNA-seq was calculated (Figure R-16A). Approximately 63% of the differentially spliced genes in *mdf-1* exhibited also significant differential gene expression (Statistical significance of the overlap  $p < 1.868e-11$ ). This means that the majority of the splicing defects in *mdf-1* caused expression changes on the mis-spliced gene.

Gene ontology (GO) term analyses of the commonly spliced and differentially upregulated genes revealed that most of these targets are involved in metabolic and biosynthetic processes. 22 genes were also included in the category “regulation of response to stress” (Figure R-16B). Based on this evidence, loss of MDF triggers splicing changes that enhance the expression of genes involved primarily in metabolic and biosynthetic processes.

The overlap between downregulated and differentially spliced genes comprised a wide range of biological processes including transcriptional regulation, cell cycle, chromosome and cytoskeleton organization and protein phosphorylation (Figure R-16C). These analyses highlight the importance of MDF for cell division, signalling and transcriptional control (Figures R-1,2 and 13). Defective splicing caused by the absence of MDF in these targets would most likely lead to the introduction of PTCs and subsequent degradation by the NMD machinery.



**B Enriched GO terms in commonly Spliced and Upregulated genes**



**C Enriched GO terms in commonly Spliced and Downregulated genes**

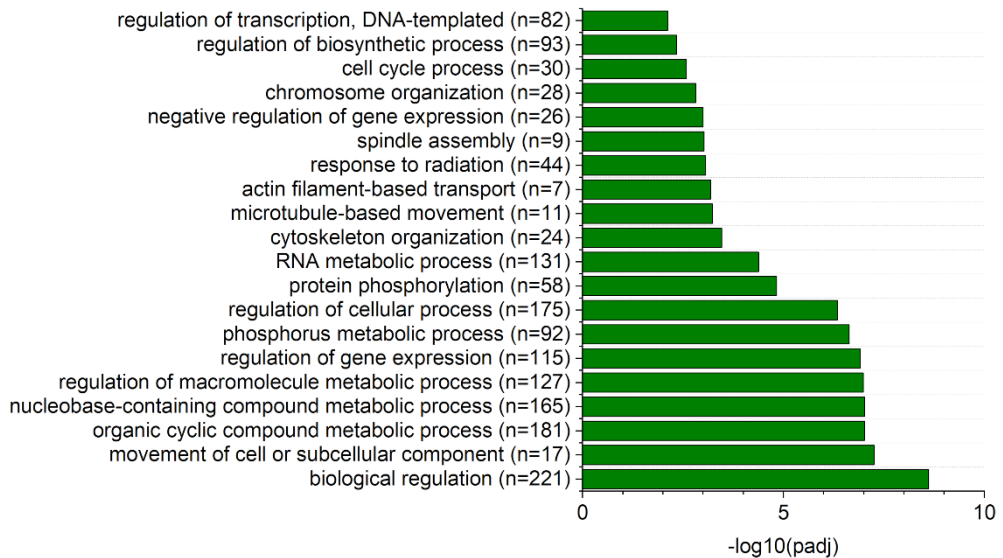


**Figure R-16. Genes involved in stress response, cell cycle and gene expression control and metabolism are commonly spliced and differentially expressed in *mdf-1* background.** (A) Venn diagram showing the overlap between differential alternative spliced (AS) genes and differential expressed genes (DEG) that were found by RNA sequencing experiments to be significantly upregulated or downregulated in *mdf-1* in comparison to WT. Percentual distributions of the only spliced and commonly spliced and transcriptionally regulated targets were calculated according to the total number of AS targets. (B) Top 20 most representative Biology Process Gene Ontology (GO) terms associated to the overlap between Upregulated and AS spliced genes (B) and Downregulated and AS spiced genes (C).

#### 4.3.5 The pleiotropic defects observed in *mdf-1* mutants correlate with the abundant differential transcriptional changes

Alternative splicing (AS) was not always linked to expression changes in the differentially spliced genes (Figure R-16A). However, based on the splicing defects reported for genes involved in transcriptional regulation (Figures R-13D and R-15C), strong changes in the transcriptional profile of *mdf-1* in comparison to WT were expected.

To analyse in more detail the transcriptional changes associated to the absence of MDF, Gene Ontology enrichment analyses for Biological Processes were also performed among the 7516 upregulated and 7872 downregulated genes found by RNA sequencing of 12-day-old *mdf-1* seedlings in comparison to WT (Figure R-17A).

Genes associated to stress responses including temperature, salt, and oxidative stress and defence responses were very abundant among the significantly upregulated genes (Figure R-17B). These findings indicate that loss of MDF leads to constitutive activation of stress conditions in accordance with *mdf-1* phenotypical analyses (Figures R-1 to 3).

The categories “RNA processing”, “RNA splicing” and “ribonucleoprotein complex assembly” were also enriched in the differentially upregulated genes. This could be a compensation mechanism of the plant to overcome the splicing deficiencies caused by the absence of MDF, since functional alterations of specific genes have been shown to alter the expression of other genes with overlapping functions to maintain cellular fitness (reviewed in El-Brolosy and Stainier, 2017).

Genes involved in Programmed Cell death were also upregulated, which suggests that the accumulated dead cells in the RAM in *mdf* mutants could be a regulated response triggered by the absence of MDF, such as the one initiated in the plant DNA damage response (DDR) upon acute DNA damage (reviewed in Nisa *et al.*, 2019).



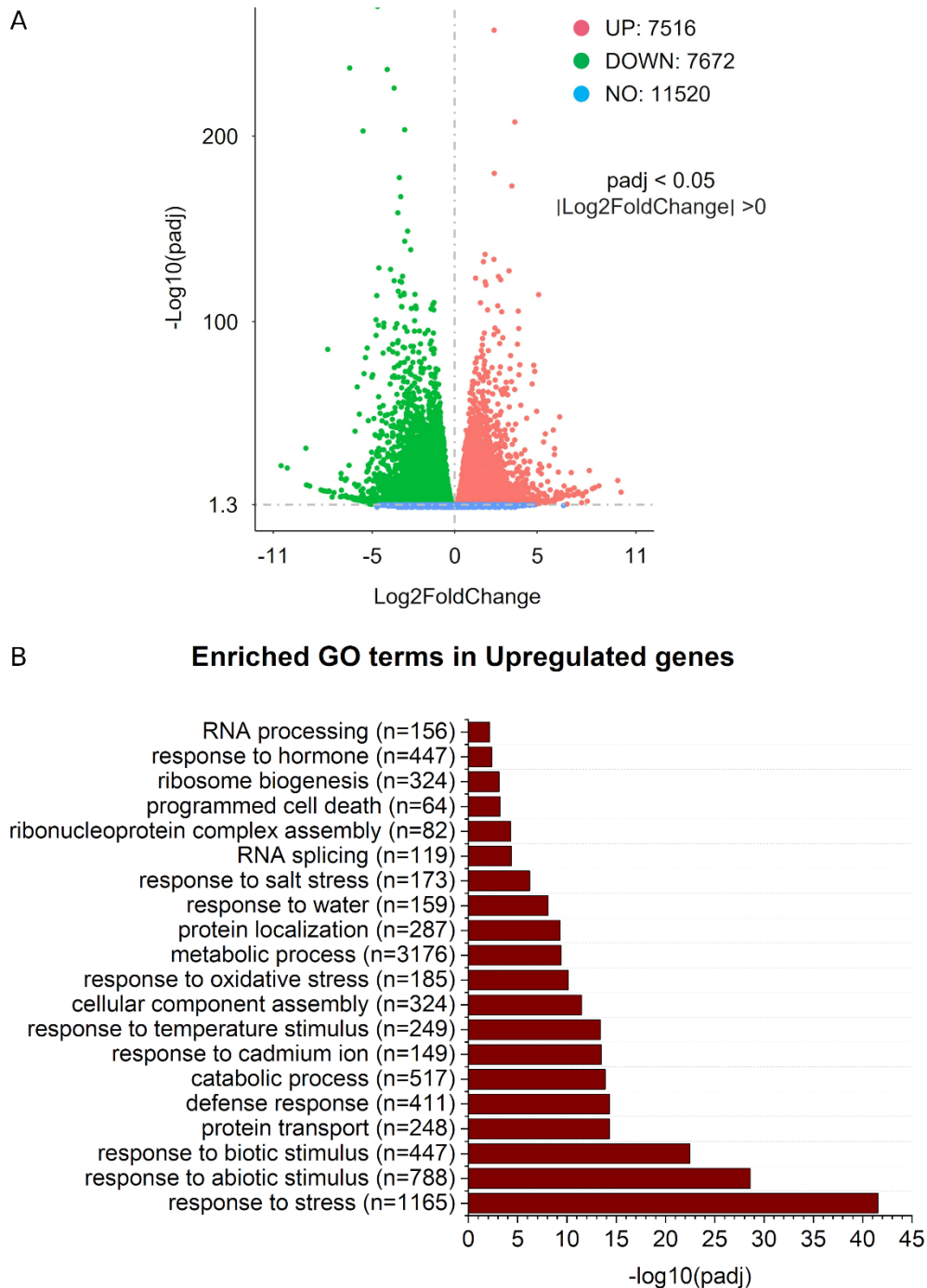


**Figure R-17.** The pleiotropic defects observed in *mdf-1* mutants correlate with the abundant differential transcriptional changes. (A) Volcano plot representing the differentially expressed genes (DEGs) upregulated (in red) and downregulated (in green) in *mdf-1* compared to WT with p values < 0.05. Blue dots indicate genes that show no differential expression. (B) 20 most representative top significant Biological Process GO terms enriched in upregulated genes in *mdf-1* compared to WT.

Interestingly, among the down-regulated genes we found a significant enrichment of pathways involved in cell division and developmental processes (Figure R-18). Some of these GO categories include “cell cycle”, “cell division”, “chromosome organization”, “meristem development” and “root and shoot system development”. These data fits with the phenotypical



observations in which cell division alterations and severe growth arrest in root and aerial tissues were documented in *mdf* mutants (Figures R-1 to 3).

As previously reported (Casson *et al.*, 2009), genes involved in auxin response and transport presented significant changes in transcript levels (Figure R-18). Additionally, the expression of genes involved in responses to DNA damage and in particular DNA repair processes, seem to be impaired in *mdf-1* background, further verifying the putative role of MDF in genome stability and the plant DDR.

Together, these data showed that loss of MDF function has a major impact on gene expression and is important for the correct expression of genes involved in cell proliferation and developmental processes, and, at the same time, leads to constitutive induction of stress responsive genes.

### Enriched GO terms in Downregulated genes

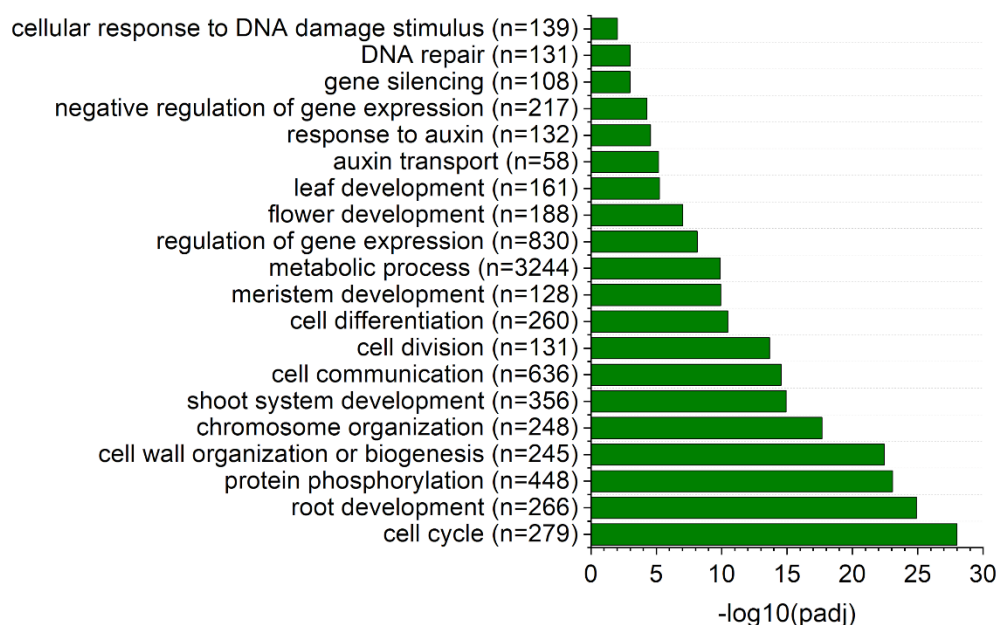


**Figure R-18. Absence of MDF leads to a reduced expression of proliferative genes and developmental processes.** 20 most representative top significant Biological Process GO terms enriched in downregulated genes in *mdf-1* compared to WT.

#### 4.3.6 MDF controls the expression of genes associated to cell cycle control upon DNA damage

The plant DNA damage response (DDR) is a mechanism that plants have evolved to ensure the DNA integrity, which, upon DNA damage, activates a signalling cascade initiated by the transcription factor SOG1 leading to cell cycle arrest, cell death and DNA repair (Yoshiyama *et al.*, 2013). Phenotypical analyses confirmed that similar responses were constitutively activated in *mdf* mutants (Figures R-1 and R-2). To gain more insight into the presumed role of MDF in genome stability, gene expression changes observed in *mdf-1* were compared to

the transcriptional program activated upon DNA damage. To this end the overlap between the 15188 differentially expressed genes (DEG) in *mdf-1* (Figure R-17A) and the DEG after incubation of Arabidopsis WT seedlings in the DSB inducing drug zeocin (Yoshiyama *et al.*, 2020) was calculated (Figure R-19).

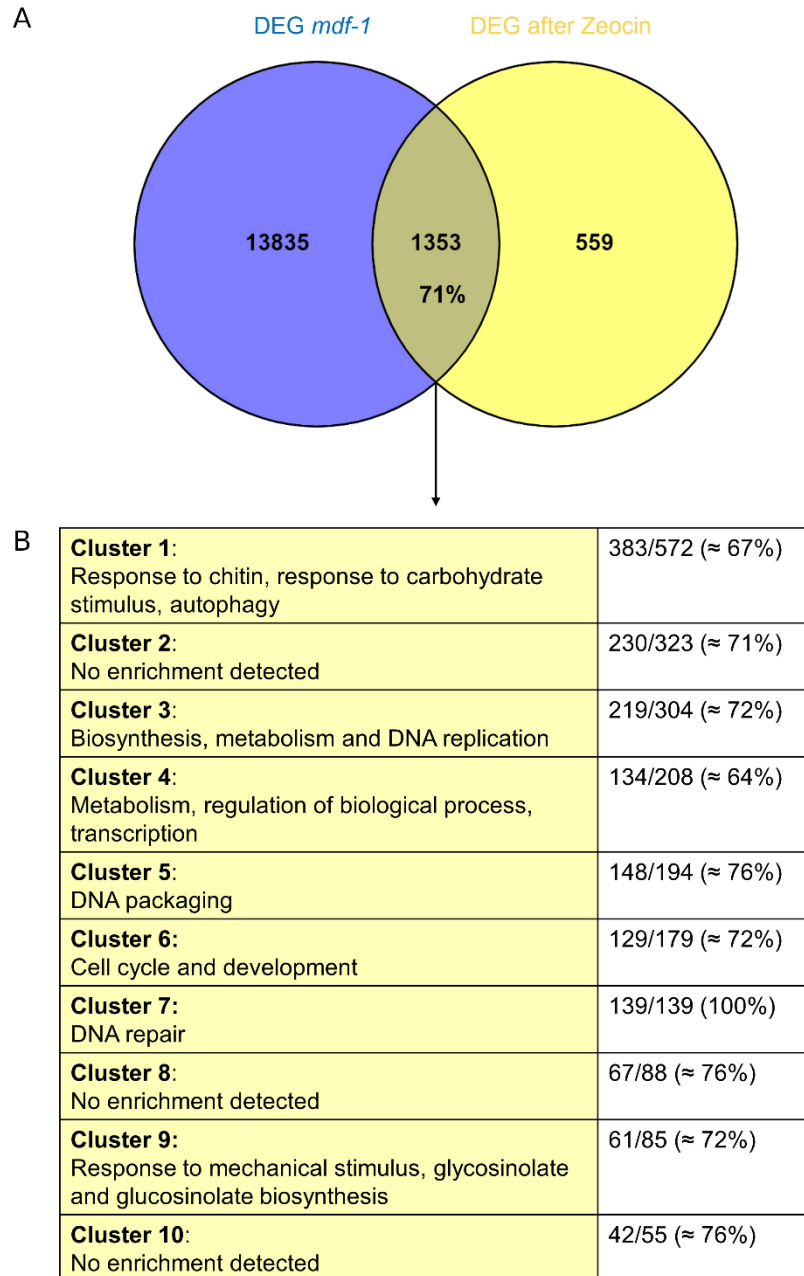


**Figure R-19. Loss of MDF induces similar transcriptional changes than zeocin incubation.** (A) Venn diagram representing the overlap between genes undergoing expression changes after zeocin incubation (Yoshiyama *et al.*, 2020) and the differentially expressed genes in *mdf-1*. (B) Quantification of the specific overlap between the genes contained in each of the 10 clusters of genes which showed transcriptional changes after zeocin incubation. Biological processes associated to each cluster are described as stated on Yoshiyama *et al.*, 2020.

Out of the 1912 targets transcriptionally induced after DNA damage (Yoshiyama *et al.*, 2020), 1353 also underwent expression changes in *mdf-1* mutant background at control conditions (Figure R-19A). This means that 71% of the total set of DEG after DNA damage induction display transcriptional changes in the absence of MDF (Statistical significance of the overlap  $p < 2.502e-47$ ).

DEG after zeocin incubation were classified into 10 clusters (Figure R-19B) (Yoshiyama *et al.*, 2020). GO term analyses of each of the clusters revealed the enrichment of various biological processes involved in the plant DNA damage response including Cell cycle in Cluster 6 or DNA repair in Cluster 7 (Yoshiyama *et al.*, 2020) (Figure R-19B). A minimum overlap of 64% was observed for every individual cluster. Thus, loss of MDF triggered expression changes in genes participating in most of the processes induced after DNA damage. Interestingly, 100% of the genes associated to DNA repair in Cluster 7 were found to be differentially expressed in *mdf-1* mutant background. Altogether these analyses indicate that loss of MDF and zeocin incubation activate a similar transcriptional program.

Additionally, the overlap between differentially expressed (15188 genes) and/or increased intron retained targets in *mdf-1* (1423 genes) and the set of 146 genes that are known as direct targets of SOG1 after DNA damage was calculated (Ogita *et al.*, 2018). 99 genes, which constituted 68% of the total set of SOG1 targets were found with a significance level of  $p < 0.005$  (Figure R-20A). As anticipated based on the central role of SOG1 in the plant DDR, the overlapping genes were involved in multiple responses altered upon DNA damage, including DNA repair and Cell cycle (Figure R-20B).

Interestingly, a significant correlation of 20% (Statistical significance of the overlap  $p < 0.024$ ) was maintained when comparing transcripts that showed either IR or strong miss expression in *mdf-1*, by only considering those genes with  $\text{Log}_2\text{Fold}$  changes above 2 (783 genes) and below -2 (1557 genes). Among them were the transcription factors ANAC044 and ANAC085, which were highly upregulated with  $\text{Log}_2\text{Fold}$  changes of 2.4 and 5.3 respectively. Moreover, RNA sequencing analyses also found ANAC085 to be differentially spliced in *mdf-1*.

ANAC044 and ANAC085 have been recently characterized as important components in the cell cycle arrest activated upon DNA damage. Increased expression of ANAC044 and ANAC085 leads to G2-specific cell cycle arrest by promoting the accumulation of R1R2R3-type MYB (Rep-MYB) transcription factors, which negatively control the expression of G2/M genes (Takahashi *et al.*, 2019). To further investigate if the lack of MDF resulted in DNA damage related-miss expression of mitotic specific genes, the set of 279 down regulated in *mdf-1* associated with the Biological Process GO term “cell cycle” (Figure R-18), were compared to the 80 loci reported to be induced after DNA damage in *myb3r1,3,5* triple mutants (Bourbouse *et al.*, 2018). 30 genes, which constitute 38% of the total of Rep-MYB DNA damage induced targets (Statistical significance of the overlap  $p < 1.798e-39$ ), were

## RESULTS

found to be transcriptionally repressed in *mdf-1* (Figure R-20C). This provides more evidence to support the putative role of MDF in DNA damage-induced cell cycle control.

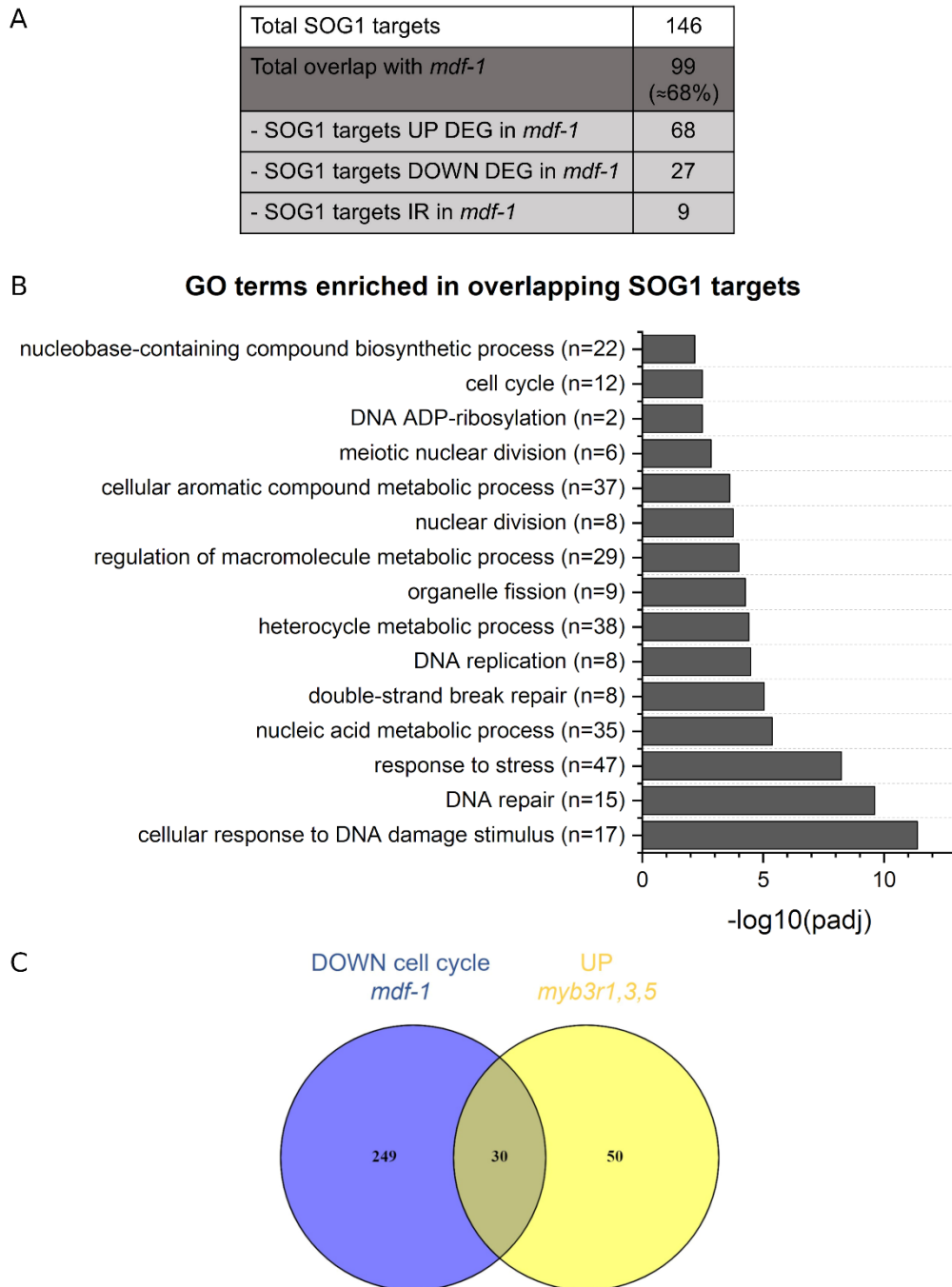


**Figure R-20. Miss expressed genes in *mdf-1* are involved in DNA damage-induced cell cycle control.** (A) Quantification of the overlap between direct SOG1 targets and genes showing IR or differential expression in *mdf-1*. (B) Biological Process GO enrichment analyses of the 99 overlapping genes found in (A). (C) Venn diagram representing the overlap between the 279 down-regulated genes in *mdf-1* associated with the GO biological process “cell cycle” and the 80 loci upregulated in *myb3r1,3,5* mutant background after DNA damage induction.

RT-qPCR experiments with 12-day-old *mdf-1*, *mdf-2*, WT and *mdf-1::pMDFMDFg* lines verified that the increased *ANAC044* and *ANAC085* expression and reduced transcript levels of G2/M specific genes were dependent on MDF. In both mutant lines the expression of *ANAC085* and *ANAC044* was significantly increased as compared to WT and the complemented line (Figure R-21A). In contrast, as anticipated, each of the seven mitotic genes tested showed an opposite expression pattern (Figure R-21B).

Surprisingly, in *mdf-1::pMDFMDFg* the downregulation of some mitotic genes (like *SCL28* and *IMK2*) was not only reversed to WT levels, but even switched to significant upregulation (Figure R-21B). This could be explained by increased *MDF* transcript levels in the complemented line in comparison to WT (Figure R-21C) and would suggest that MDF has a direct role in the transcriptional activation of these mitotic genes.

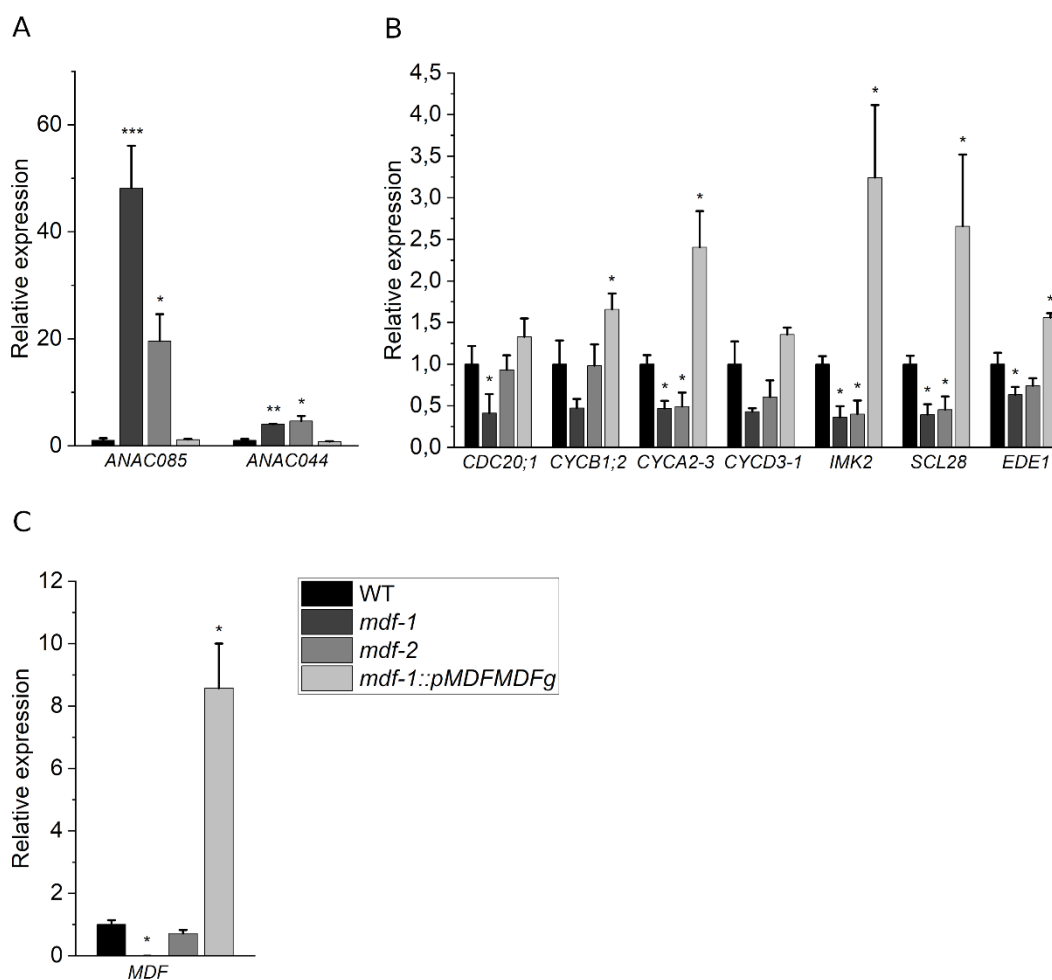


**Figure R-21. MDF controls the expression of genes associated to cell cycle control upon DNA damage.** (A-C) RT-qPCR experiments in 12-day-old WT, *mdf-1*, *mdf-2* and *mdf-1::pMDFMDFg* lines to test the expression of ANAC transcription factors (A), G2/M specific genes (B) and *MDF* (C) Average  $\pm$  Standard deviation of at least two independent biological replicates is shown. \* $P < 0.05$ ; \*\* $P < 0.005$ ; \*\*\* $P < 0.0005$  in comparison to WT as determined by a two-tailed Student's t-test.

#### 4.4 MDF acts independently or downstream from DDR regulators SOG1 and ATM

##### 4.4.1 The cell cycle and growth arrest observed in *mdf* mutants is not rescued by the absence of SOG1 and ATM

To further explore the putative function of MDF in genome stability, double mutants with *sog1-7* and *atm-2* were generated for both *mdf* mutant alleles. Phenotypical analyses of these lines would reveal whether the constitutive cell cycle arrest and cell death accumulation in the RAM of *mdf* mutants is correlated to ectopic activation of SOG1 or its upstream regulator ATM.

For this reason, the RAM of 3 DAG *mdf-1sog1-7*, *mdf-2sog1-7*, *mdf-1atm-2* and *mdf-2atm-2* double mutants was analysed by confocal microscopy (Figure R-22A). All double mutant combinations displayed a significantly lower number of dividing cells compared to WT, *sog1-7* and *atm-2* mutants (Figure R-22B). Furthermore, the shorter proximal meristem size in *mdf-1sog1-7*, *mdf-2sog1-7*, *mdf-1atm-2* and *mdf-2atm-2* was accompanied by a significantly reduced primary root length 3 DAG (Figure R-22C). While cell division and root growth retardation in *mdf-1atm-2* and *mdf-2atm-2* was equivalent to the one measured in their respective *mdf* single mutants (Figures R-22B and C), *mdf-1sog1-7* and *mdf-2sog1-7* double mutants showed a significantly slightly less pronounced cell division decrease in comparison to *mdf-1* and *mdf-2* (Figure R-22B). Moreover, the mild increase in cell division in *mdf-1sog1-7* resulted also in longer roots 3 DAG in comparison to *mdf-1* (Figure R-22C). Additionally, the combined loss of MDF and SOG or MDF and ATM had no apparent impact in later developmental stages: *mdf-1atm-2* remained dwarf after 4 weeks growth in soil (Figure R-22D) and *mdf-2sog1-7* plants retained the sterility previously reported for *mdf-2* (Figure R-22E).

These results suggest that the cell cycle and growth arrest observed in *mdf* mutants occurs independently of SOG1 and ATM. The slight significant increased number of dividing cells in the RAM of *mdfsog1-7* double mutants could be fortuitous. On the other hand, assuming that SOG1 induces cell cycle arrest independently of MDF, loss of SOG1 would relieve additional cell division suppression, resulting in more active cell division as observed in *mdf-1sog1-7* in comparison to *mdf-1*.

To understand whether the reduced cell division of *mdf-1sog1-7* and *mdf-2sog1-7* in comparison to WT was dependent on ANAC085 and ANAC044 G2/M specific cell cycle arrest, the expression of both transcription factors was tested via RT-qPCR (Figure R-22F). Significantly increased expression of both *ANAC085* and *ANAC044* was observed in *mdf-1sog1-7* and *mdf-2sog1-7* 12-day-old seedlings. Similar overexpression levels were previously seen in their respective single *mdf* mutants (Figure R-21A). Surprisingly, significantly elevated levels were also found in *sog1-7* in comparison to WT. Nevertheless,



the upregulation of *ANAC085* and *ANAC044* in *sog1-7* mutant background was much lower than in *mdf* and *mdfsog1-7* plants. These findings suggest that *ANAC085* and *ANAC044* increased expression in *mdf* mutants is not dependent on SOG1. Moreover, it indicates that *ANAC085* and *ANAC044* induction is not exclusively mediated by SOG1, since *sog1-7* loss of function mutants showed a slight upregulation at control conditions. A SOG1 independent transcriptional activation of *ANAC085* and *ANAC044* was previously shown under heat stress conditions (Takahashi *et al.*, 2019).

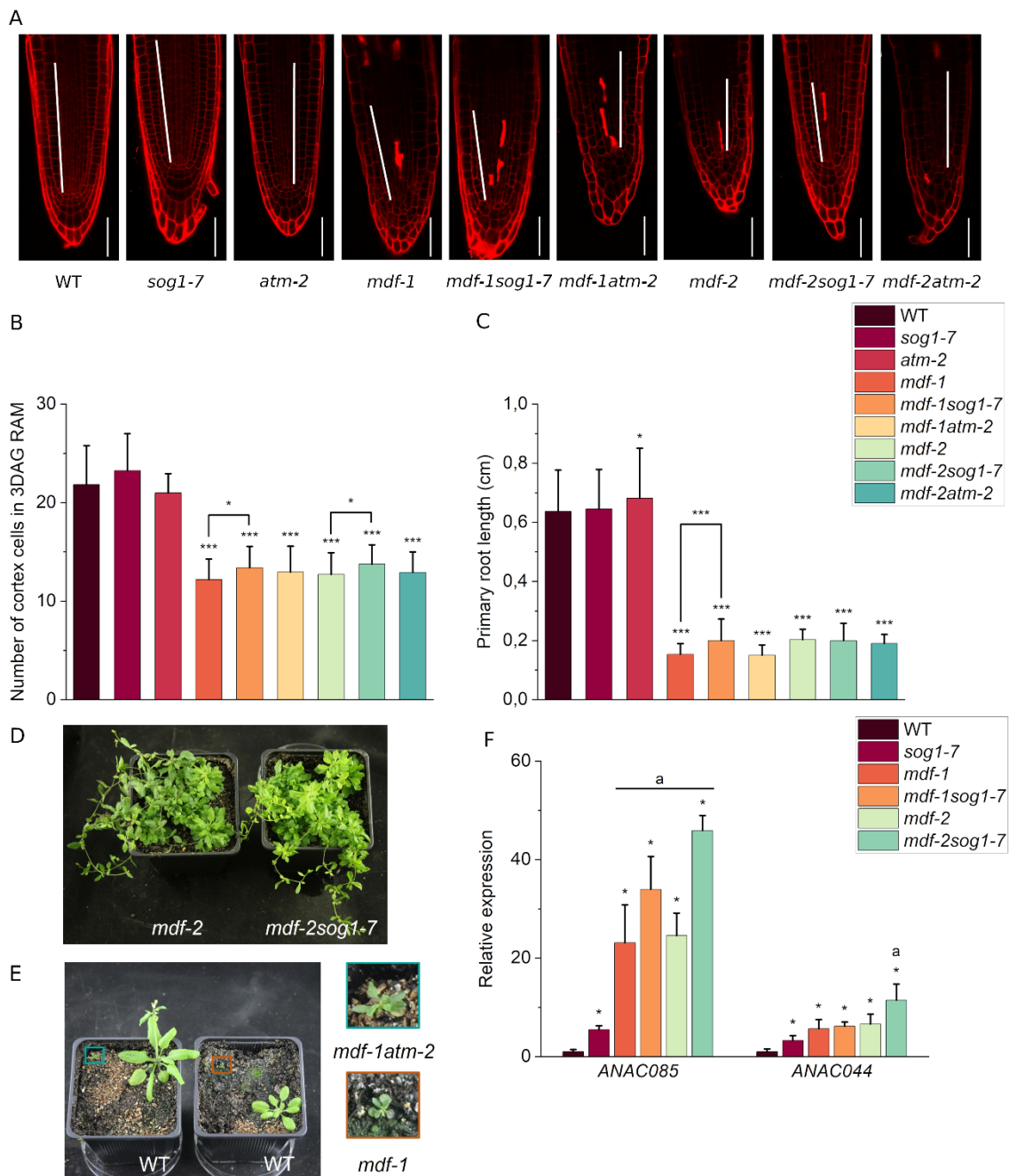


**Figure R-22.** The cell cycle and growth arrest observed in *mdf* mutants is not rescued by the absence of SOG1 and ATM. (A) Representative confocal pictures of PI-stained 3 DAG root tips of the indicated genotypes. White bar indicates the division zone. Scale bar: 50  $\mu$ m. (B) Quantification of the number of dividing cells in the cortical layer of 3 DAG seedlings of WT (n=33), *sog1-7* (n=20), *atm-2* (n=10), *mdf-1* (n=50), *mdf-1sog1-7* (n=26),

## RESULTS

*mdf-1atm-2* (n=22), *mdf-2* (n=38), *mdf-2sog1-7* (n=40) and *mdf-2atm-2* (n=38). (C) Primary root length 3 DAG of WT (n=111), *sog1-7* (n=74), *atm-2* (n=146) *mdf-1* (n=57), *mdf-1sog1-7* (n=45), *mdf-1atm-2* (n=38), *mdf-2* (n=50), *mdf-2sog1-7* (n=51) and *mdf-2atm-2* (n=37) seedlings. (D) Representative picture of 9-week-old *mdf-2* and *mdf-2sog1-7* plants. (E) Representative picture of 4-week-old WT, *mdf-1* and *mdf-1atm-2* plants. The blue and orange squares indicate the size in the original picture of the magnified zones representing *mdf-1atm-2* and *mdf-1* respectively on the right. Average  $\pm$  Standard deviation is shown. \* $P < 0.05$ ; \*\* $P < 0.005$ ; \*\*\* $P < 0.0005$  in comparison to WT, *mdf-1* and *mdf-2* as determined by a two-tailed Student's t-test. (F) RT-qPCR experiments in 12-day-old WT, *sog1-7*, *mdf-1*, *mdf-1sog1-7*, *mdf-2* and *mdf-2sog1-7* lines to test the expression of *ANAC085* and *ANAC044* transcription factors. Average  $\pm$  standard deviation of three biological replicates is represented. \* $P < 0.05$  as determined by a One-way ANOVA test post hoc Tukey Kramer in comparison to WT. "a" represents \* $P < 0.05$  as determined by a One-way ANOVA test post hoc Tukey Kramer in comparison to *sog1-7*.

### 4.4.2 The accumulation of dead cells in the RAM in *mdf* mutants occurs independently of SOG1 and ATM

Additionally, prevalence of cell death as well as cell death area in the RAM at 2 and 3 DAG were also assessed for all double mutant combinations by confocal microscopy (Figure R-23).

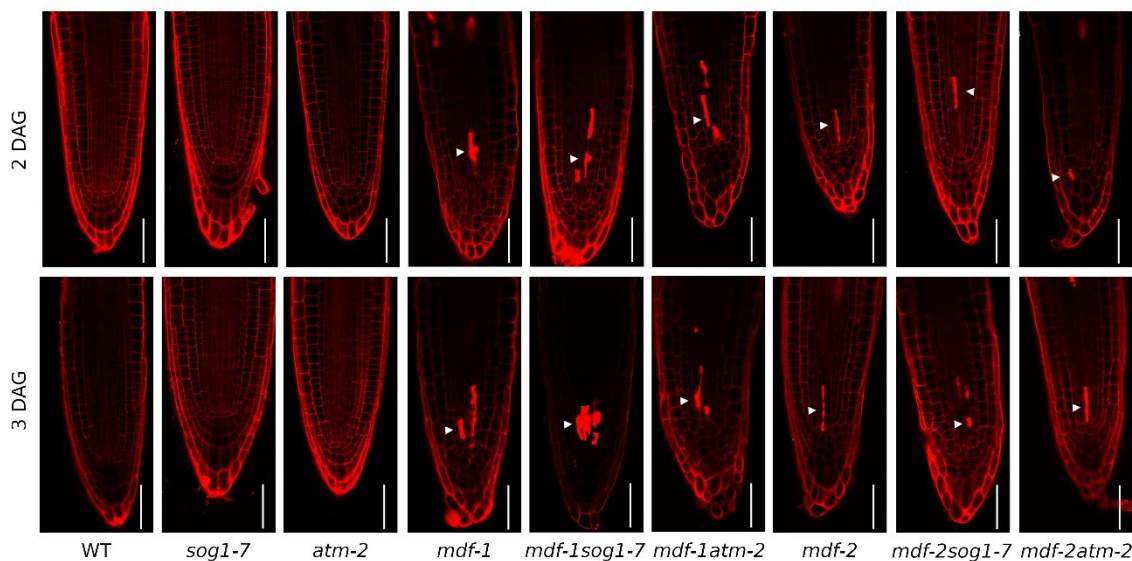


**Figure R-23.** The accumulation of dead cells in the RAM in *mdf* mutants occurs independently of SOG1 and ATM. Representative confocal pictures of PI-stained 2 and 3 DAG root tips of the indicated genotypes. Arrowheads indicate dead cells. Scale bar: 50  $\mu$ m.

Quantification of the cell death area using the Image J software revealed no drastic changes in the accumulation of dead cells in *mdfsog1-7* and *mdfatm-2* double mutants (Figure R-24A). A slight significant increase was observed for *mdf-1atm* at 2DAG and *mdf-2sog1-7* at 3DAG. Since this higher cell death accumulation was not consistent in all double mutant lines, it was not considered as relevant. However, the number of plants displaying cell death in the RAM was significantly higher in both *mdf-1sog1-7* and *mdf-1atm-2* double mutants at 2 and 3



DAG (Figure R-24B). This indicates that genome instability was further increased in the absence of SOG1 and ATM in *mdf-1* background. Furthermore, elevated occurrence of cell death in the absence of SOG1 after long term exposure to DNA damage has been correlated with inefficient activation of DNA repair processes and the occurrence of mitosis in cells with a compromised genome (Furukawa *et al.*, 2010; Johnson *et al.*, 2018). This phenomenon was also recently reported in double mutants for *MAINTENANCE OF MERISTEMS (MAIN)* and *SOG1*. *main-2sog1-7* double mutants presented increased cell death ratios than *main-2* single mutants, resembling the phenotype of *sog1-7* single mutants after long term exposure to genotoxic drugs (de Luxán-Hernández *et al.*, 2020).

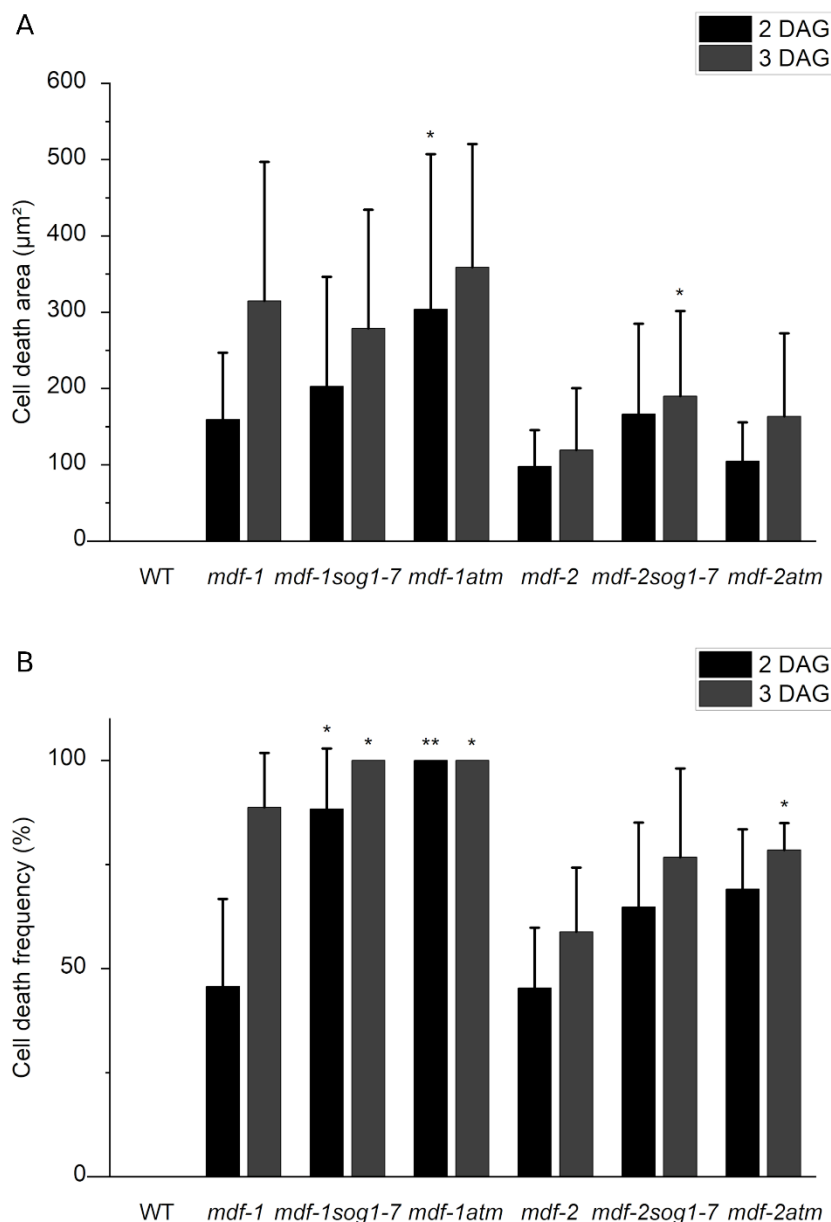


**Figure R-24.** *mdf-1sog1-7* and *mdf-1atm-2* double mutants exhibit increased cell death frequency than *mdf-1* single mutants. (A) Quantification of the cell death area and (B) percentage of plants containing dead cells in root tips of WT (n=21 and n=22), *mdf-1* (n=21 and n=95), *mdf-1sog1-7* (n=32 and n=25), *mdf-1atm-2* (n=26 and n=24), *mdf-2* (n=33 and n=59), *mdf-2sog1-7* (n=47 and n=39) and *mdf-2atm-2* (n=35 and n=46) lines at 2

## RESULTS

and 3 DAG. Statistical significance was determined in comparison to *mdf-1*. Average  $\pm$  Standard deviation is represented. \*P < 0.05; \*\*P < 0.005; \*\*\*P < 0.0005 as determined by a two-tailed Student's t-test.

### 4.4.3 Cell death accumulation in *mdf* and *mdfsog1-7* mutants is not influenced by temperature

Heat stress compromises DNA integrity mainly by the inhibition of DNA repair systems. However, in human cells it has been studied how heat stress can also directly produce different forms of DNA damage in a cell cycle stage dependent manner (Kantidze *et al.*, 2016). Upon heat stress induction, cells in G1 or G2 form double-stranded DNA breaks (DSBs), whereas single-stranded DNA breaks (SSBs) are produced in cells in S phase. Moreover, cells exposed to heat stress display an increased sensitivity to agents inducing double-stranded DNA breaks (DSBs) (Kantidze *et al.*, 2016).

In order to test whether cell death induction in *mdf* and *mdfsog1-7* double mutants was influenced by temperature, cell death area was compared at 17 and 22°C (Figure R-25).

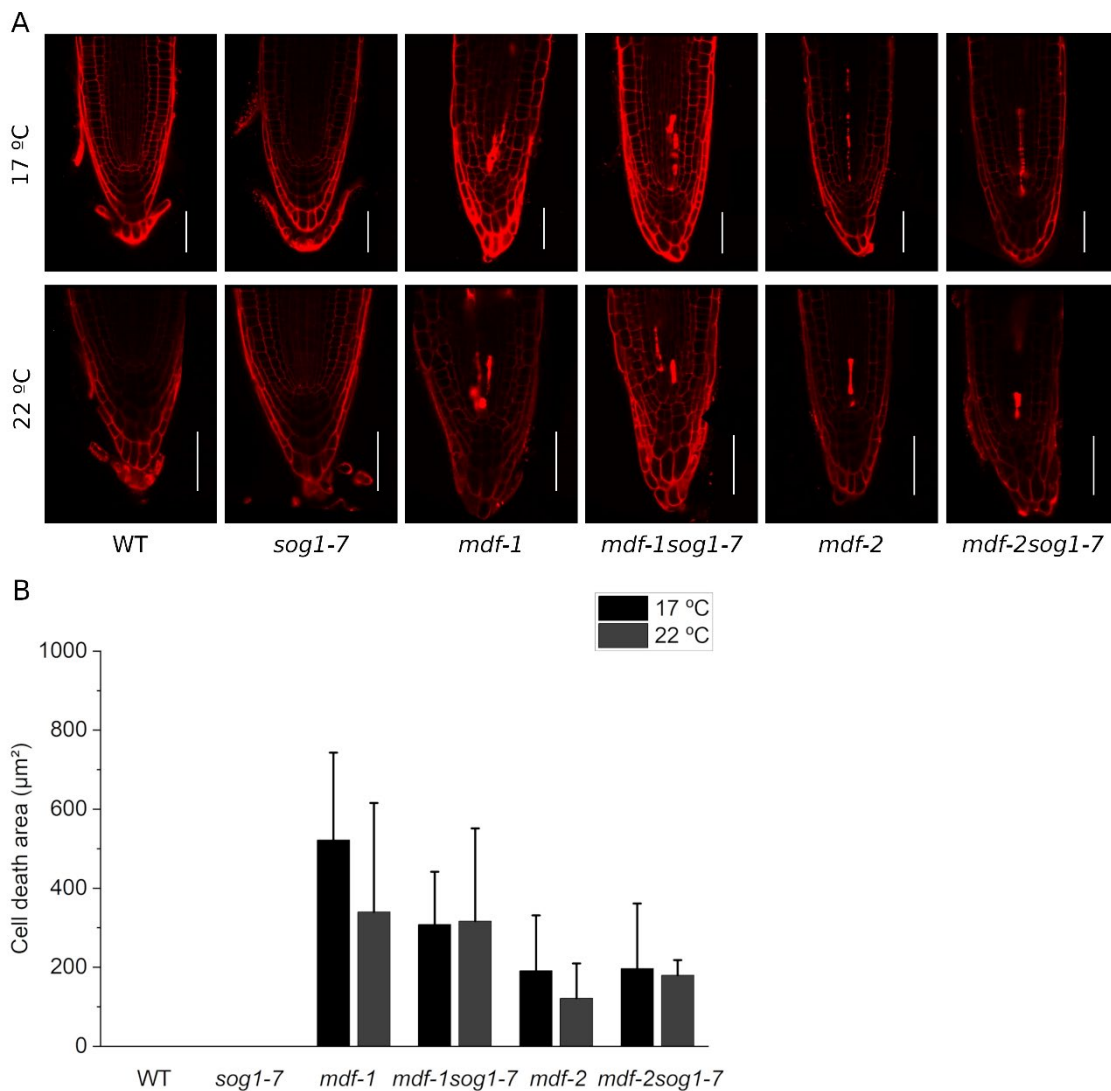


**Figure R-25. Cell death accumulation in *mdf* and *mdfsog1-7* mutants is not influenced by temperature.** (A) Representative confocal pictures of PI-stained root tips from the indicated genotypes grown for 8 days at 17°C (upper panel) and 6 days at 22 °C (lower panel). Scale bar: 50 µm. (B) Quantification of the cell death area at 17 and 22 °C from WT (n=3 and n=5), *sog1-7* (n=3 and n=5), *mdf-1* (n=5 and n=5), *mdf-1sog1-7* (n=8 and n=7), *mdf-2* (n=8 and n=6) and *mdf-2sog1-7* (n=6 and n=8) 6 and 8-day-old plants. Average ± standard deviation is represented.

No significant differences were found between both temperatures for any of the mutant lines, which suggests that low temperatures do not rescue the cell death phenotype of *mdf* mutants and that the absence of SOG1 does not influence this response. Nevertheless, further analyses should be carried out also at higher temperatures and with an increased number of plants.

#### 4.4.4 Expression of SOG1-dependent DDR genes in meristematic tissues of *mdf* mutants is influenced by SOG1

Finally, the influence of SOG1 in the expression of DNA repair genes in *mdf* background was assessed by performing RT-qPCR experiments on 3 DAG root tips of WT, *sog1-7*, *mdf* mutants and *mdfsog1-7* double mutants (Figure R-26).

While some SOG1 dependent DNA repair genes like *BREAST CANCER SUSCEPTIBILITY1 (BRCA1)*, *POLY(ADP-RIBOSE) POLYMERASE 1 (PARP1)* and *SIAMESE-RELATED 7 (SMR7)* presented a mild significant upregulation in either or both *mdf* mutants, their expression was unchanged in both *mdfsog1-7* double mutants compared to WT (Figure R-26A). Per contra, both double mutant lines showed significantly higher transcript levels than WT and *sog1-7* mutants of SOG1-independent *ETHYLENE RESPONSE FACTOR 115 (ERF115)* ERF transcription factor (Figure R-26B). ERF115 acts as a regulator of stem cell division (Heyman *et al.*, 2013) and is important for the generation of new tissue files after meristematic cell death to replace the damaged cells (Heyman *et al.*, 2016; Marhava *et al.*, 2019). Hence, increased expression of this transcription factor was expected based on the cell death accumulation and cell division defects reported in both *mdf* and *mdfsog1-7* mutants.

The mild upregulation detected for some DNA repair genes in meristematic tissue of *mdf* mutants further supports the hypothesis that the absence of MDF leads to a constitutive activation of the plant DDR. This increased DNA repair expression seems to be influenced by SOG1.

The results presented in Figures R-22 to 26 suggest that MDF acts either independently or downstream of SOG1 and ATM in its putative function in the plant DDR. Consequently, no major phenotypical differences were observed between *mdf* single mutants and double mutants additionally lacking SOG1 or ATM.

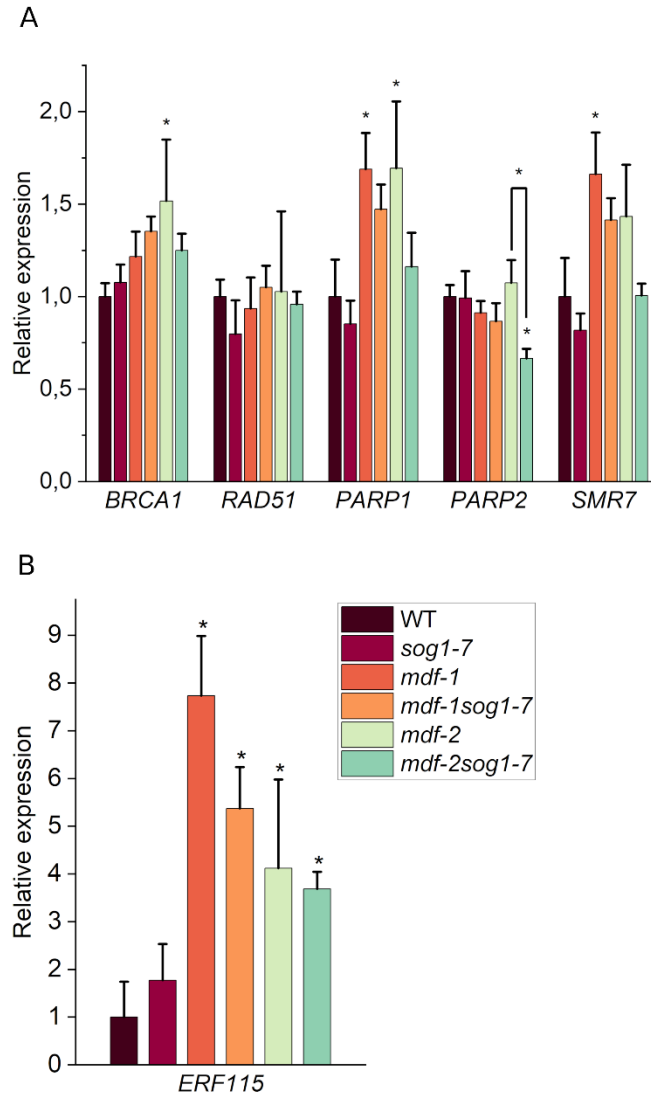


**Figure R-26. Expression of SOG1-dependent DDR genes in meristematic tissues of *mdf* mutants is influenced by SOG1.** (A-B) Expression analyses of DNA repair genes via RT-qPCRs in 3DAG root tips from the indicated genotypes in SOG1-dependent (A) and SOG1-independent (B) DDR targets. Average  $\pm$  standard deviation is represented. \* $P < 0.05$  as determined by a One-way ANOVA test post hoc Tukey Kramer in comparison to WT and *mdf-2*.

## 4.5 Analyses of the putative involvement of MDF in the plant DDR by assessing its response to different chemical treatments

To further characterize the putative role of mRNA splicing in genome stability, and in particular of MDF, sensitivity assays to different chemicals that compromise the DNA integrity (zeocin, hydroxyurea, H<sub>2</sub>O<sub>2</sub> and oryzalin) were carried out in *mdf* mutants.

In order to evaluate the prospective conserved role of pre-mRNA splicing in DNA damage control, the response to some of the drugs was also evaluated in loss of function mutants for four additional splicing factors. These were the SR-like protein SR45, the conserved splicing factor LSM8 and the SR proteins SR34 and SR34b.

SR45 was chosen due to its human homolog RNPS1, which was shown to play an important role in safeguarding genome stability and cell cycle control (Li *et al.*, 2007, Fukumura *et al.*, 2018). Additionally, lack of MDF led to decreased expression and altered splicing in *SR45* (Figure R-15). SR34 was shown to interact with SR45 (Stankovic *et al.*, 2016) and is also differentially spliced in *mdf-1* mutants. Its closest related protein SR34b is, like SR34, homologous to the human SR protein SRSF1 and has a role in Arabidopsis Cadmium tolerance regulation (Zhang *et al.*, 2014). This process has been linked to the plant DNA damage response (Wang *et al.*, 2016; Cao *et al.*, 2018; Hendrix *et al.*, 2020) and is upregulated among other stresses in the absence of MDF (Figure R-17). Lastly, the LSM8 splicing factor was chosen because of its indirect interaction with MDF (Table R-1 and Figure R-9) and its known role in AS and developmental processes after different kind of stresses (Carrasco-López *et al.*, 2017).

### 4.5.1 *mdf* mutants are hypersensitive to the DSB inducing drug zeocin

The response to double strand breaks (DSBs) was analysed by performing short and long-term experiments with zeocin, the commercial formulation of Phleomycin D1, a glycopeptide antibiotic of the bleomycin family, isolated from a mutant strain of *Streptomyces verticillus*. Its mechanism of action resides on the binding and intercalation to DNA, causing structural changes in the DNA double helix structure, leading to its functional arrest (Bérdy *et al.*, 1980).

#### 4.5.1.1 Splicing factors seem to be involved in the induction of cell cycle arrest after DNA damage treatment with zeocin

The impact of zeocin on cell division was evaluated in WT and the previously characterized T-DNA insertion mutants *mdf-1*, *mdf-2*, *sr45-1*, *sr34*, *sr34b* and *lsm8-1*. To this end, the number of cells in the cortex layer of the RAM in 3 DAG seedlings incubated ON in MS with (Z) or without zeocin (C) was compared (Figure R-27A).

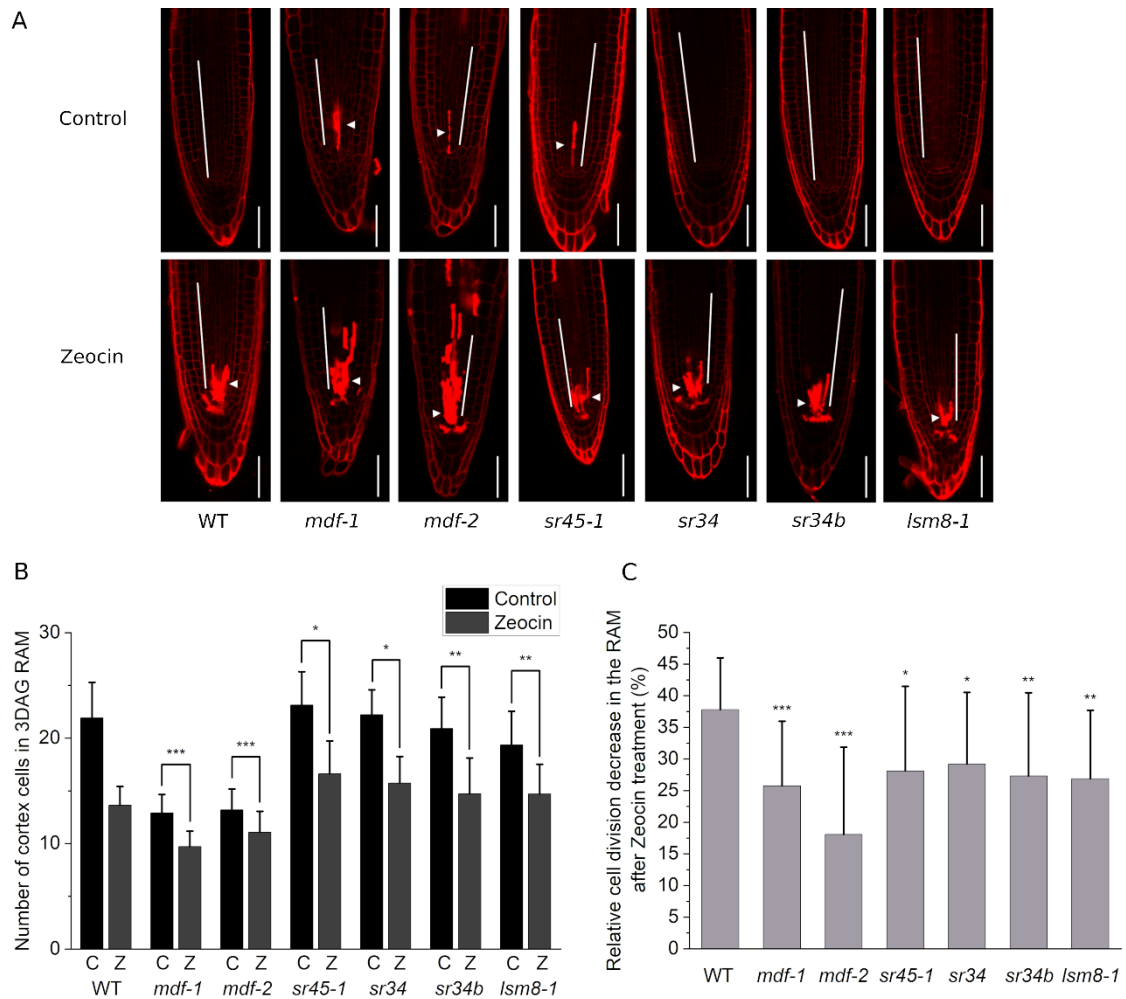


**Figure R-27. Splicing factors seem to be involved in the induction of cell cycle arrest after DNA damage treatment with zeocin.** (A) Representative confocal pictures of 3 DAG root tips of the indicated genotypes incubated ON in MS (Upper panel) or MS supplemented with zeocin 15  $\mu$ M (Lower panel). White bar indicates the division zone. Arrowheads point to dead cells. Scale bar: 50  $\mu$ m. (B) Quantification of the number of cells in the cortical layer of 3DAG RAM after ON incubation in MS (C) and MS supplemented with zeocin 15  $\mu$ M (Z) in WT (n=24 and n=30), *mdf-1* (n=22 and n=25), *mdf-2* (n=20 and n=29), *sr45-1* (n=15 and n=19), *sr34* (n=22 and n=19), *sr34b* (n=26 and n=29) and *lsm8-1* (n=17 and n=30). (C) Relative cell division decrease after zeocin treatment calculated from the data represented in (B) for the indicated genotypes. Average  $\pm$  Standard deviation is represented. \*P < 0.05; \*\*P < 0.005; \*\*\*P < 0.0005 as determined by a two-tailed Student's t-test in comparison to WT.

All lines tested exhibited a reduction in the population of dividing cells after zeocin treatment, which revealed that the response to DNA damage was not suppressed in the absence of MDF or any of the other proteins involved in pre-mRNA splicing (Figure R-27B). Nevertheless, in comparison to WT, the decrease in cell division was significantly less pronounced in all mutant lines (Figure R-27C). This suggests that specific splicing factors might be important for efficient induction of cell cycle arrest after zeocin treatment, by probably affecting the splicing of genes involved in DNA damage induced cell cycle arrest. For example, several

genes associated with cell cycle control were found to be alternatively spliced in *mdf* mutant background (Figures R-13C, R-15B and R-16C) including *CYCB2-2*, and the SOG1 direct targets *KRP6* and *ANAC085*.

#### 4.5.1.2 *mdf-1*, *sr45-1* and *lsm8-1* mutants display stronger root growth arrest than WT seedlings after DNA damage treatment with zeocin.

Changes in sensitivity to DNA damaging agents have been reported in mutant lines for genes involved in DNA damage induced cell cycle arrest. Primary root length measurements in loss of function mutants for *ANAC044* and *ANAC085* revealed a reduced primary root growth retardation in comparison to WT after treatment with different DNA damaging agents. Thus, an increased tolerance to DNA damage was reported for these lines (Takahashi *et al.*, 2019).

A similar experimental approach was followed to assess the sensitivity to zeocin in WT and the splicing mutants *mdf-1*, *mdf-2*, *sr45-1*, *sr34*, *sr34b* and *lsm8-1* (Figure R-28). To this end, seedlings were germinated on MS medium and transferred after five days to plates supplemented with zeocin. Measurement of root length at two, four, and six days after transfer (DAT) revealed that in each of the lines root growth was reduced in the presence of zeocin (Figure R-28A). Compared to WT; *mdf-1*, *sr45-1* and *lsm8-1* were significantly stronger affected by presenting complete growth arrest already four days after transfer to zeocin supplemented media. This reduced tolerance was further corroborated by phenotypical observations 14 DAT (Figure R-28B). Plants grown for 2 weeks in zeocin supplemented media were extremely arrested in comparison to WT and frequently exhibited yellowing of the leaves.

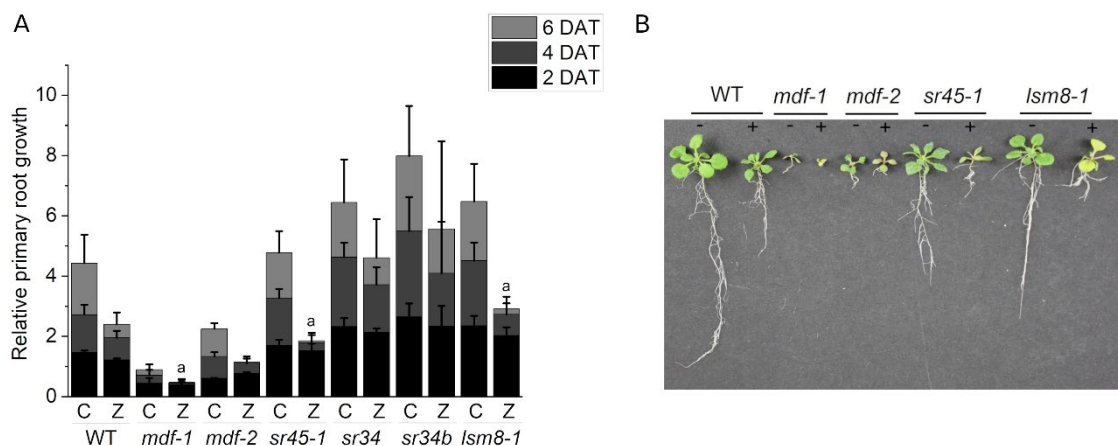


**Figure R-28.** *mdf-1*, *sr45-1* and *lsm8-1* mutants display stronger root growth arrest than WT seedlings after DNA damage treatment with zeocin. (A) Quantification of relative primary root growth in WT, *mdf-1*, *mdf-2*, *sr45-1*, *sr34*, *sr34b* and *lsm8-1* seedlings. Root length was measured at 3 DAG before transfer and at 2, 4 and 6 days after transfer (DAT) to MS medium (C) or medium supplemented with 20 $\mu$ g/mL zeocin (Z). The panel shows average ratio of root length  $\pm$  standard deviation from 2, 4 and 6 DAT/3 DAG for each line measured in at least three independent experiments (n >15 per condition and experiment). “a” represents no statistical difference between primary root length at 4 and 6 days after transfer according to a two-tailed Student’s t-test.



(B) Representative photograph of WT, *mdf-1*, *mdf-2*, *sr45-1* and *lsm8-1* seedlings at 18 DAG. At 4 DAG seedlings were transferred to MS medium (-) and MS medium supplemented with 20µg/mL zeocin (+).

The increased sensitivity in these lines could be correlated with a positive role of the three splicing factors in plant proliferation and development, in correlation with findings presented in this thesis for MDF and previously published for SR45 and LSM8 (Ali *et al.*, 2007; Perea-Resa *et al.*, 2012). At control conditions, important processes for plant development are compromised, leading to reduced growth in the three splicing mutants (Figure R-28B). Upon DNA damage, an impaired response in cell cycle arrest (Figure R-27) could be deleterious for the plant after continued exposure to zeocin, since a correct balance between stem cell maintenance and division is required to ensure the plant survival. This could explain the increased growth arrest displayed by *mdf-1*, *sr45-1* and *lsm8-1* in this experiment (Figure R-28A).

On the other hand, *sr34* and *sr34b* T-DNA insertion mutant lines showed no significant difference in the primary root growth ratio after transfer to zeocin in comparison to WT (Figure R-28A). An explanation for this could be the previously published putative genetic compensation between SR proteins and the lack of morphological defects found in neither *sr34* and *sr34b* single mutants nor *sr* quadruple mutants for SR30, SR34, SR34A and SR34B (Yan *et al.*, 2017).

#### 4.5.1.3 *mdf* mutants have an impaired response to DNA damage in the SAM

The effects of a putative defective DNA damage induced-cell cycle arrest in splicing mutants were also analysed in aerial tissues by assessing the formation of true leaves (Figure R-29A) and anchor roots (AR) in the presence of zeocin (Figure R-29B).

For the first experiment, seeds were germinated directly on MS medium and MS medium supplemented with two different concentrations of zeocin and grown horizontally under long-day conditions. Quantification of the seedlings that formed the first true leaf pair after 10 days of growth revealed that all mutant lines were more affected than the WT (Figure R-29A). True leaf formation was especially inhibited in *mdf-1*, *mdf-2*, *sr45-1* and *lsm8-1*, with a very low number of plants developing true leaves when grown in the highest zeocin concentration.

These results suggest that splicing mutants have an altered response to DNA damage also in shoot derived tissues. In accordance with the hypersensitivity reported in root growth arrest (Figure R-28A), *mdf*, *sr45-1* and *lsm8-1* mutants had an increased sensitivity to zeocin also in true leaf formation (Figure R-29A).

In the second approach to test DNA damage sensitivity in aerial tissues, the production of anchor roots at the hypocotyl was monitored at 10, 13 and 17 DAG in seedlings transferred at 4 DAG to MS medium (C) or MS medium supplemented with zeocin at a concentration of



20 $\mu$ g/mL (Z). Nearly 100% of the plants developed AR 17 DAG in both growing conditions with the exception of *mdf-1* (Figure R-29B). This developmental process was clearly delayed in *mdf-1* as previously documented in Figure R-1F. No significant changes were found in AR formation between treated and untreated plants in the WT, whereas *mdf* mutants displayed a reduction in AR formation when exposed to DNA damage. While *mdf-1* mutants started producing AR 10 DAG at control conditions, this process was delayed at least 7 days in the presence of zeocin. Moreover, in *mdf-2* plants (as symbolized by an “a” on the graph) the number of plants that formed AR was significantly reduced at 10 DAG in zeocin treated plants (Figure R-29B).

A significant difference was also observed in *lsm8-1* between both growth conditions, with a significant increase in AR production 10 DAG when grown in zeocin supplemented media (Figure R-29B).

Lastly, in *sr45-1* plants, as expected based on its delayed growth phenotype (Ali *et al.*, 2007), a reduced number of plants with AR was documented in comparison to WT at 10 DAG, independently of their growth conditions. At 13 DAG and 17 DAG an increasing trend in the production of AR was perceived in plants treated with zeocin, as described for *lsm8-1* at 10 DAG.

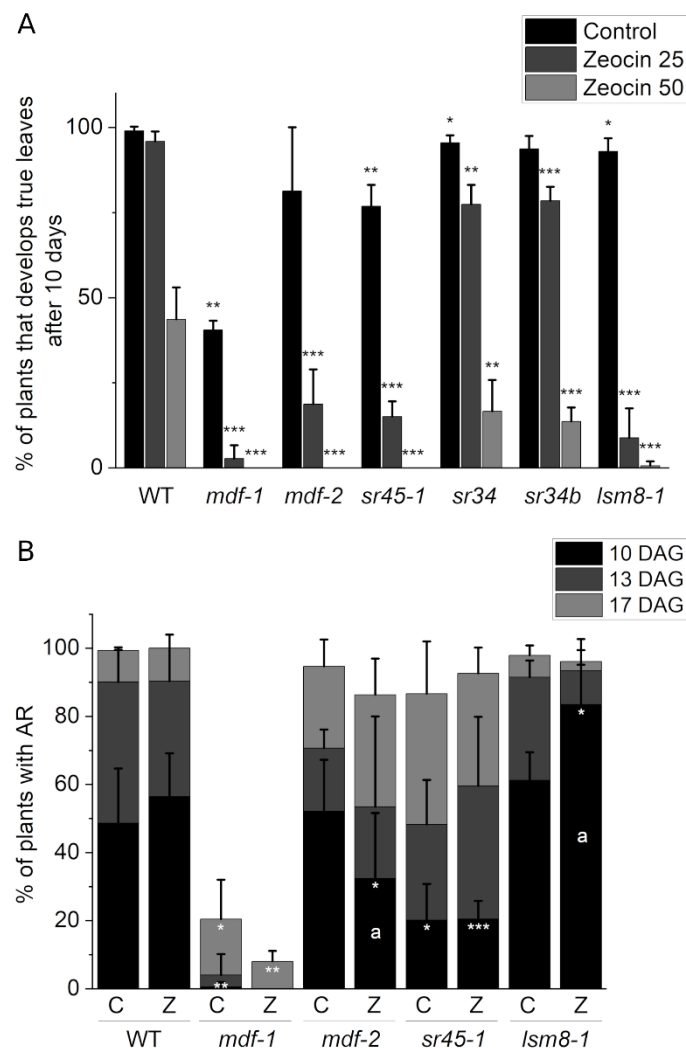


**Figure R-29. *mdf* mutants have an impaired response to DNA damage in the SAM.** (A) Percentage of plants that developed true leaves after 10 days growth on control conditions (Control) or on medium containing Zeocin 25 µg/mL (Zeocin 25) or Zeocin 50 µg/mL (Zeocin 50) for the indicated genotypes. Panel shows results from at least three independent experiments (n= at least 15 per line, condition and experiment). (B) Percentage of plants that developed anchor roots at 10, 13 and 17 DAG after transfer to MS medium (C) or MS medium supplemented with Zeocin 20 µg/mL at 4 DAG for the indicated genotypes. Panel shows results from at least three independent experiments (n= at least 15 per line, condition and experiment). Average ± standard deviation is represented. \*P < 0.05; \*\*P < 0.005; \*\*\*P < 0.0005 as determined in comparison to WT by a two-tailed Student's t-test. "a" represents statistical significance at 10 DAG between treatments in *mdf-2* and *lsm8-1*.

Adventitious root formation has been correlated with plant survival in mutants with a compromised RAM (Ühlken *et al.*, 2014). Therefore, after challenging the mutant lines to DNA damaging conditions, an increase in the development of AR was expected. A mild increasing trend was observed in both WT and *sr45-1* plants, with *sr45-1* showing this increase only at the later timepoints due to its delayed growth phenotype (Ali *et al.*, 2007). Moreover, this trend was particularly noticeable in *lsm8-1* seedlings with significantly higher number of plants producing AR after long term zeocin treatment at 10 DAG. In contrast, *mdf* mutants displayed the opposite behaviour. Since auxin transport and signalling regulate AR formation (Pacurar *et al.*, 2014), the defects reported in these biological processes in *mdf-1* (Casson *et al.*, 2009), could account for the abnormal response in these mutants. Moreover, the impaired formation of AR under constitutive DNA damaging conditions could be one of the reasons for the severe dwarf phenotype observed in the absence of MDF.

#### 4.5.1.4 MDF and SR45 are important for the correct induction of DNA repair transcripts after DNA damage

To test whether the hypersensitivity to DNA damage in *mdf-1*, *mdf-2*, *sr45-1* and *lsm8-1* was related to an altered transcriptional response to DNA damage, RT-qPCR experiments were carried out. To this end, 7-day-old seedlings were incubated for two hours in zeocin 100µM and the expression of five DDR-related genes was measured: *BREAST CANCER SUSCEPTIBILITY1 (BRCA1)*, *RAD51*, *POLY (ADP- RIBOSE)-POLYMERASE1 (PARP1)*, *POLY (ADP-RIBOSE)-POLYMERASE2 (PARP2)* and *SIAMESE-RELATED 7 (SMR7)*. Although all lines showed an increased expression of each of these genes upon zeocin treatment, the level of induction was lower in *mdf-1*, *mdf-2* and *sr45-1* than in WT, *sr34*, *sr34b* and *lsm8-1* (Figure R-30A). The reduced induction was verified especially in *sr45-1* after 6-hour incubation in bleomycin (B) (Figure R-30B), an analogous drug to zeocin also inducing DSBs. Even if the same tendency was observed, the lack of complete overlap between both drug treatments could be partially explained by the difference in incubation time. Experimental repetition with an increased number of biological replicates is required to confirm these results.

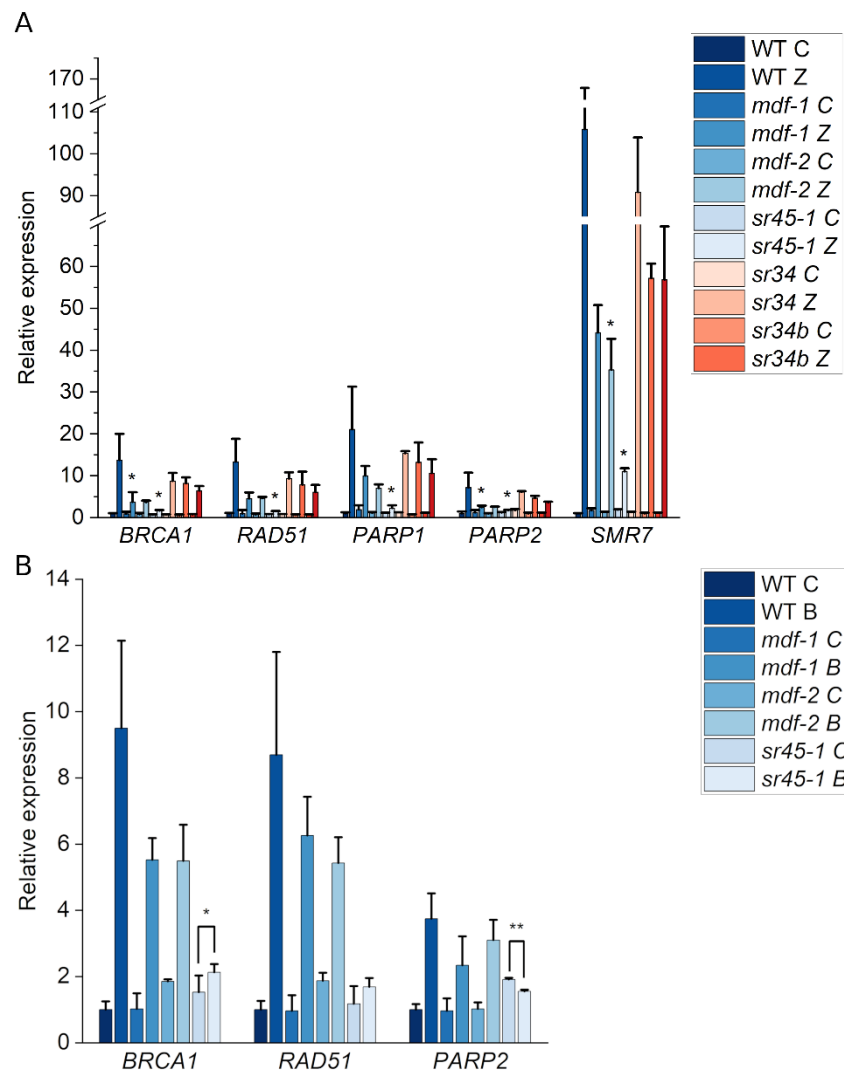


**Figure R-30. MDF and SR45 are important for the correct induction of DNA repair transcripts after DNA damage.** (A) RT-qPCR analysis showing induction of DDR-related genes in 2 biological replicates of 7-day-old seedlings of the indicated genotypes grown at control conditions (C) and after transfer to 100  $\mu$ M zeocin containing medium for 2 hours (Z). (B) RT-qPCR analysis showing induction of DDR-related genes in at least 2 biological replicates of 7-day-old seedlings of the indicated genotypes grown at control conditions (C) and after 6-hour transfer to 0,6  $\mu$ g/mL bleomycin containing medium (B). Average  $\pm$  standard deviation is represented. \* $P < 0.05$  as determined in comparison to WT by One-way ANOVA-test post hoc Tukey Kramer

Additional transcriptional analyses were performed in *mdf* mutants to confirm that the reduced expression of DDR related genes upon DNA damage induction took also place in meristematic tissues -where accumulation of dead cells was previously documented-(Figure R-31A). To this end, 3 DAG root tips incubated for two hours in MS medium (C) or MS medium supplemented with zeocin 100 $\mu$ M (Z) were used to isolate RNA in *mdf* mutants and WT seedlings. Additionally, *sog1-7*, *mdf-1sog1-7* and *mdf-2sog1-7* plants were also used to evaluate whether the reduced expression of DDR genes was SOG1 dependent.

## RESULTS

As expected, *sog1-7* and *mdfsog1-7* mutants presented no induction of DDR genes after zeocin incubation, except for *BRCA1* and *SMR7* in *mdf-2sog1-7* (Figure R-31A). This residual response could be explained by the remaining expression of the C-terminus of MDF in *mdf-2* background, which could potentially be able to partially activate the induction of these plant DDR transcripts. This also indicates that the induction of DDR genes upon DNA damage in *mdf* mutants is mostly SOG1-dependent.

All tested genes displayed an increased expression in WT and *mdf* background, but this induction was significantly lower in *mdf* mutants in *BRCA1*, *PARP2* and *SMR7* (Figure R-31A), as already observed when using complete seedlings in Figure R-30A. These new results confirm that MDF and SR45 are required for efficient transcript induction of genes involved in the plant DNA damage response, for example by modulating the splicing of DNA repair transcripts such as *RAD51D* (Figure R-15E). Moreover, this response was unchanged when using only meristematic young tissue or older complete seedlings as tissue source, suggesting that *mdf* mutants are able to respond to external DNA damage in all tissues, even those that show accumulation of dead cells.

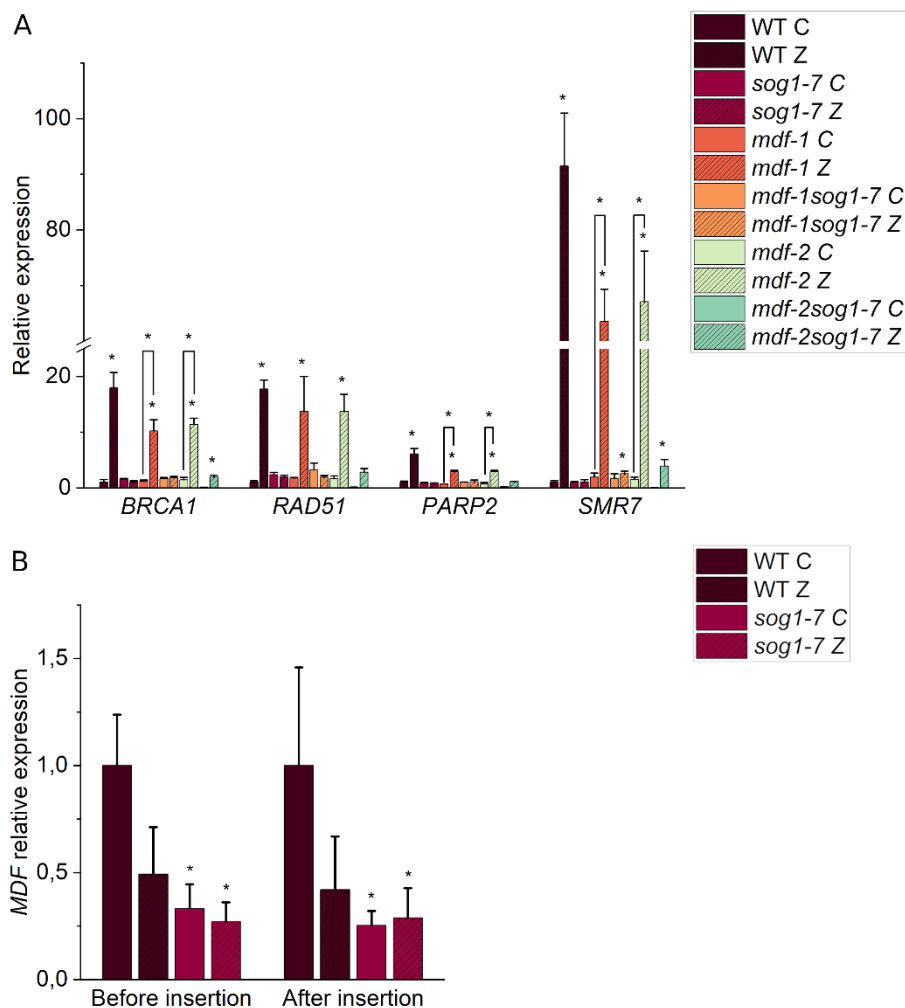


**Figure R-31.** The transcriptional response to DNA damage in *mdf* meristematic tissues is reduced and SOG1-dependent. (A) RT-qPCR analysis showing induction of DDR genes in 3 biological replicates of 3 DAG root tips

of the indicated genotypes grown at control conditions (C) and after transfer to 100  $\mu$ M zeocin containing medium for 2 hours (Z). (B) RT-qPCR analysis showing the transcript levels of *MDF* (before and after the T-DNA insertion sites in *mdf* mutants) in WT and *sog1-7* 3 DAG root tips grown at control conditions (C) and after transfer to 100  $\mu$ M zeocin containing medium for 2 hours (Z) used in (A). Primers used for this experiment were described in Figure R-5B. Average  $\pm$  standard deviation is shown. \* $P < 0.05$  as determined in comparison to WT by One-way ANOVA-test post hoc Tukey Kramer.

To determine whether the role of MDF in DNA repair transcript induction upon DNA damage was regulated at the transcriptional level, *MDF* expression was evaluated in WT and *sog1-7* root tips treated and untreated with zeocin (Figure R-31B). While no significant differences in *MDF* transcript levels were perceived in plants incubated in zeocin in comparison to control conditions for both genotypes, *sog1-7* mutants displayed lower expression than WT independently of the treatment. Hence, it could be speculated that SOG1 is important for MDF transcriptional activation, further supporting the hypothesis that MDF could act downstream of SOG1 (Figures R-22 to 26). Additionally, the lack of induction upon DNA damage in the WT indicates that MDF could be regulated after DNA damage in a post-transcriptional way. Further studies are necessary to verify this claim.

#### 4.5.1.5 DNA damage dependent accumulation of dead cells after zeocin treatment is reduced in *mdf-1* mutants

RT-qPCR experiments suggested that the reduced expression of DNA repair transcripts in *mdf* mutants was not a secondary effect of the accumulation of dead cells in the RAM, based on the similar response observed between samples only containing meristematic tissues with abundant cell death and complete seedling samples comprising all types of cells (Figures R-30A and R-31A).

To further evaluate the influence of constitutive cell death accumulation in *mdf* mutants in their response to external DNA damage, PI staining followed by confocal microscopy was carried out in 3 DAG seedlings incubated ON in Zeocin 15 $\mu$ M (Figures R-27A and R-32A). These experiments were also additionally performed in loss of function mutant for the other splicing factors.

PI staining of root tips revealed in each of the lines, including WT, a robust induction of cell death upon zeocin treatment (Figure R-32A). Moreover, consistent with the impaired induction of DNA repair genes, *sr45-1* seedlings frequently exhibited accumulation of dead cells in the division zone of the RAM at control conditions in a similar pattern as *mdf-1* and *mdf-2* (Figures R-27A and R-32A). This suggests that *mdf* and *sr45-1* seedlings present constitutive DNA damage which, due to their altered DNA repair activation upon DNA damage response, may lead to the induction of cell death in the RAM (Figures R-27A, R-30 and R-32A).

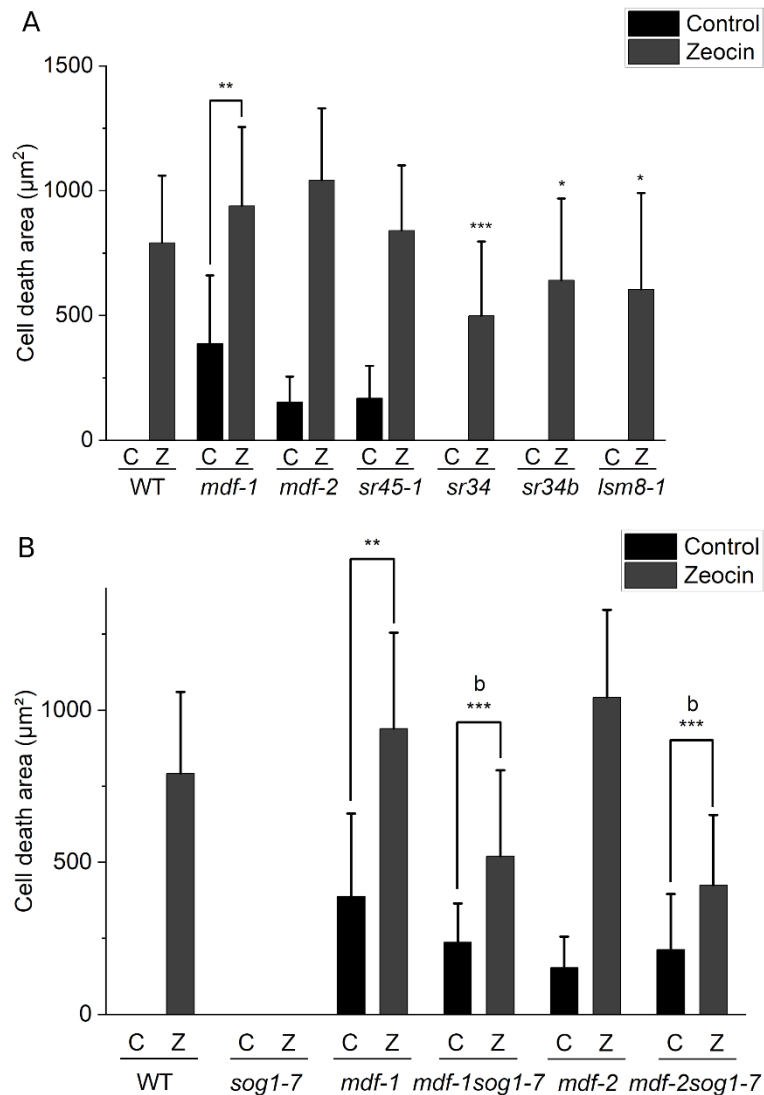


**Figure R-32.** DNA damage dependent accumulation of dead cells after zeocin treatment is reduced in *mdf-1*, *sr34*, *sr34b* and *lsm8-1* mutants. (A-B) Quantification of the cell death area in root tips of WT (n=38 and n=39), *mdf-1* (n=32 and n=35), *mdf-2* (n=31 and n=38), *sr45-1* (n=31 and n=30), *sr34* (n=31 and n=46), *sr34b* (n=33 and n=49), *lsm8-1* (n=32 and n=35), *sog1-7* (n=16 and n=19), *mdf-1sog1-7* (n=23 and n=21) and *mdf-2sog1-7* (n=27 and n=26) lines incubated ON in MS medium (C) or MS medium supplemented with Zeocin 15µM. Average ± standard deviation is represented. \*P < 0.05; \*\*P < 0.005; \*\*\*P < 0.0005 as determined in comparison to WT by a two-tailed Student's t-test. "b" represents a statistically significant reduced induction in *mdf-1sog1-7* and *mdf-2sog1-7* double mutants in comparison to *mdf-1* and *mdf-2* respectively.

Surprisingly, all splicing mutants except for *sr45-1* and *mdf-2* showed significant reduced induction of cell death after zeocin incubation in comparison to the WT (Figure R-32A). This suggests a conserved role for splicing proteins in the induction of cell death after DNA damage, which aligns with the reported presumed function of these splicing proteins also in DNA damage induced cell cycle arrest (Figure R-27). Several targets involved in programmed cell death after stress responses could also potentially be alternatively spliced or miss expressed in these mutants. This also fits with the 17 targets associated with the GO term "cellular response

to DNA damage stimulus” found in *mdf-1* RNA-seq analyses that overlapped with the set of known direct SOG1 targets (Figure R-20B).

The unaltered induction of cell death in *sr45-1* and *mdf-2* proves that merely cell death accumulation was not the cause of an impaired DNA damage response after DNA damage at the transcriptional level in these plants: *sr45-1* seedlings, which accumulate fewer dead cells in the RAM than *mdf-1* at control conditions, presented a more pronounced reduction in DNA repair transcript levels (Figure R-30). Furthermore, these results show again that *mdf-2* mutants might partially retain MDF’s function. In contrast to the other splicing factors, SR45 could not be directly involved in regulating the processes that promote the SOG1-dependent accumulation of dead cells after zeocin incubation in the RAM.

Since SOG1 is involved in the induction of cell death upon DNA damage (reviewed in Nisa *et al.*, 2019), the accumulation of dead cells after zeocin treatment was also monitored in *mdfsog1-7* double mutants in comparison to *mdf* single mutants, *sog1-7* and WT (Figure R-32B). As expected, *sog1-7* mutants did not respond to the treatment. Accordingly, *sog1-7mdf* double mutants displayed an even greater reduction in the area occupied by dead cells than *mdf-1* (Figure R-31A). This confirms that SOG1 is responsible for most of the cell death induction observed after DNA damage in *mdf* mutants. The combination of the genome instability and defective DNA repair processes presumed for *mdf* mutants and the absence of the major regulator of the plant DDR, could account for the induction of cell death still present in *mdfsog1-7* double mutants. This means that the elevated occurrence of cell death reported in *sog1-7* single mutants after long term exposure to DNA damage (Furukawa *et al.*, 2010; Johnson *et al.*, 2018) could be enhanced in *mdfsog1-7* double mutants treated with zeocin based on their putative increased genome instability at control conditions.

Alternatively, additional pathways independent of SOG1 with a role in the plant DDR, specifically in cell death induction, could be more active in the combined absence of MDF and SOG to try to compensate their loss and ensure plant survival. This would result in the increased cell death accumulation perceived in the double mutants after zeocin incubation (Figure R-32B).

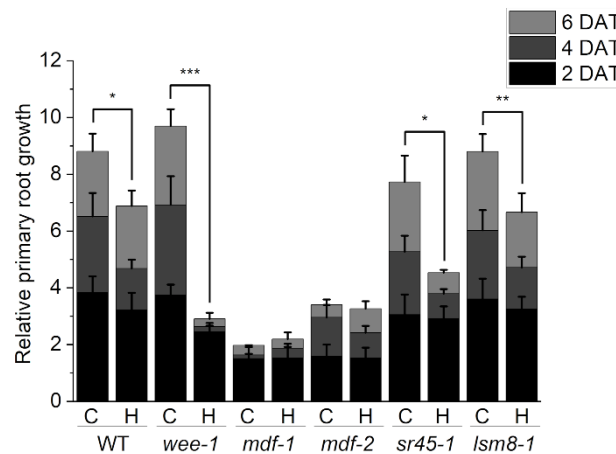
#### 4.5.2 *mdf* mutants are insensitive to the replication inhibitor Hydroxyurea

The effect of replication stress on the *mdf* phenotype was evaluated by assessing primary root growth and *MDF* induction in the presence of hydroxyurea (HU), a drug that causes depletion of deoxynucleotide triphosphates (dNTPs) (Koç *et al.*, 2004).

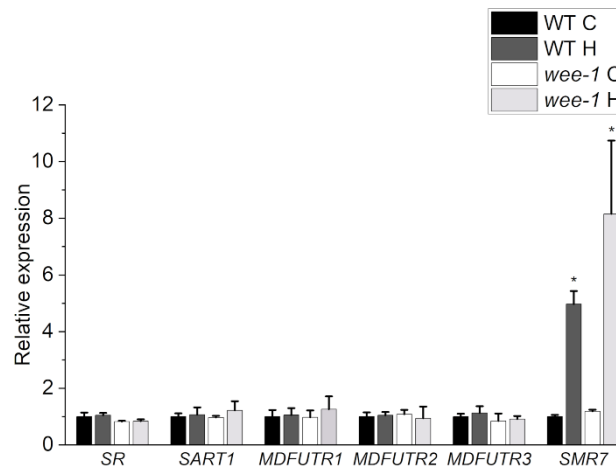
4.5.2.1 Root growth in *mdf* mutants is not affected by HU treatment

To evaluate the impact of HU on root growth, *mdf-1*, *mdf-2*, *sr45-1*, *lsm8-1* and WT plants were transferred after 5 days in light to MS medium (C) and MS medium supplemented with 1,5 mM HU (H) for 6 additional days. Relative growth 2, 4 and 6 days after transfer (DAT) is represented on the histogram (Figure R-33A). A knockout mutant for cell cycle inhibitory WEE1 kinase (*wee-1*), known to be hypersensitive to replication-inhibitory drugs, was used as a positive control (De Schutter *et al.*, 2007).

A



B



C

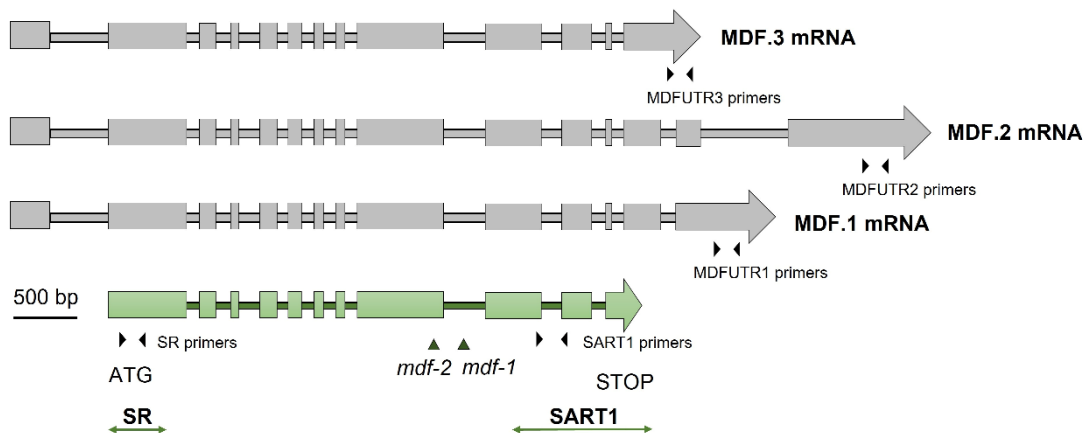




**Figure R-33. *mdf* mutants are not responsive to the replication inhibitor Hydroxyurea (HU).** (A) Quantification of relative primary root growth in WT, *wee-1*, *mdf-1*, *mdf-2*, *sr45-1* and *lsm8-1* seedlings. Root length was measured at 3 DAG before transfer and at 2, 4 and 6 days after transfer (DAT) to MS medium (C) or medium supplemented with 1,5mM HU (H). The panel shows average ratio of root length  $\pm$  standard deviation from 2, 4 and 6 DAT/3 DAG for each line measured in at least three independent experiments ( $n > 15$  per condition and experiment). \* $P < 0.05$ ; \*\* $P < 0.005$ ; \*\*\* $P < 0.0005$  as determined in comparison to control conditions by a two-tailed Student's t-test. (B) RT-qPCR analysis showing the transcript levels of different putative domains of MDF and the three splicing variants of the 3' ÚTR in *MDF* in WT and *wee-1* 7-day-old seedlings grown at control conditions (C) and after transfer to 1mM HU containing medium ON (H). Transcript levels of *SMR7* were measured as a positive control for the treatment. Average  $\pm$  standard deviation is shown. \* $P < 0.05$  as determined in comparison to WT by One-way ANOVA-test post hoc Tukey Kramer. (C) Schematical representation of the primers used in (B) to measure *MDF* expression levels. Narrow boxes represent introns and wide boxes represent exons. *MDF* CDS is shown in green, and the three different mRNA variants described in TAIR are shown in grey. Approximate position of the primer pairs used for RT-qPCR analyses are indicated with black arrowheads. Green arrowheads point to the insertion position of the *mdf-1* and *mdf-2* mutations. SR and SART1 domains predicted positions are represented with green arrows below *MDF* CDS.

WT, *wee-1*, *sr45-1* and *lsm8-1* seedlings displayed a significant reduction in primary root length after 6 days of growth in HU (Figure R-33A). This growth arrest was particularly acute in *wee-1* plants, whose relative root growth was nearly suppressed 2 DAT, demonstrating that they are hypersensitive to replication stress.

Per contra, *mdf* mutants showed no difference in root growth after transfer to HU. This could be caused by the growth arrest present in *mdf* mutants already at control conditions (Figure R-1B). However, in previous experiments following the same experimental approach, it was demonstrated that *mdf* mutants responded to zeocin, which significantly inhibited primary root growth in *mdf-1* 4DAT (Figure R-28A). Additionally, no growth reduction was also perceived in the less affected *mdf-2* mutant (Figure R-33A). Therefore, it could be speculated that *mdf* mutants are either not responsive or more tolerant to replication stress. An increased tolerance to HU treatment was already described in *rtel-1*, a knockout mutant for *DNA helicase Regulator of Telomere Length 1 (RTEL1)* (Hu *et al.*, 2015). The increased resistance to replication stress in this mutant in comparison to WT was explained by the slowdown of the DNA polymerase during S-phase due to the reduction in the pool of available dNTPs caused by HU treatment. While this slow progression is deleterious in WT and leads to large stretches of single-stranded DNA and to the accumulation of DNA breaks and damage, the hampered DNA unwinding in *rtel-1* background matches with the reduced activity of the DNA polymerase, resulting in shorter single-stranded DNA stresses and less DNA damage (Hu *et al.*, 2015).

The relationship between MDF and replication stress was further explored by measuring the transcript levels of the different putative domains of MDF (defined in the Results section 4.2.2) and the different splicing variants found in MDF 3' UTR as described in TAIR (Figure R-33B and C). To this end, RNA was isolated from WT and *wee-1* 7-day-old seedlings after

ON incubation in MS medium (C) or MS medium supplemented with HU 1,5mM (H). Additionally, the expression of *SMR7*, which is known to be induced after HU treatment in a WEE-1 independent manner (Yi *et al.*, 2014), was measured as a positive control of the methodological approach.

As expected, *SMR7* transcript levels were increased in both WT and *wee-1* lines. In contrast, no significant change was perceived neither between genotypes nor between growth conditions (Figure R-33B). Since both zeocin (Figure R-31B) and HU (Figure R-33B) treatments did not induce *MDF* expression, *MDF* is most likely not regulated after DNA damage at the transcriptional level.

#### 4.5.3 *mdf* mutants are less sensitive to the oxidative stress induced by H<sub>2</sub>O<sub>2</sub>

In addition to its effect on replication, HU has been shown to trigger the formation of reactive oxygen species (ROS) (Yi *et al.*, 2014). The putative role of ROS production in the reported tolerance of *mdf* mutants to HU was evaluated by performing long and short-term treatments with H<sub>2</sub>O<sub>2</sub>.

##### 4.5.3.1 H<sub>2</sub>O<sub>2</sub> treatment has a milder effect on primary root length and adventitious root formation in *mdf* mutants than in WT plants

One of the known effects of H<sub>2</sub>O<sub>2</sub> is its potential to act as a signalling molecule for the induction of cell division arrest by the activation of cell cycle checkpoints (Tsukagoshi, 2012). Therefore, the impact of this ROS compound on root growth arrest was assessed with two distinct experimental approaches.

On the first one, WT, *mdf-1* and *mdf-2* seedlings were transferred after 5 days in light to MS medium (C) and MS medium supplemented with H<sub>2</sub>O<sub>2</sub> 0,8 mM (H<sub>2</sub>O<sub>2</sub>). Root length was measured 7 and 10 DAT and relative root growth was calculated in relation to the root length measured before transfer (Figure R-34A). Incubation in H<sub>2</sub>O<sub>2</sub> for a week decreased the root growth of all lines. Nonetheless, this reduction was significantly less pronounced in both *mdf* mutants in comparison to WT (represented by a “b” on the histogram). After 3 additional days of ROS exposition, the differences between treated and untreated plants were milder, which suggests that, based on the light sensitivity of hydrogen peroxide, only low amounts of the chemical were still present in the media.

To examine whether H<sub>2</sub>O<sub>2</sub> influenced germination or early plant development in *mdf* mutants, a second experimental approach was carried out by directly germinating WT, *mdf-1* and *mdf-2* plants in MS medium supplemented with 0,8 mM hydrogen peroxide and monitoring their growth after 3, 5 and 12 days in light (Figure R-34B).

Long term exposure to  $H_2O_2$  decreased WT's primary root length with the strongest difference perceived after 12 days of treatment. The impact of this ROS species on *mdf* mutants was again milder: Almost no root length reduction was perceived in the mutants until day 12.

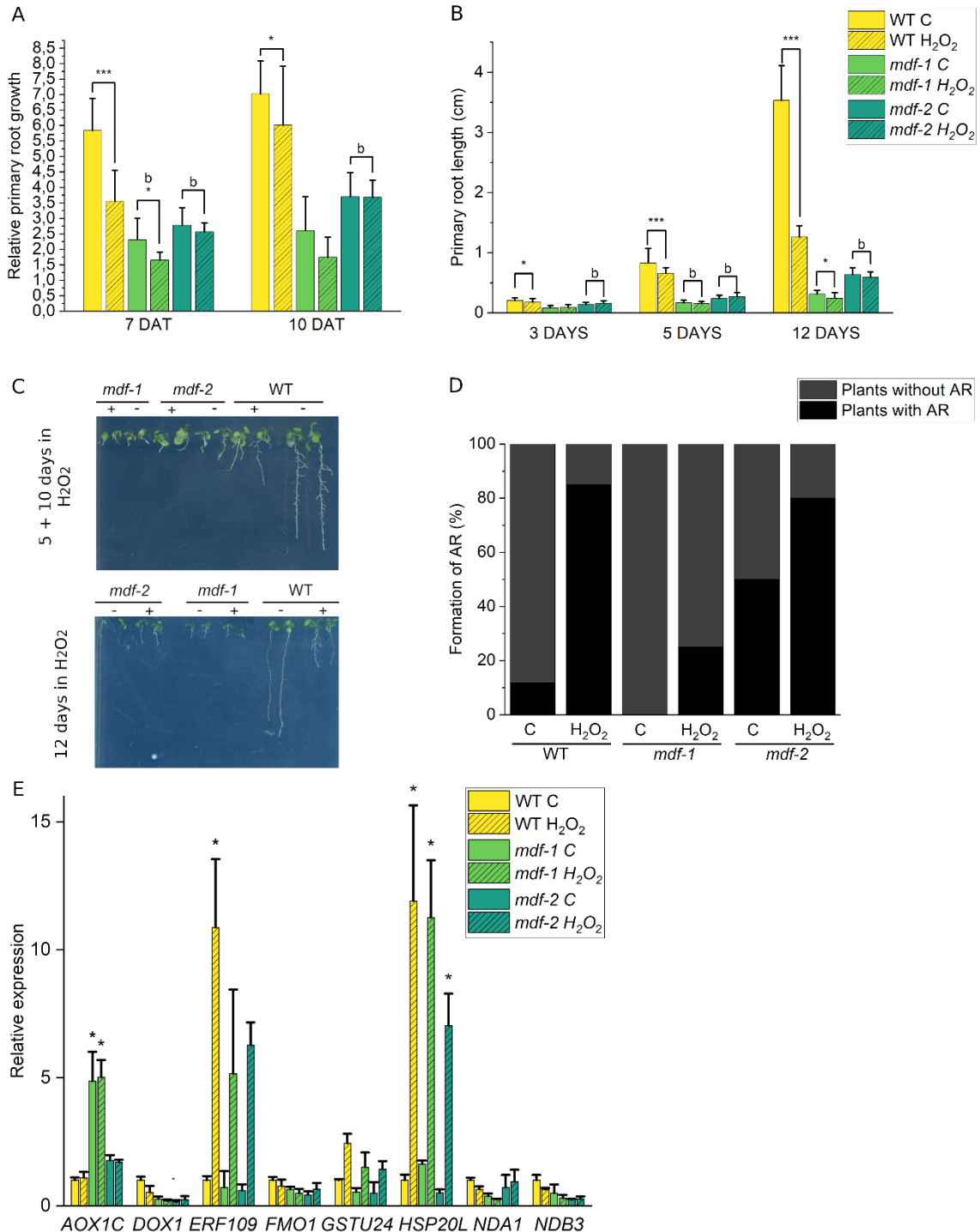


**Figure R-34. *mdf* mutants are less sensitive to the oxidative stress induced by  $H_2O_2$ .** (A) Quantification of relative primary root growth in WT, *mdf-1* and *mdf-2* seedlings. Root length was measured after 5 days in light before transfer and at 7 and 10 days after transfer (DAT) to MS medium (C) or medium supplemented with 0,8mM  $H_2O_2$  ( $H_2O_2$ ). The panel shows average ratio of root length  $\pm$  standard deviation from 7 and 10 DAT/5 days for

## RESULTS

each line in one technical replicate with a range of 4-32 plants per line and condition. (B) Quantification of primary root length in WT, *mdf-1* and *mdf-2* seedlings grown for 3, 5 and 12 days in MS medium (C) or MS medium supplemented with 0,8mM H<sub>2</sub>O<sub>2</sub> (H<sub>2</sub>O<sub>2</sub>). Average ± standard deviation of 9-48 plants per line and condition of one technical replicate is represented. \*P < 0.05; \*\*P < 0.005; \*\*\*P < 0.0005 as determined in comparison to control conditions by a two-tailed Student's t-test. "b" represents statistical difference to the reduction in root length after treatment observed in WT for the same timepoint determined by a two-tailed Student's t-test. (C) Representative scan of WT, *mdf-1* and *mdf-2* 15-day-old seedlings transferred after 5 days to MS medium (-) or MS medium supplemented with 0,8mM H<sub>2</sub>O<sub>2</sub> (+) in the upper panel and WT, *mdf-1* and *mdf-2* 12-day-old seedlings grown in MS medium (-) or MS medium supplemented with 0,8mM H<sub>2</sub>O<sub>2</sub> (+) in the lower panel. (D) Percentage of plants that formed anchor roots 10 DAT to MS medium (C) or medium supplemented with 0,8mM H<sub>2</sub>O<sub>2</sub> (H<sub>2</sub>O<sub>2</sub>). Panel shows measurements from the plants analysed in (A) for the 10 DAT timepoint and represented in the upper panel from (C). (D) RT-qPCR analyses to measure the transcript levels of the indicated ROS-inducible genes in 5-day-old WT, *mdf-1* and *mdf-2* seedlings incubated for 2 hours in MS medium (C) or MS medium supplemented with 0,5mM H<sub>2</sub>O<sub>2</sub> (H<sub>2</sub>O<sub>2</sub>). Average ± standard deviation of three biological replicates is shown. \*P < 0.05 as determined in comparison to WT by One way-ANOVA-test post hoc Tukey Kramer.

Anchor root formation was previously linked to ROS signalling. In fact, ROS species were suggested to mediate AR induction by regulating auxin biosynthesis and transport (Huang *et al.*, 2020). Since deficient AR formation was reported in *mdf-1* mutants (Figures R-1F and R-28B); in addition to primary root growth analyses, the effect of H<sub>2</sub>O<sub>2</sub> treatment on AR development was also evaluated (Figure R-34D). For this reason, the percentage of plants forming AR in the presence and absence of hydrogen peroxide 10 DAT (Figures R-34A and D) was calculated. Preliminary results based on one technical replicate suggest that H<sub>2</sub>O<sub>2</sub> has a positive influence on AR production, since all lines exhibited more AR after transfer to H<sub>2</sub>O<sub>2</sub>. This increase seems lower in *mdf* mutants, which could be related to their alterations in auxin regulation. Furthermore, the apparent increased resistance of *mdf* mutants to H<sub>2</sub>O<sub>2</sub> treatment in primary root length could also be connected to their defects in auxin signalling and transport. Additional experiments are needed to validate these data.

To verify that the higher tolerance observed in *mdf* mutants was not caused by a defective response to hydrogen peroxide, transcriptional analyses of ROS-responsive genes were carried out in 5-day-old WT, *mdf-1* and *mdf-2* seedlings incubated for 2 hours in 0,5mM H<sub>2</sub>O<sub>2</sub> (Figure R-34E). A significant induction was observed in WT plants only for *ETHYLENE RESPONSE FACTOR 109* (*ERF109*) and chaperon *HSP20-like*. Significant upregulation after H<sub>2</sub>O<sub>2</sub> incubation was confirmed in both *mdf* mutants also for *HSP20-like*. Additionally, *mdf-1* mutants displayed in both untreated and treated plants a significant increase in *ALTERNATIVE OXIDASE 1C* (*AOX1C*). The lack of statistical significance and thus discrepancy between WT and *mdf* plants in the induction of *ERF109*, could be motivated by the biological variability between replicates, especially in WT and *mdf-1* seedlings. Additionally, besides its role in ROS inhibition, *ERF109* has been suggested to retard programmed cell death (PCD) in tobacco (Bahieldin *et al.*, 2016). Therefore, it could be

speculated that the latter function could not be desirable in *mdf* background, based on the importance of the induction of cell death during the plant DDR to avoid the propagation of cells with severe genome integrity defects (Yoshiyama *et al.*, 2013; Hu *et al.*, 2016). Thus, additional mechanisms activated in the absence of MDF to ensure the plant viability, could have an inhibitory effect on *ERF109* expression, especially after additional external stress (e.g. H<sub>2</sub>O<sub>2</sub> incubation).

Lastly, the increased expression of *AOX1C* at control conditions in *mdf-1* suggests elevated ROS levels in this mutant, which could also be responsible for some of the putative DNA damage described in loss of function mutants for MDF.

These data suggests that *mdf* mutants are more tolerant to the external addition of ROS species. On one hand, a possible explanation would be the altered auxin regulation in *mdf* mutants, which would result in an impaired activation of several ROS-mediated developmental processes. On the other hand, the increased resistance could be related to the signalling function of H<sub>2</sub>O<sub>2</sub> in cell cycle arrest. Since G2/M arrest was documented in the absence of MDF (Figure R-2A), it could be speculated that the cell cycle arrest observed in *mdf* mutants is mediated by H<sub>2</sub>O<sub>2</sub>. Thus, no additional suppression could be expected.

Although two different experimental approaches confirmed this reduced sensitivity, the results comprised the findings of one technical replicate each. Therefore, experimental repetitions are required to validate the effect of ROS on *mdf* growth and AR formation.

#### 4.5.4 *mdf-1* mutants are insensitive to the microtubule depolymerizing drug oryzalin

Altered cell division has been associated with hypersensitivity to the microtubule-disrupting drug oryzalin in knockout mutants for components of the spindle assembly checkpoint (SAC) (Komaki and Schnittger, 2017). After growth in medium supplemented with oryzalin, these mutants presented elevated frequencies of cell death accompanied by increased cell death areas and reduced meristem sizes. Additionally, a significant reduction in root length was also reported (Komaki and Schnittger, 2017).

Since absence of MDF led to intron retention associated to downregulation of gene expression in targets associated to the GO terms “cell cycle”, “chromosome organization”, “cytoskeleton organization”, “spindle assembly” and “microtubule-based movement” (Figure R-16C), the relationship between microtubule depolymerization and the *mdf* phenotype was addressed by performing root length and cell death assessments in oryzalin treated seedlings.

#### 4.5.4.1 Primary root length and accumulation of dead cells in the RAM in *mdf-1* mutants is not affected by the disruption of microtubules after oryzalin treatment

The putative influence of microtubule depolymerization in the DDR mediated cell death induction and growth arrest was tested by growing WT, *sog1-7*, *mdf-1* and *mdf-2* seedlings in MS medium (C) or MS medium supplemented with oryzalin 200nM for 2 days after germination (Figure R-35A). Both WT and *sog1-7* treated seedlings exhibited a dwarf phenotype accompanied by anthocyanin accumulation in the hypocotyl, mimicking the *mdf* phenotype at control conditions. Since the *mdf* mutation is sterile, all experiments are always carried out with heterozygous plants. Therefore, the high resemblance between oryzalin treated WT and *mdf* homozygous mutants made it impossible to distinguish between heterozygous/segregating WTs and homozygous seedlings in the progeny of a *mdf* heterozygous plant grown in oryzalin 200 nM. Hence, cell death analyses were only performed in *sog1-7* and WT plants.

After growth in oryzalin, *sog1-7* and WT root tips exhibited similar cell death patterns (Figure R-35B). This suggests that cell death accumulation after oryzalin treatment is SOG1 independent and putatively unrelated to the plant DDR.

Confocal analyses were also performed with *mdf* mutants grown in a lower concentration of oryzalin. At 100 nM, homozygous and heterozygous *mdf* plants could still be phenotypically differentiated. An increase in cell death accumulation was only observed in *mdf-2* mutants, whereas *mdf-1* treated and untreated seedlings had equivalent values of cell death areas (Figure R-35C). Elevated cell death in *mdf-2* mutants after oryzalin treatment was accompanied by a significant reduction in root length (Figure R-35D). Only WT plants presented also a significant change in primary root length after long exposition to oryzalin. Thus, *sog1-7* and *mdf-1* mutants seem to be more resistant to oryzalin mediated root growth arrest at low concentrations. These phenotypical observations, in addition to the information obtained by RNA-seq, suggest that microtubule driven processes are altered and retarded in *mdf-1* background and therefore, no additional defects take place after oryzalin treatment.

The accumulation of dead cells and dwarf phenotype of WT and *sog1-7* mutants after growth in oryzalin 200 nM (Figures R-35A and B) could be motivated by a toxicity effect of the chemical at this high concentration. Confocal analyses monitoring cell death induction in WT and *sog1-7* root tips grown in oryzalin 100 nM should also be performed to evaluate whether the difference in root length reported for the WT (Figure R-35D) is associated with cell death accumulation already at this concentration.

Since the strongest response to the treatment was documented in *mdf-2* seedlings, one could speculate that this is related to the upregulation of the MDF C-terminus and 3' UTR regions (Figure R-5A). This would mean that this putative truncated MDF version could promote microtubule-destabilizing conditions and potentiate the effect of oryzalin.



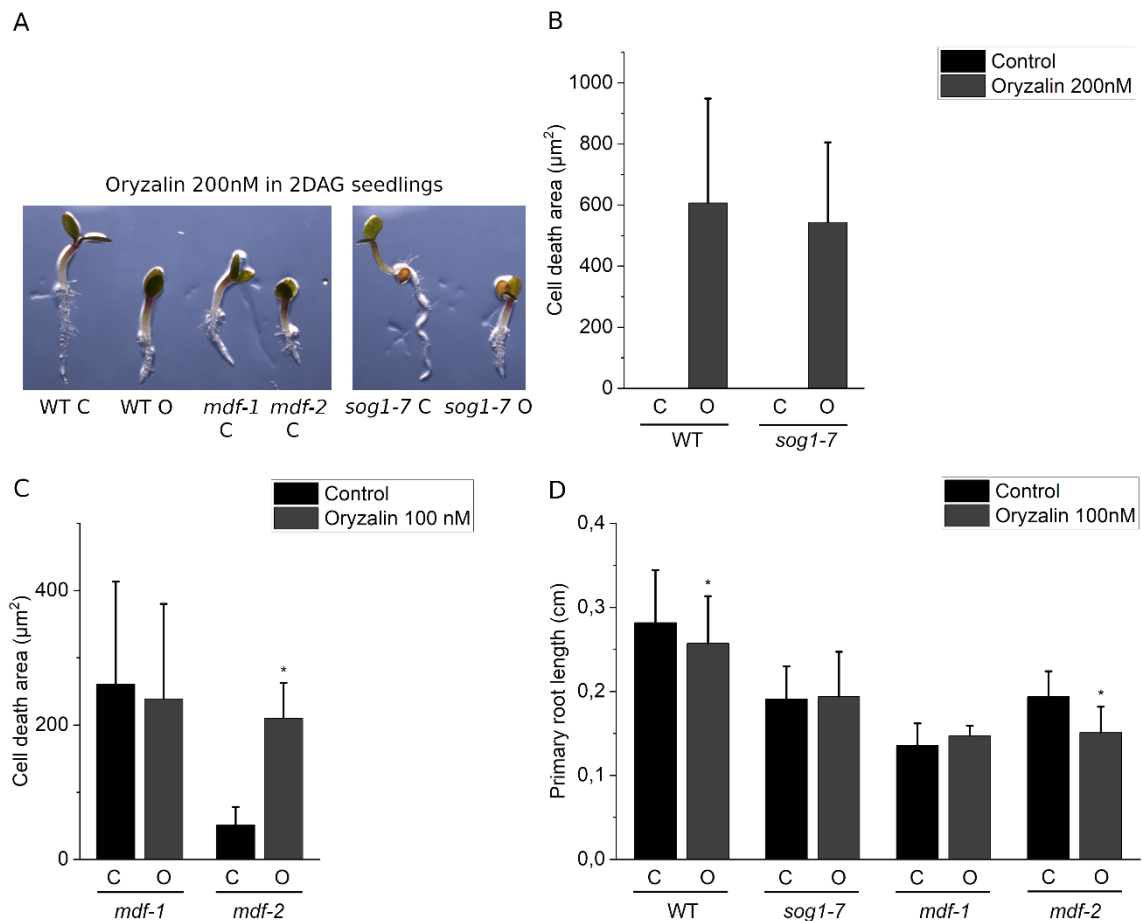


**Figure R-35. Primary root length and accumulation of dead cells in the RAM in *mdf-1* mutants is not affected by the disruption of microtubules after oryzalin treatment.** (A) Representative pictures of 2DAG WT, *mdf-1*, *mdf-2* and *sog1-7* seedlings grown in MS medium (C) or MS medium supplemented with oryzalin 200nM (O). (B) Quantification of the area of cell death in WT (n= 14) and *sog1-7* (n=13) 2 DAG seedlings represented in (A). (C) Quantification of the area of cell death in *mdf-1* (n=6 and n=8) and *mdf-2* (n=8 and n=10) 2 DAG seedlings grown in MS medium (C) or MS medium supplemented with oryzalin 100nM (O). (D) Primary root length of 2DAG WT (n=95 and n=91), *mdf-1* (n=9 and n=11), *mdf-2* (n=7 and n=9) and *sog1-7* (n=10 and n=18) seedlings grown in MS medium (C) or MS medium supplemented with oryzalin 100nM (O). Average  $\pm$  standard deviation is represented. \*P < 0.05 as determined in comparison to control conditions by a two-tailed Student's t-test.

## 4.6 The phosphorylation state of MDF influences its activity

Previous studies showed that MDF was phosphorylated at Serine 22 in an ATR/ATM dependent manner (Roitinger *et al.*, 2015; Waterworth *et al.*, 2019). To analyse the biological relevance of the phosphorylation in MDF, a phosphomimic approach was followed. This means that amino acid substitutions were performed to emulate the phosphorylation states naturally occurring in MDF. To this end, constitutively phosphorylated (35SMDF**S22**DCDS) and dephosphorylated (35SMDF**S22A**CDS) versions of MDF were generated via site directed mutagenesis (SDM) using a 35SMDFCDS construct as template.

### 4.6.1 The phosphorylation of MDF is not essential for its nuclear localization

An earlier publication reported a nuclear localization for MDF (Casson *et al.*, 2009). Co-localization studies with LSM8 (Figure R-9B) and transgenic constructs carrying MDF under its native promoter (Figure R-8A) confirmed this finding. Additionally, subnuclear localization inside the nucleolus and nuclear speckles was speculated after transient *35SMDFCDS* expression in tobacco leaves (Figure R-9B).

To understand the importance of the phosphorylation for MDF subcellular localization, a 35SMDFCDS and a constitutively dephosphorylated construct (35SMDF**S22A**CDS) were transiently transformed in Arabidopsis leaf protoplasts (Figure R-36).

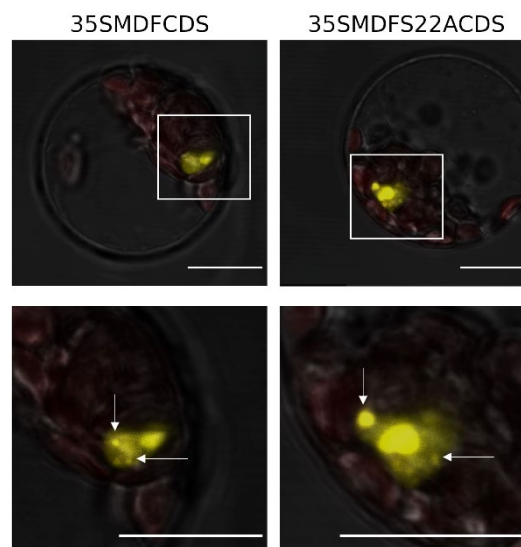


**Figure R-36. The phosphorylation of MDF is not essential for its nuclear localization.** Representative confocal pictures of transiently transformed Arabidopsis leaf protoplasts with 35SMDFCDS (left panels) and 35SMDF**S22A**CDS (right panels). MDF-derived YFP nuclear signal is represented in yellow. Chlorophyll autofluorescence is shown in red. Arrows point to putative nuclear speckles. Lower panels show amplified pictures of the regions contained in the white squares drawn in the upper panels. Scale bars: 15  $\mu$ m



Localization in the nucleoplasm and in subnuclear domains resembling nuclear speckles was observed after transient expression of both constructs. This suggests that the phosphorylation state of MDF does not influence its nuclear localization.

#### 4.6.2 The phosphorylation of MDF is important for its efficient function in cell division and growth control in the root

The importance of the phosphorylation in MDF's role in cell division control in the RAM (Figures R-1 and R-2) was evaluated in stable transformant lines carrying 35SMDFCDS non mutated and phosphomutant versions in WT and *mdf-1* background (Figure R-37). Similar YFP-derived fluorescence nuclear signal patterns were observed in all transgenic lines (Figure R-37A), suggesting that these constructs had similar levels of expression.

Quantification of the number of cells in the cortex layer of the RAM revealed no difference between non-transformed WT, *mdf-1* complemented line and WT plants transformed with either of the 35SMDFCDS constructs (Figure R-37B). Furthermore, also no significant difference was measured in primary root length between these lines (Figure R-37C). Therefore, ectopic expression of *MDFCDS* under a 35S promoter in WT background does not alter cell division nor growth in roots.

In contrast, transgenic expression of 35SMDFCDS in *mdf-1* mutant background had an impact in both cell division and root length in the RAM (Figure R-37 D and E). All stable transformants presented more dividing cells in the RAM in comparison to *mdf-1* non transformed mutants (Figure R-37D). However, this increased cell division resulted in a partial recovery of the root growth arrest, as indicated by the significant differences observed in cell division (Figure R-37D) and primary root length (Figure R-37E) between *mdf-1* transgenic lines carrying 35SMDFCDS constructs and the *mdf-1* complemented line under MDF's native promoter.

Interestingly, while significant differences were also perceived between *mdf-1::35SMDFS22A* and both *mdf-1::35SMDF* and *mdf-1::35SMDFS22D*, no changes in the number of cortex cells or primary root length were reported between *mdf-1::35SMDF* and *mdf-1::35SMDFS22D*. Since *mdf-1* seedlings expressing the dephosphomutant version of MDF had consistently fewer dividing cells and shorter root length than the other two 35SMDF transformants (Figure R-37D and E), it could be speculated that the phosphorylation of MDF influences its function during cell division in the RAM.

Surprisingly, opposite to the complemented *mdf-1* line carrying the genomic region of MDF under its native promoter, all 35SMDFCDS transgenic lines in *mdf-1* background independently of their phosphorylation status, accumulated dead cells in the RAM (Figure R-37A). Therefore, ectopic expression of *MDFCDS* does not recover the putative genome instability associated cell death induction in the RAM of *mdf-1* mutants.

## RESULTS

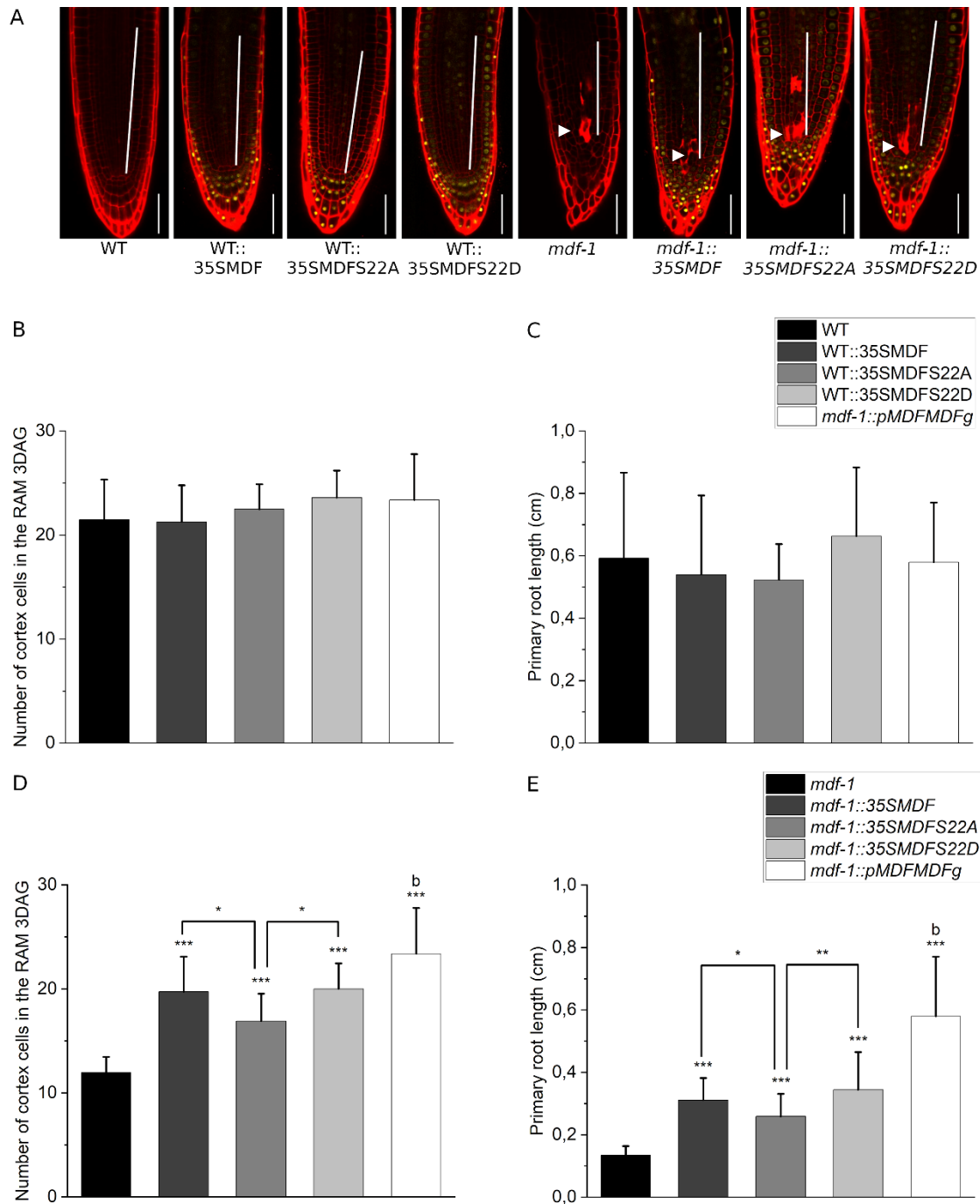


**Figure R-37.** The phosphorylation of MDF is important for its efficient function in cell division and growth control in the root. (A) Representative confocal pictures of WT and *mdf-1* 3 DAG root tips non transformed and stably transformed with 35SMDFCDS, 35SMDFS22ACDS and 35SMDFS22DCDS. Transgenic plants show a nuclear YFP-derived signal in yellow. Division zone is indicated with a white bar. Arrowheads point to dead cells. Scale bar: 50  $\mu$ m. (B) Quantification of the number of dividing cells in the cortex layer in the RAM from 3 DAG WT (n=40), WT::35SMDF (n=23), WT::35SMDFS22A (n=15), WT::35SMDFS22D (n=12) and the complemented line *mdf-1::pMDFMDFg* (n=24). (C) Quantification of the primary root length in 3 DAG WT (n=25), WT::35SMDF (n=27), WT::35SMDFS22A (n=26), WT::35SMDFS22D (n=31) and the complemented line *mdf-1::pMDFMDFg* (n=161). (D) Quantification of the number of dividing cells in the cortex layer in the RAM from 3 DAG *mdf-1* (n=36), *mdf-1::35SMDF* (n=11), *mdf-1::35SMDFS22A* (n=11), *mdf-1::35SMDFS22D* (n=16) and the complemented line *mdf-1::pMDFMDFg* (n=24). (E) Quantification of the primary root length in 3 DAG *mdf-1* (n=15), *mdf-1::35SMDF* (n=19), *mdf-1::35SMDFS22A* (n=17), *mdf-1::35SMDFS22D* (n=37) and the complemented line *mdf-1::pMDFMDFg* (n=24). Average  $\pm$  standard

deviation is represented. \* $P < 0.05$ ; \*\* $P < 0.005$ ; \*\*\* $P < 0.0005$  as determined in comparison to *mdf-1* and *mdf-1::35SMDFS22A* by a two-tailed Student's t-test. "b" represents statistical difference of all transgenic lines to the complemented line determined by a two-tailed Student's t-test.

#### 4.6.3 The phosphorylation state of MDF influences the aerial development of both *mdf* and WT transgenic plants

Overexpression (OE) of *MDF* was previously associated to ectopic meristematic activity in vegetative tissues and phenotypical alterations during seedling development including RAM absence and ectopic shoot formation (Casson *et al.*, 2009). Therefore, the aerial development of transgenic plants carrying the mutated and non-mutated constructs of 35SMDFCDS was also monitored (Figures R-38 and R-39).

In WT background, OE of 35SMDF and 35SMDFS22D led to dwarfism, with reduced rosette diameters (Figures R-38A and B) and plant statures (Figures R-38A and C) in comparison to non-transformed WT and *mdf-1* complemented lines. Per contra, no apparent phenotypical alterations were perceived in WT::35SMDFS22A transformants (Figure R-38).

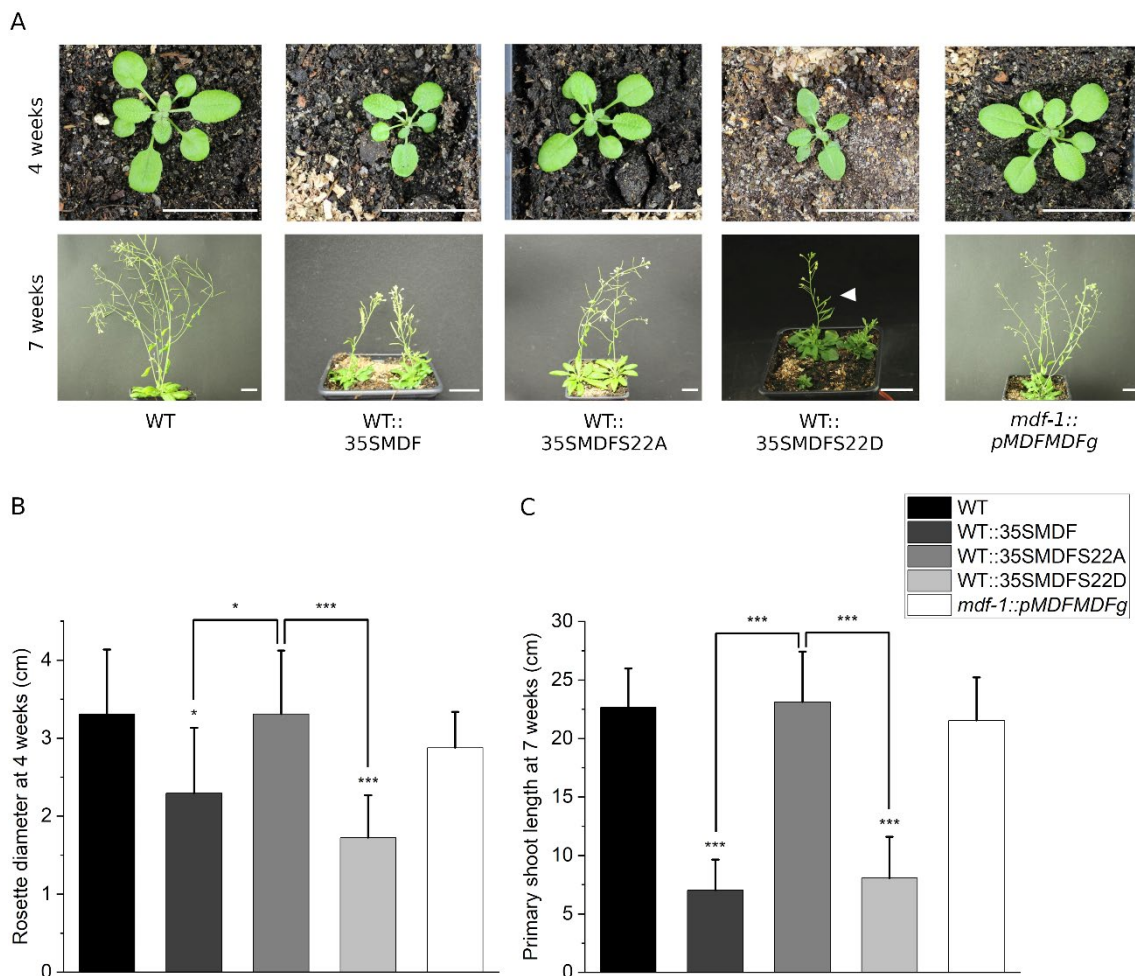


**Figure R-38.** The phosphorylation state of MDF influences aerial development in WT background. (A) Representative pictures of WT, WT::35SMDF, WT::35SMDFS22A, WT::35SMDFS22D and the complemented line *mdf-1::pMDFMDFg* 4 weeks (upper panel) and 7 weeks after germination in soil (lower panel). The white arrowhead points to the only WT::35SMDFS22D plant present in a particular pot. Scale bar:

## RESULTS

2 cm. (B) Quantification of the rosette diameter in 4-week-old WT (n=19), WT::35SMDF (n=6), WT::35SMDFS22A (n=15), WT::35SMDFS22D (n=13) and the complemented line *mdf-1::pMDFMDFg* (n=19). (C) Quantification of the primary shoot length in 7-week-old WT (n=13), WT::35SMDF (n=4), WT::35SMDFS22A (n=8), WT::35SMDFS22D (n=12) and the complemented line *mdf-1::pMDFMDFg* (n=4). Average  $\pm$  standard deviation is represented. \*P < 0.05; \*\*P < 0.005; \*\*\*P < 0.0005 as determined in comparison to WT and WT::35SMDFS22A by a two-tailed Student's t-test.

These observations suggest that the ectopic meristematic activity associated to the OE of *MDF* (Casson *et al.*, 2009) is dependent on its phosphorylation at Serine 22 and causes growth arrest not only at the seedling stage but also in later developmental stages.

This hypothesis was supported by the lack of recovery observed in *mdf-1* plants stably transformed with 35SMDFS22D, whose rosette size was indistinguishable from non-transgenic *mdf-1* lines (Figures R-39A and B). However, opposite to *mdf-1* mutants, most *mdf-1::35SMDFS22D* plants were able to shoot and flower (Figures R-39A and C).

Interestingly, *mdf-1::35SMDF* and *mdf-1::35SMDFS22A* lines exhibited partial growth recovery at the rosette stage, with significantly larger rosette diameter values than *mdf-1* non-transformed mutants (Figures R-39A and B). Moreover, at later developmental stages, transgenic expression of 35SMDFS22A in *mdf-1* background led to complete recovery of the sterility and dwarfism associated to the absence of MDF. Furthermore, no significant difference in primary shoot length was measured between *mdf-1::35SMDFS22A* and *mdf-1::pMDFMDFg* plants after 7 weeks (Figures R-39A and C). In contrast, *mdf-1::35SMDF* plants remained sterile and were significantly smaller than *mdf-1::pMDFMDFg* (Figures R-39A and C). Nevertheless, all transgenic *mdf-1::35SMDF* plants were able to form shoots and their main shoot length values were consistently larger than the ones measured in *mdf-1::35SMDFS22D* lines (Figure R-39C).

These analyses propose that OE of *MDF* in any of their variants increases shooting and rosette development in *mdf-1* background. This effect seems to be influenced by the phosphorylation status of MDF, since a complete recovery after 7 weeks was only observed in *mdf-1* mutants carrying 35SMDFS22A. Additionally, juvenile leaf development was only strongly impaired in *mdf-1::35SMDFS22D* plants.

Taking together the data gathered by OE studies in WT and *mdf-1* background, it could be speculated that MDF impacts leaf development and transition into the reproductive stage in a phosphorylation dependent manner. Dephosphorylated MDF was necessary for normal shooting and flower development, as demonstrated by the recovery and lack of phenotypical defects documented in *mdf-1* and WT transgenic plants carrying 35SMDFS22A (Figures R-38 and R-39). Correspondingly, the strongest growth alterations were observed in WT and *mdf-1* plants stably transformed with a constitutively phosphorylated version of MDF. The phenotype of plants OE *MDFCDS* in both WT and *mdf-1* background resembled the growth



alterations displayed by transgenic lines expressing *35SMDFS22D*, although slightly milder in the case of *mdf-1* transformants. This suggests that most of MDF is rapidly phosphorylated when introduced under a 35S promoter. This phosphorylation seems to positively regulate MDF's function in cell division control in the RAM (Figure R-37D), while, as previously stated, negatively influences shoot growth and flower development (Figures R-38 and R-39). Thus, the phosphorylation status of MDF could differentially regulate its role in RAM and SAM maintenance and development.

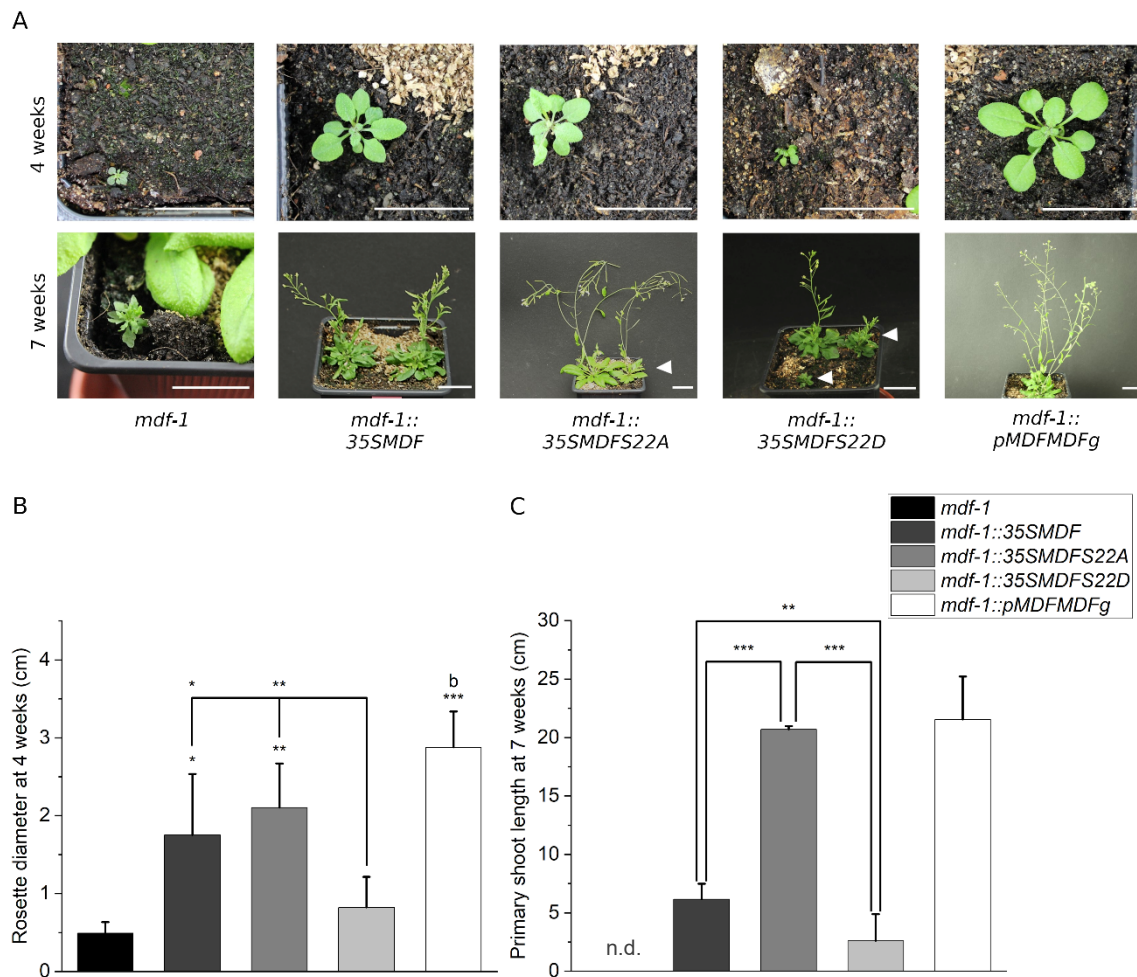


**Figure R-39.** The phosphorylation state of MDF influences aerial development in *mdf-1* background. (A) Representative pictures of *mdf-1*, *mdf-1::35SMDF*, *mdf-1::35SMDFS22A*, *mdf-1::35SMDFS22D* and the complemented line *mdf-1::pMDFMDFg* 4 weeks (upper panel) and 7 weeks after germination in soil (lower panel). The white arrowhead points to the single *mdf-1::35SMDFS22A* and the two *mdf-1::35SMDFS22D* plants present in a particular pot. Scale bar: 2 cm. (B) Quantification of the rosette diameter in 4-week-old *mdf-1* (n=12), *mdf-1::35SMDF* (n=7), *mdf-1::35SMDFS22A* (n=6), *mdf-1::35SMDFS22D* (n=5) and the complemented line *mdf-1::pMDFMDFg* (n=19). (C) Quantification of the primary shoot length in 7-week-old *mdf-1* (n=12), *mdf-1::35SMDF* (n=5), *mdf-1::35SMDFS22A* (n=3), *mdf-1::35SMDFS22D* (n=8) and the complemented line *mdf-1::pMDFMDFg* (n=4). n.d. stands for non-detected. Average  $\pm$  standard deviation is represented. \*P < 0.05; \*\*P < 0.005; \*\*\*P < 0.0005 as determined in comparison to *mdf-1*, *mdf-1::35SMDFS22D* and *mdf-1::35SMDFS22A* by a two-tailed Student's t-test. "b" represents statistical difference of all transgenic 35SMDF lines to the complemented line determined by a two-tailed Student's t-test.

#### 4.6.4 The growth arrest phenotype caused by expression of *35SMDF* in WT background is putatively dependent on ATM

A previous study reported that MDF was specifically phosphorylated after DNA damage in an ATM and/or ATR dependent manner (Roitinger *et al.*, 2015). To corroborate that the phosphorylation at Serine 22 in MDF is generated by ATM, and further analyse the significance of this posttranslational modification in its putative role in genome stability, *35SMDFCDS* constructs were also stably transformed in loss of function mutants for known components of the plant DDR: *atm-2*, *sog1-7* and *atr-2*.

##### 4.6.4.1 Transgenic lines expressing *35SMDF* in *atm-2*, *atr-2* and *sog1-7* background present no alterations in root or aerial development

A clear nuclear YFP-derived signal was observed in the RAM of all transgenic lines, confirming its stable transformation (Figure R-40A). Additionally, no apparent differences were observed in RAM organization or meristem size after stable transformation of *35SMDF* in *atm-2*, *atr-2* and *sog1-7* background (Figure R-40A).

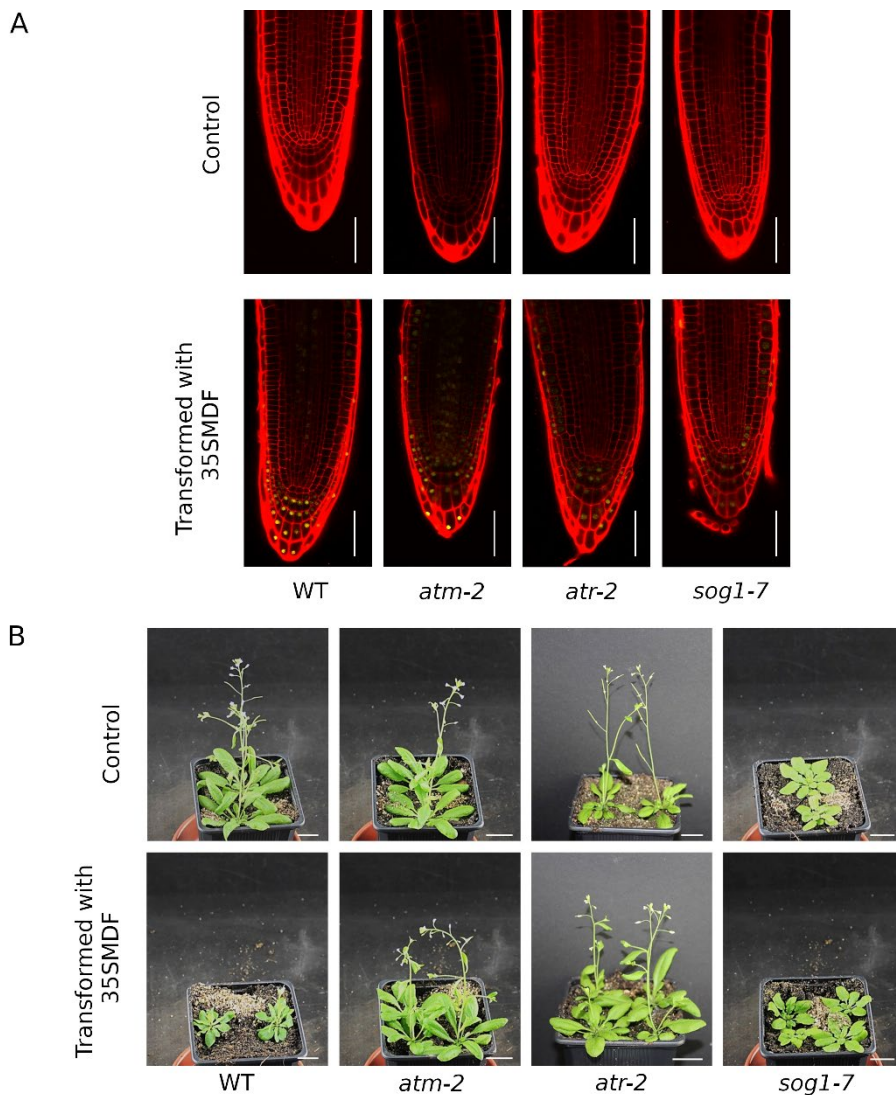


**Figure R-40. Transgenic lines expressing *35SMDF* in *atm-2*, *atr-2* and *sog1-7* background present no alterations in root or aerial development.** (A) Representative confocal pictures of WT, *atm-2*, *atr-2* and *sog1-7* 3 DAG non-transformed (upper panel) and transformed with 35SMDFCDS (lower panel). Transgenic plants show a nuclear YFP-derived signal in yellow. Scale bar: 50  $\mu$ m. (B) Representative pictures of WT, *atm-2*, *atr-2* and *sog1-7* non-transformed (upper panel) and transformed with 35SMDFCDS (lower panel) after 6 weeks in soil. Scale bar: 2 cm.

While growth arrest was verified in WT transgenic plants, ectopic expression of *MDFCDS* did not alter aerial development in *atm-2*, *atr-2* and *sog1-7* mutants (Figure R-40B), as it was observed in WT plants carrying the constitutively dephosphorylated version of MDF (Figure R-38). This suggests that the dwarfism associated to the OE of *MDF* in WT plants is dependent on ATM, ATR and SOG1. Consequently, it also provides additional evidence of the role of ATM in the phosphorylation of MDF at Serine 22 and the connection between MDF and the plant DDR. Furthermore, it highlights the importance of the phosphorylation in the regulation of MDF's activity in the SAM.

#### 4.6.4.2 Stable expression of *35SMDFS22D* in *atm-2* mutants leads to dwarfism

To confirm that the absence of phenotypical defects in vegetative tissues of *atm-2* and *sog1-7* plants after OE of *MDFCDS* (Figure R-40B) was caused by the lack of phosphorylation at Serine 22, a constitutively phosphorylated construct was introduced in both mutants (Figure R-41).

Confocal microscopy of 3 DAG root tips confirmed the stable transformation of *35SMDFS22D* (Figure R-41A). Moreover, similar nuclear YFP-derived fluorescence patterns were detected in all transgenic lines, suggesting equal levels of expression.

Analyses of the T2 from *atm-2* transformants revealed a mixed population of dwarf ( $\approx 28\%$ ) (Figure R-41B) and WT-like ( $\approx 72\%$ ) plants. Phenotypical differences were also observed in *sog1-7* T2 transgenic plants with 22% of the population displaying smaller rosette diameters and shorter stems, opposite to the close to 78% of the plants showing no growth alteration (Figure R-41B). Fluorescence was confirmed by confocal microscopy in seedlings derived from the two distinctive phenotypes in both mutant backgrounds (Data not shown). This suggests that the *35SMDFS22D* transgene was still segregating in the T2 of these lines and only plants containing both copies exhibited growth arrest (Figure R-41B).

As expected, the insertion of a constitutively phosphorylated MDF construct in both WT and *atm-2* background led to dwarfism (Figure R-41B), confirming the importance of the phosphorylation state for MDF's function in vegetative and reproductive development. These observations, together with the lack of phenotypical alterations displayed by *atm-2::35SMDF* plants (Figure R-40B), provide also further evidence of the putative role of ATM in MDF's phosphorylation.

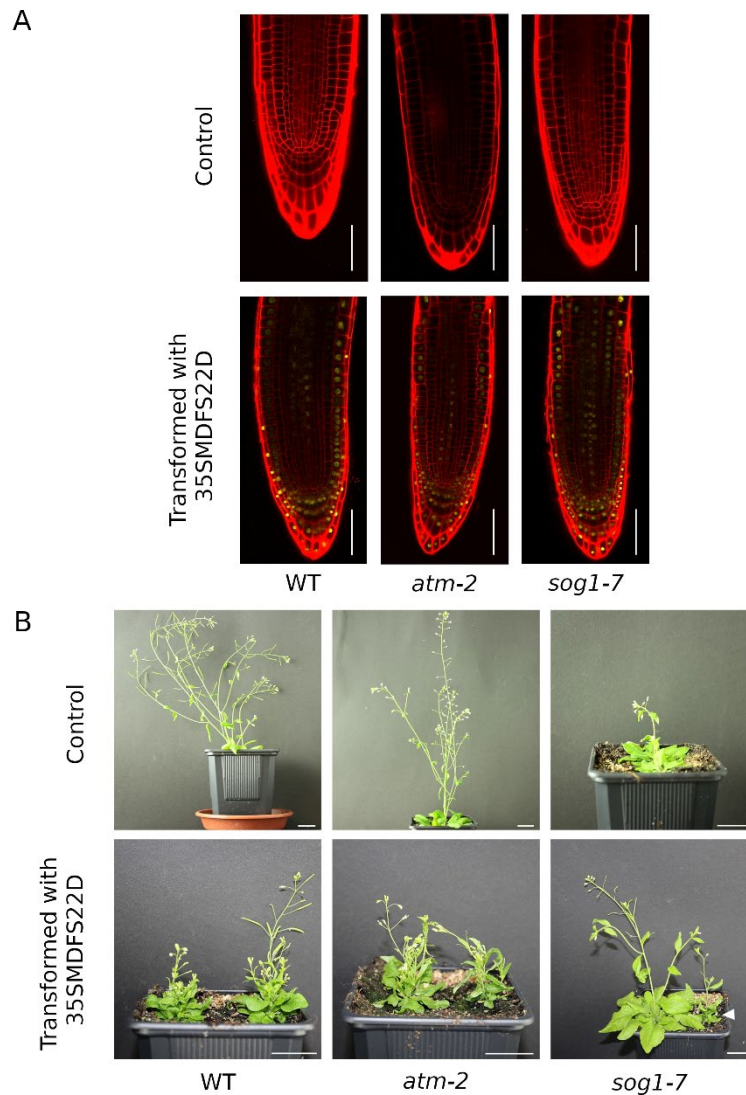


**Figure R-41.** Stable expression of *35SMDFS22D* in *atm-2* mutants leads to dwarfism. (A) Representative confocal pictures of WT, *atm-2* and *sog1-7* 3 DAG non-transformed (upper panel) and transformed with *35SMDFS22DCDS* (lower panel). Transgenic plants show a nuclear YFP-derived signal in yellow. Scale bar: 50  $\mu$ m. (B) Representative pictures of WT, *atm-2* and *sog1-7* non-transformed (upper panel) and transformed with *35SMDFCDS* (lower panel) after 7 weeks in soil. Arrowhead points to a *sog1-7::35SMDFS22D* plant displaying growth arrest opposite to the WT-like *sog1-7::35SMDFS22D* plant present in the same pot. Scale bar: 2 cm.

#### 4.6.5 The phosphorylation state of MDF does not influence the induction of cell death and DNA repair genes after DNA damage

Phenotypical analyses confirmed the biological relevance of the phosphorylation state in MDF for its function in cell division control (Figure R-37) and vegetative/reproductive development (Figures R-38 to 41). To test the impact of MDF's phosphorylation in the response to genotoxic treatments, cell death accumulation and the expression of DNA repair genes after zeocin incubation was monitored in different transgenic lines containing phosphomimic variants of *35SMDFCDS* (Figure R-42).



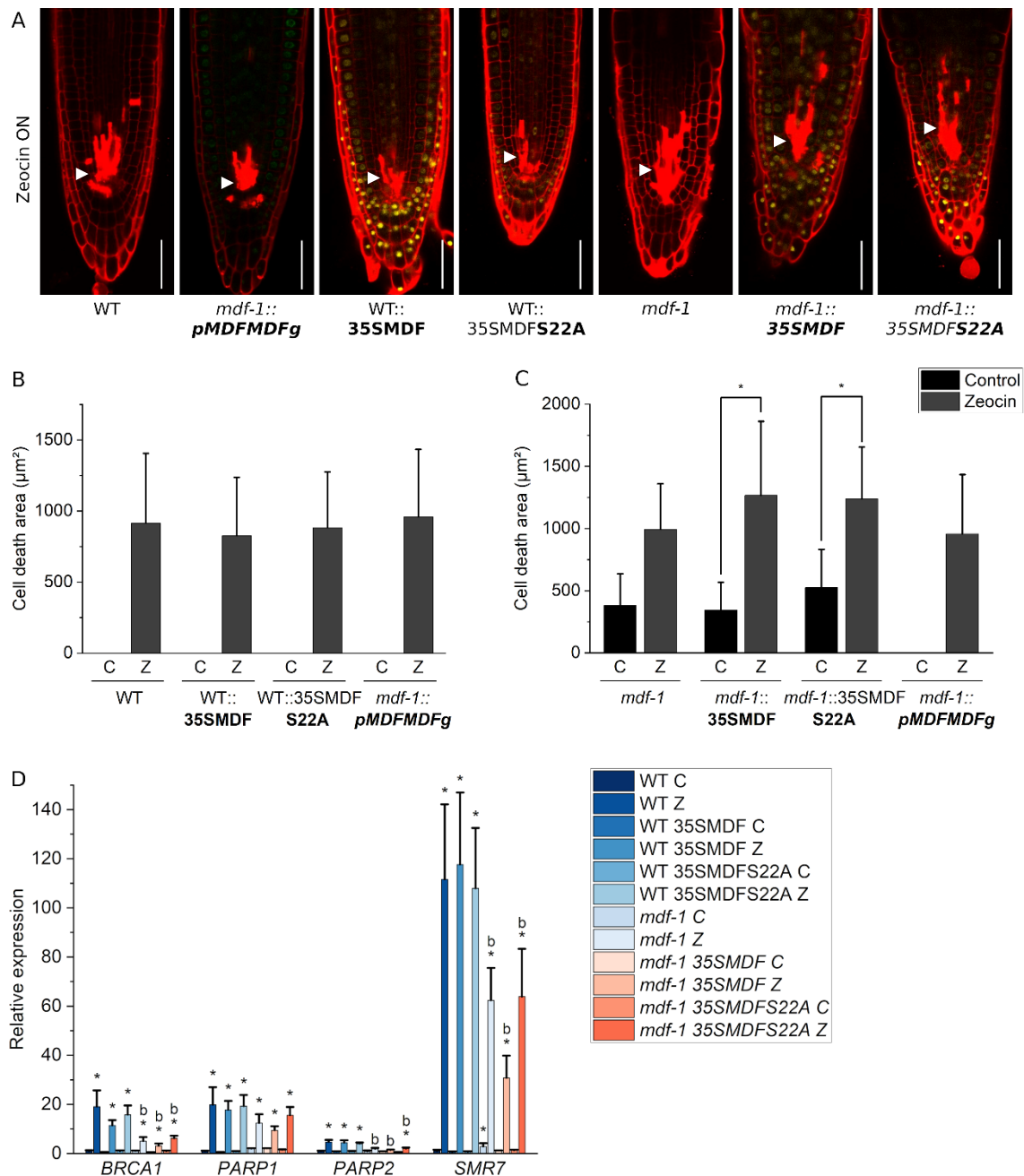


**Figure R-42. The phosphorylation state of MDF does not influence the induction of cell death and DNA repair genes after DNA damage.** (A) Representative confocal pictures of PI-stained WT and *mdf-1* 3 DAG root tips non transformed and stably transformed with 35SMDFCDS and 35SMDFS22ACDS and the *mdf-1* complemented line (*mdf-1::pMDFMDFg*) after ON incubation in zeocin 15 $\mu\text{M}$ . Transgenic plants with 35SMDFCDS constructs show a nuclear YFP-derived signal in yellow and the pMDFMDFg nuclear GFP-derived signal is detected in green. Arrowheads point to dead cells. Scale bar: 50  $\mu\text{m}$ . (B-C) Quantification of the cell death area at control conditions (C) and after ON incubation in zeocin 15 $\mu\text{M}$  (Z) in 3 DAG seedlings of WT (n=24 and n=26), WT::35SMDF (n=22 and n=24), WT::35SMDFS22A (n=29 and n=25), *mdf-1::pMDFMDFg* (n=29 and n=24), *mdf-1* (n=35 and n=38), *mdf-1::35SMDF* (n=29 and n=21) and *mdf-1::35SMDFS22A* (n=18 and n=23). Average  $\pm$  standard deviation is represented. \*P < 0.05 as determined in comparison to the increase in cell death after zeocin incubation in *mdf-1* by a two-tailed Student's t-test. (D) RT-qPCR analyses to measure the transcript levels of the indicated DDR related genes in WT and *mdf-1* 6 DAG seedlings non-transformed or transformed with the estradiol inducible 35SMDFCDS and 35SMDFS22ACDS constructs, transferred ON into estradiol 5  $\mu\text{M}$  MS containing medium and subsequently incubated for 2 hours in liquid MS medium

## RESULTS

supplemented with estradiol 20  $\mu\text{M}$  (C) or MS medium supplemented with both estradiol 20  $\mu\text{M}$  and zeocin 100  $\mu\text{M}$ . Average  $\pm$  standard deviation of two biological replicates is shown. \* $P < 0.05$  as determined in comparison to WT C by One way-ANOVA-test post hoc Tukey Kramer. “b” represents significant difference to WT Z.

As previously reported, PI-staining of root tips showed that in *mdf-1* transgenic lines for non-mutated and mutated 35SMDFCDS constructs, dead cells accumulated in the meristematic zone (Figure R-37A). To evaluate the effect of the phosphorylation on the induction of cell death upon DNA damage, cell death area after ON incubation in zeocin 15  $\mu\text{M}$  was quantified in WT (Figures R-42A and B) and *mdf-1* (Figures R-42A and C) lines stably transformed with 35SMDFCDS and 35SMDFS22A constructs. Induction in the *mdf-1* complemented line was also monitored to assess the effects of *MDF* transgene expression in *mdf-1* mutant background (Figures R-42 A-C).

Confocal experiments revealed no difference between WT, *mdf-1* complemented line and WT plants transformed with either of the 35SMDFCDS constructs (Figure R-42B). In contrast, cell death induction in *mdf-1* transgenic lines was significantly increased in comparison to *mdf-1* non-transformed seedlings (Figure R-42C). Thus, a partial recovery of the reduced induction of cell death after DNA damage treatment in the absence of *MDF* (Figure R-32) is achieved after introduction of 35SMDFCDS, as it happened with other phenotypical traits associated to the *mdf-1* mutation such as cell division and root/vegetative growth arrest (Figures R-37 and R-39). However, no significant difference was observed between *mdf-1::35SMDF* and *mdf-1::35SMDFS22A* lines, which means that the putative involvement of *MDF* in cell death induction is independent of its phosphorylation status.

Lack of *MDF* has also been linked to decreased induction of DDR-related genes after zeocin incubation (Figure R-30). To better understand the influence of *MDF* and its phosphorylation in the plant DDR transcriptional response, *MDFCDS* and *MDFS22ACDS* constructs were cloned under a 35S estradiol inducible promoter. Non-transgenic and transgenic WT and *mdf-1* lines for both constructs were transferred ON to estradiol containing MS media and subsequently incubated in liquid MS medium containing estradiol (C) or MS medium supplemented with zeocin and estradiol (Z) for 2 additional hours to induce the DNA damage response. Total RNA was isolated from these 7-day-old seedlings and the expression of *BRCA1*, *PARP1*, *PARP2* and *SMR7* was quantified via RT-qPCR (Figure R-42D). In this way, the putative correlation between 35SMDFCDS expression and the induction of DDR-related transcripts could be evaluated.

Transcriptional induction after zeocin treatment was not restored to WT levels in neither *mdf-1::35SMDF* nor *mdf-1::35SMDFS22A* lines. Additionally, OE of 35SMDF and 35SMDFS22ACDS in WT plants had no effect on the expression of DDR-related genes upon DNA damage. Assessment of *MDF* expression levels in all transgenic lines confirmed the

induction and OE of the transgenic constructs (Data not shown). These measurements corroborated that the significantly reduced levels of *BRCA1*, *PARP2* and *SMR7* in *mdf-1* transgenic lines after zeocin incubation are not caused by the lack of *35SMDFCDS* induction and subsequent expression. Thus, the lack of recovery could be motivated by the ectopic expression of *MDF* generated by the 35S promoter. Nevertheless, it could be speculated that the induction of *MDF* ON was not sufficient to efficiently respond to external DNA damage. Alternatively, endogenous DNA damage in 5 DAG *mdf-1* mutants could already be too high and putatively irreversible, resulting in a reduced activation of DNA repair processes and increased induction of cell death. Therefore, further experiments should be carried out after longer incubation times in estradiol and at earlier developmental stages. It would also be interesting to test whether the *mdf-1* transgenic *35SMDFCDS* and *35SMDFS22ACDS* lines without an inducible promoter, previously used in other experimental assessments, show WT levels of transcriptional induction of DNA repair genes after zeocin treatment.

#### 4.6.6 Splicing efficiency of MDF seems to be regulated by its phosphorylation state in a developmental related manner

Since a putative role for MDF in AS and transcriptional regulation was proofed by RNA sequencing analyses (Figures R-13, R-17 and R-18), the importance of the phosphorylation at Serine 22 for correct splicing and expression of a subset of genes was tested. To this end, transcriptional and intron retention levels of different targets were measured via RT-qPCR in WT and *mdf-1* transgenic lines carrying the non-mutated and constitutively dephosphorylated *35SMDFCDS* constructs.

##### 4.6.6.1 Splicing efficiency and transcript abundance of a subset of genes are unchanged in WT transgenic seedlings transformed with *35SMDF* constructs

Expression levels of ANAC transcription factors (Figure R-43A) and mitotic related genes (Figure R-43B), which were upregulated and downregulated respectively in *mdf-1* mutants (Figure R-21), were unchanged in WT::*35SMDF* and WT35SMDFS22A plants in comparison to WT. Correspondingly, splicing defects were not detected in both WT transgenic lines for 5 genes involved in cell cycle and splicing processes (Figure R-43C), whose increased intron retention was verified in *mdf-1* background (Figure R-15).

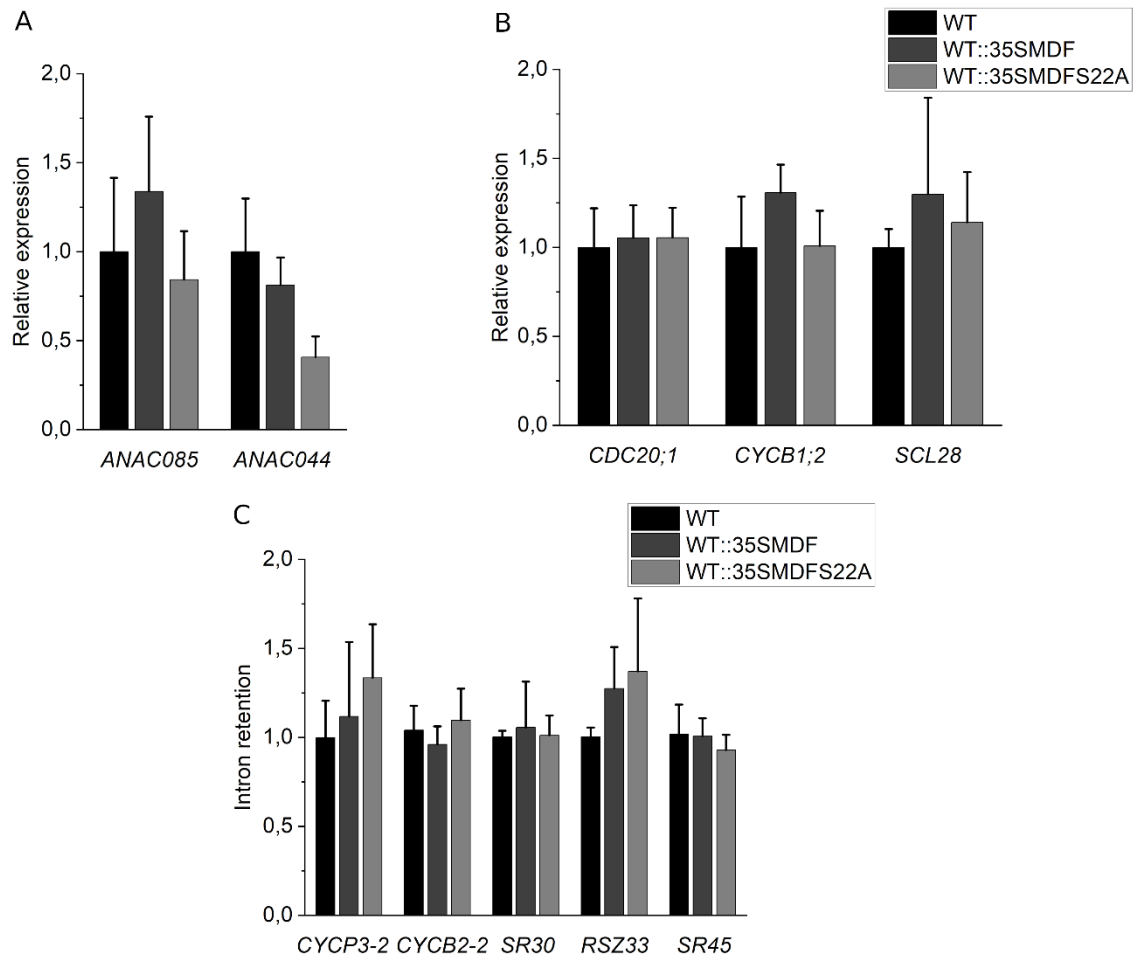


**Figure R-43.** Splicing efficiency and transcript abundance of a subset of genes are unchanged in WT transgenic seedlings transformed with 35SMDF constructs. (A-C) RT-qPCR analyses to measure the transcript levels of *ANAC085* and *ANAC044* transcription factors (A), mitotic-related genes (*CDC20;1*, *CYCB1;2*, *SCL28*) (B) and intron retention levels (C) in cell cycle associated (*CYCP3-2* and *CYCB2-2*) and splicing related (*SR30*, *RSZ33* and *SR45*) genes in 12-day-old WT, WT::35SMDF and WT::35SMDFS22A seedlings. Average  $\pm$  standard deviation of 2-3 biological replicates is represented.

#### 4.6.6.2 Splicing efficiency and transcript abundance of specific genes is affected by MDF phosphorylation state in *mdf-1* transformants containing 35SMDF construct

Finally, the putative recovery of transcriptional and AS defects caused by the absence of MDF, was tested in *mdf-1::35SMDF* and *mdf-1::35SMDFS22A* lines. RT-qPCR analyses revealed that *ANAC085* and *ANAC044* expression was restored to WT levels in both transgenic lines (Figure R-44A). Surprisingly, while in *mdf-1::35SMDFCDS* lines the expression of *CDC20;1* and *CYCA2-3* was restored to WT levels, this was not the case in *mdf-1::35SMDFS22A* seedlings for *CYCA2-3* (Figure R-44B). The retained downregulation of a cyclin in *mdf-1* plants carrying a constitutively dephosphorylated version of MDF, could account for some of the phenotypical differences observed between both stable transformants in terms of cell division and root length (Figure R-37). Additionally, splicing defects of 5

targets involved in cell cycle, DNA damage and splicing related processes were recovered to WT levels in *mdf-1::35SMDF* (Figure R-44C). Per contra, *mdf-1::35SMDFS22A* 12-day-old seedlings maintained increased intron retention levels in one RepMYB transcription factor (MYB3R3) (Figure R-44C). The importance of MYB3R3 in cell cycle arrest upon DNA damage (Bourbouse *et al.*, 2018; Takahashi *et al.*, 2019), suggests that MDF's presumed function in DNA damage induced cell division arrest could be regulated by its phosphorylation status.

Due to the phenotypic differences in shoot development between *mdf-1* transgenic lines, intron retention levels in three targets relevant for leaf and shoot development were tested in WT, *mdf-1*, *mdf-1::35SMDF* and *mdf-1::35SMDFS22A* 4-week-old leaves (Figure R-44D).

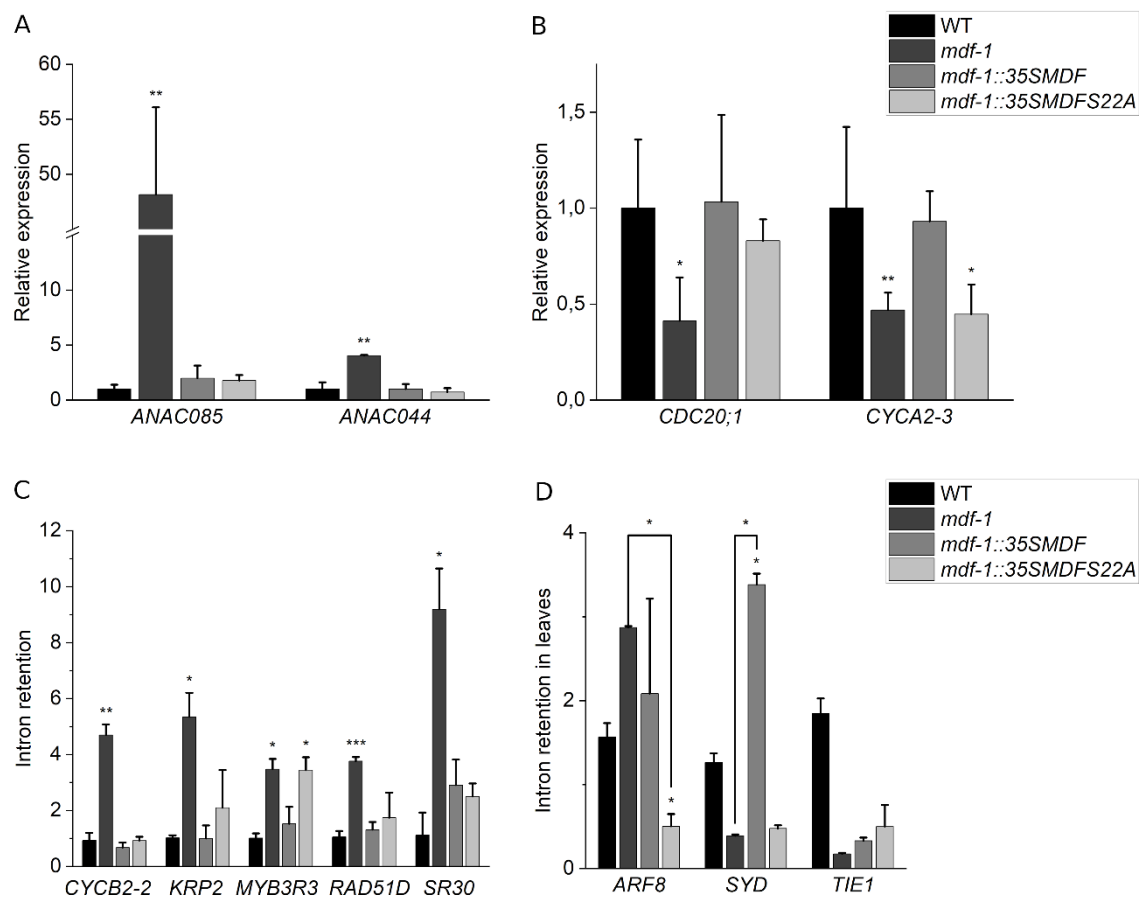


**Figure R-44. Splicing efficiency and transcript abundance of specific genes is affected by MDF phosphorylation status in *mdf-1* transformants containing 35SMDF constructs.** (A-C) RT-qPCR analyses to measure the transcript levels of *ANAC085* and *ANAC044* transcription factors (A), mitotic-related genes (*CDC20;1* and *CYCA2-3*) (B) and intron retention levels in (C) in cell cycle (*CYCB2-2* and *KRP2*), transcription (*MYB3R3*), DNA repair (*RAD51D*) and splicing related (*SR30*) genes in 12-day-old WT, *mdf-1*, *mdf-1::35SMDF* and *mdf-1::35SMDFS22A* seedlings. Average  $\pm$  standard deviation of 2-3 biological replicates is represented. \* $P < 0.05$ ; \*\* $P < 0.005$ ; \*\*\* $P < 0.0005$  as determined in comparison to WT by a two-tailed Student's t-test. (D) RT-qPCR analyses to measure intron retention levels in targets important for shoot development in 4-week-old WT, *mdf-*

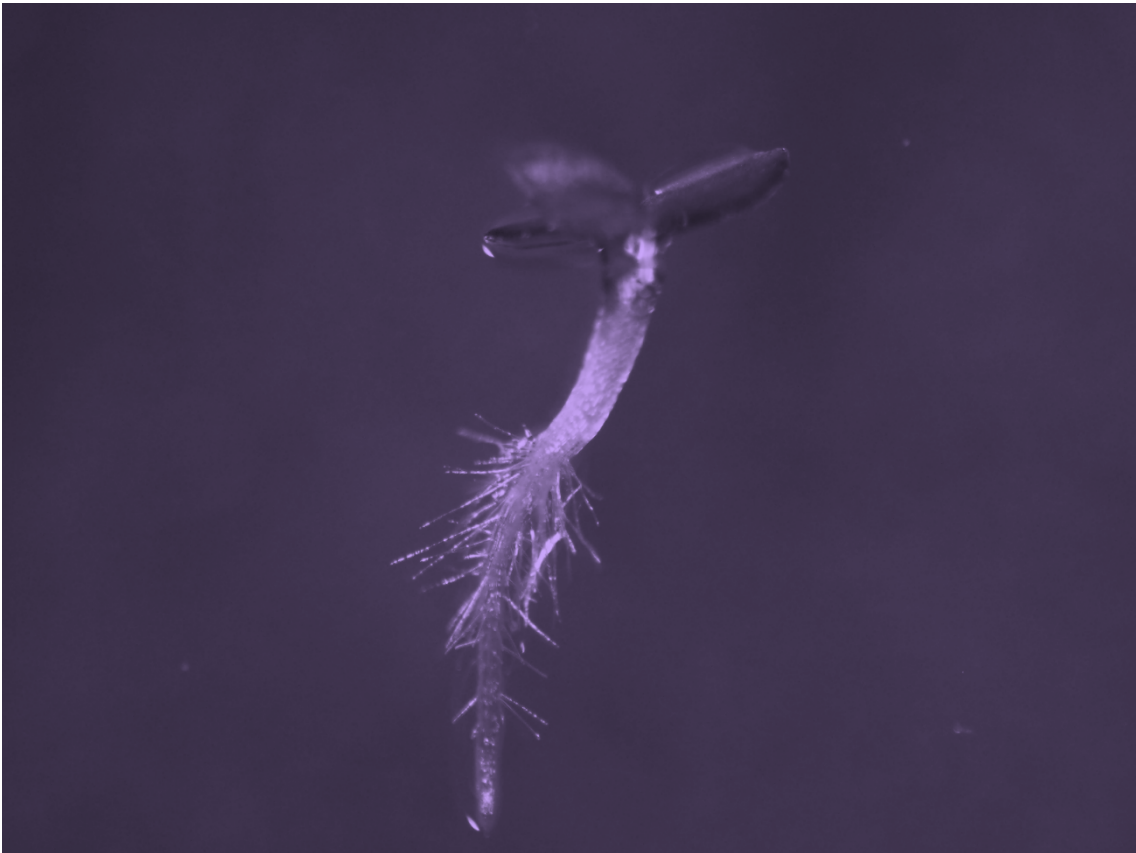
## RESULTS

1, *mdf-1::35SMDF* and *mdf-1::35SMDFS22A* leaves. Average  $\pm$  standard deviation of 2 biological replicates is represented. \*P < 0.05 as determined in comparison to WT and *mdf-1* by a two-tailed Student's t-test.

These were *AUXIN RESPONSE FACTOR 8 (ARF8)*, *SPLAYED (SYD)* and *INTERACTOR CONTAINING EAR MOTIF PROTEIN 1 (TIE1)*. While not significant, increased intron retention in *ARF8* was observed in *mdf-1* and *mdf-1::35SMDF* (Figure R-44D). In contrast, significantly reduced intron retention in comparison to both WT and *mdf-1*, and thus increased splicing efficiency, was found in rosette leaves of *mdf-1::35SMDFS22A* for *ARF8* (Figure R-44D). Additionally, only *mdf-1::35SMDF* displayed significantly increased intron retention levels in *SYD* in comparison to WT, whereas no splicing defects could be detected in both *mdf-1* and *mdf-1::35SMDFS22A* (Figure R-44D). Finally, *TIE1* mRNA splicing efficiency was equivalent in all *mdf-1* mutant lines and lower than in WT leaves (Figure R-44D).

Together these data suggest that MDF's splicing function in shoot tissues is also influenced by its phosphorylation status. While transcriptional and splicing defects were prevalent in seedlings transformed with a dephosphomutant version of MDF (Figures R-44B and C), the opposite effect was observed in leaf samples. In this context, OE of *MDFCDS* in *mdf-1* impaired mRNA splicing in the SWI2/SNF2-like protein *SYD*, which is essential for shoot apical meristem maintenance and identity (Kwon *et al.*, 2005). Surprisingly, *mdf-1* and *mdf-1::35SMDFS22A* mutants showed similar levels of intron retention than WT plants (Figure R-43D). Hence, based on the phenotypical observations (Figures R-38 and R-39) and splicing analyses of *mdf-1::35SMDF* and *mdf-1::35SMDFS22A* lines (Figure R-44D), it could be speculated that ectopic expression of phosphorylated *MDFCDS* promotes AS splicing defects in a subset of genes important for SAM maintenance, such as *SYD*, leading to developmental alterations including shorter stems and reduced rosette diameters. Therefore, it would be interesting to also evaluate splicing defects in leaves of WT transgenic plants for *35SMDF* and *35SMDFS22D* in order to confirm that dwarfism in these plants is caused by intron retention in targets important for shoot development.

# 5. DISCUSSION





## 5.1 MDF strongly impacts Arabidopsis development

Similar to mammalian SART1, which was shown to influence tissue development by its role in cell cycle regulation and transcriptional and splicing control (Henson and Taylor, 2020), the importance of MDF for normal plant development was verified by a combination of phenotypical and transcriptomic analyses.

### 5.1.1 MDF is a positive regulator of cell proliferation and plant growth

Previous studies with a CYCAT1::CDB:GUS marker found a reduced population of dividing cells associated to a shorter proximal meristem size in the root tip of *mdf-1* (Casson *et al.*, 2009). By counting the number of cortex cells in the RAM and evaluating the formation of true leaves and adventitious roots of 10-day-old seedlings, a severe cell cycle arrest was verified in the RAM of both *mdf* mutants and in the SAM of *mdf-1*. Microtubule immunostaining in root tips of both mutants confirmed the significantly higher occurrence of G2/M arrest in the absence of MDF in comparison to WT and hence, the conserved role of SART1 family proteins in cell division control in proliferating cells. The reduced expression of cell cycle associated genes in *mdf-1* mutant background verified these observations on a transcriptional level.

#### 5.1.1.1 The *mdf-2* mutant displays a slight recovery of MDF associated developmental alterations

An impaired cell division in *mdf* mutants correlated with severe primary root growth arrest, decreased size and number of rosette leaves and reduced stature. Comparison of their phenotypes revealed that *mdf-2* exhibited less severe developmental defects than *mdf-1*, especially in the SAM. In contrast to *mdf-1*, *mdf-2* was able to generate SAM-derived plant organs such as shoots and flowers.

RT-qPCR analyses showed an overexpression of the C-terminus of MDF in *mdf-2*, but not in *mdf-1*. This indicated that the expression of this truncated version of MDF in *mdf-2* might account for the phenotypic differences between both T-DNA insertion lines. Furthermore, the C-terminal domain of MDF shows the highest level of homology to SART, further suggesting that the retained expression of this domain could partially function during spliceosome assembly.

Alternatively, this putative truncated MDF protein could act as an upstream open reading frame (uORF). Previous studies in Arabidopsis showed how phenotypical differences between different mutant lines for TRIPHOSPHATE TUNNEL METALLOENZYME 3 (TTM3) were caused by the remaining expression of an uORF. This led to the expression of



Since the retained MDF truncated protein in *mdf-2* includes MDF's homologous region with MDFL (Figure D-1), it could be speculated that the overexpressed MDF C-terminal region in *mdf-2* could take over MDFL's function. Therefore, the partial recovery of cell division and developmental defects in *mdf-2* would be caused by an increase of MDFL's function. Transgenic overexpression of MDF's C-terminus and MDFL in *mdf-1* background would be helpful to validate this hypothesis.

Curiously, analyses of human SART1 revealed the existence of a short 259 aa protein isoform. While the canonical 800 aa SART1 protein isoform was found in the nuclei of most proliferating cells, this shorter human SART1 version localized predominantly in the cytosol of epithelial cancer cells (Hosokawa *et al.*, 2005). Based on the size similarity between MDFL and the short human SART1 isoform, it could be that MDFL also has a different function than MDF. In this context MDFL and MDF could hypothetically have opposite roles in cell cycle regulation and development. Therefore, the phenotypical differences between *mdf-1* and *mdf-2* could be caused by a dominant negative effect. This means that binding of the retained and highly homologous MDF C terminal region to MDFL mRNA in *mdf-2* plants, could potentially silence *MDFL* expression. Hence, a slight recovery of the cell division and splicing-derived defects would be expected, as observed in *mdf-2*. However, unlike human SART1 short isoform, MDFL is predicted to share MDF's nuclear localization (Source: Uniprot).

The importance of MDF and the putative truncated C-terminus in reproductive development was also evaluated. While the *mdf-1* mutation abolished the formation of shoots and flowers, *mdf-2* mutants generated aberrant flowers lacking stamens and thus, male sterile. Although these observations disproved the proposed lethality of both *mdf* mutations 20-25 DAG, they verified the importance of MDF in SAM maintenance and organization (Casson *et al.*, 2009). Since the acquisition of adult leaf traits is not completely repressed in both *mdf* mutants, it could be speculated that MDF is specifically important for the acquisition of flower competency at the end of the adult vegetative stage and thus, essential for the transition to reproductive development. In this way, MDF could act as a transcriptional or splicing regulator of a subset of proteins involved in this process such as FLC, FD or SOC1. Curiously, RNA seq analyses of *mdf-1* 12-day-old seedlings found a strong downregulation of *FLC* (Log<sub>2</sub>Fold -5,94) in comparison to WT, in addition to mildly reduced levels of *SOC1* (Log<sub>2</sub>Fold -0,69) and *FD* (Log<sub>2</sub>Fold -0,91). Considering FLC acts as a negative regulator of floral formation, its downregulation should theoretically promote early flowering. However, its lack of repression was not translated into higher levels of SOC1, which in complex with FD and FT is the main activator of floral meristem identity regulators. Therefore, it might be that additional factors are inhibiting *SOC1* and *FD* expression independently of FLC in the absence of MDF, leading to defective reproductive development as observed in *mdf-1* mutants. In this context, *PENNYWISE* (*PNY*) and *POUND-FOOLISH* (*PNF*) are two related BEL1-like homeobox genes, which have been described to be essential for meristem maintenance and flowering in Arabidopsis by mediating the repression of lateral organ genes (Khan *et al.*,

2015). Interestingly, significant downregulation of both *PNY* and *PNF*, which was previously related to lower FD mRNA levels (Andrés *et al.*, 2015), was found in *mdf-1* mutants. These findings suggest that miss expression of these flowering regulators might be connected to the defective formation of SAM derived organs in the absence of MDF.

FLC expression is dependent on multiple transcriptional and post-transcriptional mechanisms. These include epigenetic silencing by histone methylation, and splicing regulation (Qi *et al.*, 2019). For example, both AS in sense and antisense transcripts at the FLC locus (collectively known as COOLAIR) have been described to modulate FLC expression states (Qi *et al.*, 2019). Whether FLC lower expression in *mdf-1* mutant background is caused by defective splicing remains to be elucidated. Additionally, it should be assessed whether the reduced transcription of FLC is translated into lower protein abundance in *mdf-1*.

Future experiments should also assess whether an increased expression of *PNY* and *PNF* flowering regulators after partial activation by the MDF C-terminal region in *mdf-2* plants, is responsible for their considerable recovery in aerial tissue morphogenesis. Moreover, the aberrant “AC” flower configuration in these mutants suggested loss of “B” class function. Therefore, analyses of expression and splicing patterns of *AP3* and *PI* B class genes in *mdf-2* background could bring more insight into the function of the C-terminal domain of MDF in Arabidopsis reproductive development and flowering patterning.

#### 5.1.1.2 Loss of MDF is not lethal during embryogenesis and seed germination

*MDF* is predominantly expressed in young non differentiated cells in the basal region during the heart stage in Arabidopsis embryogenesis. In spite of its low transcription rates in early embryo stages, *MDF* is important to ensure a normal cell division pattern in the lower tier during the pre-globular stage. Consequently, *mdf-1* mutants were shown to exhibit aberrant heart stage embryo shapes (Casson *et al.*, 2005).

The coordinated antagonistic action of the HD-ZIP III and PLT gene families was shown to determine the apical-basal polarity during early embryogenesis (Smith and Long, 2010). Mis-expression of PLT genes in *mdf-1* background was previously reported (Casson *et al.*, 2009). During this work, downregulation of *PLT1* (Log<sub>2</sub>Fold -3,56) was confirmed by RNA sequencing analyses of *mdf-1* seedlings, verifying the importance of *MDF* in basal fate specification during embryogenesis in accordance with its elevated transcript levels in this region.

Previous investigations have demonstrated that the maintenance of DNA methylation patterns mostly by METHYLTRANSFERASE1 (MET1) and CHROMOMETHYLASE3 (CMT3) is critical for Arabidopsis embryogenesis and seed viability. Moreover, loss of function mutants for MET1 and CMT3 displayed, similar to *mdf-1* mutants, altered cell

divisions during embryogenesis, aberrant auxin gradient formation and mis-expression of important genes for embryo cell specification (Xiao *et al.*, 2006). Curiously, by comparing the expression profile of the 200 most up-regulated and down-regulated genes in *mdf-1* with transcriptomic data from public repositories using the GENEINVESTIGATOR® software, expression data from *met1-3* (Data set: AT-00716) showed the highest similarity. Thus, MDF could have, in addition to its role in controlling the expression of essential genes for embryo identity, an analogous function to MET1 in DNA methylation regulation during embryogenesis. Interestingly, PRP6-like STA1, another U4/U5.U6 associated splicing factor was already associated to DNA methylation processes (Dou *et al.*, 2013).

Germination assays and seed counting experiments with both *mdf-1* and *mdf-2* heterozygous plants revealed that the defective cell division pattern during early embryogenesis did not affect the viability of *mdf* homozygous seeds. These observations appoint MDF as an important but not essential regulator of cell division during embryogenesis. However, loss of SART1 family activity impacts organism survival differently in other eukaryotes. While *S. cerevisiae* Snu66 is not required for normal growth and only impacts splicing efficiency at low temperatures, Snu66 is an essential gene in *S. pombe* (Wilkinson *et al.*, 2004). Whether the presence of MDFL partially compensates the loss of MDF in Arabidopsis and consequently ensures its viability remains to be elucidated.

## 5.2 MDF acts as a splicing and transcriptional regulator

SART1 related proteins from different organisms have been described to be important for spliceosome assembly by specifically recruiting the U4/U6.U5 trisnRNP complex (Gottschalk *et al.*, 1999; Stevens and Abelson, 1999; Makarova *et al.*, 2001; Wilkinson *et al.*, 2004). In plants, MDF orthologs have been found in both eudicots and monocots, including *Medicago truncatula*, *Solanum lycopersicum* or *Zea mays* (Source: TAIR). The conservation of SART1 related proteins among the plant kingdom further indicates the biological relevance of MDF. However, to my understanding, no previous publication verified so far MDF's function in pre-mRNA splicing.

### 5.2.1 MDF is putatively associated to the U4/U6.U5 trisnRNP complex in the spliceosome

Co-IP and BiFC analyses revealed an association between MDF and LSM8, a core component of the LSM2-8 complex that is associated to the U6snRNP and functions in U6snRNA stability (Perea-Resa *et al.*, 2012). Furthermore, nuclear colocalization of both proteins was found in the nucleoplasm and presumably in nuclear speckles.

Multiple classes of “bodies” or nucleoplasm compartments have been described in animal and plant cells. Among them, the nuclear speckles have been associated to components of the pre-

mRNA splicing machinery, although other proteins such as transcription factors present also a nuclear speckled localization pattern (Lorkovic *et al.*, 2008). These subnuclear compartments are believed to act as storage and/or assembly sites from which splicing factors can be recruited to form active spliceosomal complexes at active transcription sites (Lorkovic *et al.*, 2008).

Accordingly, transient expression analyses of SR splicing factors fused to a fluorescent tag also reported a nuclear localization that showed diffuse and concentrated signals in the nucleoplasm and nuclear speckles respectively (Zhang *et al.*, 2020). Moreover, the different classes of SR proteins (Figure I-10) presented different speckle localization. This suggested that the coordinated formation of different speckles allows the plant cell to activate a more specific transcriptional and splicing response depending on the cell type and developmental stage (Lorkovic *et al.*, 2008).

In agreement with previous findings, it is very likely that both MDF and LSM8 are recruited to nuclear speckles, providing additional evidence of the predicted role of MDF in pre-mRNA splicing and its SR-related nature. The positive Co-IP and BiFC results, but lack of physical interaction reported by Y2H and FLIM-FRET experiments, suggests an indirect interaction due to their common localization inside the U4/U6-U5 trisnRNP complex in the spliceosome.

Further investigations should try to uncover the physical interactors of MDF. Promising candidates are STA1, BRR2a, and PRP3, homologous to U5-specific PRP6 and BRR2 and U4/U6 specific PRP3 human spliceosome components respectively, which were already found to interact via Y2H with human SART1 (Liu *et al.*, 2006).

Intriguingly, MDF overexpression showed also additional localization in the nucleolus, which is not common in SR-related proteins (Zhang *et al.*, 2020). As an exception, overexpression of RSZ22, another SR protein, resulted also in nucleolar localization (Tillemans *et al.*, 2005). This phenomenon was explained by proposing that RSZ22 putatively contained sequences with restricted homology to nucleolar localization signals (NoLS), that would get artefactually enhanced after ectopic RSZ22 expression. Moreover, the increased nucleolar localization after truncation of the RS domain, indicated that this domain could be partially masking the NoLS at endogenous conditions (Tillemans *et al.*, 2005).

Nucleolar signal sequence-based predictions using the Nucleolar localization sequence Detector (NoD) from Dundee university (Scott *et al.*, 2011) predicted two putative NoLS in MDF between positions 21 and 117 and between positions 386 and 411. Hence, MDF nucleolar localization could either be artificially generated by its overexpression or be related to their putative NoLS. Generation of constructs lacking MDF's presumed NoLS would be helpful to understand the biological relevance of its nucleolar localization.



## 5.2.2 The pleiotropic phenotype of *mdf* mutants is correlated with numerous expression and splicing changes

RNA sequencing experiments using 12-day-old *mdf-1* and WT seedlings revealed that absence of MDF enhanced AS changes in genes important for stress responses, gene expression, development regulation and metabolism. These observations not only provided evidence of MDF's function in pre-mRNA regulation, but also confirmed the broad spectrum of biological processes that are directly or indirectly regulated by MDF, which explains the pleiotropic phenotype of *mdf* mutants.

### 5.2.2.1 Absence of MDF impacts AS and expression levels of genes associated to stress responsive pathways

*mdf-1* mutants exhibited AS in 351 genes associated to the GO term “response to abiotic stimulus” as well as a significant transcriptional induction in 1165 targets involved in Arabidopsis stress responses. These data suggested that MDF could be important during the plant response to different stress conditions.

The link between AS and efficient and rapid stress response activation has been well studied. For example, while SR-related protein SR45 was shown to negatively regulate sugar signalling through downregulation of the ABA pathway, the transcript levels of SCL subfamily SR proteins SCL28, SCL30a and SCL33 are significantly altered after ABA treatment (Carvalho *et al.*, 2010; Cruz *et al.*, 2014). Another example is the LSM2-8 complex, whose role in AS was characterized to be essential for Arabidopsis adaptation to abiotic stress conditions including drought or salt stress (Carrasco-López *et al.*, 2017). Finally, loss of core spliceosome components also affects Arabidopsis response to different stresses since mutants for components of the tri-snRNP complex *sta1-1* and *rdm16-1* exhibit an increased hypersensitivity to ABA and salt stress (Lee *et al.*, 2006; Huang *et al.*, 2013; Du *et al.*, 2015).

MDF's direct involvement in stress response activation via AS should be further addressed by analysing the AS profile and hypersensitivity of *mdf-1* mutants after different stress treatments.

### 5.2.2.2 Regulation of pre-mRNA splicing is essential for correct plant development

As previously introduced, loss of MDF caused severe developmental defects that correlated with defective splicing of genes associated with the regulation of developmental processes. Reduced expression of genes associated to the GO terms “meristem development”, “root development”, “leaf development” or “flower development” was also found in *mdf-1* mutant background.

The importance of pre-mRNA splicing for correct plant development was previously characterized in other splicing mutants including *sr45-1* (Ali *et al.*, 2007); *lsm8-1* (Perea-



Resa *et al.*, 2012) or *hub1* (Watanabe *et al.*, 2019). The latter is a knockout mutant for UBIQUITIN-LIKE PROTEIN 5 (UBL5) also known as HOMOLOGOUS TO UBIQUITIN 1 (HUB1). HUB1 was shown to promote plant root elongation and development through pre-mRNA splicing via its interaction with PRP38 in *A. thaliana* (Watanabe *et al.*, 2019).

Partial loss of function mutants for core spliceosome U4/U5-U6 components such as RDM16 (Lv *et al.*, 2021), BRR2a (Mahrez *et al.*, 2016) and STA1 (Lee *et al.*, 2006) also exhibit developmental alterations. Some of those are similar to the phenotypical defects found in *mdf* mutants, which are also affected in a U4/U5-U6 spliceosomal component. As such, a point mutation in the sixth exon of RDM16 led to stem cell niche distortion, reduced cell division and short root in *rdm16-4* (Lv *et al.*, 2021). Regarding BRR2a, an aa exchange in the first helicase domain resulted in increased leaf serration and smaller leaves in *brr2a-2* (Mahrez *et al.*, 2016). Finally, EMS mutagenized *sta1-1* presented, similar to *mdf* mutants, increased leaf serration and smaller size in comparison to WT (Lee *et al.*, 2006).

However, unlike *mdf* mutants, *sta1-1*, *brr2a-2* and *rdm16-4* are fertile (Lee *et al.*, 2006; Mahrez *et al.*, 2016; Lv *et al.*, 2021). The milder phenotype in these three mutants could be explained by the partial functionality of the truncated and/or mutated proteins encoded by the EMS mutagenized *sta1-1*, *brr2a-2* and *rdm16-4* alleles. In this context, *rdm16-2*, which contains a T-DNA insertion in the fifth intron of RDM16, showed stronger morphological defects than *rdm16-4*, including sterility (Lv *et al.*, 2021).

Altogether these findings verified that pre-mRNA splicing plays a central role in the coordination of plant growth. They also suggest that U4/U5-U6 components are important for Arabidopsis sexual reproduction. Moreover, partial loss of function of SNU114, another U5 snRNP component, also affects Arabidopsis fertility by influencing female gametophyte development (Liu *et al.*, 2009).

### 5.2.2.3 *mdf* mutants exhibit abundant metabolic changes

Although ROS molecules are important for plant development, excessive levels result in oxidative stress, which has deleterious effects on plant fitness by triggering diverse metabolic pathways that can culminate in the induction of cell death (Sipari *et al.*, 2020). Changes in ROS homeostasis have also been shown to strongly impact Arabidopsis endogenous metabolism by promoting changes in central metabolic pathways and energy metabolism (Sipari *et al.*, 2020).

*mdf-1* mutants displayed abundant AS and transcriptional changes in genes involved in diverse metabolic processes, including “response to oxidative stress”. Additionally, loss of MDF conferred increased resistance to H<sub>2</sub>O<sub>2</sub> and increased levels of the scavenging enzyme *AOX1C* were found in *mdf-1* at normal conditions. These observations indicated that MDF could have a regulatory role in metabolic pathways, especially in ROS-related pathways. A

link between metabolism control and ROS sensitivity was previously proposed for knockout mutants for RADICAL-INDUCED CELL DEATH1 (RCD1). In this case, an increased resistance to Methyl-viologen (MV) ROS-induced toxicity was explained by the negative effect of RCD1 on reductive metabolism (Sipari *et al.*, 2020).

The cell cycle arrest phenotype documented in both *mdf* mutants would also support the hypothesis of MDF influencing ROS metabolism, since elevated levels of the H<sub>2</sub>O<sub>2</sub> ROS molecule were associated with cell division inhibition (Tsukagoshi, 2012).

Alternatively, MDF dependent putative changes in ROS metabolism could also be caused by the defective auxin signalling of *mdf* mutants (Casson *et al.*, 2009). Auxin has been characterized to coordinate many aspects of plant growth from embryogenesis to senescence (Li *et al.*, 2016) and its downstream signalling is sustained by an oscillatory feedback loop between calcium ions (Ca<sup>2+</sup>) and ROS (Mangano *et al.*, 2017). Thus, defects in auxin regulation would impact ROS homeostasis which subsequently would impair plant developmental as observed in *mdf* mutants.

#### 5.2.2.4 MDF is required for the correct splicing of regulatory genes

Although a big overlap was found between alternatively spliced and differentially expressed genes; the extremely high number of mis-expressed targets in *mdf-1* background with no associated direct splicing defect, point towards an additional indirect role of MDF in transcript regulation.

This transcriptional control could be caused by the defective splicing found in genes associated to the GO terms “gene expression”, “transcription-DNA-templated” and “regulation of gene expression”, which could putatively lead to alterations in downstream signalling cascades. Furthermore, RT-qPCR analyses confirmed increased intron retention in a subset of transcription factors such as PFA4, also known as ATbHLH112. This transcription factor regulates the expression of genes involved in abiotic stress tolerance by mediating the activation of physiological responses such as ROS scavenging pathways (Liu *et al.*, 2015). Therefore, altered PFA4 activity in *mdf-1* mutants could result in altered ROS levels and metabolic changes as previously discussed.

Additionally, previous studies reported that the SR-related SR45 protein regulates pre-mRNA splicing by coordinating the AS of other SR proteins and interacting with other regulatory proteins and spliceosomal subunits (Ali *et al.*, 2007; Zhang *et al.*, 2017). RT-qPCR analyses with *mdf* mutants confirmed increased intron retention in *SR30*, *SR45* and *RSZ33* splicing regulatory proteins. Therefore, it seems tempting to speculate that AS splicing in SR proteins including SR45 could trigger additional AS changes and be partially responsible of the strong differential expression documented in *mdf-1* mutants.

### 5.3 Loss of MDF leads to constitutive activation of the plant DDR and impaired response to DNA damaging drugs

Activation of the plant DDR after DNA damage treatment triggers cell cycle arrest, increased endoreplication, induction of DNA repair processes and accumulation of dead cells in the RAM of WT plants (Nisa *et al.*, 2019). Curiously, *mdf* mutants displayed an analogous behaviour already at control conditions, which implied that MDF could have a novel function during the plant DDR.

#### 5.3.1 MDF has a putative role in the maintenance of genome stability by modulating the AS of important DDR regulators and regulating cell proliferation

In addition to the phenotypical observations, RNA sequencing data on *mdf-1* 12-day-old seedlings revealed enrichment of AS events in genes associated to the GO terms “DNA repair” and “cellular response to DNA damage stimulus”, as well as elevated transcript levels of genes involved in “programmed cell death” and “response to cadmium ion”. The latter is relevant for the putative role of MDF in DNA damage response, since Cd-induced DNA damage has been shown to promote cell cycle arrest in Arabidopsis root tips (Cui *et al.*, 2017). Based on these observations, it can be speculated that the absence of MDF triggers the activation of DDR pathways that are normally activated upon Cd treatment. Consequently, loss of MDF would also have a genotoxic effect on the plant, probably dependent on the splicing regulation of important DDR components. One of these components could be RAD51D, a member of the RAD51 recombination and repair proteins, that displayed increased intron retention in *mdf* mutants. RAD51D together with more than other 100 DNA repair proteins, were described to be subject of AS in Arabidopsis (Nimeth *et al.*, 2020), which further supports the importance of pre-mRNA splicing control of DNA repair proteins in plants.

Additionally, MDF putative involvement in the plant DDR was assessed by comparing the expression changes found in *mdf-1* mutants against the expression changes induced after DNA damage in WT plants (Yoshiyama *et al.*, 2020). 71% of the total set of DEG triggered by DNA damage displayed transcriptional changes in the absence of MDF. A special enrichment was observed in genes associated to DNA repair processes. These observations suggested that a transcriptional program normally induced after stress conditions was constitutively activated in *mdf-1*. Consequently, absence of MDF might lead to genome instability in Arabidopsis.

To further investigate whether loss of MDF affects the expression or splicing of important regulators of the plant DDR, comparative analyses against the direct targets activated after DNA damage by SOG1 (Ogita *et al.*, 2018), the central regulator of the plant DDR (Yoshiyama *et al.*, 2013), were performed. To this end, the overlap between these targets and the differential expression changes and intron retention events found in *mdf-1* was calculated.

61% of the SOG1 targets were differentially regulated in *mdf-1*, which confirmed that some of the expression and splicing changes derived from the loss of MDF are related to DNA damage. Among the shared targets were the ANAC044 and ANAC085 proteins. These NAC transcription factors coordinate cell cycle arrest by enhancing the accumulation of Rep-MYB transcription factors, which negatively control the expression of mitosis-specific genes (Takahashi *et al.*, 2019). 30 genes out of a set of 80 loci reported to be DNA damage-induced Rep-MYB specific target genes (Bourbouse *et al.*, 2018) were found to be among the cell cycle associated downregulated genes in *mdf-1* mutants. Thus, MDF seems to control the expression of a subset of genes involved in DNA damage-induced cell cycle control. How MDF coordinates this response remains to be elucidated, although RNA sequencing data in *mdf-1* mutants suggests that it could be correlated to splicing regulation of genes associated to the GO terms “spindle assembly” or “cell cycle process”, which were shown to be both alternatively spliced and downregulated in *mdf-1* background.

Furthermore, reduced levels of human SART1 were previously associated with abnormal spindle formation and decreased chromosomal stability (Kittler *et al.*, 2004). In this context, mutations in components of the Spindle Assembly Checkpoint (SAC) in Arabidopsis led to mitotic arrest and accumulation of dead cells in the RAM (Komaki and Schnittger, 2017). The SAC is a conserved complex in eukaryotic organisms important to ensure equal chromosome segregation during cell division and is therefore essential to maintain genome stability and normal growth (Komaki and Schnittger, 2017). The pattern of dying cells in the RAM of several loss of function mutants for SAC components resembled the cell death pattern observed after DNA damage in WT plants (Komaki and Schnittger, 2017) and in *mdf* mutants at control conditions. Therefore, additional experiments are necessary to investigate whether cell death accumulation in *mdf* mutants is caused by cell cycle defects such as abnormal chromosome segregation.

Plant splicing factors have also been recently linked to cell cycle regulation during the DDR. Loss of PLEIOTROPIC REGULATORY LOCUS 1 (PRL1), a core subunit of the spliceosome activating MOS4-associated complex (MAC) complex, led to intron retention of important cell cycle genes including the *CYCD1;1* and *CYCD3;1* cyclins. Consequently, *prl1* EMS mutants exhibited delayed cell cycle progression and increased resistance to the replication stress inducing drug HU (Wang *et al.*, 2021). Hence, PRL1 was proposed to be a constitutive positive regulator of cell cycle, targeted for degradation upon replication stress through the 26S proteasome (Wang *et al.*, 2021). MDF seems to have a similar function in promoting cell cycle progression by regulating the splicing and expression of proliferation-related genes especially in meristematic cells. Thus, it could be speculated that MDF is also targeted for degradation upon DNA damage leading to reduced cell division and thereby activating the alternative endoreplication cell cycle, as observed in *mdf* mutants.

Besides its regulatory role in cell proliferation, absence of MDF was linked to the accumulation of dead cells in the root meristem and a disorganized patterning of the RAM. This additional function in the maintenance of genome stability could also be related to its splicing function. For example, *prl1-9*, a T-DNA insertion mutant for the previously mentioned PRL1, also shared these phenotypical defects with *mdf* mutants. As such, *prl9-1* presented a disorganized quiescent center (QC), aberrant cell division, reduced meristem size as well as cell death accumulation in the RAM (Ji *et al.*, 2015). Furthermore, PRL1 is, similar to MDF, proposed to control meristem size by regulating the expression of *PLETHORA* (*PLT*) transcription factors and auxin distribution by modulating PIN expression levels in the roots (Casson *et al.*, 2009; Ji *et al.*, 2015). Based on these findings, it would be relevant to further analyse the similarities between both mutants and investigate the putative common role of MDF and PRL1 in the plant DDR and in the maintenance of the RAM.

Loss of function mutants for RDM16, a core PRP3- like splicing protein necessary for the assembly of the U4/U6 snRNP, also exhibited phenotypic similarities with *mdf* mutants (Wan *et al.*, 2016). *rdm16-4* presented impaired root meristem development, reduced cell division and cell death accumulation. Additionally, they also showed mis-splicing of genes involved in cytokinin signalling and meristem patterning including transcription factors of the PLT family (Lv *et al.*, 2021). Thus, *rdm16-4* and *mdf-1* mutants showed similar developmental defects in the root, although the overall growth arrest in the absence of RDM16 was milder. This suggests that the aberrant cell division regulation in the RAM is not the only cause for the dwarf phenotype in *mdf* mutants. MDF's additional function in SAM maintenance and putative splicing control of DNA repair, metabolism, stress responses and transcription associated genes could explain the stronger developmental alterations in *mdf-1* in comparison to *rdm16-4* mutants. Additionally, as previously introduced in section 5.2.2.2, phenotypical differences between both mutant lines might be caused by the retained partial functionality of the truncated RDM16 protein in *rdm16-4* (Lv *et al.*, 2021). Hence, it would be interesting to compare the phenotype of *mdf-1* and the T-DNA insertion mutant *rdm16-2*, which, unlike *rdm16-4*, was sterile (Lv *et al.*, 2021).

### 5.3.2 *mdf* mutants exhibit altered sensitivity to genotoxic agents and SR-related proteins might have a conserved role in the plant DDR

Sensitivity assays to different DNA damaging agents were also performed to further assess the involvement of MDF in the plant DDR and its putative relation to the pleiotropic phenotype observed in *mdf* mutants.

DSB induction after zeocin treatment led to an impaired DNA damage response in the absence of MDF, as observed by the reduced cell cycle delay, cell death induction and DNA repair activation documented in *mdf-1* mutants. Furthermore, the aberrant activation of DNA damage responsive pathways, resulted in hypersensitivity to long term exposition to zeocin in

*mdf-1* seedlings, which displayed, opposite to WT plants, a complete arrest of primary root growth and true leaf formation. These observations evidence that MDF is not only important for the prevention of DNA damage by ensuring the correct pre-mRNA splicing of cell cycle and DNA repair proteins, but also in the maintenance of genome stability after exogenous application of genotoxic drugs, by contributing to an efficient activation of DNA damage response pathways. The requirement of a functional DNA damage response after long term zeocin treatment was already characterized in knockout mutants for SOG1, in which elevated cell death accumulation was correlated with inefficient activation of DNA repair processes and the occurrence of cell division in cells with a compromised genome (Furukawa *et al.*, 2010; Johnson *et al.*, 2018).

Since mammalian SR proteins have been characterized to contribute to the maintenance of genome stability by preventing the accumulation of R loops that impede replication progression and can consequently compromise the DNA integrity (Li and Manley, 2005; Xiao *et al.*, 2007; Zhang *et al.*, 2020), sensitivity assays to zeocin were also carried out with *sr34*, *sr34b* and *sr45-1* mutants.

Loss of function mutants for all SR and SR-related proteins displayed, like *mdf* mutants, a milder relative cell division arrest after zeocin incubation in comparison to WT. Moreover, cell death accumulation was also reduced in *sr34* and *sr34b* seedlings, whereas *sr45-1* presented lower transcriptional activation of DNA repair genes. Additionally, absence of SR45 resulted in accumulation of dead cells in the RAM at control conditions and increased hypersensitivity to long term zeocin treatments, as already described in *mdf* mutants. This data proposes that plant SR proteins also impact genome stability by enhancing the efficient activation of DNA damage response pathways, probably by controlling the splicing of different DDR regulators. Unlike MDF, which seems to coordinate all major responses after genotoxic treatments, other SR-related proteins differentially regulate specific DNA damage induced pathways, like cell death accumulation in the case of SR34 and SR34b and DNA repair activation in the case of SR45. This explains the stronger developmental alterations documented in the absence of MDF.

Furthermore, the accumulation of dead cells in the RAM at control conditions and defective DNA repair activation found in this study in *sr45-1* and *mdf* mutants seems to be associated with their increased sensitivity to prolonged zeocin exposure. Therefore, it could be speculated that *mdf* and *sr45-1* seedlings present constitutive DNA damage which, due to their impaired DNA repair activation, may lead to the induction of cell death in the RAM and subsequently increased sensitivity to additional exogenous DNA damage. Thus, this suggests that, as already shown for its human homolog RNA BINDING PROTEIN S1 (RNPS1) (Fukumura *et al.*, 2018), SR45 is required to maintain the integrity of spliced mRNAs and hence is important for genome stability also at endogenous conditions. In this way, SR45 could prevent the occurrence of multiple aberrant splicing events in individual pre-mRNAs, for



example associated to cell cycle or DNA repair processes. Interestingly, RNPS1 and its interaction partners SIN3-ASSOCIATED PROTEIN 18 (SAP18) and ACINUS conform the apoptosis and splicing associated (ASAP) complex, which is believed to regulate splicing during the execution of programmed cell death (Schwerk *et al.*, 2003). Recent investigations confirmed the presence of an ASAP complex in Arabidopsis, which is constituted by orthologous genes to the human components, including SR45 (Chen *et al.*, 2019). This study characterized the ASAP complex as a splicing regulator of important proteins functioning in RNA metabolism and surveillance as well as its effect on plant developmental processes such as flowering (Chen *et al.*, 2019). Additional experiments on loss of function mutants for the other components of the ASAP complex in Arabidopsis will be essential to further evaluate the role of the complex in genome stability and cell death induction.

Intriguingly, unlike in the other splicing mutants, absence of SR45 did not result in a reduction of the accumulation of dead cells in the RAM after ON zeocin incubation. This means that, in contrast to MDF, SR34 and SR34b; SR45 might not be directly involved in the regulation of pre-mRNA splicing in genes associated to programmed cell death after SOG1 transcriptional activation. Hence, the putative role of the ASAP complex in cell death induction could be SOG1 independent and therefore not relevant after short term zeocin treatment. However, it could still be responsible for the accumulation of dead cells observed at control conditions and for a putative enhancement of cell death after longer incubation times, which would justify the hypersensitivity of *sr45-1* in primary root growth and true leaf formation. Monitoring cell death accumulation in *sr45-1sog1-7* double mutants at control conditions would be necessary to verify this hypothesis.

Since recent evidence showed the importance of pre-mRNA splicing in cell cycle regulation during the DNA damage response (Lv *et al.*, 2021; Wang *et al.*, 2021), the role of conserved core spliceosome components in the maintenance of DNA integrity in plants was further analysed. For this reason, similar phenotypic assessments as in *mdf* and *sr*-related mutants were also performed for *lsm8-1* mutants. Although no dead cells were observed after PI-staining in *lsm8-1* root tips at control conditions, these mutants behaved in a similar way as *mdf* seedlings in terms of cell cycle arrest, cell death induction and long-term sensitivity after zeocin incubation. In comparison to WT, *lsm8-1* mutants showed a milder relative cell cycle inhibition and reduced accumulation of dead cells in the RAM after ON incubation in zeocin. Moreover, they displayed stronger root growth retardation and developed significantly less true leaves after long-term growth in zeocin supplemented media.

This impaired DDR could be related to its central role in AS regulation after different stress conditions (Carrasco-López *et al.*, 2017). Accordingly, LSM8 could also be specifically activated after DNA damage to coordinate the splicing of targets linked to DNA damage associated cell cycle regulation and cell death induction. Alternatively, its increased sensitivity to zeocin treatments regarding primary root growth and true leaf formation, despite WT-like



transcriptional activation of DNA repair genes, might be associated with its altered stress response phenotype as previously reported (Carrasco-López *et al.*, 2017). This means that inefficient stress response activation and execution could ultimately also alter genome integrity and enhance the effect of zeocin treatment. On the other hand, the increased sensitivity to zeocin in plant growth related biological processes could be a consequence of its known function in plant development (Perea-Resa *et al.*, 2012). Likewise, *sr45-1* and *mdf-1* long-term zeocin hypersensitivity might also be caused by the importance of SR45 (Ali *et al.*, 2007) and MDF (Casson *et al.*, 2009) in plant growth and development.

Finally, to further explore the relationship between deficient splicing and genome instability, primary root growth was also monitored after incubation with the DNA damaging agent HU, that induces replication stress by reducing the pool of available dNTPs. Relative root growth calculations revealed a strong growth arrest in WT, *sr45-1*, *lsm8-1* and the replication stress hypersensitive *wee-1*, that served as a positive control. In contrast, root growth in *mdf* mutants was unaffected after transfer to HU. These results suggest that WEE1 and MDF have opposite functions in cell cycle regulation after replicative stress. Since WEE1 is known to trigger cell cycle arrest upon DNA damage (reviewed in Gentric *et al.*, 2021), this further confirms the positive role of MDF in cell proliferation. Consequently, loss of MDF would inhibit mitotic entry and the additional slowdown of the DNA polymerase during S-phase due to the HU-induced depletion of available dNTPs, would have no additional effect on cell cycle progression and root growth. A similar phenomenon was described in the previously mentioned *prl1* splicing mutant, whose increased resistance to HU was explained by a delay in cell cycle progression caused by mis-splicing of core cell cycle regulators (Wang *et al.*, 2021). Since PRL1 was found to be phosphorylated by WEE1 upon replicative stress, leading to its ubiquitylation and subsequent degradation by the proteasome (Wang *et al.*, 2021), it might be that MDF is also a target of WEE1. Thus, it would be interesting to analyse whether the sensitivity to HU is restored or altered in *wee-1mdf-1* double mutants. Alternatively, the increased resistance of *mdf* mutants to HU could be related to the formation of ROS after HU incubation, which can negatively impact cell cycle progression (Yi *et al.*, 2014). Since RNA sequencing data in *mdf-1* mutants suggested changes in ROS metabolism, it could be speculated that the cell cycle arrest observed in *mdf* mutants is mediated by H<sub>2</sub>O<sub>2</sub>. Therefore, no additional suppression would be expected after HU treatment.

Curiously, *sr45-1* and *lsm8-1* mutants responded to exogenous application of HU in a similar way as WT plants. This indicates that SR45 and LSM8 are either not involved in cell cycle regulation upon replicative stress or have redundant functions, so that other splicing factors would compensate their loss and enable a normal response. These observations propose MDF as a major regulator of several DNA damage related responses, in accordance with the stronger developmental defects documented in *mdf* plants in comparison to other splicing mutants.

### 5.3.3 The root growth phenotype is not recovered in *mdfsog1-7* and *mdfatm-2* double mutants

Inactivation of the main components of the plant DDR in *mdf* background by generating double mutants with SOG1 or its upstream regulator ATM, did not recover the cell cycle arrest or cell death induction phenotype of *mdf* mutants at control conditions. This suggested that the root growth phenotype associated to the loss of MDF was not generated by ectopic activation of SOG1 or ATM.

Similar to *sog1-7* single mutants, *md-1fsog1-7* and *md-2fsog1-7* double mutants did not show increased levels of SOG1-dependent DNA repair targets after DNA damage treatment. However, unlike *sog1-7* single mutants, a significantly increased accumulation of dead cells was observed in the RAM after ON incubation in zeocin. Nonetheless, this response was strongly reduced in comparison to their *mdf* single mutant counterparts. These data indicated that SOG1 dependent pathways can function in the absence of MDF and are responsible for most of the rapid cell death induction and DNA repair transcriptional activation in *mdf* mutants. Therefore, MDF might prevent genome instability at control conditions independently of SOG1 and ATM. One possibility would be by promoting the expression of *ANAC085* and *ANAC044*. Increased expression of these transcription factors correlates with G2-specific cell cycle arrest by enhancing the accumulation of Rep-MYB transcription factors, which negatively control the expression of mitosis-specific genes (Takahashi *et al.*, 2019). Overexpression of *ANAC085* and *ANAC044* was found in both *mdf* and *mdfsog1-7* double mutants. For this reason, it would be interesting to analyse whether loss of MDF induces cell cycle arrest by ectopic overexpression of *ANAC085* and *ANAC044*. Therefore, it should be assessed whether *mdf-1anac085anac044* triple mutants show a recovery of the root growth phenotype.

Alternatively, MDF could act downstream of SOG1 and be negatively regulated upon DNA damage to inhibit cell cycle progression. In this case no additional root growth retardation would be expected in *mdfsog1-7* and *mdfatm-2* double mutants, as observed during this study.

In this context, as previously mentioned, targeted degradation upon DNA damage of positive regulators of cell cycle progression was already demonstrated for PRL1 (Wang *et al.*, 2021). PRL1 degradation is dependent on its phosphorylation at Serine 145 by WEE1, which promotes its ubiquitination and subsequent degradation by the proteasome (Wang *et al.*, 2021). Repression of the splicing factor PRL1 after DNA damage is linked to the activation of cell cycle checkpoints due to mis-splicing of important cell cycle regulators (Wang *et al.*, 2021).

Ubiquitin E3 ligase F-BOX-LIKE17 (FBL17) which positively regulates cell cycle by promoting the degradation of CKIs, is also repressed by WEE1 phosphorylation in response to replicative stress (Pan *et al.*, 2021). FBL17 degradation via the proteasome leads to the

accumulation of CKIs and the subsequent inhibition of CDK complexes (Gentric *et al.*, 2020; Pedroza-García *et al.*, 2022). Consequently, *fbl17* seedlings exhibit reduced proliferation in both roots and leaves and abnormal chromosomal segregation in the RAM. In contrast to *mdf* mutants, where an increase in endoreplication was shown during this study, loss of FBL17 blocks endoreplication in leaves. Interestingly, absence of FBL17 also triggers genome instability traits such as the induction of cell death and the expression of replication stress and DSB DNA repair checkpoint genes in a SOG1-independent manner (Gentric *et al.*, 2020). This function was proposed to be independent of its role in cell cycle proliferation (Noir *et al.*, 2015). Moreover, multiple DDR genes constitutively activated in the absence of FBL17 were suggested to be direct targets of the SOG1-independent RETINOBLASTOMA RELATED1 (RBR1)/E2FA transcription factor module (Gentric *et al.*, 2020). RBR1 has a conserved role in cell division mostly by binding to and thereby inhibiting the function of E2F transcription factors. This subsequently suppresses the transcription of different targets involved in cell cycle progression including FBL17 (Horvath *et al.*, 2017; Biedermann *et al.*, 2017). Knockdown mutants for RBR1 share phenotypical traits with *mdf* mutants, such as accumulation of dead cells in the RAM and hypersensitivity to DSB inducing drugs, but not to hydroxyurea (Biedermann *et al.*, 2017). However, while RBR1 negatively regulates cell cycle progression, MDF seems promote it. Therefore, *rbr1* displays no growth reduction at control conditions (Biedermann *et al.*, 2017). Besides its role in cell division control, RBR1 has also been linked to DNA repair processes during the plant DDR and, contrary to *mdf* mutants, reduced levels of RBR1 triggered a higher transcriptional activation of DDR genes after DNA damage treatment in comparison to WT plants (Biedermann *et al.*, 2017).

The similarities observed between *mdf* mutants and both *rbr1* and *fbl17*, hinted at a connection between MDF and this SOG1 independent DDR pathway. Accordingly, reduced differential expression of *RBR1*, *FBL17* and *E2FA* genes was found by RNA sequencing analyses in *mdf-1* background. Lower levels of RBR1 should theoretically result in milder E2FA inhibition and subsequently trigger a higher transcriptional activation of E2FA targets such as FBL17, which in turn promotes cell cycle proliferation. However, AS events were also found in E2FA in the absence of MDF, which suggests that the abnormal splicing of this transcription factor could impact the induction of its downstream targets. Those include not only FBL17, which would explain the cell cycle arrest in *mdf-1* background, but also genes associated to cell death induction. Since accumulation of dead cells was documented in *mdf* mutants, impaired activation of E2FA targets cannot be exclusively responsible for the genome instability traits associated to the loss of MDF. This also indicates that a putative connection between MDF and the RBR1/E2F module would most likely be restricted to their function in cell cycle regulation.

In conclusion, additional experiments are necessary to elucidate the upstream regulators of MDF during the plant DDR. Nevertheless, MDF's proposed positive function in both cell proliferation and DNA repair, which are antagonistically regulated upon DNA damage,

suggests that MDF activity is finely regulated during the plant DDR. Possible regulatory mechanisms could include negative feedback with important DDR regulators, alternative splicing or posttranslational modifications such as phosphorylation.

#### 5.4 The phosphorylation status of MDF influences Arabidopsis development

Investigations in the animal field revealed that pre-mRNA splicing and processing factors are regulated in a post-translational manner during the DDR. These modifications most frequently include phosphorylation, parylation or acetylation (Naro *et al.*, 2015). Interestingly, signalling cascades driven by phosphorylation haven been characterized to coordinate the plant DDR, with the two ATM and ATR protein kinases being the major regulators and initiators of this process (Roitinger *et al.*, 2015). In fact, previous proteomic studies identified multiple proteins regulated by their phosphorylation status upon DNA damage in an ATM and/or ATR dependent manner. Among them, 12 were linked to pre-mRNA splicing, including our protein of interest MDF (See Table I-1 in section 1.4.4).

It was therefore tempting to speculate that the activity of these group of splicing associated proteins was regulated after DNA damage, hinting at a conserved role for splicing factors in the plant DDR. Moreover, knockout mutants for some of these splicing proteins displayed genome instability defects that were similar to those seen in *mdf* mutants. For example, absence of ENHANCED SILENCING PHENOTYPE 3 (ESP3), homologous to the human PRP2 RNA splicing cofactor exhibited cell death accompanied by reduced growth (Herr *et al.*, 2006; Howles *et al.*, 2016; Zheng *et al.*, 2019). Notably, two subunits of the spliceosome associated MAC complex (MAC3A and MAC3B) important for plant development and immunity (Jia *et al.*, 2017), were also found to undergo phosphorylation changes after DNA damage (Roitinger *et al.*, 2015). This is particularly interesting based on a recent study previously mentioned that characterized the importance of the phosphorylation status of PRL1, another MAC complex subunit, in the coordination of cell cycle arrest during the plant DDR (Wang *et al.*, 2021). These observations suggest that these RNA splicing proteins are putatively regulated by changes in their phosphorylation state and constitute ideal candidates to further evaluate the function of pre-mRNA splicing during the plant DDR.

The biological relevance of the phosphorylation of MDF at Serine 22 was analysed following a phosphomimic approach in which amino acid substitutions were performed to emulate the phosphorylation states that occur naturally. To this end, constitutively phosphorylated (35SMDFS22DCDS) and dephosphorylated (35SMDFS22ACDS) versions of MDF were generated via site directed mutagenesis (SDM) using a 35SMDFCDS construct as template.

The lack of phosphorylation had no apparent impact on MDF's subnuclear localization since 35SMDFS22A derived fluorescence conserved a speckled pattern and putatively accumulated

inside the nucleolus. This is different to previous findings that showed that phosphorylation of SR and SR-related proteins was associated with changes in their subcellular localization. For instance, phosphorylation at their RS domain regulated their activity by promoting their recruitment from nuclear speckles storage sites to the nucleoplasm or facilitating their shuttling between cytoplasm and nucleus (Ali *et al.*, 2003; Huang and Steitz, 2005). As such, inhibition of phosphorylation and transcription lead to the formation of bigger speckles in SR45 (Ali *et al.*, 2003). However, since neither speckle size nor the number of formed speckles were measured, the unaltered subnuclear domain organization observed after overexpression of the dephosphomutant version of MDF could be afterwards proofed false. A reliable quantification method should be established to verify this observation. Nevertheless, assuming that, in contrast to SR45 (Ali *et al.*, 2003), the lack of phosphorylation at Serine 22 in MDF has indeed no effect on its subcellular localization, this could be caused by methodological differences between both experiments. While suppression of SR45 phosphorylation was achieved by the exogenous addition of staurosporine, a kinase inhibitor, MDF dephosphorylation state was accomplished by direct changes at the amino acid level. Thus, it could be speculated that staurosporine treatment alters additional biological treatments which could also contribute to the strong differences in speckle formation.

Phenotypical and transcriptional analyses of *mdf-1* transgenic lines stably transformed with a non-mutated MDFCDS construct under a 35S promoter and both phosphomutants revealed that the phosphorylation state of MDF influenced its function in plant development. On one hand, *mdf-1::35SMDFCDS* transgenic plants showed, in comparison to *mdf-1::35SMDFS22ACDS*, a bigger recovery of the cell division and root length defects found in *mdf-1*. On the other hand, a full recovery of the dwarf phenotype and sterility associated to the absence of MDF was only observed in transgenic *mdf-1* plants stably transformed with 35SMDFS22A. Therefore, MDF, specifically in its dephosphorylated state, seems to promote vegetative development.

This dual function could be related to the differential splicing and transcription of several genes in a phosphorylation and tissue dependent manner. For example, increased intron retention and reduced expression of *MYB3R3* and *CYCA2-3* cyclin was only retained in *mdf-1::35SMDFS22A* seedlings, whereas leaves from *mdf-1::35SMDFCDS* plants exhibited defective splicing in a protein involved in shoot apical meristem maintenance and identity. Uncovering the global transcriptional and splicing profile from *mdf-1* transgenic plants transformed with both phosphomutant versions would clarify the importance of MDF phosphorylation for target selection and splicing activity.

Opposite to *atm-2::35SMDFCDS* transformants, *atm-2::35SMDFS22D* transgenic plants displayed a strong growth arrest in aerial tissues. This suggested that the developmental function of MDF was phosphorylation dependent and probably mediated by ATM, as previously reported (Roitinger *et al.*, 2015). However, after zeocin incubation, neither cell

death induction nor DNA repair transcriptional activation were influenced by MDF phosphorylation status. Based on these analyses, it can be inferred that MDF's putative role in genome stability is likely not influenced by ATM or changes in phosphorylation.

The biological relevance of phosphorylation changes for mRNA splicing activity and plant development were previously shown in loss of function for PRE-mRNA PROCESSING 4 (PRP4) KINASE A (PRP4KA). The absence of this spliceosome-associated kinase led to diverse phenotypical alterations such as atypical rosettes, late flowering, reduced branching, and lowered seed set (Kanno *et al.*, 2018). Thus, it was proposed that PRPKA influences Arabidopsis AS by phosphorylating a subset of splicing regulators (Kanno *et al.*, 2018). Studies with MITOGEN-ACTIVATED PROTEIN KINASE 4 (MPK4), a major activator of the PAMP-induced immune response, provided recently additional evidence of the phosphorylation control of splicing activity in the context of plant stress responses. Loss of MPK4 dependent phosphorylation led to splicing changes in several splicing factors and immunity-related protein kinases (Bazin *et al.*, 2020). Therefore, not only MDF's function in plant development, but also MDF's presumed role in adaptation to stress conditions could be influenced by its phosphorylation state.

Altogether, these data provide initial evidence of a phosphorylation dependent control of MDF's splicing activity. However, additional experiments are required to further understand how MDF phosphorylation is regulated and its effect on AS on a genome-wide level. Future research could also address whether additional mechanisms beyond phosphorylation changes modulate MDF's function in genome stability.

## 5.5 Conclusions

Numerous studies in the animal field as well as recent investigations concerning the spliceosome associated MAC complex in Arabidopsis have provided supporting evidence of a conserved role for plant splicing factors in the maintenance of genome stability.

This work provided a first insight of the involvement of SR-related proteins, in particular of MDF, in the plant DDR, suggesting the following model (Figure D-2): Under control conditions MDF mediates the splicing and correct expression of genes associated to cell division and is therefore important for normal plant growth. This process would be influenced by its phosphorylation status, with the phosphorylated state being more active in the RAM, supporting root growth. On the other hand, a dephosphorylated version of MDF seems to be required in the SAM and influences the transition from vegetative to reproductive development. Additionally, the milder growth inhibition observed in *mdf-2* mutants indicated that the C-terminal part of MDF, which shows the highest homology to other SART1 family proteins, could be sufficient for MDF's activity especially during shoot development.



## DISCUSSION

Different stress conditions, including DNA damage, would potentially coordinate MDF's antagonistic roles in response to genotoxic stresses. Lack of apparent recovery of the cell cycle arrest phenotype in *mdfsog1-7* double mutants and the increased resistance to HU of *mdf* single mutants, suggested that MDF could be negatively regulated by SOG1 and/or WEE1 to inhibit cell cycle progression and putatively trigger the endocycle. On the other hand, RNA sequencing data and zeocin sensitivity assays proposed a positive role for MDF during cell death induction and DNA repair transcriptional activation. Thus, additional regulatory mechanisms might modulate MDF levels to activate different responses depending for example on the type of stress, severity of the lesion or DNA damage site (Figure D-2). Whether cell cycle and DNA repair defects associated to the loss of MDF are responsible for the induction of cell death in *mdf* mutants remains to be elucidated.

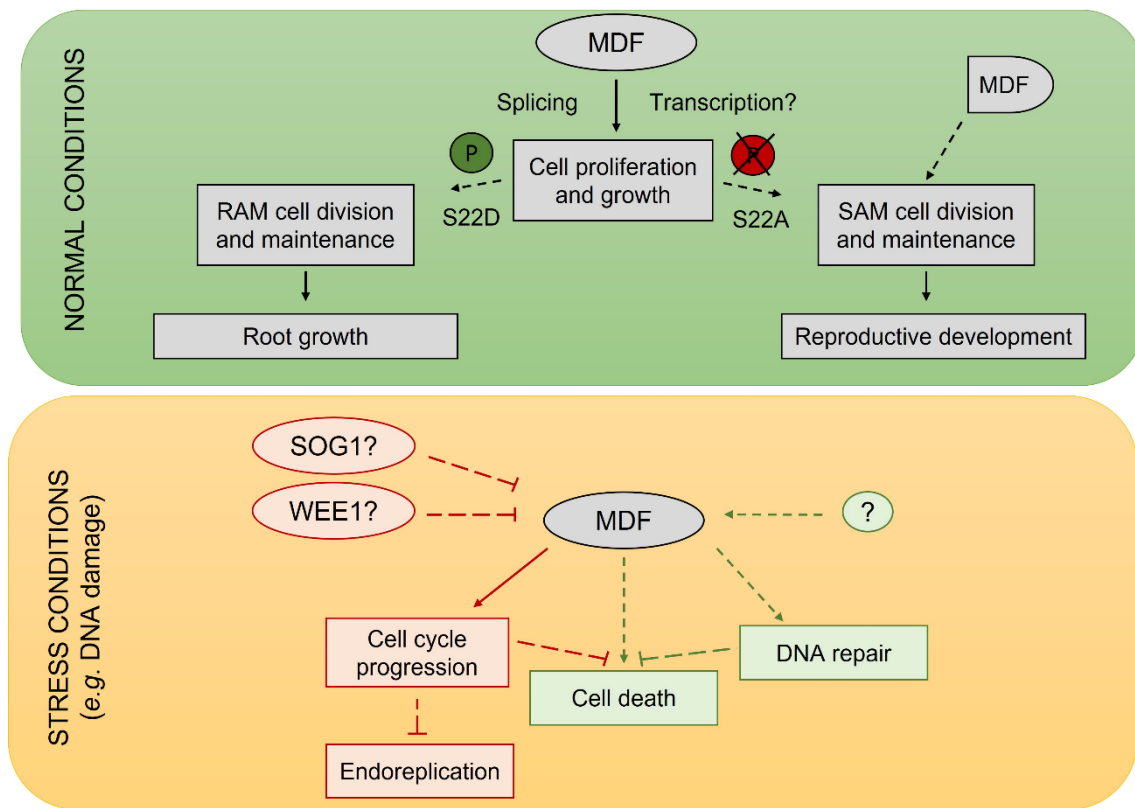
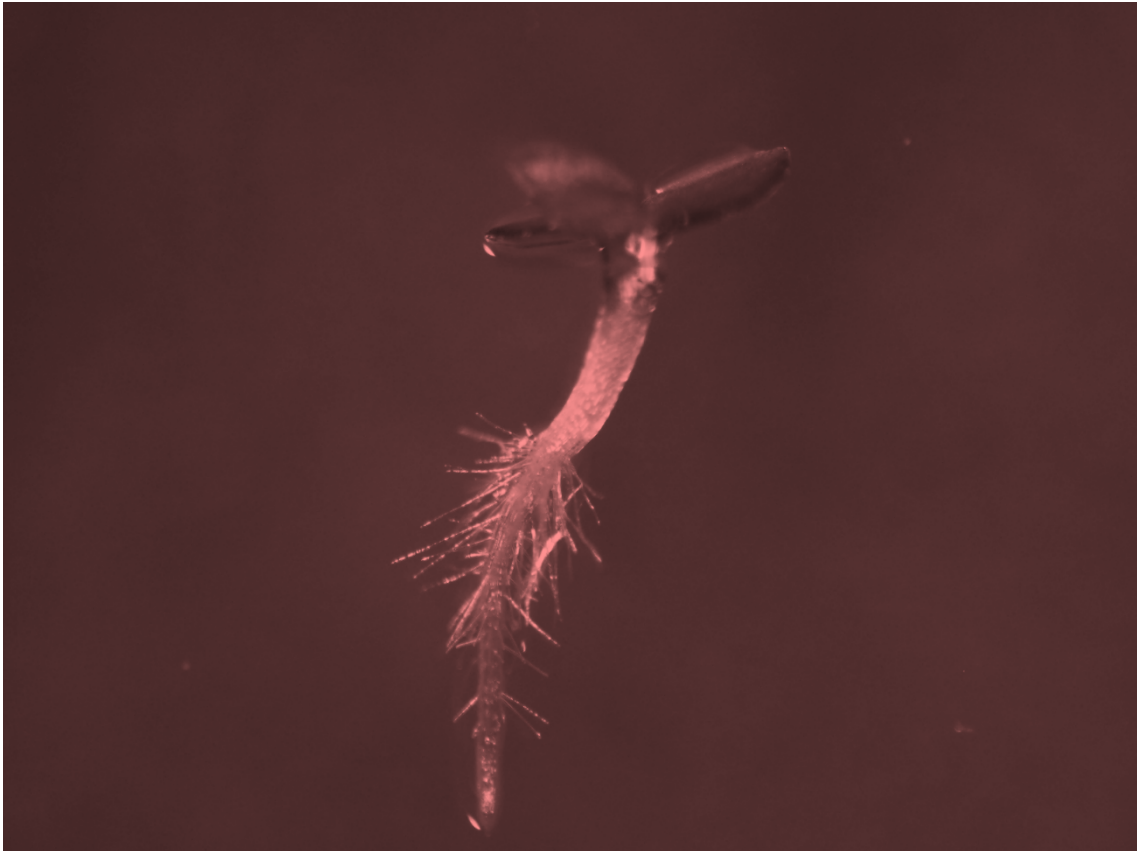


**Figure D-2. Schematic representation of the model predicting MDF's mode of action at control and under stress conditions** as described in section 5.5. MDF: MERISTEM-DEFECTIVE; SOG1: SUPPRESSOR OF GAMMA RESPONSE1. Dashed lines represent mechanisms whose regulation remains to be elucidated. Red boxes represent mechanisms activated in the absence of MDF, while green boxes represent mechanisms that might require MDF for efficient activation. A putative MDF C-terminus truncated protein is represented by the lower half on the oval used to illustrate MDF complete protein.



# 6. SUMMARY

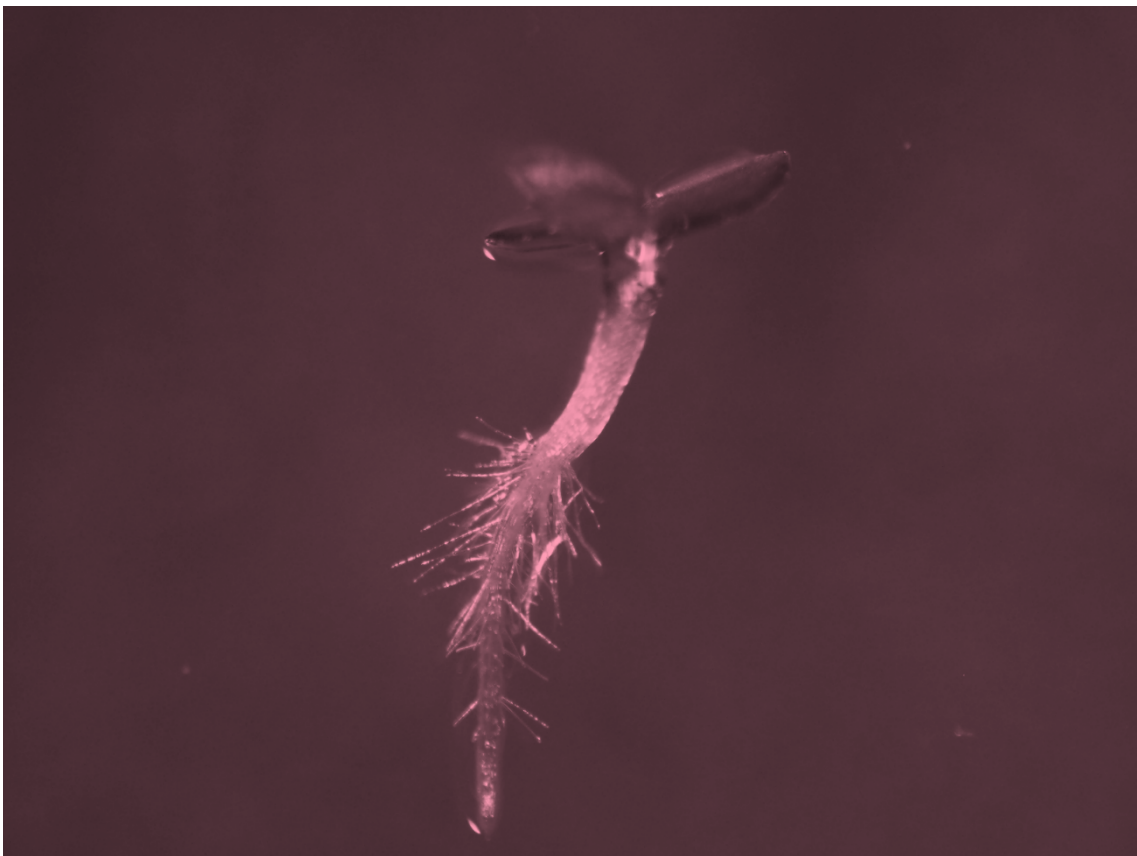


Plants have developed an elaborate DNA damage response (DDR) to cope with the exogenous environmental agents and endogenous metabolic processes that can threaten the genome integrity by inducing DNA lesions. Recent evidence suggests that, as it is already well known in animal cells, RNA binding proteins (RBPs) might also have a role in the plant DDR. The focus of this research is the SPLICEOSOME ASSOCIATED FACTOR 1 (SART1)-related splicing factor MERISTEM DEFECTIVE (MDF). MDF has been described to be involved in meristem patterning and auxin regulation. Interestingly, MDF was also shown to be phosphorylated by ATAXIATELANGIECTASIA MUTATED (ATM) and/or ATM AND RAD3-RE-LATED (ATR) – two key regulators of the plant DDR- in response to genotoxic stress. Phenotypical analyses of MDF loss of function mutants revealed strong defects in genome stability such as reduced cell division, short root phenotype or accumulation of dead cells in the root apical meristem (RAM). Moreover, RNA-sequencing analyses uncovered that *mdf-1* mutants display numerous transcription and splicing changes in genes associated to stress responses, development, cell division and metabolism. The finding that *mdf* mutants responded to short- and long-term treatments with DNA damaging agents differently than WT plants, further supported the role of MDF in coordinating stress responses (*e.g.*, DNA damage) with cell division. Additionally, preliminary assays with phosphomutant variants suggested that the phosphorylation status of MDF influenced its activity. Altogether this study proofed that MDF is localized in the spliceosome and is important for pre-mRNA splicing, cell division control and Arabidopsis development. It also provides evidence of a conserved role for splicing factors in genome stability.

Pflanzen haben eine ausgeklügelte DNA-Schadensreaktion (engl. DNA DAMAGE RESPONSE; DDR) entwickelt. Diese dient der Bewältigung von exogenen Umwelteinflüssen und endogenen Stoffwechselprozessen, die die Integrität des Genoms durch DNA-Läsionen gefährden können. Neueste Belege deuten darauf hin, dass ähnlich wie in tierischen Zellen, RNA-bindende Proteine (RBPs) auch in der pflanzlichen DDR eine Rolle spielen könnten. Im Mittelpunkt dieser Forschung steht der mit dem SPLICEOSOME ASSOCIATED 1 (SART1) verwandte Spleißfaktor MERISTEM DEFECTIVE (MDF). Es wurde beschrieben, dass MDF an der Meristemstrukturierung und der Auxinregulierung beteiligt ist. Interessanterweise konnte auch gezeigt werden, dass MDF nach genotoxischem Stress durch ATAXIATELANGIECTASIA MUTATED (ATM) und/oder ATM AND RAD3-RELATED (ATR) - zwei Schlüsselregulatoren der pflanzlichen DDR - phosphoryliert wird. Phänotypische Analysen von MDF-Funktionsverlustmutanten offenbarten starke Defekte in der Genomstabilität, wie z. B. reduzierte Zellteilung, kurze Wurzeln oder die Anhäufung von toten Zellen im Wurzelapikalmeristem (engl. ROOT APICAL MERISTEM; RAM). Des Weiteren zeigten RNA-Sequenzierungsanalysen, dass *mdf-1*-Mutanten zahlreiche Veränderungen im Transkriptions- und Spleißverhalten von Genen aufweisen, die in Stressreaktionen, Entwicklung, Zellteilung und Stoffwechsel involviert sind. Die Beobachtung, dass *mdf*-Mutanten, anders als der Wildtyp (WT), auf kurz- und langfristige Behandlungen mit DNA-schädigenden Substanzen reagierten, verdeutlicht die Rolle von MDF bei der Koordinierung von Stressreaktionen (z. B. DNA-Schäden) und Zellteilung. Darüber hinaus deuteten erste Versuche mit verschiedenen Varianten von Phosphorylierungsmutanten darauf hin, dass der Phosphorylierungszustand von MDF dessen Aktivität beeinflusst. Alles in allem beweist diese Studie, dass MDF im Spleißosom lokalisiert ist und für das Spleißen von prä-mRNA, die Kontrolle der Zellteilung und die Entwicklung von Arabidopsis wichtig ist. Sie liefert auch Hinweise auf eine konservierte Rolle von Spleißfaktoren für die Genomstabilität.



# 7. ADDITIONAL RESEARCH LINES



The results briefly described in this section are included in two publications, to which I contributed as an author in the experimental and writing process. Both manuscripts can be found in the Appendix.

### 7.1 Analyses of the impact of the MAIN/MAIL1/PP7L complex in primary root growth and genome stability

MDF was identified as one of the proteins that specifically interacted with MAIN-LIKE1 (MAIL1) after treatment with the DNA crosslinking agent mitomycin (MMC) in a Co-Immunoprecipitation (Co-IP) experiment using MAIL1- GFP as bait (Magdalena Weingartner personal communication). This interaction was confirmed during my master thesis by performing Bimolecular fluorescence complementation (BiFC) assays in *Arabidopsis* mesophyll protoplasts (Master thesis de Luxán-Hernández, 2017).

MAIL1 and its closest homolog MAINTENANCE OF MERISTEMS (MAIN) belong to a small plant-specific gene family defined by the presence of a conserved amino-transferase-like plant mobile domain (PMD). Both proteins were shown to be essential for maintenance of genome stability during cell division in stem cells and their daughter cells in the root apical meristem (RAM) (Wenig, *et al.*, 2013; Ühlken *et al.*, 2014).

In a recent publication in which I was involved (de Luxán-Hernández *et al.*, 2020. See Appendix), it was discovered that MAIL1 and MAIN acted in complex with PROTEIN PHOSPHATASE7-LIKE (PP7L). PP7L is an inactive isoform of PROTEIN PHOSPHATASE 7 (PP7) that belongs to the PP7-type family of serine/threonine phosphatases (de Luxán-Hernández *et al.*, 2020) and was characterized to be important for chloroplast development (Xu *et al.*, 2019).

By monitoring the primary root growth from 1 until 15 days after germination (DAG) of WT, *main-2*, *mail1-1*, *pp7l-1* and *pp7l-3* seedlings (Figure 2b de Luxán-Hernández *et al.*, 2020), I confirmed that absence of MAIN and MAIL1 resulted in shorter primary roots in *Arabidopsis*. Furthermore, based on the primary root growth arrest displayed by both *pp7l* mutants 3 DAG, I verified that the entire complex, including PP7L, is essential during primary root development.

In agreement with a ubiquitous expression in all plant tissues, which I demonstrated by assessing *PPTL* transcript levels in roots, seedlings, rosette leaves and flowers with RT-qPCR experiments (Figure S2d de Luxán-Hernández *et al.*, 2020), I observed a delayed development not only in the root system, but also in aerial tissues (Figure S2b de Luxán-Hernández *et al.*, 2020). These findings verified the phenotypical analyses presented in a previous publication (Xu *et al.*, 2019).

Similar to what it was shown for *mdf* mutants (Figures R-2D to F), absence of each component of the MAIN/MAIL1/PP7L complex correlated with cell death in root initials and their descendants in the root apical meristem (RAM) (Wenig, *et al.*, 2013; Ühlken *et al.*, 2014; de Luxán-Hernández *et al.*, 2020). By comparing the cell death patterns in propidium iodine (PI) stained root tips of *pptl-1sog1-7* and *pp7l-1* plants using confocal microscopy (Figure 6b de Luxán-Hernández *et al.*, 2020), I observed no apparent difference between both lines. Based on this data, it was speculated that cell death accumulation in loss of function mutants for PP7L was not induced in a SOG1 dependent manner.

Additionally, I also investigated whether *pp7l* mutants, like *main-2* and *mail1-1* (Wenig, *et al.*, 2013; Ühlken *et al.*, 2014), exhibited impaired DNA damage response (DDR) signalling. To this end, I evaluated the expression of DDR-related genes in root tips from WT, *pp7l-1* and *pp7l-3* 3 DAG by RT-qPCR (Figure 6a de Luxán-Hernández *et al.*, 2020). After normalizing the expression to WT levels, I observed that 3 out of the 4 tested genes presented a significant upregulation in both mutant lines. This confirmed that absence of PP7L, resulted in an increased transcriptional activation of DNA damage responsive genes. Therefore, the whole MAIN/MAIL1/PP7L complex seems to have a role in preserving DNA integrity in Arabidopsis.

Future studies should address whether MDF and the MAIN/MAIL1/PP7L complex function together during primary root development and maintenance of genome stability, which could explain the shared phenotypical traits between *mdf*, *main-2*, *mail1-1* and *ppt7l* mutants.

## 7.2 Assessing the importance of the Translation Elongation complex eEF1B in cell division and plant development

Cell division and plant development are influenced by post-transcriptional mechanisms that enable the plant to adapt to different endogenous and exogenous stress conditions. These processes include alternative splicing (AS), as it was previously mentioned for several splicing proteins during this thesis, but also protein synthesis and homeostasis.

In this context, a project in our department is focused on understanding how the different components of the translation elongation complex eEF1B impact Arabidopsis growth and adaptation to unfavourable abiotic conditions with special focus on heat stress. The main outcome of this investigation can be found on a manuscript recently submitted to the Journal of Experimental Botany. Its preprint form is available on the Appendix section.

My contribution to this paper includes confocal microscopy experiments with PI-stained root tips of 7-day-old WT and *eef1by1/2* double mutants that carry T-DNA insertions in the two alleles that encode the  $\gamma$  subunit of the eEF1B complex (Figure 3E Lohmann *et al.*, 2022). Quantification of the number of cortical cells within the proximal meristem revealed a



significant reduction in the population of dividing cells in *eef1bγ1/2* mutants in comparison to WT (Figure 3F Lohmann *et al.*, 2022). These data indicated that absence of the eEF1B complex  $\gamma$  subunit negatively impacts cell division in *Arabidopsis thaliana*.

Additionally, I evaluated the influence of the eEF1B complex  $\gamma$  subunit in primary root growth under increased ambient temperatures conditions. To this end, I measured the primary root length of WT, *eef1bγ1/2* and the heat shock hypersensitive *hsp101* seedlings grown for 7 days at 22 or 27°C in MS sucrose vertical plates (Figure S4C Lohmann *et al.*, 2022). Root growth was promoted in a similar degree in all lines when grown at 27°C. This was sustained by the lack of differences observed between the WT and the mutants in terms of relative root growth ratios (Figure S4C Lohmann *et al.*, 2022), which were calculated by dividing the average root length measured at 27°C between the average root length obtained at 22°C. This means that neither HEAT SHOCK PROTEIN 101 (HSP101) nor eEF1B complex  $\gamma$  subunit play an essential role in *Arabidopsis* adaptation to higher ambient temperatures.

Besides my experimental contribution I also supported the writing of this manuscript.

## ACKNOWLEDGEMENTS

This study would not have been possible without the guidance and support from my scientific supervisor and mentor Magdalena Weingartner, whose insightful suggestions and ideas elevated the quality of both the experiments and the final writing of this thesis. I will always be grateful for all your help throughout these years.

Big thanks to Stefan Hoth for welcoming me with open arms into his group and continuously encouraging me all these years to continue a career in science. I value and appreciate every scientific discussion we had and will always remember our chats in the kitchen and hallways of the IPM. Thank you also for your countless letters of recommendations and accepting to be an examiner of this thesis.

Thank you to the rest of my committee members, with special thanks to Óscar Lorenzo Sánchez for inspiring me to become a Plant Molecular Biologist researcher and granting me the first opportunity to conduct a scientific project in a laboratory. Thank you again for supporting me whenever I asked you for help and agreeing to act as a thesis examiner.

Thank you to my collaboration partners Julio Salinas, Eduardo Tranque, Pavla Binarova and Jana Chumova for your impressive scientific work and friendly disposition.

I would also like to acknowledge the contributions of different students to this project with special recognition of Hasibe Tuncay, Sotoodeh Seyedehyasaman and Anastasiia Goshina, as well as the technical and administrative support of Wiebke Hellmeyer, Judith Mehrmann, Christiane Debus, Teresa Wulf and Wenke Bahnsen.

A big thanks goes to my IPM and MPP adopted family, especially to Lisa Amelung, Giuliana Heßler, Monique Liebers, Tim Lienemann, Julia Lohmann and Linn von Pein. Each of you have been an essential support during my Hamburg journey and I know you will accompany me in my upcoming adventures.

Thank you very much to everyone who helped me both scientifically or emotionally throughout all my scientific career in Gran Canaria, Salamanca, Bonn and Hamburg. I feel very grateful for every talk, correction, email, phone call, message or hug.

**MUCHAS GRACIAS**



## REFERENCES

- Adachi, S., Minamisawa, K., Okushima, Y., Inagaki, S., Yoshiyama, K., Kondou, Y., . . . Umeda, M. (2011). Programmed induction of endoreduplication by DNA double-strand breaks in Arabidopsis. *PNAS*, *108*, 10004–10009.
- Aida, M., Beis, M., Heidstra, R., Willemsen, V., Blilou, I., Galinha, C., . . . Scheres, B. (2004). The PLETHORA Genes Mediate Patterning of the Arabidopsis Root Stem Cell Niche. *Cell*, *119*(1), 109-120.
- Ali, G., Golovkin, M., & Reddy, A. (2003). Nuclear localization and in vivo dynamics of a plant-specific serine/arginine-rich protein. *The Plant Journal*, *36*(6), 883-93.
- Ali, G., Palusa, S., Golovkin, M., Prasad, J., Manley, J., & Reddy, A. (2007). Regulation of Plant Developmental Processes by a Novel Splicing Factor. *PLoS ONE*, *5*, e471.
- Andrés, F., Romera-Branchat, M., Martínez-Gallegos, R., Patel, V., Schneeberger, K., Jang, S., . . . Coupland, G. (2015). Floral Induction in Arabidopsis by FLOWERING LOCUS T Requires Direct Repression of BLADE-ON-PETIOLE Genes by the Homeodomain Protein PENNYWISE. *Plant Physiology*, *169*, 2187–2199.
- Bahieldin, A., Atef, A., Edris, S., Gadalla, N., Ali, H., Hassan, S., . . . El-Domyati, F. (2016). Ethylene responsive transcription factor ERF109 retards PCD and improves salt tolerance in plant. *BMC Plant Biology*, *16*, 216.
- Baud, S., Boutin, J.-P., Miquel, M., Lepiniec, L., & Rochat, C. (2002). An integrated overview of seed development in Arabidopsis thaliana ecotype WS. *Plant Physiology and Biochemistry*, *40*(2), 151-160.
- Bazin, J., Mariappan, K., Jiang, Y., Blein, T., Voelz, R., Crespi, M., & Hirt, H. (2020). Role of MPK4 in pathogen-associated molecular pattern-triggered alternative splicing in Arabidopsis. *PLoS Pathogens*, *16*(4), e1008401.
- Bérdy, J., Aszalos, A., Bostian, M., & McNitt, M. (1980). *CRC Handbook of Antibiotic Compounds: Amino Acid and Peptide Antibiotics*. Boca Raton, FL: Crc Press.
- Biedermann, S., Harashima, H., Chen, P., Heese, M., Bouyer, D., Sofroni, K., & Schnittger, A. (2017). The retinoblastoma homolog RBR1 mediates localization of the repair protein RAD51 to DNA lesions in Arabidopsis. *The EMBO Journal*, *36*(9), 1279–1297.

## REFERENCES

- Bleckmann, A., Weidtkamp-Peteres, S., Seidel, C., & Simon, R. (2010). Stem cell signaling in Arabidopsis requires CRN to localize CLV2 to the plasma membrane. *Plant Physiology*, *152*(1), 166-76.
- Blilou, I., Xu, J., Wildwater, M., Willemsen, V., Paponov, I., Friml, J., . . . Scheres, B. (2005). The PIN auxin efflux facilitator network controls growth and patterning in Arabidopsis roots. *Nature*, *433*(7021), 39-44.
- Bourbousse, C., Vegesna, N., & Law, J. (2018). SOG1 activator and MYB3R repressors regulate a complex DNA damage network in Arabidopsis. *PNAS*, *115*(52), E12453–E12462.
- Bouyer, D., Heese, M., Chen, P., Harashima, H., Roudier, F., Grüttner, C., & Schnittger, A. (2018). Genome-wide identification of RETINOBLASTOMA RELATED 1 binding sites in Arabidopsis reveals novel DNA damage regulators. *PLoS Genetics*, *14*(11), e1007797.
- Boyle, E., Weng, S., Gollub, J., Jin, H., Botstein, D., Cherry, J., & Sherlock, G. (2004). GO::TermFinder—open source software for accessing Gene Ontology information and finding significantly enriched Gene Ontology terms associated with a list of genes. *Bioinformatics*, *20*(18), 3710-5.
- Breuninger, H., Rikirsch, E., Hermann, M., Ueda, M., & Laux, T. (2008). Differential Expression of WOX Genes Mediates Apical-Basal Axis Formation in the Arabidopsis Embryo. *Developmental Cell*, *14*, 867–876.
- Brown, J., & Simpson, C. (1998). SPLICE SITE SELECTION IN PLANT PRE-mRNA SPLICING. *Annual Review of Plant Physiology and Plant Molecular Biology*, *49*, 77–95.
- Canher, B., Heyman, J., Savina, M., Devendran, A., Eekhout, T., Vercauteren, I., . . . De Veylder, L. (2020). Rocks in the auxin stream: Wound-induced auxin accumulation and ERF115 expression synergistically drive stem cell regeneration. *PNAS*, *117*(28), 16667–16677.
- Cao, X., Wang, H., Zhuang, D., Zhu, H., Du, Y., Cheng, Z., . . . Liu, W. (2018). Roles of MSH2 and MSH6 in Cadmium-induced G2/M checkpoint arrest in Arabidopsis roots. *Chemosphere*, *201*, 586-594.
- Capron, A. C., Provart, N., & Berleth, T. (2009). Embryogenesis: Pattern Formation from a Single Cell. En *The Arabidopsis book* (Vol. 7). American Society of Plant Biologists.
- Carvalho, R., Domingues Carvalho, S., & Duque, P. (2010). The plant-specific SR45 protein negatively regulates glucose and ABA signaling during early seedling development in Arabidopsis. *Plant Physiology*, *154*(2), 772-83.

- Casson, S., Spencer, M., Walker, K., & Lindsey, K. (2005). Laser capture microdissection for the analysis of gene expression during embryogenesis of Arabidopsis. *The Plant Journal*, *42*, 111-123.
- Casson, S., Topping, J., & Lindsey, K. (2009). MERISTEME-DEFECTIVE, an RS domain protein, is required for the correct meristem patterning and function in Arabidopsis. *The Plant Journal*, *57*, 857-869.
- Chang, P., Hsieh, H.-Y., & Tu, S.-L. (2022). The U1 snRNP component RBP45d regulates temperature-responsive flowering in Arabidopsis. *The Plant Cell*, *34*, 834–851.
- Chaudhary, S., Khokhar, W., Jabre, I., Reddy, A., Byrne, L., Wilson, C., & Syed, N. (2019). Alternative Splicing and Protein Diversity: Plants Versus Animals. *Frontiers in Plant Science*, *10*(708).
- Chen, M.-X., Zhang, K.-L., Gao, B., Yang, J.-F., Tian, Y., Das, D., . . . Fang, Y.-M. (2020). Phylogenetic comparison of 50 splice site determination in central spliceosomal proteins of the U1-70K gene family, in response to developmental cues and stress conditions. *The Plant Journal*, *103*, 357–378.
- Chen, S., Niu, X., Guan, Y., & Li, H. (2017). Genome-Wide Analysis and Expression Profiles of the MYB Genes in *Brachypodium distachyon*. *Plant Cell Physiology*, *58*(10), 1777-1788.
- Chen, S., Rooney, T., Hu, A., Beard, H., Garrett, W., Mangalath, L., . . . Zhang, X.-N. (2019). Quantitative Proteomics Reveals a Role for SERINE/ARGININE-Rich 45 in Regulating RNA Metabolism and Modulating Transcriptional Suppression via the ASAP Complex in Arabidopsis thaliana. *Frontiers in Plant Science*, *10*(1116).
- Chen, T., Cui, P., & Xiong, L. (2015). The RNA-binding protein HOS5 and serine/arginine-rich proteins RS40 and RS41 participate in miRNA biogenesis in Arabidopsis. *Nucleic Acids Research*, *43*(17), 8283–8298.
- Cho, L.-H., Yoon, J., & An, G. (2017). The control of flowering time by environmental factors. *The Plant Journal*, *90*, 708-719.
- Clough, S., & Bent, A. (1998). Floral dip: a simplified method for Agrobacterium-mediated transformation of Arabidopsis thaliana. *The Plant Journal*, *16*(6), 735–743.
- Cruz, T., Carvalho, R., Richardson, D., & Duque, P. (2014). Abscisic acid (ABA) regulation of Arabidopsis SR protein gene expression. *International Journal of Molecular Sciences*, *15*(10), 17541-64.
- Cui, W., Wang, H., Song, J., Cao, X., Rogers, H., Francis, D., . . . Liu, W. (2017). Cell cycle arrest mediated by Cd-induced DNA damage in Arabidopsis root tips. *Ecotoxicology and Environmental Safety*, *145*, 569-574.

## REFERENCES

- Curtis, M., & Grossniklaus, U. (2003). A gateway cloning vector set for high-throughput functional analysis of genes in planta. *Plant Physiology*, *133*(22), 462–469.
- Dante, R., Larkins, B., & Sabelli, P. (2014). Cell cycle control and seed development. *Frontiers in Plant Science*, *5*(493).
- de Luxán-Hernández, C., Lohmann, J., Hellmeyer, W., Seanpong, S., Wöltje, K., Magyar, Z., . . . Weingartner, M. (2020). PP7L is essential for MAIL1-mediated transposable element silencing and primary root growth. *The Plant Journal*, *102*(4), 703-717.
- de Lyra Soriano Saleme, M., Andrade Rocha, I., & Barbosa Eloy, N. (2021). The Role of Anaphase-Promoting Complex/Cyclosome (APC/C) in Plant Reproduction. *Frontiers in Plant Science*, *12*(642934).
- De Schutter, K., Joubès, J., Cools, T., Verkest, A., Corellou, F., Babiychuk, E., . . . De Veylder, L. (2007). Arabidopsis WEE1 kinase controls cell cycle arrest in response to activation of the DNA integrity checkpoint. *The Plant Cell*, *19*, 211-225.
- Deng, X., Lu, T., Wang, L., Gu, L., Sun, J., Kong, X., . . . Cao, X. (2016). Recruitment of the NineTeen Complex to the activated spliceosome requires AtPRMT5. *PNAS*, *113*(19), 5447–5452.
- Desvoyes, B., & Gutierrez, C. (2020). Roles of plant retinoblastoma protein: cell cycle and beyond. *The EMBO Journal*, *39*(19), e105802.
- Dou, K., Huang, C.-F., Ma, Z.-Y., Zhang, C.-J., Zhou, J.-X., Huang, H.-W., . . . He, X.-J. (2013). The PRP6-like splicing factor STA1 is involved in RNA-directed DNA methylation by facilitating the production of Pol V-dependent scaffold RNAs. *Nucleic Acids Research*, *41*(18), 8489-502.
- Dramberville, A., Lauri, P., Normand, F., & Guédon, Y. (2015). Analysing growth and development of plants jointly using developmental growth stages. *Annals of Botany*, *115*, 93–105.
- Drisch, R., & Stahl, Y. (2015). Function and regulation of transcription factors involved in root apical meristem and stem cell maintenance. *Frontiers in Plant Science*, *6*(505).
- Du, J.-L., Zhang, S.-W., Huang, H.-W., Cai, T., Li, L., Chen, S., & He, X.-J. (2015). The Splicing Factor PRP31 Is Involved in Transcriptional Gene Silencing and Stress Response in Arabidopsis. *Molecular Plant*, *8*, 1053–1068.
- Dutertre, M., Sanchez, G., Barbier, J., Corcos, L., & Auboeuf, D. (2014). The emerging role of pre-messenger RNA splicing in stress responses: Sending alternative messages and silent messengers. *RNA Biology*, *8*(5), 740-747.



- Earley, K., Haag, J., Pontes, O., Opper, K., Juehne, T., Song, K., & Pikaard, C. (2006). Gateway-compatible vectors for plant functional genomics and proteomics. *The Plant Journal*, *45*(4), 616-29.
- Echevarría, C., Gutierrez, C., & Desvoyes, B. (2021). Tools for Assessing Cell-Cycle Progression in Plants. *Plant Cell Physiology*, *62*(8), 1231–1238.
- El-Brolosy, M., & Stainier, D. (2017). Genetic compensation: A phenomenon in search of mechanisms. *PLoS Genetics*, *13*(7), e1006780.
- Feke, A., Hong, J., Liu, W., & Gendron, J. (2020). A Decoy Library Uncovers U-Box E3 Ubiquitin Ligases That Regulate Flowering Time in Arabidopsis. *Genetics*, *215*, 699–712.
- Fischer, M., & Müller, G. (2017). Cell cycle transcription control: DREAM/MuvB and RB-E2F complexes. *Critical reviews in biochemistry and molecular biology*, *52*(6), 638-662.
- Forzani, C., Aichinger, E., Sornay, E., Willemsen, V., Laux, T., Dewitte, W., & Murray, J. (2014). WOX5 suppresses CYCLIN D activity to establish quiescence at the center of the root stem cell niche. *Current Biology*, *24*(16), 1939-44.
- Friml, J., Vieten, A., Sauer, M., Weijers, D., Schwarz, H., Hamann, T., . . . Jürgens, G. (2003). Efflux-dependent auxin gradients establish the apical–basal axis of Arabidopsis. *Nature*, *426*, 147-153.
- Fuchs, M., & Lohmann, J. (2020). Aiming for the top: non-cell autonomous control of shoot stem cells in Arabidopsis. *Journal of Plant Research*, *133*, 297–309.
- Fukumura, K., Inoue, K., & Mayeda, A. (2018). Splicing activator RNPS1 suppresses errors in pre-mRNA splicing: A key factor for mRNA quality control. *Biochemical and Biophysical Research Communications*, *496*, 921-926.
- Fulcher, N., & Sablowski, R. (2009). Hypersensitivity to DNA damage in plant stem cell niches. *PNAS*, *106*(49), 20984-8.
- Furukawa, T., Curtis, M., Tominey, C., Duong, Y., Wilcox, B., Aggoune, D., . . . Britt, A. (2010). A shared DNA-damage-response pathway for induction of stem-cell death by UVB and by gamma irradiation. *DNA Repair*, *9*, 940-948.
- Galinha, C., Hofhies, H., Luijten, M., Willemsen, V., Blilou, I., Heidstra, R., & Scheres, B. (2007). PLETHORA proteins as dose-dependent master regulators of Arabidopsis root development. *Nature*, *449*(7165), 1053-7.
- Galletta, B., & Rusan, N. (2015). A Yeast Two-Hybrid approach for probing protein-protein interactions at the centrosome. *Methods in Cell Biology*, *129*, 251–277.

## REFERENCES

- Garcia, V., Bruchet, H., Camescasse, D., Granier, F., Bouchez, D., & Tissier, A. (2003). AtATM is essential for meiosis and the somatic response to DNA damage in plants. *The Plant Cell*, *15*(1), 119–132.
- Gentric, N., Genschik, P., & Noir, S. (2021). Connections between the Cell Cycle and the DNA Damage Response in Plants. *International Journal of Molecular Sciences*, *22*(9558).
- Gentric, N., Masoud, K., Journot, R., Cognat, V., Chabouté, M.-R., Noir, S., & Genschik. (2020). The F-Box-Like Protein FBL17 Is a Regulator of DNA-Damage Response and Colocalizes with RETINOBLASTOMA RELATED1 at DNA Lesion Sites. *Plant Physiology*, *183*, 1295–1305.
- Gietz, R., Triggs-Raine, B., Robbins, A., Graham, K., & Woods, R. (1997). Identification of proteins that interact with a protein of interest: applications of the yeast two-hybrid system. *Molecular and Cellular Biochemistry*, *172*(1-2), 67-79.
- Gill, S., Anjum, N., Gill, R., Jha, M., & Tuteja, N. (2015). DNA Damage and Repair in Plants under Ultraviolet and Ionizing Radiations. *The Scientific World Journal*, *2015*(250158).
- Goldberg, R., de Paiva, G., & Yadegari, R. (1994). Plant Embryogenesis: Zygote to Seed. *Science*, *266*(5185), 605-614.
- Goldy, C., Pedroza-García, J.-A., Breakfield, B., & Rodriguez, R. (2021). The Arabidopsis GRAS-type SCL28 transcription factor controls the mitotic cell cycle and division plane orientation. *PNAS*, *118*(6), e2005256118.
- Gottschalk, A., Neubauer, G., Banroques, J., Mann, M., Lührmann, R., & Fabrizio, P. (1999). Identification by mass spectrometry and functional analyses of novel proteins of the yeast [U4/U6.U5] tri-snRNP. *The EMBO Journal*, *16*(16), 4535–4548.
- Guo, C., Xu, Y., Shi, M., Lai, Y., Wu, X., Wang, H., . . . Wu, G. (2017). Repression of miR156 by miR159 Regulates the Timing of the Juvenile-to-Adult Transition in Arabidopsis. *The Plant Cell*, *29*, 1293–1304.
- Gutierrez, C. (2009). The Arabidopsis Cell Division Cycle. *Arabidopsis Book*, *7*, e0120.
- Han, S.-H., Kim, J., Lee, J.-H., & Park, C.-M. (2021). Safeguarding genome integrity under heat stress in plants. *Journal of Experimental Botany*, *72*(21), 7421–7435.
- Hellemans, J., Mortier, G., De Paepe, A., Speleman, F., & Vandesompele, J. (2007). qBase relative quantification framework and software for management and automated analysis of real-time quantitative PCR data. *Genome Biology*, *8*(R19).
- Hendrix, S. (2022). Cell size matters: CDKG2 regulates endoreduplication in Arabidopsis. *The Plant Cell*, *34*, 1161–1162.

- Hendrix, S., Iven, V., Eekhout, T., Huybrechts, M., Pecqueur, I., Horemans, N., . . . Cuypers, A. (2020). Suppressor of Gamma Response 1 Modulates the DNA Damage Response and Oxidative Stress Response in Leaves of Cadmium-Exposed *Arabidopsis thaliana*. *Frontiers in Plant Science*, *11*, 366.
- Hendrix, S., Jozefczak, M., Wójcik, M., Deckers, J., Vangronsveld, J., & Cuypers, A. (2020). Glutathione: A key player in metal chelation, nutrient homeostasis, cell cycle regulation and the DNA damage response in cadmium-exposed *Arabidopsis thaliana*. *Plant Physiology and Biochemistry*, *154*, 498-507.
- Henson, H., & Taylor, M. (2020). A *sart1* Zebrafish Mutant Results in Developmental Defects in the Central Nervous System. *Cells*, *9*(2340).
- Herr, A., Molnàr, A., Jones, A., & Baulcombe, D. (2006). Defective RNA processing enhances RNA silencing and influences flowering of *Arabidopsis*. *PNAS*, *103*(41), 14994 – 15001.
- Heyman, J., Cools, T., Canher, B., Shavialenka, S., Traas, J., Vercauteren, I., . . . De Veylder, L. (2016). The heterodimeric transcription factor complex ERF115–PAT1 grants regeneration competence. *Nature plants*, *2*(16165).
- Heyman, J., Cools, T., Vandenbussche, F., Heyndrickx, K.S., Van Leene, J., . . . De Veylder, L. (2013). ERF115 controls root quiescent center cell division and stem cell replenishment. *Science*, *342*, 860-863.
- Hoekstra, F., Golovina, E., & Buitink, J. (2001). Mechanisms of plant desiccation tolerance. *Trends in Plant Science*, *6*(9), 431-438.
- Horvath, B., Kourova, H., Nagy, S., Nemeth, E., Magyar, Z., Papdi, C., . . . Scheres, B. (2017). *Arabidopsis* RETINOBLASTOMA RELATED directly regulates DNA damage responses through functions beyond cell cycle control. *The EMBO Journal*, *36*(9), 1261–1278.
- Hosokawa, M., Kadota, R., Shichijo, S., Itoh, K., Dmitriev, I., Krasnykh, V., . . . Heike, Y. (2005). Cell Cycle Arrest and Apoptosis Induced by SART-1 Gene Transduction. *Anticancer Research*, *25*, 1983-1990.
- Howles, P., Gebbie, L., Collings, D., Varsani, A., Broad, R., Ohms, S., . . . Williamson, R. (2016). A temperature-sensitive allele of a putative mRNA splicing helicase down-regulates many cell wall genes and causes radial swelling in *Arabidopsis thaliana*. *Plant Molecular Biology*, *91*, 1–13.
- Hu, Z., Cools, T., & De Veylder, L. (2016). Mechanisms Used by Plants to Cope with DNA damage. *Annual Review of Plant Biology*, *67*, 439–62.

## REFERENCES

- Hu, Z., Cools, T., Kalhorzadeh, P., Heyman, J., & De Veylder, L. (2015). Deficiency of the Arabidopsis Helicase RTEL1 Triggers a SOG1-Dependent Replication Checkpoint in Response to DNA Cross-Links. *The Plant Cell*, *27*, 149-161.
- Huang, A., Wang, Y., Liu, Y., Wang, G., & She, X. (2020). Reactive oxygen species regulate auxin levels to mediate adventitious root induction in Arabidopsis hypocotyl cuttings. *Journal of Integrative Plant Biology*, *62*(7), 912-926.
- Huang, C.-F., Miki, D., Tang, K., Zhou, H.-R., Zheng, Z., Chen, W., . . . Zhu, J.-K. (2013). A Pre-mRNA-Splicing Factor Is Required for RNA-Directed DNA Methylation in Arabidopsis. *PLoS Genetics*, *9*(9), e1003779.
- Huang, Y., & Steitz, J. (2005). SRprises along a Messenger's Journey. *Molecular Cell*, *17*, 613-615.
- Huijser, P., & Schmid, M. (2011). The control of developmental phase transitions in plants. *Development*, *138*, 4117-4129.
- Hundertmark, M., & Hinch, D. (2008). LEA (late embryogenesis abundant) proteins and their encoding genes in Arabidopsis thaliana. *BMC Genomics*, *9*(118).
- Irish, V. (2017). The ABC model of floral development. *Current Biology*, *27*, R853-R909.
- Jia, Q., Dulk-Ras, A., Shen, H., Hooykaas, P., & de Pater, S. (2013). Poly(ADP-ribose)polymerases are involved in microhomology mediated back-up non-homologous end joining in Arabidopsis thaliana. *Plant Molecular Biology*, *82*, 339-351.
- Jia, T., Zhang, B., You, C., Zhang, Y., Zeng, L., Li, S., . . . Chen, X. (2017). The Arabidopsis MOS4-Associated Complex Promotes MicroRNA Biogenesis and Precursor Messenger RNA Splicing. *The Plant Cell*, *29*, 2626-2643.
- Jiang, H.-L., Hong, J., Jiang, Y.-T., Yu, S.-X., Zhang, Y.-J., Shi, J.-X., & Lin, W.-H. (2020). Genome-Wide Association Analysis Identifies Candidate Genes Regulating Seed Number per Silique in Arabidopsis thaliana. *Plants*, *9*(585).
- Johnson, K., Dong, O., & Li, X. (2011). The evolutionarily conserved MOS4-associated complex. *Central European Journal of Biology*, *6*(5), 776-784.
- Johnson, T., Costa, A., Ferguson, A., & Frezza, C. (2018). Fumarate hydratase loss promotes mitotic entry in the presence of DNA damage after onising radiation. *Cell Death and Disease*, *9*(913).
- Kaczorowski, K., & Quail, P. (2003). Arabidopsis PSEUDO-RESPONSE REGULATOR7 Is a Signaling Intermediate in Phytochrome-Regulated Seedling Deetiolation and Phasing of the Circadian Clock. *The Plant Cell*, *15*, 2654-2665.

- Kalinina, N., Makarova, S., Makhotenko, A., Love, A., & Taliansky, M. (2018). The Multiple Functions of the Nucleolus in Plant Development, Disease and Stress Responses. *Frontiers in Plant Science*, *9*(132).
- Käll, L., Canterbury, J., Weston, J., Noble, W., & MacCoss, M. (2007). Semi-supervised learning for peptide identification from shotgun proteomics datasets. *Nature Methods*, *4*, 923–925.
- Kállai, B., Kourová, H., Chumová, J., Papdi, C., Trögelová, L., Kofronová, O., . . . Binarová, P. (2020).  $\gamma$ -Tubulin interacts with E2F transcription factors to regulate proliferation and endocycling in Arabidopsis. *Journal of Experimental Botany*, *71*(4), 1265–1277.
- Kalve, S., De Vos, D., & Beemster, G. (2014). Leaf development: a cellular perspective. *Frontiers in Plant Science*, *5*(362).
- Kalyna, M., & Barta, A. (2004). A plethora of plant serine/arginine-rich proteins: redundancy or evolution of novel gene functions? *Biochemical Society Transactions*, *32*(Pt 4), 561–564.
- Kalyna, M., Lopato, S., & Barta, A. (2003). Ectopic Expression of atRSZ33 Reveals Its Function in Splicing and Causes Pleiotropic Changes in Development. *Molecular Biology of the Cell*, *14*, 3565–3577.
- Kanno, T., Lin, W.-D., Fu, J., Chang, C.-L., Matzke, A., & Matzke, M. (2017). A Genetic Screen for Pre-mRNA Splicing Mutants of Arabidopsis thaliana Identifies Putative U1 snRNP Components RBM25 and PRP39a. *Genetics*, *207*, 1347–1359.
- Kanno, T., Venhuizen, P., Wen, T.-N., Lin, W.-D., Chiou, P., Kalyna, M., . . . Matzke, M. (2018). PRP4KA, a Putative Spliceosomal Protein Kinase, Is Important for Alternative Splicing and Development in Arabidopsis thaliana. *Genetics*, *210*, 1267–1285.
- Kantidze, O., Velichko, A., Luzhin, A., & Razin, S. (2016). Heat Stress-Induced DNA Damage. *ACTA NATURAE*, *8*; 2(29), 75-78.
- Khan, M., Ragni, L., Tabb, P., Salasini, B., Chatfield, S., Datla, R., . . . Pautot, V. (2015). Repression of Lateral Organ Boundary Genes by PENNYWISE and POUND-FOOLISH Is Essential for Meristem Maintenance and Flowering in Arabidopsis. *Plant Physiology*, *169*, 2166–2186.
- Kim, D., Jeon, J., Hwang, S., Hong, J., & Bahk, J. (2016). The C3H-type zinc finger protein GDS1/C3H42 is a nuclear-speckle-localized protein that is essential for normal growth and development in Arabidopsis. *Plant Science*, *250*, 141-153.

## REFERENCES

- Kim, D.-H., Doyle, M., Sung, S., & Amasino, R. (2009). Vernalization: Winter and the Timing of Flowering in Plants. *Annual Review of Cell and Developmental Biology*, *25*, 277–99.
- Kim, H., Nam, H., & Lim, P. (2016). Regulatory network of NAC transcription factors in leaf senescence. *Current opinion in Plant Biology*, *33*, 48–56.
- Kim, H., Oh, S., Brownfield, L., Hong, S., Ryu, H., Hwang, I., . . . Nam, H. (2008). Control of plant germline proliferation by SCF FBL17 degradation of cell cycle inhibitors. *Nature*, *455*, 1134–1138.
- Kim, K., Noh, J., Bodogai, M., Martindale, J., Yang, X., Indig, F., . . . Gorospe, M. (2017). Identification of senescent cell surface targetable protein DPP4. *Genes and development*, *31*(15), 1529–1534.
- Kittler, R., Puts, G., Pelletier, L., Poser, I., Heninger, A.-K., Drechsel, D., . . . Buchholz, F. (2004). An endoribonuclease-prepared siRNA screen in human cells identifies genes essential for cell division. *Nature*, *432*(7020), 1036–40.
- Kobayashi, K., Suzuki, T., Iwata, E., Nakamichi, N., Suzuki, T., Chen, P., . . . Ito, M. (2015). Transcriptional repression by MYB3R proteins regulates plant organ growth. *The EMBO Journal*, *34*(15), 1992–2007.
- Koç, A., Wheeler, L., Mathews, C., & Merrill, G. (2004). Hydroxyurea Arrests DNA Replication by a Mechanism That Preserves Basal dNTP Pools\*. *The Journal of Biological Chemistry*, *279*(1), 223–230.
- Köhler, A., & Hurt, E. (2007). Exporting RNA from the nucleus to the cytoplasm. *Nature Reviews Molecular Cell Biology*, *8*, 761–773.
- Komaki, S., & Schnittger, A. (2017). The Spindle Assembly Checkpoint in Arabidopsis Is Rapidly Shut Off during Severe Stress. *Developmental Cell*, *43*(2), 172–185.
- Koncz, C., deJong, F., Villacorta, N., Szakonyi, D., & Koncz, Z. (2012). The spliceosome-activating complex: molecular mechanisms underlying the function of a pleiotropic regulator. *Frontiers in Plant Science*, *3*(9), 1–12.
- Kroj, T., Savino, G., Valon, C., Giraudat, J., & Parcy, F. (2003). Regulation of storage protein gene expression in Arabidopsis. *Development*, *24*, 6065–73.
- Kumar, N., & Larkin, J. (2017). Why do plants need so many cyclin-dependent kinase inhibitors? *Plant Signaling & Behavior*, *12*(2), e1282021.
- Kwon, C., Chen, C., & Wagner, D. (2005). WUSCHEL is a primary target for transcriptional regulation by SPLAYED in dynamic control of stem cell fate in Arabidopsis. *GENES & DEVELOPMENT*, *19*, 992–1003.



- Laimbeer, F., Makris, M., & Veilleux, R. (2018). Measuring Endoreduplication by Flow Cytometry of Isolated Tuber Protoplasts. *Journal of Visualized Experiments*, *133*, e57134.
- Lamond, A., & Spector, D. (2003). Nuclear speckles: a model for nuclear organelles. *Nature Reviews Molecular Cell Biology*, *4*(8), 605-12.
- Lang, L., & Schnittger, A. (2020). Endoreplication — a means to an end in cell growth and stress response. *Current Opinion in Plant Biology*, *54*, 85–92.
- Lashbrooke, J., Cohen, H., Levy-Samocho, D., Tzfadia, O., Panizel, I., Zeisler, V., . . . Aharoni, A. (2016). MYB107 and MYB9 Homologs Regulate Suberin Deposition in Angiosperms. *The Plant Cell*, *28*, 2097–2116.
- Laux, T. (2003). The stem cell concept in plants: A matter of debate. *Cell*, *113*, 281-283.
- Lee, B.-h., Kapoor, A., Zhu, J., & Zhu, J.-K. (2006). STABILIZED1, a stress-upregulated nuclear protein, is required for pre-mRNA splicing, mRNA turnover, and stress tolerance in Arabidopsis. *The Plant Cell*, *18*, 1736–1749.
- Li, C., Potuschak, T., Colón-Carmona, A., Guitérrez, R., & Doerner, P. (2005). Arabidopsis TCP20 links regulation of growth and cell division control pathways. *PNAS*, *102*(36), 12978–12983.
- Li, S., Liu, K., Zhou, B., Li, M., Zhang, S., Zeng, L., . . . Yu, B. (2018). MAC3A and MAC3B, Two Core Subunits of the MOS4-Associated Complex, Positively Influence miRNA Biogenesis. *The Plant Cell*, *30*, 481–494.
- Li, S.-B., Xie, Z.-Z., Hu, C.-G., & Zhang, J.-Z. (2016). A Review of Auxin Response Factors (ARFs) in Plants. *Frontiers in Plant Science*, *7*(47).
- Li, X., & Manley, J. (2005). Inactivation of the SR Protein Splicing Factor ASF/SF2 Results in Genomic Instability. *Cell*, *122*, 365-378.
- Li, X., Chen, T., Li, Y., Wang, Z., Cao, H., Chen, F., . . . Liu, Y. (2019). ETR1/RDO3 Regulates Seed Dormancy by Relieving the Inhibitory Effect of the ERF12-TPL Complex on DELAY OF GERMINATION1 Expression. *The Plant Cell*, *31*, 832-847.
- Li, X., Niu, T., & Manley, J. (2007). The RNA binding protein RNPS1 alleviates ASF/SF2 depletion-induced genomic instability. *RNA*, *13*, 2108–2115.
- Liu, M., Yuan, L., Liu, N.-Y., Shi, D.-Q., Liu, J., & Yang, W.-C. (2009). GAMETOPHYTIC FACTOR 1, Involved in Pre-mRNA Splicing, Is Essential for Megagametogenesis and Embryogenesis in Arabidopsis. *Journal of Integrative Plant Biology*, *51*(3), 261–271.



## REFERENCES

- Liu, S., Rauhut, R., Vornlocher, H.-P., & Lührmann, R. (2006). The network of protein–protein interactions within the human U4/U6.U5 tri-snRNP. *RNA*, *12*, 1418–1430.
- Liu, X.-X., Guo, Q.-H., Xu, W.-B., Liu, P., & Yan, K. (2022). Rapid Regulation of Alternative Splicing in Response to Environmental Stresses. *Frontiers in Plant Science*, *13*(832177).
- Liu, Y., Ji, X., Nie, X., Qu, M., Zheng, L., Tan, Z., . . . Wang, Y. (2015). Arabidopsis AtbHLH112 regulates the expression of genes involved in abiotic stress tolerance by binding to their E-box and GCG-box motifs. *New Phytologist*, *207*, 692–709.
- Llavata Peris, C., Rademacher, E., & Weijers, D. (2010). Green beginnings - pattern formation in the early plant embryo. *Current Topics in Developmental Biology*, *91*, 1-27.
- Locascio, A., Blázquez, M., & Alabadí, D. (2013). Dynamic regulation of cortical microtubule organization through prefoldin-DELLA interaction. *Current Biology*, *23*(9), P804-809.
- Lorenzo-Orts, L., Witthoef, J., Deforges, J., Martinez, J., Loubéry, S., Placzek, A., . . . Hothorn, M. (2019). Concerted expression of a cell cycle regulator and a metabolic enzyme from a bicistronic transcript in plants. *Nature plants*, *5*, 184–193.
- Lorkovic, Z., & Hilscher, J. B. (2008). Co-localisation studies of Arabidopsis SR splicing factors reveal different types of speckles in plant cell nuclei. *Experimental Cell Research*, *314*(17), 3175-3186.
- Lv, B., Hu, K., Tian, T., Wei, K., Zhang, F., Jia, Y., . . . Ding, Z. (2021). The pre-mRNA splicing factor RDM16 regulates root stem cell maintenance in Arabidopsis. *Journal of Integrative Plant Biology*, *63*(4), 662-675.
- Ma, Y., Miotk, A., Sutikovic, Z., Ermakova, O., Wenzl, C., Medzihradzky, A., . . . Lohmann, J. (2019). WUSCHEL acts as an auxin response rheostat to maintain apical stem cells in Arabidopsis. *Nature communications*, *10*(5093).
- Mahrez, W., Shin, J., Muñoz-Viana, R., Figueroa, D., Trejo-Arellano, M., Exner, V., . . . Hennig, L. (2016). BRR2a Affects Flowering Time via FLC Splicing. *PLOS Genetics*, *12*(4), 1-25.
- Makarova, V., Makarov, E., & Lührmann, R. (2001). The 65 and 110 kDa SR-related proteins of the U4/U6.U5 tri-snRNP are essential for the assembly of mature spliceosomes. *The EMBO Journal*, *20*(10), 2553-63.
- Manara, A., DalCorso, G., Guzzo, F., & Furini, A. (2015). Loss of the Atypical Kinases ABC1K7 and ABC1K8 Changes the Lipid Composition of the Chloroplast Membrane. *Plant and Cell Physiology*, *56*(6), 1193–1204.

- Mangano, S., Denita-Juarez, S., Choi, H.-S., Marzol, E., Hwang, Y., Ranocha, P., . . . Estevez, J. (2017). Molecular link between auxin and ROS-mediated polar growth. *PNAS*, *114*(20), 5289–5294.
- Manova, V., & Gruszka, D. (2015). DNA damage and repair in plants – from models to crops. *Frontiers in Plant Science*, *6*(885).
- Marhava, P., Hoermayer, L., Yoshida, S., Marhavy, P., Benkova, E., & Friml, J. (2019). Re-activation of Stem Cell Pathways for Pattern Restoration in Plant Wound Healing. *Cell*, *177*, 957–969.
- Mayer, K., Schoof, H., Haecker, A., Lenhard, M., Jürgens, G., & Laux, T. (1998). Role of WUSCHEL in regulating stem cell fate in the Arabidopsis shoot meristem. *Cell*, *95*(6), 805-15.
- Meng, L.-S., Bao, Q.-X., Mu, X.-R., Tong, C., Cao, X., Huang, J.-J., . . . Loake, G. (2021). Glucose- and sucrose-signaling modules regulate the Arabidopsis juvenile-to-adult phase transition. *Cell Reports*, *36*(109348).
- Mishra, S., Ammon, T., Popowicz, G., Krajewski, M., Nagel, R., Ares Jr, M., . . . Jentsch, S. (2011). Role of the ubiquitin-like protein Hub1 in splice-site usage and alternative splicing. *Nature*, *474*(7350), 173–178.
- Monaghan, J., Xu, F., Gao, M., Zhao, Q., Palma, K., Long, C., . . . Li, X. (2009). Two Prp19-Like U-Box Proteins in the MOS4-Associated Complex Play Redundant Roles in Plant Innate Immunity. *PLoS Pathogens*, *5*(7), e1000526.
- Naro, C., Bielli, P., Pagliarini, V., & Sette, C. (2015). The interplay between DNA damage response and RNA processing: the unexpected role of splicing factors as gatekeepers of genome stability. *Frontiers in Genetics*, *6*(142).
- Nayeri, F. (2014). Identification of transcription factors linked to cell cycle regulation in Arabidopsis. *Plant Signaling & Behavior*, *9*(11), e972864.
- Nguyen, T., Galej, W., Bai, X.-c., Oubridge, C., Newman, A., Scheres, S., & Nagai, K. (2016). Cryo-EM structure of the yeast U4/U6.U5 tri-snRNP at 3.7 Å resolution. *Nature*, *530*(7590), 298-302.
- Nimeth, B., Riegler, S., & Kalyna, M. (2020). Alternative Splicing and DNA Damage Response in Plants. *Frontiers in Plant Science*, *11*(91).
- Ning, Y.-Q., Liu, N., Lan, K.-K., Su, Y.-N., Li, L., Chen, S., & He, X.-J. (2020). DREAM complex suppresses DNA methylation maintenance genes and precludes DNA hypermethylation. *Nature Plants*, *6*(8), 942-956.

## REFERENCES

- Nisa, M. H. (2019). The Plant DNA Damage Response: Signalling Pathways Leading to Growth Inhibition and Putative Role in Response to Stress Conditions. *Frontiers in Plant Science*, *10*(653).
- Nodine, M., Bryan, A., Racolta, A., Jerovsky, K., & Tax, F. (2011). A few standing for many: embryo receptor-like kinases. *Trends in Plant Science*, *16*(4), 211-217.
- Noir, S., Marrocco, K., Masoud, K., Thomann, A., Gusti, A., Bitrian, M., & Schnittger, A. G. (2015). The Control of Arabidopsis thaliana Growth by Cell Proliferation and Endoreplication Requires the F-Box Protein FBL17. *The Plant Cell*, *27*, 1461–1476.
- O’Malley, R., Barragan, C., & Ecker, J. (2015). A User’s Guide to the Arabidopsis T-DNA Insertional Mutant Collections. *Methods in Molecular Biology*, *1284*, 323–342.
- Ogita, N., Okushima, Y., Tokizawa, M., Yamamoto, Y., Tanaka, M., Seki, M., . . . Umeda, M. (2018). Identifying the target genes of SUPPRESSOR OF GAMMA RESPONSE 1, a master transcription factor controlling DNA damage response in Arabidopsis. *The Plant Journal*, *94*, 439–453.
- Ohtani, M., Demura, T., & Sugiyama, M. (2013). Arabidopsis ROOT INITIATION DEFECTIVE1, a DEAH-Box RNA Helicase Involved in Pre-mRNA Splicing, Is Essential for Plant Development. *The Plant Cell*, *25*, 2056–2069.
- Pacurar, D., Perrone, I., & Bellini, C. (2014). Auxin is a central player in the hormone cross-talks that control adventitious rooting. *Physiologia Plantarum*, *151*, 83–96.
- Pan, T., Qin, Q., Nong, C., Gao, S., Wang, L., Cai, B., . . . Yan, S. (2021). A novel WEE1 pathway for replication stress responses. *Nature plants*, *7*, 209–218.
- Park, S., & Harada, J. (2008). Arabidopsis embryogenesis. In *Plant Embryogenesis* (pages 3-16). Humana Press.
- Pedroza-García, J., Xiang, Y., & De Veylder, L. (2022). Cell cycle checkpoint control in response to DNA damage by environmental stresses. *The Plant Journal*, *109*, 490–507.
- Pedroza-García, J.-A., De Veylder, L., & Raynaud, C. (2019). Plant DNA Polymerases. *International Journal of Molecular Sciences*, *20*(4814).
- Perales, M., & Reddy, G. (2012). Stem cell maintenance in shoot apical meristems. *Current Opinion in Plant Biology*, *15*, 10-16.
- Perea-Resa, C., Hernández-Verdeja, T., López-Cobollo, R., Castellano, M., & Salinas, J. (2012). LSM Proteins Provide Accurate Splicing and Decay of Selected Transcripts to Ensure Normal Arabidopsis Development. *The Plant Cell*, *24*, 4930–4947.

- Pérez-Pérez, J. (2020). Anchor Root Development: A World within Worlds. *Molecular Plant*, *13*, 1105–1107.
- Perilli, S., Di Mambro, R., & Sabatini, S. (2012). Growth and development of the root apical meristem. *Current Opinion in Plant Biology*, *15*(1), 17-23.
- Petricka, J., Clay, N., & Nelson, T. (2008). Vein patterning screens and the defectively organized tributaries mutants in *Arabidopsis thaliana*. *The Plant Journal*, *56*, 251–263.
- Qi, H.-D., Lin, Y., Ren, Q.-P., Wang, Y.-Y., Xiong, F., & Wang, X.-L. (2019). RNA Splicing of FLC Modulates the Transition to Flowering. *Frontiers in Plant Science*, *10*(1625).
- Qi, J., Song, C.-P., Wang, B., Zhou, J., Kangasjärvi, J., Zhu, J.-K., & Gong, Z. (2018). Reactive oxygen species signaling and stomatal movement in plant responses to drought stress and pathogen attack. *Journal of Integrative Plant Biology*, *60*(9), 805–826.
- Raina, A., Sahu, P., Laskar, R., Rajora, N., Sao, R., Khan, S., & Ganai, R. (2021). Mechanisms of Genome Maintenance in Plants: Playing It Safe With Breaks and Bumps. *Frontiers in Plant Science*, *12*(675686).
- Reddy, A., Marquez, Y., Kalyna, M., & Barta, A. (2013). Complexity of the alternative splicing landscape in plants. *Plant Cell*, *25*(10), 3657-83.
- Reddy, A., Rogers, M., Richardson, D., Hamilton, M., & Ben-Hur, A. (2012). Deciphering the plant splicing code: experimental and computational approaches for predicting alternative splicing and splicing regulatory elements. *Frontiers in Plant Science*, *3*(18), 1-15.
- Rigo, R., Bazin, J., Romero-Barrios, N., Moison, M., Lucero, L., Christ, A., . . . Ariel, F. (2020). The *Arabidopsis* lncRNA ASCO modulates the transcriptome through interaction with splicing factors. *EMBO reports*, *21*, e48977.
- Rissel, D., & Peiter, E. (2019). Poly(ADP-Ribose) Polymerases in Plants and Their Human Counterparts: Parallels and Peculiarities. *International Journal of Molecular Sciences*, *20*(1638).
- Roitinger, E., Hofer, M., Köcher, T., Pichler, P., Novatchkova, M., Yang, J., . . . Mechtler, K. (2015). Quantitative phosphoproteomics of the ataxia telangiectasia-mutated (ATM) and ataxia telangiectasia-mutated and rad3-related (ATR) dependent DNA damage response in *Arabidopsis thaliana*. *Molecular & Cellular Proteomics*, *3*, 556-71.
- Roy, S., & Das. (2017). Homologous Recombination Defective *Arabidopsis* Mutants Exhibit Enhanced Sensitivity to Abscisic Acid. *PLOS One*, *12*(1), e0169294.

## REFERENCES

- Sarkar, A., Luijten, M., Miyashima, S., Lenhard, M., Hashimoto, T., Nakajima, K., . . . Laux, T. (2007). Conserved factors regulate signalling in *Arabidopsis thaliana* shoot and root stem cell organizers. *Nature*, *446*, 811-814.
- Scheres, B. (2007). Stem-cell niches: nursery rhymes across kingdoms. *Nature Reviews Molecular Cell Biology*, *8*(5), 345-354.
- Schlaen, R., Mancini, E., Sanchez, S., Perez-Santángelo, S., Rugnone, M., Simpson, C., . . . Yanovsky, M. (2015). The spliceosome assembly factor GEMIN2 attenuates the effects of temperature on alternative splicing and circadian rhythms. *PNAS*, *112*(30), 9382–9387.
- Schreiber, K., Bentham, A., Williams, S., Kobe, B., & Staskawicz, B. (2016). Multiple Domain Associations within the *Arabidopsis* Immune Receptor RPP1 Regulate the Activation of Programmed Cell Death. *PLoS Pathogens*, *12*(7), e1005769.
- Schütze, T., Ulrich, A., Apelt, L., Will, C., Bartlick, N., Seeger, M., . . . Wahl, M. (2016). Multiple protein–protein interactions converging on the Prp38 protein during activation of the human spliceosome. *RNA*, *22*, 265–277.
- Schwerk, C., Prasad, J., Degenhardt, K., Erdjument-Bromage, H., White, E., Tempst, P., . . . Reinberg, D. (2003). ASAP, a Novel Protein Complex Involved in RNA Processing and Apoptosis. *Molecular and Cellular Biology*, *23*(8), 2981-2990.
- Scott, M., Troshin, P., & Barton, G. (2011). NoD: a Nucleolar localization sequence detector for eukaryotic and viral proteins. *BMC Bioinformatics*, *12*(317).
- Shang, X., Cao, Y., & Ma, L. (s.f.). Alternative Splicing in Plant Genes: A Means of Regulating the Environmental Fitness of Plants. *International Journal of Molecular Sciences*, *18*(432).
- Sharma, P., Jha, A., Dubey, R., & Pessarakli, M. (2012). Reactive Oxygen Species, Oxidative Damage, and Antioxidative Defense Mechanism in Plants under Stressful Conditions. *Journal of Botany*, *2012*(217037).
- Shimotohno, A., Aki, S., Takahashi, N., & Umeda, M. (2021). Regulation of the Plant Cell Cycle in Response to Hormones and the Environment. *The Annual Review of Plant Biology*, *72*, 273–96.
- Sipari, N., Lihavanien, J., Shapiguzov, A., & Kangasjärvi, J. K. (2020). Primary Metabolite Responses to Oxidative Stress in Early-Senescing and Paraquat Resistant *Arabidopsis thaliana* *red1* (Radical-Induced Cell Death1). *Frontiers in Plant Science*, *11*(194).
- Sjogren, C., Bolaris, S., & Larsen, P. (2015). Aluminum-Dependent Terminal Differentiation of the *Arabidopsis* Root Tip Is Mediated through an ATR-, ALT2-, and SOG1-Regulated Transcriptional Response. *The Plant Cell*, *27*, 2501–2515.

- Smith, Z., & Long, J. (2010). Control of Arabidopsis apical–basal embryo polarity by antagonistic transcription factors. *Nature*, *464*, 423–426.
- Song, Y., Ito, S., & Imaizumi, T. (2013). Flowering time regulation: photoperiod- and temperature- sensing in leaves. *Trends in Plant Science*, *18*(10), 575–583.
- Spector, D., & Lamond, A. (2011). Nuclear Speckles. *Cold Spring Harbor Perspectives in Biology*, *2*, a000646.
- Srivastava, A., Tang, Y., Díaz de la Garza, R., & Blancaflor, E. (2011). The plastidial folylpolyglutamate synthetase and root apical meristem maintenance. *Plant Signaling and Behavior*, *6*(5), 751–754.
- Stankovic, N., Schloesser, M., Joris, M., Sauvage, E., Hanikenne, M., & Motte, P. (2016). Dynamic Distribution and Interaction of the Arabidopsis SRSF1 Subfamily Splicing factors. *Plant Physiology*, *170*, 1000–1013.
- Stellberger, T., Häuser, R., Baiker, A., Pothineni, V., Haas, J., & Uetz, P. (2010). Improving the yeast two-hybrid system with permutated fusions proteins: the Varicella Zoster Virus interactome. *Proteome Science*, *8*(8).
- Stellberger, T., Häuser, R., Uetz, P., & von Brunn, A. (2012). Yeast Two-Hybrid Screens: Improvement of Array-Based Screening Results by N- and C-terminally Tagged Fusion Proteins. *Functional Genomics*, *8*(15), 277–288.
- Stevens, S., & Abelson, J. (1999). Purification of the yeast U4/U6.U5 small nuclear ribonucleoprotein particle and identification of its proteins. *Proceedings of the National Academy of Sciences*, *96*, 7226–7231.
- Suetsugu, N., Takemiya, A., Kong, S.-G., Higa, T., Komatsu, A., Shimazaki, K.-i., . . . Wada, M. (2016). RPT2/NCH1 subfamily of NPH3-like proteins is essential for the chloroplast accumulation response in land plants. *PNAS*, *113*(37), 10424–10429.
- Sun, M., Zhang, Y., Wang, Q., Wu, C., Jiang, C., & Xu, J.-R. (2018). The tri-snRNP specific protein FgSnu66 is functionally related to FgPrp4 kinase in *Fusarium graminearum*. *Molecular Microbiology*, *109*(4), 494–508.
- Syed, N., Kalyna, M., Marquez, Y., Barta, A., & Brown, J. (2012). Alternative splicing in plants – coming of age. *Trends in Plant Science*, *17*(10), 616–623.
- Takahashi, N., Ogita, N., Takahashi, T., Taniguchi, S., Tanaka, M., Seki, M., & Umeda, M. (2019). A regulatory module controlling stress-induced cell cycle arrest in Arabidopsis. *eLife*, *8*, e43944.



## REFERENCES

- Takatsuka, H., Ohno, R., & Umeda, M. (2009). The Arabidopsis cyclin-dependent kinase-activating kinase CDKF;1 is a major regulator of cell proliferation and cell expansion but is dispensable for CDKA activation. *The Plant Journal*, *59*, 475–487.
- ten Hove, C., Lu, K.-J., & Weijers, D. (2015). Building a plant: cell fate specification in the early Arabidopsis embryo. *Development*, *142*, 420-430.
- Tillemans, V., Dispa, L., Remacle, C., Collinge, M., & Motte, P. (2005). Functional distribution and dynamics of Arabidopsis SR splicing factors in living plant cells. *The Plant Journal*, *41*, 567–582.
- Tsukagoshi, H. (2012). Defective root growth triggered by oxidative stress is controlled through the expression of cell cycle-related genes. *Plant Science*, *197*, 30-39.
- Ühlken, C., Horvath, B., Stadler, R., Sauer, N., & Weingartner, M. (2014). MAIN-LIKE1 is a crucial factor for correct cell division and differentiation in Arabidopsis thaliana. *The Plant Journal*, *78*(1), 107-20.
- Ühlken, C., Horvath, B., Stadler, R., Sauer, N., & Weingartner, M. (2014). MAIN-LIKE1 is a crucial factor for correct cell division and differentiations in Arabidopsis thaliana. *The Plant Journal*, *78*, 107-120.
- van Nues, R., & Beggs, J. (2001). Functional Contacts With a Range of Splicing Proteins Suggest a Central Role for Brr2p in the Dynamic Control of the Order of Events in Spliceosomes of *Saccharomyces cerevisiae*. *Genetics*, *157*, 1451–1467.
- Vanderpoole, K., Raes, J., De Veylder, L., Rouzé, P., Rombauts, S., & Inzé, D. (2002). Genome-Wide Analysis of Core Cell Cycle Genes in Arabidopsis. *The Plant Cell*, *14*, 903–916.
- Vespa, L., Couvillion, M., Spangler, E., & Shippen, D. (2005). ATM and ATR make distinct contributions to chromosome end protection and the maintenance of telomeric DNA in Arabidopsis. *Genes and Development*, *19*, 2111–2115.
- Vieira, P., & de Almeida Engler, J. (2017). Plant Cyclin-Dependent Kinase Inhibitors of the KRP Family: Potent Inhibitors of Root-Knot Nematode Feeding Sites in Plant Roots. *Frontiers in Plant Science*, *8*(1514).
- Walker, C., Wheeldon, C., & Bennet, T. (2021). Integrated dominance mechanisms regulate reproductive architecture in Arabidopsis thaliana and Brassica napus. *Plant Physiology*, *186*, 1985–2002.
- Wang, C., Tian, Q., Hou, Z., Mucha, M., Aukerman, M., & Olsen, O.-A. (2007). The Arabidopsis thaliana AT PRP39-1 gene, encoding a tetratricopeptide repeat protein with similarity to the yeast pre-mRNA processing protein PRP39, affects flowering time. *Plant Cell Reports*, *26*, 1357–1366.



- Wang, H., He, L., Song, J., Cui, W., Zhang, Y., Jia, C., . . . Liu, W. (2016). Cadmium-induced genomic instability in Arabidopsis: molecular toxicological biomarkers for early diagnosis of cadmium stress. *Chemosphere*, *150*, 258-265.
- Wang, J., Liang, Y.-p., Zhu, J.-d., Wang, Y.-x., Yang, M.-y., Yan, H.-r., . . . Zhang, X. (2021). Phototropin 1 Mediates High-Intensity Blue Light-Induced Chloroplast Accumulation Response in a Root Phototropism 2-Dependent Manner in Arabidopsis phot2 Mutant Plants. *Frontiers in Plant Science*, *12*(704618).
- Wang, L., Chen, H., Wang, C., Hu, Z., & Yan, S. (2018). Negative regulator of E2F transcription factors links cell cycle checkpoint and DNA damage repair. *PNAS*, *115*(16), E3837–E3845.
- Wang, L., Zhan, L., Zhao, Y., Huang, Y., Wu, C., Pan, T., . . . Yan, S. (2021). The ATR-WEE1 kinase module inhibits the MAC complex to regulate replication stress response. *Nucleic Acids Research*, *49*(3), 1411-1425.
- Watanabe, E., Mano, S., Nishimura, M., & Yamada, K. (2019). AtUBL5 regulates growth and development through pre-mRNA splicing in Arabidopsis thaliana. *PLoS ONE*, *14*(11), e0224795.
- Waterworth, W., Footitt, S., Bray, C., & West, C. (2016). DNA damage checkpoint kinase ATM regulates germination and maintains genome stability in seeds. *PNAS*, *113*(34), 9647-9652.
- Waterworth, W., Wilson, M., Wang, D., Nuhse, T., Warward, S., Selley, J., & West, C. (2019). Phosphoproteomic analysis reveals plant DNA damage signalling pathways with a functional role for histone H2AX phosphorylation in plant growth under genotoxic stress. *The Plant Journal*, *100*, 1007–1021.
- Weigel, D., & Jürgens, G. (2002). Stem cells that make stems. *Nature*, *415*(6973), 751-4.
- Weihmann, T., Palma, K., Nitta, Y., & Li, X. (2012). PLEIOTROPIC REGULATORY LOCUS 2 exhibits unequal genetic redundancy with its homolog PRL1. *Plant and Cell Physiology*, *53*(9), 1617–1626.
- Wenig, U., Meyer, S., Stadler, R., Fischer, S., Werner, D., Lauter, A., . . . Sauer, N. (2013). Identification of MAIN, a factor involved in genome stability in the meristems of Arabidopsis thaliana. *The Plant Journal*, *75*(3), 469 - 483.
- Wilkinson, C., Dittmar, G., Ohi, M., Uetz, P., Jones, N., & Finley, D. (2004). Ubiquitin-like Protein Hub1 Is Required for Pre-mRNA Splicing and Localization of an Essential Splicing Factor in Fission Yeast. *Current Biology*, *14*(24), 2283-2288.
- Will, C., & Lührmann, R. (2011). Spliceosome Structure and Function. *Cold Spring Harbor Perspectives in Biology*, *3*, a003707.

## REFERENCES

- Xiao, R., Sun, Y., Ding, J.-H., Lin, S., Rose, D., Rosenfeld, M., . . . Li, X. (2007). Splicing regulator SC35 is essential for genomic stability and cell proliferation during mammalian organogenesis. *Molecular and cellular biology*, *27*(15), 5393-402.
- Xiao, W., Custard, K., Brown, R., Lemmon, B., Harada, J., Goldberg, R., & Fischer, R. (2006). DNA Methylation Is Critical for Arabidopsis Embryogenesis and Seed Viability. *The Plant Cell*, *18*, 805–814.
- Xiong, F., Ren, J.-J., Yu, Q., Wang, Y.-Y., Kong, L.-J., Otegui, M., & Wang, X.-L. (2019). AtBUD13 affects pre-mRNA splicing and is essential for embryo development in Arabidopsis. *98*, 714–726.
- Yamaguchi, A., & Abe, M. (2012). Regulation of reproductive development by non-coding RNA in Arabidopsis: to flower or not to flower. *Journal of Plant Research*, *125*, 693–704.
- Yan, Q., Xia, X., Sun, Z., & Fang, Y. (2017). Depletion of Arabidopsis SC35 and SC35-like serine/arginine-rich proteins affects the transcription and splicing of a subset of genes. *PLoS Genetics*, *13*(3), e1006663.
- Yi, D., Kamei, C., Cools, T., Vanderauwera, S., Takahashi, N., Okushima, Y., . . . De Veylder, L. (2014). The Arabidopsis SIAMESE-RELATED Cyclin-Dependent Kinase Inhibitors SMR5 and SMR7 Regulate the DNA Damage Checkpoint in Response to Reactive Oxygen Species. *The Plant Cell*, *26*, 296-309.
- Yi, Y., & Jack, T. (1998). An Intragenic Suppressor of the Arabidopsis Floral Organ Identity Mutant *apetala3-1* Functions by Suppressing Defects in Splicing. *The Plant Cell*, *10*, 1465-1477.
- Yoshiyama, K. C. (2009). Suppressor of gamma response 1 (SOG1) encodes a putative transcription factor governing multiple responses to DNA damage. *PNAS*, *106*(31), 12843-12848.
- Yoshiyama, K., Aoshima, N., Takahashi, N., Sakamoto, T., Kiruma, K., Saijo, Y., . . . Kimura, S. (2020). SUPPRESSOR OF GAMMA RESPONSE 1 acts as a regulator coordinating crosstalk between DNA damage response and immune response in Arabidopsis thaliana. *Plant Molecular Biology*, *103*, 321–340.
- Yoshiyama, K., Kimura, S., Maki, H., Britt, A., & Umeda, M. (2014). The role of SOG1, a plant-specific transcriptional regulator, in the DNA damage response. *Plant Signaling and Behavior*, *9*(4), e28889-1.
- Yoshiyama, K., Kobayashi, J., Ogita, N., Ueda, M., Kimura, S., Maki, H., & Umeda, M. (2013a). ATM-mediated phosphorylation of SOG1 is essential for the DNA damage response in Arabidopsis. *EMBO reports*, *14*(9), 817-822.

- Yoshiyama, K., Sakaguchi, K., & Kimura, S. (2013b). DNA Damage Response in Plants: Conserved and Variable Response Compared to Animals. *Biology*, *2*, 1338-1356.
- Zhang, D., Chen, M.-X., Zhu, F.-Y., Zhang, J., & Liu, Y.-G. (2020). Emerging Functions of Plant Serine/Arginine-Rich (SR) Proteins: Lessons from Animals. *Critical Reviews in Plant Sciences*, *39*(2), 173–194.
- Zhang, W., Du, B., Liu, D., & Qi, X. (2014). Splicing factor SR34b mutation reduces cadmium tolerance in Arabidopsis by regulating iron-regulated transporter 1 gene. *Biochemical and Biophysical Research Communications*, *455*, 312–317.
- Zhang, X.-N., Shi, Y., Powers, J., Gowda, N., Zhang, C., Ibrahim, H., . . . Mount, S. (2017). Transcriptome analyses reveal SR45 to be a neutral splicing regulator and a suppressor of innate immunity in Arabidopsis thaliana. *BMC Genomics*, *18*(772).
- Zhang, Z., Li, W., Gao, W., Xu, M., & Guo, Y. (2020). DEAR4, a Member of DREB/CBF Family, Positively Regulates Leaf Senescence and Response to Multiple Stressors in Arabidopsis thaliana. *Frontiers in Plant Science*, *11*(367).
- Zheng, M., Yang, T., Tao, P., Zhu, C., Fu, Y., & Hsu, Y.-F. (2019). Arabidopsis GSM1 is involved in ABI4-regulated ABA signaling under high-glucose condition in early seedling growth. *Plant Science*, *287*(110183).



# 8. APPENDIX



The data presented in this thesis is partially included in the publications listed below:

- de Luxán-Hernández, C.; Lohmann, J.; Tranque, E.; Chumova, J.; Binarova, P.; Salinas, J.; Weingartner, M. (2022) MERISTEM DEFECTIVE is a conserved splicing factor and modulates cell division and stress response in Arabidopsis. *Life Science Alliance*. Manuscript in revision. ID: LSA-2022-01507-T.
- de Luxán-Hernández, C.; Lohmann, J.; Hellmeyer, W.; Seanpong, S.; Wöltje, K.; Magyar, Z.; Pettkó-Szandtner, A.; Pelissier, T.; De Jaeger, G.; Hoth, S.; Mathieu, O.; Weingartner, M. (2020) PP7L is essential for MAIL1-mediated transposable element silencing and primary root growth. *The Plant Journal*, 102, 703-717.
- Lohmann, J.; de Luxán-Hernández, C.; Gao, Y.; Zoschke, R.; Weingartner, M. (2022) The Arabidopsis Translation Elongation complex eEF1B impacts plant development and associates with heat-induced stress granules. *Journal of Experimental Botany*. Manuscript in revision. ID: JEXBOT/2022/307949.

## **MERISTEM DEFECTIVE is a conserved splicing factor and modulates cell division and stress response in Arabidopsis**

Cloe de Luxán-Hernández<sup>1</sup>, Julia Lohmann<sup>1</sup>, Eduardo Tranque<sup>2</sup>, Jana Chumova<sup>3</sup>, Pavla Binarova<sup>3</sup>, Julio Salinas<sup>2</sup> and Magdalena Weingartner<sup>1\*</sup>,

<sup>1</sup> Institute of Plant Sciences and Microbiology, University of Hamburg, Ohnhorststrasse 18, 22609 Hamburg.

<sup>2</sup> Departamento de Biotecnología Microbiana y de Plantas, Centro de Investigaciones Biológicas "Margarita Salas" (CSIC), 28040 Madrid, Spain.

<sup>3</sup> Institute of Microbiology of the Czech Academy of Sciences, Vídeňská1083, 142 20 Prague, Czech Republic.

\* To whom correspondence should be addressed. Tel: 0049 40 42816 562; Fax: 0049 40 42816 562; Email: [Magdalena.weingartner@uni-hamburg.de](mailto:Magdalena.weingartner@uni-hamburg.de)

**Running title:** MDF is a conserved plant splicing factor

### **ABSTRACT**

The coordination of cell division with stress response is essential for maintaining genome stability in plant meristems. Proteins involved in pre-mRNA splicing are important for these processes in animal and human cells. Based on its homology to the splicing factor SART1, which is implicated in the control of cell division and genome stability in human cells, we analyzed if MDF has similar functions in plants. We found that MDF associates with the spliceosomal component LSM8 and is essential for correct splicing of numerous transcripts. Loss of MDF function leads to cell division defects and cell death in meristems and was associated with upregulation of stress-induced genes and down-regulation of mitotic regulators. Our analysis of a dephosphomutant version of MDF uncovered how its activity might be controlled. The finding that the *mdf-1* mutant is hypersensitive to DNA damage treatment supports its role in coordinating stress response with cell division. Our work uncovers the conserved function of a plant splicing factor in cell division and provides novel insight into the interplay of pre-mRNA processing and genome stability in plants.

**Keywords:** cell division/genome stability/plant spliceosome/stress response



## INTRODUCTION

For plants as sessile organisms, the only way to survive in an ever-changing environment is to continuously adjust cell division and growth to environmental signals and stress conditions. This is especially important in meristematic cells, which are responsible for the continuous and error-free production of new cells for all plant organs. As in all other multicellular organisms, a conserved cell cycle machinery, which is controlled by the activities of conserved Cyclin-dependent kinases (CDK) and cyclin complexes, drives plant cells through the cell cycle. They ensure the controlled progression through the individual phases of the cell cycle namely gap phase 1 (G1), DNA replication (S), gap phase 2 (G2) and mitosis (M) (Shimotohno *et al*, 2021).

To maintain genome integrity during cell division, cells need to respond to DNA damage signals by activating the so-called DNA damage response (DDR) pathway. The DDR is controlled by two conserved kinases, ATAXIA TELANGIECTASIA MUTATED (ATM) and ATM AND RAD3-RELATED (ATR). Upon activation, they phosphorylate a plant-specific NAM-ATAF1/2-CUC2 (NAC) transcription factor, SUPPRESSOR OF GAMMA RESPONSE 1 (SOG1). Once being activated, SOG1 induces factors that lead to inhibition of cell cycle progression, activation of DNA repair (Culligan *et al*, 2006; Yi *et al*, 2014; Yoshiyama *et al*, 2009) and induction of cell death, if the cellular damage cannot be repaired (Furukawa *et al*, 2010; Johnson *et al*, 2018). SOG1-mediated cell cycle arrest was shown to occur at the G2-phase of the cell cycle through transcriptional induction of CDK inhibitors (Ogita *et al*, 2018; Yi *et al*, 2014) and the NAC transcription factors ANAC044 and ANAC085. This leads to stabilization of MYB3R repressors (Rep-MYBs) which inhibit the expression of genes required for the transition to mitosis (Takahashi *et al*, 2019).

Regulation of precursor-messenger RNA (pre-mRNA) splicing is a very effective mechanism that allows cells to rapidly adjust their transcriptional program to stressful conditions. In all eukaryotic cells, pre-mRNA splicing is catalyzed by the spliceosome, which is formed by the ordered interaction of four small ribonucleoprotein particles (snRNPs), named U1, U2, U4/U6 and U5 snRNPs, and additional splicing factors with the pre-mRNA (Will & Luhrmann, 2011). The splicing process is triggered by binding of U1 and U2 snRNPs to the 5' splice site and branching point respectively. Subsequently, pre-assembled U4/U6 snRNPs interact with U5 snRNPs to form the U4/U6.U5 tri-snRNP. Only under splicing conditions, the tri-snRNP becomes integrated into the spliceosome forming the pre-catalytic splicing complex. Major structural changes during which numerous U4/U6 and U5 snRNP-associated proteins including the LSM2-8 complex are released, lead to formation of the catalytically active spliceosome. After completion of the splicing reactions, the spliceosome is dismantled and the tri-snRNP is re-formed and takes part in new rounds of splicing (Wan *et al*, 2020; Wilkinson *et al*, 2020).

The importance of splicing proteins during DDR in animal and human cells is well established and a large part of the transcriptional reprogramming during DDR was shown to be mediated by mechanisms regulating mRNA processing and transcript stability (Boucas *et al*, 2012; Dutertre *et al*, 2011). In plants, the role of splicing factors during response and adaption to various abiotic stress conditions is well established (Laloum *et al*, 2018; Ling *et al*, 2021; Martin *et al*, 2021). For instance, for several core components of the spliceosome, such as the LSM2-8 complex or the U5-snRNP protein STABILIZED1 (STA1), a crucial role during adaption to salt and temperature stress was established (Carrasco-Lopez *et al*, 2017; Kim *et al*, 2017). In addition, serine/arginine (SR)-rich SR

proteins were shown to act as important splicing regulators during environmental responses. One prominent example is the SR-like protein SR45 that is an important regulator of developmental processes (Ali *et al*, 2007; Carvalho *et al*, 2010; Chen *et al*, 2019) and stress tolerance (Albaqami *et al*, 2019; Carvalho *et al*, 2016). However, it is not well understood to what extent plants utilize the splicing machinery for regulating DDR pathways (Nimeth *et al*, 2020).

The purified tri-snRNP from human cells contains about 30 proteins, and corresponding Arabidopsis homologs have been annotated (Koncz *et al*, 2012). One of them is MERISTEM DEFECTIVE (MDF), which is the Arabidopsis homolog to the human protein SQUAMOUS CELL CARCINOMA ANTIGEN RECOGNIZED BY T CELLS 1 (SART1). SART1 is only found in assembled tri-snRNP complexes and released from the spliceosome before its catalytic activation (Hacker *et al*, 2008). It was shown to be necessary for the association of the tri-snRNP with the pre-spliceosome, but not for the stability of the tri-snRNP itself (Makarova *et al*, 2001). Likewise, its yeast homolog SNU66 copurified with U4/ U6.U5 tri-snRNPs (Gottschalk *et al*, 1999; Stevens & Abelson, 1999) and is important for efficient pre-mRNA splicing in *Saccharomyces cerevisiae* (van Nues & Beggs, 2001). SART1 was originally identified as a tumor antigen in a range of cancers recognized by T cells (Kikuchi *et al*, 1999). Its expression was highly induced in different cancer cell lines and cancer tissue (Allen *et al*, 2012). Moreover, siRNA-based silencing revealed SART1 as an essential factor for cell division whose depletion was associated with cell division defects and induction of apoptosis (Kittler *et al*, 2004). MDF shares 38,9% overall sequence similarity with SART1. Based on its N-terminal putative RS domain containing arginine residues alternating with serine, glutamate or aspartate dipeptides, MDF is like SART1 an SR-like protein (Blencowe *et al*, 1999; Casson *et al*, 2009; Neugebauer *et al*, 1995). Published data have shown that MDF expression occurs mainly in dividing cells and that the *mdf-1* mutant showed impaired primary root development. These defects were associated with reduced cell division and cell elongation and mis-expression of genes involved in auxin regulation (Casson *et al*, 2009). Two independent phospho-proteomic screens have shown that MDF was phosphorylated at Serine 22 (S22) in proliferating cells (Roitinger *et al*, 2015; Waterworth *et al*, 2019) and this phosphorylation was increased upon DNA damage treatment (Roitinger *et al*, 2015).

In this study, we analyzed if MDF had a conserved function in pre-mRNA splicing in Arabidopsis and how this was related to its role during cell division and meristem development. We show that MDF is associated with plant tri-snRNP complexes, localizes to nuclear speckles and is important for correct splicing of numerous genes involved in developmental and signaling processes. MDF loss of function led to cell cycle arrest at the G2/M transition and increased endoreduplication levels. This phenotype was associated with altered expression of proliferation-associated genes, down-regulation of mitotic genes and constitutive upregulation of stress-related genes. Our analysis of a dephosphomutant version of MDF showed that MDF phosphorylation at S22 is important for its function in maintaining cell division activity in meristems. The interplay between pre-mRNA splicing and plant DDR was further addressed by assessing the sensitivity of mutants with impaired splicing activity to DNA damaging conditions. Thus, our work provides new insight into the role pre-mRNA processing in coordinating cell division, development and stress response in plants.

## RESULTS

## **The short root phenotype of *mdf-1* and *mdf-2* is associated with cell cycle arrest at the G2/M transition**

To assess how MDF loss of function affects cell proliferation in plants, we analyzed RAM development in WT, the two previously described T-DNA insertion lines for MDF *mdf-1* and *mdf-2* (Casson *et al.*, 2009), and a complementation line for *mdf-1* harboring a construct in which the genomic region of *MDF* including 3000 bp upstream of the start ATG was fused at the C-terminus to GFP (*mdf-1::pMDFMDFg*). Root length measurement over a time course from one to ten days after germination (dag) confirmed that in both mutants, root growth was strongly delayed compared to WT and *mdf-1::pMDFMDFg*. (Figure 1A). By confocal imaging of propidium iodide (PI) stained root tips (Figure 1B) we verified that in both *mdf* mutant lines, the cell division zone of the RAM was reduced as compared to WT and the complementation line. Quantification of the number of dividing cells in the cortical cell layer proved that the shorter meristem was due to a reduced number of dividing cells (Figure 1C). Furthermore, the PI-staining revealed that the absence of MDF lead to the accumulation of dead cells in the cell division zone of the RAM, which was not observed in the WT or the complementation line (Figure 1B and D).

Spontaneous induction of cell death is indicative for impaired genome stability and can be caused by defects during progression through mitosis (Hu *et al.*, 2016; Nisa *et al.*, 2019). To understand at which stage of cell division meristematic cells were arrested, we performed immunolabelling of microtubules in root tip cells. The quantification of microtubule arrays of six dag seedlings revealed that the number of cells showing mitotic microtubular arrays was reduced in the *mdf-1* and *mdf-2* mutants compared to WT. In contrast, the number of cells exhibiting a preprophase band marking the G2/M transition was significantly increased (Figure 1E), indicating that the transition from G2 to mitosis was impaired in the mutants. Genome instability and decreased division rates were shown to be associated with premature onset of endoreplication (Adachi *et al.*, 2011). Therefore, we measured the nuclear DNA content in 10 dag seedlings of WT, *mdf-1* and *mdf-2* by flow cytometry and found that in both mutant lines level of endoreduplication was significantly increased (Figure 1F, Figure S1A). We also assessed shoot apical meristem activity by quantifying the number of seedlings that formed true leaves at 10 dag. In this assay only *mdf-1* but not *mdf-2* showed a significant difference to WT (Figure 1G), indicating that in *mdf-1* not only root but also shoot meristem development was affected. As published previously, the insertion in *mdf-1* is located in intron 9 while in *mdf-2* lies within exon 9 (Casson *et al.*, 2009). By RT-qPCR analyses, we found that in both mutant lines the region upstream of the T-DNA insertion sites was still expressed, while the part of the gene downstream of the insertion sites, which includes the conserved SART1-domain, was not expressed in *mdf-1* but still highly accumulated in *mdf-2* (Figure S1B and C). This truncated version of MDF might still be partially functional and thus explain the phenotypic difference between *mdf-1* and *mdf-2* mutant lines (Figure 1A-G and Figure S1B). In summary, our phenotypic analyses showed that the defective meristem development in *mdf* mutants was associated with reduced cell division rates due to a G2-specific cell cycle arrest, genome instability and increased levels of endoreduplication.

## **MDF associates with U4/U6.U5 tri-snRNP proteins**

To assess if MDF as its human homolog hSART1, associates with the U4/U6.U5 tri-snRNP complexes in plant cells, we analyzed its interaction with LSM8, a core component of the tri-snRNP. LSM8 defines and confers specificity to the nuclear heteroheptameric ring complex LSM2-8 that binds and stabilizes the U6 small nuclear RNA (snRNA), which is part of the U6 snRNP and, therefore, of the U4/U6.U5 tri-snRNP complex (Beggs, 2005; Tharun, 2009). To show that MDF was associated with this complex, we performed co-immunoprecipitation (Co-IP) experiments, in which LSM8-GFP and putative interaction partners were co-immunoprecipitated using an anti-GFP antibody followed by tandem mass spectrometry (IP-MS/MS). MDF was among the proteins that specifically and abundantly co-purified with LSM8-GFP in three independent experiments (Table 1). To confirm the interaction, we performed bimolecular fluorescence complementation (BiFC) experiments using constructs harboring full-length open reading frames (ORF) of *MDF* and *LSM8* fused at the N-terminus to either the C-terminal or N-terminal half of YFP. As expected, co-expression of these constructs produced a bright YFP-derived fluorescence signal, which was mainly seen in the nucleus (Figure 2A). No fluorescence was detected in control experiments using *MDF* and *LSM1a* ORFs (Figure 2A). Next, we used fluorescence resonance energy transfer (FRET)-based fluorescence lifetime imaging to test for colocalization and physical interaction of *MDF*-GFP with *LSM8*-mCherry in tobacco leaf epidermis cells. We found that *MDF*-GFP and *LSM8*-mCherry signals overlapped in the nucleoplasm and in nuclear speckles, while only *MDF*-GFP was also concentrated in the nucleolus (Figure 2B). For FRET-FLIM measurements, constructs fused to GFP were used as donors and plasmids containing the fluorescent mCherry tag acted as acceptors. Our measurements revealed that there was no significant difference in the fluorescence lifetime of *MDF*-GFP in cells expressing *MDF*-GFP alone compared to those expressing both *MDF*-GFP and *LSM8*-mCherry. However, consistent with previous results (Perea-Resa *et al*, 2012) a significant change in fluorescence lifetime occurred upon co-expression of *LSM8*-GFP and *LSM2*-mCherry (Figure 2C). These data indicated that *LSM8* physically interacted with *LSM2*, as expected, but not with *MDF*. Additionally, Yeast Two Hybrid (Y2H) experiments were carried out confirming physical interaction between *LSM8* and *LSM2*, but not between *LSM8* and *MDF* (Figure S2). Together these data showed that *MDF* was a nuclear protein that associates with *LSM8* containing protein complexes. Its accumulation in nuclear speckles further indicated that it was part of the plant splicing complexes.

### **MDF is important for correct splicing of transcripts involved in transcriptional control and signaling**

To investigate if *MDF* loss of function was associated with defects in pre-mRNA splicing, we performed a high-coverage RNA-seq analysis on 12-days-old WT and *mdf-1* seedlings in three biological replicates. Approximately 50 million 150 base pair (bp) paired-end reads per sample were generated in a NovaSeq 6000 platform. 2945 differential splicing events corresponding to 2037 genes were identified in *mdf-1* background (Table S2-S6). Among these altered splicing events almost two third were in the category intron retention (IR: ≈64%), while the categories exon skipping, alternative 5' splice site, alternative 3' splice site and mutually exclusive exon were much less abundant (Figure 3A, Figure S3). We performed a Gene Ontology (GO) term enrichment analysis based on the biological process ontology for genes showing increased IR defects in *mdf-1* (Figure 3B, Table S7). Genes

associated with the GO terms 'transcription', 'protein phosphorylation', 'protein modification' and 'regulation of gene expression' were overrepresented. This indicated that MDF had an important function in controlling the correct splicing of transcripts involved in cellular signaling processes and transcriptional control. To gain more insight into the role of MDF in splicing regulation, we compared the altered splicing events identified in *mdf-1* with available RNA-seq data from mutants for three other components of the plant tri-snRNP in which a similar material (light grown seedlings) was used. These were *lsm8-1* (Carrasco-Lopez *et al.*, 2017), *rdm16-4* (Lv *et al.*, 2021), and *brr2a-2* (Mahrez *et al.*, 2016). The *rdm16-4* mutant has a point mutation in RDM16 encoding pre-mRNA splicing factor 3 (PRP3), which is part of the U4/U6 snRNP (Koncz *et al.*, 2012). *BRR2a* encodes a RNA helicase that is, not only part of the tri-snRNP, but also remains associated with the catalytically active spliceosome (Bessonov *et al.*, 2008). In each of these mutants, the most abundantly detected altered splicing event was IR. No representative overlap was found among the genes showing increased IR in all three mutants (Figure 3C). These data indicated that different splicing factors seem to have distinctive functions in splicing regulation. While approximately half of the detected splicing defects were specific to *mdf-1* with enrichment in the GO terms 'nucleobase-containing compound metabolic process' and 'RNA metabolic process' (Figure 3B), specific GO categories relevant for its putative role in cellular signaling and transcriptional control were shared with other splicing mutants (Figure 3B). Those were 'regulation of biological process' with *lsm8-1* (Table S8), 'protein phosphorylation' with *rdm16-4* (Table S9) and 'RNA biosynthetic process' with *brr2a-2* (Table S10). Thus, proper functioning of each of these three splicing factors, was required for splicing of those overlapping targets while correct splicing of many targets affecting RNA and DNA metabolism or stress response seemed to specifically require the function of MDF.

To validate the RNA-seq data we analyzed IR of selected targets by RT-qPCR on RNA samples isolated from 12-day-old seedlings of WT *mdf-1*, *mdf-2* and the complemented line (*mdf-1::pMDFMDFg*). Out of the analyzed genes, five were involved in cell cycle regulation (*CyclinP3-2*, *CyclinB2-2*, *KRP6*, *KRP2* and *SKP2B*) (Figure 3D), three had a role in splicing (*SR30*, *SR45* and *RSZ33*) (Figure 3E), five were known as transcriptional regulators (*PFA4*, *MYB4R1*, *MYB3R3*, *MYBL* and *REM30*) (Figure 3F) and one was associated to DNA repair processes (*RAD51D*) (Figure 3G). Among the 14 tested genes, we found for 8 genes a significant increase in intron retention in RNA samples for both *mdf-1* and *mdf-2* as compared to WT. For 6 genes, a significant difference could only be confirmed in *mdf-1* but not in *mdf-2*. Intron retention was reversed in 13 of the targets in the complemented line, further verifying that the splicing defects observed in these genes are very likely caused by the absence of MDF (Figure 3D-G). These data showed that, like its human and yeast homologs, MDF functions as pre-mRNA splicing factor in plants.

### **Loss of MDF function leads to altered expression of a large number of genes involved in stress response and cell cycle control**

To understand how loss of MDF function affected gene expression, we used our RNA-seq data to detect genome-wide transcriptional changes. We found that among the total number of differentially expressed genes 7516 were up-regulated and 7872 were down-regulated in *mdf-1* compared to WT

(Figure 4A, Table S11). A pathway enrichment analysis among the significantly upregulated genes revealed an enrichment of genes associated with stress responses. Among the top enriched GO categories were 'abiotic and biotic stimuli', 'temperature, salt and oxidative stress' and 'defense response' (Figure 4B, Table S12). Interestingly, among the down-regulated genes we found a significant enrichment of pathways involved in cell division and developmental processes. These top GO categories for down-regulated genes included 'cell cycle', 'cell division', 'chromosome organization', as well as 'cell differentiation', 'meristem development' and 'root and shoot system development' (Figure 4C, Table S13). Additionally, approximately 64% of the genes differentially intron retained in *mdf-1* background, were also among the differentially expressed genes, with the biggest overlap found among the down-regulated genes (Figure 4D). This correlated with the finding that IR might lead to introduction of a premature termination codon (PTC) and subsequent targeting of transcripts to the non-sense mediated decay (NMD) machinery, thus reducing their abundance (Filichkin *et al*, 2010). Interestingly, one of the biological processes enriched among the transcripts that were down-regulated and showed IR was 'regulation of gene expression'. Together, these data showed that loss of MDF function has a major impact on gene expression and is important for the correct expression of genes involved in cell proliferation and developmental processes, and, at the same time, leads to constitutive induction of stress response genes.

#### **MDF controls the expression of genes involved in cell cycle control during DDR**

We next aimed at understanding how the transcriptional changes in *mdf-1* might be associated with the cell division and cell death phenotype in the RAM. The DDR is a very well-studied signaling pathway in plants that, upon activation by the transcription factor SOG1, leads to cell cycle arrest, cell death and DNA repair (Yoshiyama *et al*, 2013). We therefore analyzed if a similar transcriptional program was constitutively induced in *mdf-1*. To this end we compared the transcripts that showed either increased IR or strong mis-expression in *mdf-1* by considering only those genes with Log2Fold changes above 2 (783 genes) and below -2 (1557 genes), with the set of 146 genes that are known as direct targets of SOG1 upon DNA damage (Ogita *et al.*, 2018). We found an overlap of 29 genes which constituted 20% of the total set of SOG1 target genes (Figure 5A, Table S14). Among them were the transcription factors ANAC044 and ANAC085, which were highly increased with Log2Fold changes of 2.4 and 5.3 respectively. Additionally, ANAC085 appeared to be also differentially spliced in the absence of MDF (Table S2). Increased expression of ANAC044 and ANAC085, was shown to lead to G2-specific cell cycle arrest by promoting the accumulation of Rep-MYB transcription factors, which negatively control the expression of mitosis-specific genes (Takahashi *et al.*, 2019). To further confirm mis-expression of mitosis-specific genes in *mdf-1*, we compared the set of 279 down-regulated genes in *mdf-1* that were associated with the GO term "cell cycle" (Figure 4C), with the 80 loci that were reported to be Rep-MYB specific target genes after DNA damage induction (Bourbousse *et al*, 2018) (Figure 5B, Table S15). Indeed, there was an overlap of 30 genes (38% of Rep-MYB target genes), further confirming that many genes that are mis-expressed in *mdf-1* are involved in DNA damage-induced cell cycle control. To confirm that the increased expression of ANAC044 and ANAC085 and reduced transcription of mitosis-specific genes occurred in an MDF-dependent manner, we performed RT-qPCR analyses on RNA isolated from seedlings of WT, *mdf-1*, *mdf-2* and *mdf-1::pMDFMDFg*. In

both mutant lines the expression of *ANAC085* and *ANAC044* was significantly increased as compared to WT and the complementation line (Figure 5C). In contrast, as expected, each of the seven mitotic genes tested showed an opposite expression pattern (Figure 5D). The complementation line exhibited increased levels of *MDF* (Figure 5E), which could explain why for some genes (like *SCL28* and *IMK2*), the downregulation was not only reversed to WT levels, but even switched to upregulation.

We next tested if the cell division and cell death defects of *mdf-1* were caused by ectopic activation of the DNA damage signaling component *SOG1* or its upstream regulator *ATM*. To this end, *mdf-1sog1-7* and *mdf-1atm-2* double mutants were generated by crossing with *sog1-7* and *atm-2* single mutants respectively (Garcia *et al*, 2003; Sjogren *et al*, 2015). Analysis of root growth in three day seedlings revealed that loss of *SOG1* or *ATM* function did not rescue the growth defects of *mdf-1* (Figure 6A). PI-staining of root tips showed that the organization of the RAM, including the number of dividing cells and cell death area, was unchanged in the *mdf-1sog1-7* as compared to the *mdf-1* single mutant (Figure 6B and C). However, the number of seedlings showing cell death in the meristematic zone under control conditions was significantly increased in the *mdf-1sog1-7* double mutant (Figure 6D) as compared to the *mdf-1* single mutant, indicating that genome instability was further increased in the absence of *SOG1*. Taken together, these results showed that a transcriptional program, which is normally only induced under stress conditions such as DNA damage, is constitutively activated in *mdf-1*, and thus most likely contributes to its growth arrest phenotype. Since the cell cycle arrest phenotype occurs also in the absence of *ATM* or *SOG1*, *MDF* might regulate the expression of proliferation-associated genes downstream or independent of *SOG1*.

### **The phosphorylation state of MDF influences its function during cell division control and pre-mRNA splicing**

Our data suggested that *MDF* was under control conditions important for the proper expression of proliferation-related genes required for cell division activity and growth of meristems. Interestingly, *MDF* was previously identified among the proteins that became specifically phosphorylated at S22 upon DNA damage (Roitinger *et al.*, 2015). To test if this phosphorylation influenced *MDF* activity, we used the *MDF* cDNA to generate two constructs in which either the S22 residue remained unchanged (35S::MDFYFP) or in which it was changed to alanine (35S::MDFS22AYFP) and thus could not be phosphorylated anymore. Both constructs were placed under the control of a constitutive promoter (CAMV35S), transformed into the *mdf-1* mutant, and stably transformed lines were established. We confirmed that both constructs were expressed at similar levels in the individual transgenic lines by measuring transcript abundance by RT-qPCR (Figure 7A) and protein accumulation by imaging of *MDF*-YFP-associated fluorescence in roots (Figure 7B). Analysis of root development revealed that both constructs resulted in a partial recovery of root growth. However, root length was significantly increased in the *mdf-1:p35SMDF* lines as compared to *mdf-1:p35SMDFS22A* plants (Figure 7C). We confirmed that the increased growth was due to increased cell division rates by assessing the number of dividing cells in the cortical cell layer of the RAM (Figure 7D). PI-staining of root tips showed that in transgenic lines for both constructs dead cells accumulated in the meristematic zone. However, the area of cell death was significantly increased in *mdf-1:p35SMDFS22A* seedlings (Figure 7B, 7E). These phenotypic differences demonstrated that the phosphorylation status of *MDF* indeed influenced



its ability to rescue the mutant phenotype and thus seemed to be critical for MDF activity. To assess if this was associated with splicing defects, we performed RT-qPCR experiments to analyze IR in transcripts that were found to be misspliced in *mdf-1* (Figure 3). Indeed, the IR defect was for some genes, such as *CYCB2-2* and *RAD51D*, reversed in both lines, while for others, such as in *MYB3R3*, it was only rescued in the *mdf-1::p35SMDF* line but not in *mdf-1::p35SMDFS22A* (Figure 7F). Since *MYB3R3* is involved in the repression of mitotic genes, the transcript levels of two mitotic genes downregulated in *mdf-1* background (Figure 5D) were also tested. While in *mdf-1::p35SMDF* seedlings the expression of *CDC20;1* and *CYCA2-3* was restored to WT levels, *mdf-1::p35SMDFS22A* seedlings displayed significantly reduced transcript levels of *CYCA2-3* (Figure 7G). These results suggested that the splicing activity of MDF is controlled by its phosphorylation status and that MDF might regulate splicing of specific transcripts in a phosphorylation-dependent manner.

### **Loss of conserved plant splicing factors affects DDR pathways**

We next aimed at understanding how impaired activity of conserved plant splicing factors might influence DDR signaling. To this end, we tested the sensitivity of mutant lines for three splicing factors to the double-strand breaks inducing drug zeocin. These were *mdf-1* and *mdf-2*, as well as T-DNA insertion lines for the core splicing factor *LSM8* and the SR-like protein *SR45*, which both were reported to be involved in developmental processes and abiotic stress response (Ali *et al.*, 2007; Carrasco-Lopez *et al.*, 2017; Perea-Resa *et al.*, 2012). Seedlings were germinated on MS medium and transferred after five days to plates supplemented with zeocin. Measurement of root length at two, four, and six days after transfer (DAT) revealed that in each of the lines root growth was reduced in the presence of zeocin (Figure 8A). Compared to WT, *mdf-1*, *lsm8-1* and *sr45-1* were significantly stronger affected by presenting complete growth arrest already four days after transfer to zeocin supplemented media (Figure 8B). Next, we analyzed the impact of zeocin on shoot development by growing seedlings on control medium or medium supplemented with two different concentrations of zeocin. Quantification of the seedlings that formed the first true leaf pair after 10 days of growth revealed that *mdf-1*, *mdf-2*, *lsm8-1* and *sr45-1* were significantly more affected than WT. Almost no mutant seedling was able to develop true leaves when grown in the highest zeocin concentration (Figure 8C). These results indicated that *mdf-1*, *mdf-2*, *sr45-1* and *lsm8-1* were hypersensitive to DNA damage treatment. To test whether this was due to an altered transcriptional response to DNA damage, seedlings were incubated for two hours with zeocin and used for RT-qPCR analysis of the four DDR genes: *BREAST CANCER SUSCEPTIBILITY1 (BRCA1)*, *RAD51*, *POLY (ADP-RIBOSE)-POLYMERASE1 (PARP1)* and *POLY (ADP-RIBOSE)-POLYMERASE2 (PARP2)*. Although all lines showed an increased expression of each of these genes upon zeocin treatment, the level of induction was much lower in *mdf-1*, *mdf-2* and *sr45-1* than in WT and *lsm8-1* (Figure 8D). PI staining of root tips revealed in each of the lines, including WT, a robust induction of cell death upon zeocin treatment (Figure 8E). Moreover, consistent with the impaired induction of DNA repair genes, the *sr45-1* mutant exhibited even under control conditions accumulation of dead cells in the division zone of the RAM in a similar pattern as *mdf-1* and *mdf-2* (Figure 8F). Together these results showed that MDF and SR45 seem to influence DDR signaling by modulating the transcriptional induction of DNA repair genes. Since *lsm8-1* showed a robust induction of DNA repair genes after zeocin incubation and no

spontaneous accumulation of dead cells in the RAM, the impact of zeocin treatment on root growth and true leaf formation might be associated with its altered sensitivity to abiotic stress factors (Carrasco-Lopez *et al.*, 2017).

## DISCUSSION

MDF was previously identified as an important factor for meristem development and proposed to control the expression of patterning genes (Casson *et al.*, 2009). Here we show that MDF is associated with a core component of the spliceosome and important for correct splicing of numerous transcripts in young seedlings. MDF loss of function was associated with constitutive activation of a similar transcriptional program that is in WT induced upon DNA damage. Our analysis of a dephosphomutant version of MDF indicated that the MDF phosphorylation state was important for its function in maintaining meristem activity. Moreover, we show that additional well-established mutants for plant splicing proteins are hypersensitive to DNA damage treatment underscoring the importance of alternative splicing mechanisms during plant DDR.

Since in plants a suitable *in vitro* plant-splicing system is so far not established, the individual components of the plant spliceosome were identified based on sequence similarity to human and yeast proteins (Albaqami *et al.*, 2019). MDF is known as a SART1-like protein that shares 38,9% and 25,9% overall sequence similarity with its human and yeast homologs hSART1 and ySNU66, respectively. We found that MDF was localised to nuclear speckles and interacted with the U6 snRNP bound protein LSM8, which is part of the U4/U6.U5 tri-snRNP particle. This is consistent with data from human cells showing that SART1 accumulates in the nucleoplasm, in nuclear speckles as well as in Cajal bodies in which tri-snRNP assembly occurs (Yildirim *et al.*, 2021). Moreover, human SART1 and yeast SNU66 co-purified with the U4/U6.U5 tri-snRNP complex. Y2H-based interaction studies revealed that SART1 physically interacted with the U5-associated proteins hBRR2A and hPERP6 and the U4/U6-associated protein hPRP3 while in the yeast spliceosome SNU66 interacted only with the two U5-specific yPRP8 and yBRR2 (Nguyen *et al.*, 2016). Although SART1 was suggested to act as a bridging protein between the U5 and U4/U6 snRNPs, it was found to be not essential for the assembly or the stability of the tri-snRNP and, therefore, its exact function within the spliceosome still remains to be elucidated (Liu *et al.*, 2006). Further experiments are required to identify the physical interaction partners of MDF within the plant spliceosome and its function during tri-snRNP assembly or stability.

In human cells, increased expression of SART1 in different cancer cell lines leads to cell division defects and apoptosis and correlates with altered expression of important cell cycle regulators (Hosokawa *et al.*, 2005). SART1 was also shown to be essential for cell division in breast cancer cells (Kittler *et al.*, 2004) and siRNA-mediated downregulation of SART1 resulted in increased apoptosis (Allen *et al.*, 2012). However, how these cell division related defects might be associated with altered pre-mRNA splicing is still not completely understood.

We found that under control conditions, the *mdf* mutant displays a phenotype characterised by decreased cell division rates, increased endoreduplication level and accumulation of dead cells in the

division zone of the RAM (Figure 1). The MDF phenotype resembles the phenotype of WT seedlings after induction of DNA damage and, accordingly, it also shows altered expression of genes regulated by DNA damage in plants (Ogita *et al.*, 2018; Yi *et al.*, 2014). Among the genes that are highly mis-expressed in the *mdf* mutants are the transcription factors *ANAC044* and *ANAC085* (Figure 5C), whose activation upon DNA damage promotes the stabilisation of the MYB3R transcriptional repressors, resulting in reduced expression of G2/M genes and cell cycle arrest (Takahashi *et al.*, 2019). The importance of splicing factors in cell cycle progression in plants has been suggested in a recent study in which the role of PLEIOTROPIC REGULATORY LOCUS 1 (PRL1), a conserved regulator of splicing in plants (Wang *et al.*, 2021), was analysed. Loss of PRL1 leads to IR of important cell cycle genes including the *CYCD1;1* and *CYCD3;1* cyclins and the *prl1* mutant exhibits delayed cell cycle progression and increased resistance to the replication stress inducing drug Hydroxyurea (Wang *et al.*, 2021). PRL1 was proposed to be a constitutive positive regulator of cell division that is targeted for degradation upon replication stress (Wang *et al.*, 2021). MDF seems to have a similar function in promoting cell cycle progression by regulating splicing and expression of proliferation-related genes in meristems.

Additionally, *mdf* mutants exhibit accumulation of dead cells in the root meristem and a disorganized patterning of the RAM (Figure 1B). A link between pre-mRNA splicing and maintenance of the root stem cell niche was also demonstrated by the analysis of the *rdm16-4* mutant (Lv *et al.*, 2021). RDM16 encodes the core splicing protein PRP3 that is necessary for the assembly of the U4/U6 snRNP (Wan *et al.*, 2016). The *rdm16-4* mutant showed impaired root meristem development and missplicing of genes involved in cytokinin signalling and meristem patterning such as the transcription factors of the PLETHORA (PLT) family resulting in reduced cell division rates (Lv *et al.*, 2021). Thus, *rdm16-4* and *mdf-1* mutants show to some extent similar defects in root development. However, the absence of MDF also affects shoot development (Figure 1E) and therefore MDF has additional functions necessary for plant development and survival, which might be associated with the regulation of stress-induced genes. We found that *mdf-1*, *mdf-2* and *sr45-1* mutant seedlings display a decreased induction of repair genes upon DNA stress, which might account for their increased sensitivity to zeocin. (Figure 8B and C). Interestingly, SR45 is homologous to animal RNA BINDING PROTEIN S1 (RNPS1), which is implicated in cell cycle control and maintenance of genome stability (Fukumura *et al.*, 2018; Li *et al.*, 2007). The *sr45-1* mutant of Arabidopsis was previously shown to exhibit developmental defects including delayed root growth and altered splicing of important genes for plant development (Ali *et al.*, 2007). Our finding that the *sr45-1* mutant accumulates dead cells in the RAM under control conditions and shows decreased induction of DNA repair genes upon DNA damage treatment indicates a so far unknown function for this important splicing regulator in plant DDR. However, despite the constitutive accumulation of dead cells in the RAM, *sr45-1* showed a similar induction of cell death upon DNA damage as WT. In contrast, in *mdf-1*, the relative increase of dead cells upon DNA damage is diminished. (Figure 8E). It will be interesting to test in future experiments if MDF – similar to its human homolog SART1 – is directly involved in cell death activation in dividing cells.

It was previously shown that the phosphorylation of MDF at S22 increases in seedlings upon DNA damage treatment (Roitinger *et al.*, 2015). We performed complementation experiments using a dephosphomutant version of MDF to test if the phosphorylation at S22 was important for MDF function. Indeed, we found that the dephosphomutant version of MDF was unable to fully complement the cell division phenotype of *mdf-1* (Figure 7). Splicing-related proteins have been previously identified as major phosphorylation targets in plants (de la Fuente van Bentem *et al.*, 2006). Phosphorylation of SR proteins in their RS domain was shown to alter their activity by influencing their subcellular location (Huang & Steitz, 2005). Moreover, the pre-mRNA processing 4 (PRP4) KINASE A (PRP4KA), whose loss of function was associated with several developmental defects such late flowering, reduced branching, and lowered seed set (Kanno *et al.*, 2018) was proposed to influence splicing patterns by phosphorylating a subset of splicing regulators (Kanno *et al.*, 2018). A direct link between stress response, phosphorylation and splicing was recently established by the analysis of MITOGEN-ACTIVATED PROTEIN KINASE 4 (MPK4), a major activator of the plant immune response. Absence of MPK4 leads to altered splicing of several splicing factors and immunity-related protein kinases (Bazin *et al.*, 2020). Our results provide a first insight into the mechanism by which MDF splicing activity might be controlled. However, further experiments are required to find out at a genome-wide level how the MDF phosphorylation state affects the splicing patterns in dividing tissues and how MDF phosphorylation is regulated. Together, our data suggest the following model (Figure 9): Under control conditions, MDF would promote the expression and correct splicing of genes maintaining cell division and growth in meristematic tissues. A transcriptional program that is normally induced under stress conditions would then become activated when MDF is inactive leading to cell cycle arrest, induction of endoreduplication and cell death.

## MATERIAL AND METHODS

### Plant material and growth conditions

Wild type for all experiments was the *Arabidopsis thaliana* accession Columbia (Col-0) and every mutant line used during this study was in Col-0 background. T-DNA insertion lines for *mdf-1* (SALK\_040710), *mdf-2* (SAIL\_775\_F10), *sr45-1* (SALK\_004132), *lsm8-1* (SALK\_025064) and *atm-2* (SALK\_006953) and the mutant line *sog1-7* were previously described (Ali *et al.*, 2007; Casson *et al.*, 2009; Garcia *et al.*, 2003; Perea-Resa *et al.*, 2012; Sjogren *et al.*, 2015). Double mutants for *mdf-1sog1-7* and *mdf-1atm-2* were generated by crossing. The complementation line *mdf-1::pMDFMDFg* was achieved by floral dipping (Clough & Bent, 1998) using *Agrobacterium tumefaciens* C58C1 harbouring full genomic *MDF* and promoter in the pMDC107 destination vector (Curtis & Grossniklaus, 2003). Primers for fragment amplification were described (Casson *et al.*, 2009) and used for cloning inside the pDONR221 vector (Thermo Fisher Scientific). The transgenic plants overexpressing *MDF* full-length coding sequence (CDS) were generated by amplifying *MDF* full length CDS excluding the STOP codon with primers described in Table S1 for cloning inside the pENTR-D-TOPO plasmid (Thermo Fisher Scientific) followed by LR recombination reaction with the destination vector pEG101. Final step was floral dipping using *Agrobacterium tumefaciens* C58C1 strain. The making of the *MDFS22ACDS* construct involved an additional step before LR reaction in which serine 22 was exchanged to alanine by site directed mutagenesis PCR using appropriate overlapping primers

harbouring the mutation and MDFCDS\_pENTR-D-TOPO as template. The PCR product was transformed in *Escherichia coli* TOP10 with previous DpNI incubation to avoid transformation of non-mutated plasmid. Site directed mutagenesis primers can be found in Table S1. For in vitro analyses plants were grown either on soil or on Murashige and Skoog (MS) plates containing 1% sucrose and 1% (w/v) agar in growth chambers (16 h light, 22°C/ 8 h dark, 18°C cycles). Seeds were vapor sterilized by a mixture of 2,3 mL of 32% HCl and 50 mL of NaOCl for 3 hours.

#### Growth assays and propidium iodide staining

Primary root growth was assessed by germination and growth on MS vertical plates. Plates were scanned at the indicated timepoints. Quantification was achieved using the ImageJ software. Zeocin root growth inhibition experiments were carried out by germinating plants on MS vertical plates and transferring them to control (no zeocin) and zeocin (Invitrogen) 20µg/mL for 6 additional days. Scanning was done before transfer (after 4 days in light) and 2, 4 and 6 days after transfer. Primary root length was measured at each time point and growth for each timepoint was determined by subtracting the length of the previous timepoint. Relative growth values were obtained by dividing the lengths of each timepoint by the initial root length measured before transfer. For true leaf formation experiments, plants were germinated and grown on horizontal plates containing no zeocin (Control), zeocin 25 µg/mL (Zeocin 25) and zeocin 50 µg/mL (Zeocin 50) for 10 days. Percentage of plants showing true leaves was calculated for each of the conditions in at least three independent experiments with a minimum of 20 plants per line, condition, and experiment. Propidium Iodide (PI) (Sigma-Aldrich) staining of 2 and 3 days after germination plants was performed by cutting the root tips of the plants at the desired age and incubating them for 1 min in a 10 µg/ml PI solution. For induction of cell death analyses plants were prior to PI staining transferred to liquid MS medium with or without zeocin at a concentration of 15µM overnight (ON). Number of dividing cells in the root apical meristem (RAM) was determined by counting the amount of cortex cells within the dividing zone of the RAM. Imaging was carried out using confocal microscopy and cell death area was quantified with the ImageJ software.

#### Flow cytometry

Flow cytometry was performed as described previously (Kallai *et al*, 2020). Nuclei were isolated from seedlings (Partec CyStain UV precise P kit) and analysed by flow cytometry on BD LSRII (BD Biosciences) with a solid state laser (Ex 405 nm) and 450/50 band pass filter. Data evaluation was performed in FlowJo from at least three independent experiments. Endoreduplication index (EI) was determined from percentage values of each C-level.

#### Immunofluorescence labelling

Slide preparation of squashed *Arabidopsis* roots and immunolabelling were performed as described in (Horvath *et al*, 2017). The anti- $\alpha$ -tubulin (Abcam, 1:1000) and anti-mouse Alexa Fluor 488 (1:600) Antibodies were used to visualise mitotic microtubular arrays. Chromatin was counterstained with DAPI. Microscopical analyses were performed using FV10 ASW2.0 and confocal IX-81 FV-1000 Olympus microscopes.

## Co-Immunoprecipitation experiments

Fifteen grams of 3-week-old *c-lsm8* plants (Perea-Resa *et al.*, 2012) was cross-linked with 1% formaldehyde in PBS, two times for 10 min by vacuum infiltration, followed by 5 min vacuum with glycine to a final concentration of 125 mM. Plant material was rinsed 6 times with precooled water and frozen in liquid nitrogen. Nuclei isolation was performed as reported previously (Locascio *et al.*, 2013) and LSM8-GFP was immunoprecipitated using GFP-Trap agarose system (Chromotek) following the manufacturing indications. SDS-PAGE (10% polyacrylamide) was run till the whole proteome had penetrated in the resolving gel (about 1 cm of total migration). Gels were stained with Colloidal Blue Staining Kit (Invitrogen). Each proteome was excised and divided in 2 fractions ("up" and down"). These fractions were cut in small pieces prior to manual in-gel digestion with trypsin. Excised bands were separately destained with 50 mM ammonium bicarbonate (ABC), (Sigma-Aldrich) and 50% acetonitrile (ACN), (Fisher Chemical). Samples were then reduced with 10 mM dithiothreitol (Bio-Rad) in 50 mM ABC, and alkylated with 55 mM iodoacetamide (GE Healthcare Life Sciences) in 50 mM ABC. Then, gel pieces were digested with porcine trypsin (Thermo Fisher Scientific), at a final concentration 12.5 ng/ml in 50 mM ABC, overnight at 37°C. Peptides were extracted using 100% ACN and 0.5% trifluoroacetic acid, (Sigma-Aldrich), purified using a Zip Tip (Millipore, Sigma-Aldrich), and dried (3). Finally, samples were reconstituted in 10 µl of 0.1% formic acid before their analysis by nanosystem liquid chromatography-tandem mass spectrometry (nLC-MS/MS). All peptide separations were carried out on an Easy-nLC 1000 nano system (Thermo Scientific). For each analysis, the sample was loaded into a precolumn Acclaim PepMap 100 (Thermo Scientific) and eluted in a RSLC PepMap C18, 15 cm long, 50 µm inner diameter and 2 µm particle size (Thermo Scientific). The mobile phase flow rate was 300 nL/min using 0.1% formic acid in water (solvent A) and 0.1% formic acid and 100% acetonitrile (solvent B). The gradient profile was set as follows: 0%–35% solvent B for 90 min, 35%-100% solvent B for 4 min, 100% solvent B for 8 min. Four microliters of each sample was injected. MS analysis was performed using a Q Exactive mass spectrometer (Thermo Scientific). For ionization, 2000 V of liquid junction voltage and 270 °C capillary temperature was used. The full scan method employed a  $m/z$  400–1500 mass selection, an Orbitrap resolution of 70,000 (at  $m/z$  200), a target automatic gain control (AGC) value of  $3e6$ , and maximum injection times of 100 ms. After the survey scan, the 15 most intense precursor ions were selected for MS/MS fragmentation. Fragmentation was performed with a normalized collision energy of 27 eV and MS/MS scans were acquired with a starting mass of  $m/z$  100, AGC target was  $2e5$ , resolution of 17,500 (at  $m/z$  200), intensity threshold of  $8e3$ , isolation window of 2  $m/z$  units and maximum IT was 100 ms. Charge state screening was enabled to reject unassigned, singly charged, and equal or more than seven protonated ions. A dynamic exclusion time of 20s was used to discriminate against previously selected ions. MS data were analyzed with Proteome Discoverer (version 1.4.1.14) (Thermo) using standardized workflows. Mass spectra \*.raw files were searched against Swissprot Arabidopsis thaliana (thale cress) database (14986 sequences protein entries) using Mascot (version 2.6.0, Matrix Science) search engine. Precursor and fragment mass tolerance were set to 10 ppm and 0.02 Da, respectively, allowing 2 missed cleavages, carbamidomethylation of cysteines as a fixed modification, methionine oxidation as a variable modification. Identified peptides were filtered using Percolator algorithm (Kall *et al.*, 2007) with a  $q$ -value threshold of 0.01.

## BiFC and FLIM FRET analyses

For BiFC assays, the coding sequences of *MDF*, *LSM8* and *LSM1a* were amplified from a pool of Arabidopsis cDNAs with appropriated primers, cloned into the pDONR207 vector, and then transferred to the pYFN43 and pYFC43 destination vectors for BiFC assays. These constructs were used to transform cells of *Agrobacterium tumefaciens* strain GV3101. Transient expression of fusion proteins for BiFC was analyzed by confocal microscopy, 3 days after agroinfiltration in leaves of three-week-old *Nicotiana benthamiana* plants grown at 23 °C. Analyses were performed at least in triplicate with independent samples. The constructs for FLIM-FRET assays and co-localization experiments were generated by amplifying the CDS excluding the STOP codon of each of the splicing factors by PCR and subsequent cloning into pENTR-D-TOPO for MDF and pDONR221 for LSM2 and LSM8, followed by LR recombination reaction with the destination vectors pABindGFP and pABindmCherry (Bleckmann *et al*, 2010). Constructs were transformed in *Agrobacterium tumefaciens* C58C1 and transiently expressed in 4-6 week-old *Nicotiana benthamiana* leaves. Fluorescence lifetime was acquired with a Leica TCS SP8 Confocal microscope (40× Water immersion objective). Time-correlated single photon counting was performed with picosecond resolution (PicoQuant Hydra Harp 400). Fluorophores were excited with a 470 nm (r LDHPC470B, 40 MHz) or 485 nm (LDH-D-C-485, 32 MHz) pulsed polarized diode laser with a power of 1 μW at the objective lens. For detection of emitted light, a SMD-adjusted Hybrid detector (HyD SMD3) (wavelength set to 500 – 520 nm) and a TCSPC modul PicoHarp 300 (PicoQuant) was used. Image acquisition was done at zoom 6 with a resolution of 256x256 pixel with a dwell time of 20μs, and photons were collected over 50-60 frames. Fluorescence decay was analyzed in Symphotime 64 (version 2.4; PicoQuant) using the Lifetime FRET Image analysis tool. TCSPC channels were binned by eight, count threshold was set so that the background was removed, Fluorescence decay was fitted using a multi-exponential decay, and the amplitude-weighted lifetime was considered as the sample's apparent lifetime. FRET efficiency was calculated as the lifetime of the FRET sample over the arithmetic mean of the lifetimes of the donor-only samples measured in the same experiment:  $FRET_{eff} = 1 - (T_{FRET} / T_{donor})$ . All measurements were done in three independent experiments (n = 8).

## Yeast two hybrid (Y2H) assays

Full length CDS of MDF, LSM8 and LSM2 were amplified and cloned into pDONR221 plasmids. The Gateway compatible versions of the GAL4 DNA-binding domain vector pGBT-9 (Bleckmann *et al*, 2010) and the activation domain vector pGAD424 (Clontech, www.takarabio.com) were used as destination vectors. Additionally, since LSM8 pGBT-9 gave autoactivation, full length CDS versions without the STOP codon of MDF and LSM8 were also amplified and cloned into the pDONR221 vector and recombined into the pGBKc and pGADc Y2H destination vectors (Stellberger *et al*, 2010). These vectors contain the binding and activation domain respectively C-terminally tagged, opposite to the N-terminally tagged pGBT9 and pGAD424. *Saccharomyces cerevisiae* strain AH109 was transformed as described in (Gietz *et al*, 1997). Positive transformants were selected on yeast minimal medium (SD medium: 0.66% yeast nitrogen base without amino 244 acids, 0.066% amino acid mix, 2% glucose) lacking leucine and tryptophan (SD-LW). Single positive colonies were cultured ON in liquid SD-LW at 30°C and continuous shaking. The day after a pre-culture with OD<sub>600</sub>=0.3 was



inoculated using the ON culture as the starter material. After 3h under continuous shaking at 30°C, optical density was adjusted to OD<sub>600</sub>=4 and a dilution series from 10<sup>-1</sup> to 10<sup>-3</sup> was made. Spotting of the pre-culture and dilutions was carried out on selection plates containing either SD-LW (Growth control) or SD-LWH (Interaction test). 3 colonies were tested for each of the interactions.

#### Confocal laser scanning microscopy

Detection of YFP, GFP, mCherry and PI was carried out by using the Leica TCS SP8 Confocal Platform (Leica Microsystems). Excitation wavelength of 488 nm was used for detection of GFP and YFP, while a laser light of 561 was used for excitation of mCherry and PI. The detection windows ranged from 520-540 (YFP), 496-514 (GFP), 590-630 (mCherry) and 600-636 (PI). For BiFC analyses, images were collected using a TCS SP5 confocal laser scanning microscope (Leica Microsystems). The excitation line for imaging YFP fusions was 514 nm.

#### RNA extraction and RT-qPCR analyses

Total RNA was extracted from complete seedlings of the different ages using the innuPREP Plant RNA kit (Analytik Jena Bio solutions). cDNA synthesis was carried out by using the QuantiTect® Reverse Transcription kit (QIAGEN). Rotor-Gene® SYBR® Green (QIAGEN) and the Rotor-gene-Q cyclor (QIAGEN) were used for performing the quantitative PCRs. Generated data was quality controlled and normalized to the reference genes *FASS (AT5G18580)* and *SAND (AT2G28390)* using the qbasePLUS software (Hellemans *et al*, 2007). For validation of intron retention events visualized on the IGV software, two primers pairs were designed to specifically detect intron and exon transcripts. Exon primers annealed to the exon junction, while intron-specific primers annealed inside the retained intron. Intron retention was afterwards measured by dividing intron expression by exon-specific expression. All primers are listed on Table S1.

#### RNA sequencing

Total RNA was extracted from 3 different biological replicates containing 12-day-old seedlings of WT and *mdf-1* using the innuPREP Plant RNA kit (Analytik Jena Bio solutions). RNA quality assessment, library preparation, sequencing and bioinformatic analyses were performed by Novogene Co. Integrity and quantitation of the extracted RNA were measured using the RNA Nano 6000 Assay Kit of the Bioanalyzer 2100 system (Agilent Technologies, CA, USA). With 1 µg RNA per sample as input material, sequencing libraries were subsequently generated using NEBNext® Ultra™ RNA Library Prep Kit for Illumina® (NEB) following the manufacturer's recommendations. Index codes were also added to attribute sequences to each sample. Clustering of the index-coded samples was carried out on a cBot Cluster Generation System using PE Cluster Kit cBot-HS (Illumina) following manufacturer's instructions. Afterwards, library preparations were sequenced on an Illumina NovaSeq 6000 platform and approximately 50 million 150 paired end reads per sample were generated. To ensure the high quality of the samples, only clean data was used for subsequent analyses. This was achieved after the removal of reads containing adapter and poly-N sequences and reads with low quality from the raw data. Mapping against the Arabidopsis TAIR10 reference genome was performed using the HISAT2 software. Reads Per Kilobase of exon model per Million mapped reads (RPKM) of each gene was

calculated based on the length of the gene and reads count mapped to this gene. Differential expression analyses between *mdf-1* and WT were carried out using the DESeq2 R package with the Benjamini and Hochberg's approach for adjusting p values according to the False Discovery Rate (FDR). Genes with adjusted p-value < 0.05 were considered as differentially expressed. Gene ontology (GO) enrichment analyses was performed using the GO-term finder software from Princeton University (Boyle *et al*, 2004). Alternative splicing (AS) analysis was performed with the rMATS software. Events with adjusted p-value < 0.05 were considered as alternatively spliced. Venn diagrams were generated with the online software Venny 2.1 generated by Juan Carlos Oliveros (BioinfoGP, CNB-CSIC).

## **ACKNOWLEDGEMENT**

We thank Judith Mehrmann, Sotoodeh Seyedehyasaman, Wiebke Hellmeyer, Anastasiia Goshina and Tim Lienemann for technical assistance and experimental support and to Paul Larsen (University of California, Riverside) for providing the seeds for the *sog1-7* line.

## **Disclosure and competing interests statement**

None.

## **DATA AVAILABILITY SECTION**

The genome-wide RNAseq data presented in this publication are available at Gene Expression Omnibus database GSE197898 (<https://www.ncbi.nlm.nih.gov/geo/>).

## **SUPPLEMENTARY DATA**

Supplementary Data are available online.

## **FUNDING**

This work was funded by the Deutsche Forschungsgemeinschaft (DFG) grant to M.W. [WE4506/6-1]. CL-H was recipient of a PhD fellowship from the University of Hamburg. In addition, funding was received from the Spanish Ministry of Science and Innovation to J.S. [PID2019-106987RB-I00/AEI/10.13039/5011033], from the Spanish Ministry of Science and Innovation to E.T. (FPI contract), from the Czech Academy of Science, Deutsche Akademische Austauschdienst and Bundesministeriums für Bildung und Forschung (BMBF) [CAS Mobility DAAD-19-04 and CAS Mobility DAAD-21-07] to M.W. and P.B.

## **REFERENCES**

Adachi S, Minamisawa K, Okushima Y, Inagaki S, Yoshiyama K, Kondou Y, Kaminuma E, Kawashima M, Toyoda T, Matsui M *et al* (2011) Programmed induction of endoreduplication by DNA double-strand breaks in Arabidopsis. *Proc Natl Acad Sci U S A* 108: 10004-10009  
Albaqami M, Laluk K, Reddy ASN (2019) The Arabidopsis splicing regulator SR45 confers salt tolerance in a splice isoform-dependent manner. *Plant Mol Biol* 100: 379-390  
Ali GS, Palusa SG, Golovkin M, Prasad J, Manley JL, Reddy AS (2007) Regulation of plant developmental processes by a novel splicing factor. *PLoS One* 2: e471  
Allen WL, Stevenson L, Coyle VM, Jithesh PV, Proutski I, Carson G, Gordon MA, Lenz HJ, Van Schaeybroeck S, Longley DB *et al* (2012) A systems biology approach identifies SART1 as a novel

determinant of both 5-fluorouracil and SN38 drug resistance in colorectal cancer. *Mol Cancer Ther* 11: 119-131

Bazin J, Mariappan K, Jiang Y, Blein T, Voelz R, Crespi M, Hirt H (2020) Role of MPK4 in pathogen-associated molecular pattern-triggered alternative splicing in Arabidopsis. *PLoS Pathog* 16: e1008401

Beggs JD (2005) Lsm proteins and RNA processing. *Biochem Soc Trans* 33: 433-438

Bessonov S, Anokhina M, Will CL, Urlaub H, Luhrmann R (2008) Isolation of an active step I spliceosome and composition of its RNP core. *Nature* 452: 846-850

Bleckmann A, Weidtkamp-Peters S, Seidel CA, Simon R (2010) Stem cell signaling in Arabidopsis requires CRN to localize CLV2 to the plasma membrane. *Plant Physiol* 152: 166-176

Blencowe BJ, Bowman JA, McCracken S, Rosonina E (1999) SR-related proteins and the processing of messenger RNA precursors. *Biochem Cell Biol* 77: 277-291

Boucas J, Riabinska A, Jokic M, Herter-Sprie GS, Chen S, Hopker K, Reinhardt HC (2012) Posttranscriptional regulation of gene expression-adding another layer of complexity to the DNA damage response. *Front Genet* 3: 159

Bourbousse C, Vegesna N, Law JA (2018) SOG1 activator and MYB3R repressors regulate a complex DNA damage network in Arabidopsis. *Proc Natl Acad Sci U S A* 115: E12453-E12462

Boyle EI, Weng S, Gollub J, Jin H, Botstein D, Cherry JM, Sherlock G (2004) GO::TermFinder--open source software for accessing Gene Ontology information and finding significantly enriched Gene Ontology terms associated with a list of genes. *Bioinformatics* 20: 3710-3715

Carrasco-Lopez C, Hernandez-Verdeja T, Perea-Resca C, Abia D, Catala R, Salinas J (2017) Environment-dependent regulation of spliceosome activity by the LSM2-8 complex in Arabidopsis. *Nucleic Acids Res* 45: 7416-7431

Carvalho RF, Carvalho SD, Duque P (2010) The plant-specific SR45 protein negatively regulates glucose and ABA signaling during early seedling development in Arabidopsis. *Plant Physiol* 154: 772-783

Carvalho RF, Szakonyi D, Simpson CG, Barbosa IC, Brown JW, Baena-Gonzalez E, Duque P (2016) The Arabidopsis SR45 Splicing Factor, a Negative Regulator of Sugar Signaling, Modulates SNF1-Related Protein Kinase 1 Stability. *Plant Cell* 28: 1910-1925

Casson SA, Topping JF, Lindsey K (2009) MERISTEM-DEFECTIVE, an RS domain protein, is required for the correct meristem patterning and function in Arabidopsis. *Plant J* 57: 857-869

Chen SL, Rooney TJ, Hu AR, Beard HS, Garrett WM, Mangalath LM, Powers JJ, Cooper B, Zhang XN (2019) Quantitative Proteomics Reveals a Role for SERINE/ARGININE-Rich 45 in Regulating RNA Metabolism and Modulating Transcriptional Suppression via the ASAP Complex in Arabidopsis thaliana. *Front Plant Sci* 10: 1116

Clough SJ, Bent AF (1998) Floral dip: a simplified method for Agrobacterium-mediated transformation of Arabidopsis thaliana. *Plant J* 16: 735-743

Culligan KM, Robertson CE, Foreman J, Doerner P, Britt AB (2006) ATR and ATM play both distinct and additive roles in response to ionizing radiation. *Plant J* 48: 947-961

Curtis MD, Grossniklaus U (2003) A gateway cloning vector set for high-throughput functional analysis of genes in planta. *Plant Physiol* 133: 462-469

de la Fuente van Bentem S, Anrather D, Roitinger E, Djamei A, Hufnagl T, Barta A, Csaszar E, Dohnal I, Lecourieux D, Hirt H (2006) Phosphoproteomics reveals extensive in vivo phosphorylation of Arabidopsis proteins involved in RNA metabolism. *Nucleic Acids Res* 34: 3267-3278

Dutertre M, Sanchez G, Barbier J, Corcos L, Auboeuf D (2011) The emerging role of pre-messenger RNA splicing in stress responses: sending alternative messages and silent messengers. *RNA Biol* 8: 740-747

Filichkin SA, Priest HD, Givan SA, Shen R, Bryant DW, Fox SE, Wong WK, Mockler TC (2010) Genome-wide mapping of alternative splicing in Arabidopsis thaliana. *Genome Res* 20: 45-58

Fukumura K, Inoue K, Mayeda A (2018) Splicing activator RNPS1 suppresses errors in pre-mRNA splicing: A key factor for mRNA quality control. *Biochem Biophys Res Commun* 496: 921-926

Furukawa T, Curtis MJ, Tominey CM, Duong YH, Wilcox BW, Aggoune D, Hays JB, Britt AB (2010) A shared DNA-damage-response pathway for induction of stem-cell death by UVB and by gamma irradiation. *DNA Repair (Amst)* 9: 940-948

Garcia V, Bruchet H, Camescasse D, Granier F, Bouchez D, Tissier A (2003) AtATM is essential for meiosis and the somatic response to DNA damage in plants. *Plant Cell* 15: 119-132

Gietz RD, Triggs-Raine B, Robbins A, Graham KC, Woods RA (1997) Identification of proteins that interact with a protein of interest: applications of the yeast two-hybrid system. *Mol Cell Biochem* 172: 67-79

Gottschalk A, Neubauer G, Banroques J, Mann M, Luhrmann R, Fabrizio P (1999) Identification by mass spectrometry and functional analysis of novel proteins of the yeast [U4/U6.U5] tri-snRNP. *EMBO J* 18: 4535-4548

Hacker I, Sander B, Golas MM, Wolf E, Karagoz E, Kastner B, Stark H, Fabrizio P, Luhrmann R (2008) Localization of Prp8, Brr2, Snu114 and U4/U6 proteins in the yeast tri-snRNP by electron microscopy. *Nat Struct Mol Biol* 15: 1206-1212

Hellemans J, Mortier G, De Paepe A, Speleman F, Vandesompele J (2007) qBase relative quantification framework and software for management and automated analysis of real-time quantitative PCR data. *Genome Biol* 8: R19

Horvath BM, Kourova H, Nagy S, Nemeth E, Magyar Z, Papdi C, Ahmad Z, Sanchez-Perez GF, Perilli S, Blilou I *et al* (2017) Arabidopsis RETINOBLASTOMA RELATED directly regulates DNA damage responses through functions beyond cell cycle control. *EMBO J* 36: 1261-1278

Hosokawa M, Kadota R, Shichijo S, Itoh K, Dmitriev I, Krasnykh V, Curiel DT, Takue Y, Wakasugi H, Takashima S *et al* (2005) Cell cycle arrest and apoptosis induced by SART-1 gene transduction. *Anticancer Res* 25: 1983-1990

Hu Z, Cools T, De Veylder L (2016) Mechanisms Used by Plants to Cope with DNA Damage. *Annu Rev Plant Biol* 67: 439-462

Huang Y, Steitz JA (2005) SRprises along a messenger's journey. *Mol Cell* 17: 613-615

Johnson RA, Conklin PA, Tjahjadi M, Missirian V, Toal T, Brady SM, Britt AB (2018) SUPPRESSOR OF GAMMA RESPONSE1 Links DNA Damage Response to Organ Regeneration. *Plant Physiol* 176: 1665-1675

Kall L, Canterbury JD, Weston J, Noble WS, MacCoss MJ (2007) Semi-supervised learning for peptide identification from shotgun proteomics datasets. *Nat Methods* 4: 923-925

Kallai BM, Kourova H, Chumova J, Papdi C, Trogelova L, Kofronova O, Hozak P, Filimonenko V, Meszaros T, Magyar Z *et al* (2020) gamma-Tubulin interacts with E2F transcription factors to regulate proliferation and endocycling in Arabidopsis. *J Exp Bot* 71: 1265-1277

Kanno T, Venhuizen P, Wen TN, Lin WD, Chiou P, Kalyna M, Matzke AJM, Matzke M (2018) PRP4KA, a Putative Spliceosomal Protein Kinase, Is Important for Alternative Splicing and Development in Arabidopsis thaliana. *Genetics* 210: 1267-1285

Kikuchi M, Nakao M, Inoue Y, Matsunaga K, Shichijo S, Yamana H, Itoh K (1999) Identification of a SART-1-derived peptide capable of inducing HLA-A24-restricted and tumor-specific cytotoxic T lymphocytes. *Int J Cancer* 81: 459-466

Kim GD, Cho YH, Lee BH, Yoo SD (2017) STABILIZED1 Modulates Pre-mRNA Splicing for Thermotolerance. *Plant Physiol* 173: 2370-2382

Kittler R, Putz G, Pelletier L, Poser I, Heninger AK, Drechsel D, Fischer S, Konstantinova I, Habermann B, Grabner H *et al* (2004) An endoribonuclease-prepared siRNA screen in human cells identifies genes essential for cell division. *Nature* 432: 1036-1040

Koncz C, Dejong F, Villacorta N, Szakonyi D, Koncz Z (2012) The spliceosome-activating complex: molecular mechanisms underlying the function of a pleiotropic regulator. *Front Plant Sci* 3: 9

Laloum T, Martin G, Duque P (2018) Alternative Splicing Control of Abiotic Stress Responses. *Trends Plant Sci* 23: 140-150

Li X, Niu T, Manley JL (2007) The RNA binding protein RNPS1 alleviates ASF/SF2 depletion-induced genomic instability. *RNA* 13: 2108-2115

Ling Y, Mahfouz MM, Zhou S (2021) Pre-mRNA alternative splicing as a modulator for heat stress response in plants. *Trends Plant Sci* 26: 1153-1170

Liu S, Rauhut R, Vornlocher HP, Luhrmann R (2006) The network of protein-protein interactions within the human U4/U6.U5 tri-snRNP. *RNA* 12: 1418-1430

Lv B, Hu K, Tian T, Wei K, Zhang F, Jia Y, Tian H, Ding Z (2021) The pre-mRNA splicing factor RDM16 regulates root stem cell maintenance in Arabidopsis. *J Integr Plant Biol* 63: 662-678

Mahrez W, Shin J, Munoz-Viana R, Figueiredo DD, Trejo-Arellano MS, Exner V, Siretskiy A, Grisse W, Kohler C, Hennig L (2016) BRR2a Affects Flowering Time via FLC Splicing. *PLoS Genet* 12: e1005924

Makarova OV, Makarov EM, Luhrmann R (2001) The 65 and 110 kDa SR-related proteins of the U4/U6.U5 tri-snRNP are essential for the assembly of mature spliceosomes. *EMBO J* 20: 2553-2563

Martin G, Marquez Y, Mantica F, Duque P, Irimia M (2021) Alternative splicing landscapes in Arabidopsis thaliana across tissues and stress conditions highlight major functional differences with animals. *Genome Biol* 22: 35

Neugebauer KM, Stolk JA, Roth MB (1995) A conserved epitope on a subset of SR proteins defines a larger family of Pre-mRNA splicing factors. *J Cell Biol* 129: 899-908

Nguyen THD, Galej WP, Bai XC, Oubridge C, Newman AJ, Scheres SHW, Nagai K (2016) Cryo-EM structure of the yeast U4/U6.U5 tri-snRNP at 3.7 Å resolution. *Nature* 530: 298-302

Nimeth BA, Riegler S, Kalyna M (2020) Alternative Splicing and DNA Damage Response in Plants. *Front Plant Sci* 11: 91

Nisa MU, Huang Y, Benhamed M, Raynaud C (2019) The Plant DNA Damage Response: Signaling Pathways Leading to Growth Inhibition and Putative Role in Response to Stress Conditions. *Front Plant Sci* 10: 653

Ogita N, Okushima Y, Tokizawa M, Yamamoto YY, Tanaka M, Seki M, Makita Y, Matsui M, Okamoto-Yoshiyama K, Sakamoto T *et al* (2018) Identifying the target genes of SUPPRESSOR OF GAMMA RESPONSE 1, a master transcription factor controlling DNA damage response in Arabidopsis. *Plant J* 94: 439-453

Perea-Resa C, Hernandez-Verdeja T, Lopez-Cobollo R, del Mar Castellano M, Salinas J (2012) LSM proteins provide accurate splicing and decay of selected transcripts to ensure normal Arabidopsis development. *Plant Cell* 24: 4930-4947

Roitinger E, Hofer M, Kocher T, Pichler P, Novatchkova M, Yang J, Schlogelhofer P, Mechtler K (2015) Quantitative phosphoproteomics of the ataxia telangiectasia-mutated (ATM) and ataxia telangiectasia-mutated and rad3-related (ATR) dependent DNA damage response in Arabidopsis thaliana. *Mol Cell Proteomics* 14: 556-571

Shimotohno A, Aki SS, Takahashi N, Umeda M (2021) Regulation of the Plant Cell Cycle in Response to Hormones and the Environment. *Annu Rev Plant Biol* 72: 273-296

Sjogren CA, Bolaris SC, Larsen PB (2015) Aluminum-Dependent Terminal Differentiation of the Arabidopsis Root Tip Is Mediated through an ATR-, ALT2-, and SOG1-Regulated Transcriptional Response. *Plant Cell* 27: 2501-2515

Stellberger T, Hauser R, Baiker A, Pothineni VR, Haas J, Uetz P (2010) Improving the yeast two-hybrid system with permuted fusions proteins: the Varicella Zoster Virus interactome. *Proteome Sci* 8: 8

Stevens SW, Abelson J (1999) Purification of the yeast U4/U6.U5 small nuclear ribonucleoprotein particle and identification of its proteins. *Proc Natl Acad Sci U S A* 96: 7226-7231

Takahashi N, Ogita N, Takahashi T, Taniguchi S, Tanaka M, Seki M, Umeda M (2019) A regulatory module controlling stress-induced cell cycle arrest in Arabidopsis. *Elife* 8

Tharun S (2009) Roles of eukaryotic Lsm proteins in the regulation of mRNA function. *Int Rev Cell Mol Biol* 272: 149-189

van Nues RW, Beggs JD (2001) Functional contacts with a range of splicing proteins suggest a central role for Brr2p in the dynamic control of the order of events in spliceosomes of *Saccharomyces cerevisiae*. *Genetics* 157: 1451-1467

Wan R, Bai R, Zhan X, Shi Y (2020) How Is Precursor Messenger RNA Spliced by the Spliceosome? *Annu Rev Biochem* 89: 333-358

Wan R, Yan C, Bai R, Wang L, Huang M, Wong CC, Shi Y (2016) The 3.8 Å structure of the U4/U6.U5 tri-snRNP: Insights into spliceosome assembly and catalysis. *Science* 351: 466-475

Wang L, Zhan L, Zhao Y, Huang Y, Wu C, Pan T, Qin Q, Xu Y, Deng Z, Li J *et al* (2021) The ATR-WEE1 kinase module inhibits the MAC complex to regulate replication stress response. *Nucleic Acids Res* 49: 1411-1425

Waterworth WM, Wilson M, Wang D, Nuhse T, Warward S, Selley J, West CE (2019) Phosphoproteomic analysis reveals plant DNA damage signalling pathways with a functional role for histone H2AX phosphorylation in plant growth under genotoxic stress. *Plant J* 100: 1007-1021

Wilkinson ME, Charenton C, Nagai K (2020) RNA Splicing by the Spliceosome. *Annu Rev Biochem* 89: 359-388

Will CL, Luhrmann R (2011) Spliceosome structure and function. *Cold Spring Harb Perspect Biol* 3

Yi D, Alvim Kamei CL, Cools T, Vanderauwera S, Takahashi N, Okushima Y, Eekhout T, Yoshiyama KO, Larkin J, Van den Daele H *et al* (2014) The Arabidopsis SIAMESE-RELATED cyclin-dependent kinase inhibitors SMR5 and SMR7 regulate the DNA damage checkpoint in response to reactive oxygen species. *Plant Cell* 26: 296-309

Yildirim A, Mozaffari-Jovin S, Wallisch AK, Schafer J, Ludwig SEJ, Urlaub H, Luhrmann R, Wolfrum U (2021) SANS (USH1G) regulates pre-mRNA splicing by mediating the intra-nuclear transfer of tri-snRNP complexes. *Nucleic Acids Res* 49: 5845-5866

Yoshiyama K, Conklin PA, Huefner ND, Britt AB (2009) Suppressor of gamma response 1 (SOG1) encodes a putative transcription factor governing multiple responses to DNA damage. *Proc Natl Acad Sci U S A* 106: 12843-12848

Yoshiyama KO, Sakaguchi K, Kimura S (2013) DNA damage response in plants: conserved and variable response compared to animals. *Biology (Basel)* 2: 1338-1356

## TABLE AND FIGURES LEGENDS

Table 1. Mass spectrometry results of MDF protein co-immunoprecipitating with LSM8-GFP. Results of the MS analyses showing the Score, coverage and sequence of the peptides that were identified for MDF in each of the three Co-IP experiments using LSM8-GFP as bait.

Figure 1. The short root phenotype of *mdf-1* and *mdf-2* is associated with cell cycle arrest at the G2/M transition. (A) Primary root length from 1 until 10 days after germination (dag) of WT (n=62, 137, 97, 74, 74, 75, 75, 74 and 75), *mdf-1* (n=48, 65, 69, 55, 53, 41, 50, 44 and 45), *mdf-2* (n=46, 57, 63, 51, 51, 51, 50, 52, 49 and 50) and *mdf-1::pMDFMDFg* (n=72, 160, 161, 166, 223, 68, 66, 63 and 148). Statistical significance was determined in comparison to WT and *mdf-1*. (B) Representative confocal images of propidium iodide-stained root tips of WT, *mdf-1*, *mdf-2* and *mdf-1::pMDFMDFg* 3 dag seedlings. Asterisk shows the quiescent center (QC). Arrowhead marks dead cells. White bar indicates the division zone. Scale bar: 50  $\mu$ m. (C) Number of dividing cells in the cortical layer of 3 dag seedlings of WT (n=40), *mdf-1* (n=36), *mdf-2* (n=21) and *mdf-1::pMDFMDFg* (n=24). Statistical significance was determined in comparison to WT. (D) Quantification of the cell death area of root tips of WT (n=21 and n=22), *mdf-1* (n=21 and n=95), *mdf-2* (n=33 and n=59) and *mdf-1::pMDFMDFg* (n=19 and n=25) lines at 2 and 3 dag. (E) Analyses of immunolabeled mitotic microtubular arrays in root tips of WT (n=348), *mdf-1* (n=269) and *mdf-2* (n=284) 6 dag seedlings. Percentual distribution of cells accumulated in G2/M with preprophase bands (G2/M - pre-prophase), pro, meta and anaphase spindle (mitosis) and with phragmoplast (cytokinesis) was determined. (F) Endoreduplication index determined from flow cytometry data measured in WT (n=7), *mdf-1* (n=3) and *mdf-2* (n=4) 10 dag seedlings. (G) Percentage of plants developing true leaves after 10 days for WT, *mdf-1* and *mdf-2*. Average of at least 4 independent experiments with at least 20 plants per line, condition, and experiment is represented. Average  $\pm$  Standard deviation is represented. \*P < 0.05; \*\*P < 0.005; \*\*\*P < 0.0005 as determined by a two-tailed Student's t-test.

Figure 2. MDF interacts with LSM8 and localises to nuclear speckles. (A) Representative confocal images of BiFC assays showing reconstitution of YFP fluorescence in the nucleus of epidermal cells of *Nicotiana benthamiana* leaves in which nYFP-MDF and cYFP-LSM8 as well as cYFP-MDF and nYFP-LSM8 are co-expressed. No fluorescence is seen upon co-expression of nYFP-MDF and cYFP-LSM1a or cYFP-MDF and nYFP-LSM1a. Upper panels show fluorescence images and lower panels show bright field images. Scale bar: 75  $\mu$ m. (B) Representative confocal images showing GFP (green) and mCherry (red)-derived fluorescence upon co-expression of MDF-GFP and LSM8-mCherry in *Nicotiana benthamiana* leaf epidermis cells. MDF localises to the nucleolus (arrow) and co-localizes with LSM8-mCherry in the nucleoplasm and nuclear speckles (arrowheads). Scale bar: 9,7  $\mu$ m. (C) Box graphs representing FLIM-FRET efficiencies (%) measured in *Nicotiana benthamiana* leaf epidermis cells expressing LSM8-GFP alone or in combination with LSM2-mCherry or MDF-GFP alone or together with LSM8-mCherry. FRET efficiency was significantly higher in samples co-expressing LSM8-GFP and LSM2-mCherry (\*P < 0.0001; two-tailed Student's t-test).

Figure 3. MDF is important for correct splicing of transcripts involved in transcriptional control and signalling. (A) Quantification of alternative splicing (AS) events (ES: Exon skipping, MXE: Mutually exclusive exon, A5'SS: Alternative 5' splice site, A'3SS: Alternative 3' splice site, IR: Intron retention) identified in *mdf-1* in respect to WT. (B) 20 most representative top significant Biological Process GO terms enriched in intron retained targets identified in *mdf-1*. Colouring indicates enriched Biological Processes found in targets showing IR in *mdf-1* and *lsm8-1* (yellow), *mdf-1* and *rdm16-4* (green) and *mdf-1* and *brr2a-2* (red). (C) Venn diagram representing the overlap between significantly increased IR targets between *mdf-1*, *lsm8-1*, *rdm16-4* and *brr2a-2*. (D-G) RT-qPCR analysis to confirm increased IR events found by RNA-seq in seedlings of WT, *mdf-1*, *mdf-2* and *mdf-1::pMDFMDFg* on genes involved in cell cycle (D), pre-mRNA splicing (E), transcription (F) and DNA repair (G). Captures from the IGV software corresponding to the read coverage tracks for *mdf-1* and WT are represented below each graph. Big boxes represent exons and small boxes represent introns. Intron retention events verified by RT-qPCR are highlighted in orange. Average  $\pm$  Standard deviation of at least two independent biological replicates is represented. \*P < 0.05; \*\*P < 0.005; \*\*\*P < 0.0005 in comparison to WT as determined by a two-tailed Student's t-test.

Figure 4. Loss of *MDF* function leads to altered expression of a large number of genes involved in stress response and cell cycle control. (A) Volcano plot representing the differentially expressed genes (DEGs) upregulated (in red) and downregulated (in green) in *mdf-1* compared to WT with p values < 0.05. Blue dots indicate genes that show no differential expression. (B) 20 most representative top significant Biological Process GO terms enriched in upregulated genes in *mdf-1* compared to WT. (C) 20 most representative top significant Biological Process GO terms enriched in downregulated genes in *mdf-1* compared to WT. (D) Venn diagram representing the overlap between intron retained and differentially expressed genes and its percentual distribution.

Figure 5. *MDF* loss of function alters the expression of genes involved in cell cycle control during DDR. (A) Quantification of the overlap between direct SOG1 targets and genes showing IR, or a  $|\text{Log}_2\text{Fold}|$  change value > 2 in *mdf-1* background. (B) Venn diagram representing the overlap between the 279 down-regulated genes in *mdf-1* associated with the GO biological process "cell cycle" and the 80 loci upregulated in *myb3r1,3,5* mutant background after DNA damage induction. (C-D) RT-qPCR analysis of transcriptional changes found by RNA-seq in seedlings of WT, *mdf-1*, *mdf-2* and *mdf-1::pMDFMDFg* on the transcription factors *ANAC085* and *ANAC044* (C) and mitosis-related genes (D). (E) *MDF* expression measured by RT-qPCR in seedlings of WT, *mdf-1*, *mdf-2* and *mdf-1::pMDFMDFg*. Average  $\pm$  Standard deviation of at least two independent biological replicates is shown. \*P < 0.05; \*\*P < 0.005; \*\*\*P < 0.0005 in comparison to WT as determined by a two-tailed Student's t-test.

Figure 6. Root growth arrest in *mdf-1* occurs independently of SOG1 and ATM. Primary root length of 3 dag seedlings of WT (n= 110), *mdf-1* (n= 57), *mdf-1sog1-7* (n= 45), *mdf-1atm-2* (n= 38), *sog1-7* (n= 74) and *atm-2* (n= 146) plants. Statistical significance was determined in comparison to WT. (B) Representative confocal images of PI-stained root tips of WT, *sog1-7*, *mdf-1* and *mdf-1sog1-7* in 3 dag seedlings. Arrowhead marks dead cells. Scale bar: 50  $\mu\text{m}$ . (C-D) Quantification of the cell death area of root tips and of the frequency of seedlings showing cell death in WT (n=21 and n=22), *mdf-1* (n=21



and n=95) and *mdf-1sog1-7* (n=32 and n=25) lines at 2 and 3 dag. Statistical significance was determined in comparison to *mdf-1*. Average  $\pm$  Standard deviation is represented. \*P < 0.05; \*\*P < 0.005; \*\*\*P < 0.0005 as determined by a two-tailed Student's t-test.

Figure 7. The phosphorylation state of MDF influences its function during cell division control and pre-mRNA splicing. (A) *MDF* expression by RT-qPCR in WT, *mdf-1*, *mdf-1::p35SMDF* and *mdf-1::p35SMDFS22A* 12 dag seedlings (n=3). Statistical significance was determined in comparison to WT. (B) Representative confocal images of PI-stained root tips of WT, *mdf-1*, *mdf-1::p35SMDF* and *mdf-1::p35SMDFS22A* 3 dag seedlings. Arrowhead marks dead cells. Arrow marks nuclei showing YFP associated fluorescence. White bar indicates the division zone. Scale bar: 50  $\mu$ m. (C) Primary root length of 3 dag seedlings of WT (n= 25), *mdf-1* (n= 15), *mdf-1::p35SMDF* (n=19) and *mdf-1::p35SMDFS22A* (n=17). Statistical significance was determined in comparison to WT and *mdf-1*. (D) Number of dividing cells in the cortical layer of 3dag seedlings of WT (n=40), *mdf-1* (n=36) *mdf-1::p35SMDF* (n=10) and *mdf-1::p35SMDFS22A* (n=10). Statistical significance was determined in comparison to WT and *mdf-1*. (E) Quantification of cell death area in 3 dag seedlings of WT (n=24), *mdf-1* (n=35) *mdf-1::p35SMDF* (n=29) and *mdf-1::p35SMDFS22A* (n=19). Statistical significance was determined in comparison to *mdf-1*. (F-G) RT-qPCR analysis to confirm increased IR and downregulation events found by RNA-seq in WT, *mdf-1*, *mdf-1::p35SMDF* and *mdf-1::p35SMDFS22A* in samples of 12 dag seedlings (n=2-3). Statistical significance was determined in comparison to WT. Average  $\pm$  Standard deviation is represented. \*P < 0.05; \*\*P < 0.005; \*\*\*P < 0.0005 as determined by a two-tailed Student's t-test.

Figure 8. Mutant lines for *MDF*, *LSM8* and *SR45* exhibit increased sensitivity to zeocin treatment. (A) Representative photograph of WT, *mdf-1*, *mdf-2*, *sr45-1* and *lsm8-1* seedlings at 18 dag. At 4dag seedlings were transferred to MS medium (-) and MS medium supplemented with 20 $\mu$ g/mL zeocin (+). (B) Quantification of relative primary root growth of seedlings of WT, *mdf-1*, *mdf-2*, *sr45-1* and *lsm8-1*. Root length was measured at 3 dag before transfer and at 2, 4 and 6 days after transfer (dat) to MS medium (C) or medium supplemented with 20 $\mu$ g/mL zeocin (Z). The panel shows ratio of root length from 2, 4 and 6 dat/3dag for each line measured in at least three independent experiments (a minimal of 20 plants per line, condition and experiment were measured). "a" represents no statistical difference between primary root length at 4 and 6 days after transfer according to a two-tailed Student's t-test. (C) Percentage of plants that developed true leaves at 10 dag grown on control conditions (Control) or on medium containing Zeocin 25  $\mu$ g/mL (Zeocin 25) or Zeocin 50  $\mu$ g/mL (Zeocin 50) for WT, *mdf-1*, *mdf-2*, *sr45-1* and *lsm8-1*. Panel shows results from at least three independent experiments (at least 20 plants per line, condition and experiment) \*P < 0.05; \*\*P < 0.005; \*\*\*P < 0.0005 as determined in comparison to WT by a two-tailed Student's t-test. (D) RT-qPCR analysis showing induction of DNA repair genes in 2 biological replicates of 6 dag seedlings of WT, *mdf-1*, *mdf-2*, *sr45-1* and *lsm8-1* grown at control conditions (C) and after transfer to 100  $\mu$ M zeocin containing medium for 2 hours (Z). \*P < 0.05 as determined in comparison to WT by One way ANOVA-test post hoc Tukey Kramer. (E) Quantification of cell death area in seedlings that were at 2 dag incubated for 24 hours in MS medium (C) or in medium containing 15  $\mu$ M zeocin (Z) for WT (n=38 and n=39), *mdf-1* (n=32 and n=35), *mdf-2* (n=31 and n=38), *sr45-1* (n=31 and n=30) and *lsm8-1* (n=32 and n=35). \*P < 0.05; \*\*P < 0.005; \*\*\*P <

0.0005 as determined in comparison to WT by a two-tailed Student's t-test. Average  $\pm$  Standard deviation is shown. (F) Representative confocal images of PI-stained root tips of 3 day seedlings of WT, *mdf-1*, *sr45-1* and *lsm8-1* grown on MS medium. Arrowhead marks dead cells. White bar indicates the division zone. Scale bar: 50  $\mu$ m.

Figure 9. Schematic representation of MDF's mode of action. Under control conditions, MDF is expressed in meristematic cells and promotes the correct splicing and expression of genes maintaining cell division and growth. In the absence of *MDF*, a transcriptional program is activated that leads to cell cycle arrest and promotes endoreplication, cell death and increased expression of stress genes. The same response is induced in WT upon DNA stress. How MDF activity might be modulated by stress response pathways still remains to be established as indicated by a dotted arrow

#### DatasetEV:

Table S1. List of primers used for the different experiments.

Table S2. List of differential IR events in *mdf-1* vs WT.

Table S3. List of differential ES events in *mdf-1* vs WT.

Table S4. List of differential A5'SS events in *mdf-1* vs WT.

Table S5. List of differential A3'SS events in *mdf-1* vs WT.

Table S6. List of differential MXE events in *mdf-1* vs WT.

Table S7. List of enriched Biological Process associated GO terms in increased IR genes in *mdf-1*.

Table S8. List of enriched Biological Process associated GO terms in commonly IR genes between *mdf-1* and *lsm8-1*.

Table S9. List of enriched Biological Process associated GO terms in commonly IR genes between *mdf-1* and *rdm16-4*.

Table S10. List of enriched Biological Process associated GO terms in commonly IR genes between *mdf-1* and *brr2a-2*.

Table S11. List of Differentially expressed genes in *mdf-1* vs WT.

Table S12. List of enriched Biological Process associated GO terms in DEG upregulated in *mdf-1*.

Table S13. List of enriched Biological Process associated GO terms in DEG downregulated in *mdf-1*.

Table S14. Overlap between DEG with  $|\text{Log2Fold}| > 2$  and targets with increased IR in *mdf-1* and SOG1 DNA damaged induced direct targets.

Table S15. Overlap between Cell cycle related genes in *mdf-1* and *myb3r1,3,5* mutants.

#### Appendix:

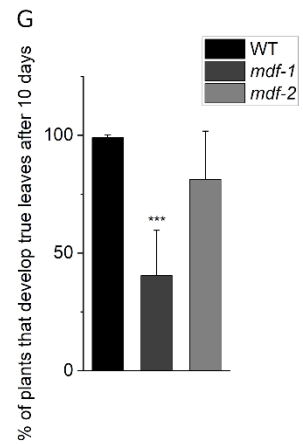
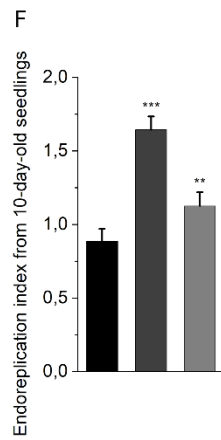
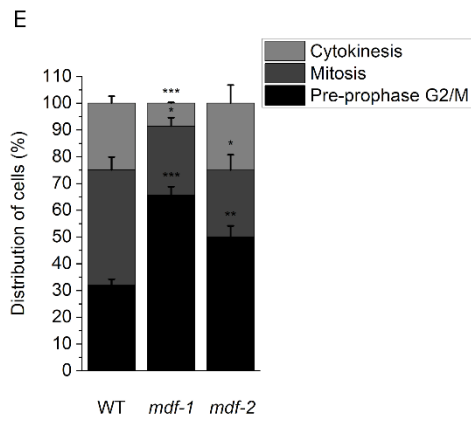
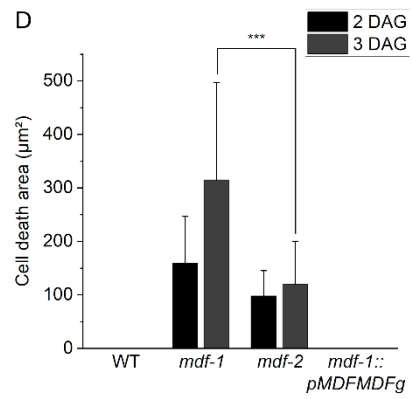
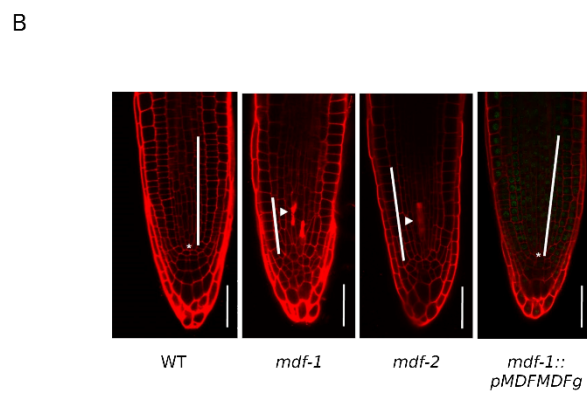
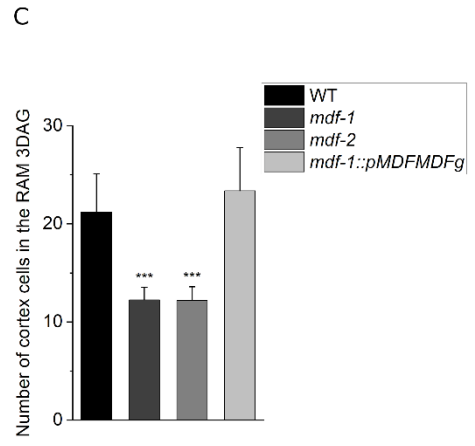
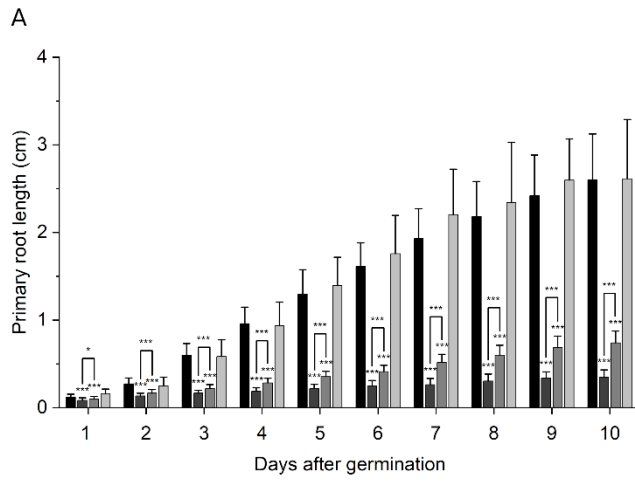
Figure S1. Analysis of *mdf-1* and *mdf-2* mutant seedlings. (A) Representative DNA content histograms determined by flow cytometry of WT (n=6), *mdf-1* (n=3) and *mdf-2* (n=3) 10 dag seedlings. (B) RT-qPCR analysis of *MDF* expression in 3 biological replicates of 3 dag root tips of WT, *mdf-1* and *mdf-2*. \*P < 0.05 as determined in comparison to WT by One way ANOVA-test post hoc Tukey Kramer. Average  $\pm$  Standard deviation is shown. (C) Schematic representation of *MDF* coding sequence. Big light green boxes represent exons and small dark green boxes represent introns. T-DNA insertion positions for *mdf-1* and *mdf-2* are represented by green arrowheads. Black arrowheads indicate approximate annealing positions of the primers used for testing *MDF* expression before and after the T-DNA insertion. The dashed line on the reverse primer for testing the expression after the T-DNA insertion shows that this primer only binds to exonic regions.

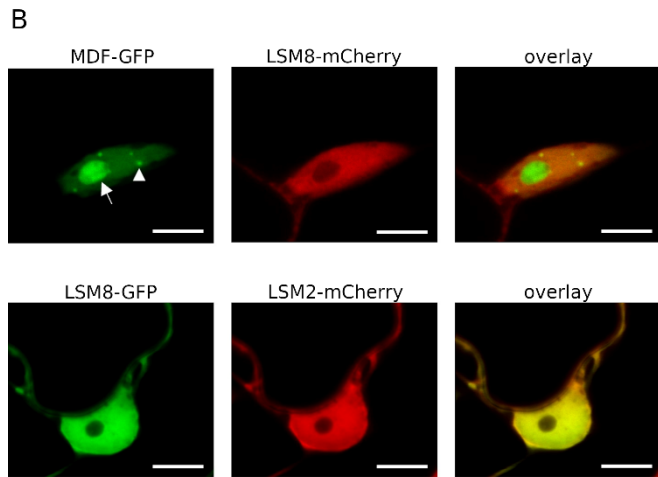
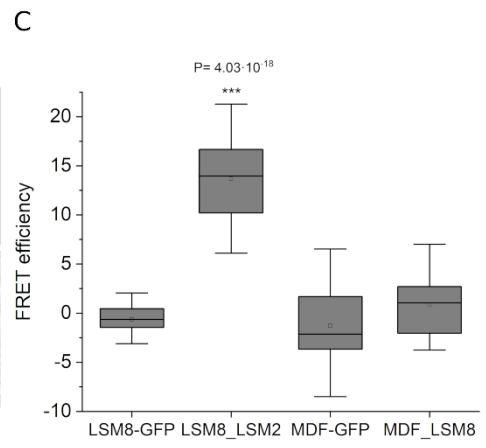
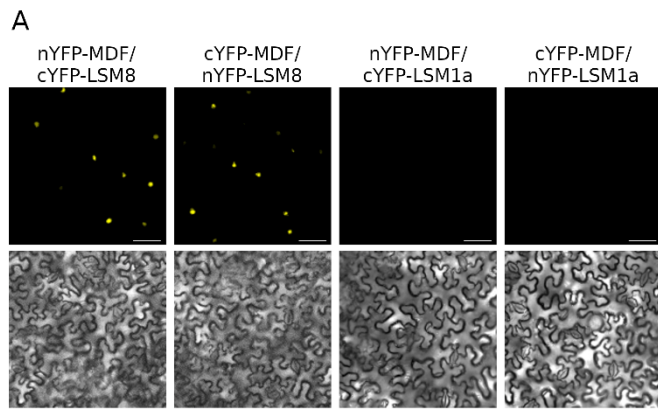
Figure S2. Yeast-two-hybrid (Y2H) assay confirming physical interaction between LSM8 and LSM2 but not between LSM8 and MDF. Growth of serial dilutions of yeast colonies was followed on medium without tryptophan and leucine (+HIS) and selective medium without tryptophan, leucine and histidine (-HIS) supplemented with 3-amino-1,2,4-triazole (3-AT). BD: DNA-binding domain; AD: activation domain; N: N-terminally tagged; C: C-terminally tagged. Interactions with BD and AD vectors containing Citrine were used as negative controls. Interaction between LSM8 and LSM2 was used as positive control. LSM8 shows autoactivation in the BD vector.

Figure S3. Quantification and percentual distribution of targets showing alternative splicing. (A) Number and percentage of AS events identified in *mdf-1* in respect to WT. Specific targets are defined as targets subject of one form of AS that do not contain other forms of AS. (ES: Exon skipping, MXE: Mutually exclusive exon, A5'SS: Alternative 5' splice site, A3'SS: Alternative 3' splice site, IR: Intron retention) (B) Venn diagram showing the overlap between differentially expressed genes and genes that show increased intron retention in *mdf-1* as compared to WT.

Table 1

<b>R1</b>	Accession	Description	Score	Coverage
	Q9LFE0	SART-1 family protein DOT2 OS=Arabidopsis thaliana GN=DOT2 PE=1 SV=1 - [DOT2_ARATH]	162,4486099	6,59
		A2	Sequence	Protein Group Accessions
		High	GLNEGGDNVDAASSGK	Q9LFE0
		High	IQGQTTHTFEDLNSSAK	Q9LFE0
		High	NSDTPSQSVQR	Q9LFE0
		High	EASALDLQNR	Q9LFE0
<b>R2</b>	Accession	Description	Score	Coverage
	Q9LFE0	SART-1 family protein DOT2 OS=Arabidopsis thaliana GN=DOT2 PE=1 SV=1 - [DOT2_ARATH]	198,5233817	7,93
		A2	Sequence	Protein Group Accessions
		High	GLNEGGDNVDAASSGK	Q9LFE0
		High	IFEEQDNLNQGENEDGEDGEHLGKVK	Q9LFE0
		High	NSDTPSQSVQR	Q9LFE0
		High	VVEGGAVILTLK	Q9LFE0
<b>R3</b>	Accession	Description	Score	Coverage
	Q9LFE0	SART-1 family protein DOT2 OS=Arabidopsis thaliana GN=DOT2 PE=1 SV=1 - [DOT2_ARATH]	210,6966728	12,2
		A2	Sequence	Protein Group Accessions
		High	GLNEGGDNVDAASSGK	Q9LFE0
		High	IFEEQDNLNQGENEDGEDGEHLGKVK	Q9LFE0
		High	NSDTPSQSVQR	Q9LFE0
		High	mLPQYDEAATDEGIFLDAK	Q9LFE0
		High	VVEGGAVILTLK	Q9LFE0
		High	KPESEDVFmEEDVAPK	Q9LFE0

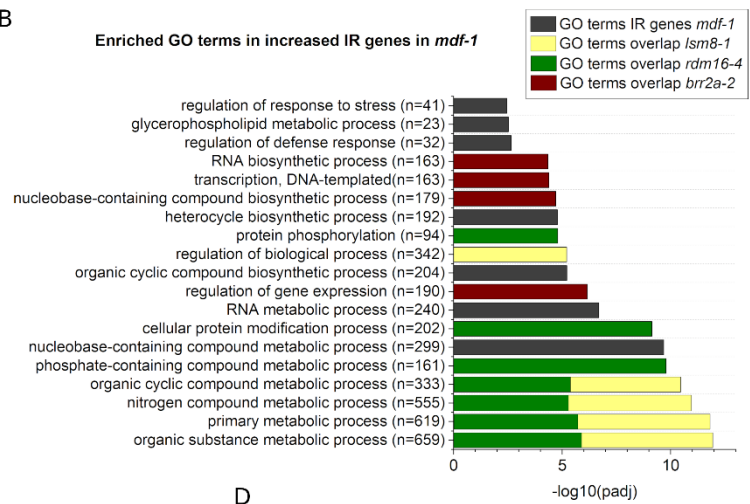




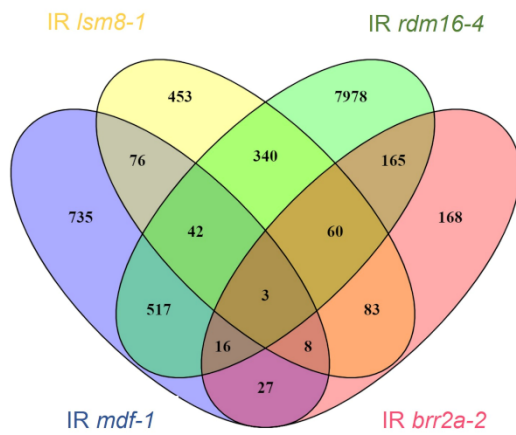
A

ES	379 (≈13%)
MXE	53 (≈2%)
A5'SS	296 (≈10%)
A3'SS	323 (≈11%)
IR	1894 (≈64%)
<b>Total AS events</b>	<b>2945</b>

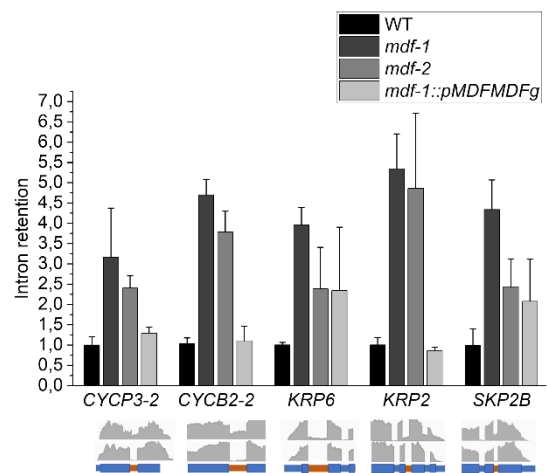
B



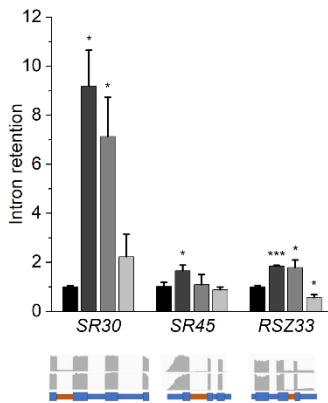
C



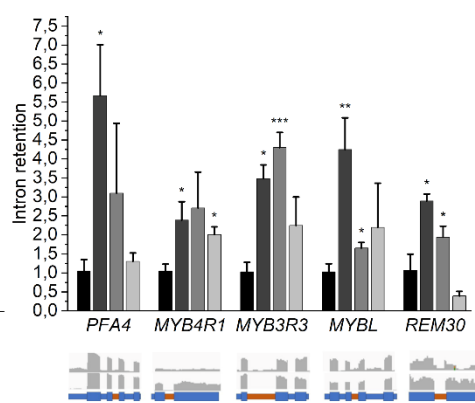
D



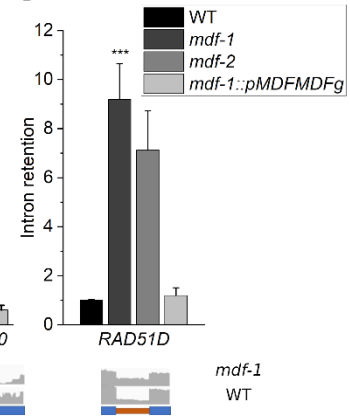
E

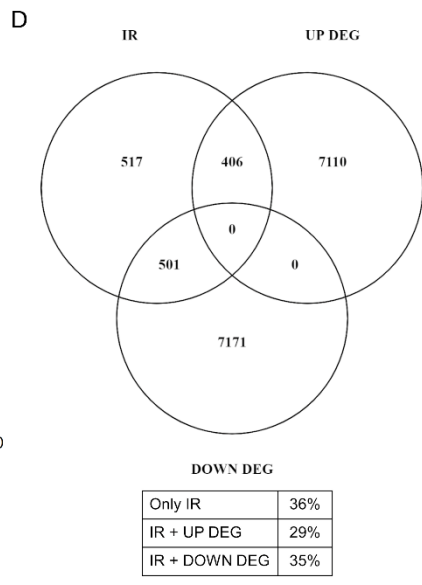
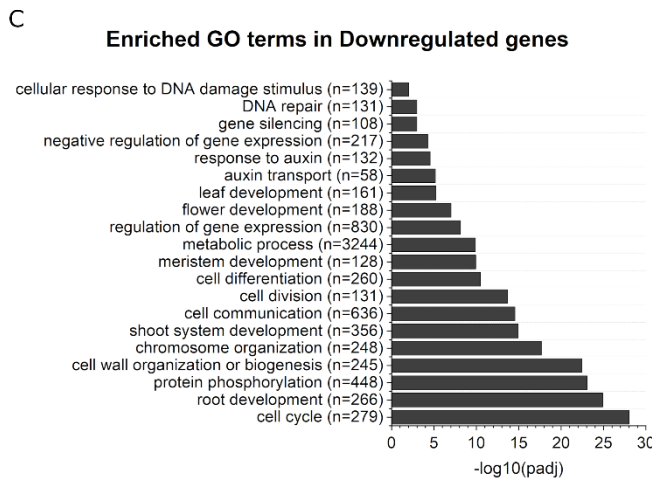
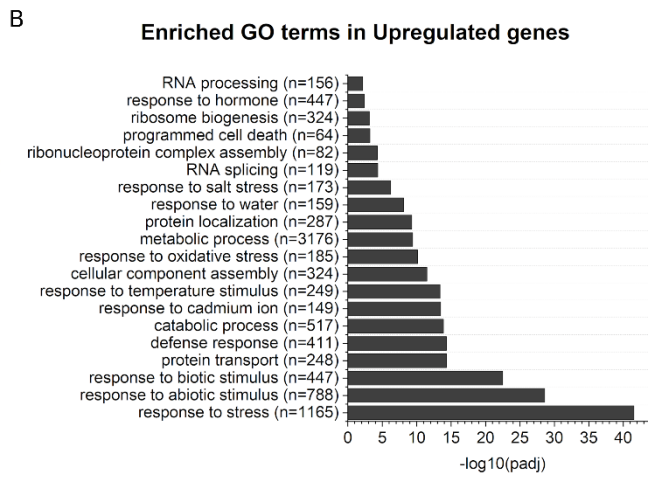
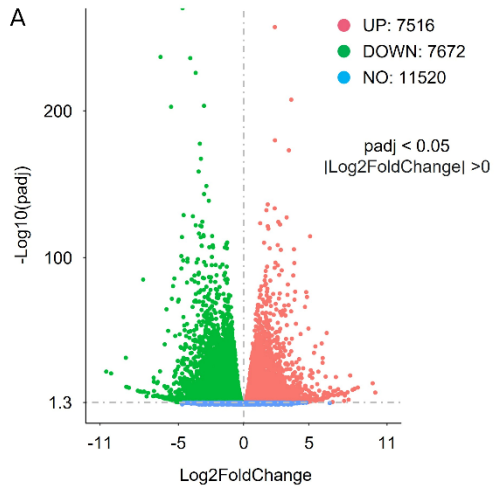


F



G



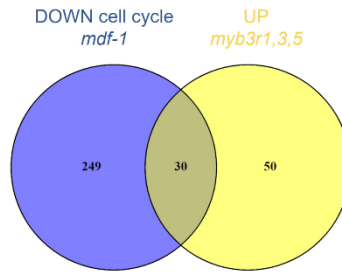




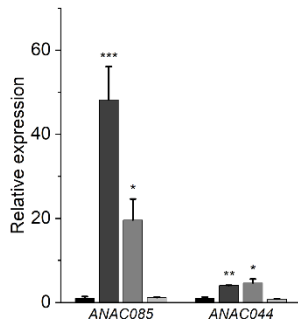
A

Total SOG1 targets	146
Total overlap with <i>mdf-1</i>	29 (=20%)
SOG1 targets UP DEG in <i>mdf-1</i>	17
SOG1 targets DOWN DEG in <i>mdf-1</i>	5
SOG1 targets IR in <i>mdf-1</i>	9

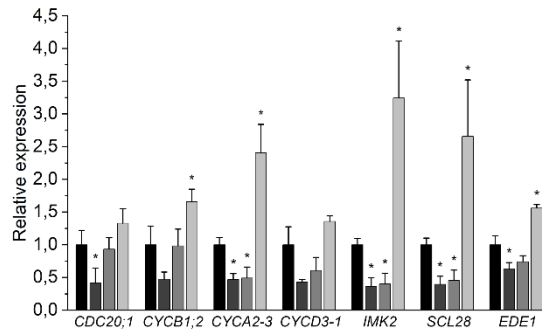
B



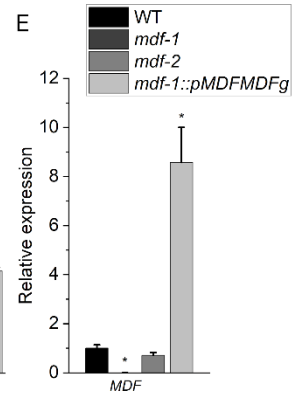
C



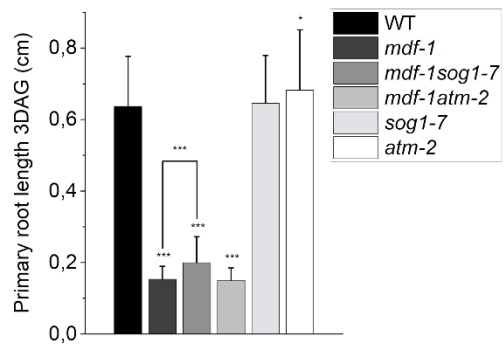
D



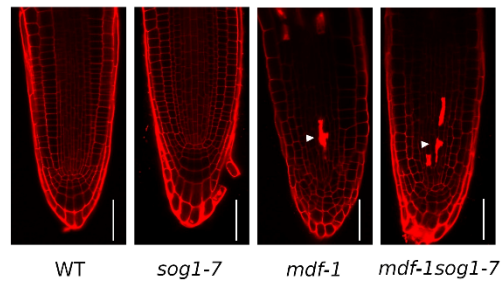
E



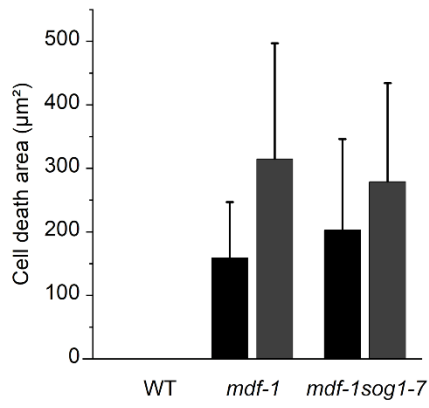
A



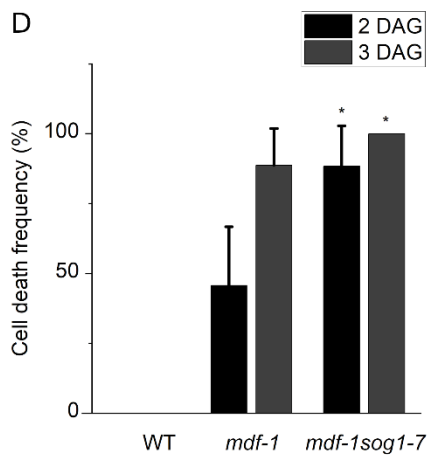
B

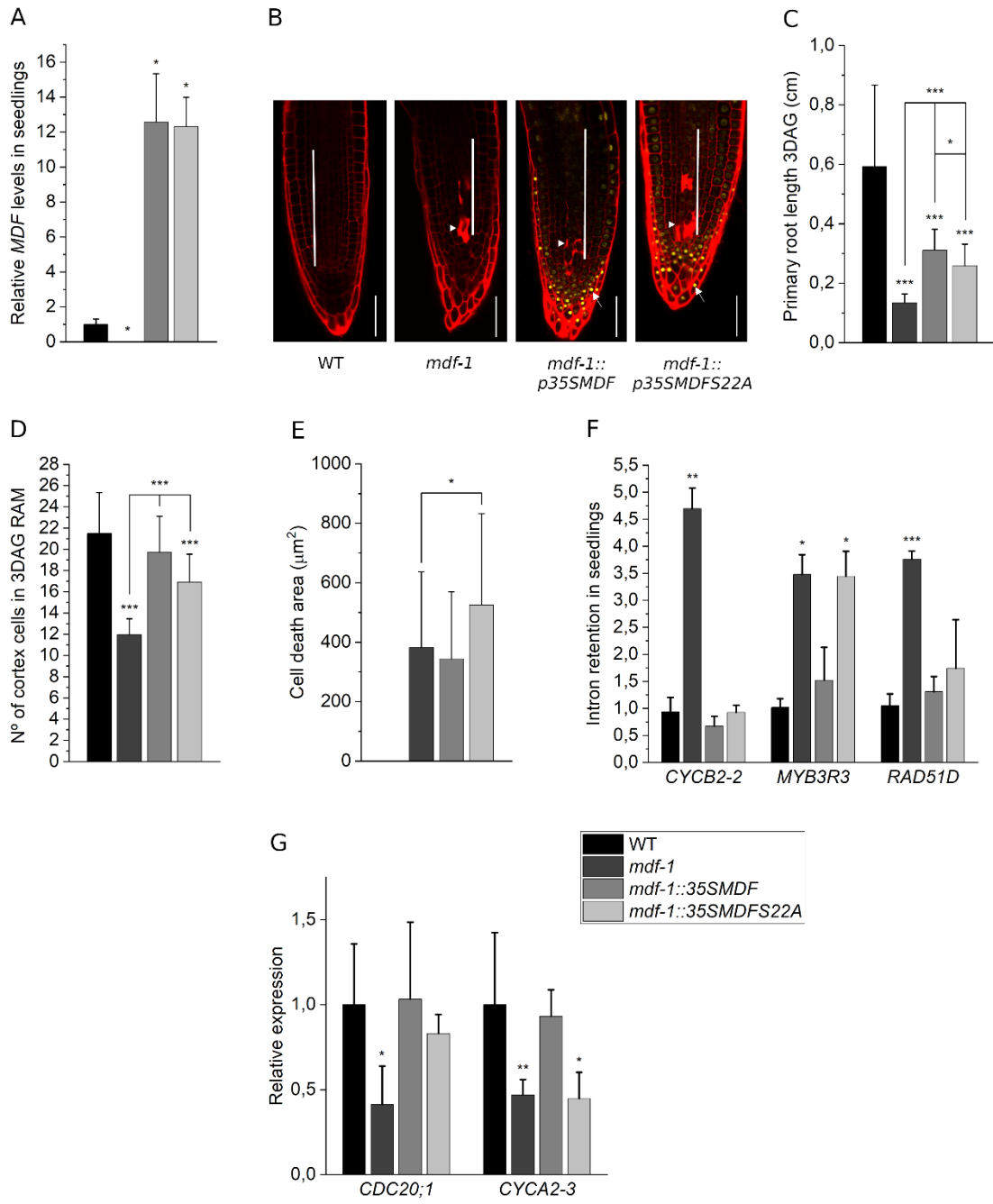


C

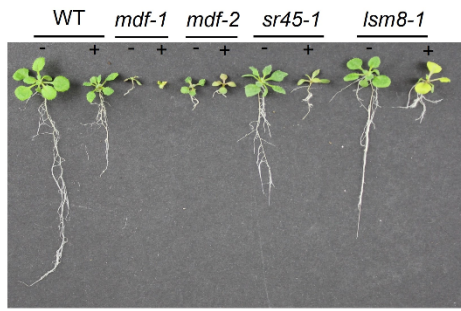


D

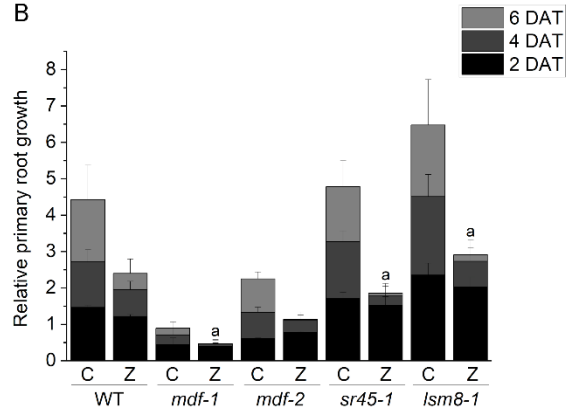




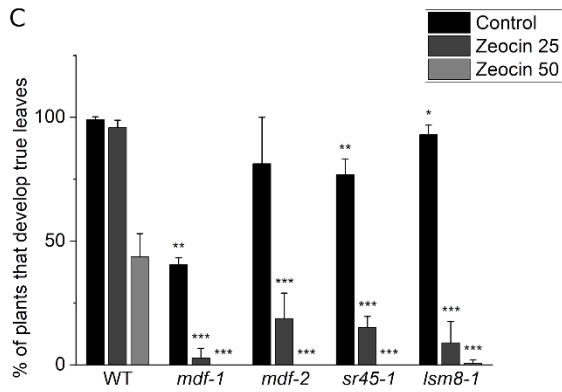
A



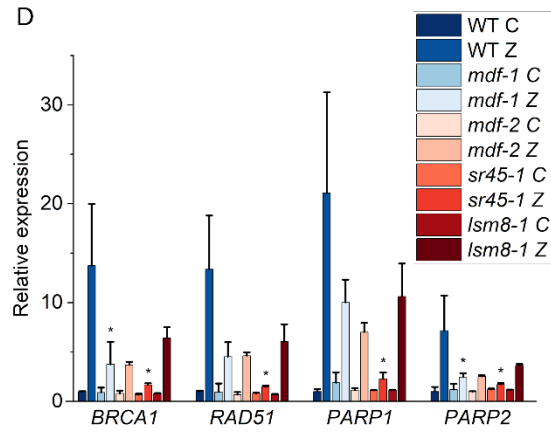
B



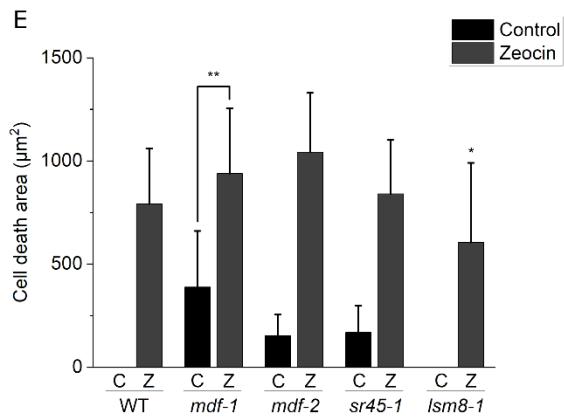
C



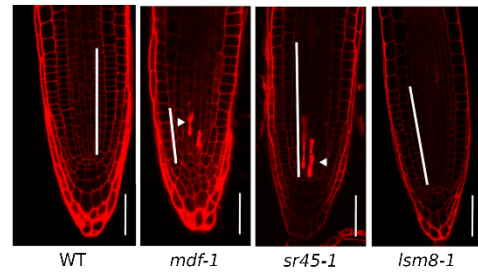
D

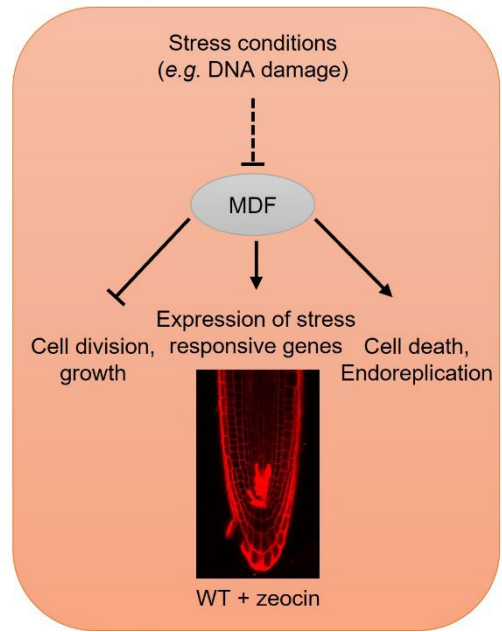
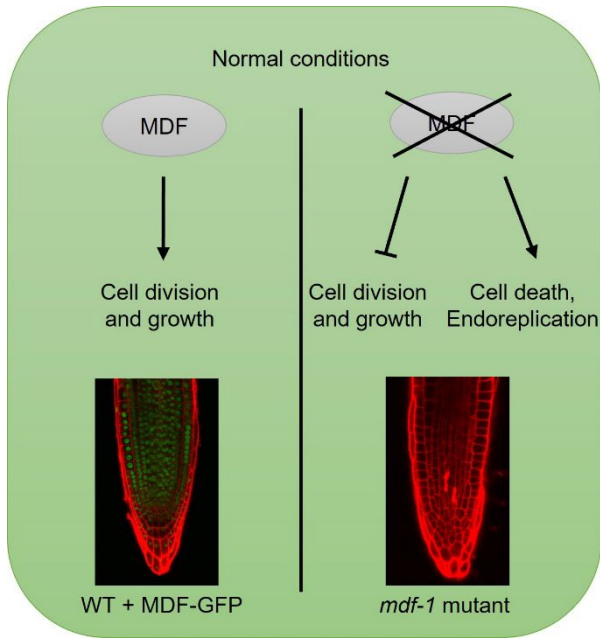


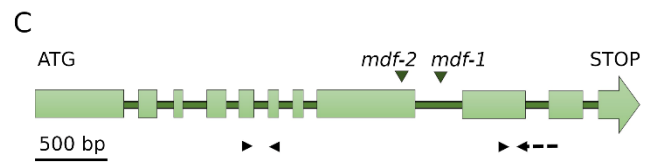
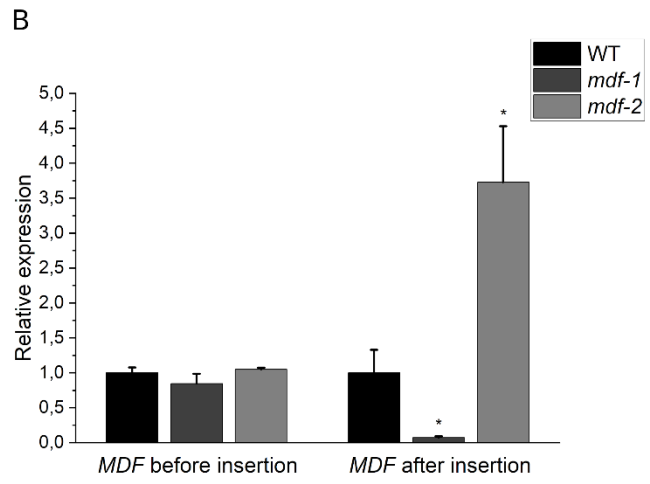
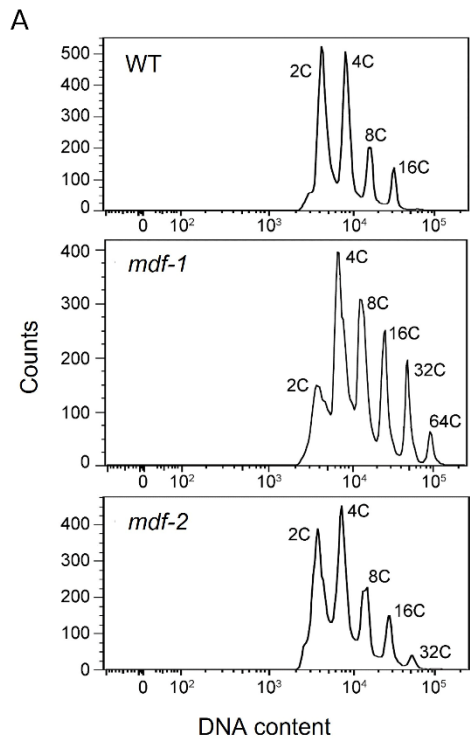
E

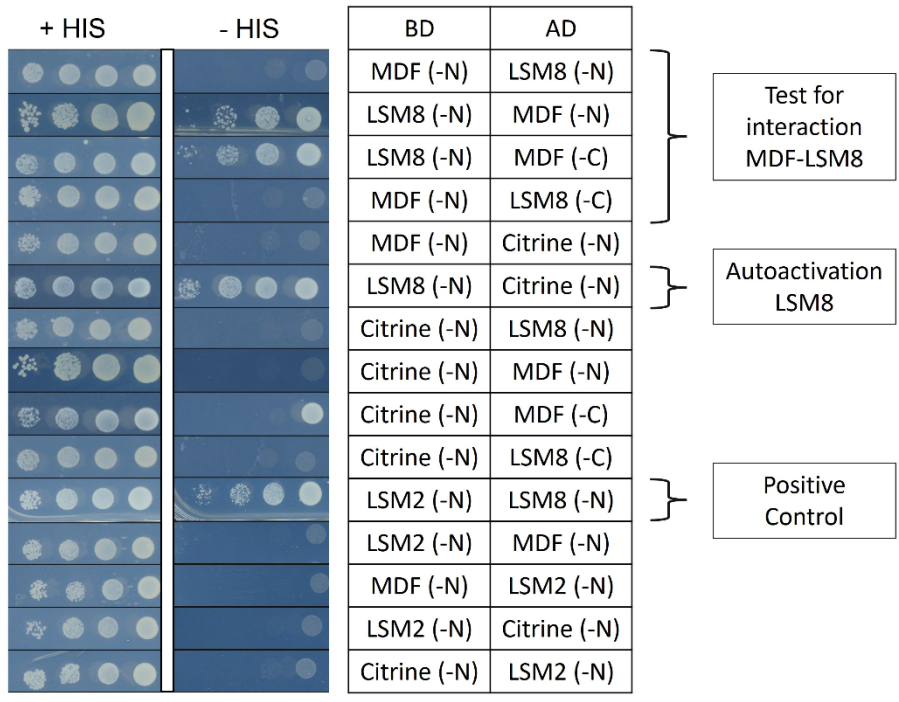


F





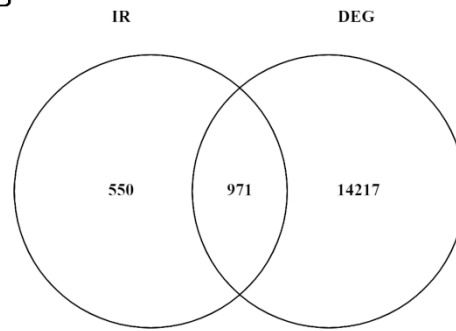




A


ES+MXE+A5SS+A3SS	801 ( $\approx 40\%$ )
Specific targets	516 ( $\approx 25\%$ )
IR	1521 ( $\approx 75\%$ )
Specific targets	1236 ( $\approx 61\%$ )
<b>Total targets</b>	<b>2037</b>

B





# PP7L is essential for MAIL1-mediated transposable element silencing and primary root growth

Cloe de Luxán-Hernández<sup>1</sup>, Julia Lohmann<sup>1</sup>, Wiebke Hellmeyer<sup>1</sup>, Senoch Seanpong<sup>1</sup>, Kerstin Wöltje<sup>1</sup>, Zoltan Magyar<sup>2</sup>, Aladár Pettkó-Szandtner<sup>2,3</sup>, Thierry Pélissier<sup>4</sup>, Geert De Jaeger<sup>5,6</sup>, Stefan Hoth<sup>1</sup>, Olivier Mathieu<sup>4</sup> and Magdalena Weingartner<sup>1,\*</sup> 

<sup>1</sup>Molecular Plant Physiology, Institute for Plant Science and Microbiology, Universität Hamburg, Hamburg 22609, Germany,

<sup>2</sup>Institute of Plant Biology, Biological Research Centre, Szeged 6726, Hungary,

<sup>3</sup>Laboratory of Proteomics Research, Biological Research Centre, Temesvári krt. 62, 6726 Szeged, Hungary,

<sup>4</sup>GReD – CNRS UMR6293 – Inserm U1103, Université Clermont Auvergne, UFR de Médecine, Clermont-Ferrand Cedex, France,

<sup>5</sup>VIB Center for Plant Systems Biology, 9052 Gent, Belgium, and

<sup>6</sup>Department of Plant Biotechnology and Bioinformatics, Ghent University, Technologiepark 71, 9052 Gent, Belgium

Received 21 March 2019; revised 22 November 2019; accepted 4 December 2019; published online 17 December 2019.

\*For correspondence (e-mail magdalena.weingartner@uni-hamburg.de).

## SUMMARY

The two paralogous *Arabidopsis* genes *MAINTENANCE OF MERISTEMS (MAIN)* and *MAINTENANCE OF MERISTEMS LIKE1 (MAIL1)* encode a conserved retrotransposon-related plant mobile domain and are known to be required for silencing of transposable elements (TE) and for primary root development. Loss of function of either *MAIN* or *MAIL1* leads to release of heterochromatic TEs, reduced condensation of pericentromeric heterochromatin, cell death of meristem cells and growth arrest of the primary root soon after germination. Here, we show that they act in one protein complex that also contains the inactive isoform of PROTEIN PHOSPHATASE 7 (PP7), which is named PROTEIN PHOSPHATASE 7-LIKE (PP7L). PP7L was previously shown to be important for chloroplast biogenesis and efficient chloroplast protein synthesis. We show that loss of *PP7L* function leads to the same root growth phenotype as loss of *MAIL1* or *MAIN*. In addition, *pp7l* mutants show similar silencing defects. Double mutant analyses confirmed that the three proteins act in the same molecular pathway. The primary root growth arrest, which is associated with cell death of stem cells and their daughter cells, is a consequence of genome instability. Our data demonstrate so far unrecognized functions of an inactive phosphatase isoform in a protein complex that is essential for silencing of heterochromatic elements and for maintenance of genome stability in dividing cells.

**Keywords:** *Arabidopsis thaliana*, meristems, root growth architecture, DNA repair and processing, transcriptional regulation.

## INTRODUCTION

Almost all cells of the plant body descend from small populations of self-renewing stem cells that are maintained within meristems. The stem cell niche of the root apical meristem (RAM) is located at the growing tip of the root and consists of a small group of rarely dividing quiescent centre (QC) cells, which are believed to act as organizers and as long-term reservoirs of stem cells (Heidstra and Sabatini, 2014). The cells directly adjacent to the QC are named root initials and maintain a stem cell-like character. They are able to renew themselves and to produce daughter cells, which undergo several rounds of rapid cell divisions until reaching the elongation zone, in which they gradually become differentiated (Wendrich *et al.*, 2017a).

During cell division, the status and integrity of the DNA is constantly monitored and detection of DNA damage leads to activation of the two conserved checkpoint kinases ATAXIATELANGICTASIA MUTATED (ATM) and ATM AND RAD3-RELATED (ATR), which are known to phosphorylate the transcription factor SUPPRESSOR OF GAMMA-RESPONSE 1 (SOG1) in plants (Sancar *et al.*, 2004; Yoshiyama *et al.*, 2013). Once being activated, SOG1 orchestrates the DNA damage response (DDR) involving delayed cell cycle progression by transcriptional induction of cell cycle inhibitors and activation of DNA repair by induction of DNA repair factors (Culligan *et al.*, 2006; Yoshiyama *et al.*, 2009; Yi *et al.*, 2014). In addition, SOG1 induces programmed cell death (PCD) specifically in root initials to prevent accumulation and propagation of

deleterious mutations (Furukawa *et al.*, 2010; Johnson *et al.*, 2018). New pools of stem cells are then replenished by activation of cell division in QC cells, which allows the formation of a new stem cell niche that sustains root growth (Heyman *et al.*, 2013; Hu *et al.*, 2016). Therefore, treatment of Arabidopsis seedlings with DNA damaging agents such as zeocin or bleomycin or with ionizing radiation leads to activation of DDR, resulting in a transient arrest of root growth and induction of cell death specifically in root initials and their immediate descendants (Fulcher and Sablowski, 2009; Furukawa *et al.*, 2010). In agreement, impaired root growth and spontaneous cell death in the RAM was also described for mutants with defects in DNA replication, DNA repair, or chromatin assembly. Examples are mutants lacking components of the mediator complex (Raya-Gonzalez *et al.*, 2018) or with disrupted function of the homologue of yeast *DNA Replication Helicase/Nuclease 2* (Jia *et al.*, 2016), as well as mutants with impaired function of histone chaperone complexes (Ma *et al.*, 2018) or with defects in structural components of the chromatin (Diaz *et al.*, 2019).

We have previously characterized the *MAINTENANCE OF MERISTEMS (MAIN)* gene family, which is defined by a conserved amino-transferase-like plant mobile domain (PMD) of unknown function (Uhlken *et al.*, 2014a). Two members of this gene family, namely *MAIN* and *MAIN-LIKE 1 (MAIL1)* are important for maintenance of genome stability in dividing cells of the RAM. Our published data showed that the single loss-of-function *main-2* and *mail1-1* mutants displayed very strong developmental defects, in particular a short-root phenotype due to growth arrest of the primary root soon after germination. This phenotype was associated with reduced cell division and precocious differentiation in the RAM, death of stem cells and their progenitor cells, and progressive loss of QC identity (Wenig *et al.*, 2013; Uhlken *et al.*, 2014b). Moreover, genome-wide expression analyses revealed that several TE-encoded loci that were mainly localized in pericentromeric heterochromatin were overexpressed in both mutants. Constitutive heterochromatin is in all eukaryotes highly condensed, transcriptionally inactive and enriched with different kinds of repeated sequences and TEs, while the gene-rich euchromatin is more relaxed and transcriptionally active (Fransz and de Jong, 2002). Condensation of heterochromatin is, in most plant cells, mediated by high levels of cytosine methylation and repressive histone modifications (Du *et al.*, 2015). In addition, silencing is ensured by factors that control proper chromatin condensation and thus act independently of DNA methylation (Moissiard *et al.*, 2012; Feng and Michaels, 2015; Wang *et al.*, 2017). The overexpressed loci in *main* and *mail1-1* exhibited no changes in the pattern of DNA methylation and histone modification (Uhlken *et al.*, 2014a,b; Ikeda *et al.*, 2017). This suggested that they may be involved in heterochromatin

silencing by influencing chromatin structure and function (Ikeda *et al.*, 2017).

Apart from *MAIN* and *MAIL1*, the *MAIN* gene family contains two additional members named *MAIN-LIKE2 (MAIL2)* and *MAIN-LIKE3 (MAIL3)*. Whereas *MAIN*, *MAIL1*, and *MAIL2* encode very similar proteins, *MAIL3* encodes a larger protein that contains an additional phosphatase domain. For that reason, *MAIL3* also groups with the plant-specific PP7-type family of serine/threonine phosphatases (Uhrig *et al.*, 2013). In Arabidopsis, the PP7-type subfamily has three members: the founding member PROTEIN PHOSPHATASE 7 (PP7), *MAIN-LIKE 3 (MAIL3)*, and an inactive isoform encoded by the At5g10900 locus, which is named PP7L (Uhrig *et al.*, 2013) (Xu *et al.*, 2019). The function of *MAIL3* is unknown and T-DNA insertion lines for *MAIL3* are indistinguishable from wild-type (Uhlken *et al.*, 2014b). PP7 was identified as an important modulator of light signalling by influencing the expression of nuclear-encoded sigma factors (SIG), which are important regulators of chloroplast gene expression (Moller *et al.*, 2003; Genoud *et al.*, 2008; Sun *et al.*, 2012). Recently, T-DNA insertion mutants for *PP7L* have been shown to exhibit impaired chloroplast development specifically during young seedling development. This was associated with impaired chloroplast ribosome accumulation and reduced protein synthesis in chloroplasts. However, the mechanism by which *PP7L* influences chloroplast translation is still unknown (Xu *et al.*, 2019). Here, we aimed at understanding the molecular mechanisms of *MAIN* and *MAIL1* action. We show that *MAIN* and *MAIL1* interact with each other and with *PP7L*. Loss-of-function alleles for *PP7L* displayed the same developmental defects as *mail1-1* and *main-2* mutants, including growth arrest of the primary root and cell death in the RAM. Moreover, *PP7L* mutant lines showed mis-expression of a subset of heterochromatic TE-encoded loci, which are also mis-expressed in *mail1-1* and *main-2*. Double mutant analyses confirmed that *MAIN*, *MAIL1* and *MIPP* acted in the same pathway and suggest that *MAIL3* might influence the silencing activity of this complex. In addition, we show evidence that the primary root growth defects in these mutants were caused by genome instability.

## RESULTS

### *MAIL1* interacts with *MAIN* and *PP7L*

To gain insight into molecular functions of *MAIN* family proteins, we searched for proteins interacting with *MAIL1*. To this aim, co-immunoprecipitation (Co-IP) experiments were performed using *mail1-1* mutant seedlings expressing a *MAIL1-green fluorescent protein (GFP)* fusion from the endogenous *MAIL1* promoter (*mail1-1/pMAIL1::MAIL1-GFP*), which fully complemented the

mutant phenotype (Uhlken *et al.*, 2014b). MAIL1-GFP and putative interaction partners were identified by immunoprecipitation followed by tandem mass spectrometry (IP-MS/MS). In parallel, two control Co-IP experiments using a line expressing GFP (*p35S::GFP*) were performed. MAIN and PROTEIN PHOSPHATASE 7-LIKE (PP7-L), which is encoded by the *At5g10900* gene, were among the proteins that specifically and most abundantly co-purified with MAIL1-GFP in each of the three experiments (Table S1). We performed reverse Co-IP experiments to confirm these co-purifications using seedlings expressing PP7L-GFP from its native promoter as bait. Indeed, peptides for MAIN and MAIL1 were most abundantly identified in the co-immunoprecipitates of PP7L-GFP in the three independent experiments (Table S1). Therefore, MAIN, MAIL1, and PP7L belong to the same protein complex in plant cells. Yeast-two-hybrid (Y2H) experiments were performed to further address the physical interaction of MAIL1 with MAIN and of MAIL1 with PP7L. A full-length construct of MAIL1 showed strong interaction with PP7L and weaker interaction with MAIN (Figure 1a). In contrast, a truncated version of MAIL1, in which the non-conserved C-terminal domain was deleted (MAIL1 $\Delta$ C), did not interact with PP7L showing that the conserved PMD domain of MAIL1 was not sufficient for this interaction (Figure 1a,b). To confirm the observed interactions *in planta*, we performed bimolecular fluorescence complementation (BiFC) experiments using the pBiFCt-2in1 vector system in Arabidopsis leaf protoplasts (Grefen and Blatt, 2012). Constructs harbouring full-length open reading frames of *MAIL1* and *MAIN*, *MAIL1* and *PP7L*, or *MAIN* and *PP7L*, which were fused at the N-terminus to each half of the *yellow fluorescent protein (YFP)* resulted in a bright YFP-derived fluorescence signal, which was mainly seen in the nucleus (Figure 1c). No fluorescence was detected in control experiments, in which PP7L fused to the C-terminal half of YFP and no protein fused to the N-terminal half of YFP was expressed (Figure 1c). We have previously shown that GFP fusion proteins of MAIL1 or MAIN were exclusively localized to the nucleus (Wenig *et al.*, 2013; Uhlken *et al.*, 2014a,b). In contrast, the PP7L-GFP fusion protein was reported to be localized to the nucleus and to the cytoplasm (Xu *et al.*, 2019). We therefore analyzed the co-localization of PP7L-GFP and MAIL1-mCherry in tobacco leaf epidermis cells, in which both constructs were simultaneously expressed from estradiol-inducible promoters. We found that the MAIL1-GFP signal was confined to the nucleus while PP7L-mCherry derived fluorescence accumulated in both the nucleus and the cytoplasm (Figure 1d). Taken together, these results showed that MAIL1 physically interacted with MAIN and with PP7L, and that this complex localized to the nucleus, while PP7L by itself accumulated also in the cytoplasm.

### Loss-of-function mutants for PP7L phenocopy *mail1-1* mutants

To test the biological significance of the interaction between MAIL1 and PP7L, we obtained T-DNA insertion lines for *PP7L* from the SALK collection (Alonso *et al.*, 2003), which were previously characterized and named *pp7l-1* and *pp7l-3* (Xu *et al.*, 2019). Our phenotypic analysis of seedlings revealed that homozygous *pp7l-1* and *pp7l-3* mutants displayed the similar primary root growth defect as the *mail1-1* and *main-2* mutant (Figure 2a). By measuring root length of seedlings growing for 15 days on vertical agar plates, we found that growth arrest of the primary root occurred in *mail1-1*, *pp7l-1* and *pp7l-3* at 3 days after germination (dag), while in *main-2* the primary root continued to grow, although much slower than the wild-type primary root (Figure 2b). Confocal microscopy of propidium iodide (PI)-stained root tips of seedlings at 3 dag revealed that the impaired growth of the primary root was associated with a reduced size of the cell division zone and early onset of cell differentiation (Figure 2c). Furthermore, PI staining that specifically marks dead cells due to impaired membrane integrity demonstrated that each of these mutant lines exhibited cell death of stem cells and their descendants. At 3 dag, seedlings of *mail1-1*, *pp7l-1* and *pp7l-3* were indistinguishable from each other and displayed numerous dead cells in the cell division zone and a disorganized cellular pattern of the RAM. In contrast, in the *main-2* mutant, the cellular organization of the RAM was maintained and only in about 50% of the seedlings ( $n = 40$ ) individual dead cells were observed (Figure 2c). It was previously shown that embryo development was unaltered in the *mail1-1* mutant and that the defects in the RAM occurred only after onset of germination (Uhlken *et al.*, 2014b). We therefore examined embryo development of *pp7l-1* and *pp7l-3* mutants and found no difference from wild-type at any stage of development (Figure S1a,b). Moreover, the cellular pattern of the RAM was indistinguishable from wild-type in mature seeds of both *pp7l-1* and *pp7l-3* mutant lines (Figure S1c). In a next step, we analyzed root tips of germinating seeds and found that during the process of radicle emergence (growth stage 0.50; Boyes *et al.*, 2001) numerous dead cells accumulated in the cell division zone of the RAM in the *pp7l-1*, *pp7l-3*, and *mail1-1* mutants. In contrast, in the *main-2* mutant most of the germinating seeds examined resembled wild-type and only in 12% of all roots ( $n = 35$ ) dead cells were detected (Figure 2d). These analyses demonstrated that *pp7l-1* and *pp7l-3* showed the identical root growth defects as *mail1-1* whereas, in *main-2*, the same defects also occurred, but at a later developmental stage. Despite the growth arrest of the primary root, *pp7l-1* and *pp7l-3* mutant lines were able to sustain shoot growth by forming anchor roots, which seemed to take over the function of

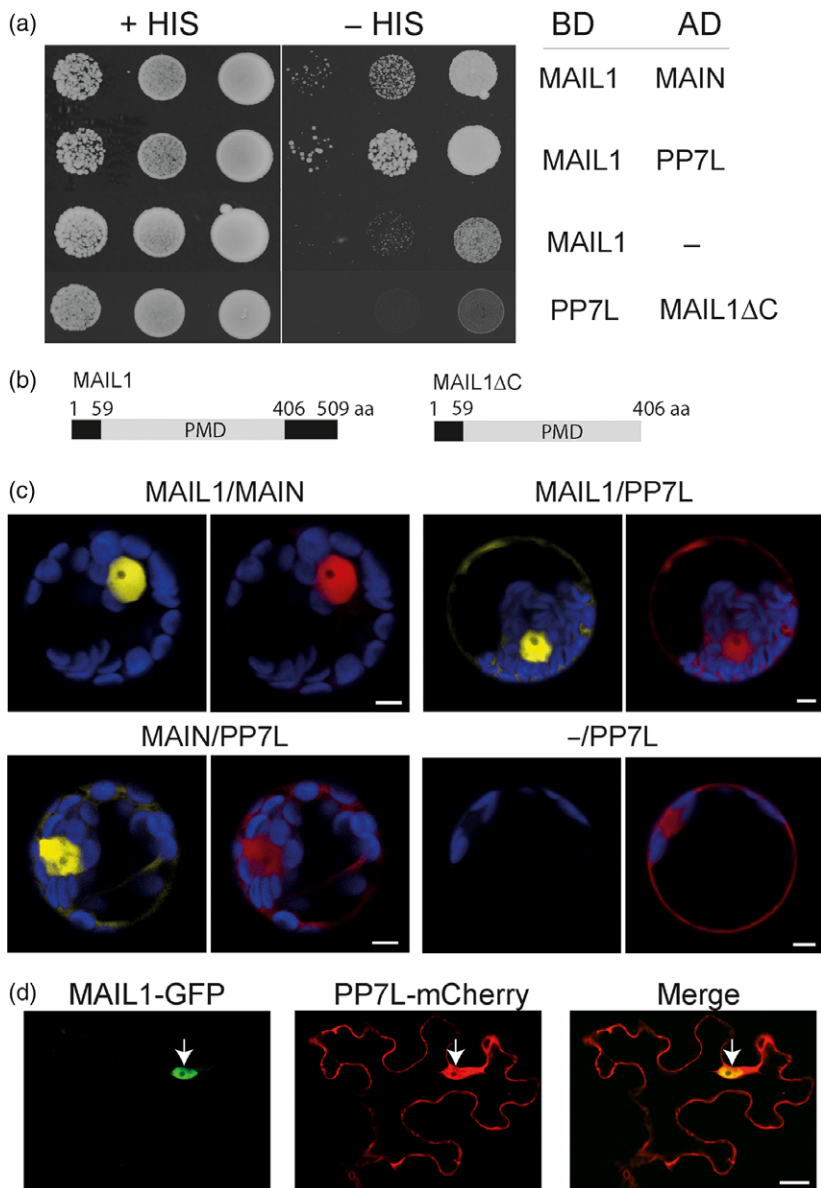


**Figure 1.** MAIL1 interacts with PP7L and with MAIN. (a) Yeast-two-hybrid (Y2H) assay showing the interaction of MAIL1 with PP7L and with MAIN. Growth of serial dilutions of yeast colonies was verified on medium without tryptophan and leucine (+HIS) and selective medium without tryptophan, leucine and histidine (-HIS) supplemented with 3-amino-1,2,4-triazole (3-AT). BD, DNA-binding domain; AD, activation domain. An empty AD-containing vector was used as the control.

(b) Structure of the MAIL1 full-length protein and the truncated version of MAIL1 (MAIL1ΔC) with the plant mobile domain (PMD) highlighted in grey.

(c) BiFC assays showing that Arabidopsis leaf protoplasts transfected with pBiFCt-2in1-NN (MAIL1/MAIN), pBiFCt-2in1-NN (MAIL1/PP7L) or pBiFCt-2in1-NN (MAIN/PP7L) showed a yellow fluorescent protein (YFP)-derived fluorescence signal in the nucleus (arrows). Protoplasts transfected with a control construct (pBiFCt-2in1-NN (-/PP7L)) showed no YFP-derived fluorescence. Red: red fluorescent protein (RFP)-derived fluorescence as a control for successful transfection. Blue: autofluorescence of chloroplasts. Yellow: YFP-derived fluorescence. Scale bars, 5 μm.

(d) Representative confocal images of *Nicotiana benthamiana* epidermis cells co-expressing MAIL1-green fluorescent protein (GFP) and PP7L-mCherry showing that MAIL1-GFP-derived fluorescence (green) is confined to the nucleus and PP7L-mCherry-derived fluorescence (red) is seen in the nucleus and in the cytoplasm. Arrows point to the nucleus. Scale bar, 25 μm.

the primary root, as previously described for *mail1-1* (Uhlken *et al.*, 2014b). Both *pp7l* mutant lines formed rosettes of smaller size than wild-type and were delayed in development (Figure S2a) (Xu *et al.*, 2019). They produced the same number of rosette leaves before onset of flowering as wild-type, and during shoot and flower formation no phenotypic alterations were detected (Figure S2b,c). We assessed the tissue-specific *PP7L* expression pattern in wild-type plants and found that *PP7L* was ubiquitously expressed in all tissues tested including roots (Figure S2d). In conclusion, these analyses showed that *PP7L* was, like *MAIN* and *MAIL1*, essential for primary root growth during post-germination development in addition to its previously established function during chloroplast development in leaves (Xu *et al.*, 2019).

### PP7L is involved in silencing of TEs

Previously, RNA-sequencing (RNA-seq) analyses revealed that loss of *MAIL1* or *MAIN* induced release of silencing of numerous TEs belonging to both DNA transposon and retrotransposon classes. In addition, the expression of several protein-coding genes known to be epigenetically regulated was increased (Ikeda *et al.*, 2017). To test if *PP7L* was also involved in silencing of TEs, we selected six of those loci including two CACTA-like transposase family genes (*At1g36680* and *At5g33395*), the Mutator-like transposable element MULE gene *At2g15810*, the protein-coding gene *AT3g29639*, which was shown to be epigenetically regulated (Kurihara *et al.*, 2008), the DNA/HARBINGER transposon encoded gene *At4g04293* (*ATIS112A*) and the Gypsy



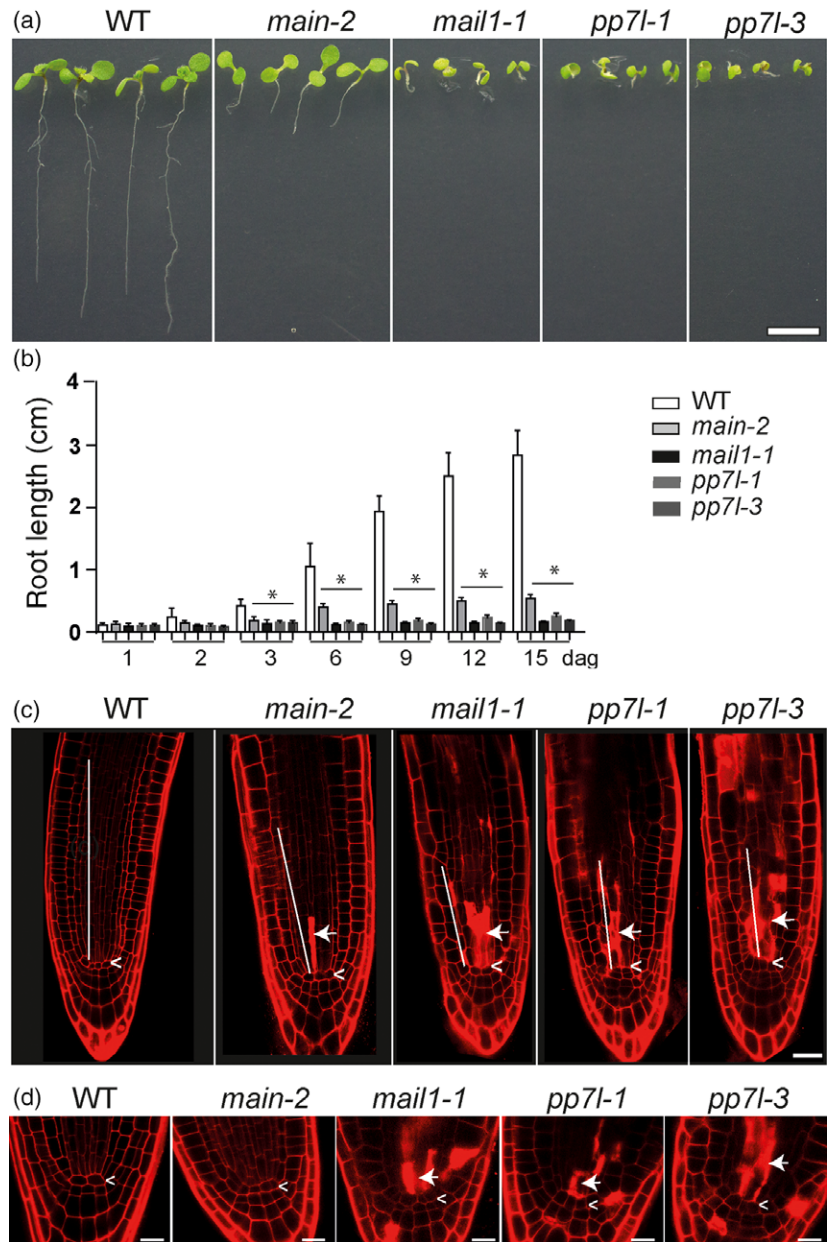
**Figure 2.** *pp7l-1* and *pp7l-3* showed similar developmental defects as *mail1-1* and *main-2*.

(a) Representative images of wild-type, *main-2*, *mail1-1*, *pp7l-1*, and *pp7l-3* seedlings at 8 days after germination (dag). Scale bar, 0.7 cm.

(b) Wild-type and mutant seedlings were grown on vertical plates and root lengths were measured at indicated days after germination (dag). The mean of the root length of three independent experiments is shown. Graphs represent mean  $\pm$  SE ( $n = 80-100$ ). Asterisk indicate significant difference to wild-type ( $P < 0.05$ ).

(c) Confocal images of propidium iodide (PI)-stained root tips of wild-type, *mail1-1*, *main-2*, *pp7l-1* and *pp7l-3* at 3 dag showing reduced size of the meristematic zone of the root apical meristem (RAM) (indicated by a white line) and accumulation of dead cells proximal to the quiescent centre (QC) in *mail1-1*, *main-2*, *pp7l-1*, and *pp7l-3* mutants. Arrows point to intensely stained, dead cells; arrowheads mark the position of the QC. Scale bar, 25  $\mu$ m.

(d) Confocal images of PI-stained root tips of germinating seeds (24–48 h in light) of the indicated genotypes showing accumulation of dead cells around the QC (marked by arrowhead) in *mail1-1*, *pp7l-1* and *pp7l-3* but not in wild-type or *main-2*. Arrows point to intensely stained, dead cells. Scale bars, 12.5  $\mu$ m.



LTR-retrotransposon encoded locus *ATHILA* (*At3TE58495*). In the following, we tested by RT-qPCR whether these loci were also mis-expressed in *pp7l-1* and *pp7l-3*. Indeed, each of the six loci was significantly increased compared with wild-type in seedlings of *pp7l-1* and *pp7l-3* and they were expressed at similar levels when compared with *mail1-1* and *main-2* (Figure 3a). To ensure that the release of silencing was due to loss of *PP7L* function we analyzed the expression of these loci in a complementation line for *pp7l-1* (*pp7l-1C*). In this line, a construct carrying the genomic sequence of *PP7L* fused at the C-terminus to GFP was expressed under its native promoter on the *pp7l-1* mutant background. In *pp7l-1C*, the expression of each of the

tested loci was reduced to wild-type levels (Figure 3a). We also confirmed that the primary root was fully restored in seedlings of *pp7l-1C* grown on Murashige and Skoog plates (Figure 3b). Confocal imaging of root tips revealed that there was no cell death in the division zone of the RAM of *pp7l-1C* seedlings and a *PP7L*-GFP-derived signal was observed in all cells of the root tip (Figure 3c). To further confirm that *PP7L* was involved in TE silencing, we analyzed the recently published RNA-seq dataset for *pp7l-1* (Xu *et al.*, 2019) for TE expression and found that 11 TE-encoded loci were among the significantly increased transcripts. Notably, 10 of these loci were among the transcripts that were also found as upregulated in the

published RNA-seq datasets for *mail1-1* and *main-2* (Ikeda *et al.*, 2017) (Figure 3d and Table S2). It should be noted that two of the loci that showed significant increase in both *pp7l-1* and *pp7l-3* in our RT-qPCR experiments, namely At1g6680 and At3TE58495, were not detected as significantly upregulated in the *pp7l-1* RNA-seq data. This difference might be explained by the different growth conditions or age of the sampled seedlings: for the *pp7l-1* RNA-seq analysis 4-day-old seedlings were used, whereas we used samples of 6-day-old seedlings. Taken together, these data demonstrated that loss of *PP7L* function caused not only the same root growth phenotype as loss of *MAIL1* or *MAIN*, but that *PP7L* was also important for the silencing of TE-encoded transcripts that were commonly controlled by *MAIN* and *MAIL1*.

#### **MAIL1, MAIN, and PP7L function in the same molecular pathway**

To confirm that *PP7L* acted in the same pathway as *MAIL1* and *MAIN*, we generated *pp7l-1 mail1-1* and *pp7l-1 main-2* double mutants. We found that seedlings of both double mutant combinations showed growth arrest of the primary root and were phenotypically indistinguishable from the respective single mutant parents (Figure 4a). This indicated that *MAIL1*, *MAIN*, and *PP7L* function in the same pathway to support root growth. In a next step, we examined the expression levels of the six selected TE loci in both double mutant combinations and compared these to the respective single mutant parents (Figure 4b). We found no significant increase in the expression level of none of the tested loci in both double mutant lines compared with the single mutant parents, indicating that there was no additive effect on the strength of silencing release in the double mutant lines. However, we found that four loci were even significantly lower expressed in the *pp7l-1 main-2* double mutant compared with *pp7l-1*, and one of these was also reduced in the *pp7l-1 mail1-1* double mutant (Figure 4b). This might be explained by alternative silencing pathways, which try to compensate for loss of *MAIN/MAIL1/PP7L* activity and which might be more effective in the absence of two components of the complex. We have previously shown that the release of silencing in the *mail1-1* and *main-2* mutant was associated with impaired heterochromatin condensation (Ikeda *et al.*, 2017). By measuring chromocentre area in DAPI-stained nuclei we found a similar expansion of chromocentres in *pp7l-1* as we previously found for *mail1-1* (Ikeda *et al.*, 2017) and this was unchanged in the *pp7l-1 mail1-1* double mutant (Figure S3). Together, our results showed that the tested double mutant combinations had no general additive effect on silencing release and heterochromatin condensation, suggesting that *PP7L*, *MAIL1*, and *MAIN* acted in the same silencing pathway.

#### **MAIL3 does not affect the root growth phenotype, but seems to influence PP7L-mediated TE silencing**

The *MAIL3* protein represents a long isoform of *PP7*. It contains a PMD domain sharing 34% identity with the PMD domain of *MAIL1* and a *PP7*-like phosphatase domain sharing 39% identity with the phosphatase domain of *PP7L* (Figure 5a). In a complex with *MAIL1* and/or *MAIN* proteins, *PP7L* may therefore form a protein similar to *MAIL3*. In contrast with *MAIL3*, however, *PP7L* is missing essential amino acids within its catalytic domain (Figure S4). Consequently, it is annotated as an inactive isoform (Farkas *et al.*, 2007). It has been shown that inactive phosphatase homologues can modulate or regulate signalling pathways of real phosphatases by acting as pseudophosphatases that bind to specific residues of their substrates and, in this way, protect these from becoming dephosphorylated by the real phosphatase (Reiterer *et al.*, 2014). We therefore wanted to test whether *MAIL3* affects the function of the *MAIN/MAIL1/PP7L* complex. For instance, *PP7L* might act as a negative regulator of the *MAIL3* phosphatase by binding to its (so far unknown) substrates and thereby preventing their de-phosphorylation. In this case, the *PP7L* mutant phenotype would be due to ectopic activity of *MAIL3* and should be rescued in a *mail3-2* mutant background. We therefore generated double mutants between *pp7l-3* and *mail3-2* and also between *mail1-1* and *mail3-2*. As shown previously, the *mail3-2* mutant has, like the *pp7l-3* mutant, a T-DNA insertion within the phosphatase domain (Figure 5a). The *mail3-2* mutant did neither show any defect in development nor release of gene silencing (Uhlken *et al.*, 2014b; Ikeda *et al.*, 2017). We found that primary root growth arrest in the *pp7l-3 mail3-2* and in the *mail3-2 mail1-1* double mutant was indistinguishable from the arrest in *pp7l-3* or in *mail1-1*, indicating that the absence of *MAIL3* did not influence the root growth defects (Figure 5b). In a next step, we tested whether the silencing activity of *MAIL1* or *PP7L* was altered in the absence of *MAIL3*. RT-qPCR analyses revealed that each of the six tested loci was still significantly increased in expression in both double mutant combinations compared with wild-type or to the *mail3-2* single mutant (Figure 5c). However, whereas there was no significant difference in expression level of any of the tested loci between *mail1* and *mail3-2 mail1-1*, the expression level of four loci was significantly reduced in the *mail3-2 pp7l-3* double mutant compared with the *pp7l-3* single mutant (Figure 5c). This result indicated that *MAIL3* does influence silencing activity of loci that are controlled by *PP7L*. Loss of *MAIL3* might either allow for more efficient residual silencing activity of *MAIN* and *MAIL1* in the absence of *PP7L* or enable alternative silencing pathways to become more effective.

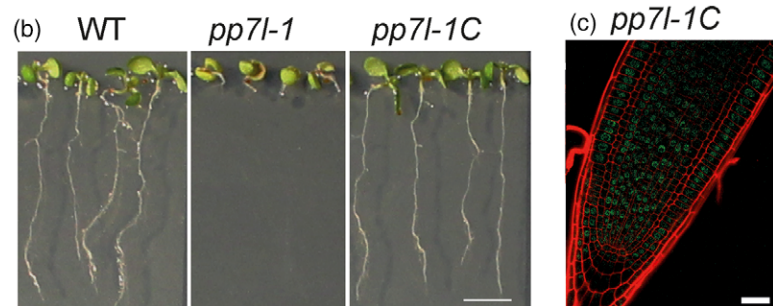
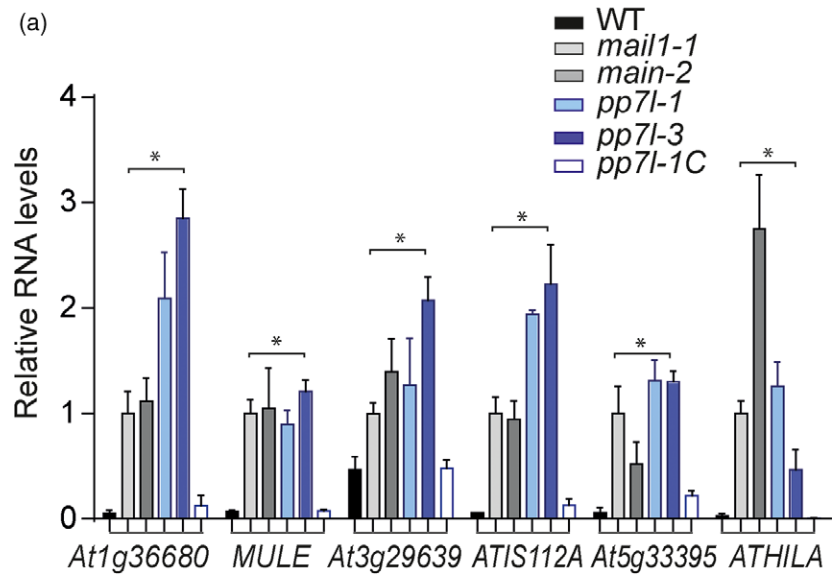
**Figure 3.** Loss of PP7L function lead to release of transposable element (TE) silencing.

(a) RT-qPCR analysis on RNA isolated from 7 days after germination (dag) seedlings of the indicated genotypes for six loci that were upregulated in *mail1-1* and *main-2*. Transcript levels are represented relative to those in *mail1-1*, which were set to 1. Values represent the mean from three biological replicates  $\pm$  SE. Asterisk indicates means differing significantly from wild-type ( $P < 0.05$ ).

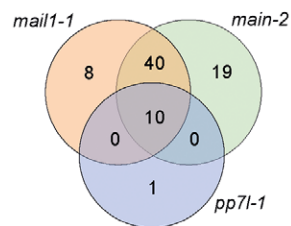
(b) Phenotype of 10-dag seedlings of wild-type (left), *pp7l-1* (centre) and *pp7l-1* mutants complemented with a ProPP7L:PP7L-green fluorescent protein (GFP) construct (*pp7l-1C*), in which the short-root phenotype was restored. Scale bar, 0.5 cm.

(c) Representative confocal image of a propidium iodide (PI)-stained root tip of *pp7l-1C* at 7 dag showing that root apical meristem (RAM) organization was restored. A faint PP7L-GFP-derived signal (green) was seen in all cells of the root tip. Scale bar, 25  $\mu$ m.

(d) Venn diagram showing overlap of TEs that were significantly increased in *mail1-1*, *main-2*, and *pp7l-1*.



(d) Up-regulated TEs



### The cell death in the RAM was caused by genome instability

Having established that MAIN, MAIL1, and PP7L acted in the same complex to prevent primary root growth arrest, accumulation of dead cells in the RAM, and release of TE silencing, we next aimed at understanding the mechanisms causing the observed mutant phenotypes. It is well established that activation of PCD in root initials is an important response to DNA damage (Hu *et al.*, 2016) and that spontaneous cell death in the RAM is a characteristic feature of mutants with impaired genome stability (Nisa *et al.*, 2019). If cell death in *pp7l-1* and *pp7l-3* mutants was due to impaired genome stability, we would expect that the

expression of DDR-related genes would be increased. To test this, we performed RT-qPCR analyses on RNA isolated from root tips of *pp7l-1* and *pp7l-3* seedlings, in which cell death was detected. Indeed, out of the four genes tested, three showed significantly increased expression in both mutant lines compared with wild-type (Figure 6a). These are the DNA repair gene *POLY (ADP-RIBOSE)-POLYMERASE1 (PARP1)*, the cell cycle inhibitor *SIAMESE-RELATED (SMR7)*, and the *ETHYLEN RESPONSE FACTOR 115 (ERF115)*, a transcription factor that is known to become activated after DNA damage-induced cell death in meristematic cells. The DNA repair gene *RAD51* that is involved in homologous recombination-mediated DNA repair



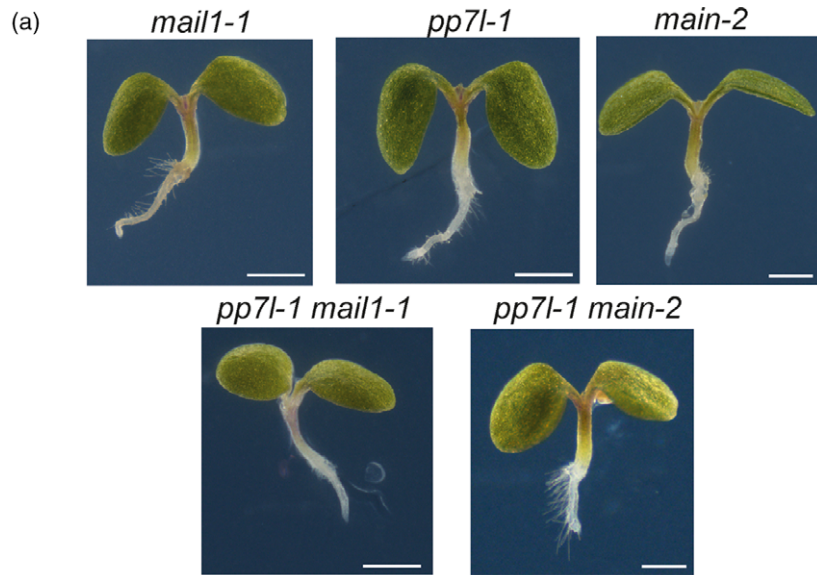
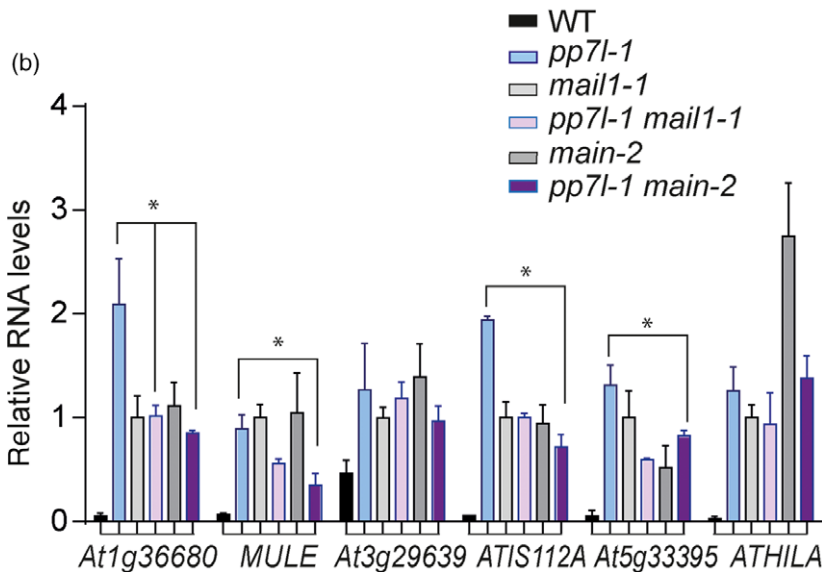


**Figure 4.** MAIL1, MAIN, and PP7L act in the same pathway.

(a) Representative photographs of 6 days after germination (dag) seedlings of the indicated genotypes showed that both double mutant combinations displayed the same phenotype as the single mutant parents. Scale bar, 1 mm.

(b) RT-qPCR analysis on RNA isolated from 7-dag seedlings of the indicated genotypes for the six selected loci showing that silencing strength was not increased in both double mutant combinations but at four loci reduced in *pp7l-1 main-2* compared with *pp7l-1*. Transcript levels are represented relative to those in *mail1-1*, which were set to 1. Values represent mean from three biological replicates  $\pm$  SE. Asterisk indicates significant difference. ( $P < 0.05$ ).



(Amiard *et al.*, 2013) was not increased in both mutant lines, indicating that this repair pathway might not be activated. A similar increased expression of DDR-related genes was previously shown to occur in root tips of *main-2* (Wenig *et al.*, 2013) and *mail1-1* (Uhlken *et al.*, 2014b) seedlings. The transcription factor SOG1 is an important regulator of DDR and is known to be required for induction of cell death in root initials upon DNA damage (Yoshiyama *et al.*, 2013). This cell-type-specific PCD is seen after a 20-h treatment with the radiometric drug zeocin in wild-type, but not in *SOG1*-deficient lines such as *sog1-1* (Yoshiyama *et al.*, 2013) or *sog1-7* (Figure S4) (Sjogren *et al.*, 2015). To test whether cell death in *pp7l* mutants was caused by constitutive activation of *SOG1* and thus could be rescued by inactivation of *SOG1*, we crossed the *pp7l-1* mutant onto the

*sog1-7* mutant background. In PI-stained root tips of 3 dag seedlings we scored the fractions of roots showing either no cell death, cell death exclusively in one or two root initials or cell death in many cells of the RAM (Figure 6b,c). As expected, almost no cell death was observed in wild-type plants and in the *sog1-7* single mutants. In contrast, the *pp7l-1* mutant exhibited cell death in numerous cells across the mitotic zone of the RAM. This cell death pattern was almost unchanged in *pp7l-1 sog1-7* double mutants, indicating that cell death occurred independently of *SOG1*. In parallel, we analyzed a *main-2 sog1-7* double mutant. Whereas in the *main-2* single mutant the majority of seedlings showed no cell death or cell death confined to one or two root initials (Figure 6b,c), the *main-2 sog1-7* double mutant displayed in almost 100% of the roots death in



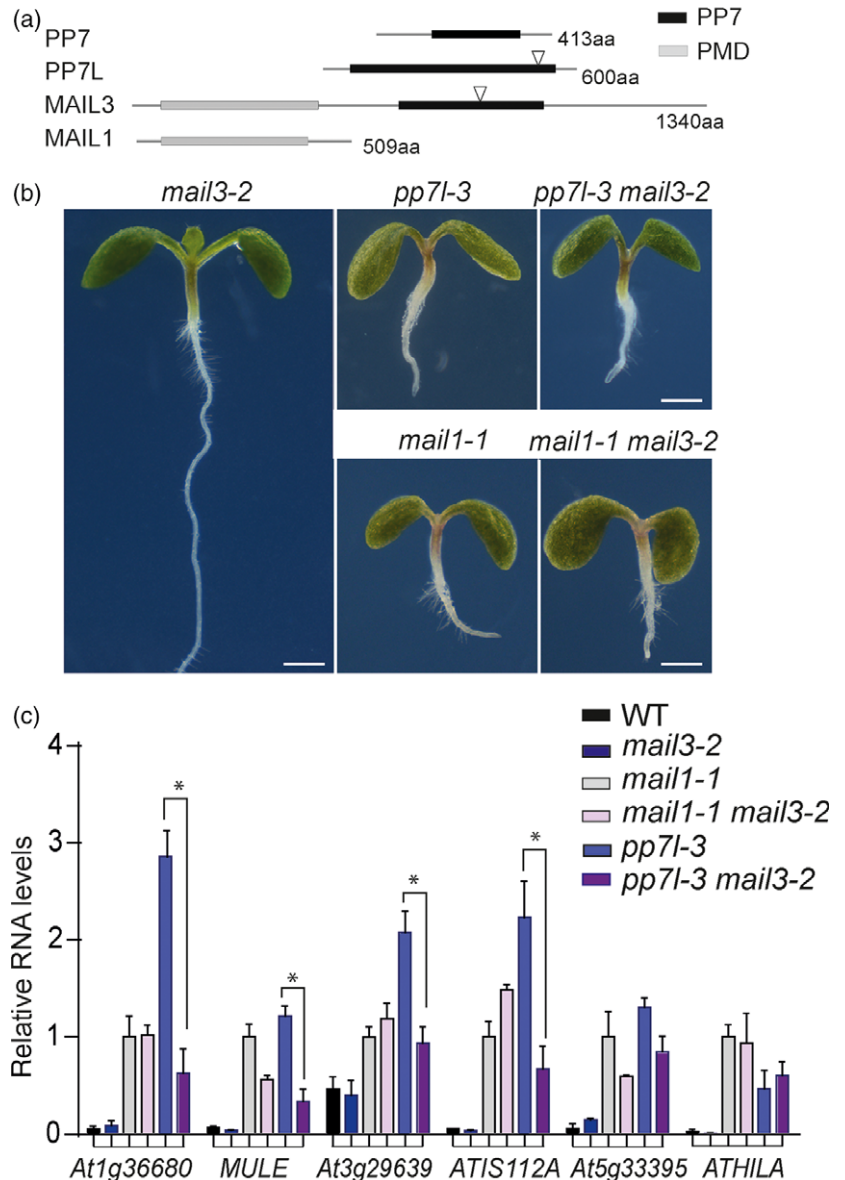
**Figure 5.** The phenotype of *pp7l-3* was unchanged on the *mail3-2* mutant background.

(a) Architecture of the PP7 (black) and PMD (grey) domain-containing proteins. Triangles indicate the position of the T-DNA insertion in *mail3-2* and *pp7l-3*.

(b) Representative photographs of 6 days after germination (dag) seedlings of the indicated genotypes showing that the short-root phenotype was unchanged in both double mutant combinations compared with the respective single mutants. Scale bar, 1 mm.

(c) RT-qPCR analysis on RNA isolated from 7-dag seedlings of the indicated genotypes for six heterochromatic loci showing that RNA levels were significantly reduced at four loci in the *pp7l-3 mail3-2* double mutant compared with *pp7l-3* while there was no significant difference between *mail1-1 mail3-2* and *mail1-1*. Transcript levels are represented relative to those in *mail1-1*, which were set to 1.

Values represent mean from three biological replicates  $\pm$  SE. Asterisk indicates significant difference ( $P < 0.05$ ).



many cells that were randomly distributed across the mitotic zone of the RAM (Figure 6b,c). The cell death pattern of the *main-2 sog1-7* double mutant was similar to that seen in *SOG-1* deficient lines after long-term exposure to genotoxic drugs (Figure S5). This *SOG-1* independent cell death was suggested to be a consequence of DNA repair processes not being efficiently activated and thus mitosis proceeding in the presence of damaged DNA (Furukawa *et al.*, 2010; Johnson *et al.*, 2018). This supported the conclusion that the cell death was caused by genome instability. In a next step, we tested whether *main-2* and *pp7l-1* were both able to transcriptionally respond to DNA damage treatment. To this end, seedlings of wild-type, *main-2* and *pp7l-1* were incubated for 2 h with the DNA damaging drug zeocin and used for RT-qPCR analysis of four well established DDR genes: *RAD51*, *BREAST CANCER SUSCEPTIBILITY1*

(*BRCA1*), *POLY (ADP-RIBOSE)-POLYMERASE2 (PARP2)* and *SIAMESE-RELATED 7 (SMR7)*. Both mutant lines showed a robust induction of each of these genes upon zeocin treatment, indicating that DDR signalling was not impaired (Figure 6d). Taken together, these results showed that loss of function of the MAIN/MAIL1/PP7L complex was associated with genome instability and consequent cell death in dividing cells. This cell death occurred through a pathway that acts independent of *SOG1* signalling.

## DISCUSSION

### MAIN, MAIL1, and PP7L act in one protein complex

MAIL1 and MAIN belong to a small protein family that is characterized by the PMD domain, a conserved protein motif that is also found in several different transposon

encoded genes. The molecular function of this domain is still unknown. Single loss-of-function mutations for *MAIN* and *MAIL1* caused similar phenotypes (Wenig *et al.*, 2013; Uhlken *et al.*, 2014a,b), and these phenotypes were not changed in *main-2 mail1-1* double mutants. It was therefore suggested that the two proteins may act as a heterodimer (Ikeda *et al.*, 2017). Here, we showed that *MAIN* and *MAIL1* indeed act in the same protein complex and that *PP7L* is part of this complex (Figure 1). Each of these three proteins contains a predicted nuclear localization signal (Kosugi *et al.*, 2009). Interestingly, we found that *PP7L* localized to the nucleus and to the cytoplasm, whereas *MAIN* and *MAIL1* were exclusively localized to the nucleus (Figure 1), suggesting that interaction between the three proteins does only occur in the nucleus. It will be interesting to test how the intracellular localization of *PP7L* is regulated and whether its cytoplasmic accumulation serves a specific function.

### PP7L is required for primary root development

*PP7L* belongs to the *PP7*-type family of serine–threonine phosphatases, which has a characteristic organization of its catalytic domain (Farkas *et al.*, 2007). *PP7* is known as an important regulator of light signalling. A loss-of-function allele of *PP7* displayed hypersensitivity to red light, and this phenotype was dependent on the presence of its interaction partner nucleotide-diphosphate kinase (*NDPK2*) (Genoud *et al.*, 2008). *PP7* was also shown to positively regulate the blue light-induced stomatal opening by interacting and dephosphorylating the zinc-finger protein *HYPERSENSITIVE TO RED AND BLUE1* (*HRB1*). Together *PP7* and *HRB1* seem to be part of a larger protein complex, which forms in a blue light-dependent manner (Sun *et al.*, 2012). Recently, three T-DNA insertion lines for *PP7L* (*pp7l-1*, *pp7l-2* *pp7l-3*) were characterized and it was shown that *PP7L* is important for chloroplast biogenesis during development of cotyledons and the first pair of true leaves (Xu *et al.*, 2019). Each of these lines showed an increased accumulation of anthocyanins, a reduced photosynthetic activity, and delayed chloroplast development. This was associated with a reduced production of chloroplast proteins, and it was suggested that *PP7L* is involved post-transcriptional control of chloroplast gene expression (Xu *et al.*, 2019). In this study, we found that *pp7l-1* and *pp7l-3* mutants were also impaired in primary root development and showed growth arrest of the primary root, associated with cell death of dividing cells in the RAM. This cell death occurred in *pp7l-1* and *pp7l-3* during the process of germination (Figure 2) and thus even before the chloroplast development phenotype in cotyledons was observed (Xu *et al.*, 2019). We assume that the function of *PP7L* in chloroplast development is independent from its function in root development. However, further analyses are required to clarify this in future. The root growth

phenotype of *pp7l* mutants was very similar to that of the single *mail1-1* or *main-2* mutants. We conclude that the presence of each of these three proteins is required for the function of the *MAIL1/MAIN/PP7L* protein complex in root development. Our double mutant analyses revealed no changes in the developmental phenotype in none of the combinations tested (*mail1-1 main-2*, *mail1-1 pp7l-1* and *main-2 pp7l-3*) (Figure 4), demonstrating that these three proteins function in the same molecular pathway. These analyses further confirmed that the observed phenotype is due to loss of *MAIL1/MAIN/MIPP* complex activity and not a consequence of ectopic accumulation of any of these three proteins in the absence of one interaction partner.

### Potential role of PP7L in TE silencing

*PP7L* loss-of-function mutants did not only show the same root developmental defects as *mail1-1* and *main-2* but also release of the same TE-encoded loci. We show that only a subset of the loci that are commonly controlled by *MAIN* and *MAIL1* was also mis-expressed in *pp7l-1*. One model to explain this could be that *MAIL1* and *MAIN* act as a heterodimer to control silencing of heterochromatic loci. The association of *PP7L* to this heterodimer might be required for efficient silencing on a specific subset of the *MAIN/MAIL1* controlled loci. It will be interesting to test in future experiments which domains are important for the interactions between these three proteins and how *PP7L* association influences the conformation of *MAIN* and *MAIL1* proteins.

Due to mutations of essential amino acids within the serine/threonine-specific protein phosphatase signature, *PP7L* is annotated as catalytically inactive isoform, whereas *MAIL3* and *PP7* are both annotated as active phosphatases (Farkas *et al.*, 2007). It was tempting to speculate that a phosphatase-inactive *MIPP* acts as a negative regulator of *MAIL3*. Our double mutant analyses revealed that the root phenotype of *mail1-1* and *pp7l-3* was unaltered in the *mail3-2* mutant background (Figure 5b). However, the absence of *MAIL3* did lead to a reduced expression level of several loci in the *pp7l-3* background (Figure 5c), whereas no changes were observed in the *mail1-1* background. One interpretation could be that *MAIL3* influences the silencing efficiency of the *MAIN/MAIL1* heterodimer only in the absence of *PP7*, for instance by destabilizing their interaction. Alternatively *MAIL3* might influence the activity of alternative silencing pathways that try to compensate for the loss of *MAIN/MAIL1/PP7L*-mediated silencing.

### How does the MAIL1/MAIN/PP7L complex control root growth and TE silencing?

We found that the first defect that was observed in the developing RAM of *mail1-1*, *main-2*, *pp7l-1*, and *pp7l-3* mutants was cell death of root initials and their descendants. This was especially obvious in the *main-2* mutant,

**Figure 6.** Analysis of DNA damage response (DDR) signalling and cell death in *pp7l* mutants.

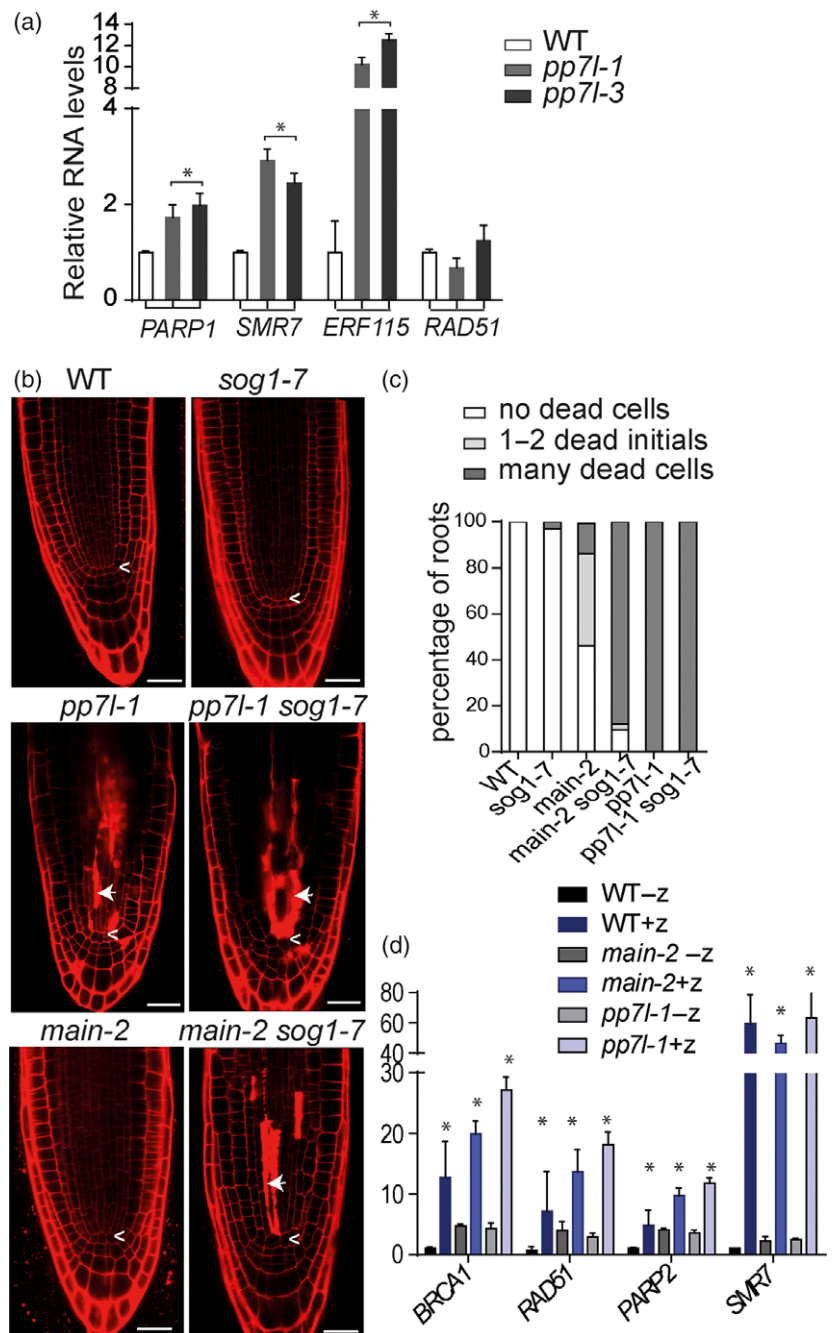
(a) RT-qPCR analysis on RNA from root tips of 3 days after germination (dag) seedlings showed increased expression of DDR-related genes in *pp7l-1* and *pp7l-3*. Transcript levels are represented relative to those in wild-type, which were set to 1. Values represent mean from three biological replicates  $\pm$  SE. Asterisk indicates significant difference from wild-type ( $P < 0.05$ ).

(b) Representative confocal images of propidium iodide (PI)-stained root tips of 3 dag seedlings of the indicated genotypes. Arrows point to dead cells, arrowheads indicate the quiescent centre (QC). Scale bar, 25  $\mu$ m.

(c) Quantification of roots of 3 dag seedlings showing no cell death, cell death in one or two root initials or cell death in many cells of the root apical meristem (RAM) of the indicated genotypes. Values represent mean from at least four biological replicates ( $n = 40-50$ ).

(d) RT-qPCR analysis of DDR-related genes in 7-dag seedlings of the indicated genotypes with or without 2 h of zeocin (100  $\mu$ M) treatment showed a robust transcriptional response to DNA damage in *main-2* and *pp7l-1*. Transcript levels are represented relative to those in wild-type without treatment, which were set to 1.

Values represent the mean from three biological replicates  $\pm$  SE. Asterisk indicate means differing significantly from the respective control without zeocin treatment ( $P < 0.05$ ).



in which the cell death phenotype occurred at a later stage than in *mail1-1* and *pp7l* mutants (Figure 2). Moreover, published data showed that growth arrest of the primary root of *main-2* and *mail1-1* was associated with typical symptoms of active DDR such as reduced cell division, precocious cell differentiation in the RAM and increased expression of DNA repair genes (Wenig *et al.*, 2013; Uhlken *et al.*, 2014a,b). SOG1 is known to be activated upon DNA damage and on the one hand induces cell-type-specific PCD in root initials. On the other hand, SOG1 is essential

for efficient activation of DNA repair pathways (Yoshiyama *et al.*, 2017). By analyzing *pp7l-1 sog1-7* and *main-2 sog1-7* double mutant lines (Figure 6), we established that cell death in the RAM was not induced by the SOG1 pathway. Moreover, the finding that the *main-2 sog1-7* double mutant showed more cell death than the *main-2* single mutant suggests that SOG1-mediated activation of DNA repair pathways is essential for cell survival during the first days after germination. We thus suggest that loss of function of *MAIN* and of its interaction partners *MAIL1* and

MIPP leads to genome instability and constitutive DNA damage resulting in root growth arrest. Recently, it was shown that in parallel to SOG1 another pathway involving the E2F transcription factors and RETINOBLASTOMA RELATED 1 (RBR1) controls the transcriptional response to DNA damage and the induction of cell death (Horvath *et al.*, 2017; Nisa *et al.*, 2019). It will be interesting to test whether this pathway is involved in the induction of cell death in the mutants described here. The next obvious question is how genome instability and the consequent defects in the RAM are connected with release of TE silencing. So far, release of TE silencing has not been associated with specific defects in the RAM. For instance loss of function of the chromatin remodelling factor DECREASED IN DNA METHYLATION (DDM1), which leads to high expression of numerous TEs due to loss of DNA methylation, is associated with accumulation of additional mutations in *ddm1-1* inbred lines (Tsukahara *et al.*, 2009). However, the *ddm1-1* mutant does not show any specific defects in root growth when grown under standard conditions (Choi *et al.*, 2019). One explanation could be that reduced compaction of pericentromeric heterochromatin, which was observed in *mail1-1*, *main-2*, and *pp7l-1* nuclei (Figure S3) and which was proposed to be responsible for release of silencing of pericentromeric heterochromatin (Ikeda *et al.*, 2017), might also lead to defects in chromatin integrity during cell divisions in the RAM. However, the fact that the severity of the root phenotype does not correlate with the release of silencing phenotype, for instance the *pp7l-1* mutant lines show a stronger cell death phenotype but a weaker silencing defect compared with *main-2*, suggests that this is not the case. It seems more likely that the MAIN/MAIL1/PP7L complex functions in several different pathways and that the silencing defects occur independently from the meristem defects.

## EXPERIMENTAL PROCEDURES

### Plant material and growth conditions

*Arabidopsis thaliana* accession Columbia (Col) was used as the wild-type and all mutants are on the Col background. Plants were grown either in potting soil or on a solid medium containing half-strength Murashige and Skoog salts, 1% sucrose and 1% (w/v) agar in growth chambers (16 h light, 22°C/8 h dark, 18°C cycles). The T-DNA insertion lines SALK\_018295 (*mipp-1*) and SALK\_022053 were obtained through the Nottingham Arabidopsis Stock Centre. Primer pairs for genotyping are described in Table S2 (Alonso *et al.*, 2003). The T-DNA insertion lines for MAIN and MAIL1 and the *sog1-7* mutant have been described previously (Wenig *et al.*, 2013; Uhlken *et al.*, 2014a,b; Sjogren *et al.*, 2015; Ikeda *et al.*, 2017).

### Co-immunoprecipitation

Transgenic seedlings expressing MAIL1-GFP, MIPP-GFP or GFP were grown for 6 days and 3 g material was used for each GFP pull down. MS analysis was performed on a Q-Exactive Orbitrap

and quantitative analysis was carried out using MAXQUANT and PERSEUS software. Protocols are described in Wendrich *et al.* (2017b).

### Plasmid construction

To create the complementation construct for *mipp-1* the genomic fragment of MIPP including the putative promoter sequence (310 bp upstream of Start-ATG) and excluding the STOP codon was amplified by PCR from genomic DNA and cloned into the pENTR-D-TOPO plasmid (www.thermofisher.com/) and sequenced. By LR recombination reaction, the fragment was inserted into the destination vector pMDC107 (Curtis and Grossniklaus, 2003) yielding ProPP7L-PP7L-GFP. For subcellular localization analysis, the full-length coding sequence (CDS) of MIPP and MAIL1 excluding the STOP codon was amplified by PCR and cloned into pDONR221, followed by LR recombination reaction with the destination vector pABindGFP (Bleckmann *et al.*, 2010). For Y2H assays, the full-length CDS of MAIN, MAIL1 and PP7L and the truncated version of MAIL1 (MAIL1ΔC) were amplified by PCR and cloned into pENTR-D-TOPO and the fragments were recombined into Gateway-compatible versions of the GAL4 DNA-binding domain vector pGBT-9 (Bleckmann *et al.*, 2010) and the activation domain vector pGAD424 (Clontech, www.takarabio.com) by LR recombination reaction. For BiFC analysis the full-length CDS of MAIN, MAIL1 and PP7L were amplified with primers adding recombination sites and cloned into pDONR221L1L4 or pDONR221L3L2 (Grefen and Blatt, 2012) and subsequently, by LR recombination reactions, inserted into BiFC-2in1-NN. All primers are listed in Table S2.

### Transgenic plants and transient expression in leaves

The constructs were transformed into *Agrobacterium tumefaciens* C58C1. To generate transgenic plants *Agrobacterium* was resuspended in 3 ml of transformation buffer containing 5% sucrose and 0.05% silwet L-77, and used for plant transformation by the floral dip method (Clough and Bent, 1998). For transient expression, the plasmid-containing agrobacteria were cultivated overnight at 28°C, harvested by centrifugation, and the pellet was resuspended in sterile water to a final OD<sub>600</sub> of 1. The *Agrobacterium* suspension was infiltrated into leaves of 4- to 6-week-old *Nicotiana benthamiana* plants using a needleless 2-ml syringe.

### Transformation of yeast cells

Transformation of the yeast strain AH109 was carried out according to (Gietz *et al.*, 1997). In brief, the binding and activation domain vectors were transformed simultaneously and the cells were spread on yeast minimal medium (SD medium: 0.66% yeast nitrogen base without amino acids, 0.066% amino acid mix, 2% glucose) lacking leucine and tryptophan (SD-L-W). After 3 d of incubation at 29°C, overnight cultures of single colonies were grown in double dropout medium (SD-L-W) under continuous shaking for 24 h at 29°C. The optical density was set to an OD<sub>600</sub> of 4 and a dilution series from 10<sup>-1</sup> to 10<sup>-3</sup> was dripped on selection agar plates lacking histidine (SD-L-W-H) and containing 0.5 mM 3-amino-1,2,4-triazole (3-AT) as well as on SD-L-W medium as a control.

### Protoplast isolation and transformation

Protoplast isolation was carried out as previously described with minor changes (Drechsel *et al.*, 2011). Mesophyll protoplasts were isolated from leaves of 6-week-old plants in protoplasting buffer (500 mM sorbitol, 1 mM CaCl<sub>2</sub>, 0.25% macerozym R10, 1% cellulase R10, 10 mM MES-KOH, pH 5.7). The protoplast transformation was performed with 150 μl protoplasts, 20 μg plasmid DNA and 165 μl



PEG-Ca buffer (40% PEG 4000, 200 mM sorbitol, 100 mM CaCl<sub>2</sub>). The transformation sample was mixed completely by gently rotating the tube and was incubated for 30 min at room temperature in the dark. To stop this process, the sample was diluted with W5 buffer (154 mM NaCl, 125 mM CaCl<sub>2</sub>, 5 mM KCl, 5 mM glucose, 2 mM MES, pH 5.7) in three steps of 500 µl, 1 ml and 1.5 ml. The sample was centrifuged at 60 g for 3 min (without brake) and was washed with 3 ml W5 buffer twice. The protoplasts were incubated for 24 h at room temperature in the dark and fluorescence signals were analyzed by confocal laser scanning microscopy.

### Root growth assay and propidium iodide staining

For the analysis of root growth, plants were germinated and grown on vertical plates. The plates were scanned every 3 days and measurement of root length was carried out using IMAGEJ software (<http://imagej.nih.gov/ij/>). The final values were calculated by determining the arithmetic mean of the root length values of three biological replicates, which were themselves the average of at least 20–30 plants. For treatment with zeocin, seedlings were transferred to liquid medium containing zeocin or, as control, no zeocin and incubated for the indicated time. Staining of cell wall and dead cells was performed by submerging seedling for 1 min in a 10 µg/ml PI/water solution and imaging was carried out using confocal microscopy.

### Analysis of embryos and mature seeds

For analysis of embryonic development, seeds were excised from green siliques and cleared in Hoyer's solution (100 g chloral hydrate, 5 ml glycerol, 30 ml H<sub>2</sub>O, 7.5 g gum arabic) overnight. Embryos were examined by confocal laser scanning microscopy using a differential interference contrast filter. For mPS-PI staining of mature seeds, dry seeds were incubated in water overnight and seeds with an opened seed coat were selected for further treatment. The seeds were treated as described in Truernit *et al.* (2008). In short, seeds were fixed (50% methanol, 10% acetic acid) at 4°C overnight, followed by an overnight treatment with 1% SDS and 0.2 N NaOH at RT. After bleaching using sodium hypochlorite solution (2.5% active chloride) for 5 min, seeds were treated with 1% periodic acid for 40 min at RT, and then stained with Schiff's reagent containing 100 µg/ml PI for 2 h. After two washing steps, seeds were destained in a chloral hydrate solution (4 g chloral hydrate, 1 ml glycerol, 2 ml water), covered with Hoyer's solution and incubated for 3 days before imaging by confocal microscopy.

### Confocal laser scanning microscopy

To detect fluorescence of YFP, GFP or red fluorescent protein (RFP) confocal laser scanning microscopy was applied using the Leica TCS SP8 Confocal Platform (Leica Microsystems, Wetzlar, Germany). For excitation of YFP and GFP, laser light of 488 nm and for RFP of 561 nm was used. The detection windows ranged from 520 to 540 nm (YFP), 496–511 nm (GFP), 569–591 nm (RFP) and 690–708 nm for detection of chlorophyll auto-fluorescence.

### Cytological analysis of nuclei

Determination of chromocentre area was performed on DAPI-stained nuclei from 4-week-old rosette leaves, as previously described (Ikeda *et al.*, 2017).

### Expression analysis

Total RNA was extracted from Arabidopsis seedlings or inflorescence material using the innuPREP Plant RNA kit (Analytik Jena

BioSolutions, [www.analytik-jena.de](http://www.analytik-jena.de)). cDNA synthesis was performed using a QuantiTect® Reverse Transcription Kit (QIAGEN, <http://www.qiagen.com>). The cDNA was used either for semiquantitative PCR experiments or for quantitative PCR using a RotorGene 2000 (Corbett Research, <http://www.corbettlifescience.com>). Target-specific efficiencies were calculated as the mean of all reaction-specific efficiencies for a given target. Data were quality-controlled, normalized against two reference genes, and statistically evaluated using QBASEPLUS 3.0 (Hellemans *et al.*, 2007). Primers used for genotyping, semiquantitative reverse transcriptase polymerase chain reaction (RT-PCR) and qRT-PCR are listed in Table S3.

### RNA-seq analysis

Previously published RNA-seq data of *pp7l-1* mutants (4-day-old seedlings, three replicates; (Xu *et al.*, 2019)), *mail1-1* and *main* mutants (3-week-old seedlings, two replicates; (Ikeda *et al.*, 2017)), and corresponding wild-types were mapped on the *Arabidopsis thaliana* genome (TAIR10) using STAR (Dobin *et al.*, 2013) allowing multimapping reads. Read counting was performed with featureCounts (Liao *et al.*, 2014) on 'transposable element' TAIR10 annotations. Differentially expressed TEs (Benjamini-Hochberg adjusted *P*-values < 0.05) were subsequently identified using DESeq2 (Love *et al.*, 2014). TEs with ≥10% of the sequence overlapping a protein-coding gene annotation were not considered in the analysis.

### ACCESSION NUMBERS

Sequence data from this article can be found in the EMBL/GenBank libraries under the accession numbers: *MAIL1* (At2g25010), *MAIL3* (At1g48120), *MAIN* (At1g17930), *PP7L* (At5g10900), *PP7* (At5g63870).

### ACKNOWLEDGEMENTS

We thank Judith Mehrmann, Teresa Wulf, Sotoodeh Seyede-hyasaman, and Zsuzsanna Darula for technical assistance and experimental support and to Paul Larsen (University of California, Riverside) for providing the seeds for the *sog1-7* line. This work was funded by the Deutsche Forschungsgemeinschaft (DFG) grant to MW (WE 4506/6-1). C.L.-H. was supported by a UHH fellowship, work in the Mathieu lab was supported by CNRS, Inserm, and Université Clermont Auvergne and AP-Sz was supported by the GINOP-2.3.2-15-2016-00032.

### CONFLICT OF INTEREST

The authors declare no conflicts of interest.

### AUTHOR CONTRIBUTIONS

CL-H, JL, SS, and KW designed and performed experiments. WH and TP performed experiments. ZM and AP-S performed experiments and analyzed data. GJ, OM, and SH analyzed data. MW conceived this project, designed experiments, analyzed data and wrote the manuscript.

### SUPPORTING INFORMATION

Additional Supporting Information may be found in the online version of this article.

**Figure S1.** Embryo development was unaffected in *pp7l-1* and *pp7l-3*.

**Figure S2.** Shoot development of *pp7l-1* and *pp7l-3*.

**Figure S3.** Impaired chromocentre condensation in *pp7l-1*.

**Figure S4.** PP7L is an inactive phosphatase.

**Figure S5.** Cell death pattern in the RAM of wild-type and *sog1-7* after zeocin treatment.

**Table S1.** Number of peptides identified by LC-MS/MS for co-immunoprecipitating proteins.

**Table S2.** Gene lists used to generate the diagram in Figure 3(d).

**Table S3.** Primer list.

## REFERENCES

- Alonso, J.M., Stepanova, A.N., Leisse, T.J. *et al.* (2003) Genome-wide insertional mutagenesis of *Arabidopsis thaliana*. *Science*, **301**, 653–657.
- Amiard, S., Gallego, M.E. and White, C.I. (2013) Signaling of double strand breaks and deprotected telomeres in Arabidopsis. *Front. Plant Sci.* **4**, 405.
- Bleckmann, A., Weidtkamp-Peters, S., Seidel, C.A. and Simon, R. (2010) Stem cell signaling in Arabidopsis requires CRN to localize CLV2 to the plasma membrane. *Plant Physiol.* **152**, 166–176.
- Boyes, D.C., Zayed, A.M., Ascenzi, R., McCaskill, A.J., Hoffman, N.E., Davis, K.R. and Gorch, J. (2001) Growth stage-based phenotypic analysis of Arabidopsis: a model for high throughput functional genomics in plants. *Plant Cell*, **13**, 1499–1510.
- Choi, S.H., Ryu, T.H., Kim, J.I., Lee, S., Lee, S.S. and Kim, J.H. (2019) Mutation in DDM1 inhibits the homology directed repair of double strand breaks. *PLoS ONE*, **14**, e0211878.
- Clough, S.J. and Bent, A.F. (1998) Floral dip: a simplified method for Agrobacterium-mediated transformation of *Arabidopsis thaliana*. *Plant J.* **16**, 735–743.
- Culligan, K.M., Robertson, C.E., Foreman, J., Doerner, P. and Britt, A.B. (2006) ATR and ATM play both distinct and additive roles in response to ionizing radiation. *Plant J.* **48**, 947–961.
- Curtis, M.D. and Grossniklaus, U. (2003) A gateway cloning vector set for high-throughput functional analysis of genes in planta. *Plant Physiol.* **133**, 462–469.
- Diaz, M., Pecinkova, P., Nowicka, A., Baroux, C., Sakamoto, T., Gandha, P.Y., Jerabkova, H., Matsunaga, S., Grossniklaus, U. and Pecinka, A. (2019) The SMC5/6 complex subunit NSE4A is involved in DNA damage repair and seed development. *Plant Cell*, **31**, 1579–1597.
- Dobin, A., Davis, C.A., Schlesinger, F., Drenkow, J., Zaleski, C., Jha, S., Batut, P., Chaisson, M. and Gingeras, T.R. (2013) STAR: ultrafast universal RNA-seq aligner. *Bioinformatics*, **29**, 15–21.
- Drechsel, G., Bergler, J., Wippel, K., Sauer, N., Vogelmann, K. and Hoth, S. (2011) C-terminal armadillo repeats are essential and sufficient for association of the plant U-box armadillo E3 ubiquitin ligase SAUL1 with the plasma membrane. *J. Exp. Bot.* **62**, 775–785.
- Du, J., Johnson, L.M., Jacobsen, S.E. and Patel, D.J. (2015) DNA methylation pathways and their crosstalk with histone methylation. *Nat. Rev. Mol. Cell Biol.* **16**, 519–532.
- Farkas, I., Dombradi, V., Miskai, M., Szabados, L. and Koncz, C. (2007) Arabidopsis PPP family of serine/threonine phosphatases. *Trends Plant Sci.* **12**, 169–176.
- Feng, W. and Michaels, S.D. (2015) Accessing the inaccessible: the organization, transcription, replication, and repair of heterochromatin in plants. *Annu. Rev. Genet.* **49**, 439–459.
- Franz, P.F. and de Jong, J.H. (2002) Chromatin dynamics in plants. *Curr. Opin. Plant Biol.* **5**, 560–567.
- Fulcher, N. and Sablowski, R. (2009) Hypersensitivity to DNA damage in plant stem cell niches. *Proc. Natl Acad. Sci. USA*, **106**, 20984–20988.
- Furukawa, T., Curtis, M.J., Tominey, C.M., Duong, Y.H., Wilcox, B.W., Aggoune, D., Hays, J.B. and Britt, A.B. (2010) A shared DNA-damage-response pathway for induction of stem-cell death by UVB and by gamma irradiation. *DNA Repair (Amst)*, **9**, 940–948.
- Genoud, T., Santa Cruz, M.T., Kulicic, T., Sparla, F., Fankhauser, C. and Mettraux, J.P. (2008) The protein phosphatase 7 regulates phytochrome signaling in Arabidopsis. *PLoS ONE*, **3**, e2699.
- Gietz, R.D., Triggs-Raine, B., Robbins, A., Graham, K.C. and Woods, R.A. (1997) Identification of proteins that interact with a protein of interest: applications of the yeast two-hybrid system. *Mol. Cell Biochem.* **172**, 67–79.
- Grefen, C. and Blatt, M.R. (2012) A 2in1 cloning system enables ratiometric bimolecular fluorescence complementation (rBiFC). *Biotechniques*, **53**, 311–314.
- Heidstra, R. and Sabatini, S. (2014) Plant and animal stem cells: similar yet different. *Nat. Rev. Mol. Cell Biol.* **15**, 301–312.
- Hellemans, J., Mortier, G., De Paepe, A., Speleman, F. and Vandesompele, J. (2007) qBase relative quantification framework and software for management and automated analysis of real-time quantitative PCR data. *Genome Biol.* **8**, R19.
- Heyman, J., Cools, T., Vandenbussche, F. *et al.* (2013) ERF115 controls root quiescent center cell division and stem cell replenishment. *Science*, **342**, 860–863.
- Horvath, B.M., Kourova, H., Nagy, S. *et al.* (2017) Arabidopsis RETINOBLASTOMA RELATED directly regulates DNA damage responses through functions beyond cell cycle control. *EMBO J.* **36**, 1261–1278.
- Hu, Z., Cools, T. and De Veylder, L. (2016) Mechanisms used by plants to cope with DNA damage. *Annu. Rev. Plant Biol.* **67**, 439–462.
- Ikeda, Y., Pelissier, T., Bourguet, P., Becker, C., Pouch-Pelissier, M.N., Pogorelnik, R., Weingartner, M., Weigel, D., Deragon, J.M. and Mathieu, O. (2017) Arabidopsis proteins with a transposon-related domain act in gene silencing. *Nat. Commun.* **8**, 15122.
- Jia, N., Liu, X. and Gao, H. (2016) A DNA2 homolog is required for DNA damage repair, cell cycle regulation, and meristem maintenance in plants. *Plant Physiol.* **171**, 318–333.
- Johnson, R.A., Conklin, P.A., Tjahjadi, M., Missirian, V., Toal, T., Brady, S.M. and Britt, A.B. (2018) SUPPRESSOR OF GAMMA RESPONSE1 links DNA damage response to organ regeneration. *Plant Physiol.* **176**, 1665–1675.
- Kosugi, S., Hasebe, M., Tomita, M. and Yanagawa, H. (2009) Systematic identification of cell cycle-dependent yeast nucleocytoplasmic shuttling proteins by prediction of composite motifs. *Proc. Natl Acad. Sci. USA*, **106**, 10171–10176.
- Kurihara, Y., Matsui, A., Kawashima, M. *et al.* (2008) Identification of the candidate genes regulated by RNA-directed DNA methylation in Arabidopsis. *Biochem. Biophys. Res. Commun.* **376**, 553–557.
- Liao, Y., Smyth, G.K. and Shi, W. (2014) featureCounts: an efficient general purpose program for assigning sequence reads to genomic features. *Bioinformatics*, **30**, 923–930.
- Love, M.I., Huber, W. and Anders, S. (2014) Moderated estimation of fold change and dispersion for RNA-seq data with DESeq2. *Genome Biol.* **15**, 550.
- Ma, J., Liu, Y., Zhou, W., Zhu, Y., Dong, A. and Shen, W.H. (2018) Histone chaperones play crucial roles in maintenance of stem cell niche during plant root development. *Plant J.* **95**, 86–100.
- Moissiard, G., Cokus, S.J., Cary, J. *et al.* (2012) MORC family ATPases required for heterochromatin condensation and gene silencing. *Science*, **336**, 1448–1451.
- Moller, S.G., Kim, Y.S., Kunkel, T. and Chua, N.H. (2003) PP7 is a positive regulator of blue light signaling in Arabidopsis. *Plant Cell*, **15**, 1111–1119.
- Nisa, M.U., Huang, Y., Benhamed, M. and Raynaud, C. (2019) The plant DNA damage response: signaling pathways leading to growth inhibition and putative role in response to stress conditions. *Front. Plant Sci.* **10**, 653.
- Raya-Gonzalez, J., Oropeza-Aburto, A., Lopez-Bucio, J.S., Guevara-Garcia, A.A., de Veylder, L., Lopez-Bucio, J. and Herrera-Estrella, L. (2018) MED1ATOR18 influences Arabidopsis root architecture, represses auxin signaling and is a critical factor for cell viability in root meristems. *Plant J.* **96**, 895–909.
- Reiterer, V., Evers, P.A. and Farhan, H. (2014) Day of the dead: pseudokinases and pseudophosphatases in physiology and disease. *Trends Cell Biol.* **24**, 489–505.
- Sancar, A., Lindsey-Boltz, L.A., Unsal-Kacmaz, K. and Linn, S. (2004) Molecular mechanisms of mammalian DNA repair and the DNA damage checkpoints. *Annu. Rev. Biochem.* **73**, 39–85.
- Sjogren, C.A., Bolaris, S.C. and Larsen, P.B. (2015) Aluminum-dependent terminal differentiation of the Arabidopsis root tip is mediated through an ATR-, ALT2-, and SOG1-regulated transcriptional response. *Plant Cell*, **27**, 2501–2515.
- Sun, X., Kang, X. and Ni, M. (2012) Hypersensitivity to red and blue 1 and its modification by protein phosphatase 7 are implicated in the control of Arabidopsis stomatal aperture. *PLoS Genet.* **8**, e1002674.
- Truernit, E., Bauby, H., Dubreucq, B., Grandjean, O., Runions, J., Barthelmy, J. and Palauqui, J.C. (2008) High-resolution whole-mount imaging of three-dimensional tissue organization and gene expression enables

- the study of Phloem development and structure in Arabidopsis. *Plant Cell*, **20**, 1494–1503.
- Tsukahara, S., Kobayashi, A., Kawabe, A., Mathieu, O., Miura, A. and Kakutani, T.** (2009) Bursts of retrotransposition reproduced in Arabidopsis. *Nature*, **461**, 423–426.
- Uhlken, C., Horvath, B., Stadler, R., Sauer, N. and Weingartner, M.** (2014a) MAIN-LIKE1 is a crucial factor for correct cell division and differentiation in *Arabidopsis thaliana*. *Plant J.* **78**, 107–120.
- Uhlken, C., Hoth, S. and Weingartner, M.** (2014b) MAIL1 is essential for development of the primary root but not of anchor roots. *Plant Signal Behav.* **9**, e976477.
- Uhrig, R.G., Labandera, A.M. and Moorhead, G.B.** (2013) Arabidopsis PPP family of serine/threonine protein phosphatases: many targets but few engines. *Trends Plant Sci.* **18**, 505–513.
- Wang, J., Blevins, T., Podicheti, R., Haag, J.R., Tan, E.H., Wang, F. and Pikaard, C.S.** (2017) Mutation of Arabidopsis SMC4 identifies condensin as a corepressor of pericentromeric transposons and conditionally expressed genes. *Genes Dev.* **31**, 1601–1614.
- Wendrich, J.R., Boeren, S., Moller, B.K., Weijers, D. and De Rybel, B.** (2017a) In vivo identification of plant protein complexes using IP-MS/MS. *Methods Mol. Biol.* **1497**, 147–158.
- Wendrich, J.R., Moller, B.K., Li, S., Saiga, S., Sozzani, R., Benfey, P.N., De Rybel, B. and Weijers, D.** (2017b) Framework for gradual progression of cell ontogeny in the Arabidopsis root meristem. *Proc. Natl Acad. Sci. USA*, **114**, E8922–E8929.
- Wenig, U., Meyer, S., Stadler, R., Fischer, S., Werner, D., Lauter, A., Melzer, M., Hoth, S., Weingartner, M. and Sauer, N.** (2013) Identification of MAIN, a factor involved in genome stability in the meristems of *Arabidopsis thaliana*. *Plant J.* **75**, 469–483.
- Xu, D., Marino, G., Klingl, A., Enderle, B., Monte, E., Kurth, J., Hiltbrunner, A., Leister, D. and Kleine, T.** (2019) Extrachloroplastic PP7L functions in chloroplast development and abiotic stress tolerance. *Plant Physiol.* **180**, 323–341.
- Yi, D., Alvim Kamei, C.L., Cools, T. et al.** (2014) The arabidopsis SIAMESE-RELATED cyclin-dependent kinase inhibitors SMR5 and SMR7 regulate the DNA damage checkpoint in response to reactive oxygen species. *Plant Cell*, **26**, 296–309.
- Yoshiyama, K., Conklin, P.A., Huefner, N.D. and Britt, A.B.** (2009) Suppressor of gamma response 1 (SOG1) encodes a putative transcription factor governing multiple responses to DNA damage. *Proc. Natl Acad. Sci. USA*, **106**, 12843–12848.
- Yoshiyama, K.O., Kobayashi, J., Ogita, N., Ueda, M., Kimura, S., Maki, H. and Umeda, M.** (2013) ATM-mediated phosphorylation of SOG1 is essential for the DNA damage response in Arabidopsis. *EMBO Rep.* **14**, 817–822.
- Yoshiyama, K.O., Kaminoyama, K., Sakamoto, T. and Kimura, S.** (2017) Increased phosphorylation of Ser-Gln sites on SUPPRESSOR OF GAMMA RESPONSE1 strengthens the DNA damage response in *Arabidopsis thaliana*. *Plant Cell*, **29**, 3255–3268.





1 **Title Page**

2  
3  
4 **The Arabidopsis Translation Elongation complex eEF1B impacts plant development**  
5 **and associates with heat-induced stress granules**

6  
7 Julia Lohmann<sup>1</sup>, Cloe de Luxán-Hernández<sup>1</sup>, Yang Gao<sup>2</sup>, Reimo Zoschke<sup>2</sup>, Magdalena  
8 Weingartner<sup>1</sup>

9  
10 <sup>1</sup> Institute of Plant Sciences and Microbiology, University of Hamburg, Ohnhorststrasse 18,  
11 22609 Hamburg.

12  
13 <sup>2</sup> Max Planck Institute of Molecular Plant Physiology, Am Mühlenberg 1, 14476 Potsdam-  
14 Golm.

15  
16 Email: julia.lohmann@uni-hamburg.de

17 cloe.de.luxan.hernandez@studium.uni-hamburg.de

18 YGao@mpimp-golm.mpg.de

19 zoschke@mpimp-golm.mpg.de

20 magdalena.weingartner@uni-hamburg.de (corresponding author, orcid ID: 0000-  
21 0003-0962-4728)

22  
23 Date of submission:

24 Number of Tables: 0

25 Number of Figures: 8

26 Word count: 5259 (max 5500)

27  
28 Supplementary Material:

29 Number of Tables: 1

30 Number Figures: 6

31  
32 Running title: Role of eEF1B in plant development and heat stress response  
33  
34  
35  
36  
37  
38  
39  
40  
41  
42

43 **HIGHLIGHT** (30 words)

44  
45 The eEF1By subunit is essential for growth and development at standard conditions. The  
46 rapid localisation of eEF1B subunits to cytoplasmic foci might allow adaption of translation  
47 rates to heat stress.  
48  
49

50  
51  
52  
53  
54  
55  
56  
57  
58  
59  
60  
61  
62  
63  
64  
65  
66  
67  
68  
69  
70  
71  
72  
73  
74  
75  
76  
77  
78  
79  
80  
81  
82

**ABSTRACT** (200 words)

The important role of translational control for maintenance of proteostasis is well documented in plants, but the exact mechanisms that coordinate translation rates during plant development and stress response are not well understood. In Arabidopsis, the translation elongation complex eEF1B consists of three subunits: eEF1B $\alpha$ , eEF1B $\beta$  and eEF1B $\gamma$ . While eEF1B $\alpha$  and eEF1B $\beta$  have a conserved GTP/GDP exchange function, the function of eEF1B $\gamma$  is still unknown. By generating Arabidopsis mutants with strongly reduced eEF1B $\gamma$  levels, we revealed its essential role during plant growth and development and analysed its impact on translation. To explore the function of the eEF1B subunits at high temperature stress, we analysed their dynamic localisation as GFP-fusions under control and heat stress conditions. Each of these fusion proteins accumulated in heat-induced cytoplasmic foci and co-localised with the stress-granule marker PAB8-mCherry. Quantification of cytoplasmic foci demonstrated that eEF1B $\beta$  accumulates more often and more efficiently in stress granules than the other two subunits. Co-expression analyses revealed that eEF1B $\beta$  promoted cytoplasmic foci formation and protein-protein-interaction studies indicated that eEF1B $\beta$  seems to be important for eEF1B complex assembly. These data provide new insight into the mechanisms that allow for rapid adaption of translation rates during heat stress response.

**KEYWORDS:**

Arabidopsis thaliana, cytoplasmic foci, plant development, heat stress, stress granules, thermotolerance, translation elongation.

**ABBREVIATIONS:** Cycloheximide (CHX), eukaryotic translation elongation factor 1 (eEF1), glutathione-S-transferase (GST), HEAT-SHOCK PROTEIN101 (HSP101), hygromycin B (HYG), Poly-(A)-binding protein (PAB), small heat shock proteins (sHSPs), stress granules (SGs), yeast-two-hybrid (Y2H).

## 83 INTRODUCTION

84

85 Protein biosynthesis is a fundamental process that drives growth, cell division and develop-  
86 ment of all organisms. The importance of a coordinated protein translation during stress re-  
87 sponse and for maintenance of protein homeostasis is well documented in plants  
88 (Merchante, 2017). Thus, a tight regulation of the three phases of translation (initiation, elon-  
89 gation and termination) is necessary for plant survival and adaption. Initiation is the most  
90 intensively studied step that can be regulated in many different ways such as phosphoryla-  
91 tion of individual translation initiation factors and RNA binding proteins or by changes in ribo-  
92 somal protein composition (Browning and Bailey-Serres, 2015; Jackson et al., 2010;  
93 Merchante et al., 2017). More recently, the control of translation elongation was also shown  
94 to be critical for regulating protein biosynthesis and downstream protein folding and modifica-  
95 tion processes (Schuller and Green, 2018; Stein and Frydman, 2019). Translation elongation  
96 is executed by the eukaryotic TRANSLATION ELONGATION FACTOR 1A (eEF1A) complex  
97 which delivers GTP and the required aminoacyl-tRNA to the A-site of the ribosome. Codon-  
98 anticodon recognition between the mRNA in the A-site and the aminoacyl-tRNA leads to  
99 GTP hydrolysis and release of eEF1A-GDP. The subsequent regeneration of eEF1A-GTP is  
100 catalyzed by the GDP/GTP exchange activity of the eukaryotic TRANSLATION ELONGA-  
101 TION FACTOR 1B (eEF1B) complex. In Arabidopsis, the eEF1B complex consists of three  
102 subunits named eEF1B $\alpha$ , eEF1B $\beta$  and eEF1B $\gamma$ . Each of these subunits is encoded by two  
103 genes and the encoded proteins show a very high degree of similarity (Le Sourd et al.,  
104 2006). The precise combination and conformation of the protein complex in plants is still un-  
105 known. Homologies to other well-studied organisms have led to the canonical functions of  
106 eEF1B subunits becoming the accepted understanding. eEF1B $\alpha$  and eEF1B $\beta$  subunits are  
107 believed to be necessary for recharging eEF1A due to their guanine exchange factor activity  
108 (Le Sourd et al., 2006). In contrast, the molecular function of the eEF1B $\gamma$  subunit is less  
109 clear. It has a conserved N-terminal domain that contains two glutathione S-transferase  
110 (GST)-like motifs and a highly conserved C-terminal domain of so far unknown function (Le  
111 Sourd et al., 2006). The human eEF1B $\gamma$  was shown to be able to bind both eEF1B $\alpha$  and  
112 eEF1B $\beta$  simultaneously through its N-terminal domain and it was suggested to act as a  
113 structural protein that keeps the eEF1B complex in its correct conformation (Mansilla et al.,  
114 2002). Apart from a study in rice showing that eEF1B $\gamma$  exhibits low GST activity (Kobayashi  
115 et al., 2001), the function of eEF1B $\gamma$  in plants has not been studied in plants so far.

116 Exposure of plants to above-optimal temperature leads to a global inhibition of protein syn-  
117 thesis rates, which reduces the production and accumulation of newly formed potentially  
118 damaged proteins (Cherkasov et al., 2013; Ivanov et al., 2019). Additionally, heat stress  
119 causes the formation of cytoplasmic stress granules (SGs). SGs are known to contain trans-  
120 lation-stalled mRNA molecules and mRNA binding proteins that are believed to protect the  
121 mRNAs from degradation. SGs contain also components of the translation machinery such  
122 as translation initiation factors, ribosomal proteins and Poly(A)-binding proteins (PAB) and  
123 thus store partially assembled translation initiation complexes (Protter and Parker, 2016;  
124 Weber et al., 2008). Upon stress relief, SGs become disassembled and stored mRNAs can  
125 be used to reactivate translation or they become degraded. The processes of SG-  
126 disassembly, re-initiation of translation and protein disaggregation are supported by chaper-  
127 ones and disaggregases, such as HEAT SHOCK PROTEIN 101 (HSP101) (Chantarachot  
128 and Bailey-Serres, 2018; Weber et al., 2008). The exact mechanisms that coordinate rapid  
129 inhibition of translation during temperature increase and re-initiation of translation after stress  
130 relief are still not well understood in plants (Cherkasov et al., 2013; Ivanov et al., 2019).

131 Moreover, the role of SGs during these processes and how their formation is controlled is still  
132 unclear and an active area of research.

133 A recent mass spectrometry study revealed that all three subunits of the eEF1B complex are  
134 present in heat-induced stress granules of *Arabidopsis* seedlings (Kosmacz et al., 2019). The  
135 eEF1B subunits were also shown to be bound to small heat shock proteins (sHSPs) upon  
136 heat stress and to co-localise with sHSPs in heat-induced cytoplasmic aggregates. Further-  
137 more, the disaggregase HSP101 was important for re-solubilisation of eEF1B complex com-  
138 ponents after recovery from heat stress (McLoughlin et al., 2016; McLoughlin et al., 2019).  
139 These data suggested that the eEF1B complex might be especially heat-labile and that its  
140 components may be important for translational control during stress and/or stress recovery  
141 (McLoughlin et al., 2016).

142 Here, we aimed at understanding the so far unknown function of eEF1B $\gamma$  and the role of the  
143 eEF1B complex in stress responses. We performed a first functional analysis of the eEF1B $\gamma$   
144 subunit in *Arabidopsis*. Our interaction studies revealed that not eEF1B $\gamma$  but eEF1B $\beta$  seems  
145 to be important for eEF1B complex assembly in plants by being able to bind to the two other  
146 subunits. Using T-DNA insertion lines, we have established a double mutant line with  
147 strongly reduced eEF1B $\gamma$  protein levels. This mutant line showed delayed development, re-  
148 duced cell division rates and altered polysome profiles indicating that eEF1B $\gamma$  is important for  
149 efficient protein biosynthesis during standard growth conditions. We also analysed the heat  
150 sensitivity of the mutant line and found that it showed a similar thermotolerance as the WT.  
151 The *in vivo* localisation of the eEF1B subunits revealed that each of the eEF1B subunits rap-  
152 idly accumulated in cytoplasmic foci and co-localised with the stress granule marker PAB8  
153 upon high temperature stress. Interestingly, we found that eEF1B $\beta$  accumulated faster and  
154 more efficiently in cytoplasmic foci than the other two subunits. This rapid sequestration of  
155 eEF1B $\beta$  might interfere with eEF1B complex assembly and thus contribute to deceleration of  
156 translation as soon as temperatures rise.

157

158

## 159 **MATERIALS and METHODS**

160

### 161 MATERIALS and METHODS

162

#### 163 Plant material and growth conditions

164 All plants used in this study were in the *Arabidopsis thaliana* accession Columbia (Col0)  
165 background. The T-DNA insertion lines SAIL\_450\_F07 (*eef1by1-1*), GABI\_920E04 (*eef1by1-2*),  
166 GABI\_041E07 (*eef1by2-1*) and GABI\_473B05 (*eef1by2-2*), as well as the previously de-  
167 scribed *hsp101* mutant (Hong and Vierling, 2001; McLoughlin et al., 2019) were ordered from  
168 the Nottingham *Arabidopsis* Stock Centre. The *eef1by1-2 eef1by2-2 (eef1by1/2)* double mu-  
169 tant was obtained by crossing the respective single mutants. The complementation lines  
170 (p35S::YFP-eEF1B $\gamma$ 2, p35S::YFP-eEF1B $\beta$ 1 and p35S::YFP-eEF1B $\gamma$ 2 $\Delta$ N in *eef1by1/2*) were  
171 generated by floral painting (Clough and Bent, 1998) using *Agrobacterium tumefaciens*  
172 GV3101 harbouring full length coding sequence (CDS) or truncated version of eEF1B $\beta$ 1 or  
173 eEF1B $\gamma$ 2 in the pEarleyGate104 vector (Earley et al., 2006). The GFP reporter line contained  
174 a plasmid harbouring the coding sequence of GFP placed under the control of the 35S pro-  
175 moter. Primers for PCR-based genotyping are listed in Table S1. Plants were grown either  
176 on soil or on Murashige and Skoog (MS) medium containing 1% sucrose in liquid culture or  
177 with 1% (w/v) agar on plates in growth chambers (16 h light, 22°C/ 8 h dark, 18°C cycles). To  
178 test seed germination, seeds were sown on MS plates, stratified for three days and observed

179 every 12h after transfer to light. Seeds were counted as germinated when the radical  
180 emerged through the seed coat.

181

## 182 Heat stress assays

183 For analysis of seed germination after heat stress, seeds were stratified for three days in 1  
184 ml of liquid MS medium in tubes. Tubes with stratified seeds were subjected to 3.5 h at 45°C  
185 in a thermoincubator before sowing on solid MS plates. Seed germination was checked every  
186 24 h. For seedling-based heat stress assays, MS plates were placed in a temperature-  
187 controlled hot-air incubator. Root growth and hypocotyl elongation assays were performed as  
188 described previously (McLoughlin et al., 2016). For analysis of root growth after heat stress,  
189 seedlings were grown for 4d in light on MS plates in a vertical position. The following heat  
190 stress conditions were applied: 1.5 h at 38°C, 2 h at 22°C, 2 h at 45°C. Root tips were  
191 marked on the plates before seedlings were allowed to recover for 5d. Photographs were  
192 taken and root growth after application of heat stress was measured using ImageJ software  
193 (<http://imagej.nih.gov/ij/>). To analyse hypocotyl elongation, seedlings were grown for 2.5d in  
194 the dark, heat-stressed (1.5 h at 38°C, 2 h at 22°C, 3 h at 45°C), then the hypocotyl tips were  
195 marked and seedlings were grown again for 2.5d in the dark. Hypocotyl elongation after heat  
196 stress was measured again with ImageJ software. For seedling survival rate, seven-days-old  
197 seedlings grown on horizontal placed MS plates were heat-stressed (1.5 h at 38°C, 2 h at  
198 22°C, 2.5 h at 45°C) and allowed to recover for 5d before taking photographs. Seedling sur-  
199 vival was defined by growth of green true leaves. For long-term acquired thermotolerance,  
200 6d-old seedlings grown on horizontal placed MS plates were pre-heat treated (3h 30 min at  
201 38°C), allowed to recover for 2 days at 22°C, then heat treated again (100min at 45°C). Sev-  
202 en days after the second heat treatment, photographs were taken. Plant survival were evalu-  
203 ated regarding the presence of expanded green leaves. For ambient temperature stress,  
204 plants were germinated under control conditions (24h), then grown at control conditions  
205 (22°C) or under ambient temperature stress (27°C) on vertical placed MS plates for 7 days.  
206 Root length was measured using ImageJ software.

207

## 208 Root growth assay and propidium iodide and FM4-64 staining

209 For quantitative measurement of primary root length, seeds were stratified and grown for the  
210 indicated times on vertical MS plates. Root length was measured using ImageJ software. For  
211 treatment with translation inhibitors, seeds were germinated and grown on MS plates sup-  
212 plemented with cycloheximide (0.05  $\mu$ M or 0.1  $\mu$ M) or hygromycin B (10 mg/ml or 20 mg/ml).  
213 Root growth on translation inhibitors was normalized to root growth under standard condi-  
214 tions, resulting in relative root length. Propidium iodide (PI) staining of root tips was done in  
215 the following way: root tips were cut from seven-days-old seedlings and incubated for 1 min  
216 in 10  $\mu$ g/ml PI solution and imaged using confocal microscopy. The number of dividing cells  
217 within the root meristem was defined by counting the number of cortical cells within the meri-  
218 stem. FM4-64 staining was performed on first true leaves of 7d old seedlings. Leaves were  
219 stained for 30 min and washed twice in water and imaged using confocal microscopy.

220

## 221 Plasmid construction

222 For Y2H assays, the full length CDS of *eEF1B $\alpha$ 2* (AT5G19510), *eEF1B $\beta$ 1* (AT1G30230),  
223 *eEF1B $\gamma$ 1* (AT1G09640) and *eEF1B $\gamma$ 2* (AT1G57720) including the STOP were amplified by  
224 PCR and cloned into pENTR-D-TOPO or pDONR221 vectors (Thermo Fisher Scientific).  
225 After confirmation of the correct fragment by sequencing, Gateway LR Clonase II Enzyme  
226 mix (Thermo Fisher Scientific) was used to generate expression constructs in GAL4 DNA-  
227 binding domain vector pGBT-9 and the activation domain vector pGAD424 (Clontech). To

228 generate truncated versions of eEF1B $\gamma$ 1 and eEF1B $\gamma$ 2, full length constructs were used as  
229 templates for PCR amplification. Primers were designed so that predicted functionally do-  
230 mains should be conserved. For creation of YFP- and MYC-fusion constructs used in Co-IP  
231 experiments, LR reaction was used for recombination into pEarleyGate104 or  
232 pEarleyGate203 vectors (Earley et al., 2006). GFP and mCherry fusion constructs used in  
233 localisation studies were created by PCR amplification of the respective full length CDS with-  
234 out the STOP codon, cloned into pDONR221 and subsequent LR reaction into pABindGFP  
235 or pABindmCherry (Bleckmann et al., 2010). All primers are listed in Table S1.  
236

### 237 Y2H assays

238 Yeast strain AH109 was transformed with the respective gene-containing pGBT9 and  
239 pGAD424 vector according to (Gietz et al., 1997). Selection of positive transformants was  
240 performed on yeast minimal medium (SD medium: 0.66% yeast nitrogen base without amino  
241 acids, 0.066% amino acid mix, 2% glucose) lacking leucine and tryptophan (SD-LW). Yeast  
242 colonies were tested for plasmid insertion by colony PCR. Single positive colonies were used  
243 for overnight cultures grown in liquid SD-LW under continuous shaking for 16-18h at 30°C.  
244 Overnight culture was used to inoculate a pre-culture with OD<sub>600</sub>=0.3 and yeast was grown  
245 for 3h under continuous shaking at 30°C. Optical density was adjusted to OD<sub>600</sub>=4 and a  
246 dilution series from 10<sup>-1</sup> to 10<sup>-3</sup> was spotted on selection plates containing either SD-LW for  
247 growth control or SD-LWH for test of interaction. Data is representative for at least two inde-  
248 pendent experiments.  
249

### 250 Protoplast transformation

251 Protoplast isolation and transformation was performed as previously described with several  
252 adjustments (Yoo et al., 2007). Plants used for protoplast isolation were grown in short day  
253 conditions (8 h light, 22°C/16 h dark, 18°C cycles). Leaves from 6-weeks-old plants were cut  
254 in small stripes and incubated in enzyme-containing protoplasting buffer (500 mM sorbitol, 1  
255 mM CaCl<sub>2</sub>, 0.25% macerozym R10, 1% cellulase R10, 10 mM MES- KOH, pH 5.7) for 2 h at  
256 26°C with 40 rpm in the dark. Isolated protoplasts were washed twice in MaMG buffer (450  
257 mM sorbitol, 15 mM MgCl<sub>2</sub>, 5 mM MES-KOH, pH 5.7). For protoplast transformation, 300 $\mu$ l  
258 protoplast suspension was carefully mixed with 25  $\mu$ g plasmid DNA and 330  $\mu$ l PEG-Ca buff-  
259 er (40% PEG 4000, 200 mM mannitol, 100 mM CaCl<sub>2</sub>) and incubated for 30 min in the dark.  
260 To eliminate PEG, protoplasts were washed twice in 3 ml wash buffer (154 mM NaCl, 125  
261 mM CaCl<sub>2</sub>, 5 mM KCl, 5 mM glucose, 2 mM MES, pH 5.7) and finally left in 3 ml wash buffer  
262 for overnight incubation. Gene expression from estradiol-inducible pABind vectors was in-  
263 duced by addition of 50  $\mu$ M estradiol to the protoplasts for overnight incubation. Protoplast  
264 samples for Co-IP were collected from 1.5 ml protoplast suspension. The amounts of plasmid  
265 DNA, PEG-Ca and W5 buffer were adjusted accordingly.  
266

### 267 Protein extraction and Co-Immunoprecipitation

268 Frozen plant material was snap-frozen in liquid nitrogen and grinded to fine powder. Per 0.1  
269 g plant material, 200  $\mu$ l of RIPA buffer (25 mM Tris, 150 mM NaCl, 0.1 % SDS, 0.5 % Sodium  
270 deoxycholate, 1 % Triton X-100, cOmplete™ protease inhibitor cocktail (1:1000, Roche)) was  
271 added, carefully mixed and incubated for 30 min on ice. After centrifugation (8000 rpm, 20  
272 min, 4°C), supernatant was collected. Protein concentration was determined by Bradford  
273 Assay (Pierce Detergent Compatible Bradford Assay Kit) and 40  $\mu$ g of protein were mixed  
274 with 5x SDS loading dye and boiled for 5 min at 95°C. For co-immunoprecipitation, N-  
275 terminally YFP-tagged eEF1B subunits (in pEG104) were co-expressed with MYC-tagged  
276 eEF1B $\beta$ 1 or eEF1B $\gamma$ 2 (pEG203) in Arabidopsis protoplasts. After 24 h incubation, proto-



277 plasts were harvested by centrifugation at 14000 rpm for 5 s. Protoplast pellet was resus-  
278 pended in 250  $\mu$ l Lysis buffer (10 mM Tris, 150 mM NaCl, 0.5 mM EDTA, 0.1 % Triton X-100,  
279 cOMplete™ protease inhibitor cocktail (1:1000, Roche) and incubated for 15 min at 4°C. Af-  
280 ter centrifugation (14000 rpm, 10 min, 4°C), supernatant was transferred to a new tube. 45  $\mu$ l  
281 of supernatant were mixed with 5x SDS loading dye, boiled at 95°C for 5 min and used as  
282 “Input” sample. Remaining supernatant was diluted 1:5 with wash buffer (10mM Tris, 150  
283 mM NaCl, 0.5 mM EDTA) and added to 15  $\mu$ l GFP-Trap® Magnetic Agarose (Chromotek).  
284 Incubation and washing of beads were performed according to the manufacturer’s protocol.  
285 Beads were boiled at 95°C for 10 min in 50  $\mu$ l 2x SDS loading dye for elution.

286

#### 287 SDS-PAGE and Immunoblot Analysis

288 Denatured protein samples were loaded on 10 % (w/v) polyacrylamide gels for protein sepa-  
289 ration via SDS-PAGE. Proteins were transferred to a nitrocellulose membrane by semi-dry  
290 blotting. Primary antibodies used for immunoblotting were: anti-MYC-HRP (1:1000, R951-25,  
291 Thermo Scientific), anti-GFP (1:5000, G1544, Sigma), anti-EF1By (1:3000, AS10676,  
292 Agrisera), anti-Actin (1:1000, A0480, Sigma). As secondary antibodies, anti-rabbit-HRP  
293 (1:5000, 4750.1, Carl Roth) or anti-mouse-HRP (1:5000, A4416, Sigma) were applied.  
294 Chemiluminescent signal was visualized with Pierce™ ECL Western Blotting Substrate and  
295 detected at ChemiDoc Imaging System (BioRad). Quantification of western blots was per-  
296 formed by comparing band intensities using ImageJ software.

297

#### 298 SunSET method

299 SunSET method was performed as previously described (Van Hoewyk, 2016) with several  
300 modifications. Briefly, seeds were germinated and grown in liquid MS culture for 7 days un-  
301 der continuous shaking at 50 rpm in growth chambers. Seedlings were either pretreated with  
302 10  $\mu$ M or 100  $\mu$ M CHX for 4h or directly treated with 100  $\mu$ M Puromycin for 2h. Seedlings  
303 were washed three times for 5 min in water before snap-freezing in liquid nitrogen. Proteins  
304 were extracted, quantified and immunoblotted as described above. Antibodies used were  
305 anti-puromycin (1:1000, PMY-2A4, University of Iowa) and anti-mouse-HRP (1:2500, A4416,  
306 Sigma).

307

#### 308 Polysome analysis

309 Polysome analysis was performed according to a published procedure (Barkan, 1998) with  
310 some modifications: 4 ml lysate prepared from 400 mg frozen Arabidopsis tissue was loaded  
311 onto a 1-ml sucrose cushion (30% (w/v) sucrose, 100 mM KCl, 40 mM Tris acetate, pH 8.0,  
312 15 mM MgCl<sub>2</sub>, 5 mM 2-mercaptoethanol, 100  $\mu$ g ml<sup>-1</sup> chloramphenicol and 100  $\mu$ g ml<sup>-1</sup>  
313 cycloheximide) and centrifuged for 1.5 h at 4 °C and 303,800 g to pellet large  
314 ribonucleoproteins (RNPs, monosomes and polysomes). Subsequently, mRNAs from this  
315 pellet were size-separated according to their ribosome-loading by ultracentrifugation for 4 h  
316 at 4 °C and 169,000 g in previously described sucrose density gradients (Barkan, 1998). A  
317 density gradient fractionation system (Teledyne ISCO) was used to document a continuous  
318 UV absorbance profile at 254 nm for the sucrose gradient. Briefly, the bottom of the ultracen-  
319 trifuge tube containing the sucrose gradient was pierced to allow the subsequent introduction  
320 of a dense chase buffer (65% (w/v) sucrose), which raised the gradient through the UV de-  
321 tector and into the collection tubes by a peristaltic pump.

322

#### 323 Confocal laser scanning microscopy and Image Analysis

324 Confocal laser scanning microscopy was performed using the Leica TCS SP8 Confocal Plat-  
325 form (Leica Microsystems). Excitation wavelength of 476 nm was used for GFP and 561 nm

326 was used for mCherry/RFP. Emission was detected as follows: 498-514 nm for GFP, 590-  
327 630 nm for mCherry/RFP and 712-724 nm for auto-fluorescence of chloroplasts. All proto-  
328 plast images are shown as 2D maximum intensity projection from z-stacks. Cytoplasmic foci  
329 quantification from confocal images of protoplasts was performed using ImageJ version  
330 1.53n (<https://imagej.nih.gov/ij/index.html>). Pearson and Spearman's rank correlation coefficient  
331 were calculated using the ImageJ Plugin Coloc2 to analyze colocalization. Coefficient  
332 values can vary from -1 (negative correlation) to +1 (positive correlation). Frequency of  
333 colocalisation was calculated as percentage of foci showing both GFP- and mCherry-  
334 fluorescence compared to the total number of foci inside a protoplast. GFP-fluorescent foci,  
335 mCherry-fluorescent foci and foci showing both fluorophors were counted using the ImageJ  
336 Plugin Cell Counter. Size of foci was quantified using ImageJ macro 'Analyze particles', only  
337 foci with a size between 0,05 – 5  $\mu\text{m}^2$  were counted.

338

339 Gene expression and BioAnalyzer analysis

340 For semi-quantitative and quantitative PCR and BioAnalyzer analysis, RNA was extracted  
341 from seven-days-old seedlings grown on MS plates using the innuPREP Plant RNA kit  
342 (Analytik Jena Bio solutions). For BioAnalyzer analysis, RNA was analyzed using an Agilent  
343 2100 BioAnalyzer System (Agilent technologies) according to manufacturer's directions. For  
344 PCR analysis, RNA was transcribed to cDNA using the QuantiTect® Reverse Transcription  
345 kit (QIAGEN). DreamTaq Polymerase (Thermo Scientific) was used to perform semi-  
346 quantitative RT-PCR. qPCR experiments were performed using Rotor-Gene® SYBR® Green  
347 (QIAGEN) and a Rotorgene-Q cycler (QIAGEN). Generated data was quality controlled and  
348 normalized to the reference genes *FASS* (AT5G18580) and *SAND* (AT2G28390) using  
349 qbasePLUS 3.0 software (Hellemans et al., 2007). Primers are listed in Table S1.

350

351

## 352 Results

### 353 Interaction of the individual eEF1B subunits in Arabidopsis

354 The interactions between the individual subunits of the eEF1B complex have so far not been  
355 studied in plants. To test if eEF1B $\alpha$ , eEF1B $\beta$  and eEF1B $\gamma$  were present in one complex in  
356 Arabidopsis we performed co-immunoprecipitation experiments. To this end, MYC-tagged  
357 versions of eEF1B $\beta$ 1 or eEF1B $\gamma$ 1 were co-expressed with YFP-tagged eEF1B $\alpha$ 2 or  
358 eEF1B $\gamma$ 2 in protoplasts. Each subunit of the eEF1B complex is encoded by two genes. We  
359 chose for those experiments the sequence of eEF1B $\alpha$ 2 and of eEF1B $\beta$ 1 since according to  
360 the eFP Browser (Klepikova et al., 2016) these two genes were higher expressed in all tis-  
361 sues than eEF1B $\alpha$ 1 and eEF1B $\beta$ 2. The two genes encoding the eEF1B $\gamma$  subunit showed  
362 similar expression levels and therefore both of these genes were used for interaction studies.  
363 YFP-tagged proteins were enriched by incubation with GFP-antibody coupled beads and co-  
364 precipitated proteins were identified by immunoblotting. As expected, MYC-eEF1B $\beta$ 1 was  
365 efficiently co-eluted with YFP-eEF1B $\alpha$ 2 and YFP-eEF1B $\gamma$ 2 and MYC-eEF1B $\gamma$ 1 co-  
366 precipitated with YFP-eEF1B $\alpha$ 2 while no co-precipitation was observed with Citrine, which  
367 served as negative control (Fig. 1A). Interestingly, MYC-eEF1B $\gamma$ 1 also interacted with YFP-  
368 eEF1B $\gamma$ 2 (Fig. 1A). To analyze the physical interactions between individual subunits, we per-  
369 formed Yeast-two-hybrid (Y2H) assays. Full-length eEF1B $\beta$ 1 interacted with full-length  
370 eEF1B $\alpha$ 2, eEF1B $\gamma$ 1 and eEF1B $\gamma$ 2, whereas no interaction was found between eEF1B $\alpha$ 2 and  
371 eEF1B $\gamma$ 1 or eEF1B $\gamma$ 2 (Fig. 1B). This was unexpected since in other organisms it was shown  
372 that eEF1B $\gamma$  was able to bind to the other subunits and thus proposed to be the structural  
373 component of the complex (Jeppesen et al., 2003; Mansilla et al., 2002; Sasikumar et al.,

374 2012). In contrast to our Co-IP results, we did not observe an interaction between eEF1By1  
375 and eEF1By2 in Y2H, indicating that the two eEF1By proteins do not form heterodimers. The  
376 plant eEF1By1 protein contains, like its human counterpart, an N-terminal domain with two  
377 GST-like domains (GST\_N and GST\_C) and a conserved C-terminal domain (C-term) (Fig.  
378 1C). From the human eEF1By homologs, it is known that the N-terminus mediates interaction  
379 with the two other subunits (Mansilla et al., 2002). Since the human and the Arabidopsis  
380 eEF1By protein sequences share only 41% identity, we tested, if the N-terminus of  
381 AteEF1By was necessary for the interaction with eEF1B $\beta$ . Therefore, we cloned truncated  
382 versions of eEF1By1 and eEF1By2 into vectors for Y2H assays, which were either lacking  
383 the C-terminal domain (eEF1By1 $\Delta$ C and eEF1By2 $\Delta$ C) or the N-terminal domain  
384 (eEF1By1 $\Delta$ N and eEF1By2 $\Delta$ N) as schematically shown in Figure 1C. Consistent with the  
385 studies in human cells, we found that the two eEF1By constructs containing the C-terminus  
386 did not interact with eEF1B $\beta$ , while the N-terminus of eEF1By was sufficient for an interaction  
387 with eEF1B $\beta$  (Fig. 1D). Overall, our co-immunoprecipitation showed that the three eEF1B  
388 subunits are part of one complex in planta. Opposite to what was reported in studies with  
389 animal cells, the Y2H assays indicated that eEF1B $\beta$  might be the core component of the  
390 eEF1B complex in Arabidopsis, as it is able to bind to both other subunits.

391

### 392 **Impaired eEF1By-function leads to developmental defects**

393 To examine the function of eEF1By in plants, we characterised two T-DNA insertion lines for  
394 both eEF1By-encoding genes. The T-DNA insertions in eEF1By1 were localised to intron 1  
395 in *eef1by1-1* (SAIL\_450\_F07) and to exon 7 in *eef1by1-2* (GABI\_920E04). In *eEF1By2*, the  
396 T-

397 DNA inserts were localised to exon 7 in line *eef1by2-1* (GABI\_041E07) and the 3'-UTR in  
398 line

399 *eef1by2-2* (GABI\_473B05) (Fig. 2A). We confirmed that none of the homozygous mutant  
400 lines

401 produced any eEF1By full-length mRNA of the gene harbouring the insertion except for line  
402 *eef1by1-1* (Fig. 2B). Moreover, since the insertions in *eEF1By2* were located just before the  
403 STOP codon (*eef1by2-1*) and in the 3'UTR (*eef1by2-2*), we analysed its expression by RT-  
404 qPCR. These analyses revealed that *eEF1By2* mRNA levels were reduced to 30% in  
405 *eef1by2-1* and 20% in *eef1by2-2* relative to WT levels (Fig. 2C). The single mutant lines did  
406 not exhibit any phenotypic alterations compared to WT (Fig. 2D) indicating that eEF1By1 and  
407 eEF1By2 might act redundantly. Therefore, we generated double mutant lines. The only  
408 combination yielding homozygous double mutant plants was *eef1by1-2 eef1by2-2*, hereafter  
409 referred to as *eef1by1/2*. We confirmed that eEF1By protein levels were significantly de-  
410 creased in protein extracts of *eef1by1/2*, in which only 20% of WT protein levels were de-  
411 tected in immunoblots

412 using an eEF1By-specific antibody (Fig. 3A). In contrast to the single mutant lines, the  
413 *eef1by1/2* double mutant showed a pleiotropic developmental phenotype. Seed germination  
414 was retarded and occurred about 24 hours later than in WT (Fig. 3B). Seedlings exhibited  
415 reduced primary root length at 4, 7 and 10 days after germination (dag), when compared to  
416 WT (Fig. 3C and 3D). Since root length of 10 days-old *eef1by1/2* mutants equalled that of  
417 seven-days-old WT seedlings (Fig. 3D), growth retardation rather than growth arrest caused  
418 the short primary root phenotype in the double mutant. Analysis of propidium iodide (PI)  
419 stained root tips revealed that the number of dividing cells was significantly reduced in the  
420 proximal meristem of seedlings at 7dag in the double mutant compared to WT (Fig. 3E and  
421 3F). Moreover, 13 dag seedling exhibited a drastically reduced formation of lateral roots (Fig.  
422 3G). The delay in development was similarly present in above-ground tissue. 26 days-old

423 soil-grown double mutants were smaller compared to WT (Fig. 3H). The double mutant  
424 showed a delayed formation (Fig. 3I) and growth of rosette leaves (Fig. S1A and B). Shoot  
425 development (Fig. S1C) and the transition to flowering occurred also delayed (Fig. S1D).  
426 Adult plants reached the same size as WT, further confirming that development was delayed  
427 but not arrested in the mutant line. Siliques of the double mutant line produced a reduced  
428 number of viable seeds due to abortion of about 20 % of the seeds (Fig. S1E and F), indicat-  
429 ing a defect in embryogenesis. To demonstrate that the observed phenotype was due to re-  
430 duced eEF1B $\gamma$  levels, we generated a complementation construct harbouring a Pro35S-YFP-  
431 eEF1B $\gamma$ 2 fusion construct, which was transformed into the *eef1by1/2* mutant background.  
432 The expression of this YFP-eEF1B $\gamma$ 2 fusion construct in the complementation line  
433 (*eef1by1/2-C*) was confirmed by immunoblotting (Fig. 3A). In this line, all aspects of the dou-  
434 ble mutant phenotype as shown for root length, lateral root formation and rosette growth  
435 were largely rescued (Fig. 3C, 3D, 3G, 3H and 3I). Together these analyses revealed that  
436 the two eEF1B $\gamma$ -encoding genes acted redundantly and that impaired eEF1B $\gamma$  function af-  
437 fected numerous developmental processes, especially those that are associated with rapid  
438 cell proliferation. To evaluate the impact of the interaction between eEF1B $\gamma$  and eEF1B $\beta$  on  
439 eEF1B $\gamma$ 's developmental function, additional complementation studies were performed. As  
440 we found in our Y2H assay that the N-terminus of eEF1B $\gamma$  was essential for the interaction  
441 with eEF1B $\beta$ , we generated a complementation construct harbouring the N-terminally trun-  
442 cated version of eEF1B $\gamma$  (Pro35S-YFP-eEF1B $\gamma$ 2 $\Delta$ N) and transformed it into the *eef1by1/2*  
443 double mutant background. Analysis of root growth parameters in these transgenic plants  
444 revealed that the truncated eEF1B $\gamma$ 2 $\Delta$ N was not able to complement the phenotype (Fig.  
445 S2). This indicated that the ability of eEF1B $\gamma$  to interact with the other components of the  
446 eEF1B complex was necessary for its function and thus that most probably the *eef1by1/2*  
447 mutant phenotype was due to reduced activity of the whole eEF1B complex.

448

#### 449 **Role of eEF1B $\gamma$ during protein synthesis**

450 To investigate, if the growth defects of *eef1by1/2* were due to impaired protein synthesis  
451 rates, we assayed the sensitivity of WT and mutant seedlings to the translation inhibitors  
452 cycloheximide (CHX) and hygromycin B (HYG). Both of these compounds are known to in-  
453 hibit the translation elongation process (Kurepa et al., 2010). We expected that treatment  
454 with low concentrations of a compound that interfered with the same process that was consti-  
455 tutively affected in the double mutant line should have a weaker effect in the double mutant  
456 than in the WT. As expected, root length of WT seedlings grown for four days on MS-plates  
457 containing low concentrations of cycloheximide was significantly reduced. At a concentration  
458 of 0.05  $\mu$ M CHX, WT roots showed only 81% and at 0.1  $\mu$ M CHX only 50% of root length that  
459 was reached at standard conditions. In contrast, root length of the *eef1by1/2* double mutant  
460 was almost not affected at 0.05  $\mu$ M CHX, and at 0.1  $\mu$ M CHX only reduced to 90% as com-  
461 pared to standard conditions (Fig. 4A) and thus significantly less affected than in the WT.  
462 We obtained a similar result by treatment of seedlings with hygromycin B (Fig. 4A). The  
463 lower sensitivity of the double mutant to both of these compounds suggested that an im-  
464 paired translation rate accounted for the reduced growth phenotype.

465 To analyse translation activity in a more direct manner, we analysed polysome-bound and  
466 thus translationally active mRNAs on sucrose gradients in leaves of 24-days-old WT and  
467 mutant plants. The polysome profiles revealed higher peaks for all fractions (monosomes,  
468 disomes and polysomes) (Fig. 4C) in the mutant samples compared to WT. The significantly  
469 increased total peak area indicated that the mutant line accumulated more mRNAs associ-  
470 ated with ribosomal complexes than the WT (Fig. 4D). To test if this was associated with an  
471 increased abundance of ribosomes we isolated total RNA from the same samples and de-

472 termed the relative amount of ribosomal RNA (rRNA) using a BioAnalyzer. Indeed, quantifi-  
473 cation of the peak area for 18S and 28S rRNA revealed that the amount of 28S rRNA was  
474 significantly increased in the mutant compared to the WT (Figure 4E). To investigate if this  
475 over-accumulation of ribosomal complexes was due to an increased cell number per leaf  
476 area we analysed the first true leaves of seven days-old seedlings by FM4-64 staining of cell  
477 walls. We found that cell number and thus cell size was not significantly different in WT and  
478 mutant samples, indicating that the mutant produced more ribosomal complexes per cell  
479 (Fig. 4F; Fig. S3E). Further analysis of the polysome profiles revealed that the double mutant  
480 showed a significantly higher ratio of polysomal to monosomal RNAs than the WT (Fig. 4G).  
481 A higher fraction of polysomal RNA would be expected to lead to a higher overall protein  
482 synthesis rate. We therefore assessed the protein synthesis rate in WT and mutant samples  
483 using the SunSET method (Van Hoewyk, 2016). To this end seven days-old seedlings were  
484 treated with puromycin, which is an analog of aminoacyl-tRNAs and transferred onto elongat-  
485 ing polypeptide chains. The puromycin-labeled proteins were detected by western blotting  
486 using a puromycin-specific antibody and the intensity of the bands is a measure for the total  
487 protein synthesis rate. We found that WT and mutant samples showed a similar pattern of  
488 puromycin-labeled proteins (Fig. 4H) indicating that the total protein synthesis rate was not  
489 changed in the mutant line. As proof of concept, seedlings were treated prior to the puromy-  
490 cin incubation with the translation inhibitor CHX, which efficiently blocked translation and  
491 resulted in no detection of puromycin-labeled proteins. We concluded from these results that  
492 despite the increased number of ribosomes and accumulation of polysome-associated  
493 mRNA molecules, protein synthesis rate was not increased in the mutant line. This result  
494 indicates that the average ribosome transit time on mRNAs is increased which would be in-  
495 dicative for impaired translation elongation or termination.

496

#### 497 **Reduced eEF1By function did not influence heat sensitivity**

498 At high temperature stress eEF1By proteins were shown to become insoluble and to interact  
499 with sHSPs, which enabled their rapid resolubilisation during recovery from heat stress  
500 (McLoughlin et al., 2016; McLoughlin et al., 2019). It was therefore suggested that eEF1By  
501 proteins might be specifically heat sensitive and that their activity might be required for re-  
502 covery of translation activity after heat stress (McLoughlin et al., 2016). We therefore used  
503 the established double mutant line to test if eEF1By activity was important during high tem-  
504 perature stress. We analyzed basal thermotolerance by quantifying the germination rate of  
505 seeds that were incubated for 3.5 hours at 45°C. This treatment reduced the germination rate  
506 of WT and the *eef1by1/2* mutant to a similar level (Fig. 5A). In contrast, the *hsp101* mutant,  
507 which is impaired in HSP101 function and was used as a heat sensitive control line (Hong  
508 and Vierling, 2001; McLoughlin et al., 2019), was much more affected (Fig. 5A). We next  
509 investigated acquired heat tolerance by quantifying hypocotyl elongation in etiolated seed-  
510 lings (Fig. 5B), root growth of four-days-old light-grown seedlings (Fig. 5C) and survival rate  
511 of seven-days-old seedlings (Fig. 5D) using the following treatment: acclimation at 38°C for  
512 90 min followed by 120 min at room temperature and subsequent heat incubation at 45°C for  
513 . In each of these assays, the *eef1by1/2* mutant line behaved in a similar way as the WT,  
514 while the *hsp101* mutant was much more severely affected. The *eef1by1/2* double mutant  
515 but not the *hsp101* mutant showed also a similar behavior as WT in assays for long-term  
516 acquired thermotolerance (LAT) (Fig. S4A and B). Upon growth at increased ambient tem-  
517 perature, the *hsp101* and the *eef1by1/2* line behaved like WT (Fig. S4C and D). In conclu-  
518 sion, our data showed that reduced eEF1By function did not interfere with response to and  
519 recovery from heat stress.

520

521 **Each component of the eEF1B complex co-localises with PAB8 in heat stress induced**  
522 **cytoplasmic foci**

523 Each of the three eEF1B subunits was found in the list of proteins that accumulated in heat-  
524 induced SGs of seedlings based on mass spectrometric analyses (Kosmacz et al., 2019). In  
525 order to validate this result, we used GFP-fusion constructs of eEF1B $\alpha$ , eEF1B $\beta$  and eEF1B $\gamma$   
526 that were co-expressed with PAB8-mCherry, a well established marker for SGs (Tabassum  
527 et al., 2020), in Arabidopsis protoplasts. All fusion constructs were expressed under the con-  
528 trol of the estradiol-inducible 35S promotor. We confirmed the integrity of the fusion con-  
529 structs during expression in protoplasts by immunoblotting using GFP and RFP- specific an-  
530 tibodies (Fig. S5). Co-localization of the three eEF1B-GFP fusion proteins with PAB8-  
531 mCherry showed that under control conditions, each of the proteins was uniformly distributed  
532 in the cytoplasm. After incubation of protoplasts at 42°C for one hour, cytoplasmic foci were  
533 observed (Fig. 6A). The GFP signal of each of the eEF1B subunit fusion constructs largely  
534 co-localized with PAB8-mCherry in cytoplasmic foci. This co-localization was analysed by  
535 calculating the Pearson correlation and Spearman's rank coefficients. For all combinations  
536 the coefficients were close to 1, which indicates a high co-localization between the proteins  
537 (Fig. 6B). Additionally, we counted the frequency of cytoplasmic foci, which showed co-  
538 localisation of each of the GFP fusion proteins with PAB8-mCherry. Although the frequency  
539 of co-localization was higher than 50% for all three subunits, eEF1B $\beta$ 1-GFP showed the  
540 highest co-localization frequency with PAB8-mCherry (Fig. 6C). To show that the observed  
541 stress granules are not only formed in protoplasts but also in intact plant tissues, we ana-  
542 lysed stably transformed plants constitutively expressing the following constructs: *p35S:YFP-*  
543 *eEF1B $\beta$ 1* or *p35S:YFP-eEF1B $\gamma$ 2*. As control, we used plants stably expressing *p35S:GFP*.  
544 Analysis of root tip epidermis cells of 4 dag seedlings revealed a uniformly distributed fluo-  
545 rescence in the cytoplasm for each construct under control conditions. Upon incubation at  
546 42°C for 20 minutes, YFP-tagged eEF1B $\beta$ 1 and eEF1B $\gamma$ 2 accumulated in cytoplasmic foci  
547 while the fluorescence signal of cells expressing free GFP remained unchanged. Moreover,  
548 analysis of the same roots after recovery for 12 hours at 22°C revealed that cytoplasmic foci  
549 were not visible anymore and the fluorescence was again uniformly distributed in the cyto-  
550 plasm (n=30 per line, measured in 3 independent experiments) (Fig. S6).

551 Our findings confirm that all eEF1B subunits are recruited to cytoplasmic stress granules  
552 upon heat stress. However, the size and number of the cytoplasmic foci formed by the indi-  
553 vidual subunits varied strongly. To quantify this observation we measured the number and  
554 size of foci in 30 protoplasts from three independent experiments. Representative pictures of  
555 protoplasts for each construct are shown in Figure 7A. Interestingly, this analysis revealed an  
556 increased size and number of foci in protoplasts expressing eEF1B $\beta$ 1-GFP or PAB8-  
557 mCherry than in protoplasts expressing eEF1B $\alpha$ 2-GFP or eEF1B $\gamma$ 2-GFP (Fig. 7B and C).  
558 Our Y2H experiments showed that eEF1B $\beta$  was the only subunit able to physically interact  
559 with the two other subunits. Therefore, we next analysed if the presence of eEF1B $\beta$  influ-  
560 enced the recruitment of eEF1B $\alpha$  or eEF1B $\gamma$  into stress granules by co-expressing eEF1B $\alpha$  or  
561 eEF1B $\gamma$  with eEF1B $\beta$  in protoplasts. Interestingly, we observed that eEF1B $\alpha$ 1 or eEF1B $\gamma$ 2  
562 accumulated more often in cytoplasmic foci, when they were co-expressed together with  
563 eEF1B $\beta$  compared to co-expression of eEF1B $\alpha$  with eEF1B $\gamma$ 2 or of eEF1B $\gamma$ 2 with eEF1B $\alpha$   
564 (Fig. 8A). We quantified this observation by counting how many foci per cell showed either  
565 GFP or mCherry fluorescence or both signals in protoplasts co-expressing the following  
566 combinations: eEF1B $\alpha$ 2-GFP and eEF1B $\beta$ 1-mCherry, eEF1B $\alpha$ 2-GFP and eEF1B $\gamma$ 2-  
567 mCherry, eEF1B $\beta$ 1-GFP and eEF1B $\gamma$ 2-mCherry, eEF1B $\gamma$ 2-GFP and eEF1B $\alpha$ 1-mCherry (Fig.  
568 8B). These findings indicated that eEF1B $\beta$  not only accumulates more efficiently in SGs than  
569 the two other subunits but also seems to promote recruitment of the two other subunits to

570 stress granules. It seems tempting to speculate that this might be an additional mechanism  
571 contributing to adjustment of protein translation rates to increasing temperatures.

572

573

## 574 **DISCUSSION**

575

576 In plants, the response to environmental stresses is not only controlled at the transcriptional  
577 level but also involves rapid adaption of translation rates in order to maintain protein homeo-  
578 stasis. An immediate response to increased temperature stress is the rapid inhibition of  
579 translation and the formation of SGs (Chantarachot and Bailey-Serres, 2018; Maruri-Lopez et  
580 al., 2021). Several lines of evidence have suggested that the eEF1B complex might be in-  
581 volved in these processes in plants. Here we addressed the function of one component of  
582 the eEF1B complex using Arabidopsis mutants with reduced expression of the eEF1By sub-  
583 unit. Analysis of this mutant line revealed that eEF1By is essential for normal growth and  
584 development at control conditions and influences ribosome abundance and polysome pro-  
585 files. We also tested the ability of the established mutant line to adapt to increased tempera-  
586 ture stress and examined the dynamic localisation of each of the three eEF1B subunits at  
587 increased temperature.

588

### 589 **The role of eEF1By during growth, development and translation**

590 Unlike eEF1B $\alpha$  and eEF1B $\beta$ , eEF1By lacks guanine nucleotide exchange activity and was  
591 therefore proposed to act as structural protein that is important for scaffolding of the eEF1B  
592 complex (Le Sourd et al., 2006). Our Y2H data showed that plant eEF1By also required its  
593 conserved N-terminal domain for interaction with the other eEF1B subunits. However, unlike  
594 in human cells, plant eEF1By physically interacted only with the eEF1B $\beta$  subunit. We found  
595 that eEF1B $\beta$  was able to physically interact with the other two subunits and thus might, apart  
596 from being guanine nucleotide exchange protein, also be important for eEF1B complex as-  
597 sembly in plants (Fig. 1). Although eEF1By does not seem to serve as structural component,  
598 it might still act as a scaffolding protein that controls the intracellular localization or enhances  
599 the activity of the eEF1B complex. So far, not much was known about specific functions of  
600 individual eEF1B subunits in plants. In Arabidopsis, a T-DNA insertion line for one of the two  
601 homologous genes encoding the eEF1B $\beta$  subunit was characterized (Hossain et al., 2012)  
602 and shown to exhibit a dwarf phenotype associated with defects in cell wall formation  
603 (Hossain et al., 2012). For the two other eEF1B subunits no loss of function mutant analyses  
604 have - at least to our knowledge - so far been published in plants. Structural analyses of the  
605 human eEF1B complex revealed that the presence of eEF1By enhanced the catalytic activity  
606 of eEF1B $\alpha$  (Trosiuk et al., 2016). In yeast, the eEF1B complex has two subunits, namely  
607 eEF1B $\alpha$  and eEF1By. While eEF1B $\alpha$  is essential for growth and survival (Hiraga et al.,  
608 1993), deletion of eEF1By did not result in any obvious defects in protein synthesis or growth  
609 at control conditions (Kinzy et al., 1994). Nonetheless, its absence impaired response to oxi-  
610 dative stress and lead to defects in protein turnover and accumulation of cytotoxic proteins  
611 under conditions of oxidative stress (Olarewaju et al., 2004).

612 Our analysis of the *eef1by1/2* double mutant line uncovered an essential function for the  
613 eEF1By subunit during normal growth and cell division in plants. The analysis of polysome  
614 profiles and protein synthesis rates revealed that the *eef1by1/2* double mutant contained a  
615 higher number of ribosomes per cell (Fig. 4) and more polysome associated mRNAs while  
616 total protein synthesis rates remained unchanged. A similar effect was previously described  
617 to occur in yeast upon treatment with oxidative stress and was suggested to indicate attenu-  
618 ated translation elongation and termination (Shenton et al., 2006). It is tempting to speculate



619 that reduced eEF1By levels lead to disturbed translation kinetics through reduced availability  
620 of EF1A:aa-tRNA:GTP ternary complexes and thus impaired translation elongation effi-  
621 ciency. Translation elongation kinetics is known to be influenced by many different factors,  
622 including codon usage, mRNA secondary structures and ribosome stalling signals (Rodnina  
623 and Wintermeyer, 2016). Deceleration of translation can on the one hand enable proper fold-  
624 ing of nascent protein chains, which is especially important for long proteins. On the other  
625 hand, it can reduce translational fidelity and lead to frame shifting or amino acid mis-  
626 incorporation (Stein and Frydman, 2019). Our phenotypic analyses revealed that the mutant  
627 line showed significantly delayed development of all organs, while the final size and shape of  
628 adult plants was unaffected (Fig. 3). It is likely but still needs to be proven that the retarded  
629 growth phenotype of the *eef1by1/2* mutant line is due to altered translation kinetics and/or  
630 impaired protein homeostasis. A similar growth phenotype was previously reported for other  
631 mutants affected in general protein biosynthesis such as mutants for the RNA binding protein  
632 PUM23 that is involved in rRNA processing (Abbasi et al., 2010) and the translation initiation  
633 factor subunits eIF3h (Kim et al., 2004) or eIF5B (Zhang et al., 2017). Interestingly, the Ara-  
634 bidopsis eEF1By protein contains, like many other metazoan eEF1By proteins, two consen-  
635 sus CDK phosphorylation sites. One of these sites is located in the N-terminal domain that is  
636 required for interaction with eEF1Bβ (Fig. 1C). In mammalian cells, it was shown that during  
637 mitosis eEF1By becomes phosphorylated to control translation rates in a spatiotemporal  
638 manner (Kalous et al., 2020). It will be interesting to test in future experiments, if eEF1By  
639 phosphorylation occurs also in plants during mitosis and serves a similar function.

640

#### 641 **The role of the eEF1B complex during heat stress**

642 In order to test if eEF1By activity was important for heat stress recovery, we analysed the  
643 thermotolerance of the *eef1by1/2* mutant line. We found that plants impaired in eEF1By ac-  
644 tivity presented the same thermosensitivity as WT. Thus, eEF1By does not seem to be a  
645 limiting factor for rapid recovery of protein synthesis rates after heat-induced translational  
646 arrest. Nevertheless, several reports suggested that the eEF1B complex might be involved in  
647 heat stress response as a component of stress granules. First, eEF1By was found to accu-  
648 mulate in stress granules after robust heat shock in yeast (Grousl et al., 2013). Second, in  
649 plants, eEF1Bβ and eEF1By were shown to be bound to sHSPs and to co-localise with them  
650 in heat-induced cytoplasmic foci. After recovery, the HSP101 disaggregase was shown to be  
651 required for resolubilisation of eEF1B subunits (McLoughlin et al., 2016). Third, in an inde-  
652 pendent study the three eEF1B subunits were found as components of heat-induced stress  
653 granules (Kosmacz et al., 2019). It was therefore suggested that eEF1Bs are either them-  
654 selves thermally-labile proteins or that they bind to other thermally-labile proteins  
655 (McLoughlin et al., 2016).

656 Here we showed that each of the eEF1B subunits co-localized with the stress granule marker  
657 PAB8 upon heat stress (Fig. 6). Interestingly, we found that eEF1Bβ accumulated in foci of  
658 increased size and number compared to eEF1Bα and eEF1By (Fig. 7). Moreover, the heat-  
659 induced accumulation of eEF1Bα-GFP or eEF1By-GFP in cytoplasmic foci was promoted by  
660 co-expression of eEF1Bβ-mCherry (Fig. 8). Our interaction data indicated that eEF1Bβ ap-  
661 pears to be the core subunit connecting eEF1Bα and eEF1By. This suggests that the rapid  
662 association of eEF1Bβ with foci might ensure efficient disassembly of the eEF1B complex  
663 and thus downregulation of translation upon heat stress. A similar effect has been observed  
664 in yeast, in which certain elongation factors including eEF1By2 accumulated in cytoplasmic  
665 foci already upon mild heat shock and it was hypothesized that these fast aggregating trans-  
666 lation elongation factors served as 'nucleation site' for assembling stress granule compo-  
667 nents (Grousl et al., 2013). Several reports have shown that so-called nucleating proteins

668 can promote stress granule formation (Panas et al., 2016). Most SG-nucleating proteins have  
669 distinct properties, e.g. intrinsically disordered protein regions or low complexity sequences  
670 like prion-like domains, which facilitate liquid-liquid phase separation (Fomicheva and Ross,  
671 2021; Panas et al., 2016). So far, none of these properties has been described for any of the  
672 eEF1B subunits. Therefore, further experiments are needed to investigate the exact nature  
673 and role of eEF1B $\beta$ -associated foci during stress response. Recent research in human cells  
674 indicated that localization of mRNA in stress granules does not only lead to global  
675 downregulation of translation, but also promotes targeted translation of specific transcripts  
676 necessary for stress response (Maruri-Lopez et al., 2021; Mateju et al., 2020; Wilbertz et al.,  
677 2019). Whether the rapid temperature-induced recruitment of the eEF1B complex to SGs is  
678 also involved in these processes in plants remains to be analyzed.

679  
680

### 681 **SUPPLEMENTARY DATA**

682 Supplementary data are available at *JXB* online.

683 Table S1: List of primers used in this study.

684 Figure S1: Phenotype of the *eef1by1/2* double mutant, *eef1by1* and *eef1by2* single mutants.

685 Figure S2: The truncated version of eEF1B $\gamma$  (YFP-eEF1B $\gamma$  $\Delta$ N) does not complement the  
686 phenotype of the *eef1by1/2* double mutant.

687 Figure S3: Quantification of rRNA levels and cell size in WT and mutant plants.

688 Figure S4: The *eef1by1/2* mutant does not display altered thermotolerance.

689 Figure S5: Integrity of GFP- and mCherry-fusion proteins.

690 Figure S6: eEF1B $\beta$ 1 and eEF1B $\beta$ 2 accumulate in stress granules in Arabidopsis roots after  
691 heat stress.

692

### 693 **ACKNOWLEDGEMENTS**

694 We thank Wiebke Hellmeyer, Judith Mehrmann, Teresa Wulf and Zhijian Zhang for technical  
695 assistance. Special thanks go to Mahsa Nasimi, Felix Christian Thies and Florian Pomrehn  
696 for experimental support and technical assistance. We thank Dr. Justin Lee (IPB, Halle) for  
697 providing the plasmid pUBN-RFP-PAB8. The antibody PMY-2A4 developed by Jonathan  
698 Yewdell was obtained from the Developmental Studies Hybridoma Bank, created by the  
699 NICHD of the NIH and maintained at The University of Iowa, Department of Biology, Iowa  
700 City, IA 52242. This work was funded by the Deutsche Forschungsgemeinschaft (DFG) grant  
701 to MW (WE4506/6-1). CLH was supported by a UHH fellowship.

702

### 703 **AUTHOR CONTRIBUTIONS**

704 MW and JL designed the project.

705 JL, CLH, YG, and RZ performed experiments and analyzed data.

706 MW acquired funding.

707 MW, JL and CLH wrote the manuscript.

708

### 709 **DATA AVAILABILITY STATEMENT**

710 All data supporting the findings of this study are available within the paper and within its sup-  
711 plementary materials published online. The data supporting the findings of this study are  
712 available from the corresponding author, (Magdalena Weingartner), upon request.

### **REFERENCES**

- Abbasi, N., H.B. Kim, N.I. Park, H.S. Kim, Y.K. Kim, Y.I. Park, and S.B. Choi. 2010. APUM23, a nucleolar Puf domain protein, is involved in pre-ribosomal RNA processing and normal growth patterning in Arabidopsis. *Plant J* 64:960-976.
- Barkan, A. 1998. Approaches to investigating nuclear genes that function in chloroplast biogenesis in land plants. *Method Enzymol* 297:38-57.
- Bleckmann, A., S. Weidtkamp-Peters, C.A. Seidel, and R. Simon. 2010. Stem cell signaling in Arabidopsis requires CRN to localize CLV2 to the plasma membrane. *Plant Physiol* 152:166-176.
- Browning, K.S., and J. Bailey-Serres. 2015. Mechanism of cytoplasmic mRNA translation. *Arabidopsis Book* 13:e0176.
- Chantarachot, T., and J. Bailey-Serres. 2018. Polysomes, Stress Granules, and Processing Bodies: A Dynamic Triumvirate Controlling Cytoplasmic mRNA Fate and Function. *Plant Physiol* 176:254-269.
- Cherkasov, V., S. Hofmann, S. Druffel-Augustin, A. Mogk, J. Tyedmers, G. Stoecklin, and B. Bukau. 2013. Coordination of translational control and protein homeostasis during severe heat stress. *Curr Biol* 23:2452-2462.
- Clough, S.J., and A.F. Bent. 1998. Floral dip: a simplified method for Agrobacterium-mediated transformation of Arabidopsis thaliana. *Plant J* 16:735-743.
- Earley, K.W., J.R. Haag, O. Pontes, K. Opper, T. Juehne, K. Song, and C.S. Pikaard. 2006. Gateway-compatible vectors for plant functional genomics and proteomics. *Plant J* 45:616-629.
- Fomicheva, A., and E.D. Ross. 2021. From Prions to Stress Granules: Defining the Compositional Features of Prion-Like Domains That Promote Different Types of Assemblies. *Int J Mol Sci* 22:
- Gietz, R.D., B. Triggs-Raine, A. Robbins, K.C. Graham, and R.A. Woods. 1997. Identification of proteins that interact with a protein of interest: applications of the yeast two-hybrid system. *Mol Cell Biochem* 172:67-79.
- Grousl, T., P. Ivanov, I. Malcova, P. Pompach, I. Frydlova, R. Slaba, L. Senohrabkova, L. Novakova, and J. Hasek. 2013. Heat Shock-Induced Accumulation of Translation Elongation and Termination Factors Precedes Assembly of Stress Granules in *S. cerevisiae*. *Plos One* 8:
- Hellemans, J., G. Mortier, A. De Paepe, F. Speleman, and J. Vandesompele. 2007. qBase relative quantification framework and software for management and automated analysis of real-time quantitative PCR data. *Genome Biol* 8:R19.
- Hiraga, K., K. Suzuki, E. Tsuchiya, and T. Miyakawa. 1993. Cloning and Characterization of the Elongation-Factor Ef-1-Beta Homolog of Saccharomyces-Cerevisiae - Ef-1-Beta Is Essential for Growth. *Febs Lett* 316:165-169.
- Hong, S.W., and E. Vierling. 2001. Hsp101 is necessary for heat tolerance but dispensable for development and germination in the absence of stress. *Plant J* 27:25-35.
- Hossain, Z., L. Amyot, B. McGarvey, M. Gruber, J. Jung, and A. Hannoufa. 2012. The translation elongation factor eEF-1Bbeta1 is involved in cell wall biosynthesis and plant development in Arabidopsis thaliana. *Plos One* 7:e30425.

- Ivanov, P., N. Kedersha, and P. Anderson. 2019. Stress Granules and Processing Bodies in Translational Control. *Cold Spring Harb Perspect Biol* 11:
- Jackson, R.J., C.U. Hellen, and T.V. Pestova. 2010. The mechanism of eukaryotic translation initiation and principles of its regulation. *Nat Rev Mol Cell Biol* 11:113-127.
- Jeppesen, M.G., P. Ortiz, W. Shepard, T.G. Kinzy, J. Nyborg, and G.R. Andersen. 2003. The crystal structure of the glutathione S-transferase-like domain of elongation factor 1B gamma from *Saccharomyces cerevisiae*. *J Biol Chem* 278:47190-47198.
- Kalous, J., D. Jansova, and A. Susor. 2020. Role of Cyclin-Dependent Kinase 1 in Translational Regulation in the M-Phase. *Cells* 9:
- Kim, T.H., B.H. Kim, A. Yahalom, D.A. Chamovitz, and A.G. von Arnim. 2004. Translational regulation via 5' mRNA leader sequences revealed by mutational analysis of the Arabidopsis translation initiation factor subunit eIF3h. *Plant Cell* 16:3341-3356.
- Klepikova, A.V., A.S. Kasianov, E.S. Gerasimov, M.D. Logacheva, and A.A. Penin. 2016. A high resolution map of the Arabidopsis thaliana developmental transcriptome based on RNA-seq profiling. *Plant J* 88:1058-1070.
- Kobayashi, S., S. Kidou, and S. Ejiri. 2001. Detection and characterization of glutathione S-transferase activity in rice EF-1betabeta'gamma and EF-1gamma expressed in *Escherichia coli*. *Biochem Biophys Res Commun* 288:509-514.
- Kosmacz, M., M. Gorka, S. Schmidt, M. Luzarowski, J.C. Moreno, J. Szlachetko, E. Leniak, E.M. Sokolowska, K. Sofroni, A. Schnittger, and A. Skiryycz. 2019. Protein and metabolite composition of Arabidopsis stress granules. *New Phytol* 222:1420-1433.
- Le Sourd, F., S. Boulben, R. Le Bouffant, P. Cormier, J. Morales, R. Belle, and O. Mulner-Lorillon. 2006. eEF1B: At the dawn of the 21st century. *Biochim Biophys Acta* 1759:13-31.
- Mansilla, F., I. Friis, M. Jadidi, K.M. Nielsen, B.F. Clark, and C.R. Knudsen. 2002. Mapping the human translation elongation factor eEF1H complex using the yeast two-hybrid system. *Biochem J* 365:669-676.
- Maruri-Lopez, I., N.E. Figueroa, I.E. Hernandez-Sanchez, and M. Chodasiewicz. 2021. Plant Stress Granules: Trends and Beyond. *Front Plant Sci* 12:722643.
- Mateju, D., B. Eichenberger, F. Voigt, J. Eglinger, G. Roth, and J.A. Chao. 2020. Single-Molecule Imaging Reveals Translation of mRNAs Localized to Stress Granules. *Cell* 183:1801-1812 e1813.
- McLoughlin, F., E. Basha, M.E. Fowler, M. Kim, J. Bordowitz, S. Katiyar-Agarwal, and E. Vierling. 2016. Class I and II Small Heat Shock Proteins Together with HSP101 Protect Protein Translation Factors during Heat Stress. *Plant Physiol* 172:1221-1236.
- McLoughlin, F., M. Kim, R.S. Marshall, R.D. Vierstra, and E. Vierling. 2019. HSP101 Interacts with the Proteasome and Promotes the Clearance of Ubiquitylated Protein Aggregates. *Plant Physiol* 180:1829-1847.
- Merchante, C., A.N. Stepanova, and J.M. Alonso. 2017. Translation regulation in plants: an interesting past, an exciting present and a promising future. *Plant J* 90:628-653.
- Olarewaju, O., P.A. Ortiz, W.Q. Chowdhury, I. Chatterjee, and T.G. Kinzy. 2004. The translation elongation factor eEF1B plays a role in the oxidative stress response pathway. *RNA Biol* 1:89-94.

- Panas, M.D., P. Ivanov, and P. Anderson. 2016. Mechanistic insights into mammalian stress granule dynamics. *J Cell Biol* 215:313-323.
- Protter, D.S.W., and R. Parker. 2016. Principles and Properties of Stress Granules. *Trends Cell Biol* 26:668-679.
- Rodnina, M.V., and W. Wintermeyer. 2016. Protein Elongation, Co-translational Folding and Targeting. *J Mol Biol* 428:2165-2185.
- Sasikumar, A.N., W.B. Perez, and T.G. Kinzy. 2012. The many roles of the eukaryotic elongation factor 1 complex. *Wiley Interdiscip Rev RNA* 3:543-555.
- Schuller, A.P., and R. Green. 2018. Roadblocks and resolutions in eukaryotic translation. *Nat Rev Mol Cell Biol* 19:526-541.
- Shenton, D., J.B. Smirnova, J.N. Selley, K. Carroll, S.J. Hubbard, G.D. Pavitt, M.P. Ashe, and C.M. Grant. 2006. Global translational responses to oxidative stress impact upon multiple levels of protein synthesis. *J Biol Chem* 281:29011-29021.
- Stein, K.C., and J. Frydman. 2019. The stop-and-go traffic regulating protein biogenesis: How translation kinetics controls proteostasis. *J Biol Chem* 294:2076-2084.
- Tabassum, N., L. Eschen-Lippold, B. Athmer, M. Baruah, M. Brode, L.D. Maldonado-Bonilla, W. Hoehenwarter, G. Hause, D. Scheel, and J. Lee. 2020. Phosphorylation-dependent control of an RNA granule-localized protein that fine-tunes defence gene expression at a post-transcriptional level. *Plant J* 101:1023-1039.
- Trosiuk, T.V., V.F. Shalak, R.H. Szczepanowski, B.S. Negrutskii, and A.V. El'skaya. 2016. A non-catalytic N-terminal domain negatively influences the nucleotide exchange activity of translation elongation factor 1B $\alpha$ . *FEBS J* 283:484-497.
- Van Hoewyk, D. 2016. Use of the non-radioactive SUNSET method to detect decreased protein synthesis in proteasome inhibited Arabidopsis roots. *Plant Methods* 12:20.
- Weber, C., L. Nover, and M. Fauth. 2008. Plant stress granules and mRNA processing bodies are distinct from heat stress granules. *Plant J* 56:517-530.
- Wilbertz, J.H., F. Voigt, I. Horvathova, G. Roth, Y. Zhan, and J.A. Chao. 2019. Single-Molecule Imaging of mRNA Localization and Regulation during the Integrated Stress Response. *Mol Cell* 73:946-958 e947.
- Yoo, S.D., Y.H. Cho, and J. Sheen. 2007. Arabidopsis mesophyll protoplasts: a versatile cell system for transient gene expression analysis. *Nat Protoc* 2:1565-1572.
- Zhang, L., X. Liu, K. Gaikwad, X. Kou, F. Wang, X. Tian, M. Xin, Z. Ni, Q. Sun, H. Peng, and E. Vierling. 2017. Mutations in eIF5B Confer Thermosensitive and Pleiotropic Phenotypes via Translation Defects in Arabidopsis thaliana. *Plant Cell* 29:1952-1969.

## FIGURE LEGENDS

**Figure 1: eEF1B $\beta$  physically interacts with eEF1B $\alpha$  and eEF1B $\gamma$**

**(A)** Co-immunoprecipitation of MYC-tagged eEF1B $\beta$ 1 and eEF1By1 with YFP-tagged eEF1B $\alpha$ 2, eEF1By2 or Citrine, which was used as negative control. Proteins were transiently expressed in protoplasts. The YFP-tagged proteins were enriched from protein extracts using GFP-trap beads (IP). Co-precipitating MYC-tagged proteins were detected by anti-MYC immunoblotting (Co-IP). The data are representative for three independent replicates.

**(B)** Y2H assay showing physical interaction between the subunits of the eEF1B complex. A serial dilution of yeast colonies was spotted on medium lacking tryptophan and leucine (+HIS) as growth control and on selective medium additionally lacking histidine (-HIS) to test for protein-protein interaction. Citrine was used as negative control. BD: DNA-binding domain. AD: Activation domain. **(C)** Structure of eEF1By1 and eEF1By2 proteins and the truncated versions used for Y2H assays in (D). P indicates the position of the conserved CDK-phosphorylation sites. **(D)** Y2H assay showing the interaction of eEF1B $\beta$ 1 with eEF1By1 $\Delta$ C and eEF1By2 $\Delta$ C but not with eEF1By1 $\Delta$ N and eEF1By2 $\Delta$ N. The data are representative for at least two independent replicates.

**Figure 1: Characterisation of T-DNA insertion lines for *eEF1By1* and *eEF1By2*.**

**(A)** Gene structure of *eEF1By1* and *eEF1By2* showing exons (black boxes), introns (black lines), UTRs (white boxes), T-DNA insertion sites (filled, vertical arrowheads) and the annealing sites of the primers used for RT-qPCR (filled, horizontal arrowheads) and RT-PCR (filled and white arrowheads (3'UTRrev)). **(B)** Agarose gel picture of RT-PCR analysis on RNA isolated from seedlings of WT and the indicated mutant lines. The following primer sets were used: *eef1by1*fw and *eef1by1\_3'UTRrev* for *eEF1By1* expression and *eef1by2*fw and *eef1by2\_3'UTRrev* for *eEF1By2* expression. Primers for *UBIQUITIN* were used as reference. **(C)** RT-qPCR analysis on RNA isolated from 7-days-old seedlings of WT and mutant lines. The primers are indicated in (A). Transcript levels are represented relative to those in WT, which were set to 1. Values represent the mean from three biological replicates. Asterisks indicate means differing significantly from WT (two-tail Student's *t* test; \* *P* < 0.05; \*\* *P* < 0.01; \*\*\* *P* < 0.001). **(D)** Phenotype of 24-days-old seedlings of WT and the indicated single mutant lines.

**Figure 3: Phenotype of the *eef1by1/2* double mutant and the complementation line.**

**(A)** Immunoblot of protein extracts from 10-days-old seedlings of WT, the *eef1by1/2* mutant, which showed a significantly reduced expression and the complementation line (*eef1by1/2-C*), which showed expression of the YFP-eEF1By fusion protein. Immunoblot analysis was performed using antibodies recognising eEF1By and ACTIN as loading control. **(B)** Seed germination of WT, *eef1by1/2* and the single mutant lines. Values represent means  $\pm$ SE from three independent experiments (*n*≥25). **(C)** Representative images of 7-days-old seedlings of WT, the *eef1by1/2* double mutant, the complementation line and the single mutant lines. Seedlings were grown on vertical plates. **(D)** Seedlings of the indicated genotypes were grown on vertical plates and root length was analysed at the indicated timepoints using ImageJ software. Values represent the means  $\pm$ SE from four independent experiments (*n*=20). **(E)** Confocal images of PI-stained root tips of WT and *eef1by1/2* at seven dag showing reduced size of the meristematic zone of the RAM (indicated by a white line). **(F)** Quantification of dividing cells in the cortical cell layer of the RAM of WT and *eef1by1/2*. Data represent means  $\pm$ SE from four independent experiments (*n*=30). **(G)** Quantification of lateral roots formed in 10-days-old seedlings of the indicated genotypes grown on vertical plates. Values represent the means  $\pm$ SE from four biological replicates (*n*=20). **(H)** Representative photographs of 26 days-old plants of the indicated genotypes grown on soil. **(I)** Seedlings of the indicated genotypes were grown on horizontal plates and seedlings exhibiting true leaves

were quantified at indicated time points. Values represent means  $\pm$ SE from four independent experiments (n= 30). Scalebar represents in (C) 1 cm, in (E) 60  $\mu$ m, and in (H) 2 cm. Asterisks in (A, D, F, G and I) indicate means differing significantly from WT (two-tail Student's *t* test; \* *P* < 0.05; \*\* *P* < 0.01; \*\*\* *P* < 0.001).

**Figure 4: Analysis of translation and protein synthesis rates.**

Relative root growth of seedlings of the indicated genotypes grown on MS medium supplemented with 0.05  $\mu$ M or 0.1  $\mu$ M cycloheximide (CHX) **(A)** or 10 mg/L or 20 mg/L hygromycin B (HYG) **(B)**. The average root length of untreated seedlings was set to 1 for each line. Values represent means  $\pm$ SE from three independent experiments (n $\geq$ 20). Asterisk indicate means differing significantly from the relative root growth of WT (two-tail *t* test; \*\* *P* < 0.01 and \* *P* < 0.05). **(C)** Polysome profiles of cell lysates prepared from 24 days-old-leaves of WT and the *eef1by1/2* mutant. The ribonucleoprotein particles were separated by sucrose gradient sedimentation and analysed by absorbance measurement at 254 nm. Data represent means from three independent experiments. **(D)** Analysis of the total amount of mRNA associated with ribosomal complexes by quantification of the total peak area of polysome profiles shown in (C). Values represent means  $\pm$ SE from the three independent experiments. **(E)** Quantification of 18S and 28S rRNA peaks of electropherograms (shown in Figure S3A) obtained from BioAnalyzer analysis of total RNA from WT and mutant samples. Data represent means  $\pm$ SE from the three independent experiments. **(F)** Quantification of cell number per 1mm<sup>2</sup> counted from confocal images of adaxial epidermal leaf cells from 7 days old seedlings stained with FM4-64 (representative images are shown in Figure S3B). Data represent means  $\pm$ SE from 10 individual seedlings (n=30). **(G)** Ratio of polysomal to monosomal and subunit-associated rRNAs calculated from the peak areas as indicated by dashed boxes in (C). **(H)** Detection of puromycin-labeled proteins by immunoblotting. 7 days-old seedlings grown in liquid MS medium, where either left untreated (Control), treated with puromycin (100  $\mu$ M; 2h) or first treated with 10 or 100  $\mu$ M CHX (4h) to inhibit translation, followed by puromycin treatment. Proteins were extracted and detected with a puromycin-specific antibody. Membranes were Ponceau stained for equal loading control. The data are representative for three independent replicates.

**Figure 5: Thermotolerance phenotype of WT and mutant plants.**

**(A)** Seed germination of WT and mutant lines at control conditions and after heat treatment of imbibed seeds for 3,5 h at 45°C (HS). Germination rates were determined at indicated time points after treatment. Values represent means  $\pm$ SE of two biological replicates (n=50). **(B)** Acquired thermotolerance measured by hypocotyl elongation under control conditions or after heat treatment (HS). Seedlings were grown for 2,5 days in the dark and heat-treated for: 90 min at 38°C, 120 min at 22°C, and 180 min at 45°C. Hypocotyl elongation was measured 2,5 days after the treatment. Left panel shows hypocotyl length and right panel shows ratio of hypocotyl length from HS/Control. Values represent means  $\pm$ SE of three biological replicates (n $\geq$ 20). **(C)** Acquired thermotolerance measured by root growth under control conditions or after heat treatment (HS). Seedlings of the indicated genotypes were grown for 4 days on vertical plates and heat-treated for: 90 min at 38°C, 120 min at 22°C, and 120 min at 45°C. Root length was measured 5 days after heat treatment. Left panel shows root length and right panel shows ratio of root length from HS/Control. Data represent means  $\pm$ SE from three independent experiments (n $\geq$ 15) **(D)** Acquired thermotolerance analysed by assessing seedling survival rate. Seedlings were grown for 7 days at control conditions before heat treatment (90 min at 38°C, 120 min at 22°C, and 120 min at 45°C). Five days after heat treatment photographs (left) were taken and seedling survival rate (right



panel) was scored by counting the number of seedlings that showed green leaves. Data represent means  $\pm$ SE from three independent experiments ( $n \geq 30$ ). Asterisk indicate means differing significantly from the WT (two-tail t test; \*\*  $P < 0.01$  and \*  $P < 0.05$ ).

**Figure 6: eEF1B subunits colocalize with PAB8 in cytoplasmic foci after heat stress.**

(A) Representative confocal images of protoplasts transiently co-expressing PAB8-mCherry and eEF1B $\alpha$ 2-GFP, eEF1B $\beta$ 1-GFP or eEF1B $\gamma$ 2-GFP at control conditions or after heat treatment (42°C, 60 min) showing that each eEF1B subunit accumulated in cytoplasmic foci after heat stress. Scale bar is 10  $\mu$ m. (B) Pearson correlation coefficient and Spearman's rank correlation value calculated from 25 protoplasts for each combination after heat treatment using ImageJ Coloc2. (C) Frequency of colocalisation between foci for each of the combinations shown in (A). Foci were counted using ImageJ Cell Counter. Data represent means  $\pm$ SE from three independent experiments ( $n=25$ ).

**Figure 7: The individual eEF1B subunits accumulate in stress granules of different number and size.**

(A) Representative confocal images of protoplasts transiently expressing eEF1B $\alpha$ 2-GFP, eEF1B $\beta$ 1-GFP or eEF1B $\gamma$ 2-GFP or PAB8-mCherry after heat treatment (42°C, 60 min) showing that cytoplasmic foci formation was more pronounced in cells expressing eEF1B $\beta$ 1-GFP or PAB8-mCherry compared to the other constructs. Scale bar is 10  $\mu$ m. (B) Quantification of the number of cytoplasmic foci per cell in protoplasts expressing the indicated constructs after heat treatment (42°C, 60 min). Cytoplasmic foci were counted using ImageJ software. Data represent means  $\pm$ SE from three independent experiments ( $n=30$ ). (C) Quantification of the size of cytoplasmic foci in protoplasts expressing the indicated constructs after heat treatment (42°C, 60 min). Cytoplasmic foci were measured using ImageJ software. Data represent means  $\pm$ SE from three independent experiments ( $n=30$ ).

**Figure 8: Co-expression eEF1B $\beta$ 1-GFP increases accumulation of eEF1B $\alpha$ 2-GFP and eEF1B $\gamma$ 2-GFP in stress granules after heat stress.**

(A) Representative confocal images of protoplasts transiently co-expressing the following constructs after heat treatment (42°C, 60 min): eEF1B $\alpha$ 2-GFP and eEF1B $\beta$ 1-mCherry, eEF1B $\alpha$ 2-GFP and eEF1B $\gamma$ 2-mCherry, eEF1B $\beta$ 1-GFP and eEF1B $\gamma$ 2-mCherry or eEF1B $\gamma$ 2-GFP and eEF1B $\beta$ 1-mCherry. Formation of cytoplasmic foci is enhanced, when eEF1B $\beta$ 1 is co-expressed. (B) Quantification of foci per cell showing only GFP-fluorescence, only mCherry-fluorescence or both in protoplasts described in (A). Foci were counted using ImageJ Cell Counter. Data represent means  $\pm$ SE from three independent experiments ( $n=25$ ).

**Figure S1: Phenotype of *eef1by1/2* double mutant and single mutants.**

(A) Representative photograph of leaves from 28 days-old soil-grown plants. Scale bar is 1 cm. (B) Quantification of the size of the biggest rosette leaf (leaf number 9 to 12) of 26 days-old soil-grown plants. Values represent means  $\pm$ SE ( $n=35$ ). (C) Representative photograph of flowering plants of the indicated genotypes. (D) Quantification of leaves formed by soil-grown plants of the indicated genotypes at the time point of floral transition. Values represent means  $\pm$ SE ( $n=40$ ). (E) Representative photographs of siliques of WT and the *eef1by1/2* double mutant. Scale bar is 2 mm. (F) Quantification of seeds or empty spots per silique. Values represent means  $\pm$ SE ( $n=30$ ). Asterisks in (B,D,F) indicate means differing significantly from WT (two-tail Student's t test; \*  $P < 0.05$ ; \*\*  $P < 0.01$ ; \*\*\*  $P < 0.001$ ).

**Figure S2: The truncated version of eEF1By (YFP-eEF1ByΔN) does not complement the phenotype of the *eef1by1/2* double mutant.**

(A) Representative photograph of 7 days-old seedlings of the indicated genotypes grown on vertical plates. Scale bar is 1 cm. (B) Measurement of root length of seedlings of the indicated genotypes. Plants were grown on vertical plates and root length was analyzed using ImageJ software. Values represent means  $\pm$ SE from three independent experiments (n=15). (C) Quantification of lateral root formation of seedlings grown on vertical plates. Values represent means  $\pm$ SE from three independent experiments (n=15).

**Figure S3: Quantification of rRNA levels and cell size in WT and mutant plants.**

(A) Representative electropherograms of WT and *eef1by1/2* mutant total RNA samples generated by a BioAnalyzer (Agilent). The quantification is shown in Figure 3E. (B) Representative confocal images of adaxial epidermal leaf cells of 7 days-old seedlings stained with FM4-64. Scale bar is 10  $\mu$ M. Quantifications are shown in Figure 3F.

**Figure S4: The *eef1by1/2* mutant does not display altered thermotolerance.**

(A) Long-term acquired thermotolerance (LAT) of WT and *eef1by1/2* double mutant. Seedlings were grown for 6 days at control conditions before first heat treatment (3h 30 min at 38°C), allowed to adapt for 2 days at 22°C, then heat treated a second time (100 min at 45°C). Seven days after the second heat treatment, photographs were taken. (B) Quantification of LAT experiment described in (A) by counting the percentage of plants showing expanded green leaves. Data represent means  $\pm$ SE from three independent experiments (n $\geq$ 30). Asterisk indicate means differing significantly from the WT (two-tail t test; \*\*\* P < 0.001). (C) Measurement of root length of WT and the *eef1by1/2* mutant grown at control conditions (22°C) or at increased ambient temperature (27°C) on vertical plates for 7 days. Data represent means  $\pm$ SE from three independent experiments (n $\geq$ 30). Asterisk indicate means differing significantly from WT (two-tail t test; \*\*\* P < 0.001). (D) Data shown in (C) presented as ratio of root length at ambient temperature/control.

**Figure S5: Integrity of GFP- and mCherry-fusion proteins.**

Immunoblot of protein extracts from protoplasts transiently expressing eEF1B $\alpha$ 2-GFP, eEF1B $\beta$ 1-GFP, eEF1By2-GFP, free GFP or PAB8-mCherry. Immunoblot analysis was performed using a GFP or RFP-specific antibody. Ponceau staining was performed as loading control. The data are representative for three independent replicates.

**Figure S6: eEF1B $\beta$ 1 and eEF1By2 accumulate in stress granules in Arabidopsis roots after heat stress.**

Representative confocal images of root cells of 4 dag seedlings expressing YFP-eEF1B $\beta$ 1, YFP-eEF1By2 or free GFP. Seedlings were photographed at control conditions, after heat treatment (20 min, 42°C) and after recovery (12 hours at 22°C after heat treatment). In all seedlings analyzed the fluorescence associated with YFP-eEF1B $\beta$ 1 (n=35) or YFP-eEF1By2 (n= 32) accumulated in cytoplasmic foci after heat treatment, while no foci were observed in seedlings expressing free GFP (n=32). Imaging of the same roots after recovery revealed that the cytoplasmic foci were disassembled (n= 32 for each construct). Scale bar is 23 $\mu$ m. Data were collected in three independent experiments.

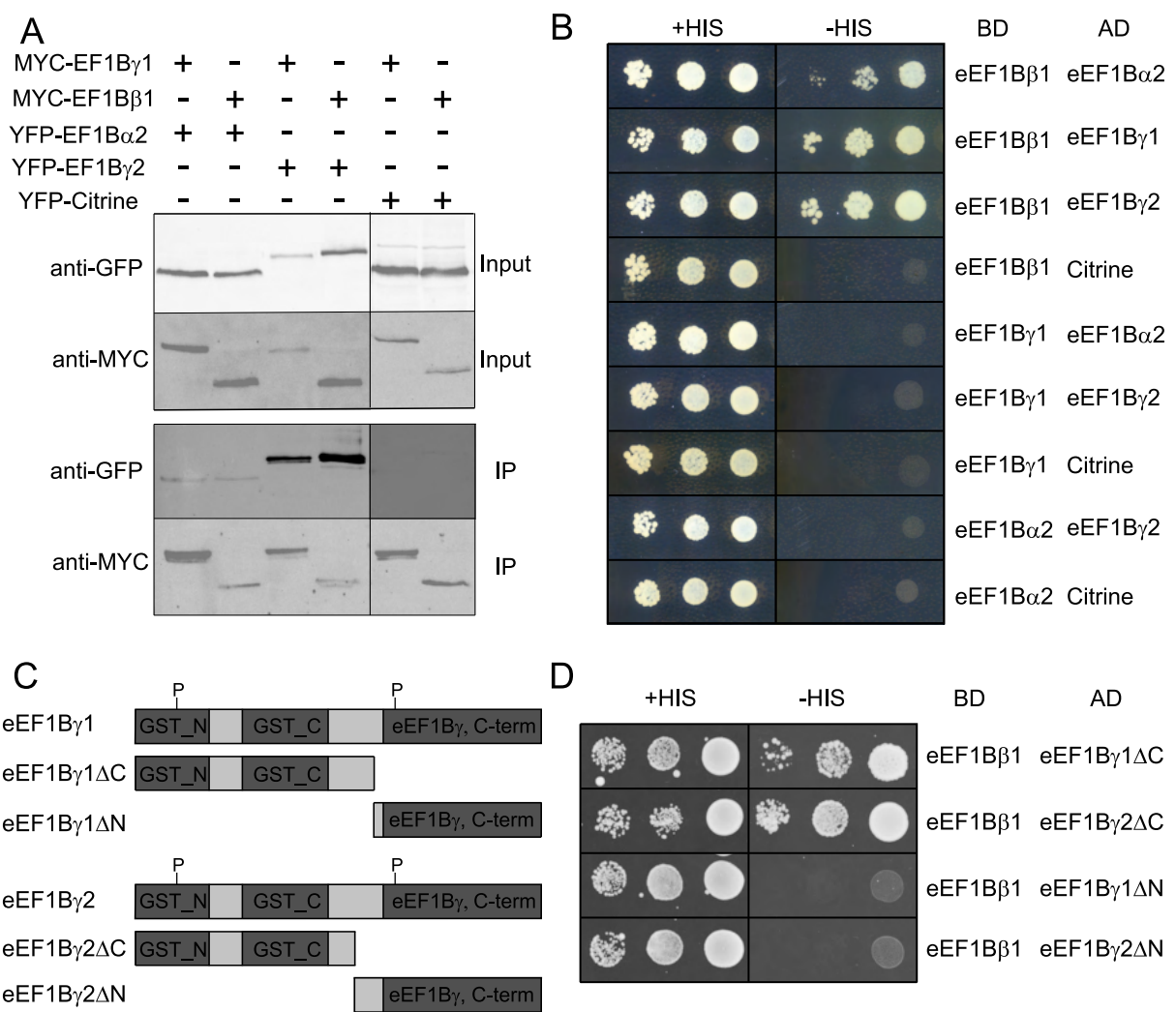


### Figure 1: eEF1B $\beta$ physically interacts with eEF1B $\alpha$ and eEF1B $\gamma$

**(A)** Co-immunoprecipitation of MYC-tagged eEF1B $\beta$ 1 and eEF1B $\gamma$ 1 with YFP-tagged eEF1B $\alpha$ 2, eEF1B $\gamma$ 2 or Citrine, which was used as negative control. Proteins were transiently expressed in protoplasts. The YFP-tagged proteins were enriched from protein extracts using GFP-trap beads (IP). Co-precipitating MYC-tagged proteins were detected by anti-MYC immunoblotting (Co-IP). The data are representative for three independent replicates.

**(B)** Y2H assay showing physical interaction between the subunits of the eEF1B complex. A serial dilution of yeast colonies was spotted on medium lacking tryptophan and leucine (+HIS) as growth control and on selective medium additionally lacking histidine (-HIS) to test for protein-protein interaction. Citrine was used as negative control. BD: DNA-binding domain. AD: Activation domain. **(C)** Structure of eEF1B $\gamma$ 1 and eEF1B $\gamma$ 2 proteins and the truncated versions used for Y2H assays in (D). P indicates the position of the conserved CDK-phosphorylation sites. **(D)** Y2H assay showing the interaction of eEF1B $\beta$ 1 with eEF1B $\gamma$ 1 $\Delta$ C and eEF1B $\gamma$ 2 $\Delta$ C but not with eEF1B $\gamma$ 1 $\Delta$ N and eEF1B $\gamma$ 2 $\Delta$ N. The data are representative for at least two independent replicates.

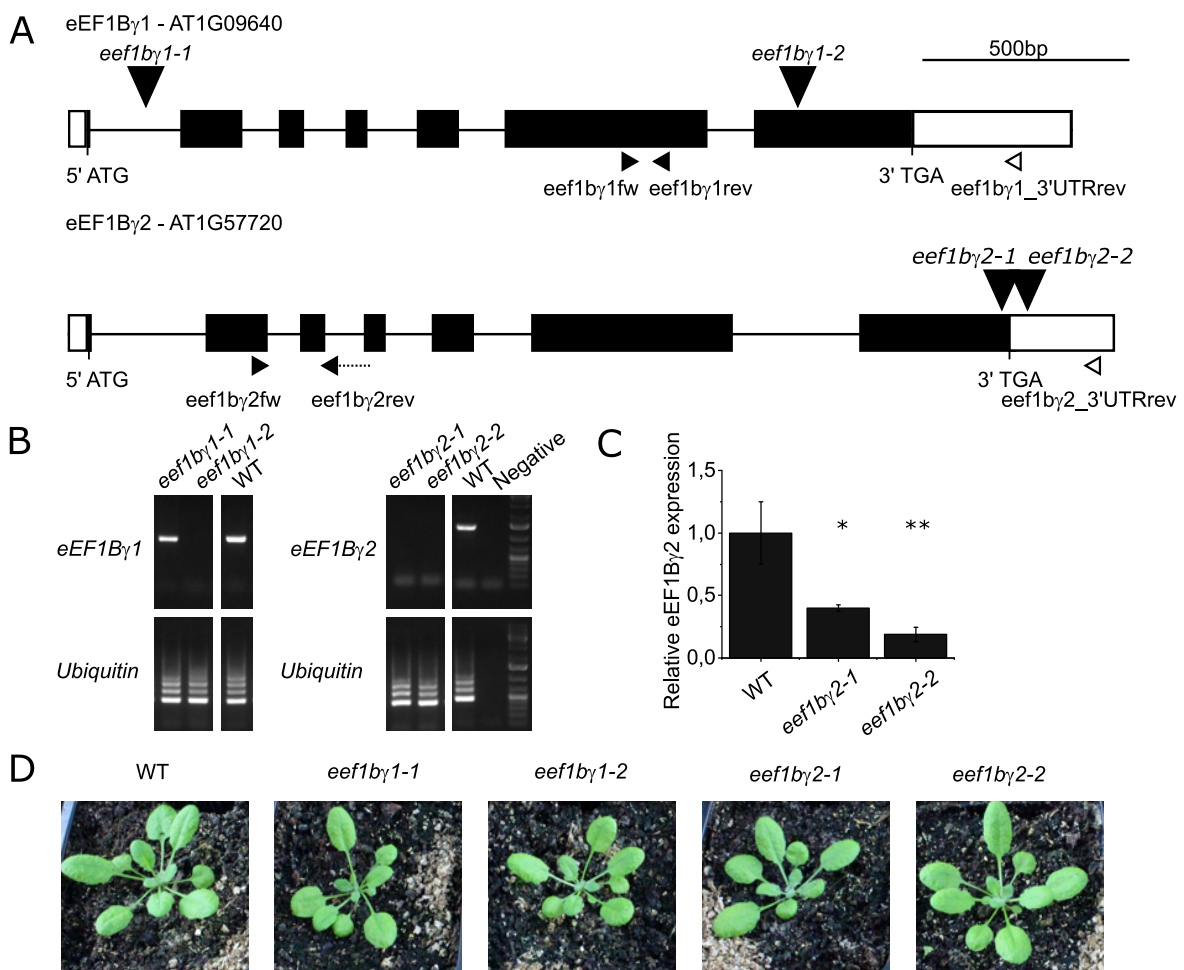


**Figure 2: Characterisation of T-DNA insertion lines for *eEF1Bγ1* and *eEF1Bγ2*.**

**(A)** Gene structure of *eEF1Bγ1* and *eEF1Bγ2* showing exons (black boxes), introns (black lines), UTRs (white boxes), T-DNA insertion sites (filled, vertical arrowheads) and the annealing sites of the primers used for RT-qPCR (filled, horizontal arrowheads) and RT-PCR (filled and white arrowheads (3'UTRrev)). **(B)** Agarose gel picture of RT-PCR analysis on RNA isolated from seedlings of WT and the indicated mutant lines. The following primer sets were used: *eef1bγ1fw* and *eef1bγ1\_3'UTRrev* for *eEF1Bγ1* expression and *eef1bγ2fw* and *eef1bγ2\_3'UTRrev* for *eEF1Bγ2* expression. Primers for *UBIQUITIN* were used as reference. **(C)** RT-qPCR analysis on RNA isolated from 7-days-old seedlings of WT and mutant lines. The primers are indicated in (A). Transcript levels are represented relative to those in WT, which were set to 1. Values represent the mean from three biological replicates. Asterisks indicate means differing significantly from WT (two-tail Student's *t* test; \*  $P < 0.05$ ; \*\*  $P < 0.01$ ; \*\*\*  $P < 0.001$ ). **(D)** Phenotype of 24-days-old seedlings of WT and the indicated single mutant lines.

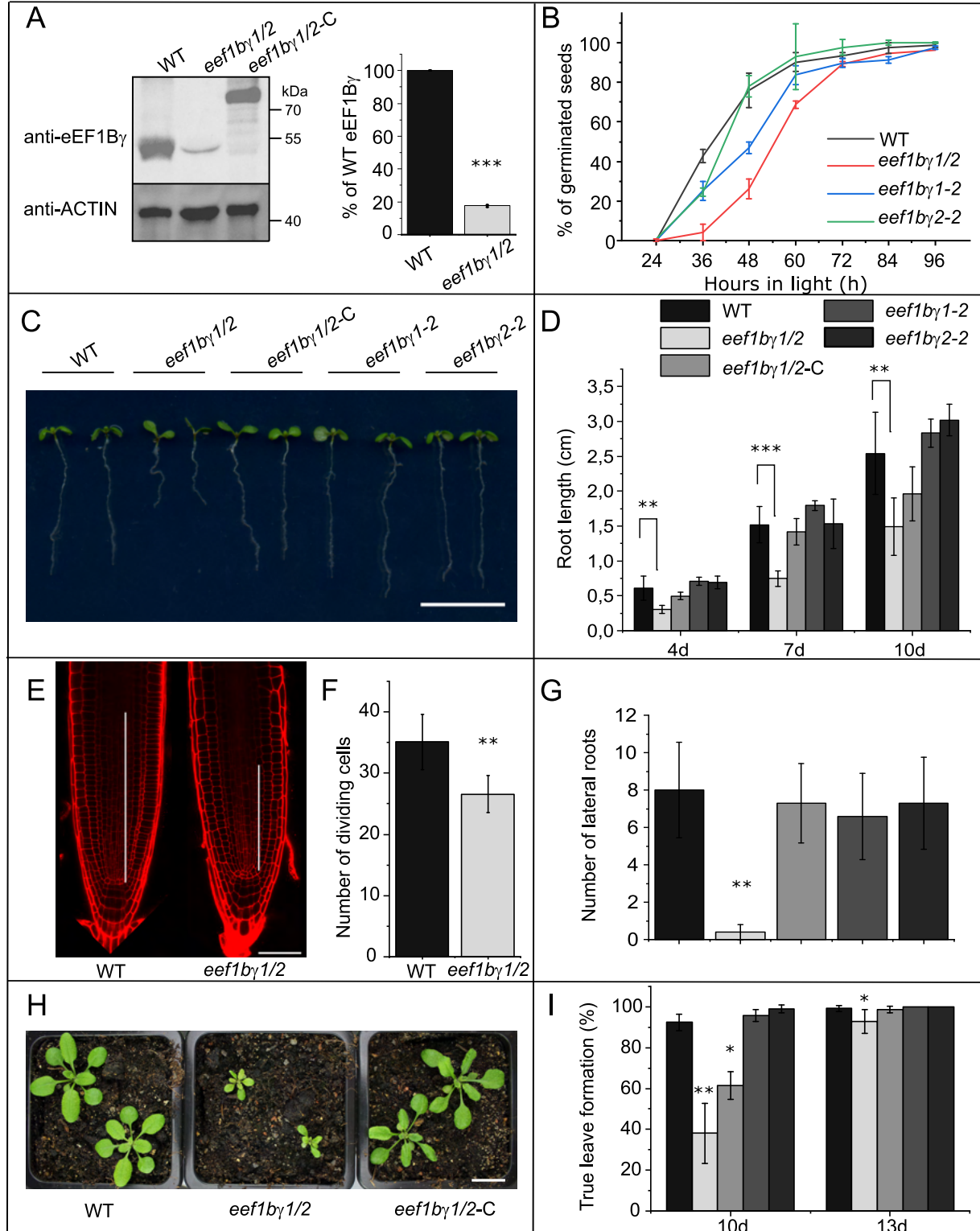


**Figure 3: Phenotype of the *eef1b $\gamma$ 1/2* double mutant and the complementation line.**

**(A)** Immunoblot of protein extracts from 10-days-old seedlings of WT, the *eef1b $\gamma$ 1/2* mutant, which showed a significantly reduced expression and the complementation line (*eef1b $\gamma$ 1/2-C*), which showed expression of the YFP-eEF1B $\gamma$  fusion protein. Immunoblot analysis was performed using antibodies recognising eEF1B $\gamma$  and ACTIN as loading control. **(B)** Seed germination of WT, *eef1b $\gamma$ 1/2* and the single mutant lines. Values represent means  $\pm$ SE from three independent experiments ( $n \geq 25$ ). **(C)** Representative images of 7-days-old seedlings of WT, the *eef1b $\gamma$ 1/2* double mutant, the complementation line and the single mutant lines. Seedlings were grown on vertical plates. **(D)** Seedlings of the indicated genotypes were grown on vertical plates and root length was analysed at the indicated timepoints using ImageJ software. Values represent the means  $\pm$ SE from four independent experiments ( $n=20$ ). **(E)** Confocal images of PI-stained root tips of WT and *eef1b $\gamma$ 1/2* at seven dag showing reduced size of the meristematic zone of the RAM (indicated by a white line). **(F)** Quantification of dividing cells in the cortical cell layer of the RAM of WT and *eef1b $\gamma$ 1/2*. Data represent means  $\pm$ SE from four independent experiments ( $n=30$ ). **(G)** Quantification of lateral roots formed in 10-days-old seedlings of the indicated genotypes grown on vertical plates. Values represent the means  $\pm$ SE from four biological replicates ( $n=20$ ). **(H)** Representative photographs of 26 days-old plants of the indicated genotypes grown on soil. **(I)** Seedlings of the indicated genotypes were grown on horizontal plates and seedlings exhibiting true leaves were quantified at indicated time points. Values represent means  $\pm$ SE from four independent experiments ( $n=30$ ). Scalebar represents in (C) 1 cm, in (E) 60  $\mu$ m, and in (H) 2 cm. Asterisks in (A, D, F, G and I) indicate means differing significantly from WT (two-tail Student's *t* test; \*  $P < 0.05$ ; \*\*  $P < 0.01$ ; \*\*\*  $P < 0.001$ ).



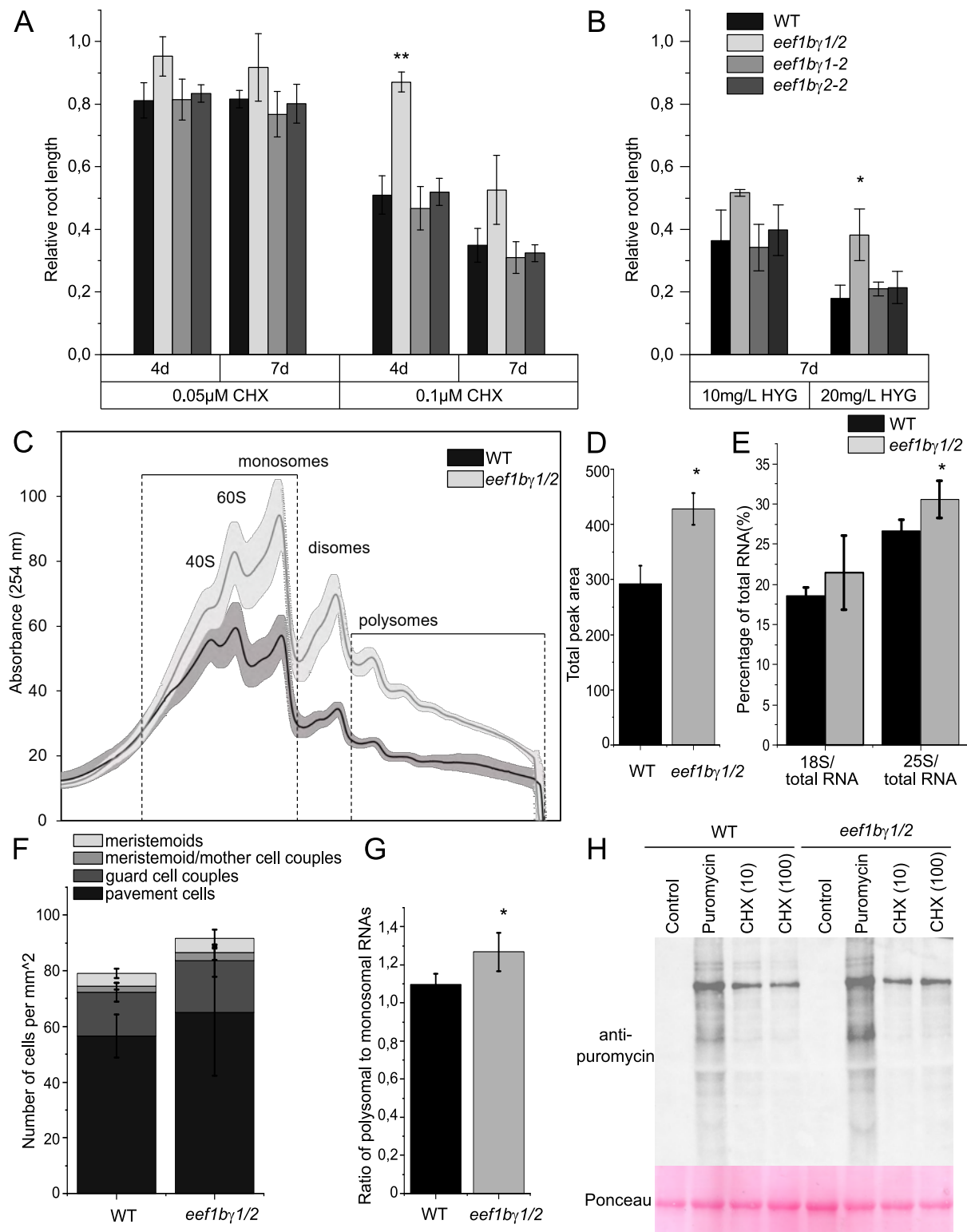


**Figure 4: Analysis of translation and protein synthesis rates.**

Relative root growth of seedlings of the indicated genotypes grown on MS medium supplemented with 0.05  $\mu$ M or 0.1  $\mu$ M cycloheximide (CHX) (A) or 10 mg/L or 20 mg/L hygromycin B (HYG) (B). The average root length of untreated seedlings was set to 1 for each line. Values represent means  $\pm$ SE from three independent experiments ( $n \geq 20$ ). Asterisk indicate means differing significantly from the relative root growth of WT (two-tail t test; \*\*  $P < 0.01$  and \*  $P < 0.05$ ). (C) Polysome profiles of cell lysates prepared from 24 days-old-leaves of WT and the *eef1b $\gamma$ 1/2* mutant. The ribonucleoprotein particles were separated by sucrose gradient sedimentation and analysed by absorbance measurement at 254 nm. Data represent means from three independent experiments. (D) Analysis of the total amount of mRNA associated with ribosomal complexes by quantification of the total peak area of polysome profiles shown in (C). Values represent means  $\pm$ SE from the three independent experiments. (E) Quantification of 18S and 28S rRNA peaks of electropherograms (shown in Figure S3A) obtained from BioAnalyzer analysis of total RNA from WT and mutant samples. Data represent means  $\pm$ SE from the three independent experiments. (F) Quantification of cell number per 1mm<sup>2</sup> counted from confocal images of adaxial epidermal leaf cells from 7 days-old-seedlings stained with FM4-64 (representative images are shown in Figure S3B). Data represent means  $\pm$ SE from 10 individual seedlings ( $n=30$ ). (G) Ratio of polysomal to monosomal and subunit-associated rRNAs calculated from the peak areas as indicated by dashed boxes in (C). (H) Detection of puromycin-labeled proteins by immunoblotting. 7 days-old seedlings grown in liquid MS medium were either left untreated (Control), treated with puromycin (100  $\mu$ M; 2h) or first treated with 10 or 100  $\mu$ M CHX (4h) to inhibit translation, followed by puromycin treatment. Proteins were extracted and detected with a puromycin-specific antibody. Membranes were Ponceau stained for equal loading control. The data are representative for three independent replicates.

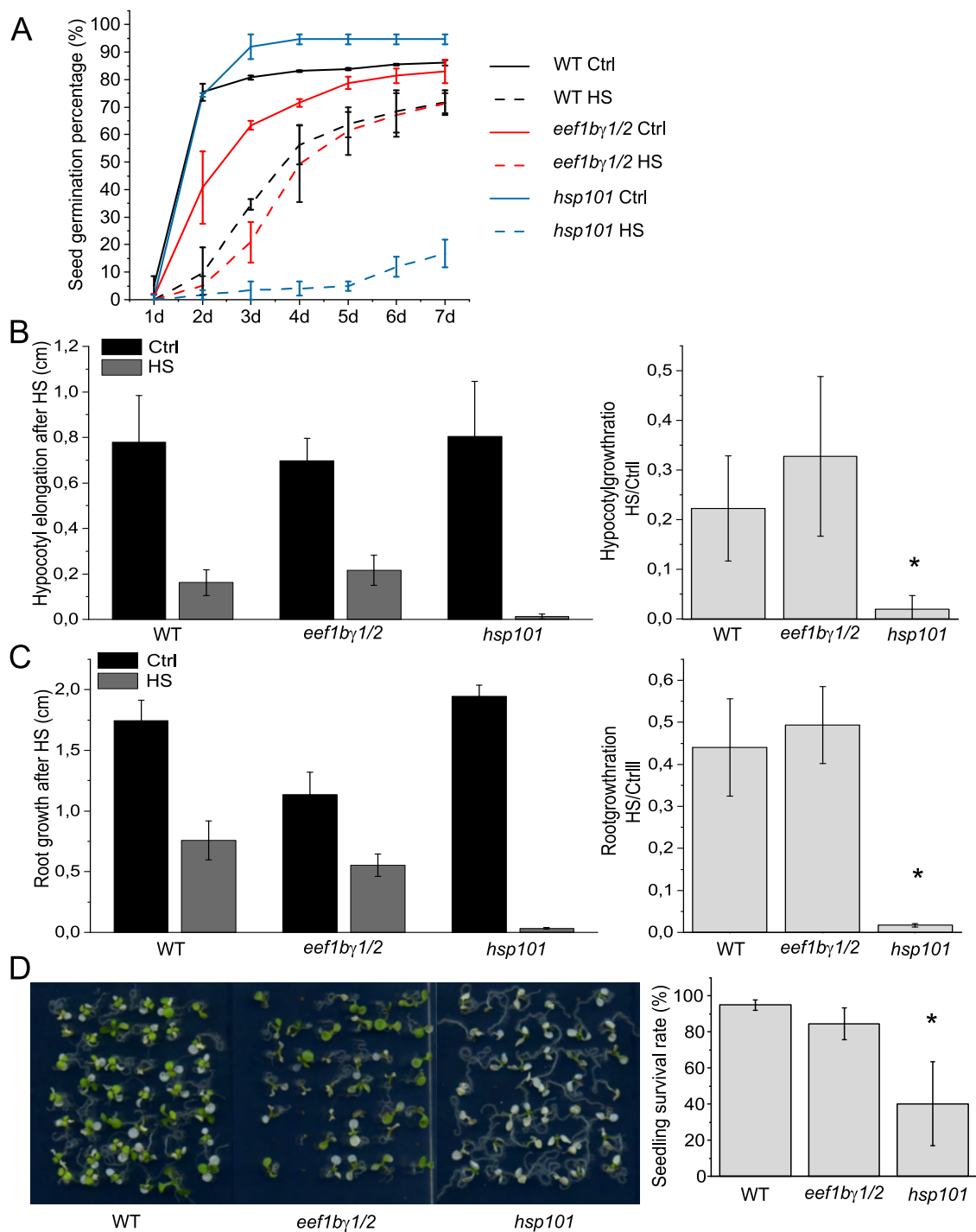


**Figure 5: Thermotolerance phenotype of WT and mutant plants.**

**(A)** Seed germination of WT and mutant lines at control conditions and after heat treatment of imbibed seeds for 3,5 h at 45°C (HS). Germination rates were determined at indicated time points after treatment. Values represent means  $\pm$ SE of two biological replicates (n=50). **(B)** Acquired thermotolerance measured by hypocotyl elongation under control conditions or after heat treatment (HS). Seedlings were grown for 2,5 days in the dark and heat-treated for: 90 min at 38°C, 120 min at 22°C, and 180 min at 45°C. Hypocotyl elongation was measured 2,5 days after the treatment. Left panel shows hypocotyl length and right panel shows ratio of hypocotyl length from HS/Control. Values represent means  $\pm$ SE of three biological replicates (n $\geq$ 20). **(C)** Acquired thermotolerance measured by root growth under control conditions or after heat treatment (HS). Seedlings of the indicated genotypes were grown for 4 days on vertical plates and heat-treated for: 90 min at 38°C, 120 min at 22°C, and 120 min at 45°C. Root length was measured 5 days after heat treatment. Left panel shows root length and right panel shows ratio of root length from HS/Control. Data represent means  $\pm$ SE from three independent experiments (n $\geq$ 15) **(D)** Acquired thermotolerance analysed by assessing seedling survival rate. Seedlings were grown for 7 days at control conditions before heat treatment (90 min at 38°C, 120 min at 22°C, and 120 min at 45°C). Five days after heat treatment photographs (left) were taken and seedling survival rate (right panel) was scored by counting the number of seedlings that showed green leaves. Data represent means  $\pm$ SE from three independent experiments (n $\geq$ 30). Asterisk indicate means differing significantly from the WT (two-tail t test; \*\* P < 0.01 and \* P < 0.05).

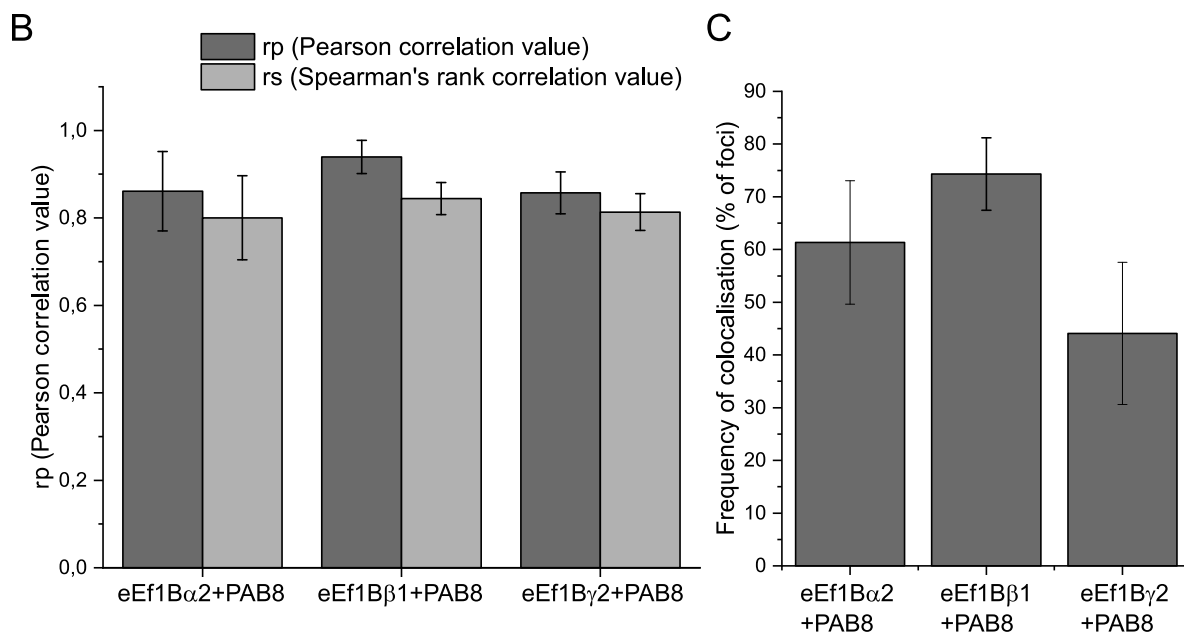
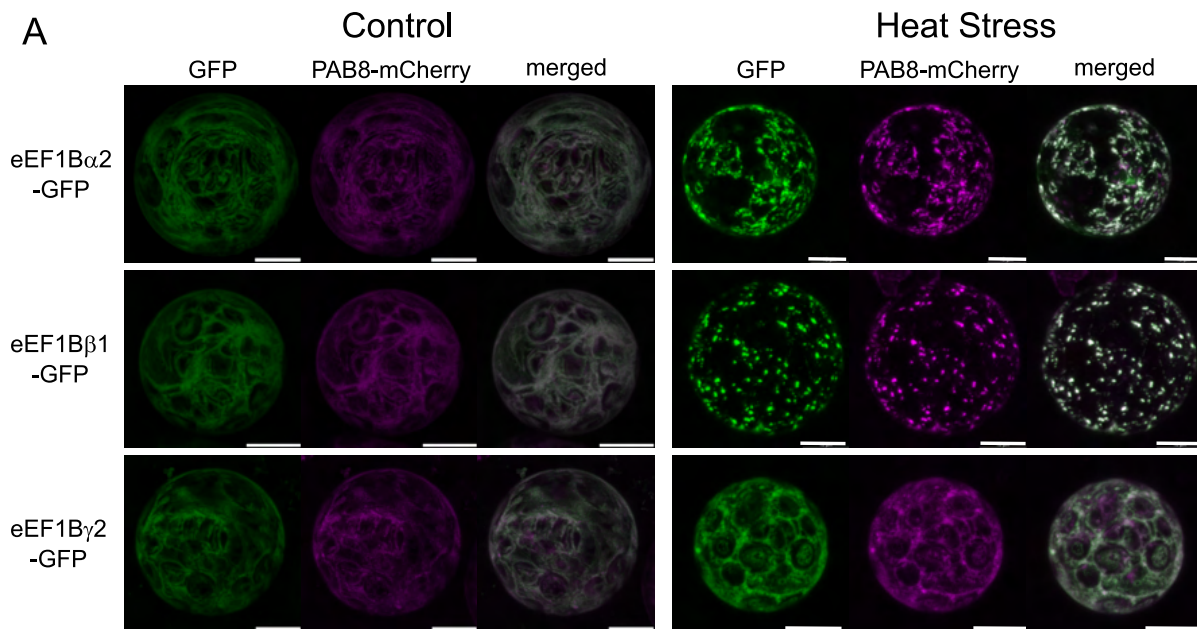


**Figure 6: eEF1B subunits colocalize with PAB8 in cytoplasmic foci after heat stress.**

**(A)** Representative confocal images of protoplasts transiently co-expressing PAB8-mCherry and eEF1B $\alpha$ 2-GFP, eEF1B $\beta$ 1-GFP or eEF1B $\gamma$ 2-GFP at control conditions or after heat treatment (42°C, 60 min) showing that each eEF1B subunit accumulated in cytoplasmic foci after heat stress. Scale bar is 10  $\mu$ m. **(B)** Pearson correlation coefficient and Spearman's rank correlation value calculated from 25 protoplasts for each combination after heat treatment using ImageJ Coloc2. **(C)** Frequency of colocalisation between foci for each of the combinations shown in (A). Foci were counted using ImageJ Cell Counter. Data represent means  $\pm$ SE from three independent experiments (n=25).



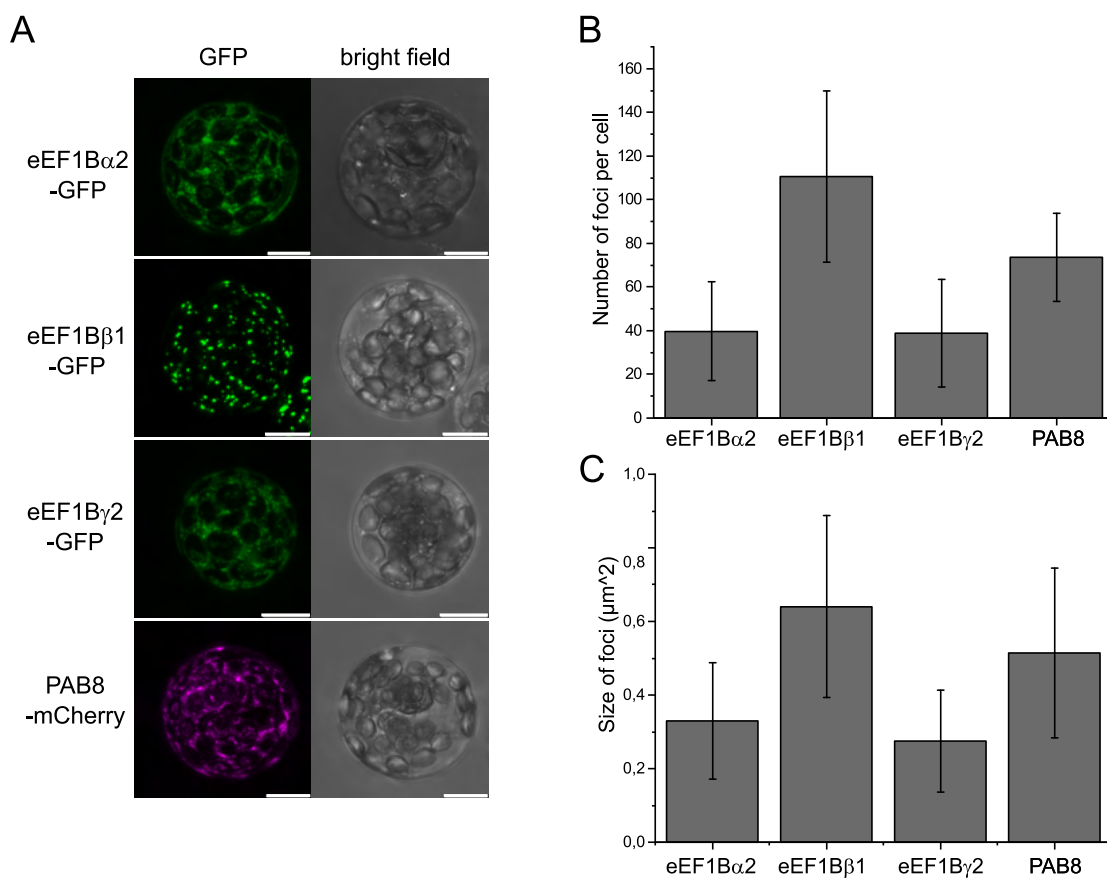


**Figure 7: The individual eEF1B subunits accumulate in stress granules of different number and size.**

**(A)** Representative confocal images of protoplasts transiently expressing eEF1B $\alpha$ 2-GFP, eEF1B $\beta$ 1-GFP or eEF1B $\gamma$ 2-GFP or PAB8-mCherry after heat treatment (42°C, 60 min) showing that cytoplasmic foci formation was more pronounced in cells expressing eEF1B $\beta$ 1-GFP or PAB8-mCherry compared to the other constructs. Scale bar is 10  $\mu\text{m}$ . **(B)** Quantification of the number of cytoplasmic foci per cell in protoplasts expressing the indicated constructs after heat treatment (42°C, 60 min). Cytoplasmic foci were counted using ImageJ software. Data represent means  $\pm$ SE from three independent experiments (n=30). **(C)** Quantification of the size of cytoplasmic foci in protoplasts expressing the indicated constructs after heat treatment (42°C, 60 min). Cytoplasmic foci were measured using ImageJ software. Data represent means  $\pm$ SE from three independent experiments (n=30).

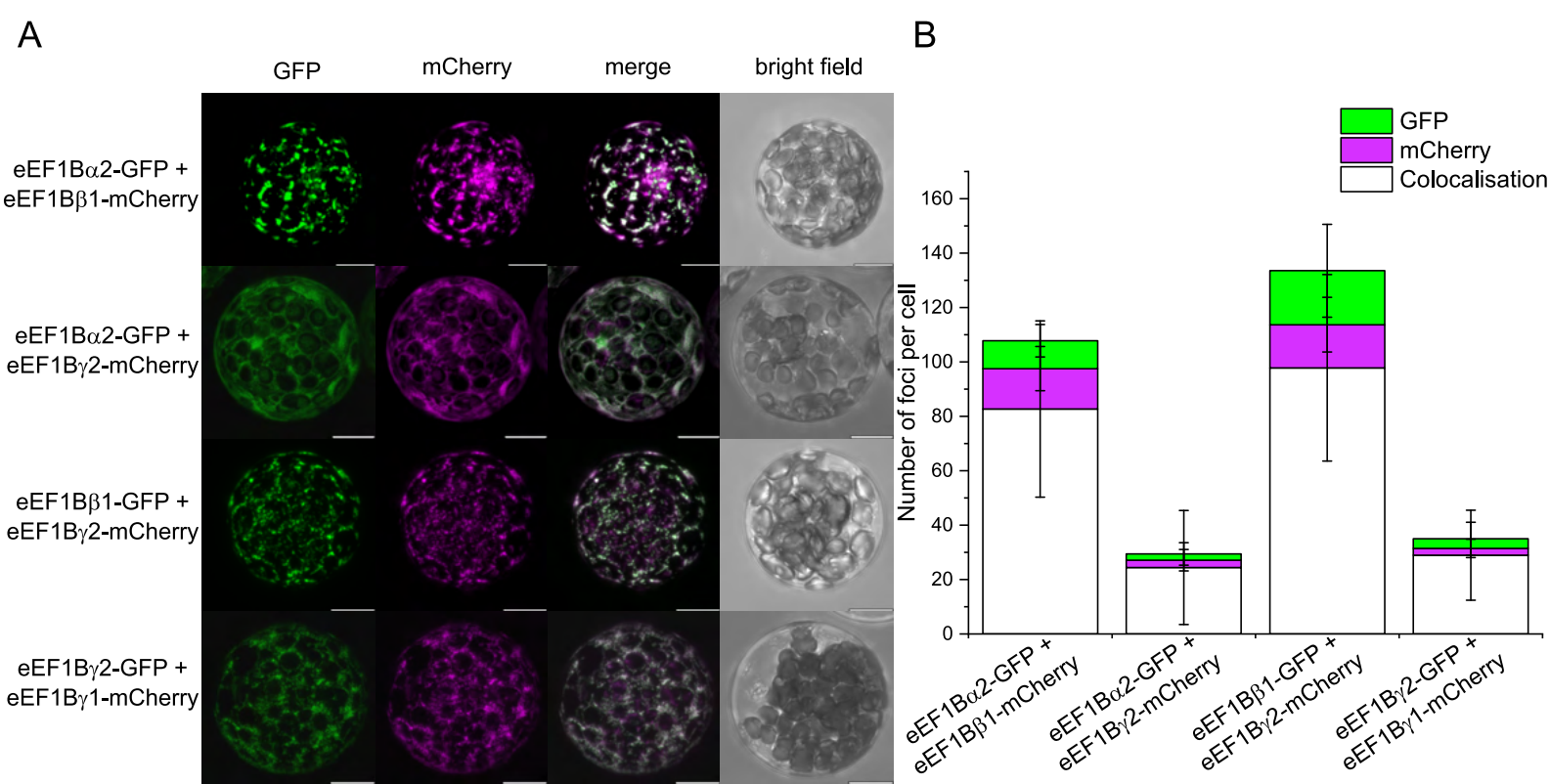


**Figure 8: Co-expression of eEF1B $\beta$ 1-GFP increases accumulation of eEF1B $\alpha$ 2-GFP and eEF1B $\gamma$ 2-GFP in stress granules after heat stress.**

**(A)** Representative confocal images of protoplasts transiently co-expressing the following constructs after heat treatment (42°C, 60 min): eEF1B $\alpha$ 2-GFP and eEF1B $\beta$ 1-mCherry, eEF1B $\alpha$ 2-GFP and eEF1B $\gamma$ 2-mCherry, eEF1B $\beta$ 1-GFP and eEF1B $\gamma$ 2-mCherry or eEF1B $\gamma$ 2-GFP and eEF1B $\gamma$ 1-mCherry. Formation of cytoplasmic foci is enhanced, when eEF1B $\beta$ 1 is co-expressed. **(B)** Quantification of foci per cell showing only GFP-fluorescence, only mCherry-fluorescence or both in protoplasts described in (A). Foci were counted using ImageJ Cell Counter. Data represent means  $\pm$ SE from three independent experiments (n=25).

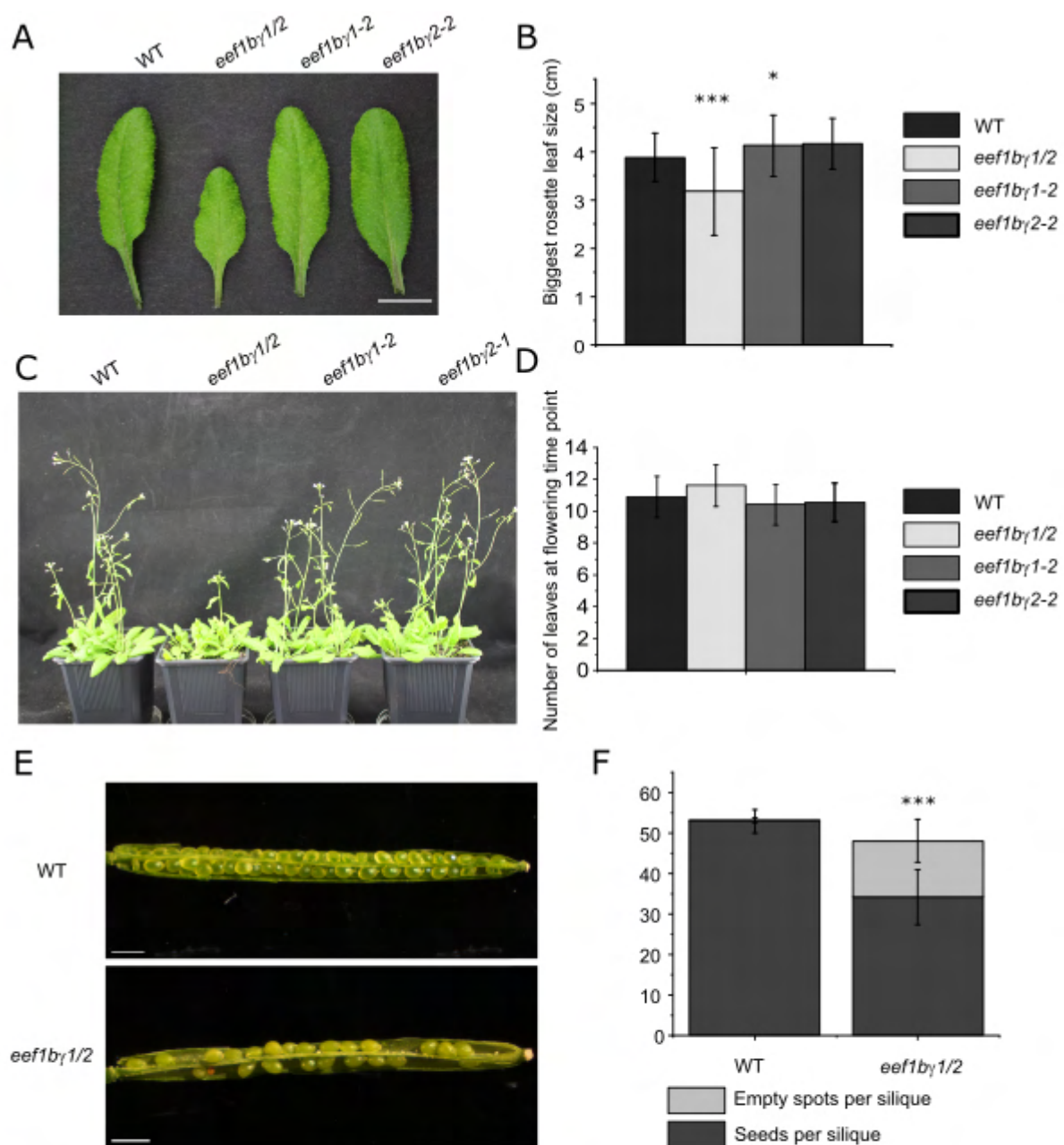


**Figure S1: Phenotype of *eef1by1/2* double mutant and single mutants.**

**(A)** Representative photograph of leaves from 28 days-old soil-grown plants. Scale bar is 1 cm. **(B)** Quantification of the size of the biggest rosette leaf (leaf number 9 to 12) of 26 days-old soil-grown plants. Values represent means  $\pm$ SE (n=35). **(C)** Representative photograph of flowering plants of the indicated genotypes. **(D)** Quantification of leaves formed by soil-grown plants of the indicated genotypes at the time point of floral transition. Values represent means  $\pm$ SE (n=40). **(E)** Representative photographs of siliques of WT and the *eef1by1/2* double mutant. Scale bar is 2 mm. **(F)** Quantification of seeds or empty spots per silique. Values represent means  $\pm$ SE (n=30). Asterisks in (B,D,F) indicate means differing significantly from WT (two-tail Student's t test; \* P < 0.05; \*\* P < 0.01; \*\*\* P < 0.001).

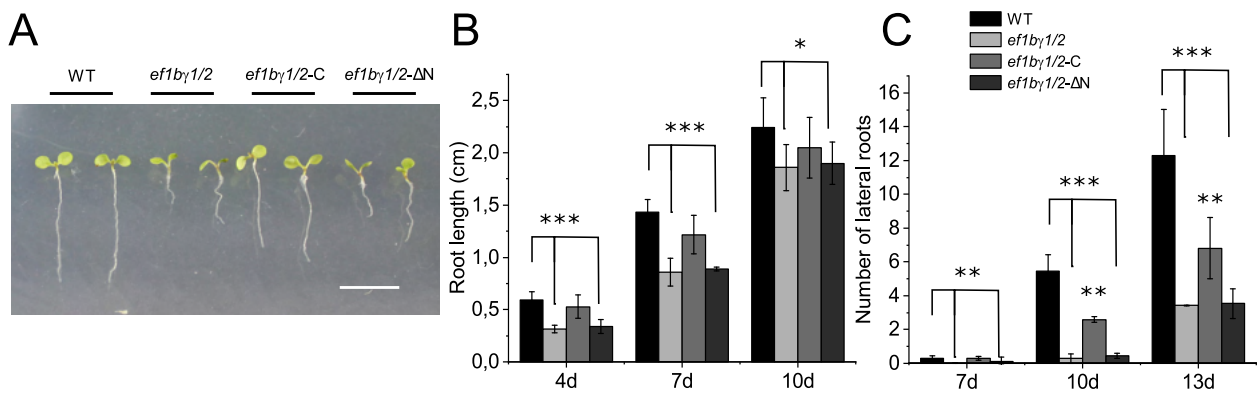


**Figure S2: The truncated version of eEF1B $\gamma$  (YFP-eEF1B $\gamma$  $\Delta$ N) does not complement the phenotype of the *eef1bγ1/2* double mutant.**

(A) Representative photograph of 7 days-old seedlings of the indicated genotypes grown on vertical plates. Scale bar is 1 cm. (B) Measurement of root length of seedlings of the indicated genotypes. Plants were grown on vertical plates and root length was analyzed using ImageJ software. Values represent means  $\pm$ SE from three independent experiments (n=15). (C) Quantification of lateral root formation of seedlings grown on vertical plates. Values represent means  $\pm$ SE from three independent experiments (n=15).

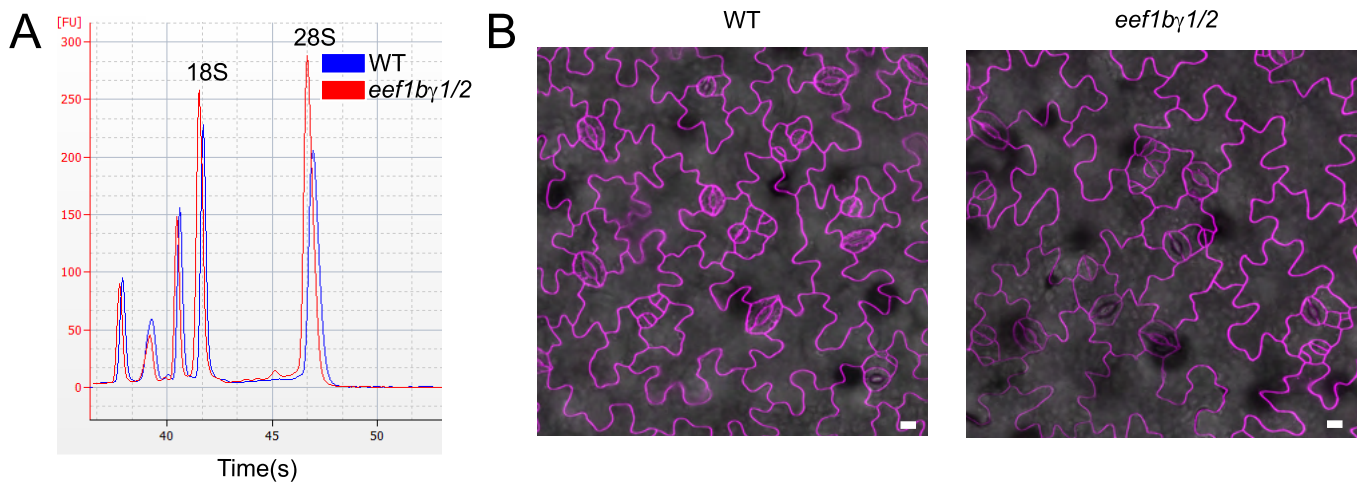


**Figure S3: Quantification of rRNA levels and cell size in WT and mutant plants.**

(A) Representative electropherograms of WT and *eef1bγ1/2* mutant total RNA samples generated by a BioAnalyzer (Agilent). The quantification is shown in Figure 3E. (B) Representative confocal images of adaxial epidermal leaf cells of 7 days-old seedlings stained with FM4-64. Scale bar is 10  $\mu$ m. Quantifications are shown in Figure 3F.



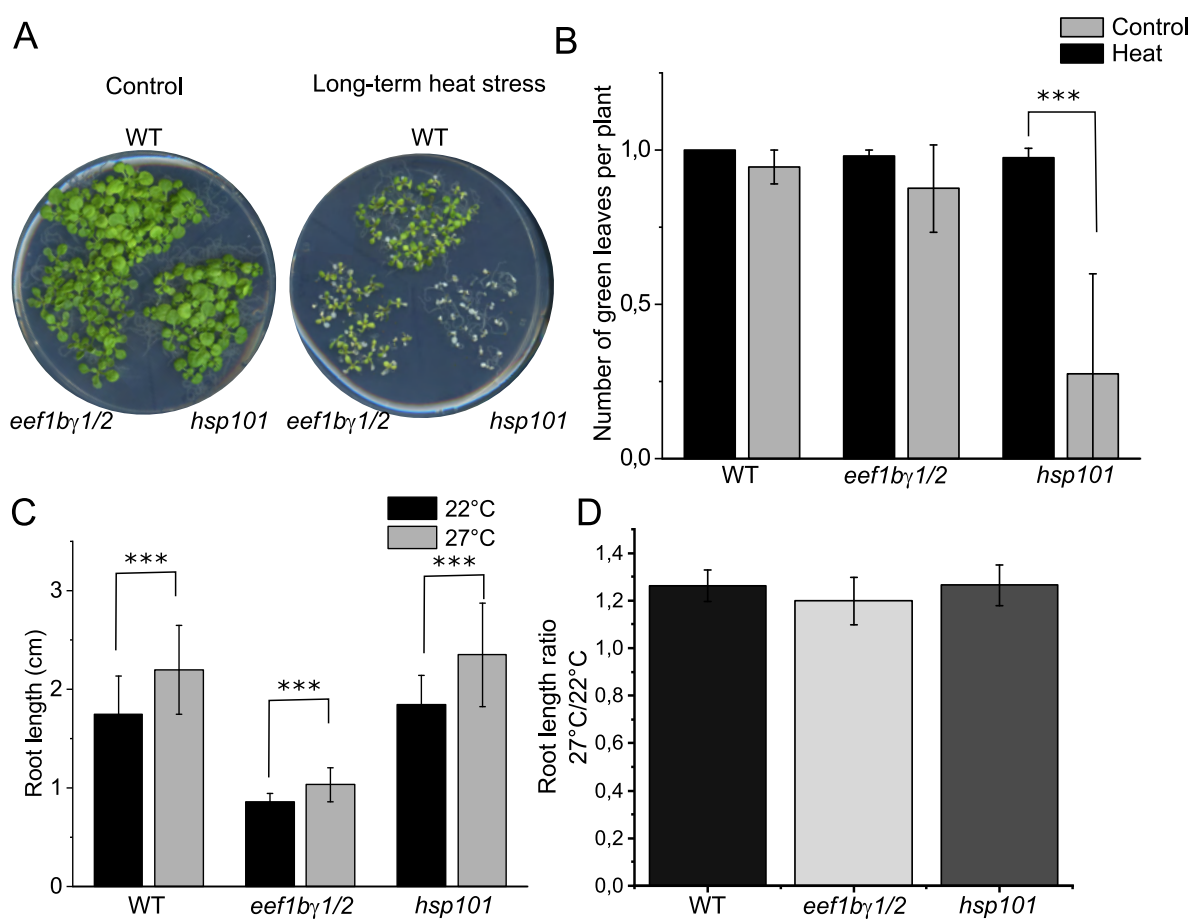


**Figure S4: The *eef1b $\gamma$ 1/2* mutant does not display altered thermotolerance.**

**(A)** Long-term acquired thermotolerance (LAT) of WT and *eef1b $\gamma$ 1/2* double mutant. Seedlings were grown for 6 days at control conditions before first heat treatment (3h 30 min at 38°C), allowed to adapt for 2 days at 22°C, then heat treated a second time (100 min at 45°C). Seven days after the second heat treatment, photographs were taken. **(B)** Quantification of LAT experiment described in (A) by counting the percentage of plants showing expanded green leaves. Data represent means  $\pm$ SE from three independent experiments ( $n \geq 30$ ). Asterisks indicate means differing significantly from the WT (two-tail t test; \*\*\*  $P < 0.001$ ). **(C)** Measurement of root length of WT and the *eef1b $\gamma$ 1/2* mutant grown at control conditions (22°C) or at increased ambient temperature (27°C) on vertical plates for 7 days. Data represent means  $\pm$ SE from three independent experiments ( $n \geq 30$ ). Asterisks indicate means differing significantly from WT (two-tail t test; \*\*\*  $P < 0.001$ ). **(D)** Data shown in (C) presented as ratio of root length at ambient temperature/control.

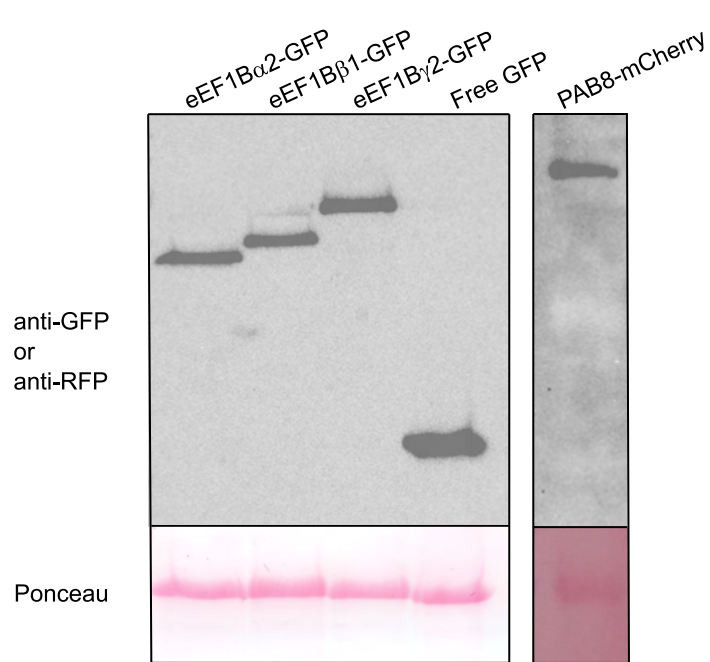


**Figure S5: Integrity of GFP- and mCherry-fusion proteins.**

Immunoblot of protein extracts from protoplasts transiently expressing eEF1B $\alpha$ 2-GFP, eEF1B $\beta$ 1-GFP, eEF1B $\gamma$ 2-GFP, free GFP or PAB8-mCherry. Immunoblot analysis was performed using a GFP or RFP-specific antibody. Ponceau staining was performed as loading control. The data are representative for three independent replicates.

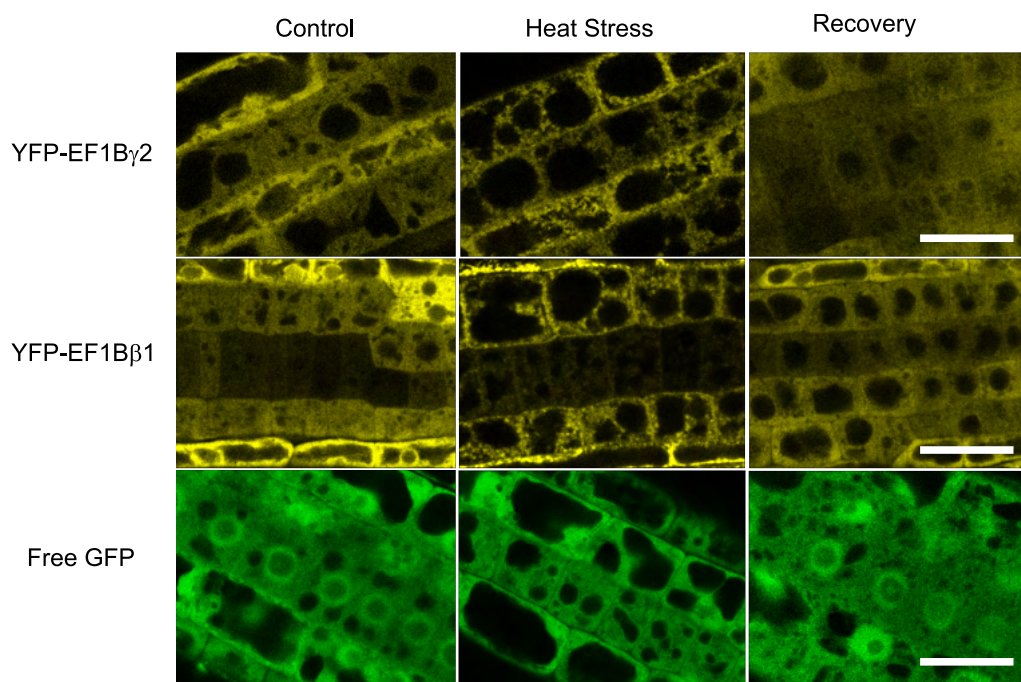


**Figure S6: eEF1B $\beta$ 1 and eEF1B $\gamma$ 2 accumulate in stress granules in Arabidopsis roots after heat stress.**

Representative confocal images of root cells of 4 dag seedlings expressing YFP-eEF1B $\beta$ 1, YFP-eEF1B $\gamma$ 2 or free GFP. Seedlings were photographed at control conditions, after heat treatment (20 min, 42°C) and after recovery (12 hours at 22°C after heat treatment). In all seedlings analyzed the fluorescence associated with YFP-eEF1B $\beta$ 1 (n=35) or YFP-eEF1B $\gamma$ 2 (n= 32) accumulated in cytoplasmic foci after heat treatment, while no foci were observed in seedlings expressing free GFP (n=32). Imaging of the same roots after recovery revealed that the cytoplasmic foci were disassembled (n= 32 for each construct). Scale bar is 23  $\mu$ m. Data were collected in three independent experiments.

## Eidesstattliche Versicherung

Hiermit erkläre ich an Eides statt, dass ich die vorliegende Dissertationsschrift selbst verfasst und keine anderen als die angegebenen Quellen und Hilfsmittel benutzt habe.

Hamburg, den 12.07.2022

Cloe de Luxán Hernández

A handwritten signature in black ink that reads "Cloe de Luxán Hernández". The signature is written in a cursive style and is enclosed within a hand-drawn, irregular oval shape.